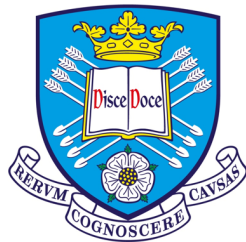


Investigating a role for C9orf72 in mitochondrial quality control

by

Emma Frances Smith

Submitted for the degree of Doctor of Philosophy (PhD)



The
University
Of
Sheffield.

Sheffield Institute for Translational Neuroscience

University of Sheffield

November 2018

Abstract

Mitochondria are vital for the production of energy in the form of ATP and the regulation of many cellular metabolic pathways, including calcium buffering and apoptosis. Due to their high metabolic requirements and extreme polarisation, neurons are especially dependent on the correct localisation and function of their mitochondria. Accordingly, neurons are selectively vulnerable to disturbance of mitochondrial quality control pathways. Mitochondrial dysfunction is strongly implicated in neurodegenerative disorders including amyotrophic lateral sclerosis (ALS) and frontotemporal dementia (FTD).

A GGGGCC hexanucleotide repeat expansion in the first intron of the *C9orf72* gene is currently the most common genetic defect associated with both ALS and FTD. It is unclear how the repeat expansion leads to disease. However, disease has been shown to correlate with reduced *C9orf72* expression, indicating that loss of function may play a role in disease pathogenesis. *C9orf72* encodes two protein isoforms, which we and others have previously shown to play a role in the autophagy pathway. We previously identified several mitochondrial proteins as interacting partners of *C9orf72* using a Y2H screen. This thesis aimed to explore the role of the interaction between *C9orf72* and mitochondria.

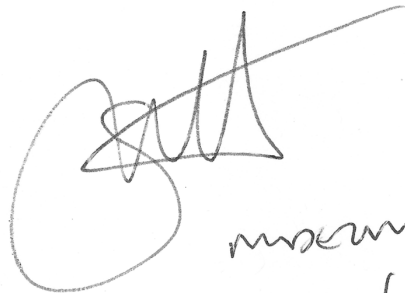
We found *C9orf72* to be located in the mitochondrial intermembrane space and to interact with proteins of the inner mitochondrial membrane and the cytosolic DUB, USP8, previously shown to regulate mitochondrial quality control. *C9orf72* was found to regulate the dynamics of the mitochondrial network and the clearance of damaged mitochondria through the mitophagy pathway. Indeed, siRNA knockdown of *C9orf72* impaired the clearance of damaged mitochondria. Supporting the role of an imbalance in mitochondrial dynamics in disease, *C9orf72* ALS/FTD patient iAstrocytes displayed altered mitochondrial dynamics.

Thus, *C9orf72* haploinsufficiency, leading to reduced levels of the *C9orf72* protein and impaired mitochondrial quality control, could lead to the accumulation of damaged organelles, which may contribute to ALS/FTD pathogenesis.

Statement from Professor Christopher McDermott, Head of Department of Neuroscience

The following PhD thesis '*Investigating a role for C9orf72 in mitochondrial quality control*' submitted to the University of Sheffield by E. F. Smith contains published material from the review article 'The Role of Mitochondria in Amyotrophic Lateral Sclerosis'. This was published in *Neuroscience Letters* (DOI:10.1016/j.neulet.2017.06.052), under a Creative Commons Attribution License (CC BY).

Permission has been given by the co-authors Professor P. J. Shaw and Dr K. J. De Vos for the reuse of the material in this thesis. E. F. Smith wrote the manuscript and prepared the figures, Professor P. J. Shaw critically read the manuscript and Dr K. J. De Vos provided feedback and edited the manuscript. Given the contribution that E. F. Smith made towards the original manuscript, I am happy that reuse of the material in this thesis is appropriate.



Christopher McDermott
24/10/18

Acknowledgements

I would first like to thank my supervisors Dr Kurt De Vos and Dr Andrew Grierson for their continual support and guidance throughout this project. Their enthusiasm, encouragement and help with the preparation of this thesis have been invaluable. I would also like to thank the Motor Neurone Disease Association (MNDA) for funding this PhD project.

I would like to express my gratitude to the patients and families who provided fibroblasts and to Dr Laura Ferraiuolo and her team for culturing these and providing the iAstrocytes. I would like to thank Dr Heather Mortiboys for sharing her protocol for the measurement of mitochondrial membrane potential. Furthermore, I would also like to thank Dr Guillaume Hautbergue and Dr Adrian Higginbottom for sharing their expertise and reagents.

I would also like to thank all past and present members of the De Vos/Grierson lab groups, for their support, friendship and for accommodating my idiosyncrasies. A special thank you to Yolanda and Becky for their willingness to help and listen. I also am extremely grateful to Chris for his extensive help with experimental techniques and for always being available to discuss science, lab life and beyond.

Finally, I would like to thank my parents and brothers for always only being a phone call or message away to provide encouragement and diversion, and Mathew for his constant companionship and patience.

Without all of you this would not have been possible. Thank you!

Contents

Abstract	i
Acknowledgements	v
Contents	vii
Table of Figures.....	xii
Table of Tables.....	xv
Abbreviations.....	xvi
Chapter 1. Introduction	1
1.1 Amyotrophic lateral sclerosis and frontotemporal dementia	1
1.1.1 Pathological features of ALS and FTD.....	2
1.1.2 Genetics of ALS and FTD	3
1.1.3 Mechanisms of disease in ALS.....	8
1.1.3.1 Glutamate excitotoxicity	8
1.1.3.2 Neuroinflammation.....	9
1.1.3.3 Dysregulated RNA metabolism.....	9
1.1.3.4 Dysfunctional proteostasis	10
1.1.3.5 Mitochondrial dysfunction.....	13
1.1.3.5.1 Defective mitochondrial respiration and ATP production	16
1.1.3.5.2 Oxidative stress.....	19
1.1.3.5.3 Calcium mishandling	21
1.1.3.5.4 Pro-apoptotic signaling.....	23
1.2 Impaired mitochondrial dynamics in ALS.....	24
1.2.1 Aberrant mitochondrial fission and fusion events	24
1.2.2 Impaired axonal transport of mitochondria.....	29
1.2.3 Disrupted mitochondrial quality control	32
1.2.3.1 PINK1/Parkin dependent mitophagy	33
1.2.3.2 Parkin independent mitophagy pathways	38
1.2.3.3 Mitophagy feeds into the canonical autophagy pathway that is impaired in ALS	41
1.3 C9orf72-related ALS/FTD	42
1.3.1 The C9orf72 gene	42
1.3.2 C9orf72 is a DENN domain containing protein involved in membrane trafficking events.....	43
1.3.2.1 The role of C9orf72 in autophagy	47
1.3.2.2 The role of C9orf72 in lysosome biology.....	50
1.3.2.3 The role of C9orf72 in the regulation of synaptic function.....	51
1.3.2.4 Additional unexplored functions of C9orf72	51
1.3.3 A repeat expansion in C9orf72 is associated with ALS/FTD	52

1.3.3.1	Toxic RNA gain of function.....	54
1.3.3.2	Toxic protein gain of function	56
1.3.3.3	C9orf72 loss of function.....	58
1.3.3.4	In vitro patient models	61
1.3.3.5	Genetic modifiers of C9orf72 ALS/FTD.....	62
1.4	Hypothesis and aims of the PhD.....	63
Chapter 2.	Materials and Methods.....	65
2.1	Cell culture	65
2.1.1	Cell lines.....	65
2.1.2	Patient derived iAstrocytes.....	65
2.1.3	DNA plasmid transfection.....	67
2.1.4	siRNA transfection	70
2.1.5	Induction of mitophagy	71
2.2	Cloning of plasmid DNA.....	71
2.2.1	Site directed mutagenesis.....	71
2.2.2	Restriction digest of plasmid DNA.....	73
2.2.3	Agarose gel electrophoresis.....	73
2.2.4	Gel elution of purified linear DNA.....	74
2.2.5	Ligation.....	74
2.2.6	Transformation	74
2.2.7	Colony PCR	75
2.2.8	Preparation of glycerol stocks	76
2.2.9	Preparation of plasmid DNA from bacteria.....	76
2.3	Protein biochemistry.....	76
2.3.1	Cell harvesting and lysis	76
2.3.2	Bradford assay	77
2.3.3	Immunoprecipitation.....	77
2.3.4	Polyacrylamide gel electrophoresis and immunoblot.....	78
2.3.4.1	SDS-PAGE.....	78
2.3.4.1.1	Tris-Glycine SDS-PAGE.....	78
2.3.4.1.2	Tris-Tricine SDS-PAGE	78
2.3.4.2	Transfer to membrane.....	79
2.3.4.3	Immunoblot.....	79
2.3.4.4	Quantification of band intensities	81
2.3.5	Cellular fractionation	81
2.3.5.1	Mitochondrial enriched fractions.....	81
2.3.5.2	Purification of mitochondria by sucrose gradient.....	82

2.3.5.3	Isolation of mitochondria from rat liver	82
2.3.6	Mitochondrial sub-organelle analysis	83
2.3.6.1	Membrane integration	83
2.3.6.2	OMM localisation	83
2.3.6.3	IMS localisation	83
2.4	Immunofluorescence microscopy	84
2.4.1	Immunostaining	84
2.4.2	Proximity Ligation Assay	86
2.4.3	Image acquisition and analysis	86
2.4.3.1	Image acquisition	86
2.4.3.2	Quantification of mitochondrial morphological parameters	86
2.4.3.3	Quantification of PLA	90
2.4.3.4	Quantification of Parkin recruitment	91
2.4.3.5	Quantification of mitophagy	92
2.4.4	Analysis of mitochondrial membrane potential	93
2.4.4.1	Plating	93
2.4.4.2	TMRM dye loading	93
2.4.4.3	Automated image acquisition	93
2.4.4.4	Automated analysis of TMRM staining	93
2.5	RT-qPCR	94
2.5.1	RNA extraction	94
2.5.2	Reverse transcription of RNA to cDNA	94
2.5.3	RT-qPCR	95
2.6	In vitro binding assay	96
2.6.1	Production of GST-tagged proteins	96
2.6.2	Polyacrylamide gel and Coomassie stain to check GST expression	96
2.6.3	In vitro binding assay	97
2.6.3.1	In vitro translation in reticulocytes	97
2.6.3.2	Bacterial lysis	97
2.6.3.3	Binding assay	98
2.7	Online bioinformatics tools	98
2.7.1	TMHMM	98
2.7.2	MitoMiner	98
2.7.3	Clustal Omega	99
2.8	Statistical analysis	99
Chapter 3.	Investigating the interaction between C9orf72 and mitochondrial proteins	100
3.1	Introduction	100

3.2	C9orf72 interacts with mitochondrial proteins	101
3.2.1	Transient expression of C9orf72 in cell lines	106
3.2.2	Ornithine Aminotransferase	108
3.2.3	Cytochrome c oxidase subunit 6c	110
3.2.4	ATP Synthase	114
3.2.5	TIM23 complex.....	116
3.3	C9orf72 localises to mitochondria	118
3.4	Investigating the sub-mitochondrial localisation of C9orf72	121
3.4.1	C9orf72 is a peripheral mitochondrial protein	121
3.4.2	C9orf72 is localised in the mitochondrial intermembrane space	123
3.5	Targeting C9orf72 to the mitochondrial intermembrane space	128
3.5.1	Class I IMS protein import.....	128
3.5.2	Class II IMS protein import.....	131
3.5.3	Class III IMS protein import.....	136
3.6	Discussion.....	139
Chapter 4. Investigating the role of the C9orf72 protein in mitochondrial function and dynamics 144		
4.1	Introduction	144
4.2	C9orf72 protein levels alter mitochondrial network dynamics	144
4.2.1	C9orf72 regulates fission/fusion of the mitochondrial network.....	148
4.2.2	Increased C9orf72 expression leads to mitochondrial network fragmentation without altering mitochondrial membrane potential.....	151
4.2.3	Mitochondrial fragmentation occurring upon increased C9orf72 levels is a result of the activation of mitophagy	152
4.3	C9orf72 regulates mitochondrial clearance via mitophagy	157
4.3.1	C9orf72 regulates the recruitment of Parkin to mitochondria	159
4.3.2	C9orf72 is not required for the degradation of OMM proteins.....	164
4.3.3	C9orf72 is recruited to mitochondria upon mitochondrial damage.....	167
4.4	C9orf72 ALS patient iAstrocytes display altered mitochondrial dynamics .	168
4.4.1	C9orf72 patient iAstrocytes have fragmented mitochondrial networks ..	169
4.4.2	Parkin recruitment is delayed in C9orf72 patient iAstrocytes.....	171
4.5	Discussion.....	173
Chapter 5. Investigating the role of the interaction between C9orf72 and USP8 in mitophagy 178		
5.1	Introduction	178
5.2	C9orf72 interacts with USP8.....	180
5.3	C9orf72 and USP8 do not have connected roles in maintaining mitochondrial dynamics.....	187

5.3.1	Knockdown of USP8 does not affect C9orf72 induced fragmentation of the mitochondrial network.....	187
5.3.2	The recruitment of Parkin is differentially regulated by C9orf72 and USP8	189
5.4	Discussion	199
Chapter 6.	Discussion.....	204
6.1	Introduction	204
6.2	The role of the C9orf72 protein in maintaining mitochondrial function.....	205
6.2.1	C9orf72 in mitochondrial function and mitophagy.....	205
6.2.2	Rab GTPases in mitochondrial dynamics and mitophagy	209
6.2.3	The role of the C9orf72 and USP8 interaction.....	212
6.3	Defective mitochondrial dynamics in ALS.....	213
6.3.1	ALS proteins interact with mitochondria and mediate mitochondrial dysfunction.....	213
6.3.2	Import of mitochondrial proteins in ALS.....	215
6.3.3	Structural alterations of mitochondrial networks in ALS.....	215
6.3.4	Defective mitochondrial quality control in ALS.....	217
6.4	Future Directions	222
References	225

Table of Figures

Figure 1.1 The ALS-FTD spectrum.....	7
Figure 1.2 Autophagy is impaired in ALS	13
Figure 1.3 Defective mitochondrial respiration, ATP production and oxidative stress. 18	
Figure 1.4 Loss of calcium homeostasis in ALS	22
Figure 1.5 Pro-apoptotic signalling	24
Figure 1.6 Aberrant mitochondrial fission and fusion in ALS	28
Figure 1.7 Disrupted axonal transport in ALS.....	32
Figure 1.8 Parkin dependent mitophagy is impaired in ALS.....	37
Figure 1.9 Parkin independent mitophagy is impaired in ALS	41
Figure 1.10 The C9orf72 protein contains DENN domains	44
Figure 1.11 Rab GTPases activity is mediated by GAPs and GEFs	45
Figure 1.12 The C9orf72/SMCR8/WDR41 complex interacts with Rab GTPases in autophagy	50
Figure 1.13 The C9orf72 gene is linked to a GGGGCC repeat expansion in intron 1 in ALS/FTD	52
Figure 1.14 The repeat expansion in C9orf72 leads to ALS through 3 different potential disease mechanisms	54
Figure 2.1 Mitochondrial sub-organelle fractionation.....	84
Figure 2.2: Quantification of mitochondrial morphology	88
Figure 2.3: Binary connectivity add-on to quantify mitochondrial network connectivity	89
Figure 2.4: Quantification of PLA puncta per cell	90
Figure 2.5 Quantification of Parkin recruitment	91
Figure 2.6: Quantification of mitophagy.....	92
Figure 2.7: Coomassie stained polyacrylamide gel verifying the expression of GST-tagged proteins	97
Figure 3.1 Myc-tagged C9orf72 constructs express efficiently in cells	107
Figure 3.2 C9orf72 does not interact with OAT	109
Figure 3.3 C9orf72L and C9orf72DdD but not C9orf72S interact with COX6C	111
Figure 3.4 C9orf72L, C9orf72S and C9orf72DdD interact with COX6C in situ.....	113
Figure 3.5 C9orf72 interacts with the ATP Synthase complex	115
Figure 3.6 C9orf72 interacts with the TIM23 complex	117
Figure 3.7 Overexpressed C9orf72 localises to mitochondria	119
Figure 3.8 Endogenous C9orf72 is located in mitochondria	120
Figure 3.9 C9orf72 is not predicted to contain a transmembrane domain.....	122
Figure 3.10 C9orf72L is a peripheral mitochondrial protein.....	123
Figure 3.11 Optimisation of Proteinase K and PMSF conditions.....	125
Figure 3.12 Optimisation of digitonin permeabilisation of the OMM	126

Figure 3.13 C9orf72L resides in the mitochondrial IMS	127
Figure 3.14 Class I IMS protein import.....	129
Figure 3.15 Class II IMS protein import.....	132
Figure 3.16 The C9orf72 protein contains conserved cysteine residues.....	134
Figure 3.17 Knockdown of CHCHD4 does not affect C9orf72 levels or its localisation in mitochondria	135
Figure 3.18 Class III IMS protein import.....	136
Figure 3.19 COX6C is required for the mitochondrial localisation of C9orf72S.....	137
Figure 3.20 Overexpression of COX6C does not affect mitochondrial C9orf72 levels	138
Figure 4.1 Overexpression of C9orf72 leads to the fragmentation of the mitochondrial network	146
Figure 4.2 Reduced levels of C9orf72 lead to increased mitochondrial networking...	147
Figure 4.3 Increased C9orf72 levels do not affect the level of fusion protein Mfn2, but induces Drp1 translocation to mitochondria.....	149
Figure 4.4 The reduction of C9orf72 levels promotes mitochondrial network fusion through increased Mfn2 levels.....	151
Figure 4.5 Increased C9orf72 levels do not influence mitochondrial membrane potential	152
Figure 4.6 The fragmentation of the mitochondrial network upon increased levels of C9orf72L requires the ULK1 initiation complex	155
Figure 4.7 ULK1 is recruited to mitochondria by an increase in C9orf72L levels.....	157
Figure 4.8 Reduced levels of C9orf72 impair mitophagy.....	158
Figure 4.9 An increased C9orf72 level recruits Parkin to mitochondria.....	161
Figure 4.10 The loss of C9orf72 leads to reduced mitochondrially located Parkin at later stages of mitophagy.....	163
Figure 4.11 Loss of C9orf72 does not impair the degradation of OMM proteins during mitophagy	167
Figure 4.12 C9orf72 is recruited to mitochondrial upon mitochondrial damage	168
Figure 4.13 C9orf72 patient iAstrocytes display fragmented mitochondrial networks	170
Figure 4.14 C9orf72 patient iAstrocytes have delayed Parkin recruitment.....	172
Figure 5.1 C9orf72 interacts with USP8	180
Figure 5.2 The generation and expression of USP8 fragments	182
Figure 5.3 C9orf72 interacts with the USP domain of USP8.....	184
Figure 5.4 C9orf72L interacts with the Rhodanese and USP domains of USP8.....	186
Figure 5.5 Knockdown of USP8 does not prevent C9orf72L overexpression induced fragmentation of the mitochondrial network.....	188
Figure 5.6 Knockdown of USP8 impairs Parkin recruitment.....	189
Figure 5.7: The predicted translocation of Parkin ^{WT} and Parkin ^{3xKR} in mitophagy.	191
Figure 5.8: Parkin translocation to mitochondria requires K27, K48 and K76 independently of USP8 activity	193

Figure 5.9 Cells unable to form K6- linked ubiquitin chains are equally affected by USP8 knockdown in their ability to recruit Parkin	196
Figure 5.10 Overexpression of C9orf72 does not rescue the USP8 knockdown delay in Parkin translocation	197
Figure 5.11 Knockdown of C9orf72 does not affect the USP8 knockdown delay in Parkin translocation	199
Figure 6.1 A model suggesting how the C9orf72 complex regulates the engulfment of damaged mitochondria by the autophagosome	207
Figure 6.2 C9orf72 may regulate Rab GTPases governing mitochondrial dynamics	212
Figure 6.3 Mitochondrial damage establishes a pathological cycle	214

Table of Tables

Table 1-1 Known major genetic causes of ALS.....	5
Table 1-2 Impact of ALS genes on mitochondrial function	15
Table 1-3 C9orf72 and the C9orf72/SMCR8/WDR41 complex interact with Rab GTPases.....	46
Table 2-1 C9orf72 patient and matched control iAstrocyte lines	66
Table 2-2 Plasmid DNA constructs.....	67
Table 2-3 Transfection reagents and conditions	69
Table 2-4 siRNA sequences.....	70
Table 2-5 siRNA transfection conditions	71
Table 2-6 Primers used for site directed mutagenesis and PCR elongation times	72
Table 2-7 Composition of restriction digests	73
Table 2-8 PCR mix for colony PCR.....	75
Table 2-9 Primers used for colony PCR.....	75
Table 2-10 Composition of Tris-Glycine polyacrylamide gels.....	78
Table 2-11 Composition of Tris-Tricine polyacrylamide gels.....	79
Table 2-12 Primary antibodies used in immunoblotting.....	80
Table 2-13 Primary antibodies used in immunofluorescence.....	85
Table 2-14 Secondary antibodies used in immunofluorescence	85
Table 2-15 Sequences of primers used for RT-qPCR.....	95
Table 2-16 Master mix for RT-qPCR.....	96
Table 3-1 Mitochondria associated hits from C9orf72 yeast two-hybrid screens	102
Table 3-2 Mitochondrial interacting partners of C9orf72L identified in mass spectrometry screens (Dr Guillaume Hautbergue, SITraN, Sheffield).....	103
Table 3-3 Mitochondrial interacting partners of C9orf72L from the published proteomics screens.....	103
Table 3-4 C9orf72 is not predicted to contain a mitochondrial targeting sequence....	130

Abbreviations

aa	Amino acids
Ab	Antibody
AD	Alzheimer's disease
ADP	Adenosine diphosphate
ALR	Augmenter of Liver Regeneration
ALS	Amyotrophic lateral sclerosis
AMPK	AMP activated protein kinase
APS	Ammonium persulphate
ATP	Adenosine triphosphate
AU	Arbitrary unit
BNIP3	BCL2 Interacting Protein 3
BSA	Bovine serum albumin
C9orf72	Chromosome 9 open reading frame 72
C9orf72DdD	C9orf72 DENN and dDENN domains
C9orf72L	C9orf72 long isoform
C9orf72S	C9orf72 short isoform
Ca ²⁺	Calcium
CCCP	Carbonyl cyanide m-chlorophenyl hydrazone
CCS	Copper chaperones for SOD
COX IV	Cytochrome c oxidase IV
COX6C	Cytochrome c oxidase subunit 6c
cDNA	complementary DNA
CHCHD4	Coiled-Coil-Helix-Coiled-Coil-Helix Domain Containing 4
CNS	Central nervous system
CRISPR	Clustered Regularly Interspaced Short Palindromic Repeats
ddH ₂ O	Double distilled water
dDENN	downstream DENN

DENN	Differentially expressed in normal and neoplasia
DFCP1	Double FYVE domain-containing protein 1
DM1	Myotonic Dystrophy Type 1
DMEM	Dulbecco's modified Eagle's medium
DMPK	Dystrophia Myotonica Protein Kinase
DNA	Deoxyribonucleic acid
dNTPs	Deoxynucleotides
DPR	Dipeptide repeat
dsDNA	double stranded DNA
DUB	Deubiquitinating enzyme
ECL	Enhanced chemiluminescence
EDTA	Ethylenediaminetetraacetic acid
EGFR	Epidermal Growth Factor Receptor
EGTA	ethylene glycol-bis(β -aminoethyl ether)-N,N,N',N'-tetraacetic acid
ER	Endoplasmic reticulum
ERV1	Growth factor, Augmenter Of Liver Regeneration
ETC	Electron transport chain
EV	Empty vector
fALS	Familial ALS
FBS	Foetal bovine serum
FIP200	FAK Family Kinase-Interacting Protein of 200 kDa
FL	Full Length (protein)
FTD	Frontotemporal Dementia
FUNDC1	FUN14 Domain Containing 1
FUS	Fused in Sarcoma
fwd	Forward primer
GAP	GTPase activating protein
GEF	Guanine exchange factor

h	Hour
HD	Huntington's Disease
HSP60	Heat Shock Protein 60
IMM	Inner Mitochondrial Membrane
IMS	Intermembrane Space
kb	Kilobase
kDa	Kilo Dalton
LIR	LC3 interacting region
LUT	Look Up Table
MAM	Mitochondria Associated Membranes
MDV	Mitochondria Derived Vesicle
MEF	Mouse embryonic fibroblast
Mfn	Mitofusin
MIA40	Mitochondrial Intermembrane Space Import And Assembly 40 Homolog (S. Cerevisiae)
MICOS	Mitochondrial Contact Site and Cristae Organising System
min	Minute
MIT	Microtubule Interacting and Trafficking domain
mito	Mitochondria
mL	Millilitre
mM	Millimolar
MMP	Mitochondrial Membrane Potential
MND	Motor Neuron Disease
MnSOD	Manganese-containing Superoxidase dismutase
mtDNA	Mitochondrial DNA
mTOR	Mammalian target of Rapamycin
mTORC1	mTOR complex 1
MVB	Multivesicular Body

NDP52	Nuclear Dot Protein 52
NIX	BCL2 Interacting Protein 3 Like
nm	Nanometre
nM	Nanomolar
NTC	Non-targeting Control
O/A	Oligomycin and Antimycin A
OAT	Ornithine Aminotransferase
O.D.	Optical Density
OMM	Outer Mitochondrial Membrane
OPTN	Optineurin
OXPHOS	Oxidative Phosphorylation
p62	Sequestosome 1
PBS	Phosphate buffered saline
PCR	Polymerase chain reaction
PD	Parkinson's Disease
PEI	Polyethylenimine
PHB2	Prohibitin 2
PINK1	PTEN-induced kinase 1
PK	Proteinase K
PLA	Proximity Ligation Assay
pmol	Picomole
PMSF	Phenylmethylsulfonyl fluoride
Poly-GA	Poly-glycine-alanine DPR
Poly-GP	Poly-glycine-proline DPR
Poly-GR	Poly-glycine-arginine DPR
Poly-PA	Poly-proline-alanine DPR
Poly-PR	Poly-proline-arginine DPR
PTPIP51	Protein Tyrosine Phosphatase-Interacting Protein 51

PVDF	Polyvinylidene fluoride
RT-qPCR	Quantitative real time polymerase chain reaction
RAN	Repeat associated non-ATG
rev	Reverse primer
RHO	Rhodanese domain
RIPA	Radioimmunoprecipitation assay
RNA	Ribonucleic acid
ROI	Region of interest
ROS	Reactive oxygen species
rpm	Revolutions per minute
s	Second
sALS	Sporadic ALS
SDS	Sodium dodecyl sulphate
siRNA	Small interfering RNA
SMCR8	Smith-Magenis Syndrome Chromosome Region, Candidate 8
SOD1	Cu/Zn superoxide dismutase 1
SQSTM1	Sequestosome 1
TARDP	TAR DNA binding protein
TB	Terrific broth
TBK1	TANK-binding kinase 1
TDP-43	TAR DNA-Binding Protein-43
TFEB	Transcription Factor EB
TIM	Translocase of the inner membrane
TMRM	Tetramethylrhodamine, methyl ester
TOM	Translocase of the outer membrane
Ub	Ubiquitin
UBD	Ubiquitin binding domain
uDENN	upstream DENN

ULK1	Unc-51 like autophagy activating kinase 1
UPS	Ubiquitin proteasome system
USP	Ubiquitin specific protease domain
USP8	Ubiquitin specific protease 8
VAPB	Vesicle-associated membrane protein-associated protein B
VCP	Valosin containing protein
WDR41	WD Repeat Domain 41
WT	Wild type
x g	Relative Centrifugal Force (times gravity)
Y2H	Yeast 2-hybrid
μg	Microgram
μL	Microlitre
μm	Micrometre
μM	Micromolar

Chapter 1. Introduction

1.1 Amyotrophic lateral sclerosis and frontotemporal dementia

Motor neuron disease (MND) describes a group of neurological disorders characterised by the selective loss of motor neurons. Amyotrophic Lateral Sclerosis (ALS), the most common MND, is characterised by a progressive degeneration of both upper and lower motor neurons, resulting in muscle atrophy, gradual paralysis and death, usually as a result of respiratory failure. ALS has a worldwide prevalence of 4 – 6 in 100,000, with differences noted between populations (Chiò et al., 2013; Mehta et al., 2016). For instance, the incidence of ALS in European and North American populations was reported to be 1.8 per 100,000, whereas the incidence in eastern Asia was reported to be 0.8 per 100,000 (Marin et al., 2017). The average age of onset of ALS is 55 – 65 years of age, however familial cases of ALS are frequently associated with early onset (Orsini et al., 2015). Familial cases of ALS (fALS) account for around 10 % of all ALS cases, with the remaining 90 % showing no familial inheritance pattern and are referred to as sporadic disease (sALS). The mean survival of an affected individual is 2 – 3 years from diagnosis, with only 25 % and 5 – 10 % surviving 5 and 10 years post diagnosis, respectively (Kiernan et al., 2011).

ALS is characterised into two subtypes depending on site of disease onset. Limb onset ALS is characterised with initial weakness in the limbs, leading to difficulties in moving and carrying out daily tasks. Limb onset is frequently asymmetrical, affecting a single limb in the first instance and accounts for around 70 % of ALS cases (Kiernan et al., 2011). A second group of ALS patients present with initial difficulties with swallowing or speech, termed bulbar onset ALS. Whether the patient originally presents with limb or bulbar onset ALS, the degeneration of motor neurons leads to gradual paralysis affecting the whole body and ultimately the respiratory system leading to respiratory failure (reviewed in Kiernan et al., 2011; Zarei et al., 2015). ALS patients experience difficulties swallowing leading to malnutrition which may potentiate muscle wasting. Due to an earlier degeneration of muscles involved in swallowing, bulbar onset ALS patients frequently have a shorter survival time (reviewed in Chio et al., 2009). In addition, a patient's psychological health has been promoted as a contributing factor to disease. Depression and anxiety are frequently reported by ALS patients, with low mood found to lead to faster disease progression and a shorter survival time (reviewed in Kiernan et al., 2011).

Frontotemporal dementia (FTD) is a common cause of dementia in adults under the age of 65, with a prevalence of 3 – 26 per 100,000 in the UK population aged 45 – 65 years

(Bang et al., 2015). FTD is characterised by neurodegeneration of both the frontal and temporal cortex. Degeneration results in changes in language use and understanding, and personality changes which include increased disinhibition, apathy and abnormal emotional responses (Bang et al., 2015). FTD is categorised into 3 variants according to symptom onset and progression; behavioural variant FTD, non-fluent primary progressive aphasia and semantic variant primary progressive aphasia (Bang et al., 2015). Initially it was considered that unlike in other forms of dementia, FTD patients did not present with any memory impairment not associated with inattention due to reduced executive function. However, more recently, it has become apparent that both long- and short-term memory are affected in FTD, although the exact memory deficit depends on the FTD variant (reviewed in Hornberger and Piguet, 2012). A family history of dementia is reported in 41 % of FTD cases (Rohrer et al., 2009). Death of an individual affected with FTD usually occurs 8 years following onset and is often due to secondary infections (Bang et al., 2015).

ALS shows a degree of clinical overlap with FTD. Around 50 % of ALS patients display behavioural and personality changes associated with FTD and up to 25 % of ALS cases present with clinically diagnosed FTD. Similarly, while approximately 15 % of FTD patients go on to develop ALS, about half display some degree of motor involvement (Swinnen and Robberecht, 2014). The development of ALS occurs more frequently in patients with behavioural variant FTD (Bang et al., 2015).

1.1.1 Pathological features of ALS and FTD

ALS patients who do not have a dementia co-morbidity, do not display gross alterations in brain morphology. However, the spinal cord of ALS patients displays atrophy of the anterior nerve roots. Microscopically, atrophy of motor neurons is observed in the anterior horn of the spinal cord, the lower cranial motor nuclei of the brainstem and the Betz cells of the motor cortex (reviewed in Saberi et al., 2015).

Pathologically, proteinaceous inclusions are a hallmark of ALS. ALS post-mortem tissue displays the presence of 3 distinct protein inclusions. Lewy body-like hyaline inclusions and skein-like inclusions, filamentous inclusions comprised of peripherin and which are ubiquitin positive, are found in the surviving spinal and medullar neurons (Lowe et al., 1988; Mizusawa, 1993; Xiao et al., 2006). These inclusions may form as a result of the aggregation of neurofilament proteins due to defective protein turnover (Migheli et al., 1994). ALS patient post-mortem tissues also display the presence of Bunina bodies (Okamoto et al., 1993), proteinaceous inclusions comprised of cystatin C and transferrin (Okamoto et al., 2008), in the cytoplasm and dendrites surviving lower motor neurons

(Kuroda et al., 1990), which are specific to ALS pathology. Furthermore, an increased prevalence of axonal spheroids, consisting of peripherin and hyperphosphorylated neurofilament, in the proximity of axon hillocks is found in ALS (Corbo and Hays, 1992; Migheli et al., 1993). Although axonal spheroids are a feature of ageing, they are more prevalent in ALS and may represent an early pathological change (Sasaki et al., 1989).

The majority of sALS and fALS cases present with protein inclusions which are positive for TAR DNA-binding protein 43 (TDP-43), which itself can be mutated in ALS (Mackenzie et al., 2007; Pesiridis et al., 2009). Further ubiquitin, sequestosome 1 (p62) and TDP-43 positive inclusions are also observed in sALS and some fALS cases (Arai et al., 2006). Finally many of the mutant forms of proteins associated with ALS have been found to produce inclusions, including the ALS mutant forms of Superoxide dismutase 1 (SOD1), TDP-43, Fused in Sarcoma (FUS) and Optineurin (OPTN) (Blokhuis et al., 2012).

Overt atrophy of the frontal and temporal lobes is observed in FTD patients. Different patterns of degeneration are associated with each variant of FTD and may account for the differences in disease presentation (Bang et al., 2015; Mackenzie and Neumann, 2016; Mohandas and Rajmohan, 2009). In addition to the atrophy, FTD patients display gliosis and changes in microvasculature of the affected brain regions (Bang et al., 2015).

FTD is associated with the accumulation of proteinaceous inclusions. TDP-43 inclusions are a prevalent feature of FTD and are similar to those observed in ALS (Arai et al., 2006; Neumann et al., 2006). In both ALS and FTD, these inclusions are indicative of the mislocalisation of TDP-43 from the nucleus to the cytosol. Secondly, accumulations of hyperphosphorylated tau is a feature of a group of neurodegenerative diseases (tauopathies), which includes FTD, and account for 40 % of frontotemporal lobar degeneration (FTLD) cases (Mackenzie and Neumann, 2016). The cellular localisation and identity of the cells displaying tau inclusions have been reported to be due to the extent of tau hyperphosphorylation and the tau isoforms found in the inclusions (reviewed in Lee et al., 2001).

1.1.2 Genetics of ALS and FTD

To date mutations in over 20 genes have been associated with ALS (Table 1-1; Ref: <http://alsod.iop.kcl.ac.uk/home.aspx>; (Abel et al., 2012)), including *SOD1* (Rosen et al., 1993), TAR DNA binding protein (*TARDBP*) (Sreedharan et al., 2008), *FUS* (Kwiatkowski Jr et al., 2009; Vance et al., 2009), and Chromosome 9 open reading frame 72 (*C9orf72*) (DeJesus-Hernandez et al., 2011; Renton et al., 2011). Together mutations in these genes account for approximately 60 % of fALS and 11 % of sALS cases.

Therefore, the genetic basis of a significant number of ALS cases remains to be determined. The mutation identified in *C9orf72* is the most common cause of ALS that has been identified to date, accounting for around 40 % of fALS and 6 % of sALS in Western countries (reviewed in Renton et al., 2014).

In addition to the genes listed in Table 1-1, a number of rare variants and ALS risk factors have been identified. These include *NEFH* (Figlewicz et al., 1994), *PRPH* (Gros-Louis et al., 2004; Leung et al., 2004), *SPAST* (Meyer et al., 2005) and *ELP3* (Simpson et al., 2009) which play a role in cytoskeleton architecture; *UNC13A* (van Es et al., 2009), *DCTN1* (Puls et al., 2003), *TUBA4* (Smith et al., 2014) and *ANXA11* (Smith et al., 2017a) which regulate vesicle trafficking; *TAF15* (Ticozzi et al., 2011) and *TIA1* (Mackenzie et al., 2017) which are involved in RNA metabolism; *LMNB* (Johnson et al., 2014b) involved in maintaining the nuclear envelope, *SQSTM1/p62* (Fecto et al., 2011) and *TBK1* (Freischmidt et al., 2015) involved in the targeting of cellular substrates for degradation by the autophagy pathway; *CCNF* (Williams et al., 2016) involved in proteostasis; *DAO* (Millecamps et al., 2010; Mitchell et al., 2010) involved in oxidative stress pathways; *NEK1* (Kenna et al., 2016) and *C21orf2* (van Rheenen et al., 2016) involved in the DNA damage response.

The genes found to be mutated in ALS have been implicated in a wide range of cellular pathways, suggesting that ALS may be a multi-factorial disease (reviewed in Ferraiuolo et al., 2011; Taylor et al., 2016). Possible pathogenic mechanisms underlying motor neuron degeneration include RNA metabolism dysregulation, excitotoxicity, disruption of proteostasis, oxidative stress, and mitochondrial dysfunction. Due to the complex aetiology observed in ALS, it is likely that multiple of these mechanisms are concurrently involved in disease. This leads to the possibility that these mechanisms may interact and influence reciprocally their dysfunction.

Table 1-1 Known major genetic causes of ALS

The genes identified in ALS and the cellular processes affected in disease (Ref: <http://alsod.iop.kcl.ac.uk/home.aspx>).

Locus	Gene	Chromosome	Gene name	Cellular processes affected in disease	Reference
ALS1	<i>SOD1</i>	21q22.11	Cu/Zn superoxide dismutase 1	Oxidative stress, axonal transport, mitochondrial function, endosome trafficking	(Rosen et al., 1993)
ALS2	<i>Alsin</i>	2q33.2	Alsin	ESCRT, vesicle trafficking	(Hentati et al., 1994)
ALS3	<i>ALS3</i>	18q21	Unknown	-	(Hand et al., 2002)
ALS4	<i>SETX</i>	9q34.13	Senataxin	RNA metabolism, DNA metabolism	(Zhao et al., 2009)
ALS5	<i>SPG11</i>	15q14	Spastic paraplegia 11	DNA metabolism	(Orlacchio et al., 2010)
ALS6	<i>FUS</i>	16p11.2	Fused in Sarcoma	RNA metabolism	(Kwiatkowski Jr et al., 2009; Vance et al., 2009)
ALS7	<i>ALS7</i>	20p13	Unknown	-	(Sapp et al., 2003)
ALS8	<i>VAPB</i>	20q13.33	Vesicle-associated membrane protein-associated protein B	Axonal transport, calcium buffering, UPR	(Nishimura et al., 2004)
ALS9	<i>ANG</i>	14q11.1	Angiogenin	RNA metabolism, DNA metabolism	(Greenway et al., 2004)

Locus	Gene	Chromosome	Gene name	Cellular processes affected in disease	Reference
ALS10	<i>TARDBP</i>	1p36.22	TAR DNA binding protein	RNA metabolism	(Sreedharan et al., 2008)
ALS11	<i>FIG4</i>	6q21	FIG4 Phosphoinositide 5-Phosphatase	Autophagy, ER-Golgi network, ESCRT	(Chow et al., 2009)
ALS12	<i>OPTN</i>	10p13	Optineurin	Autophagy, ER-Golgi network, vesicle trafficking	(Maruyama et al., 2010)
ALS13	<i>ATXN2</i>	12q23-24.1	Ataxin 2	RNA metabolism	(Elden et al., 2010)
ALS14	<i>VCP</i>	9p13	Valosin-containing protein	Autophagy, vesicle trafficking	(Johnson et al., 2010)
ALS15	<i>UBQLN2</i>	Xp11.21	Ubiquilin 2	Autophagy	(Deng et al., 2011)
ALS16	<i>SIGMAR1</i>	9p13	Sigma non-opioid intracellular receptor 1	ER-Golgi network	(Al-Saif et al., 2011)
ALS17	<i>CHMP2B</i>	3p12.1	Chromatin modifying protein 2B	ESCRT, vesicle trafficking	(Parkinson et al., 2006)
ALS18	<i>PFN1</i>	17p13.3	Profilin 1	Cytoskeleton architecture	(Wu et al., 2012)
ALS19	<i>ERBB4</i>	2q33.3-q34	Erb-B2 receptor tyrosine kinase 4	Cytoskeleton architecture	(Takahashi et al., 2013)
ALS20	<i>hnRNPA1</i>	12q13.1	Heterogeneous nuclear riboprotein A1	RNA metabolism	(Kim et al., 2013a)
ALS21	<i>MATR3</i>	5q31.2	Matrin 3	RNA metabolism	(Johnson et al., 2014b)

Locus	Gene	Chromosome	Gene name	Cellular processes affected in disease	Reference
ALS-FTD1	<i>C9orf72</i>	9p21.2	Chromosome 9 open reading frame 72	Autophagy, RNA processing	(DeJesus-Hernandez et al., 2011; Renton et al., 2011)
ALS-FTD2	<i>CHCHD10</i>	22q11.23	Coiled-coil-helix-coiled-coil-helix domain containing 10	Mitochondrial function	(Johnson et al., 2014a)

Abbreviations: ESCRT - endosomal sorting complexes required for transport, RNA - ribonucleic acid, DNA - deoxyribonucleic acid, UPR - unfolded protein response, ER - endoplasmic reticulum

Forty-one percent of FTD patients display a family history of dementia, although only 10 % show a pattern consistent with autosomal dominant inheritance (Rohrer et al., 2009). The main genetic causes of FTD include mutations in Tau (*MAPT*), Progranulin (*GRN*) and *C9orf72*, which together account for around 60 % of familial disease (Le Ber, 2013). Mutations in *C9orf72* mutations account for 25 % of familial cases, making it the most common cause of both FTD and ALS (Bang et al., 2015). Mutations in a number of ALS genes are also rare genetic causes of FTD; these include *VCP*, *CHMP2B*, *FUS*, *TARDBP*, *SQSTM1/p62*, *UBQLN2*, *TBK1* and *OPTN* (reviewed in Bang et al., 2015; Mackenzie and Neumann, 2016). The overlap between both the genetics and clinical features of FTD and ALS suggest a spectrum of disease (Figure 1.1).

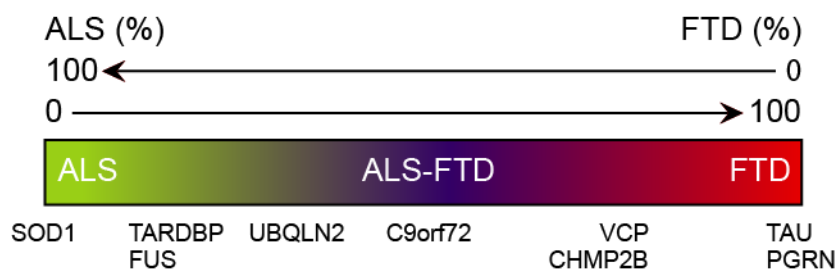


Figure 1.1 The ALS-FTD spectrum

Whilst mutations in *SOD1* produce exclusively an ALS phenotype, and those in *TAU* and *PGRN* exclusively an FTD phenotype, mutations in several genes have been

identified to present either as ALS or FTD. Most consistently, the repeat expansion of the C9orf72 gene is the most common genetic cause of both ALS and FTD.

1.1.3 Mechanisms of disease in ALS

A number of disrupted cellular processes are thought to contribute to the pathogenesis of ALS. Below are briefly explored some of the most commonly observed cellular dysfunctions found in ALS, including glutamate excitotoxicity, neuroinflammation, dysregulated RNA metabolism and proteostasis, and mitochondrial dysfunction.

Due to the overlap in clinical features and pathology, many of the mechanisms proposed to contribute to ALS are thought to contribute to FTD. Tauopathy is additionally linked to the development of altered mitochondrial dynamics, oxidative stress, cytoskeleton alterations and dysregulation of the nucleoskeleton leading to gene expression changes (reviewed in Orr et al., 2017).

1.1.3.1 Glutamate excitotoxicity

Neurotransmission underlies the functioning of the central nervous system (CNS). The major excitatory neurotransmitter of the CNS is L-glutamate which is removed from the synaptic cleft following neurotransmission by astrocytes, where it is degraded and recycled back to the neuron (Featherstone, 2010). L-glutamate release elicits an action potential in the post-synaptic neuron, through the activation of NMDA and AMPA receptors leading to the influx of sodium (Na^{2+}) and calcium (Ca^{2+}). Elevated and persistent Ca^{2+} influx into the post-synaptic neuron can induce neuronal death, termed excitotoxicity (reviewed in Dong et al., 2009).

Excitotoxicity has been linked to ALS (reviewed in Foran and Trotti, 2009; Van Den Bosch et al., 2006). Synaptic L-glutamate levels are elevated in ALS patients, suggesting defective re-uptake by astrocytes (Rothstein et al., 1992). Elevated synaptic L-glutamate can lead to further stimulation of post-synaptic receptors and excitotoxicity. Motor neurons express a high number of Ca^{2+} permeable AMPA receptors at the postsynaptic terminal, which results in a greater vulnerability to excitotoxicity through excessive Ca^{2+} influx during excitatory neurotransmission events (Shaw and Eggett, 2000; Van Den Bosch et al., 2000; Williams et al., 1997). In addition, motor neurons have reduced cytosolic buffering capacity as they express low levels of Ca^{2+} buffering proteins such as parvalbumin and calbindin D-28k, which makes them more reliant on mitochondria for Ca^{2+} buffering (Alexianu et al., 1994; reviewed in Grosskreutz et al., 2010; Ince et al., 1993; Palecek et al., 1999; Tadic et al., 2014). ALS neurons display decreased mitochondrial associated Ca^{2+} buffering capacity (explored further in

1.1.3.5.3), which potentiates the persistence in elevated Ca^{2+} in post-synaptic neurons and excitotoxicity (reviewed in Jaiswal, 2013; Smith et al., 2017b). Together this provides a potential link between elevated Ca^{2+} levels and cell type vulnerability in ALS (Van Den Bosch et al., 2000).

1.1.3.2 Neuroinflammation

An abnormal activation of the immune system is a common feature of neurodegenerative diseases (reviewed in Chen et al., 2016a), including ALS (reviewed in Liu and Wang, 2017). Indeed, a self-perpetuating cycle may be established, which promotes neurodegeneration. Activation of the immune response, including microglial activation, leads to the generation of reactive oxygen species (ROS) and a pro-inflammatory environment which may result in neuronal death. Neuronal death may then consequently result in the release of signals that lead to further microglial activation (reviewed in Chen et al., 2016a).

Evidence of an abnormally activated immune response is observed in ALS patient post-mortem tissue. The infiltration of activated microglia has been identified in ALS patients and *in vitro* models of SOD1 and C9orf72 ALS (Corcia et al., 2012; Gargiulo et al., 2016; O'Rourke et al., 2016; Turner et al., 2004). It is unclear if the infiltration is a primary feature of disease or as a result of the axonal dying back mechanism. Astrocytes act as neurotrophic support cells which regulate the neuroinflammatory process (reviewed in Colombo and Farina, 2016). In culture, ALS patient derived iAstrocytes do not support motor neurons to the same extent as control astrocytes (Meyer et al., 2014). Indeed, metabolic changes in astrocyte function have been reported to contribute to motor neuron death (reviewed in Liu and Wang, 2017). The dysfunction of microglia and astrocytes in ALS support a non-cell autonomous disease mechanism (reviewed in Chen et al., 2018). The activation of the immune response in ALS is not restricted to the CNS. In the periphery reduced levels of regulatory T-cells are reported, with lower levels associated with a more rapid disease progression (Beers et al., 2011; Henkel et al., 2013).

1.1.3.3 Dysregulated RNA metabolism

A common feature of ALS cases, with the exception of SOD1 and FUS linked ALS, is the presence of TDP-43 positive inclusions. TDP-43 is an RNA-binding protein that normally localises to the nucleus, where it is involved in transcription and splicing. In ALS, TDP-43 is mislocalised to the cytosol. The loss of the nuclear function of TDP-43 is proposed to lead to altered expression of nuclear encoded proteins (reviewed in

Scotter et al., 2015). Similarly, ALS-linked mutations in the RNA-binding and processing protein FUS lead to dysregulation of transcription and splicing events, through the mislocalisation of FUS to the cytosol (reviewed in Shang and Huang, 2016). In addition, the loss of nuclear TDP-43 and FUS also leads to the dysregulation of miRNAs resulting in further changes in gene expression (Dini Modigliani et al., 2014; Freischmidt et al., 2013).

Cytosolic accumulations of TDP-43 and FUS can result in the formation of RNA-rich stress granules in the cytosol (reviewed in Aulas and Vande Velde, 2015). Under normal conditions, stress granule formation is a dynamic protective mechanism triggered by cellular stress, following which the RNAs contained are either stored, degraded or translated (reviewed in Protter and Parker, 2016). However prolonged stress granule formation leads to sequestration of RNA binding proteins and changes in gene expression. Persistent stress granules are proposed to prime the formation of insoluble protein aggregates, which are a common feature in ALS (reviewed in Aulas and Vande Velde, 2015).

In C9orf72-linked ALS/FTD, in addition to the TDP-43 mislocalisation related changes in RNA metabolism, patients display the presence of RNA foci, which arise from the repeat expansion itself (DeJesus-Hernandez et al., 2011). The impact of these RNA foci in C9orf72 ALS/FTD will be discussed further in 1.3.3.1. How changes in RNA metabolism may contribute to ALS pathogenesis has been reviewed extensively elsewhere (Barmada, 2015; Kapeli et al., 2017; Liu et al., 2017).

1.1.3.4 Dysfunctional proteostasis

Proteostasis, the maintenance of a healthy pool of functional proteins, is achieved through the degradation of misfolded and aggregated proteins by the proteasome and acidic lysosomes (reviewed in Boya et al., 2013; Tanaka, 2009). As such, proteostasis underlies cellular homeostasis and dysfunctional proteostasis is associated with the development of neurodegenerative disease (reviewed in Labbadia and Morimoto, 2015). Due to their post-mitotic nature, neurons are particularly vulnerable to disturbances in proteostasis (reviewed in Son et al., 2012).

Protein aggregates are a hallmark of ALS pathology, with all patient cases and many disease models displaying some degree of protein mislocalisation and aggregation (Blokhuis et al., 2013). Accumulations of proteins in ALS are likely to overwhelm the systems designed to clear dysfunctional proteins and lead to cellular stress (reviewed in Ramesh and Pandey, 2017). Indeed, alterations in the mechanisms evolved to maintain proteostasis have been reported in ALS, including decreased activity and

protein folding by chaperones, the induction of endoplasmic reticulum (ER) stress and the unfolded protein response (UPR), decreased proteasome function and impaired autophagy (reviewed in Medinas et al., 2017; Shahheydari et al., 2017; Webster et al., 2017). Ultimately, defects in proteostasis may contribute to other ALS disease mechanisms, including mitochondrial dysfunction and neuroinflammation.

The autophagy pathway is responsible for the bulk degradation of cytosolic proteins and organelles through fusion with the lysosome (Figure 1.2). Briefly, the initiation of autophagosome biogenesis is regulated by the Unc-51 like autophagy activating kinase 1 (ULK1) initiation complex, comprised of ULK1, FAK Family Kinase-Interacting Protein of 200 kDa (FIP200), Autophagy Related 13 (ATG13) and Autophagy Related 101 (ATG101) (Ganley et al., 2009; Hosokawa et al., 2009; Mercer et al., 2009). The ULK1 initiation complex is regulated by mammalian target of rapamycin complex 1 (mTORC1) and AMP-activated protein kinase (AMPK) (Kim et al., 2011; Laker et al., 2017; Tian et al., 2015). The activation of ULK1 results in its translocation to the nascent phagophore (Hara et al., 2008; Karanasios et al., 2013). Contributing further to the nucleation of the autophagosome, the PI3K complex, consisting of Beclin1, Vps14, Vps34 and ATG14L, is also recruited to the nascent phagophore. The PI3K complex converts phosphatidylinositol to PI3P, promoting the elongation of the phagophore membrane (Matsunaga et al., 2009; Zhong et al., 2009). The extension of the phagophore membrane is achieved through the additional retrieval of ATG9A membranes (Zhou et al., 2016). The ATG5-12 and PE-LC3 ubiquitin-like conjugation systems elongate and complete the encapsulation of the phagophore (Mizushima et al., 1998). In mammals both the LC3 and GABARAP subfamilies undergo PE conjugation (Weidberg et al., 2010), but may play distinct roles in autophagy progression (reviewed in Schaaf et al., 2016).

Cargos destined for the autophagosome are targeted by the autophagy receptors, including p62 and OPTN, which interact with poly-ubiquitin chains on the substrate via their ubiquitin-like domains (reviewed in Shaid et al., 2013). The autophagy receptors additionally possess LC3-interacting regions (LIR), which interacts with LC3-II found on the growing phagophore (reviewed in Birgisdottir et al., 2013).

Following the completion of the autophagosome membrane, the autophagosome undergoes transport and fusion to the lysosome. Autophagosome contents are degraded by acidic hydrolases and the constituents released into the cytosol for recycling (reviewed in Nakamura and Yoshimori, 2017)

Defects in the autophagy pathway have been reported to be widespread in ALS (Figure 1.2) (reviewed in Ramesh and Pandey, 2017; Webster et al., 2017). The C9orf72 protein has been shown to mediate the translocation of the ULK1 initiation complex to the phagophore during initiation (Figure 1.2) (Sellier et al., 2016; Webster et al., 2016a; Yang et al., 2016). As C9orf72 haploinsufficiency may contribute to disease, the initiation of autophagy is thought to be impaired in C9orf72 ALS/FTD (discussed later in sections 1.3.2.1 and 1.3.3.3) (reviewed in Webster et al., 2016b). Furthermore, the retrieval of ATG9A membranes has been shown to be regulated by the Rab GTPase Rab7 (Yamano et al., 2018). Interestingly, the C9orf72 protein has been shown to interact with Rab7 (Farg et al., 2014; Frick et al., 2018). It is currently unknown whether this interaction is relevant for the retrieval of ATG9A membranes, or whether this is affected in C9orf72 ALS/FTD.

The trafficking of the PI3K complex is mediated by the Rab GTPase Rab5, which is regulated by its effector Alsln (Ravikumar et al., 2008). ALS-linked mutations in Alsln result in decreased activation of the PI3K complex and decreased autophagosome formation (Figure 1.2) (Hadano et al., 2001; Hadano et al., 2010; Otomo et al., 2011).

The delivery of substrates to the autophagosome, including mitochondria, is dependent on their association with LC3. ALS-linked mutations in OPTN, TBK1, p62 and UBQLN2 lead to impaired delivery of substrates to the autophagosome (Figure 1.2) (reviewed in Majcher et al., 2015; Webster et al., 2017).

The VCP protein has been shown to play a role in the degradation of proteins by the proteasome (reviewed in Avci and Lemberg, 2015; Meyer and Wehl, 2014), reduced VCP activity has also been shown to result in a decreased maturation of autophagosomes (Figure 1.2) (Ju et al., 2009; Tresse et al., 2010). As ALS linked mutations in VCP are likely to result in loss of function (reviewed in Tang and Xia, 2016), VCP-linked ALS may also be associated with decreased autophagosome maturation.

Finally, ALS and FTD-linked mutations in the axonal retrograde transport proteins Tubulin, Dynein and Dynactin and proteins involved in lysosome biogenesis pathways contribute to the accumulation of autophagic cargos (Figure 1.2) (reviewed in Webster et al., 2017).

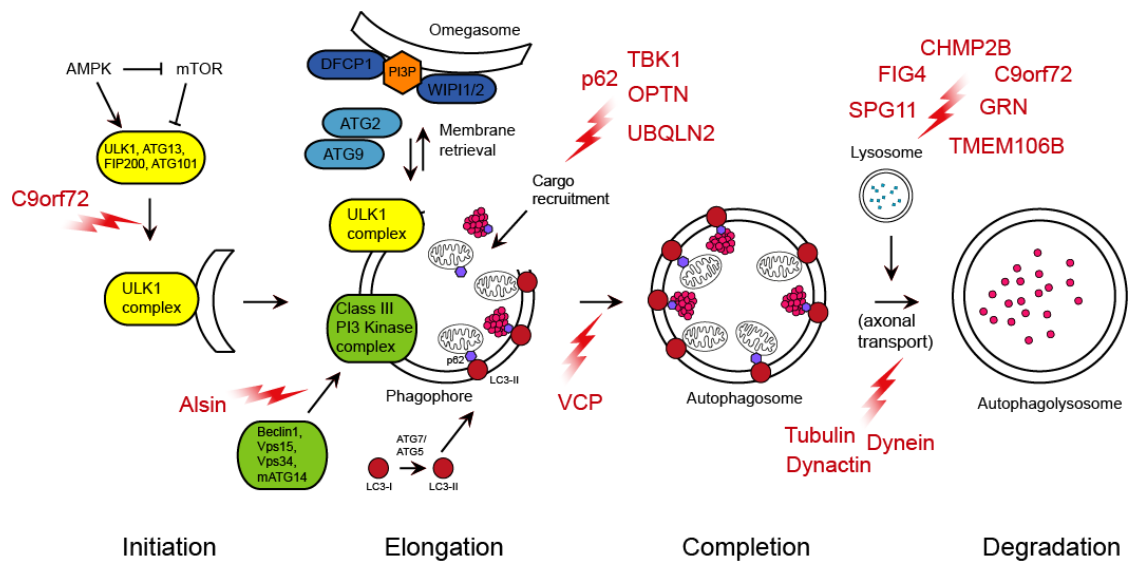


Figure 1.2 Autophagy is impaired in ALS

The autophagy pathway is responsible for the clearance of damaged organelles and proteins. The AMPK and mTOR axes regulate the initiation of autophagy. Upon induction of autophagy, the ULK1 initiation complex is recruited to the phagophore. Elongation of the nascent phagophore is mediated by the PI3K complex and the retrieval of additional ATG9A membranes. Cargos are delivered to the autophagosome via autophagy receptors including p62 and OPTN through their interaction with LC3-II on the nascent phagophore. Completed autophagosomes are transported and fuse to lysosomes, which results in the degradation of autophagy substrates. Degraded autophagic substrates, namely amino acids, are recycled back to the cytosol. ALS-linked mutations (indicated in red) impair the progression of autophagy at multiple stages, and lead to the accumulation of damaged proteins and organelles. Please refer to main text for further details.

1.1.3.5 Mitochondrial dysfunction

During normal ageing, mitochondrial quality decreases leading to accumulations of damaged and poorly functioning organelles (reviewed in Shi et al., 2018a; Sun et al., 2016). The general decline in mitochondrial function may be a contributing factor in the onset and progression of neurodegenerative diseases. Indeed, dysfunction of mitochondria is a prevalent feature of neurodegenerative disease including Alzheimer's (AD), Huntington's (HD), Parkinson's (PD) diseases and ALS (reviewed in Evans and Holzbaur, 2018; Guedes-Dias et al., 2016; Kerr et al., 2017; Park et al., 2018; Smith et al., 2017b).

Structurally altered and aggregated mitochondria, with a swollen and vacuolated appearance, were one of the first changes observed in ALS patient motor neurons (Atsumi, 1981; Sasaki and Iwata, 2007) and in Bunina bodies (Hart et al., 1977). Furthermore, mitochondrial structure and the mitochondrial network appears to be disrupted in most if not all models of familial ALS (reviewed in Smith et al., 2017b). Moreover, the structural damage to mitochondria and fragmentation of the mitochondrial network was reported to occur in early disease stages in *in vivo* models of ALS. This indicates that mitochondrial morphological alterations occur potentially as a source of degenerations rather than a consequence and may contribute to ongoing degenerating phenotype (Magrané et al., 2014; Vande Velde et al., 2011; Wang et al., 2013).

A number of proteins that have been linked to familial and sporadic ALS, including SOD1, TDP-43, FUS, C9orf72, and the C9orf72 GGGGCC repeat expansion-associated glycine/arginine (GR) dipeptide repeat protein (DPR), have been shown to interact with mitochondria (Blokhuys et al., 2016; Deng et al., 2015; Higgins et al., 2002; Lopez-Gonzalez et al., 2016; Mattiazzi et al., 2002; Wang et al., 2016). Several of these interactions have been shown to deleteriously affect mitochondrial function (reviewed in Smith et al., 2017b).

Many of the identified ALS genes have a role in mitochondrial-associated functions. Evidence gathered from *in vitro* and *in vivo* disease models and from patient studies strongly implicates the dysfunction of mitochondria as a core ALS disease component (Table 1-2) (reviewed in Khalil and Liévens, 2017; Smith et al., 2017b). Furthermore, with the possible exception of RNA toxicity, mitochondrial dysfunction appears to be directly or indirectly linked to all of the postulated “non-mitochondrial” mechanisms of toxicity associated with ALS, including excitotoxicity, loss of protein homeostasis and defective axonal transport.

Table 1-2 Impact of ALS genes on mitochondrial function

Potential impact of pathogenic variants of ALS genes on mitochondrial function
(Reference: <http://alsod.iop.kcl.ac.uk/home.aspx>, adapted from (Smith et al., 2017b)).

Gene	Protein	Potential consequence of mutation on mitochondrial function
<i>SOD1</i>	Cu, Zn superoxide dismutase 1	Mutant protein aggregates in IMS; decreased ATP generation; increased cellular ROS and ROS induced cellular damage; imbalance in Ca ²⁺ homeostasis; induction of apoptosis via VDAC inhibition and Bcl-2 binding; disrupted mitochondrial architecture; impaired mitochondrial network dynamics and axonal transport; impaired mitochondrial clearance by mitophagy; disrupted ER-mitochondria contacts
<i>ALS2</i>	Alsin	Reduced autophagosome formation and decreased mitophagy
<i>FUS</i>	RNA-binding protein FUS	Decreased ATP generation; increased ROS levels; loss of Ca ²⁺ homeostasis and disruption of ER-mitochondria contacts; reduced mitophagy-related gene expression; disrupted mitochondrial architecture; impaired mitochondrial transport via disrupted kinesin gene expression
<i>VAPB</i>	Vesicle-associated membrane protein-associated protein B	Impaired Ca ²⁺ homeostasis; decreased anterograde axonal transport; disrupted ER-mitochondria contacts
<i>TARDBP</i>	TAR DNA-binding protein 43	TDP-43 aggregates in mitochondria and disrupts mtDNA transcription; decreased ATP generation; impaired Ca ²⁺ homeostasis and disrupted ER-mitochondria contacts; disrupted mitochondrial architecture; altered mitochondrial network dynamics and impaired mitochondrial axonal transport; reduced mitophagy related gene expression; impaired mitochondrial clearance by mitophagy
<i>OPTN</i>	Optineurin	Reduced mitochondrial clearance by mitophagy
<i>VCP</i>	Valosin-containing protein	Decreased ATP levels; mitochondrial uncoupling; reduced mitochondrial clearance by mitophagy
<i>SIGMAR1</i>	Sigma non-opioid intracellular receptor 1	Reduced ATP generation; disrupted ER-mitochondria contacts; dysregulated Ca ²⁺ homeostasis; reduced axonal transport

Gene	Protein	Potential consequence of mutation on mitochondrial function
<i>C9orf72</i>	Chromosome 9 open reading frame 72	DPR proteins interact with mitochondrial ribosomal proteins; altered MMP; increased cellular ROS levels; poly(GR) DPR induced oxidative stress; impaired autophagy; disrupted mitochondrial architecture and altered mitochondrial network dynamics
<i>CHCHD10</i>	Coiled-coil-helix-coiled-coil-helix domain containing 10	Disrupted mitochondrial architecture; decreased electron transport chain activity
<i>SQSTM1</i>	p62/Sequestosome 1	Reduced mitochondrial clearance by mitophagy; reduced MMP
<i>TBK1</i>	TANK-binding kinase 1	Reduced mitochondrial clearance by mitophagy

Abbreviations: IMS - intermembrane space, ATP - adenosine triphosphate, ROS - reactive oxygen species, ER - endoplasmic reticulum, mtDNA - mitochondrial DNA, DPR - dipeptide repeat protein, MMP - mitochondrial membrane potential

ALS associated mitochondrial dysfunction comes in many guises, including defective oxidative phosphorylation (OXPHOS), excessive ROS generation and ROS induced damage, impaired Ca^{2+} buffering capacity and defective mitochondrial dynamics (reviewed in Smith et al., 2017b). These perturbations are explored briefly below and the impaired mitochondrial dynamics in ALS will be discussed further in section 1.2, due to their relevance to this thesis.

1.1.3.5.1 Defective mitochondrial respiration and ATP production

Reductions in cellular respiration and ATP production are well documented in ALS. In post-mortem spinal cord of sporadic ALS patients the activity of all electron transfer chain (ETC) complexes, complex I, II, III, and IV, were found to be reduced (Figure 1.3) (Borthwick et al., 1999; Wiedemann et al., 2002). In addition, the activity of complexes I and IV were found to be to be impaired in skeletal muscle (Crugnola et al., 2010; Vielhaber et al., 2000; Wiedemann et al., 1998) while complex I activity and ATP levels were reduced in lymphocytes of sporadic ALS patients (Ghiasi et al., 2012).

Studies into the activity of the ETC and ATP production in *SOD1 in vitro* and *in vivo* studies have revealed conflicting results. For instance, *SOD1 G93A* transgenic mice displayed impaired ATP synthesis and depressed mitochondrial respiration rates in the brain and spinal cord, which were found well before disease onset and persist throughout the course of the disease (Kirkinezos et al., 2005; Mattiazzi et al., 2002).

Associated with these changes, decreased complex I+III, II+III and IV activity were observed in the spinal cord of 17-week old symptomatic SOD1 G93A transgenic mice (Mattiuzzi et al., 2002). Additionally, complex IV activity was reduced in forebrain mitochondria isolated from presymptomatic, symptomatic and end-stage SOD1 G93A transgenic mice (Kirkinezos et al., 2005; Mattiuzzi et al., 2002). Analysis of mutant SOD1 ALS cell models recaptured the defects found in SOD1 G93A mice. SOD1 I113T patient fibroblast lines showed reduced oxidative phosphorylation compared to non-disease controls (Allen et al., 2014). Stable low level expression of SOD1 G93A or G37R in NSC34 motor neuron-like cell lines reduced the activity of complex II and IV (Coussee et al., 2011; Menzies et al., 2002) accompanied by reduced mitochondrial membrane potential (MMP) (Richardson et al., 2013) while doxycycline induced expression of SOD1 G93A, A4V, H46R, H80R, D90A, or D123H in the same cell line caused a decrease in complex I, II+III and IV activity which was accompanied by reduced cellular ATP levels (Ferri et al., 2006). In contrast to these studies, Bowling et al. found increased complex I activity in post-mortem frontal cortex of familial ALS patients with a SOD1 A4V mutation (Bowling et al., 1993) and the same lab reported an increase in complex I activity in the forebrain of SOD1 G93A mice (Browne et al., 1998). Similarly, others found no evidence for reduced mitochondrial respiration via complex I or II in presymptomatic SOD1 G93A transgenic mice (Damiano et al., 2006). It is not readily apparent what accounts for the discrepancy between these studies, but these measurements are particularly sensitive to variations in experimental conditions and differences between the SOD1 G93A strains cannot be excluded. Nevertheless, despite differences between studies and cell models, the overarching trend is that ALS mutant SOD1 decreases ETC activity and causes impaired ATP production. Moreover, the presymptomatic occurrence of OXPHOS disruption in SOD1 G93A transgenic mice suggests it may have a causative role in this ALS model.

Defective mitochondrial respiration and ATP production has also been observed in models of non-SOD1 related familial ALS. Depolarisation of mitochondria was described in NSC-34 cells expressing wild type or mutant TDP-43 (Q331K and M337V) and primary motor neurons expressing TDP-43 M337V (Duan et al., 2010; Hong et al., 2012; Lu et al., 2012; Wang et al., 2013). In NSC-34 cells TDP-43 associated MMP reduction was accompanied by decreased complex I activity (Figure 1.3) (Lu et al., 2012). Similarly, in TDP-43 G298S and A382T patient fibroblasts reduced MMP was accompanied by decreased complex I activity, reduced oxygen consumption and decreased ATP levels (Wang et al., 2016). However, this may not always be the case

as others reported reduced MMP, but no changes in mitochondrial respiration or ATP content in 3 independent TDP-43 A382T patient fibroblast lines (Onesto et al., 2016).

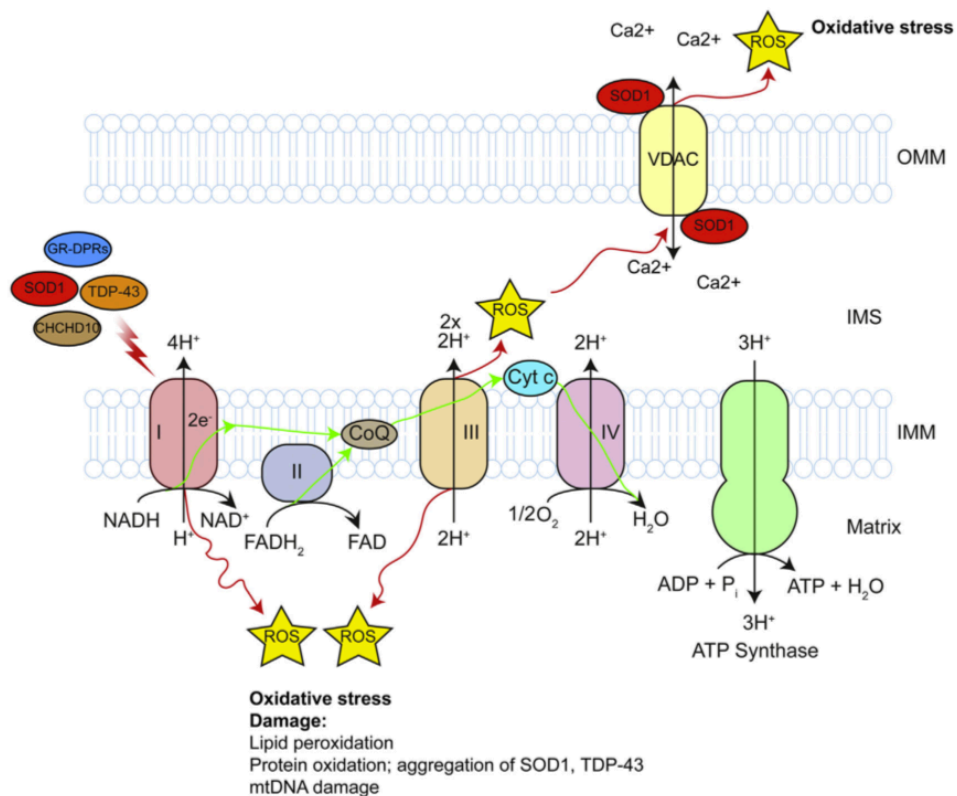


Figure 1.3 Defective mitochondrial respiration, ATP production and oxidative stress

The activity of the electron transport chain is required for the generation of cellular ATP. The activity of the complexes involved in the electron transport chain have been shown to be decreased in SOD1, TDP-43 and CHCHD10-related ALS. This results in decreased MMP and ATP generation, and increased generation of ROS. See text for details. Figure taken from (Smith et al., 2017b), under the terms of the Creative Commons Attribution License (CC BY).

As was the case for TDP-43, overexpression of wild type or mutant FUS P525L caused a drop in MMP in HEK293 cells (Deng et al., 2015) and ATP production was impaired upon expression of wild-type or ALS mutant FUS R521C or R518K in NSC-34 cells (Stoica et al., 2016). Similarly overexpression of the Sig1R E102Q mutant in N2A cells reduced ATP production (Tagashira et al., 2014). Decreased MMP was further observed in SQSTM1 knockout MEFs and in SH-SY5Y, mouse cortical neurons and astrocytes in which VCP expression was reduced using siRNA to model ALS-associated loss of function mutants in p62 and VCP respectively (Bartolome et al., 2013; Seibenhener et al., 2013). In case of VCP the same results were obtained in VCP R155C, R155H and

R191Q ALS patient fibroblast lines (Bartolome et al., 2013). In these cell models of VCP-associated ALS the decrease in MMP was accompanied by a decrease in ATP levels but increase in the rate of mitochondrial respiration and oxygen consumption, suggesting that depletion of MMP is due to uncoupling rather than ETC activity deficits (Bartolome et al., 2013). Finally, analysis of fibroblasts from patients with mutations in the mitochondrial protein CHCHD10 revealed impaired ETC activity at complexes I, II, III and IV which was accompanied by a severe bioenergetics deficit (Figure 1.3) (Bannwarth et al., 2014; Genin et al., 2016).

Despite differences in mechanisms and specific observations depending on the models studied, decreased ETC activity and ATP levels emerge as a common feature in ALS. It is conceivable that, in line with the high energy demands of neurons, gradual depletion of ATP due to reduced respiration may trigger degeneration.

1.1.3.5.2 Oxidative stress

Reactive oxygen species (ROS) are a natural by-product of oxidative phosphorylation. The ETC is responsible for the majority of ROS produced in a cell, with free radicals, mainly superoxide anion ($O_2^{\cdot-}$), produced at complexes I, II and III as a result of incomplete, premature reduction of oxygen (reviewed in Murphy, 2009; Turrens, 2003). Dismutation of $O_2^{\cdot-}$, a reaction catalysed by SOD1 and SOD2, gives rise to H_2O_2 which can further generate hydroxyl anions (OH^{\cdot}) by partial reduction. $O_2^{\cdot-}$ can also react with nitric oxide (NO^{\cdot}) to form peroxynitrate ($ONOO^-$). ROS generated in cells can act as signalling molecules, but when excessively produced can lead to cellular damage to DNA, proteins and lipids and result in reduced efficiency of cellular processes, induce inflammatory pathways, excitotoxicity, protein aggregation and ER stress or cell death (reviewed in Gandhi and Abramov, 2012; Kim et al., 2015a). By proximity, mitochondria are particularly susceptible to ROS induced damage to mtDNA, proteins and lipids. Especially mtDNA appears vulnerable and this is exacerbated by limited DNA repair mechanisms in mitochondria. Resultant mitochondrial damage has been shown to affect mitochondrial function and is implicated in ageing (reviewed in Andersen, 2004; Cui et al., 2012).

Increased levels of ROS and ROS-associated damage have been widely reported in ALS (reviewed in Barber and Shaw, 2010). Increased markers of ROS damage have been found in biofluids of patients with sporadic ALS (Bogdanov et al., 2000; Mitsumoto et al., 2008; Simpson et al., 2004; Smith et al., 1998) as well as in post-mortem tissue (Chang et al., 2008; Fitzmaurice et al., 1996; Shaw et al., 1995; Shibata et al., 2001).

Oxidative damage to DNA, RNA, proteins and lipids has been widely reported in SOD1 G93A rodent and cell models (reviewed in Barber and Shaw, 2010). mRNA oxidation has been shown to precede motor neuron degeneration and cause reduced expression of the encoded proteins in SOD1 G93A transgenic mice (Chang et al., 2008). Interestingly, mRNAs coding for ETC complexes and ATP synthase were selectively susceptible to oxidation (Chang et al., 2008). Furthermore, SOD1 itself is a target of oxidative damage (Andrus et al., 1998) and this has been linked to its misfolding and aggregation (Rakhit et al., 2002). Since misfolded, aggregated SOD1 has been shown to disrupt mitochondrial function and increase superoxide production (Israelson et al., 2010; Pickles et al., 2013; Pickles et al., 2016), a vicious cycle mechanism emerges in which mitochondrial damage and oxidative stress caused by misfolded SOD1 leads to exacerbation of SOD1 misfolding and downstream mitochondrial damage. Interestingly, using monoclonal antibodies to misfolded SOD1, misfolded wild type SOD1 species been shown to be present in sporadic ALS patients (Bosco et al., 2010; Brotherton et al., 2012) although this has been disputed by others (Ayers et al., 2014).

Oxidative damage has also been proposed to promote aggregation of TDP-43 via cysteine oxidation and disulphide bond formation and acetylation (Cohen et al., 2015; Cohen et al., 2012). In agreement, treatment of COS-7 cells with 4-hydroxynonenal (HNE), which is produced in cells by lipid peroxidation, was shown to cause insolubilisation, phosphorylation, and partial cytosolic localisation of TDP-43, which may contribute to its aggregation (Kabuta et al., 2015). Overexpression of wild type and mutant TDP-43 M337V and Q331K or its C-terminal fragments in NSC34 have been shown to increase ROS and cause oxidative damage (Hong et al., 2012). In addition to these deleterious effects TDP-43 also appears to have a protective function in response to oxidative stress. Indeed, oxidative stress has been shown to induce recruitment of TDP-43 to stress granules (Colombrita et al., 2009; McDonald et al., 2011; Meyerowitz et al., 2011).

Other ALS-associated proteins that have been linked to oxidative stress include FUS P525L which has been shown to augment ROS levels when overexpressed in HEK293 cells (Deng et al., 2015), and poly(GR) DPRs arising from the C9orf72 repeat expansion have been shown to increase oxidative stress (Figure 1.3) (Lopez-Gonzalez et al., 2016). Interestingly as was the case for TDP-43, an oxidative environment increased FUS inclusions, again pointing toward a detrimental feed-forward loop (Finelli et al., 2015).

1.1.3.5.3 Calcium mishandling

Loss of Ca^{2+} homeostasis has been observed in *in vitro* and *in vivo* models of mutant SOD1, VAPB, TDP-43, and FUS-related ALS and in the motor nerve terminals ALS patients (Carri et al., 1997; Damiano et al., 2006; De Vos et al., 2012; Mórotz et al., 2012; Siklós et al., 1996; Siklos et al., 1998; Stoica et al., 2014; Stoica et al., 2016; Van Den Bosch et al., 2000). In SOD1 G93A transgenic mice, a significant decrease in mitochondrial Ca^{2+} loading capacity in the CNS was observed long before disease onset, suggesting an early loss of Ca^{2+} buffering may be causal in disease (Damiano et al., 2006).

Loss of ER–mitochondria communication has emerged as a major cause of loss of Ca^{2+} homeostasis in ALS. An estimated 5 – 20 % of mitochondria are closely associated with the ER at contact sites called mitochondria-associated ER membranes (MAM). Several protein complexes that tether ER to mitochondria have been proposed, including homo and heterotypic interactions between mitofusin 1 and 2, interaction of IP₃R with VDAC via Grp75, and the integral ER protein VAPB that binds to PTPIP51 on the outer mitochondrial membrane. Among other functions, ER–mitochondria contact sites allow Ca^{2+} exchange between the two organelles (reviewed in Manfredi and Kawamata, 2016; Paillusson et al., 2016). Disruption of ER–mitochondria interactions have been reported in mutant SOD1, SIGMAR1, TDP-43, and FUS-related ALS (Figure 1.4) (Bernard-Marissal et al., 2015; Stoica et al., 2014; Stoica et al., 2016). In case of mutant TDP-43 and FUS-related ALS, reduced ER–mitochondria communication was caused by a GSK3 β -dependent reduction in VAPB-PTPIP51 interaction (Stoica et al., 2014; Stoica et al., 2016). In contrast, ALS mutant VAPB P56S was shown to have greater affinity for PTPIP51 and to increase ER–mitochondria association (De Vos et al., 2012). However, since VAPB expression is down-regulated because of reduced expression of the VAPB P56S mutant in ALS8 patient-derived iPSC neurons (Mitne-Neto et al., 2011), it is likely that in VAPBP65S-related ALS ER–mitochondria contacts are actually decreased as well. In SIGMAR1 knockout mice which model loss of Sig1R1 function, the interaction between IP₃R and VDAC was decreased in motor neurons (Bernard-Marissal et al., 2015). Interestingly VAPB expression levels in the spinal cord of sporadic ALS cases are significantly lower compared to healthy controls (Anagnostou et al., 2010). Thus, disrupted ER-mitochondria communication may be a general feature in ALS.

In ALS mutant FUS and TDP-43 models, reduced ER–mitochondria communication leads to reduced Ca^{2+} uptake in mitochondria and an associated rise in cytosolic Ca^{2+} upon triggering of Ca^{2+} release from the ER (Stoica et al., 2014; Stoica et al., 2016).

Similarly, in *SIGMAR1* knockout mice cytosolic Ca^{2+} levels were elevated and the time to return to basal levels was significantly longer (Bernard-Marissal et al., 2015).

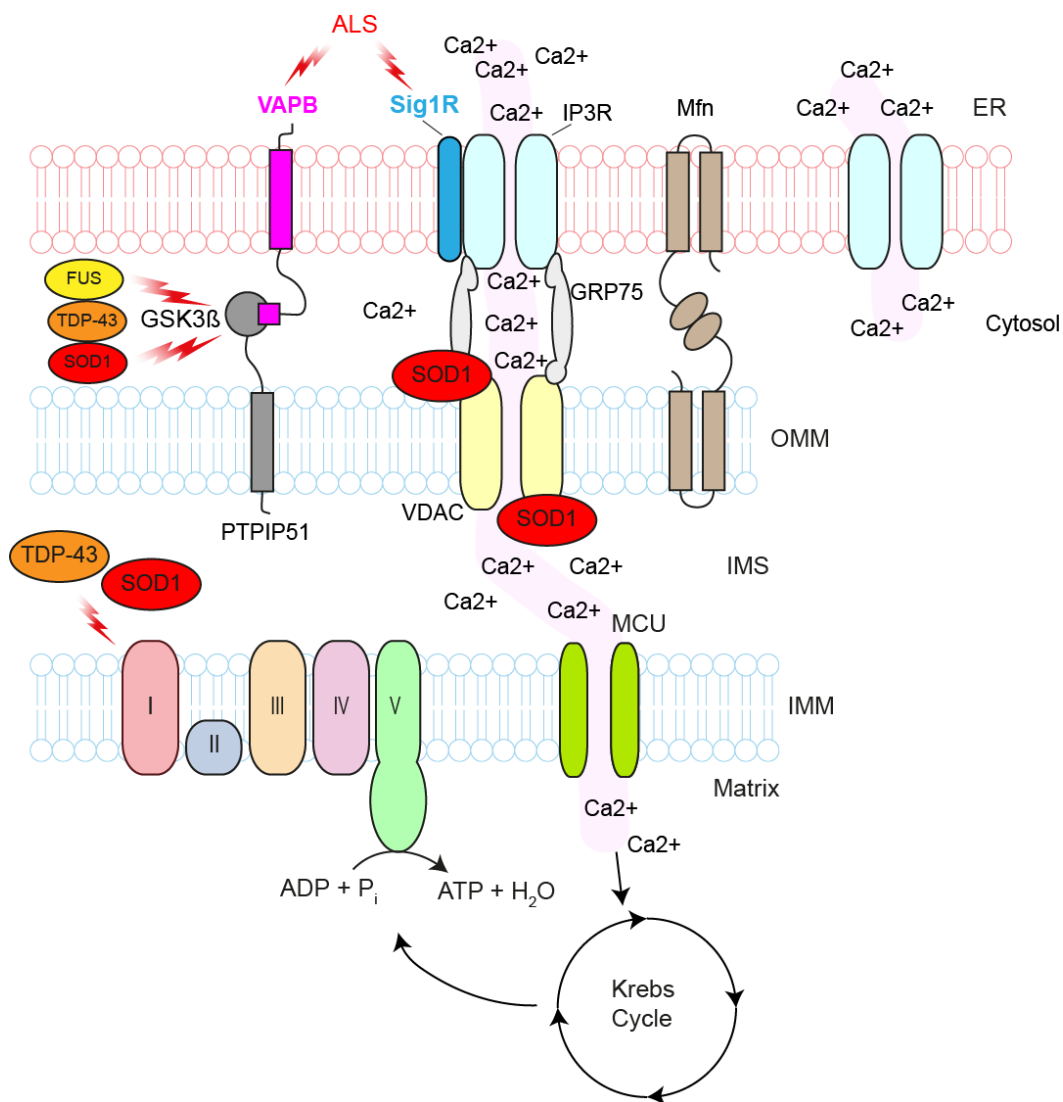


Figure 1.4 Loss of calcium homeostasis in ALS

Calcium homeostasis is achieved through the exchange of Ca^{2+} between the ER and mitochondria at ER-mitochondria contacts. ER-mitochondria contacts are disrupted in SOD1, TDP-43, VAPB, Sig1R and FUS ALS. Disruption of the contacts may lead to increases in cytosolic Ca^{2+} levels and disruption of Ca^{2+} dependent cellular processes, including axonal transport, ATP generation and protein homeostasis. MCU, mitochondrial Ca^{2+} uniporter. See text for details. Figure taken from (Smith et al., 2017b), under the terms of the Creative Commons Attribution License (CC BY).

Dysregulation of Ca^{2+} possibly by miscommunication between ER and mitochondria contacts may be a primary cause of motor neuron death in ALS and contribute to excitotoxicity (as discussed in 1.1.3.1). In addition, mitochondrial Ca^{2+} regulates ATP

production by activating the rate-limiting enzymes of the Krebs cycle and regulates oxidative phosphorylation and ATP synthesis to match local energy demand (Figure 1.4). As discussed above, reduced ATP production is a common feature in ALS (1.1.3.5.1). Diminished ATP levels may directly impact on axonal transport of mitochondria, vesicles and other cargoes by starving molecular motors of ATP. At the same time, elevated levels of cytosolic Ca^{2+} may disrupt axonal transport of mitochondria by interacting with the mitochondrial kinesin-1 receptor MIRO1 and in turn exacerbate axonal transport deficits and local ATP levels. Indeed elevated cytosolic Ca^{2+} levels were shown to disrupt axonal transport of mitochondria in ALS mutant VAPB P56S expressing neurons (reviewed in De Vos and Hafezparast, 2017; Mórotz et al., 2012). Furthermore, loss of Ca^{2+} homeostasis may contribute to a number of other ALS-associated toxic mechanisms, such as axonal transport defects and oxidative stress, and loss of protein homeostasis (reviewed in Barber and Shaw, 2010; De Vos and Hafezparast, 2017; Webster et al., 2017).

1.1.3.5.4 Pro-apoptotic signaling

Apoptosis is a last resort mechanism employed by cells upon suffering irreparable damage (reviewed in Ashkenazi and Salvesen, 2014). Apoptosis serves to remove a damaged cell from the environment in a controlled manner so as to not induce large-scale degeneration. Mitochondria are integral to apoptosis. Upstream apoptotic signalling cascades converge on mitochondria to bring about cytochrome c release, which activates downstream executioner caspases (Figure 1.5) (reviewed in Ashkenazi and Salvesen, 2014). Apoptosis is regulated by pro- and anti- apoptotic proteins of the Bcl-2 family, which regulate the release of caspase-activating factors from mitochondria (reviewed in Ashkenazi and Salvesen, 2014; Walensky, 2006). ALS mutant SOD1 has been shown to directly influence apoptotic signalling by interaction with Bcl-2. Wild-type and ALS mutant SOD1 (A4V, G37R, G41D and G85R) have been shown to bind the anti-apoptotic factor Bcl-2 in spinal cord samples (Pasinelli et al., 2004). When bound to mutant SOD1, the BH3 domain of Bcl-2 is exposed and this causes a pro-apoptotic gain of function of the Bcl-2 protein in both cell and animal models of mutant SOD1 G93A ALS and in mutant SOD1 A4V patient spinal cord (Figure 1.5) (Pedrini et al., 2010). The toxic mutant SOD1–Bcl-2 complex inhibits mitochondrial permeability to ADP and induces mitochondrial hyperpolarization due to reducing the interaction of SOD1 and VDAC1 (Figure 1.3, Figure 1.5) (Tan et al., 2013).

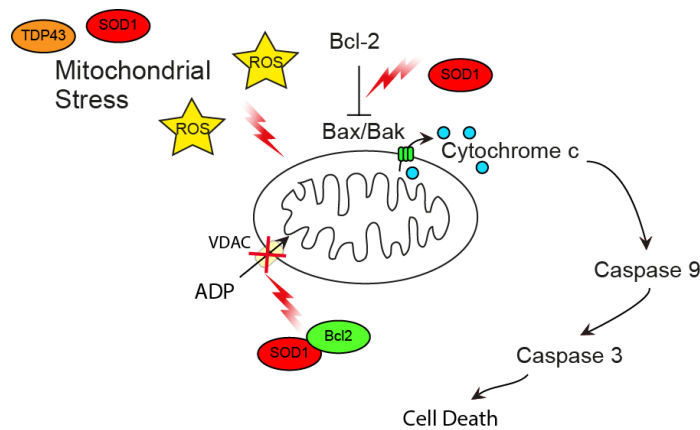


Figure 1.5 Pro-apoptotic signalling

Mitochondrial stress is increased due to dysfunctional cellular pathways resulting in increased ROS generation, and mitochondrial damage. Mutant SOD1 contributes to apoptotic signalling in ALS by binding the anti-apoptotic factor Bcl-2 and promoting a pro-apoptotic conformation of the protein. The Bcl2-SOD1 complex inhibits VDAC ADP permeability and induces mitochondrial hyperpolarisation. See text for details. Figure taken from (Smith et al., 2017b), under the terms of the Creative Commons Attribution License (CC BY).

1.2 Impaired mitochondrial dynamics in ALS

Mitochondria are dynamic organelles that undergo fission and fusion events and directed transport. Furthermore, mitochondrial function is vital for many aspects of cellular health, therefore the maintenance of a healthy pool of mitochondria underpins homeostasis. Owing to the activity of the OXPHOS machinery and the generation of ROS therefrom, mitochondria are susceptible to high levels of damage to mitochondrial DNA (mtDNA), proteins and lipids. Therefore, many cellular pathways have been identified that monitor mitochondrial health and act to recover or remove damaged mitochondria. Several lines of research indicate that impaired mitochondrial dynamics may contribute to the aetiology of ALS.

1.2.1 Aberrant mitochondrial fission and fusion events

Mitochondria exist as part of a dynamic network. An individual mitochondrion can fuse to and fission from the network according to the cellular environment, promoting normal function.

Fusion of a mitochondrion to the network allows for the sharing of mtDNA, proteins and metabolites, as well as the equilibration of the MMP. Fusion of a mitochondrion with a decreased MMP, and therefore reduced ATP synthesis, to the wider mitochondrial

network, dissipates the decrease in MMP and restores ATP generation. The dissipation of small changes in MMP alongside the exchange of proteins results in a more uniform distribution of mitochondrial damage across the mitochondrial population. This mechanism would prevent the accumulation of irreparable mitochondrial damage, which would result in the organelle being removed from the cell by mitophagy (discussed in 1.2.3). In this way, mitochondrial fusion events are often reported as being pro-survival and overall are more energy efficient for the cell (reviewed in Tilokani et al., 2018; Youle and van der Bliek, 2012).

Mitochondrial fusion is controlled by GTPases that are located in both the outer mitochondrial membrane (OMM) and inner mitochondrial membrane (IMM). Mitofusins 1 and 2 (Mfn1, Mfn2) mediate the fusion of the OMM. Mfn1/2 are OMM proteins which are involved in the tethering of mitochondria and ER at MAM, but also tether mitochondria together during fusion events (Ishihara et al., 2004; Koshiba et al., 2004). The interaction between Mitofusins via their coil-coil domains results in apposition of the OMM of the interacting mitochondria. Although Mfn1 and Mfn2 are proposed to play similar roles in mitochondrial tethering, they may have specific roles in the fusion of OMM (reviewed in Benard and Karbowski, 2009). The precise mechanism of OMM fusion is not yet known, however changes in OMM mechanics may underlie the fusion event (reviewed in Schrepfer and Scorrano, 2016). OPA1 is responsible for the fusion of IMM. OPA1 activity not only requires GTP hydrolysis but the electrochemical gradient established by the OXPHOS machinery. OPA1 undergoes proteolytic cleavage by PARL, Yme1, paraplegin and the m-AAA protease complex resulting in several isoforms that function at different stages of mitochondrial fusion (reviewed in Benard and Karbowski, 2009). Long isoform of OPA1 (L-OPA1) is inserted into the IMM and forms homodimers with IMM localised L-OPA1 on incoming mitochondria. IMM tethering then results in fusion of the IMM membranes (Del Dotto et al., 2017). In addition, L-OPA1 found on the IMM on one mitochondrion can interact with cardiolipin found on the second mitochondrion and induce IMM fusion (Ban et al., 2017). The interactions between IMM are likely stabilised by cleaved products of OPA1 which are found in the intermembrane space (IMS) (Del Dotto et al., 2017).

Multiple proteins have been identified that aid in the regulation of mitochondrial fusion events (reviewed in Benard and Karbowski, 2009). Mitofusin-binding protein has been reported to inhibit fusion, potentially by inhibiting the hydrolysis of GTP by Mfn1/2 until the mitochondria are fully docked (Eura et al., 2006). Stomatin-like protein 2 has been suggested to be involved in the processing of OPA1 (Merkwirth et al., 2008) and interacts with Mfn2 (Hajek et al., 2007), suggesting co-regulation of the OMM and IMM

fusion events. mitoPLD is involved in the conversion of cardiolipin to phosphatidic acid in the OMM. mitoPLD may be inserted into the interacting mitochondria and bring about changes in OMM lipid properties which aid in mitochondrial fusion events (Choi et al., 2006). Finally, proteins involved in apoptotic pathways also influence mitochondrial fusion. Indeed, mitochondrial fragmentation is required for the progression of apoptosis. Both Bax and Bak, pro-apoptotic Bcl-2 proteins, regulate the formation and stability of the Mfn complex (Brooks et al., 2007; Karbowski et al., 2006).

Fission of the mitochondrial network is important for cell division, survival and death (reviewed in Tilokani et al., 2018; Youle and van der Bliek, 2012). During the mitosis G2 phase, mitochondria are prepared for segregation into daughter cells. Fragmentation of the mitochondrial network is an important step in apoptosis. The separation of a single mitochondrion from the network also occurs to promote mitochondrial motility and to isolate damaged mitochondria destined for degradation by mitophagy.

ER-mitochondria contact sites are frequently observed to become sites of mitochondrial fission events. At MAM, the ER wraps around mitochondria and produces an initial constriction of the organelle. The mitochondrial fission GTPase Dynamin 1 like (Drp1) is subsequently recruited to these constriction sites where it oligomerises. Drp1 is recruited to the OMM surface by the OMM proteins Mff, Fis1, MiD49 and MiD51 (Losen et al., 2013; reviewed in Pagliuso et al., 2018). Notably, Mff has been found to be enriched at the ER constriction sites and may provide a mechanism for localised Drp1 recruitment (Friedman et al., 2011). Furthermore, MAM sites are enriched in cardiolipin which has been reported to promote the recruitment and activation of Drp1 during mitochondrial fission (Francy et al., 2017). GTP hydrolysis by Drp1 leads to increased constriction of the mitochondrion (reviewed in Hatch et al., 2014; Kraus and Ryan, 2017). Fission of the mitochondria is achieved through the assembly of Dynamin 2 at the Drp1 constriction site (Lee et al., 2016b). The control of Drp1 mediated fission events occurs through post-translational modifications of Drp1. These modifications include activating and inactivating phosphorylation of Drp1; ubiquitin mediated control of Drp1 turnover; Drp1 S-nitrosylation leading to enhanced GTPase activity; a SUMOylation induced increase in Drp1 stabilisation; and O-GlyNAcylation mediated increases in GTP binding (reviewed in Otera et al., 2013; Pagliuso et al., 2018).

Evidence points towards imbalances in the fission/fusion cycling of the mitochondrial network in ALS (Figure 1.6). In SOD1 G93A expressing SH-SY5Y and NSC-34 cell models, a decrease in OPA1 and increase in Drp1 levels resulting in a fragmented mitochondrial network were reported (Ferri et al., 2010). *In vivo*, the levels of Mfn1 and OPA1 progressively decreased while the levels of P-Drp1 and Fis1 were unaffected in

the spinal cord of SOD1 G93A transgenic mice (Liu et al., 2013). In contrast, in SOD1 G93A mouse muscle fibres there was no reported change in Mfn1, Mfn2 or Drp1 levels (Luo et al., 2013). Interestingly, overexpression of a dominant negative Drp1 inhibits SOD1 G93A induced mitochondrial fragmentation and partially rescues cell death in cortical neurons (Song et al., 2013). In addition, inhibition of the interaction between Drp1 and Fis1 prevented mitochondrial alterations and improved survival in SOD1 G93A mice, suggesting that Drp1 activation may contribute to disease pathogenesis (Joshi et al., 2018).

Overexpression of wild type TDP-43 and to a greater extent ALS mutants TDP-43 Q331K and M337V resulted in reduced mitochondrial length in primary motor neurons which was sensitive to Mfn2 levels (Wang et al., 2013). Transgenic mice expressing wild type TDP-43 exhibited increased levels of Fis1 and activated Drp1 phosphorylated at Ser616 and a reduction in Mfn1, which correlated with aberrant mitochondrial morphology and clustering (Xu et al., 2010). In contrast, the same group reported no changes in the levels of phospho-S616 Drp1, Fis1 or Mfn1 in mutant TDP-43 M337V transgenic mice, despite a similar mitochondrial phenotype (Xu et al., 2011). It is possible that different pathways lead to fragmentation of the mitochondrial network in wild type and mutant TDP-43 transgenic mice, or, alternatively, that external factors linked to disease such as changes in apoptotic factors result in mitochondrial fragmentation. Nevertheless, analysis of TDP-43 A382T patient fibroblasts showed that Fis1 levels were significantly increased compared to control cells (Onesto et al., 2016). In *Drosophila*, overexpression of wild type TDP-43 led to a decrease in Mfn/Marf. Interestingly, similar to the reports in SOD1 G93A mice, increasing levels of Mfn/Marf or inactivation of Drp1 rescued the motor phenotype of wild type and ALS-linked TDP-43 G298S expressing *Drosophila* (Khalil et al., 2017). A similar rescue of mitochondrial fragmentation by overexpression of Mfn2 was observed in TDP-43 M337V expressing primary motor neurons (Wang et al., 2013). The levels of IMM fusion protein OPA1 was found to be dysregulated in TDP-43 A315T but not wild type mice (Stribl et al., 2014). Together this points to dysregulated mitochondrial fission/fusion cycling in both SOD1 and TDP-43 ALS.

Counterintuitively, mitochondrial network fragmentation in C9orf72 patient fibroblasts was associated with an increase in Mfn1 levels (Onesto et al., 2016). It is possible that Mfn1 expression is increased to compensate for dysregulation of other fusion and fission factors which remain to be identified.

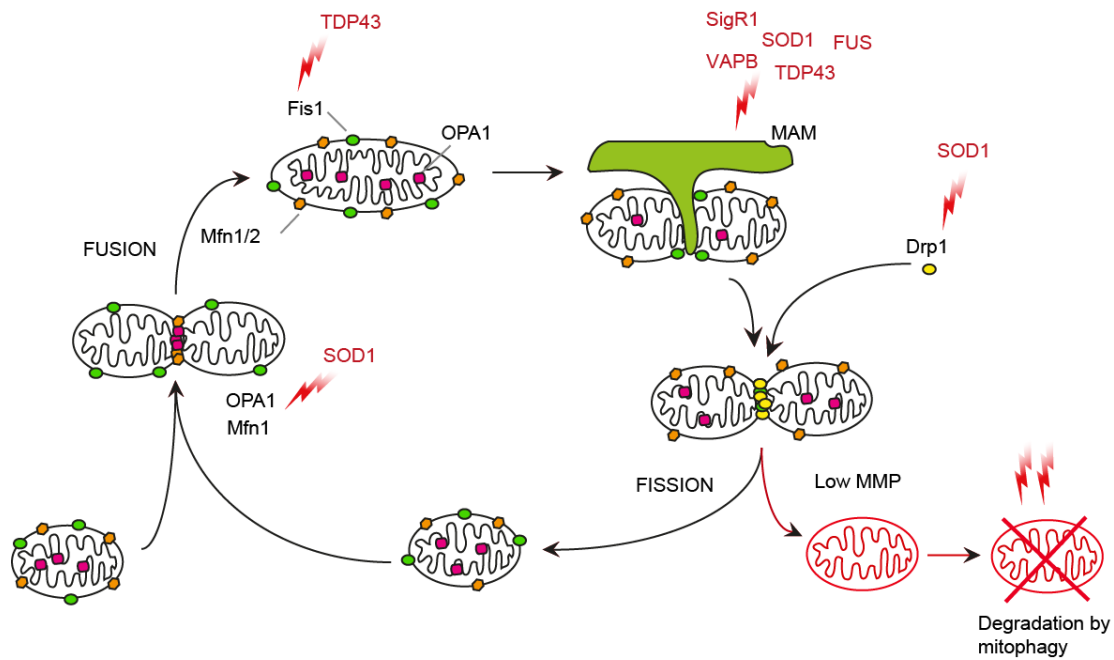


Figure 1.6 Aberrant mitochondrial fission and fusion in ALS

Mitochondrial network dynamics are required for correct mitochondrial function. Mitochondrial fission is promoted in SOD1 and TDP-43 ALS by increases in the fission factors Fis1 and Drp1 and a decrease in the fusion factors Mfn1 and OPA1. Decreased ER–mitochondria contact sites may also lead to decreased mitochondrial fission events. Finally, dysfunctional removal of damaged organelles through the mitophagy pathway may also contribute to accumulation of fragmented mitochondria. Figure adapted from (Smith et al., 2017b), under the terms of the Creative Commons Attribution License (CC BY).

ER-mitochondria contact sites have been shown to regulate mitochondrial morphology (Friedman et al., 2011). ER-mitochondria contacts sites are commonly found to be reduced in various ALS models, including SOD1, TDP-43, FUS, VAPB and SIGMAR1 (reviewed in Smith et al., 2017b). Consistent with reduced fission, decreased ER–mitochondria contacts in motor neurons of SIGMAR1 knockout correlated with elongated mitochondria (Bernard-Marissal et al., 2015), whereas, in VAPB P56S overexpressing cells increased ER–mitochondria contacts correlated with fragmented mitochondria (De Vos et al., 2012). However, in SOD1, TDP-43 and FUS ALS models, reduced ER–mitochondria contacts appear to correlate with fragmented mitochondria (De Vos et al., 2007; Fukunaga et al., 2015; Stoica et al., 2014; Stoica et al., 2016; Wang et al., 2013; Watanabe et al., 2016). Therefore, there is no straightforward causal relation of ALS-associated disruption of ER–mitochondria contacts and changes in mitochondrial network morphology.

The relevance of exacerbated mitochondrial fission in the aetiology of ALS is not clear. Perhaps, smaller mitochondria which tend to be less energetically favourable and more prone to accumulating ROS induced damage if they cannot fuse back to the network (Hoitzing et al., 2015), may exacerbate mitochondrial damage. Thus, the fragmented mitochondrial network observed may correlate directly with the reduced MMP, ATP levels and increased ROS reported in ALS. Alternatively, mitochondrial fragmentation may reflect mitophagy defects.

1.2.2 Impaired axonal transport of mitochondria

Motor neurons are highly polarized cells and require membrane-bound vesicles, organelles, proteins, lipids and RNA to be transported from the soma to the axon terminal and *vice versa*. Impaired axonal transport of mitochondria is a well-documented phenomenon in ALS (reviewed in De Vos et al., 2008; De Vos and Hafezparast, 2017). In fact, axonal transport defects are one of the earliest events in ALS motor neurons, indicating that they may be a primary cause of motor neuron loss.

Long distance transport of mitochondria is mediated by the molecular motors kinesin-1 (previously referred to as conventional kinesin or KIF5) and cytoplasmic dynein that move along microtubules. Kinesin-1 moves toward the faster growing plus end of microtubules whereas cytoplasmic dynein moves toward the opposite minus end. Because axonal microtubules are uniformly orientated with their plus ends pointing away from the cell body, kinesin-1 transports mitochondria toward the axon terminal (anterograde transport) and cytoplasmic dynein ferries mitochondria to the cell body (retrograde transport) (Figure 1.7).

Defects in both anterograde and retrograde transport of mitochondria have been reported in a number of *in vitro* and *in vivo* experimental models. ALS mutant SOD1 G93A, A4V, G85R or G37R caused reduced anterograde but not retrograde axonal transport mitochondria in cultured cortical neurons and an identical phenotype was observed in embryonic motor neurons isolated from SOD1 G93A transgenic mice (De Vos et al., 2007). Similarly, overexpression of the ALS mutant VAPB P56S caused a selective block in anterograde transport of mitochondria (Mórotz et al., 2012). Reduced overall mitochondrial transport was observed in primary motor neurons expressing wild-type TDP-43 and to a greater extent ALS mutant TDP-43 Q331K or M337V (Wang et al., 2013) and in Sig1R deficient motor neurons (Bernard-Marissal et al., 2015). Interestingly, normal levels of axonal transport of mitochondria were reported in cortical neurons expressing wild type or mutant TDP-43 M337V or A315T at 5–7 days in culture, suggesting a possible cell type specificity (Alami et al., 2014).

Subsequent time-lapse recordings in single axons in the intact sciatic nerve of presymptomatic SOD1 G93A and TDP-43 A315T transgenic mice and rats confirmed deficits in axonal transport of mitochondria *in vivo* (Bilsland et al., 2010; Magrané et al., 2014; Magrané et al., 2012; Marinković et al., 2012).

Mitochondrial transport defects result in redistribution of mitochondria in axons. *In vitro*, the number of axonal mitochondria was significantly reduced and the remaining mitochondria were spaced further apart in primary neurons expressing ALS mutant SOD1 (De Vos et al., 2007). *In vivo* the number of axonal mitochondria was reduced in motor neurons of early symptomatic SOD1 G37R and SOD1 G85R transgenic mice and the motor axon terminals of SOD1 G93A transgenic rats and TDP-43 transgenic mice (Magrané et al., 2012; Shan et al., 2010; Vande Velde et al., 2011). Furthermore, the distribution of the remaining mitochondria was no longer homogeneous throughout the axons with abnormal mitochondrial clusters observed along the axon (Magrané et al., 2014; Shan et al., 2010; Sotelo-Silveira et al., 2009; Vande Velde et al., 2011). Similar mislocalisation and aggregation of mitochondria has been observed in the soma, dendrites and proximal axons in human spinal cord sections from ALS patients, suggesting that disruption to mitochondrial transport is a general phenomenon in ALS (Sasaki and Iwata, 2007).

A number of possible mechanisms underlying mitochondrial axonal transport defects have been proposed. In rare cases, pathogenic mutations in the axonal transport machinery, such as cytoplasmic dynein, kinesin-1 and α -tubulin directly disrupt axonal transport. In most cases, however, the disruption of axonal transport of mitochondria appear to be indirect; proposed mechanisms include microtubule destabilization, pathogenic kinase signaling, protein aggregation, and mitochondrial damage (reviewed in De Vos and Hafezparast, 2017).

Axonal transport of mitochondria is controlled by the integral OMM protein MIRO1 (reviewed in Devine et al., 2016). MIRO1 is an atypical Rho GTPase comprised of two GTPase domains separated by two calcium-binding E-helix-loop-F-helix (EF)-hand motifs (Fransson et al., 2006). MIRO1 is anchored in the OMM and connects mitochondria to kinesin-1 and cytoplasmic dynein via the adapter proteins TRAK1 and 2 (Brickley et al., 2005; Brickley and Stephenson, 2011; Glater et al., 2006; MacAskill et al., 2009a; Morlino et al., 2014; van Spronsen et al., 2013).

MIRO1 regulates mitochondrial trafficking in response to physiological Ca^{2+} stimuli and mitochondrial damage. Binding of Ca^{2+} to the MIRO1 EF-hand motifs modulates the interaction of kinesin-1 with MIRO1 and impedes anterograde transport of mitochondria

(Macaskill et al., 2009b; Wang and Schwarz, 2009). During mitophagy, PINK1 phosphorylates MIRO1 in response to mitochondrial damage (Shlevkov et al., 2016; Wang et al., 2011; Weihofen et al., 2009). Phosphorylation marks MIRO1 for Parkin-dependent manner proteasomal degradation and results in detachment of kinesin-1 from mitochondria and arrested mitochondrial movement (Wang et al., 2011).

Mitochondrial Ca^{2+} handling is dysregulated in ALS. Hence ALS-associated mitochondrial axonal transport defects may be the direct result of aberrant calcium-mediated regulation of MIRO1. In agreement with such a mechanism, increased cytosolic Ca^{2+} levels are elevated in cellular models and in motor neurons from transgenic ALS models (Mórotz et al., 2012; Siklos et al., 1998) and, at least in case of VAPB P56S there is direct evidence that elevated Ca^{2+} disrupts transport of mitochondria via MIRO1 (Figure 1.7) (Mórotz et al., 2012). Similarly, ALS mutant SOD1, TDP-43, and Sig1R-associated reductions in ER-mitochondria contacts result in transiently elevated cytosolic Ca^{2+} levels due to reduced calcium-uptake in mitochondria and show axonal transport deficits, but the possible involvement of MIRO1 remains to be determined (Bernard-Marissal et al., 2015; Stoica et al., 2014; Watanabe et al., 2016).

Decreased levels of MIRO1 have been reported in SOD1 G93A and TDP-43 M337V transgenic mice as well as in the spinal cord of ALS patients (Zhang et al., 2015a). Since both SOD1 G93A and TDP-43 M337V damage mitochondria, these results suggest that ALS-associated mitochondrial damage leads to halting of mitochondrial transport via PINK1/Parkin-dependent degradation of MIRO1.

In some cases, ALS-associated proteins may directly affect the axonal transport machinery. Both TDP-43 and FUS have been shown to regulate the expression of several kinesins, including kinesin-1 and TDP-43 binds TRAK1 mRNA (Colombrita et al., 2012; Polymenidou et al., 2011; Xiao et al., 2011). ALS-mutant SOD1 directly binds to cytoplasmic dynein in SOD1 G93A and G37R cell and mouse models and the interaction becomes more prevalent through disease progression (Shi et al., 2010; Tateno et al., 2009; Zhang et al., 2007). Thus, in the case of mutant SOD1 axonal transport defects may in part be due to sequestration of dynein.

There are several ways in which defective axonal transport of mitochondria may contribute to disease. Defective axonal transport of mitochondria may lead to imbalances in ATP generation and Ca^{2+} buffering at the post synaptic terminal. In conjunction with mitochondrial damage this may cause the dying back of the axon, a feature implicated in ALS (Figure 1.7) (Moloney et al., 2014). Retrograde transport

defects are associated with defects in the removal of damaged organelles by mitophagy, which could explain the mitochondrial aggregates found in the axons of ALS patients (Okamoto et al., 1990; Sasaki and Iwata, 1996). Furthermore, defective axonal transport of mitochondria may also affect the transport of other axonal cargoes such as signaling endosomes which appear closely linked to ALS pathology (reviewed in De Vos and Hafezparast, 2017).

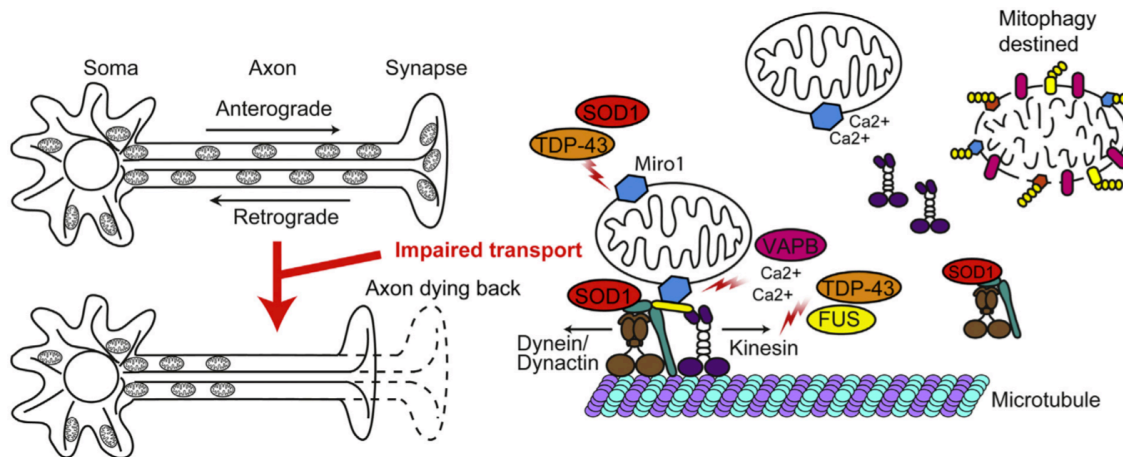


Figure 1.7 Disrupted axonal transport in ALS

Neurons depend on axonal transport of mitochondria for their ATP requirement and Ca^{2+} buffering. Axonal transport of mitochondria is impaired in ALS. *MIRO1*, an OMM protein involved in mitochondrial trafficking, is reduced in *SOD1* and *TDP-43*-associated ALS. Mutant *SOD1* binds the dynein/dynactin complex required for retrograde transport sequestering it in the cytosol. *FUS* and *TDP-43* are proposed to regulate kinesin expression levels. Increases in cytosolic Ca^{2+} levels due to decreased ER–mitochondria contacts in *SOD1*, *TDP-43*, *FUS*, *Sig1R* and *VAPB*-related ALS may contribute to detachment of the mitochondria from kinesin, through aberrant *MIRO1* regulation. Loss of mitochondria from the axon terminal may lead to the dying back of the axon. See text for details. Figure taken from (Smith et al., 2017b), under the terms of the Creative Commons Attribution License (CC BY).

1.2.3 Disrupted mitochondrial quality control

Mitochondria that are extensively damaged and that cannot be recovered by normal reshuffling of the mitochondrial network are removed from the cell by a specialised branch of the autophagy pathway, called mitophagy. Mitophagy can result in either the removal of an entire mitochondrion from the cell, or in the removal of damaged mitochondrial components. Although mitophagy employs many of the same proteins as

autophagy and joins the canonical autophagy pathway at the latter stages, the targeting of mitochondria for degradation is achieved by a specific subset of cellular proteins.

As discussed above, the accumulation of fragmented, rounded mitochondria is a common feature in ALS and may indicate failure of mitophagy to clear damaged mitochondria (1.1.3.5, Table 1-2) (reviewed in Hamacher-Brady and Brady, 2016).

1.2.3.1 PINK1/Parkin dependent mitophagy

The most well characterised mitophagy pathway is the PTEN induced kinase 1 (PINK1)/Parkin dependent pathway. This was initially propelled by the identification of multiple pathogenic mutations in *PINK1* and *Parkin* in early onset forms of recessive PD (Klein and Westenberg, 2012).

PINK1 is a serine threonine kinase which is targeted to mitochondria through an N-terminal mitochondrial localisation sequence. PINK1 is imported through the translocase of the outer membrane (TOM20) complex and recognised by the translocase of the inner membrane (TIM23) complex. In healthy mitochondria, PINK1 undergoes partial import through the TIM23 complex. The N-terminal presequence is cleaved in the matrix by MPP. In addition, Presenilins-associated rhomboid-like protein (PARL) cleaves PINK1 in the IMS. PARL cleavage of PINK1 results in the generation of an unstable PINK1 protein, with an N-terminal Phe residue. N-terminal Phe residues act as cellular signals for ubiquitination and the subsequent degradation of proteins via the N-end rule (reviewed in Dissmeyer et al., 2018). Cleaved PINK1 is retro-transported back into the cytosol and is rapidly degraded by the N-end rule pathway by the proteasome (Yamano and Youle, 2013). Hence when mitochondria are healthy, PINK1 is maintained at low levels. Upon mitochondrial damage, MMP is lost, which perturbs mitochondrial import through TIM23, hence preventing PINK1 import (reviewed in Dudek et al., 2013). Furthermore, PINK1 cleavage by PARL is inhibited upon loss of MMP (Jin et al., 2010). This leads to the accumulation of full length PINK1 associated with the TOM20 complex on the OMM (reviewed in Pickles et al., 2018).

Full length PINK1 auto-phosphorylates resulting in its activation (Okatsu et al., 2012). PINK1 also phosphorylates ubiquitin residues that are found on the OMM. Phosphorylation of ubiquitin at Ser65, leads to the recruitment of the E3 ligase Parkin to the OMM of damaged mitochondria (Kazlauskaitė et al., 2014). Parkin is phosphorylated by PINK1 at Ser65 of its ubiquitin-like domain (Shiba-Fukushima et al., 2012). Ser65 phosphorylation leads to a conformational change in Parkin and an increase in its E3 ligase activity (reviewed in Gladkova et al., 2018). This results in the ubiquitination of its targets on the OMM, including Mfn1/2 involved in mitochondrial fusion events, MIRO1

involved in mitochondrial transport, the TOM complex involved in mitochondrial protein import, and voltage dependent anion channels (VDAC) (Figure 1.8) (reviewed in Durcan and Fon, 2015; Yamano et al., 2016). VDAC has been proposed to act as a docking site for Parkin on mitochondria (Sun et al., 2012). The formation of ubiquitin chains by Parkin on OMM proteins produces a feed forward mechanism, as it provides further substrates for PINK1 phosphorylation, reinforcing the progress of mitophagy. However, the progression of mitophagy via ubiquitination of OMM substrates is also under repression by de-ubiquitinating enzymes (DUB): ubiquitin-specific peptidase 30 (USP30) and ubiquitin-specific peptidase 15 (USP15) (Cornelissen et al., 2014; Cunningham et al., 2015). These remove ubiquitin chains from mitochondria and oppose the progression of mitophagy. This is thought to be a mechanism for keeping basal mitophagy in check (reviewed in Durcan and Fon, 2015).

The ubiquitination of OMM substrates serves 2 functions. Firstly, ubiquitinated cargoes are recognised by the Type II AAA+ ATPase Valosin containing protein (VCP). VCP is involved in a multitude of processes, but its main function is to dislodge damaged ubiquitinated proteins from large protein complexes and membranes for degradation in by the proteasome (reviewed in Avci and Lemberg, 2015; Meyer and Wehl, 2014). VCP is recruited to the OMM of damaged mitochondria following Parkin recruitment and extracts ubiquitinated Mfn1 and Mfn2 from the OMM to allow their degradation by the proteasome (Tanaka et al., 2010). As such, VCP is essential for mitophagy (Kim et al., 2013b). Removal of the proteins involved in mitochondrial fusion and motility from the OMM results in the isolation of the damaged mitochondrion from the network.

The second function of ubiquitin chains is to recruit the autophagosome machinery to the damaged mitochondria. Ubiquitin chains on damaged mitochondria are recognised by the ubiquitin binding domain (UBD) of the mitophagy adaptor proteins: OPTN, nuclear dot protein 52 (NDP52), sequestosome 1 (p62), neighbour of BRAC1 gene 1 (NBR1) and Tax1 binding protein 1 (TAX1BP1) (reviewed in Pickles et al., 2018; Rogov et al., 2014). A certain level of redundancy exists between the mitophagy adaptor proteins. For instance, expression of OPTN is able to compensate for loss of NDP52 (Lazarou et al., 2015). Furthermore, although p62 has been reported to be recruited to mitochondria during mitophagy, it is not essential for the clearance of damaged organelles (Narendra et al., 2010b; Okatsu et al., 2010). This suggests that clearance of mitochondria is a multifaceted mechanism and underlines its importance in the maintenance of cellular homeostasis. In addition to the UBD required for the recognition of ubiquitin, the mitophagy adaptor proteins contain LIR domains. The LIR recruits LC3 positive autophagosomes to the mitochondrion for its subsequent engulfment and degradation

through the canonical autophagy pathway (Figure 1.2) (reviewed in Birgisdottir et al., 2013). The interaction between the mitophagy adaptor proteins, LC3 and damaged mitochondria is regulated by TANK binding kinase 1 (TBK1). TBK1 phosphorylates OPTN Ser177 increasing its interaction with LC3 (Wild et al., 2011a). Activated TBK1 subsequently phosphorylates OPTN at Ser473 and Ser513, which increases the affinity of OPTN for ubiquitin and phospho-ubiquitin chains on OMM substrates (Heo et al., 2015; Lazarou et al., 2015; Richter et al., 2016). TBK1 activity has also been shown to phosphorylate NDP52, p62 and TAX1BP1 in their UBD to promote their interaction with ubiquitin chains and enhance mitochondrial clearance (Wild et al., 2011a).

TDP-43 and FUS directly regulate the expression of Parkin (Lagier-Tourenne et al., 2012; Polymenidou et al., 2011). Loss of TDP-43 or FUS was shown to decrease Parkin levels (Figure 1.8) (Lagier-Tourenne et al., 2012) and consistent with loss of TDP-43 function in the nucleus, decreased Parkin protein levels were observed in sporadic ALS spinal cord motor neurons containing cytoplasmic TDP-43 aggregates (Lagier-Tourenne et al., 2012). Parkin protein levels were also found to be decreased in TDP-43 A513T transgenic mice (Stribl et al., 2014) but this was not observed by others (Hebron et al., 2013). Thus, since cytosolic TDP-43 aggregation is a near universal phenomenon in ALS, loss of Parkin may impair mitophagy in most ALS cases. Furthermore TDP-43 accumulates in mitochondria and causes mitochondrial damage (Wang et al., 2016). Therefore, a two-hit scenario emerges in which loss of mitophagy exacerbates the consequences of mitochondrial damage. Of note, Parkin has been shown to ubiquitinate TDP-43 and to promote its translocation from the nucleus to the cytosol in an HDAC6-dependent process (Hebron et al., 2013). Even though the latter is likely to reflect the role of Parkin and HDAC6 in aggrephagy rather than mitophagy, it does emphasise a close link between Parkin and TDP-43 that merits further examination.

Missense mutations in VCP cause of 1 - 2 % of familial ALS cases as well as inclusion body myopathy (IBM) with Paget's disease (PDB) and FTD (Johnson et al., 2010; Koppers et al., 2012). Although it is not exactly known how disease-associated mutations in VCP alter its cellular functions, most mutations appear to convey varying degrees of loss of function (reviewed in Tang and Xia, 2016). Consistent with loss of function, MEFs expressing mutant VCP A232E do not clear mitochondria following damage, despite labelling with Parkin (Figure 1.8) (Kim et al., 2013b). Interestingly, not unlike Parkin, VCP has been linked to TDP-43 metabolism. In SH-SY5Y cells expressing mutant VCP (R95G, R155H/C, R191Q, A232E), TDP-43 redistributed from the nucleus to the cytoplasm (Gitcho et al., 2009). Similarly, in VCP R152H or A229E transgenic *Drosophila* and spinal cord motor neurons of VCP R155H or A232E transgenic mice,

the expression of mutant VCP induced TDP-43 pathology (Custer et al., 2010). Furthermore, in *Drosophila*, TBPH, the fly homolog of TDP-43 was identified as a genetic modifier that suppressed mutant VCP toxicity, indicating that VCP toxicity is at least in part mediated by a toxic gain of function of TDP-43 (Custer et al., 2010). A possible explanation for this genetic interaction is that accumulation of cytoplasmic TDP-43 exacerbates loss of mitochondrial quality control by mutations in VCP.

Mutations in the *OPTN*, *SQSTM1* and *TBK1* genes have been associated with ALS (Figure 1.8) (Fecto et al., 2011; Freischmidt et al., 2015; Maruyama et al., 2010; reviewed in Renton et al., 2014). ALS-associated mutations in these genes appear cause loss of function phenotypes. The ALS-associated *OPTN* E478G mutation maps to the UBD of *OPTN* and is no longer recruited to damaged mitochondria (Shen et al., 2015; Wong and Holzbaur, 2014). Along the same lines, the ALS-associated L341V mutation in p62 maps to the LIR domain and disrupts interaction with LC3 (Goode et al., 2016). The ALS mutant forms of *TBK1*; *TBK1* del690-713 and E696K, prevent the interaction between *TBK1* and *OPTN* and impair clearance of LC3 labelled autophagic cargos (Heo et al., 2015; Lazarou et al., 2015). Furthermore, the expression of *TBK1* E696K did not rescue *TBK1* knockdown induced defects in LC3 recruitment to mitochondria, suggesting ALS mutant *TBK1* also impairs mitophagy (Moore and Holzbaur, 2016). Finally, the activation of *TBK1* is dependent on the upstream activity of PINK1/Parkin, which as discussed above, is affected in ALS (Heo et al., 2015; Lazarou et al., 2015).

Despite a large amount of research concentrating on the Parkin dependent pathway mechanisms, the relevance of Parkin in basal mitophagy has been called into question. Much of the work carried out to investigate Parkin dependent mitophagy has employed chemical agents to induce mitochondrial damage and may not reflect mitophagy *in vivo*. PINK1 knockout mice were shown to have no defect in mitochondrial turnover compared to wild type animals (McWilliams et al., 2018). Moreover, PINK1 and Parkin knockout *Drosophila* models do not display defects in the basal levels of mitophagy (Lee et al., 2018b). This suggests that neither PINK1 nor Parkin are essential to maintain mitochondrial health in *in vivo* models. Interestingly, Parkin was shown to play a role in the maintenance of mitochondria in the cell body but not in the motor axon in an *in vivo* *Drosophila* model (Sung et al., 2016). Therefore, compartmentalised mitophagy events may underlie mitochondrial health in neurons and warrant further investigation. Furthermore, despite evidence of overexpressed but not endogenous Parkin recruitment occurring upon the induction of mitochondrial damage, the mechanisms of mitochondrial

quality control active in neurons are still poorly understood (reviewed in Cummins and Gotz, 2017; Martinez-Vicente, 2017).

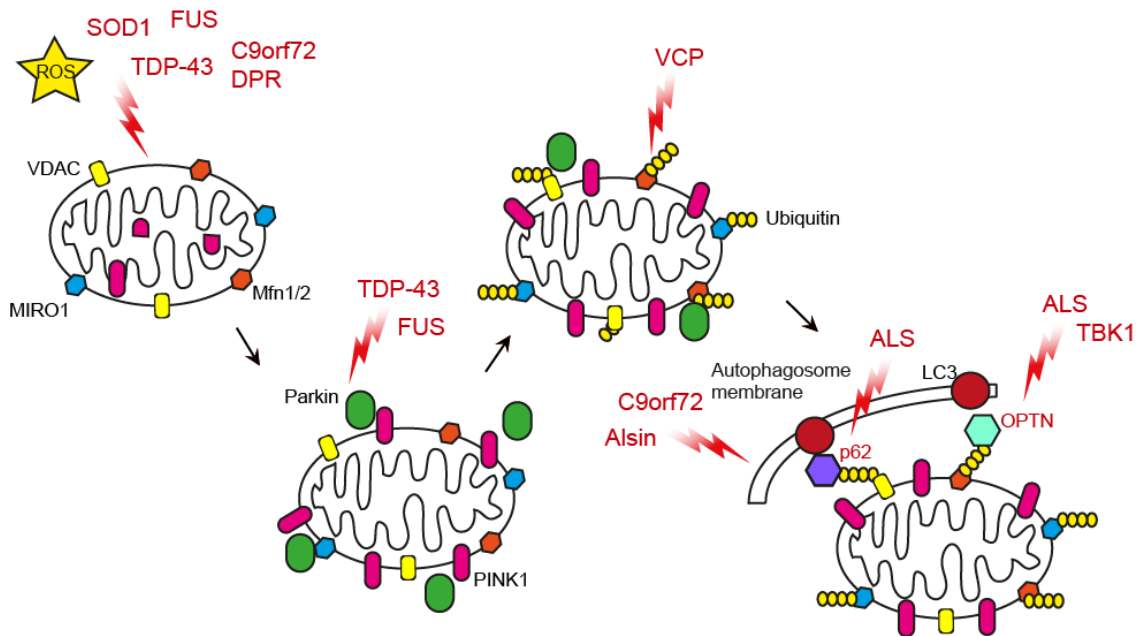


Figure 1.8 Parkin dependent mitophagy is impaired in ALS

Parkin dependent mitophagy removes dysfunctional mitochondria from the cell. Upon mitochondrial damage the loss of MMP results in the cessation of PINK1 import and cleavage in mitochondria. Full length PINK1 accumulates on the OMM, where it phosphorylates ubiquitin chains. Parkin is recruited to phosphorylated ubiquitin chains and is itself phosphorylated by PINK1, resulting in an increase in the E3 ligase activity of Parkin. Parkin ubiquitinates OMM proteins involved in mitochondrial fusion and motility, which are subsequently removed from the OMM by VCP and are degraded by the proteasome. Ubiquitin chains on the OMM lead to the recruitment of the autophagy machinery and canonical autophagy ensues. Elevated ROS and aggregates of mutant ALS protein which associate with mitochondria lead to mitochondrial stress and induction of mitophagy. Mitophagy is impaired at several stages in ALS (indicated in red). Mutant TDP-43 and FUS levels may affect Parkin levels. The removal of ubiquitinated OMM proteins may be impaired by ALS-linked mutations in VCP. Recognition of ubiquitinated mitochondrial cargos may be impaired by mutations in p62, OPTN and TBK1. Other ALS genes including Alsln and C9orf72, which are linked to autophagy, have been implicated in mitochondrial clearance. For further details please refer to the main text. Figure adapted from (Smith et al., 2017b), under the terms of the Creative Commons Attribution License (CC BY).

1.2.3.2 Parkin independent mitophagy pathways

In addition to the Parkin dependent mitophagy explored above, additional mechanisms leading to the removal of damaged mitochondria have been identified. It is perhaps not surprising that alternative mechanisms for mitochondrial quality control have evolved, due to the importance of mitochondrial function for cellular homeostasis. Therefore, a certain degree of redundancy is to be expected in the system.

Most straightforwardly, proteins found on the OMM can act directly as mitophagy receptors and interact with LC3 via a LIR domain. This is the case for BCL2 Interacting Protein 3 Like (NIX), BCL2 Interacting Protein 3 (BNIP3) and FUN14 Domain Containing 1 (FUNDC1) proteins that are involved in hypoxia induced mitophagy, where both NIX and BNIP3 are upregulated (Liu et al., 2012; Shi et al., 2014; Sowter et al., 2001). NIX has also been implicated in mitochondrial clearance during the maturation of erythrocytes (Schweers et al., 2007). Interaction of the OMM receptor protein with LC3/GABARAP leads directly to mitochondria being targeted to autophagosomes (Figure 1.9). Additional OMM proteins mediate the recruitment of LC3 autophagosomes indirectly. Choline dehydrogenase (CHDH) accumulates on the OMM upon mitochondrial depolarisation and interacts with p62. p62 subsequently recruits LC3 to mitochondria (Park et al., 2014). Furthermore Fis1, implicated in mitochondrial fission, interacts with TBC1 domain family members 15 and 17 (TBC1D15/TBC1D17) which are mitochondrial Rab GTPase activating proteins (GAP). The TBC1D15/17 complex interacts with LC3/GABARAP to recruit autophagosomes via Rab7 (Figure 1.9) (Yamano et al., 2014; Yamano et al., 2018).

Spinal cord motor neurons of SOD1 G93A mice were shown to have reduced BNIP3 expression (Rogers et al., 2017). This may lead to the decreased recognition of damaged organelles and an accumulation of fragmented mitochondria, as reported in the SOD1 G93A animal models (Dal Canto and Gurney, 1994; De Vos et al., 2007; Higgins et al., 2003; Magrané et al., 2009). As noted above, ALS-linked mutations in p62 impair the interaction between p62 and LC3 (Goode et al., 2016), which may also result in defective Parkin independent mitophagy clearance of mitochondria in ALS. Rab7 has been shown to interact with C9orf72 (Farg et al., 2014; Frick et al., 2018). Due to the structure of the C9orf72 protein (discussed subsequently 1.3.2), C9orf72 may regulate the trafficking and activity of Rab7 in mitophagy. As C9orf72 haploinsufficiency may lead to ALS/FTD (DeJesus-Hernandez et al., 2011), this may result in impaired clearance of mitochondria via the Fis1 pathway. Thus, Parkin independent mitophagy mechanisms may also be affected in ALS, although further evidence is required to determine the extent of its contribution to disease pathogenesis.

Proteins found inside mitochondria have also been shown to be involved in the recruitment of the autophagy machinery to damaged organelles. These proteins would become accessible to the autophagy machinery found in the cytosol upon the rupture of the mitochondrial membranes, a feature of both Parkin dependent and independent mitophagy (Yoshii et al., 2011). For instance, Prohibitin 2 (PHB2) an IMM protein, was shown to interact with LC3 via a LIR following rupture of the OMM (Figure 1.9) (Wei et al., 2017). TDP-43 was found to interact with PHB2 and to be involved in the expression of PHB2 during mitophagy (Davis et al., 2018). It will be interesting to determine the effect of ALS mutations in TDP-43 and the effect of TDP-43 mislocalisation on PHB2 mediated clearance of mitochondria.

The mechanisms discussed above have been shown to result in the removal of an entire damaged mitochondrion. However, it is likely that *in vivo* mitochondria are also maintained by selective removal of damaged mitochondrial components, as part of cellular homeostasis. This would indeed appear to be a more energetically favourable mechanism to maintain mitochondrial health, as it would not require the biogenesis of new organelles.

Under basal conditions, OMM proteins are ubiquitinated. The ubiquitin labelled proteins are then removed from the OMM by VCP and degraded by the proteasome. Although this mechanism is also involved in Parkin dependent mitophagy, it may also maintain OMM proteins in basal conditions. Mitochondrial substrates of the proteasome that are maintained in this manner are thought to include TOM subunits, PINK1 and the OMM proteins involved in mitochondrial fusion events (reviewed in Shanbhag et al., 2012). As noted above, ALS linked mutations in VCP are associated with loss of function (reviewed in Tang and Xia, 2016). In addition, the proteasome may degrade misfolded proteins encoded by the nuclear genome destined for mitochondrial import. These can be intercepted by the proteasome quality control system and targeted directly for degradation by the 26S proteasome (reviewed in Shanbhag et al., 2012). As noted above (1.2.3.1), the function of the proteasome is impaired in ALS, leading to the accumulation of ubiquitinated substrates (reviewed in Bendotti et al., 2012; Webster et al., 2017), which would impair basal levels of mitochondrial maintenance.

Mitochondrial proteins synthesised and folded in the mitochondrial matrix are also subject to quality control pathways. Unfolded proteins in the mitochondrial matrix trigger the mitochondrial unfolded protein response (UPR^{mt}). Triggering of UPR^{mt} induces transcription of nuclear genes encoding the mitochondrial chaperones and proteases which refold or remove damaged mitochondrial proteins (reviewed in Shpilka and Haynes, 2017). UPR^{mt} was shown to be active in both SOD1 G93A mice and a SOD1

G93A mouse model where the mutant SOD1 was targeted exclusively to the mitochondrial IMS (Riar et al., 2017). Although the activation of UPR^{mt} may represent a mechanism by which the cell attempts to restore mitochondrial function, excessive activation may trigger cell death where the mitochondrial proteins cannot be repaired (reviewed in Münch, 2018).

Recently a mitochondrial quality control pathway activated by low level stress in neurons was described. Upon ROS induced damage, mitochondrial proteins and lipids become oxidised and are segregated on the mitochondrial membranes. A section of mitochondrial membrane corresponding to the OMM only or to both OMM and IMM has been revealed be removed from the mitochondrion. The mitochondrial derived vesicles (MDV) bud off from the surface of the mitochondrion and are delivered directly to the lysosome via the multivesicular body (MVB) (late endosome) (Figure 1.9) (McLelland et al., 2014; Soubannier et al., 2012a). Damaged mitochondria released syntaphilin (SNPH) which resulted in the immobilisation of the damaged mitochondrion (Kang et al., 2008). SNPH vesicles formed in a Parkin and Drp1 independent manner and budded from axonal mitochondria. The vesicles were then transported to the soma and degraded by lysosomes (Lin et al., 2017). MDV have been reported to maintain mitochondria in normal growth conditions but may be upregulated by mitochondrial damage including hypoxia (Soubannier et al., 2012a). In stress induced mitophagy, the formation of MDV has been shown to be dependent on the activity of Parkin dependent mitophagy, and may form an additional, more rapid mechanism by which mitochondria are maintained by mitophagy (McLelland et al., 2014; Sugiura et al., 2014). Moreover, the formation of MDV has been shown to participate in mitochondrial mediated immunity events (Matheoud et al., 2016) and form exosomes that are released from the neuron (reviewed in Torralba et al., 2016). An increased number of MDV was reported in SOD1 G93A mouse ventral root axons, indicating mitochondrial stress that occurred prior to the activation of Parkin dependent mitophagy (Lin et al., 2017).

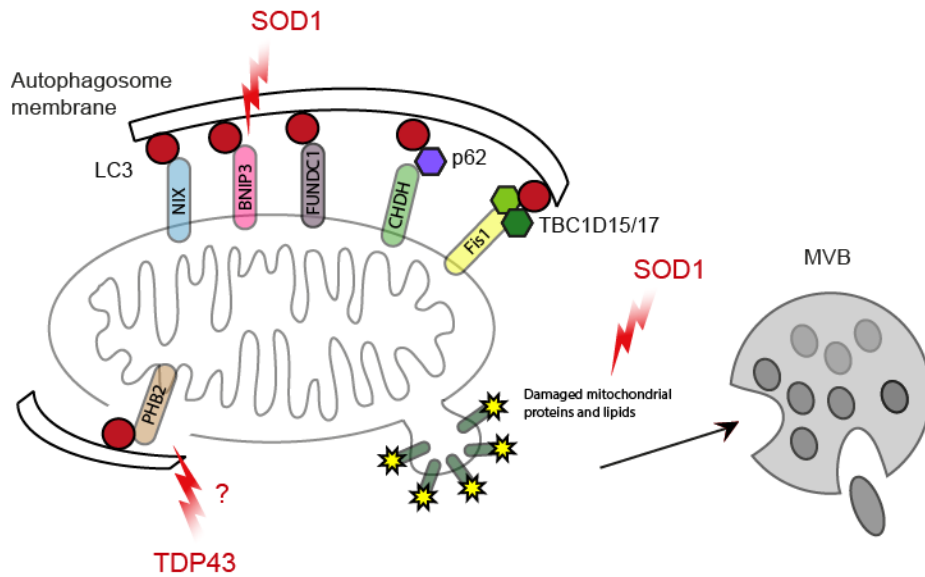


Figure 1.9 Parkin independent mitophagy is impaired in ALS

Mitochondrial proteins of the OMM (NIX, FUNDC1, BNIP3) recruit the LC3 autophagosome directly. CHDH and Fis1 recruit adaptor proteins which interact with LC3. ALS linked mutations in SOD1, TDP-43, SQSTM1/p62 and C9orf72 may impair Parkin independent mitophagy. Prohibitin 2 (PHB2) of the IMM interacts with LC3 upon rupture of the OMM. TDP-43 regulates the expression of PHB2, which may be affected in ALS. Non-whole organelle quality control is achieved by the budding of a damaged portion of mitochondrial membranes containing damaged lipids and proteins from the mitochondrial surface. MDVs are transported to the multivesicular body (MVB). An increase in MDV formation is found in SOD1 ALS. For further details please refer to the main text.

1.2.3.3 Mitophagy feeds into the canonical autophagy pathway that is impaired in ALS

Downstream of the labelling of damaged mitochondria with LC3, the mitophagy pathways joins the canonical autophagy pathway (reviewed in Yoshii and Mizushima, 2015). Autophagy deficient cells display accumulations of damaged mitochondria (Narendra et al., 2008). As autophagy is impaired in ALS, it is likely that these defects may lead to a decrease in the removal of damaged mitochondria, leading to the accumulations of damaged mitochondria observed in patient tissue and ALS models (1.1.3.5).

Site specific generation of autophagosomes around mitochondria promote their clearance. Indeed, the ULK1 initiation complex has been shown to be recruited to damaged mitochondria in both PINK1/Parkin and FUNDC1 mitophagy pathways,

indicating that site specific initiation of autophagy at damaged mitochondria may occur (Itakura et al., 2012; Wu et al., 2014). AMPK has been shown to phosphorylate ULK1 at Ser555 during hypoxia and thereby promote its recruitment to damaged mitochondria (Tian et al., 2015). Contributing further to the nucleation of the autophagosome during mitophagy and dependent on the prior recruitment of ULK1 and ATG9A, the PI3K complex, is also recruited to damaged mitochondria. AMBRA1 has been shown to interact with Parkin and activate the PI3K complex to enhance mitochondrial clearance (Van Humbeeck et al., 2011), although localisation of AMBRA1 to the OMM has also been shown to induce mitophagy in the absence of Parkin (Strappazzon et al., 2015).

Downstream of ULK1 and PI3K complex activation, double FYVE domain-containing protein 1 (DFCP1), a protein normally found diffusely on ER and Golgi membranes localises to the omegasome where it binds PI3P (Axe et al., 2008; Wong and Holzbaur, 2014). Recruitment of DFCP1 may initialise mitochondrial localised phagophores and assists in the recruitment of LC3 to damaged mitochondria (Axe et al., 2008). Indeed, the recruitment of DFCP1 to the omegasome is dependent on the recruitment of OPTN and NDP52 to mitochondria (Lazarou et al., 2015).

As noted previously (1.1.3.4), autophagy progression is impaired in ALS (reviewed in Webster et al., 2017). The general impairment of autophagy in ALS will lead to impaired clearance of damaged mitochondria. Corticospinal motor neurons of *Alsin* knockout mice exhibit fused mitochondria engulfed by vacuole structures, consistent with failure to remove damaged mitochondria by mitophagy (Gautam et al., 2016; Hadano et al., 2006). Furthermore, the delivery of substrates to the autophagosome, including mitochondria, is dependent on their association with LC3. ALS-linked mutations in OPTN, TBK1, p62 and UBQLN2 lead to impaired delivery of substrates, including mitochondria, to the autophagosome (reviewed in Majcher et al., 2015; Webster et al., 2017).

1.3 C9orf72-related ALS/FTD

1.3.1 The C9orf72 gene

The *C9orf72* gene is located on the short arm of chromosome 9 at position 21.2. The *C9orf72* gene contains 11 exons and is predicted to encode 3 transcript variants, from which 2 protein isoforms are produced. Variant 1, corresponding to exons 2 – 6, produces the C9orf72 short isoform (C9orf72S), a protein comprised of 222 amino acids. Variants 2 and 3 correspond to exons 2 – 11 and produce the C9orf72 long isoform (C9orf72L), a protein of 481 amino acids.

1.3.2 C9orf72 is a DENN domain containing protein involved in membrane trafficking events

As described above, the C9orf72 gene is predicted to encode 2 C9orf72 protein isoforms: C9orf72L and C9orf72S. C9orf72 mRNA has been shown to be expressed ubiquitously, indicating that C9orf72 may be expressed in most tissues [<https://www.proteinatlas.org/ENSG00000147894-C9orf72/tissue>] (Uhlen et al., 2015). C9orf72 expression levels have been shown to vary depending on cell type. C9orf72 mRNA levels have been reported to be high in myeloid cells and to be elevated in microglia compared to neurons in adult mouse brain (O'Rourke et al., 2016). However the full picture remains unclear as it has also been reported that C9orf72 expression is higher in motor neurons compared to oligodendrocyte and astrocytes at a 2.5 : 1 : 1 ratio (Jiang et al., 2016).

Computational analysis of the C9orf72L protein suggests C9orf72 shares structural homology with the differentially expressed in normal and neoplasia (DENN) family of proteins (Levine et al., 2013; Zhang et al., 2012). C9orf72L was found to contain the tripartite DENN domain, a typical feature of DENN proteins consisting of an N-terminal upstream DENN (uDENN) domain (amino acids 23 – 104), a central DENN domain (amino acids 200 – 343) and a C-terminal downstream DENN (dDENN) domain (amino acids 370 – 464) (Figure 1.10). Although the 3 DENN domains have distinct sequences and evolutionary conservation, the 3 domains are always associated, potentially as a result of structural or functional requirements (Levivier et al., 2001). DENN proteins frequently function as guanine exchange factors (GEF) for Rab-GTPases that are involved in membrane trafficking events and autophagy (Hutagalung and Novick, 2011; Marat et al., 2011; reviewed in Zhen and Stenmark, 2015). Interestingly, the C9orf72S isoform corresponds to the N-terminal portion of C9orf72L, i.e. the first 222 amino acids, and contains the uDENN domain only (Figure 1.10). It is unclear how the function of the C9orf72S protein is affected by this altered DENN domain structure.

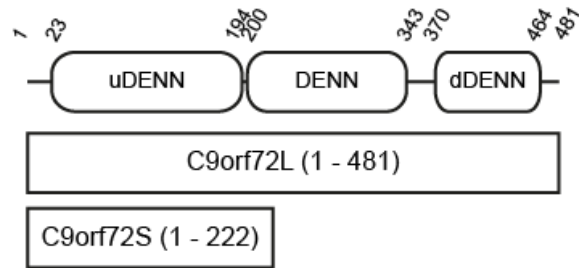


Figure 1.10 The C9orf72 protein contains DENN domains

The C9orf72 protein is predicted to contain the 3 domains found in a typical DENN protein: a N-terminal longin (uDENN) domain, a central DENN domain and a C-terminal alpha (dDENN) domain. Based on sequence alignment, the C9orf72S isoform is predicted to lack the majority of the central DENN domain and the terminal d-DENN domain found in C9orf72L.

As a DENN domain containing protein, C9orf72 has been proposed to act in Rab GTPase cascades, which control membrane trafficking events (reviewed in Zhen and Stenmark, 2015). Briefly, a Rab GTPase cycles between GDP and GTP bound forms. DENN domain containing proteins tend to be Rab GEFs. Rab GEFs activate the Rab GTPase by mediating the exchange of GDP for GTP. Conversely, Rabs are inactivated by the hydrolysis of GTP to GDP which is enhanced by the activity of GTPase-activating protein (GAP). Rab effectors bind the GTP bound Rab and mediate the localisation and activity of the Rab. Trafficking of newly synthesised inactive Rabs to the membrane is mediated by an initial interaction with Rab escort protein (REP), which presents the Rab to geranylgeranyl transferase (GGT) for prenylation. The prenylated Rab then enters the Rab GTPase cycle. Post inactivation of the Rab by a GAP, the Rab is subsequently recognised by Rab GDP dissociation inhibitor (GDI), which results in the extraction of the inactive Rab from the membrane. The interaction between GDI displacement factor (GDF) and the Rab GEF result in the insertion of the Rab into the membrane and its subsequent activation (Figure 1.11) (reviewed in Brighthouse et al., 2010; Grosshans et al., 2006). To mediate membrane trafficking events, Rab GTPases act in Rab cascades, where the upstream Rab and its effector mediate the recruitment of the downstream Rab's GEF, whilst the downstream Rab recruits the GAP for the upstream Rab (reviewed in Pfeffer and Kellogg, 2017).

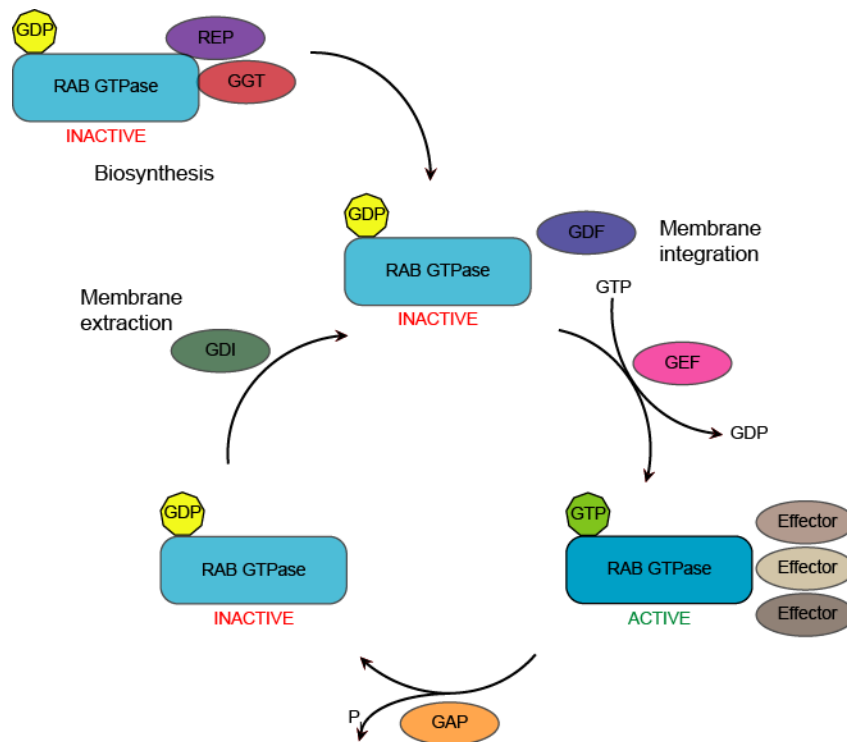


Figure 1.11 Rab GTPases activity is mediated by GAPs and GEFs

Rab GTPases cycle between active GTP bound and inactive GDP bound forms. GDP-bound Rab is targeted to specific membranes by its GEF and effector proteins where it is activated by the GEF through the exchange of GDP for GTP. The GAP stimulates the hydrolysis of GTP by the Rab resulting in its inactivation. The inactive Rab is removed from the membrane by GDI.

C9orf72L has been shown to display a diffuse cytosolic localisation, whereas C9orf72S appeared to be localised to the nuclear membrane (Davidson et al., 2017; Farg et al., 2014; Xiao et al., 2015). Hence it appears that the C9orf72 isoforms may have different localisations and may therefore have distinct subcellular roles.

To identify the cellular function of the C9orf72 protein, investigations into the interacting partners of C9orf72 were performed. C9orf72 was found to be in a complex with Smith-Magenis Syndrome Chromosome Region candidate 8 (SMCR8) and WD repeat domain 41 (WDR41) (Amick et al., 2016; Sellier et al., 2016; Sullivan et al., 2016; Yang et al., 2016). Like C9orf72, SMCR8 was found to be a DENN domain containing protein (Levine et al., 2013; Zhang et al., 2012), which may also play a role in membrane trafficking events. Indeed, the complex containing C9orf72 and SMCR8 supports the function of these proteins in Rab cascades (Sellier et al., 2016; reviewed in Webster et al., 2016b). Interestingly, the interaction between C9orf72 and SMCR8 has been shown to be important to maintain the stability of the two interacting partners (Amick et al.,

2016; Ugolino et al., 2016; Zhang et al., 2018). In contrast, WDR41 is a member of the WD-repeat containing protein family, members of which frequently act as scaffolds for protein complexes, due to their ability to bind both proteins and lipids. Hence WDR41 may be important in regulating the stability and cellular localisation of the C9orf72/SMCR8 complex (Amick et al., 2018).

Consistent with the DENN function of the C9orf72 and SMCR8 proteins, either C9orf72 or the C9orf72/SMCR8/WDR41 complex have been identified to interact with and regulate several Rab GTPases (Table 1-3). Investigations into the nature of the interactions between C9orf72 or the C9orf72/SMCR8/WDR41 complex and the identified Rab GTPases in relation the function of some of these Rabs have been performed. This identified several cellular membrane trafficking pathways to be regulated by the C9orf72/SMCR8/WDR41 complex, although the final picture remains unclear.

Table 1-3 C9orf72 and the C9orf72/SMCR8/WDR41 complex interact with Rab GTPases

Rab GTPase	Characterisation of interaction	Reference
Rab1a	C9orf72 (co-loc, co-IP), C9orf72 complex (co-IP)	(Farg et al., 2014; Frick et al., 2018; Webster et al., 2016a)
Rab3	C9orf72 complex (co-IP)	(Frick et al., 2018)
Rab5	C9orf72 (co-IP), C9orf72 complex (co-IP), C9orf72 (co-loc)	(Aoki et al., 2017; Farg et al., 2014; Frick et al., 2018)
Rab6a	C9orf72 complex (co-IP)	(Sellier et al., 2016)
Rab7	C9orf72 complex (co-IP), C9orf72 (co-loc, co-IP)	(Farg et al., 2014; Frick et al., 2018)
Rab8a	C9orf72 (co-IP), C9orf72 complex (co-IP)	(Sellier et al., 2016)
Rab10	C9orf72 (co-IP), C9orf72 complex (co-IP)	(Aoki et al., 2017; Frick et al., 2018)
Rab11	C9orf72 (co-loc, co-IP)	(Farg et al., 2014)
Rab12	C9orf72 complex (co-IP)	(Sellier et al., 2016)
Rab13	C9orf72 (co-IP), C9orf72 complex (co-IP)	(Aoki et al., 2017; Frick et al., 2018)
Rab15	C9orf72 (co-IP), C9orf72 complex (co-IP)	(Aoki et al., 2017; Frick et al., 2018)

Rab GTPase	Characterisation of interaction	Reference
Rab18	C9orf72 (co-IP)	(Aoki et al., 2017)
Rab19	C9orf72 (co-IP)	(Aoki et al., 2017)
Rab25	C9orf72 complex (co-IP)	(Sellier et al., 2016)
Rab27a	C9orf72 (co-IP)	(Aoki et al., 2017)
Rab28	C9orf72 (co-IP)	(Aoki et al., 2017)
Rab29	C9orf72 (co-IP)	(Aoki et al., 2017)
Rab33a	C9orf72 complex (co-IP)	(Sellier et al., 2016)
Rab38	C9orf72 (co-IP), C9orf72 complex (co-IP)	(Sellier et al., 2016)
Rab39a	C9orf72 complex (co-IP)	(Sellier et al., 2016)
Rab39b	C9orf72 complex (co-IP)	(Sellier et al., 2016)
Rab40a	C9orf72 (co-IP)	(Aoki et al., 2017)
Rab42	C9orf72 (co-IP)	(Aoki et al., 2017)

Abbreviations: co-loc: co-localisation, co-IP: co-immunoprecipitation

1.3.2.1 The role of C9orf72 in autophagy

Consistent with a role for the C9orf72 protein in autophagy, C9orf72 was found to co-localise with LC3 positive autophagosome structures (Farg et al., 2014) and knockdown of C9orf72 impaired the initiation of autophagy (Webster et al., 2016a). Furthermore, C9orf72 has been shown to interact with the proteins of the autophagy initiation complex: ULK1, FIP200, ATG13 and ATG101 (Webster et al., 2016a; Yang et al., 2016).

During the initiation stages of autophagy, C9orf72 was found to act as an effector for Rab1a regulating the recruitment of the ULK1 initiation complex to the phagophore (Sullivan et al., 2016; Webster et al., 2016a; Yang et al., 2016). Indeed, the knockdown of C9orf72 impaired the translocation of the ULK1 initiation complex to the phagophore which led to impaired clearance of autophagic cargos (Sellier et al., 2016; Webster et al., 2016a). Interestingly, the initiation of autophagy has previously been implicated in ALS. ALS-linked mutations in Alsin, a GEF for Rab5, led to decreased autophagosome formation (Topp et al., 2004).

Consistent with the DENN protein properties of both C9orf72 and SMCR8 and a Rab GTPase cascade, the C9orf72/SMCR8/WDR41 complex may regulate the initiation and the downstream maturation step of autophagy (reviewed in Webster et al., 2016b). The recruitment of Rab1a to the initiation site by C9orf72 may mediate the co-trafficking of the C9orf72 interacting partner SMCR8. Indeed, upstream Rabs and their effector mediate the recruitment of the downstream Rab GEFs. The C9orf72/SMCR8/WDR41 complex was shown to display GEF activity towards Rab8a and Rab39b (Sellier et al., 2016), which act in autophagosome elongation and maturation (Pilli et al., 2012; Sato et al., 2014; Seto et al., 2013). The GEF activity towards Rab8a and Rab39b was shown to be conveyed by SMCR8 (Sellier et al., 2016), indicating the presence of Rab GTPase cascade (Figure 1.12B). Rab8a and Rab39b have also been shown to interact with OPTN and p62, suggesting that the C9orf72/SMCR8/WDR41 complex may also be involved in site specific targeting of autophagosome initiation (Pilli et al., 2012; Sellier et al., 2016; Webster et al., 2016b). Furthermore, SMCR8 is phosphorylated by both TBK1 and ULK1, regulating its activity and driving site specific autophagy initiation (Pilli et al., 2012; Sellier et al., 2016; Wild et al., 2011b).

The C9orf72/SMCR8/WDR41 complex has been shown to interact with additional Rab GTPases that have been implicated in the autophagy pathway (Table 1-3) (Aoki et al., 2017; Sellier et al., 2016): Rab12 involved in autophagosome trafficking (Xu et al., 2015); Rab38 (a paralog of the interacting Rab Rab32) (Hirota and Tanaka, 2009), Rab33a (a paralog of the interacting Rab Rab33b) (Itoh et al., 2008) and Rab18 (Feldmann et al., 2017) shown to play a role in autophagosome formation (Figure 1.12A). This may suggest further involvement of the C9orf72/SMCR8/WDR41 complex in Rab cascades in autophagy that warrant future investigation.

C9orf72 was also shown to co-localise with Rab7, Rab7L1 (Rab29) and Rab11 which are involved in the maturation of autophagosomes and in endocytic transport (Figure 1.12A) (Aoki et al., 2017; Farg et al., 2014; Gutierrez et al., 2004; Szatmari et al., 2014; reviewed in Webster et al., 2016b). This suggested that C9orf72 may play a role in membrane trafficking events. Despite some evidence suggesting that C9orf72 may be involved in the trafficking of endocytic vesicles, the mechanism has not yet been fully elucidated (Farg et al., 2014).

C9orf72 has also been implicated in other autophagy-linked pathways. C9orf72 has been shown to interact with the heat-shock chaperone HSC70, which plays a role in aggregophagy (Sellier et al., 2016). Furthermore, C9orf72 interacts with p62, which targets stress granules for autophagic clearance (Guo et al., 2014). The knockdown of both C9orf72 and p62 resulted in delayed clearance of stress granules, which were shown to

accumulate in C9orf72 ALS/FTD patient cerebellum and hippocampus (Chitiprolu et al., 2018). These additional autophagy-linked functions of C9orf72 warrant further study as they may provide links between C9orf72 disease mechanisms and the other cellular pathology observed in ALS.

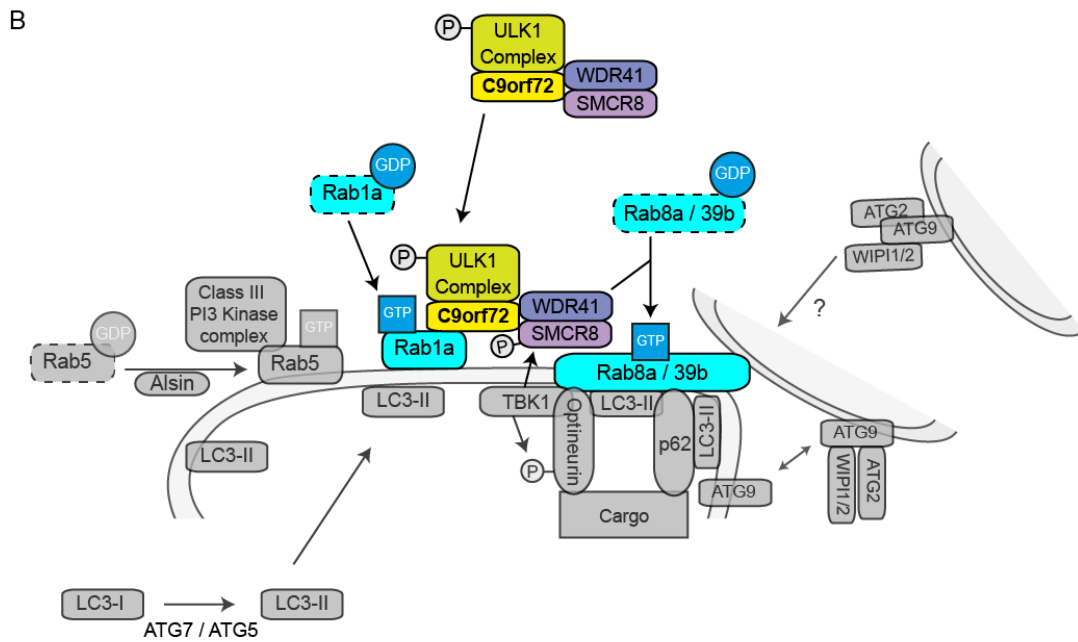
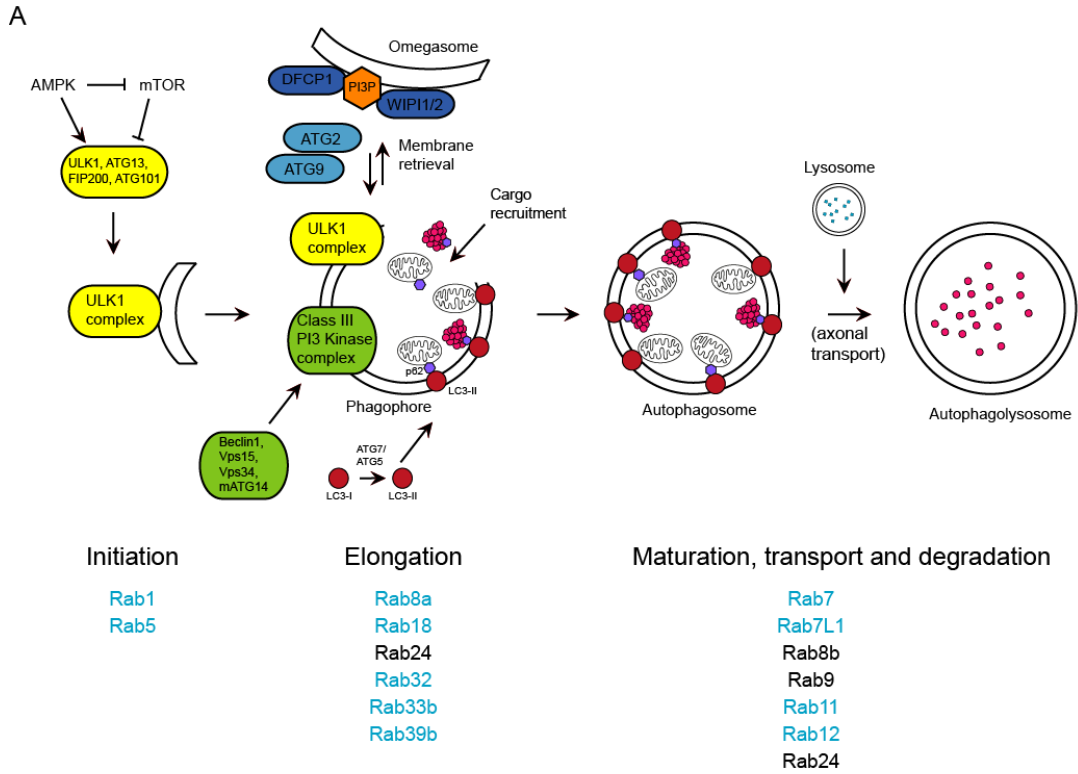


Figure 1.12 The C9orf72/SMCR8/WDR41 complex interacts with Rab GTPases in autophagy

A) Rab GTPases play important roles in the membrane trafficking steps of autophagy, including during initiation, autophagosome membrane elongation and the transport of the autophagosome to the lysosome. The Rab GTPases that have been shown to interact with and therefore may be regulated by the C9orf72/SMCR8/WDR41 complex are shown in blue. B) The C9orf72/SMCR8/WDR41 complex is involved in the initiation of autophagy in a Rab cascade. C9orf72 regulates the recruitment of the ULK1 initiation complex via Rab1a. The complex subsequently acts as a GEF for the downstream Rabs Rab8a and Rab39b which are involved in the elongation of the autophagosome membrane via the retrieval of ATG9 membranes. Through interactions with p62 and OPTN, Rab8a and Rab39b may promote site directed autophagosome formation. For further details please refer to main text. Figure adapted from (Webster et al., 2016b), under the terms of the Creative Commons Attribution License (CC BY).

1.3.2.2 The role of C9orf72 in lysosome biology

Previously it had been described that both SMCR8 and WDR41 localised to lysosomal membranes (Schroder et al., 2007). More recently, C9orf72 was also found to be recruited to lysosomes upon amino acid starvation (Amick et al., 2016). Consistent with a role for WDR41 in the regulation of the C9orf72/SMCR8 complex, WDR41 was found to interact with C9orf72 and regulate its recruitment to lysosomes (Amick et al., 2018). Knockdown of SMCR8 and C9orf72 resulted in enlarged lysosome vesicles, suggesting lysosomal dysfunction (Amick et al., 2016). Lysosomal dysfunction is additionally a prevalent feature of C9orf72 and SMCR8 knockout mouse models. Both C9orf72 and SMCR8 knockout mice were shown to display higher levels of the lysosomal protein Lamp1 on the surface of macrophages, thereby indicating that C9orf72 and SMCR8 may play a role in the lysosomal exocytosis (Zhang et al., 2018). Furthermore, C9orf72 knockout mice display microglia and macrophages with enlarged lysosomes, which may promote the pro-inflammatory state reported in these mice (O'Rourke et al., 2016; Sullivan et al., 2016) (discussed later in 1.3.3.3).

The transcription of genes encoding both autophagy and lysosomal proteins is under the transcriptional control of Transcription Factor EB (TFEB), which is stimulated upon starvation. Briefly, the inhibition of mTOR upon starvation results in the translocation of TFEB to the nucleus and the transcription of genes involved in autophagy and lysosome biogenesis (reviewed in Napolitano and Ballabio, 2016; Settembre et al., 2012). Loss of C9orf72 has been shown to result in dysregulation of the mTOR signalling pathway,

which may lead to lysosomal dysfunction. Loss of C9orf72 resulted in decreased mTORC1 activity and subsequently in an increase in TFEB levels and its translocation to the nucleus, leading to an increase in lysosome biogenesis (Ugolino et al., 2016).

Following starvation, the activation of mTOR via amino acid availability results in the phosphorylation of the ribosomal protein S6 kinase, resulting in the promotion of cell proliferation and the attenuation of autophagosome and lysosome biogenesis (reviewed in Magnuson et al., 2012). The knockdown of C9orf72 led to impaired mTORC1 signalling in response to refeeding following amino acid starvation, which may potentiate the lysosomal defects (Amick et al., 2016; Amick et al., 2018; Jung et al., 2017; Ugolino et al., 2016). Interestingly, a similar phenotype was observed in WDR41 knockout cells, which was rescued by the targeting of C9orf72 to the lysosome (Amick et al., 2018). This indicated that the lysosomal role of C9orf72 is dependent on its localisation which is driven by WDR41 (Amick et al., 2016; Amick et al., 2018).

1.3.2.3 The role of C9orf72 in the regulation of synaptic function

C9orf72 has been shown to be enriched in synaptosome fractions and located in synapses in hippocampal mossy fibre terminals (Atkinson et al., 2015; Frick et al., 2018). The synaptic function of the C9orf72 protein remains unclear. C9orf72 was found to interact with the Rab3 family (Frick et al., 2018), that is responsible for the transport of presynaptic neurotransmitter containing vesicles to the active zone, which underlies neurotransmission events (reviewed in Binotti et al., 2016; Schluter et al., 2006). In addition, C9orf72 has been shown to potentially regulate neuronal growth. GTPases are involved in the regulation of axonal growth and in synapse plasticity, via the regulation of actin filaments. The assembly of actin filaments is regulated by cofilin (reviewed in Spence and Soderling, 2015). C9orf72 knockdown primary motor neurons resulted in higher levels of inactive cofilin, which led to decreased actin dynamics and axonal growth (Sivadasan et al., 2016).

1.3.2.4 Additional unexplored functions of C9orf72

Finally, in addition to the interacting partners of C9orf72 explored above, proteomics screens have identified numerous other proteins as potential interacting partners of C9orf72 (Blokhuis et al., 2016; Sellier et al., 2016; Sullivan et al., 2016). GO biological process analysis suggested that C9orf72 may play a role in protein folding, mitochondrial membrane organisation and in cellular transport events (Blokhuis et al., 2016). Therefore, the C9orf72 protein may have further cellular roles that are as of yet

unexplored, but which may inform on the cellular pathways involved in C9orf72 ALS/FTD pathogenesis.

1.3.3 A repeat expansion in C9orf72 is associated with ALS/FTD

A GGGGCC hexanucleotide repeat expansion in the first intron of the *C9orf72* gene is the most common genetic defect associated with both ALS and FTD (DeJesus-Hernandez et al., 2011; Renton et al., 2011; reviewed in Renton et al., 2014) (Table 1-1). The repeat expansion in *C9orf72* accounts for 34.2 % and 25.9 % of familial ALS and FTD cases respectively (Van Blitterswijk et al., 2012). Healthy individuals may present with up to 30 GGGGCC repeats, which is not considered to be pathogenic. However, ALS and FTD patients with the repeat expansion in *C9orf72* may have hundreds to thousands of GGGGCC repeats in this intron (DeJesus-Hernandez et al., 2011; Renton et al., 2011). It has been reported that the length of the repeat expansion correlates with age of disease onset (Gijssels et al., 2015) and disease duration in FTD (Suh et al., 2015). However, this was subsequently proposed to be linked to the patients having additional ALS/FTD risk factors (reviewed in Haeusler et al., 2016; Xi et al., 2015).

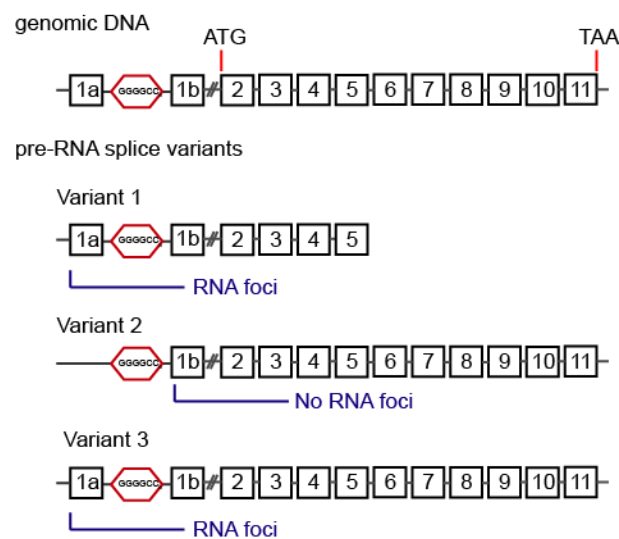


Figure 1.13 The *C9orf72* gene is linked to a GGGGCC repeat expansion in intron 1 in ALS/FTD

The GGGGCC repeat expansion associated with ALS/FTD is located in the first intron of C9orf72. The C9orf72 gene produces 3 splice variants which encode two protein isoforms: C9orf72S from variant 1, and C9orf72L from variants 2 and 3. With the inclusion of exon 1a in both variants 1 and 3, these pre-RNAs contain the repeat expansion sequence and could lead to the production of the RNA foci and DPRs associated with C9orf72 ALS/FTD.

The length of the GGGGCC repeat expansion has been shown to vary between brain regions in C9orf72 repeat expansion carriers (Beck et al., 2013). Shorter repeat lengths have been reported in patient cerebellum compared those found in frontal cortex or in blood (Van Blitterswijk et al., 2013). This somatic variability has been attributed to the formation of G-quadruplexes in the repeat expansion DNA (Zhou et al., 2015), which decrease replication efficiency and increase repeat instability, leading to both expansion and contraction of the repeat (Thys and Wang, 2015). Somatic instability has been proposed to contribute to the incomplete penetrance and phenotypic heterogeneity associated with the C9orf72 repeat expansion (Beck et al., 2013). A longer repeat length in the cerebellum has been associated with a decrease in survival post disease onset (Van Blitterswijk et al., 2013).

The mechanism by which the GGGGCC repeat expansion in C9orf72 causes ALS and FTD is currently unknown. Three main hypotheses have been put forward based on evidence from other repeat expansion diseases; an RNA gain of function toxicity, a protein gain of function toxicity and a loss of function through C9orf72 haploinsufficiency (Figure 1.14) (reviewed in Gendron and Petrucelli, 2018; Todd and Petrucelli, 2016). It is possible that no single mechanism leads to disease outright and that interplay between C9orf72 repeat expansion mechanisms and other cellular dysfunctions contribute to disease progression.

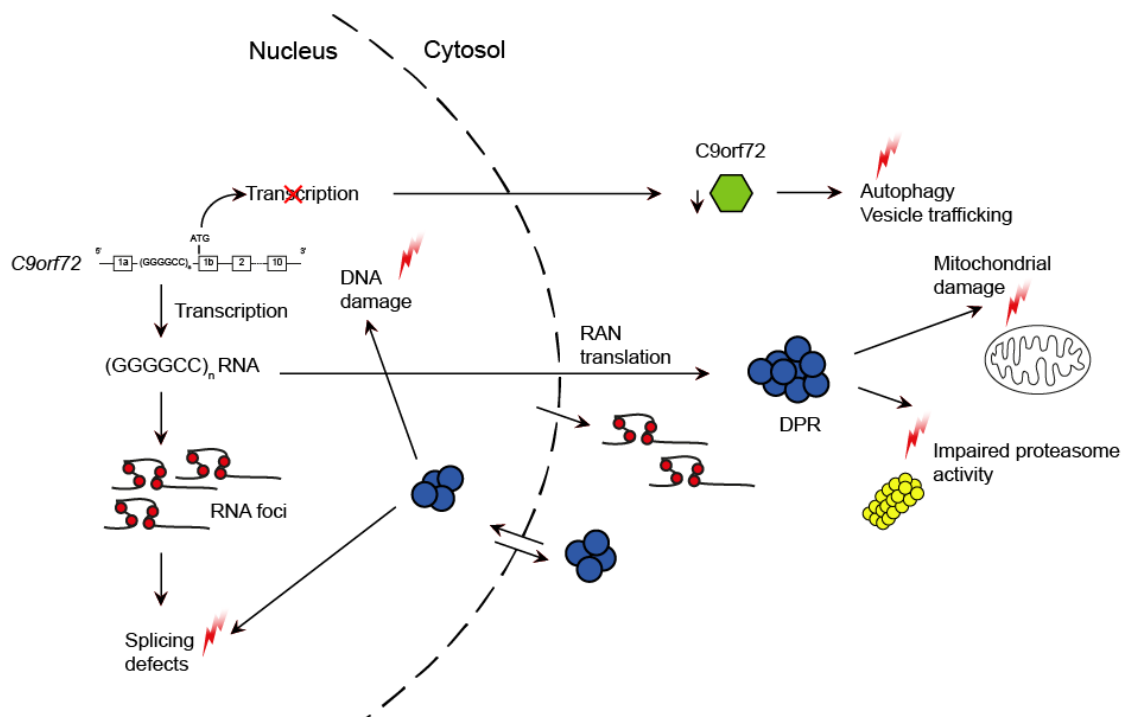


Figure 1.14 The repeat expansion in C9orf72 leads to ALS through 3 different potential disease mechanisms

Three distinct mechanisms have been proposed to cause disease in the C9orf72 repeat expansion patients. 1) RNA toxicity - RNA foci bind and sequester RNA binding proteins, nuclear export factors and splicing machinery leading to altered splicing and expression of nuclear encoded genes. RNA foci also lead to nucleolar stress and their presence in the cytosol results in excitotoxicity. 2) Protein toxicity - The C9orf72 repeat expansion mRNA is aberrantly exported into the cytosol where it is translated in a repeat-associated non-AUG (RAN) manner resulting in the production of DPR proteins, which form cytoplasmic and nuclear aggregates. The poly-GA polypeptides induce protein stress, whereas the poly-GR and poly-PR polypeptides induce nucleolar stress and disrupt splicing events. 3) C9orf72 haploinsufficiency - C9orf72 mRNA and protein levels are reduced in C9orf72 ALS/FTD patients, leading to disruptions in membrane trafficking and autophagy. See text for details.

1.3.3.1 Toxic RNA gain of function

A toxic RNA gain of function is common in many non-coding repeat expansion diseases including spinocerebellar ataxia type 8 (SCA8), type 1 myotonic dystrophy (DM1) and Huntington disease like-2 (HDL2) (reviewed in Sicot and Gomes-Pereira, 2013). DM1 is caused by an expanded CTG repeat in the dystrophin myotonia protein kinase gene (Cooper et al., 2009). The CTG expansion is retained in the nucleus, leading to the formation of discrete RNA foci. These foci sequester RNA binding proteins such as the splicing factor muscleblind-like protein 1, resulting in downstream splicing defects which give rise directly to the disease (Mankodi et al., 2002).

RNA foci have been reported in the frontal cortex, hippocampus, cerebellum and spinal cord of C9orf72 ALS/FTD patients (Cooper-Knock et al., 2014; DeJesus-Hernandez et al., 2011; Mizielinska et al., 2013). These foci have been shown to originate from both the sense and antisense RNA strands (Haeusler et al., 2014) and arise from the transcription of both variants 1 and 3, due to the inclusion of the intron located between exons 1a and 1b (Figure 1.13) (reviewed in Haeusler et al., 2016). The presence of antisense foci correlated with the presence of mislocalised TDP-43 (Cooper-Knock et al., 2015b). Furthermore, the presence of RNA foci in the frontal cortex region of C9orf72 patients was shown to correlate strongly with disease onset (Mizielinska et al., 2013). The RNA foci are frequently reported in the nucleus but have also been found in the cytoplasm (Donnelly et al., 2013; Lagier-Tourenne et al., 2013; Mizielinska et al., 2013). Finally, RNA foci in *Drosophila* models of C9orf72 have been shown to be present in

distal neurites and associate with proteins involved in transport and local translation of RNA containing granules (Burguete et al., 2015).

Both the RNA and DNA of the repeat expansion of C9orf72 have been shown to be structurally organised into G-quadruplexes, a secondary structure comprising a stack of guanine rich DNA/RNA stabilised by hydrogen bonds around a central cation (Conlon et al., 2016; Zhou et al., 2015). C9orf72 repeat expansion G-quadruplexes have been shown to sequester hnRNP-H and alter splicing events in ALS brain (Conlon et al., 2016). Interestingly, small molecules that bind and stabilise G-quadruplexes have been shown to reduce RNA foci and DPR burden (arising from protein toxicity; 1.3.3.2), and lead to an elongation in lifespan in a repeat expansion *Drosophila* model (Simone et al., 2018).

Many groups have concentrated on investigating the abnormal binding of nuclear proteins to the RNA foci. This abnormal binding leads to the sequestration of nuclear proteins and reduces their ability to function in normal RNA processing (reviewed in Barker et al., 2017; Todd and Petrucelli, 2016). The binding of adenosine deaminase, RNA-specific, B2 (ADARB2) to the RNA foci may lead to increased sensitivity to excitotoxicity (Donnelly et al., 2013). Additionally the accumulation of abortive RNA transcripts bound to nucleolin induce nucleolar stress (Haeusler et al., 2014). Furthermore, the RNA foci have been found to bind and sequester mRNA export proteins; ALYREF (Cooper-Knock et al., 2014), Pur-alpha (Sareen et al., 2013), hnRNP A3 (Mori et al., 2013b), hnRNP H/F (Cooper-Knock et al., 2014), hnRNP A1 (Cooper-Knock et al., 2014; Sareen et al., 2013) and RanGAP1 (Zhang et al., 2015b), along with the splicing factors hnRNP H (Cooper-Knock et al., 2014), ASF/SF2 (Reddy et al., 2013), SRSF1 and SRSF2 (Cooper-Knock et al., 2014; Rossi et al., 2015). The binding of the repeat expansion to the export proteins may result in the aberrant export of C9orf72 mRNA from the nucleus to the cytosol where non-ATG initiated translation occurs (discussed in 1.3.3.2). In addition, binding of C9orf72 mRNA to the export adaptors may prevent the normal export of other mRNAs resulting in further cellular dysfunction (Rossi et al., 2015). Finally, the sequestration of splicing proteins by the RNA foci could lead to altered expression and splicing profiles of many nuclear encoded proteins. This includes the splicing defects in genes previously linked to ALS (*ATXN2* and *FUS*) that have been reported in C9orf72 ALS patient cerebellum (Prudencio et al., 2015).

A challenge for researchers dissecting the models of C9orf72 repeat expansion is the differentiation between RNA and protein toxicity (reviewed in Batra and Lee, 2017; Gitler and Tsuiji, 2016; Moens et al., 2017). Experimental models expressing the GGGGCC repeat expansion have been shown to result in the formation of both sense and

antisense RNA foci, but also display aggregates indicative of protein toxicity (Freibaum et al., 2015; Mizielinska et al., 2014; Tran et al., 2015). Indeed, expression of the pure repeat has been shown to be toxic in *in vitro* cellular, Drosophila and Zebrafish models (reviewed in Moens et al., 2017). In mouse models however, the evidence is not as clear. Reports of ALS pathology, including TDP-43 aggregation and motor and cognitive dysfunction have been reported by some groups, but not by others (reviewed in Batra and Lee, 2017; Moens et al., 2017). The reasons for differences between the models generated may be due to expression levels and the genetic background of the mice (Batra and Lee, 2017).

In order to investigate the RNA toxicity hypothesis alone, repeat only RNA models have been generated. The insertion of STOP codons in every frame of the repeat expansion suppresses protein translation (and thereby protein toxicity), whilst not affecting the expression of the repeat RNA (Mizielinska et al., 2014). In Drosophila, expression of repeat only RNA did not lead to toxicity in comparison to the expression of pure GGGGCC RNA, despite the formation of RNA foci (Mizielinska et al., 2014). A second model consisting of a GGGGCC repeat in an intron also produced nuclear sense RNA foci but did not lead to neurodegeneration (Tran et al., 2015). Together these reports suggested that RNA toxicity did not lead directly to neurodegeneration. In contrast, expression of interrupted GGGGCC repeats in neurons in an inducible Drosophila model resulted in neurodegeneration (Zhang et al., 2015b). In addition, expression of intronic repeats in primary cortical and motor neurons resulted in the formation of RNA foci in the absence of protein toxicity, which was toxic to the cell (Wen et al., 2014). Therefore, RNA toxicity may play a role in C9orf72 repeat expansion in some models, but not in others and may depend on the cell type in which the repeats are expressed. Hence, it remains unclear if and how RNA toxicity is linked to disease in C9orf72 ALS/FTD patients.

1.3.3.2 Toxic protein gain of function

In several repeat expansion diseases including SCA8, DM1 and HD, the repeat expansion has been shown to undergo non-ATG initiated translation, termed repeat-associated non-AUG (RAN) translation. RAN translation occurs in all reading frames and results in the production of toxic proteins that are formed of repetitive peptide sequences (reviewed in Green et al., 2016).

The C9orf72 repeat expansion has been shown to be RAN translated resulting in the formation of 5 DPR species. The DPRs arise from the transcription of both variants 1 and 3, due to the inclusion of the intron located between exons 1a and 1b (Figure 1.13)

(reviewed in Haeusler et al., 2016). Sense transcripts produce poly-glycine-alanine (GA), poly-glycine-arginine (GR) and poly-glycine-proline (GP) DPRs. Poly-proline-arginine (PR), poly-proline-alanine (PA) and poly-glycine-proline (GP) DPRs arise from the antisense transcripts. The DPRs are prone to aggregation in the cell and form inclusions that are positive for p62 and ubiquitin but negative for TDP-43 across the CNS of C9orf72 ALS patients (Ash et al., 2013; Gendron et al., 2013; Mori et al., 2013a; Mori et al., 2013c; Zu et al., 2013). In patient tissues poly-GA inclusions have been found to be the most abundant, whereas poly-AP and poly-PR inclusions are rarely observed (Davidson et al., 2014; Gendron et al., 2013; Mackenzie et al., 2015). No consistent correlation between the presence of DPR pathology and ALS progression or neurodegeneration have been identified (Davidson et al., 2014; MacKenzie et al., 2013; Mackenzie et al., 2015). The aggregation of the DPRs may therefore constitute a protective role by sequestering small dipeptide repeat species and may not be disease relevant. Following this notion, the levels of soluble poly-GP in cerebellum was shown to correlate with cognitive impairment (Gendron et al., 2015).

The DPR inclusions have been shown to interact with and sequester cellular proteins and alter cellular function (reviewed in Todd and Petrucelli, 2016). Poly-GA inclusions have been revealed to bind Unc119, a protein involved in axonal maintenance and branching. Unc119 levels have been shown to reduce upon poly-GA expression in neurons which could lead to a decrease in membrane trafficking events (May et al., 2014). Poly-GA was also shown to interact with subunits of the proteasome, suggesting that it may alter protein homeostasis (Zhang et al., 2014). Indeed, aggregating DPRs along with the frequent p62 and ubiquitin staining observed in C9orf72-related ALS cases, suggest an impairment of protein turnover via the ubiquitin proteasome system or autophagy (Cooper-Knock et al., 2012; Stewart et al., 2012). The poly-GA DPR has also been suggested to display properties similar to prion proteins, forming toxic amyloids. These have the propensity to spread from cell to cell and could underlie the progression of neurodegeneration in C9orf72 ALS/FTD (Zhou et al., 2017).

The arginine containing DPRs (poly-GR and poly-PR) display a strong nuclear localisation, potentially as they resemble arginine rich nuclear import sequences (Kwon et al., 2014; Tao et al., 2015; Wen et al., 2014; Zu et al., 2013). Arginine containing DPRs have been shown to play a role in the formation and regulation of membrane-less organelles, including the nucleolus, nuclear pore complex, nuclear speckles and stress granules via the binding of low complexity domain (LCD) containing proteins (Lee et al., 2016c; Lin et al., 2016). Knockdown of a number of LCD interacting partners of poly-GR and poly-PR DPRs reduced DPR mediated pathology (Lee et al., 2016c). Consistent

with a role in the formation of membrane-less organelles, poly-GR and poly-PR DPRs were found to localise to the nucleolus, which resulted in a decrease in translation, rRNA synthesis and biogenesis of ribosomes (Kwon et al., 2014). In addition, the expression of poly-GR and poly-PR has been shown to decrease in the localisation of other proteins to the membrane-less organelles (Lee et al., 2016c). These changes may underlie the changes in splicing seen in poly-GR and poly-PR models (Kanekura et al., 2016; Kwon et al., 2014). Furthermore, poly-GR and poly-PR have been shown to interact with proteins involved in components of the nuclear pore and trafficking machinery. This may lead to changes in nucleocytoplasmic transport that have been reported in C9orf72 ALS patient models (Boeynaems et al., 2016; reviewed in Freibaum and Taylor, 2017; Jovicic et al., 2015; Lee et al., 2016c). Finally, the expression of poly-GR DPRs has been shown to induce DNA damage, which was linked to increased levels of ROS generation. Poly-GR DPRs interact with mitochondrial ribosomal proteins inducing mitochondrial dysfunction; including the hyperpolarisation and increased ROS generation (Lopez-Gonzalez et al., 2016).

Expression of the C9orf72 repeat expansion DPRs in cell and animal models have been reported to result in varying degrees of toxicity. To differentiate between the RNA and protein mediated toxicity, a number of DPR only models have been generated, which take advantage of codon degeneracy. These models result in the production of specific DPR species without the GGGGCC associated RNA foci/toxicity. Expression of poly-GR and poly-PR of lengths between 20 and 400 repeats have been consistently shown to induce toxicity in number of cell, Drosophila and mouse models (reviewed in Gitler and Tsuiji, 2016; Moens et al., 2017). Mild toxicity of the remaining DPR species of 20 to 400 length repeats have been reported in 3 studies but are not consistently observed. This may owe to the models examined, repeat length and application of the DPR (exogenous application versus induced expression) (reviewed in Moens et al., 2017). Therefore, it appears that DPRs, especially poly-GR and poly-PR, may contribute to cellular toxicity in C9orf72 ALS/FTD.

1.3.3.3 C9orf72 loss of function

Haploinsufficiency arises from the loss of normal expression of a gene from one of the two alleles, resulting in a reduction in the expression of the protein. Haploinsufficiency can arise from a number of defects including missense mutations in the gene, gene deletion, mRNA instability and transcriptional repression. Several repeat expansion diseases including fragile X syndrome and Friedreich ataxia are associated with haploinsufficiency (reviewed in La Spada and Taylor, 2010). ALS and FTD patients with

the repeat expansion in C9orf72 have been shown to have reduced mRNA levels encoding the C9orf72 protein in lymphoblast and frontal cortex (Belzil et al., 2013; DeJesus-Hernandez et al., 2011). Subsequently, the level of the C9orf72 protein was shown to be reduced in C9orf72 ALS patient frontal, motor cortex, temporal cortex and cerebellum (Frick et al., 2018; Waite et al., 2014; Xiao et al., 2015). This suggests that haploinsufficiency of the C9orf72 protein may contribute to disease pathogenesis.

Several mechanisms leading to the reduction in C9orf72 expression have been reported. The G-quadruplex structure adopted by the repeat expansion DNA has been shown to impair transcription (Haeusler et al., 2014). Reduced C9orf72 mRNA may also be as a result of hypermethylation of the CpG island 5' of the C9orf72 promoter region (Xi et al., 2013). CpG island hypermethylation acts as a repressor of gene transcription and is a common feature in cancer (reviewed in Sproul and Meehan, 2013). The presence of hypermethylation of the CpG island is associated with reduced RNA foci and DPR pathology (Liu et al., 2014). This suggests that the downregulation of C9orf72 transcription may be a protective factor in disease. C9orf72 expression has also been shown to be affected by histone binding. Trimethylation of histones H3 and H4 led to an increase in binding of histones to the repeat expansion and transcriptional repression (Belzil et al., 2013). Finally, the RNA and DNA of the C9orf72 repeat expansion has been shown to be structurally organised into R-loops (Haeusler et al., 2014; Reddy et al., 2013). R-loops are comprised of a DNA:RNA hybrid and is associated with a non-template single strand of DNA. R-loop formation is important for the regulation of gene expression, but also has implications for the stability of the genome (reviewed in Groh et al., 2014; Skourti-Stathaki and Proudfoot, 2014). In C9orf72 ALS, the formation of R-loops led to transcript abortion and thereby potentially C9orf72 haploinsufficiency (Haeusler et al., 2014).

Evidence suggests that in C9orf72 ALS patients the expression of specific transcripts is altered. Variants 1 and 2 were found to be significantly downregulated in C9orf72 patient cerebellum and frontal cortex, but variant 3 levels were unaffected (DeJesus-Hernandez et al., 2011; Fratta et al., 2013; Van Blitterswijk et al., 2015; Waite et al., 2014). In the case of variant 1, the decrease in mRNA was linked to a decrease in the use of the promoter that is upstream of exon 1a. In the case of variant 2, the repeat expansion is proposed to lie within the promoter sequence and hence lead to the decrease in transcription (Sareen et al., 2013). Interestingly, increased expression of variant 1 was associated with increased survival in C9orf72 carriers, which supports a role for C9orf72 haploinsufficiency in disease (Van Blitterswijk et al., 2015).

Reduced transcription of C9orf72 leads to decreases in protein levels and impact upon pathways in which the C9orf72 protein is active. C9orf72 patient cell models have been shown to display defects in autophagy and the oxidative stress response (Chitiprolu et al., 2018; Webster et al., 2016a; Webster et al., 2016b). This suggested that although transcriptional repression may alleviate the RNA and protein toxicity burden in C9orf72 ALS/FTD disease, reduced levels of C9orf72 may lead to cellular defects associated with the function of the C9orf72 protein itself and that haploinsufficiency may contribute to disease pathogenesis. Indeed, knockdown of C9orf72 in cell models has been shown to result in the aggregation of p62 (Sellier et al., 2016; Webster et al., 2016a), similar to the inclusions found in C9orf72 ALS/FTD patients (Cooper-Knock et al., 2012; Stewart et al., 2012). Furthermore, the delayed clearance of stress granules upon C9orf72 knockdown were similar to those shown to accumulate in C9orf72 ALS/FTD patient cerebellum and hippocampus (Chitiprolu et al., 2018).

Whether C9orf72 haploinsufficiency contributes to neurodegeneration has been investigated in a number of *in vivo* and *in vitro* C9orf72 models (reviewed in Gitler and Tsuiji, 2016; Moens et al., 2017). Recently, the survival of C9orf72 ALS patient iPSC motor neurons was shown to be dependent on the level of C9orf72 protein, suggesting that C9orf72 haploinsufficiency contributes to disease progression (Shi et al., 2018b). C9orf72 knockout *C. elegans* and *D. rerio* models displayed motor defects suggestive of a role for C9orf72 in ALS related motor neuron degeneration (Ciura et al., 2013; Therrien et al., 2013). Contrastingly, the majority of C9orf72 knockout mice generated do not consistently show an effect on either survival or motor function (reviewed in Gitler and Tsuiji, 2016; Moens et al., 2017). Indeed, only two C9orf72 knockout mouse models have a mild motor phenotype (Atanasio et al., 2016; Jiang et al., 2016). In addition, the C9orf72 knockout mice showed no overt signs of neurodegeneration and did not present with the classical TDP-43 pathology that is associated with ALS (reviewed in Moens et al., 2017). This indicated that C9orf72 haploinsufficiency may not lead directly to neurodegeneration or the development of ALS linked pathology.

The overt characteristics of C9orf72 knockout mice, are consistent with an immunological defect rather than a neurological phenotype. C9orf72 knockout mice developed splenomegaly and lymphadenomegaly, accompanied by autoimmunity and increased levels of inflammation (Atanasio et al., 2016; Burberry et al., 2016; Jiang et al., 2016; O'Rourke et al., 2016; Sudria-Lopez et al., 2016; Sullivan et al., 2016). This may support a role for the C9orf72 in the regulation of the immune system, which is of growing interest in the neurodegenerative field due to the growing association between dysregulation of immune responses and neurodegeneration (reviewed in Labzin et al.,

2018; Lall and Baloh, 2017). The correct functioning of the autophagy pathway is required to regulate the innate and adaptive immune responses (reviewed in Levine et al., 2011; Netea-Maier et al., 2016). Indeed, both *AMPK* and *ULK1* knockout mice develop splenomegaly, similar to that of the *C9orf72* knockout mice (Honda et al., 2014; Zhu et al., 2014). Furthermore, *C9orf72* knockout mice display an increase in pro-inflammatory cytokines including IL-1 β (O'Rourke et al., 2016), a phenotype previously associated with the autophagy deficient *ATG16L* knockout mice (Saitoh et al., 2008). Together these indicate a potential role for *C9orf72* in the regulation of immune-related autophagy, which may be relevant for disease pathogenesis.

1.3.3.4 *In vitro* patient models

Several groups have used *in vitro* *C9orf72* ALS/FTD patient cell models to investigate the role of the above mechanisms in disease, the relevance of cell type specific pathology and to develop therapeutic strategies (reviewed in Selvaraj et al., 2017). *C9orf72* ALS patient neurons and astrocyte models were shown to display RNA foci, although RNA foci numbers were lower in astrocytes than in neurons (Mizielinska et al., 2013). Similarly, both neuron and astrocyte *C9orf72* ALS patient models have been shown to display DPR aggregates (Zu et al., 2013) (Ferraiuolo lab, University of Sheffield, unpublished data). Knockdown of the nuclear export adaptor SRSF1 in *C9orf72* ALS patient iNeurons improved their survival and decreased DPR production. Surprisingly, the survival of motor neurons in co-culture with *C9orf72* ALS patient iAstrocytes was improved by the knockdown of SRSF1 in the iAstrocytes, indicating that repeat expansion linked changes in the astrocyte may impair their ability to support neurons (Hautbergue et al., 2017). Finally, despite differences in levels of expression of *C9orf72* in astrocytes and neurons (Jiang et al., 2016; O'Rourke et al., 2016), both have been shown to display reduced *C9orf72* protein levels, consistent with haploinsufficiency, in *C9orf72* ALS patient models (Fomin et al., 2018; Webster et al., 2016a).

C9orf72 ALS patient derived neuron models have been shown to display defects in proteostasis and mitochondrial function; including increased ROS generation, impaired calcium buffering and altered MMP (Dafinca et al., 2016; Lopez-Gonzalez et al., 2016; Webster et al., 2016a). To date the same level of investigation has not been completed in *C9orf72* ALS patient astrocyte models. However, the study of astrocytes in ALS patient models has gained traction, due to the non-cell autonomous nature of ALS (reviewed in Chen et al., 2018). Astrocytes support neuronal function, synaptic function and maintenance through the secretion of extracellular vesicles that contain specific

micro RNAs (miRNA) (Gosselin et al., 2013; reviewed in Schratt, 2009). C9orf72 ALS patient derived astrocytes are unable to support the growth of motor neurons to the same extent as healthy control derived astrocytes (Meyer et al., 2014). C9orf72 ALS patient derived iAstrocytes were subsequently shown to have impaired extracellular vesicle formation and altered miRNA vesicular content, which led to the decreased survival of co-cultured motor neurons (Varcianna et al., 2019). C9orf72 ALS patient astrocytes were shown to have increased levels of intracellular glutamate, indicating that glutamate metabolism may be impaired (Fomin et al., 2018). Impaired glutamate metabolism by astrocytes may lead to impaired neurotransmission and promote excitotoxicity (reviewed in Van Den Bosch et al., 2006). C9orf72 ALS patient iAstrocytes were also shown to be more glycolytic than iAstrocytes derived from healthy controls. Furthermore, C9orf72 ALS patient iAstrocytes were also shown to have an adenosine metabolism defect, which stemmed from decreased levels of adenosine deaminase. Supplementation with inosine to promote glycolysis, rescued the C9orf72 ALS patient astrocyte-associated toxicity towards motor neurons. This indicated that disrupted metabolism in astrocytes may contribute to C9orf72 ALS pathogenesis (Allen et al., 2019). It is currently unclear how the repeat expansion in C9orf72 results in the above changes in astrocytic function, although C9orf72 haploinsufficiency has been proposed to lead to the changes in glutamate homeostasis (Fomin et al., 2018; Shi et al., 2018b).

1.3.3.5 Genetic modifiers of C9orf72 ALS/FTD

Several genes have been identified that are genetic modifiers of C9orf72 ALS/FTD, which impact on age of onset and survival. The age of onset of both ALS and FTD was delayed by 4.42 and 3.95 years in C9orf72 ALS/FTD patients which were homozygous for the minor alleles of prion protein (*PRNP*) or which were homozygous or heterozygous for the minor alleles in metallothionein 1 E (*MT-1e*) respectively. Conversely age of onset was lower for C9orf72 ALS/FTD patients that carried the minor allele of ubiquitin-associated protein 1 (*UBAP1*) (Van Blitterswijk et al., 2014b). A shorter survival post onset in C9orf72 FTD patients was associated with the minor allele *MT-1e*, elongator acetyltransferase complex subunit 3 (*ELP3*) and apolipoprotein E (*APOE*). A shorter survival was associated with C9orf72 ALS patients carrying the minor allele of unc-13 homologue A, *C. elegans* (*UNC13A*), however survival was extended by the minor allele delta-aminolevulinate dehydratase (*ALAD*) (Van Blitterswijk et al., 2014b).

A single nucleotide polymorphism in *TMEM106B* is also a genetic modifier of C9orf72 ALS/FTD. The *TMEM106B* minor allele was shown to prevent C9orf72 repeat expansion patients from developing FTD but not ALS, whilst the major allele, itself a risk factor for

FTD delayed onset and increased age at death of C9orf72 patients (Gallagher et al., 2014; Van Blitterswijk et al., 2014a). The modifier of C9orf72 ALS/FTD, TMEM106B is also involved in lysosome trafficking and function. Overexpression of TMEM106B in cells results in the accumulation of swollen lysosomes (Stagi et al., 2014). Interestingly, this phenotype does not occur upon knockdown of C9orf72 (Busch et al., 2016). This highlights the possible functional importance of this pathway in the development of neurodegenerative conditions.

Repeat expansion diseases display disease anticipation, whereby the disease severity increases, and onset is earlier in successive generations. Disease anticipation is attributed to the dynamic and unstable nature of the repeat expansion and is associated with both HD and DM1 (Harper et al., 1992; Ridley et al., 1988). Disease anticipation is thought to contribute to earlier onset in successive generations of C9orf72 ALS/FTD patients (Van Mossevelde et al., 2017), although additional data is required to fully understand this mechanism.

1.4 Hypothesis and aims of the PhD

A repeat expansion in the first intron of the *C9orf72* gene was identified as the most common genetic defect associated with ALS and FTD (DeJesus-Hernandez et al., 2011; Renton et al., 2011). Although research has focussed on identifying the mechanism by which the repeat expansion results in disease, no single causative link has been established. The proposed mechanisms include both RNA and protein toxic gain of function and C9orf72 haploinsufficiency. The C9orf72 protein has been shown to be involved in the regulation of the autophagy quality control pathway (Amick et al., 2016; Sellier et al., 2016; Sullivan et al., 2016; Webster et al., 2016a; Yang et al., 2016). C9orf72 ALS/FTD patients were shown to display defects in autophagy (Webster et al., 2016a). We hypothesised that C9orf72 haploinsufficiency may contribute to C9orf72 ALS/FTD and understanding the function of C9orf72 further may uncover disease related mechanisms.

Using a yeast two-hybrid and mass spectrometry coupled immunoprecipitation approaches, we identified numerous proteins which potentially interact with C9orf72. A number of the identified interacting partners were mitochondrial proteins. Hence, we hypothesised that C9orf72 may be found on mitochondria and interact with mitochondrial protein complexes.

Mitochondrial health is paramount to the survival of cells especially long-lived cells such as neurons. Mitochondrial dysfunction is a prevalent feature of neurodegenerative diseases including ALS (reviewed in Smith et al., 2017b). Recently, C9orf72 ALS/FTD

patient models have been shown to display signs of mitochondrial dysfunction (Dafinca et al., 2016; Lopez-Gonzalez et al., 2016; Onesto et al., 2016). The correct functioning of mitochondria is maintained through the import of nuclear encoded proteins into mitochondria and dynamic mitochondrial events. Mitochondrial health is underlined by the fission/fusion cycling of the mitochondrial network and the removal of damaged mitochondria through the mitophagy arm of the autophagy pathway. As mitochondrial quality control is regulated by the autophagy pathway and C9orf72 has been implicated in the regulation of autophagy, we hypothesised that C9orf72 may play a role in maintaining mitochondrial quality control and that this may be involved in C9orf72 ALS/FTD pathogenesis.

In order to investigate the above hypotheses, the following aims were established:

- To investigate the interaction between C9orf72 and the mitochondrial proteins identified in interacting partner screens.
- To characterise the nature of the interaction between C9orf72 and mitochondria.
- To determine the functional relevance of the interaction between C9orf72 and mitochondria, including whether C9orf72 plays a role in mitochondrial quality control.
- To explore whether the mitochondrial role of the C9orf72 protein is relevant in C9orf72 ALS/FTD.

Chapter 2. Materials and Methods

2.1 Cell culture

2.1.1 Cell lines

HEK293, C9orf72^{KO} CRISPR HEK293 (generated in house by Dr Christopher Webster, and characterised by Dr Yolanda Gibson and described below), HeLa, EYFP-Parkin HeLa (a gift from Dr Alex Whitworth (Cambridge) made in Dr Jon Lane's lab (Bristol)) and CV1 cells were cultured in Dulbecco's modified Eagle's medium (DMEM) (Sigma-Aldrich) supplemented with 10 % fetal bovine serum (FBS) (LSP) and 1 mM sodium pyruvate (Sigma-Aldrich) at 37 °C in a 5 % CO₂ incubator. Cell lines were sub-cultured twice weekly, to a confluency of 100 %. All cell lines were subjected to monthly testing for mycoplasma contamination.

The C9orf72^{KO} CRISPR HEK293 line was characterised by Dr Yolanda Gibson (unpublished data). HEK293 have been shown to be hypotriploid (Bylund et al., 2004) and our parental HEK293 line was found to possess 3 C9orf72 alleles. The C9orf72^{KO} CRISPR HEK293 line was found to have a deletion in each allele of C9orf72; of either 4, 10 or 35 bp, each of which resulted in a premature STOP codon. The knockout of C9orf72 was confirmed by qPCR and C9orf72 immunoblot.

Flp-In FLAG-C9orf72L and Sham HEK293 lines were a generous gift from Dr Adrian Higginbottom (SITraN, Sheffield). To maintain selection and repression of the transgene, Flp-In FLAG-C9orf72L or Sham HEK293 lines were maintained in DMEM (Sigma-Aldrich) supplemented with 10 % Tetracycline-free FBS (Biosera), 100 µg/µL Hygromycin B (Invitrogen) and 15 µg/µL Blastidicin S HCl (InvivoGen). Cell lines were sub-cultured twice weekly, to a confluency of 100 %. For induction of transgene expression, cells were swapped to DMEM (Sigma-Aldrich) supplemented with 10 % Tetracycline-free FBS (Biosera), 100 µg/µL Hygromycin B (Invitrogen) and 10 µg/mL Tetracycline (Invitrogen). Tetracycline-induction was performed 24 h prior to cell harvesting.

2.1.2 Patient derived iAstrocytes

Human skin fibroblast samples were obtained from Professor Pamela Shaw, from the Sheffield tissue bank. Informed consent was obtained from subjects prior to sample collection (Study number STH16573, Research Ethics Committee reference 12/YH/0330).

The differentiation of patient fibroblasts to iAstrocytes was carried out by the members of Dr Laura Ferraiuolo's lab (SITraN, Sheffield), according to the protocol described in (Meyer et al., 2014). Information regarding patient matching and disease status are listed in Table 2-1.

Briefly, patient fibroblasts were transduced with Oct3/4, Sox2, Klf4, and c-Myc. The following day the medium on the cells was changed to DMEM (Gibco) with 10 % FBS (Life Science Production), to allow cells to recover. Seventy-two h post infection, the media on the cells was changed to DMEM/F12 (Gibco) culture medium containing 1 % N2 (Gibco), 1 % B27 (Gibco), 20 ng/mL FGF2 (Peprotech), 20 ng/mL EGF (Peprotech), and 5 µg/mL heparin (Sigma) to promote the conversion of fibroblasts to NPC. 7 days post infection, cells displayed morphological changes consistent with NPC characteristics. iNPC cells were maintained in DMEM/F12, 1 % N2, 1 % B27, and 40 ng/mL FGF2.

To differentiate iNPCs to iAstrocytes, iNPCs were seeded onto fibronectin coated dishes and grown in DMEM containing 10 % FBS and 0.3 % N2 for a minimum of 7 days. iAstrocytes were immunostained with astrocytic markers Vimentin, CD44, S100b and GFAP.

Table 2-1 C9orf72 patient and matched control iAstrocyte lines

Line ID	Gender	Age at biopsy (years)	Ethnicity	Genotype	Mutation	Time until death following biopsy (months)
C - 155	Male	40	Caucasian	Non-ALS control	-	-
P - 183	Male	49	Caucasian	fALS	C9orf72	27
C - 3050	Male	65	Caucasian	Non-ALS control	-	-
P - 78	Male	66	Caucasian	fALS	C9orf72	31.7
C - 209	Female	69	Caucasian	Non-ALS control	-	-
P - 201	Female	66	Caucasian	fALS	C9orf72	19.4

The length of the repeat expansion in C9orf72 was confirmed by Southern blotting to be over 1000 repeats in lines P - 183, P - 78 and P - 201.

2.1.3 DNA plasmid transfection

HeLa and HEK293 cells were transfected with plasmid DNA with Lipofectamine 2000 (Invitrogen) according to the manufacturer's instructions, or with polyethylenimine (PEI) (Polysciences, stock 1 mM, 3 μ L PEI / μ g DNA). Briefly, Lipofectamine 2000 or PEI was diluted in Opti-MEM (Gibco) and incubated 5 min at room temperature. Separately, DNA was diluted in Opti-MEM. Lipofectamine 2000/PEI was then added to the DNA and mixed by pipetting. DNA/Lipofectamine 2000 or DNA/PEI mixes were incubated at room temperature for 20 min. DNA mixes were then added directly to cells in culture medium. Patient derived iAstrocytes were transfected with Lipofectamine 2000 as described above.

For the transfection of CV1 cells, DNA was diluted in Opti-MEM and Turbofect (Thermo Fisher Scientific) transfection reagent was added directly to the diluted DNA. Tubes were immediately vortexed for 5 s and subsequently incubated for 20 min at room temperature. DNA containing mixes were then added to cells in culture medium.

Information regarding DNA plasmids used in transfections is listed in Table 2-2. The amount of DNA and transfection reagent used for transfections are listed in Table 2-3. The media was changed on cells 5.5 h post-transfection to limit cytotoxicity. Cells were used for experimentation 24 h post transfection.

Table 2-2 Plasmid DNA constructs

DNA construct	Attribution
pCI-neo	Promega
pEGFP-C2	Clontech
pRK5-Myc-C9orf72L	In house (Dr Kurt De Vos)
pRK5-Myc-C9orf72S	In house (Dr Kurt De Vos)
pRK5-Myc-C9orf72DdD	In house (Dr Kurt De Vos)
pRK5-HA-C9orf72L	In house (Miss Emma Smith)
pRK5-HA-C9orf72S	In house (Miss Emma Smith)
pRK5-HA-C9orf72DdD	In house (Miss Emma Smith)
pEGFPc2-C9orf72L	In house (Dr Kurt De Vos)
pEGFPc2-C9orf72S	In house (Dr Kurt De Vos)
pEGFP-USP8	Prof Sylvie Urbe (Liverpool)

DNA construct	Attribution
pCI-neo-Myc-USP8	In house (Miss Emma Smith)
pCI-neo-Myc-USP8 ^{MIT}	In house (Miss Emma Smith)
pCI-neo-Myc-USP8 ^{MIT-RHO}	In house (Miss Emma Smith)
pCI-neo-Myc-USP8 ^{RHO}	In house (Miss Emma Smith)
pCI-neo-Myc-USP8 ^{USP}	In house (Miss Emma Smith)
pCI-neo-Myc-USP8 ^{RHO-USP}	In house (Miss Emma Smith)
pRK5-HA-Ubiquitin ^{WT}	Dr Ted Dawson (Baltimore) via Addgene (plasmid 17608)
pRK5-HA-Ubiquitin ^{K6R}	In house (Miss Emma Smith)
pEYFPc1-Parkin	Dr Alex Whitworth (Cambridge)
pEYFPc1-Parkin ^{K27R, K48R, K76R}	In house (Miss Emma Smith)
pcDNA3.1-Parkin-Myc/His	Dr Mark Cookson (NIH)
pAcGFP1-Mito	Clontech
pcDNA3.1-Mfn2-Myc/His	Prof David Chan (Caltech) via Addgene (plasmid 23213)
pRK5-Myc-MIRO1	Prof Pontus Aspenström (Stockholm)
pCMV6-OAT-Myc/DDK	Origene
pCMV6-COX6C-Myc/DDK	Origene

Table 2-3 Transfection reagents and conditions

Transfection reagent	Plate size	DNA per well (μg)	Transfection reagent per well (μL)	Transfection mix per well (μL)
Lipofectamine 2000	96 well	0.1	0.2	10
	24 well	0.5	1	50
	12 well	1	2	100
	6 well	2	4	200
	T75 flask	10	20	1,000
	10 cm ² dish	10	20	1,000
PEI	24 well	0.5	1.5	50
	12 well	1	3	100
	6 well	2	6	200
	T75 flask	10	30	1,000
	10 cm ² dish	10	30	1,000
Turbofect	24 well	1	2	50
	12 well	2	4	100
	6 well	4	8	200

2.1.4 siRNA transfection

Small interfering RNA (siRNA) for knockdown experiments was obtained from Sigma-Aldrich (Table 2-4). EYFP-Parkin HeLa, HeLa and HEK293 cells were transfected with siRNA using Lipofectamine RNAiMAX (Invitrogen, 6 pmol siRNA per 24 well) according to the manufacturer's instructions. Briefly, Lipofectamine RNAiMAX was diluted in Opti-MEM and incubated 5 min at room temperature. siRNA was diluted in nuclease free water (Qiagen) to a concentration of 10 μ M. Diluted siRNA was subsequently diluted in Opti-MEM as required (Table 2-5). Lipofectamine RNAiMAX mix was then added to the siRNA in Opti-MEM and incubated 20 min at room temperature. siRNA/Lipofectamine RNAiMAX mix was then added to cells in culture medium. Media was changed 5.5 h post-transfection.

Cells were used for experimentation 4 days following siRNA transfection. When subsequent plasmid DNA transfection was required, this was performed on day 3, 24 h before cells were used in experimentation.

Table 2-4 siRNA sequences

siRNA	Sequence
NTC	MISSION siRNA Universal Negative Control #1 (SIC001)
C9orf72 #2	GUGCUAUAGAUGUAAAGUU[dT][dT]
C9orf72 #D	GAUCAGGGUCAGAGUAUUA[dT][dT]
USP8 #1	UGAAAUACGUGACUGUUUA[dT][dT]
USP8 #2	UAUCUAUACUGUCCUGUCC[dT][dT]
COX6C #1	GUAAAGUAAUCUUGGAAUA[dT][dT]
COX6C #5	GUUUCGUGUGGCUGAUCAA[dT][dT]
CHCHD4 #1	CCAUCUUGACCUUGAGUAU[dT][dT]
CHCHD4 #2	CCAUUACCCAAGAACGUUU[dT][dT]
FIP200 #1	CAAGUUAGAGGUUGAACUU[dT][dT]
FIP200 #2	GAUCUUAUGUGAUCGUCCA[dT][dT]
ULK1 #1	CACUUUAUGCAUAUAGAGA[dT][dT]

Table 2-5 siRNA transfection conditions

Transfection reagent	Plate size	siRNA per well (pmol)	Transfection reagent per well (μL)	Transfection mix per well (μL)
Lipofectamine	24 well	6	0.6	50
RNAiMAX	12 well	12	1.2	100
	6 well	24	2.4	200
	T75	150	15	1,000

2.1.5 Induction of mitophagy

Mitophagy was induced in cells by incubation with 10 μM or 20 μM Carbonyl cyanide m-chlorophenyl hydrazone (CCCP) (Sigma-Aldrich) for the indicated time period (0 – 4 h). Alternatively, mitophagy was induced by incubation with a combination of 4 μM Antimycin A (Sigma-Aldrich) and 10 μM Oligomycin (Sigma-Aldrich) for the indicated time period (0 – 23 h).

2.2 Cloning of plasmid DNA

2.2.1 Site directed mutagenesis

Primers for mutagenesis were designed using the QuikChange primer design tool (Agilent) and purchased from Sigma-Aldrich. Mutagenesis was performed according to the manufacturer's protocol using a QuikChange Lightning Kit (Agilent, 210518). Briefly, 75 ng DNA was amplified and mutated with 125 ng of the designed mutagenesis primer (Table 2-6).

Amplification was performed in a thermocycler using the following parameters: 2 min 95 °C, followed by 18 cycles of 95 °C for 20 s to melt dsDNA, 60 °C for 10 s to anneal primers and an elongation step at 68 °C of 30 s per kb of plasmid to be amplified (Table 2-6). Parental DNA, lacking the mutation, was digested by incubation with Dpn1 enzyme 10 min at 37 °C. Plasmid DNA was transformed into XL-10 Gold Ultracompetent cells, as described in 2.2.6. All constructs harbouring a mutation generated in house were verified by sequencing.

Table 2-6 Primers used for site directed mutagenesis and PCR elongation times

Construct	Primer	Sequence (5' - 3')	Elongation time (min)
pCl-neo Myc-USP8 MIT-STOP	fwd rev	CTTAAATTAAGATATGAAGAAGCTTAAGTCCGG AAAAAACTTGAGGAAA TTTCCTCAAGTTTTTTCCGGACTTAAGCTTCTTC ATATCTTAATTTAAG	4.5
pCl-neo Myc-USP8 RHO-STOP	fwd rev	TTGTTATCCCCAGTATACAACATAGGCTAAGGT CACTCCACC GGTGGAGTGACCTTAGCCTATGTTGTATACTGG GGATAACAA	4.5
pCl-neo Myc-USP8 Xho1-RHO	fwd rev	CATCCATTATAATCAAGCTGATGTTTTTCTCGAG CATCATTGTGTATAGTTCCTTTGCTGTG CACAGCAAAGGAACTATACACAATGATGCTCGA GAAAAACATCAGCTTGATTATAATGGATG	4.5
pCl-neo Myc-USP8 Xho1-USP	fwd rev	CCTAAGTTACGAAGTCCAGTAAGCTCGAGTCCA GAACCTCCAAAACAGGA TCCTGTTTTTGGAGGTTCTGGACTCGAGCTTAC TGGACTTCGTAAGTACTAGG	4.5
EYFP- Parkin K27R	fwd rev	CAACCACCTCCCTGAGCTGGAAGATGCTGGTG T ACACCAGCATCTTCCAGCTCAGGGAGGTGGTT G	3.5
EYFP- Parkin K48R	fwd rev	ATTCCTCAGCTCCCTCCCTGCGAAAATCACACG CGTGTGATTTTCGCAGGGAGGGAGCTGAGGAA T	3.5
EYFP- Parkin K76R	fwd rev	TTCATTTCTTGACCTCTTCTCCACGGTCTCTGC AC GTGCAGAGACCGTGGAGAAGAGGTCAAGAAAT GAA	3.5

Construct	Primer	Sequence (5' - 3')	Elongation time (min)
pRK5 Ubiquitin K6R	HA- fwd rev	TCTTACCAGTCAGGGTCCTCACGAAGATCTGCA TG CATGCAGATCTTCGTGAGGACCCTGACTGGTA AGA	2.5

2.2.2 Restriction digest of plasmid DNA

For sub-cloning of a cDNA into a new vector, 1 µg of plasmid DNA (insert) or 3 µg plasmid DNA (destination vector) was digested using the required restriction enzymes (obtained from Thermo Fisher Scientific) (Table 2-7). The digest was performed to cut insert from existing vector and to open the recipient destination vector. Digests were performed in FastDigest buffer (Thermo Fisher Scientific) at 37 °C for 15 min. To prevent re-ligation, the destination vector was de-phosphorylated using FastAP Thermosensitive Alkaline Phosphatase (Thermo Fisher Scientific) for 15 min at 37 °C. Digested DNA was run on an agarose gel for purification, as described in 2.2.3.

Table 2-7 Composition of restriction digests

	DNA (destination vector)	DNA (insert)
DNA	3 µg	1 µg
10 X FD buffer	1 X	1 X
Restriction enzyme 1	1.5 µL	0.5 µL
Restriction enzyme 2	1.5 µL	0.5 µL
Fast AP	3 µL	N/A

2.2.3 Agarose gel electrophoresis

Separation of DNA products on agarose gels was performed during gel excision for vector cloning (2.2.2) and during colony polymerase chain reaction (PCR) screening (2.2.7). DNA from a restriction digest or colony PCR DNA product was run on a 1 % agarose gel (1 % agarose (Bioline), 0.002 % ethidium bromide in TAE buffer (40 mM Tris, 20 mM acetic acid, 1 mM EDTA pH 8)), for 40 min at 100 V in TAE buffer. Bands

were visualised on a Syngene G:Box UV box. The size of DNA products was estimated using Hyperladder 1kb or Hyperladder 25bp (Bioline) as required.

2.2.4 Gel elution of purified linear DNA

Following the running of restriction digested products on an agarose gel, bands corresponding to the insert and vector were excised from the gel using a scalpel under a UV light box.

Excised DNA was eluted from the gel using a GenElute kit (Sigma-Aldrich, NA1111-1KT) according to the manufacturer's protocol. Briefly, excised bands were dissolved in gel solubilisation buffer at 55 °C for 10 min. Isopropanol was added to the dissolved gel and the sample passed through a spin column at 14,000 x g for 1 min. The column was washed in wash buffer at 14,000 x g for 1 min and dried by centrifugation at 14,000 x g for 1 min. DNA was eluted from the column using GelElute solution at 14,000 x g for 1 min. The concentration of the eluted DNA was determined on a NanoDrop ND-1000 Spectrophotometer.

2.2.5 Ligation

Ligation was performed by incubating linearised insert and vector at a 3:1 molar ratio using the Quick Ligation kit (M2200, NEB). DNA for vector and insert were diluted in nuclease free water (Qiagen) and 2 X Quick Ligase buffer to a final volume of 19 µL. One µL of Quick Ligase enzyme was added and the reaction incubated for 15 min at room temperature.

2.2.6 Transformation

Plasmid DNA was transformed into XL-10 Gold Ultracompetent cells (Agilent) according to the manufacturer's protocol. Briefly, bacteria were thawed gently on ice and 20 µL transferred to a pre-chilled tube. One µL β-mercaptoethanol was added to improve competency. One µL of ligated plasmid was incubated with the bacteria for 30 min on ice, followed by a heat shock at 42 °C in a heat block for 45 s. Bacteria were returned to ice for 2 min. Five hundred µL of pre-warmed LB broth (Thermo Fisher Scientific) was added to the transformed bacteria, which were subsequently incubated 1 h at 37 °C on a shaker. Transformed bacteria were then plated onto pre-warmed LB agar (Thermo Fisher Scientific) plates containing Ampicillin (100 µg/mL, Melford) or Kanamycin (30 µg/mL, Sigma-Aldrich) as required, and grown overnight at 37 °C.

2.2.7 Colony PCR

Colony PCR was used to ascertain the incorporation of insert into the destination vector following the ligation step. Sixteen colonies per transformation were selected to undergo screening. A master mix containing 500 nM of the required primers and 5 X FirePol (Solis Biodyne, 04-12-00115) was produced for all required reactions (Table 2-8). The sequences of primers used are found in Table 2-9. Single colonies were picked, streaked to a copy plate and added to the PCR mix in a 96 well format. Streak plates were incubated at 37 °C. PCR amplification was performed in a thermocycler using the following parameters: 5 min 95 °C, followed by 35 cycles of 95 °C for 40 s to melt dsDNA, 55 °C for 45 s to anneal primers and an elongation step at 72 °C of 1 min per kb of plasmid to be amplified, a final elongation step of 10 min at 72 °C was included.

PCR product was run on a 1 % agarose gel for 40 min at 100 V and imaged on a SynGene G:Box (as described previously, 2.2.3). Colonies containing insert were grown in LB broth supplemented with the appropriate antibiotic (Ampicillin (100 µg/mL) or Kanamycin (30 µg/mL)) overnight at 37 °C with constant shaking. Plasmid DNA was isolated from bacterial cultures as described subsequently (2.2.9).

Table 2-8 PCR mix for colony PCR

	Single well (µL)	Master mix (µL)
5 X FirePol	2	32
Fwd primer (10 µM)	0.5	8
Rev primer (10 µM)	0.5	8
Water	7	112

Table 2-9 Primers used for colony PCR

Primer	Sequence (5' – 3')
T7EEV	AAGGCTAGAGTACTTAATACGA
SP6	TATTTAGGTGACACTATAG
T3	ATTAACCCTCACTAAAGGGA

2.2.8 Preparation of glycerol stocks

Five hundred μL of overnight LB broth culture of transformed bacteria was added to 500 μL of 50 % glycerol and briefly vortexed. Glycerol stocks were stored at $-80\text{ }^{\circ}\text{C}$.

2.2.9 Preparation of plasmid DNA from bacteria

Bacterial colonies were streaked from glycerol stocks onto LB agar plates containing the appropriate antibiotic (Ampicillin (100 $\mu\text{g}/\text{mL}$) or Kanamycin (30 $\mu\text{g}/\text{mL}$)) and grown overnight at $37\text{ }^{\circ}\text{C}$ in a warm room. The following morning single colonies were picked into 1 mL starter cultures of LB broth containing the appropriate antibiotic (Ampicillin (100 $\mu\text{g}/\text{mL}$) or Kanamycin (30 $\mu\text{g}/\text{mL}$)) and grown at $37\text{ }^{\circ}\text{C}$ in a warm room with constant shaking. Eight h subsequently the starter cultures were expanded to 5 mL cultures which were grown overnight at $37\text{ }^{\circ}\text{C}$ in a warm room with constant shaking.

DNA was extracted from bacteria using a NucleoSpin plasmid kit (Macherey-Nagel, 740588.250), according to the manufacturer's instructions. Briefly, bacteria were pelleted by centrifugation at $3,893\text{ x g}$ for 10 min. Bacterial pellets were resuspended in A1 buffer and subjected to SDS/alkaline lysis by addition of A2 buffer for 5 min. The lysis was neutralized by addition of A3 buffer and bacterial debris pelleted by centrifugation at $11,000\text{ x g}$ for 10 min. The supernatant was transferred to a spin column and centrifuged 1 min at $11,000\text{ x g}$. DNA was washed once in AW buffer 1 min at $11,000\text{ x g}$ and once in A4 buffer containing ethanol 1 min at $11,000\text{ x g}$. The column was dried by centrifugation for 2 min at $11,000\text{ x g}$. The column was eluted by the addition of elution buffer and incubation at room temperature for 1 min followed by centrifugation at $11,000\text{ x g}$ for 1 min. DNA concentration was determined on a Nanodrop ND-1000 Spectrophotometer.

2.3 Protein biochemistry

2.3.1 Cell harvesting and lysis

Cells were collected in trypsin EDTA (Lonza) and pelleted at 400 x g for 4 min. After two phosphate-buffered saline (PBS) (137 mM NaCl, 2.7 mM KCl, 8.1 mM Na_2HPO_4 , 1.5 mM KH_2PO_4) washes, cells were lysed in RIPA buffer (50 mM Tris HCl pH 6.8, 150 mM NaCl, 1 mM EDTA, 1 mM EGTA, 0.1 % SDS, 0.5 % deoxycholic acid, 1 % Triton X-100 and 1 X protease inhibitor cocktail (Thermo Fisher Scientific)) for 30 min on ice and clarified by centrifugation at $15,000\text{ x g}$ for 30 min at $4\text{ }^{\circ}\text{C}$. Protein concentration was determined by Bradford protein assay (2.3.2). Samples were made up in 5 X sample loading buffer (5 X buffer: 300 mM Tris-HCl pH 6.8, 10 % SDS, 25 % glycerol, 25 % β -

mercaptoethanol, 0.01 % bromophenol blue; final sample buffer concentration (1 X): 60 mM Tris-HCl pH 6.8, 2 % SDS, 5 % glycerol, 5 % β -mercaptoethanol, 0.002 % bromophenol blue) (Laemmli, 1970) and stored at -20 °C.

2.3.2 Bradford assay

Protein concentration was determined by Bradford assay (Bradford, 1976). Protein samples were diluted 1:100 in Bradford reagent (Bio-Rad). A bovine serum albumin (BSA) standard (100 mg/mL, Sigma-Aldrich) was similarly diluted in Bradford reagent. Serial dilutions of both samples and standards were plated on a 96-well plate and read at 595 nm on a platereader (PHERAstar FS, BMG Labtech). Conformational change of the Coomassie Brilliant Blue G-250 in the Bradford reagent upon binding to protein results in a shift of absorbance from 465 nm to 595 nm. Samples with a higher protein concentration exhibit a proportional increase in absorbance at 595 nm. A standard curve was plotted on a scatter chart of absorbance against concentration for the protein standard. Considering where there was a linear relationship between protein concentration and absorbance, a line of best fit was obtained from the graph. The equation of the line was used to determine the concentration of experimental samples.

2.3.3 Immunoprecipitation

Cells were collected in trypsin EDTA and pelleted at 400 x g for 4 min, and subsequently washed twice in PBS. Cells were lysed in modified ice cold BRB80 (80 mM K-PIPES pH 6.8, 1 mM MgCl₂, 1 mM EDTA, 1 % NP-40, 150 mM NaCl and 1 X protease inhibitor cocktail) for 1 h at 4 °C with constant rotation. Lysates were clarified by centrifugation 15,000 x g for 30 min prior to determination of protein concentration by Bradford assay (2.3.2). 0.5 – 1 mg of protein lysate was incubated overnight at 4 °C with 1 - 2 μ g primary antibody with constant rotation. Protein G sepharose beads (17-0618-01, GE Healthcare) were washed 3 times by resuspending in BRB80 followed by centrifugation at 3,000 x g for 30 s. Washed protein G sepharose beads were diluted in BRB80 to produce a 50 % bead slurry. For antibody capture, 20 μ L of 50 % bead slurry was incubated with the protein lysate for 2 h at 4 °C with constant rotation. Bead-antibody complexes were washed 5 times in BRB80 at 3,000 x g for 30 s. Beads were eluted by boiling in 2 X sample buffer for 5 min. Samples were analysed by SDS-PAGE and immunoblot (as described in 2.3.4).

2.3.4 Polyacrylamide gel electrophoresis and immunoblot

2.3.4.1 SDS-PAGE

Polyacrylamide gels were run in the 4-gel Mini-PROTEAN Tetra cell system (BioRad). The size of protein bands was estimated by the running of a protein ladder alongside experimental samples. The Precision Plus Protein™ All Blue Protein Standard (1610373, Bio-Rad) ladder provided a range of 10 – 250 kDa with reference bands at 25, 50 and 75 kDa. All samples were boiled for 5 min at 100 °C prior to loading on polyacrylamide gels.

2.3.4.1.1 Tris-Glycine SDS-PAGE

Protein lysates were separated by SDS-PAGE on single percentage (10 % or 12 % acrylamide) or 4 - 20 % gradient (Invitrogen) Tris-Glycine polyacrylamide gels at 100 V in running buffer (25 mM Tris, 192 mM glycine, 0.1 % SDS).

Table 2-10 Composition of Tris-Glycine polyacrylamide gels

	10 % gel	12 % gel
Acrylamide (37.5:1 acrylamide:bis-acrylamide)	10 %	12 %
Tris pH 8.8	375 mM	375 mM
SDS	0.1 %	0.1 %
APS	0.1 %	0.1 %
TEMED	0.001 %	0.001 %

2.3.4.1.2 Tris-Tricine SDS-PAGE

For endogenous COX6C immunoblot, where the resolution of a 8.8 kDa protein was required, protein lysates were separated by SDS-PAGE on 16 % Tris-Tricine polyacrylamide gels, according to the method adapted from (Schagger, 2006). Gels were ran at 70 V in running buffer (anode buffer: 100 mM Tris, 22.5 mM HCl; cathode buffer: 100 mM Tris, 100 mM Tricine, 0.1 % SDS).

Table 2-11 Composition of Tris-Tricine polyacrylamide gels

	16 % gel
AB-3 (acrylamide-bisacrylamide)	16.5 % T, 1 % C
3 X Gel buffer	1 X (Final: 1 M Tris, 333 mM HCl, 0.1 % SDS, pH 8.45)
APS	0.1 %
TEMED	0.002 %

2.3.4.2 Transfer to membrane

Proteins separated by SDS-PAGE were transferred to 0.45 μ m nitrocellulose (GE Healthcare), 0.2 μ m nitrocellulose (Bio-Rad), 0.45 μ m PVDF (Immobilon) or 0.2 μ m PVDF (Bio-Rad) membranes. PVDF membranes were activated in methanol prior to transfer. Briefly, polyacrylamide gels were placed into a cassette in direct contact with the membrane and sandwiched between sheets of filter paper and sponge. Cassettes were placed in the transfer tank so that the gel was towards the cathode and the membrane towards the anode, leading to the transfer of proteins from the gel to the membrane. Transfer was performed at 100 V for 1 h in transfer buffer (25 mM Tris, 192 mM glycine, 20 % methanol).

Membranes were subject to reversible Ponceau S (0.1 % Ponceau S, 5 % acetic acid) staining following transfer, to identify successful transfer and gauge protein loading equivalence. Ponceau S stain was removed by washing the membrane in water.

2.3.4.3 Immunoblot

Membranes were blocked in 5 % fat-free milk (Marvel) in TBST (20 mM Tris HCl pH 7.5, 137 mM NaCl, 0.1 % Tween-20) at room temperature for 1 h. Membranes were probed with primary antibodies in blocking buffer for 1 h at room temperature or overnight at 4 °C. The identity of primary antibodies used are outlined in Table 2-12. Membranes were washed 3 times 10 min in TBST at room temperature. Membranes were subsequently incubated 1 h with secondary HRP-conjugated antibodies at room temperature (anti-rabbit HRP (P0448, Dako, 1:5,000) or anti-mouse HRP (P0447, Dako, 1:5,000)). After 3 10 min TBST washes, the membranes were prepared for imaging with SuperSignal West Pico Chemiluminescent (ECL) substrate (Thermo Scientific) according to the manufacturer's instructions. Briefly, a 1:1 ratio of the stable peroxide and

luminol/enhancer solutions were added to the membrane and incubated with constant rocking for 5 min.

Imaging was performed on a SynGene G:Box or onto ECL film (GE healthcare) and developed in a dark room using developer and fix solutions (Ilford). For manual developing, membranes were placed into a developing cassette and film placed on the membrane. The exposed film was then placed in developer solution for 1 min. The film was then washed in water and placed in fix solution for 2 min. Films were then washed in water and dried at room temperature.

Table 2-12 Primary antibodies used in immunoblotting

Antibody Target	Supplier	Product code	Host Species	Dilution
anti-FLAG	Sigma-Aldrich	F315.2MG	Mouse	1:2,000
anti-Myc	Cell Signaling	2276S	Mouse	1:2,000
anti-Myc	Abcam	ab9106	Rabbit	1:2,000
anti-GFP	Clontech	632380	Mouse	1:4,000
anti-GFP	Clontech	632377	Rabbit	1:1,000
anti-HA	Sigma-Aldrich	H6908	Rabbit	1:1,000
anti-HA	Sigma-Aldrich	H9658	Mouse	1:2,000
anti-GAPDH	Cell Signaling	2118	Rabbit	1:2,000
anti-Tubulin	Sigma-Aldrich	T9026	Mouse	1:10,000
anti-Tubulin	Abcam	ab4074	Rabbit	1:10,000
anti-COX IV	Cell Signaling	4850	Rabbit	1:2,000
anti-TOMM20	BD Biosciences	612278	Mouse	1:1,000
anti-MnSOD	Enzo	ADI-SOD-110	Rabbit	1:1,000
anti-Mfn2	Sigma-Aldrich	M6444	Rabbit	1:1,000
anti-Mfn1	Abcam	ab57602	Mouse	1:2,000
anti-ATP5A	Abcam	ab14748	Mouse	1:5,000
anti-HSP60	Sigma-Aldrich	H3524	Mouse	1:2,000
anti-PTPIP51	Sigma-Aldrich	HPA009975	Rabbit	1:1,000

Antibody Target	Supplier	Product code	Host Species	Dilution
anti-COX6C	Abcam	ab110267	Mouse	1:1,000
anti-TIMM23	BD Biosciences	611222	Mouse	1:2,000
anti-Cytochrome c	Abcam	ab110325	Mouse	1:1,000
anti-CHCHD4	Proteintech	21090-1-AP	Rabbit	1:1,000
anti-TIMM9	Proteintech	11479-1-AP	Rabbit	1:500
anti-USP8	Sigma-Aldrich	HPA004869	Rabbit	1:1,000
anti-C9orf72	Proteintech	25757-1-AP	Rabbit	1:1,000
anti-Drp1	BD Biosciences	611112	Mouse	1:1,000
anti-ULK1	Cell Signaling	8054	Rabbit	1:1,000
anti-FIP200	Sigma-Aldrich	SAB4200135	Rabbit	1:500

2.3.4.4 Quantification of band intensities

Quantification of signal intensities was performed using ImageJ/FIJI software (Abramoff et al., 2004). A region of interest (ROI) was drawn around the bands to be quantified. The intensity of the bands was extracted using the analyse gels function, and the area under the curve taken as signal intensity. Signal intensities were normalised to a loading control.

2.3.5 Cellular fractionation

2.3.5.1 Mitochondrial enriched fractions

Mitochondria were isolated from cells by differential centrifugation to produce a mitochondrial enriched fraction, as described in (Vance, 1990). Cells were collected in trypsin EDTA and pelleted at 400 x g for 4 min. Pellets were washed twice in PBS and once in mitochondrial isolation buffer (220 mM mannitol, 70 mM sucrose, 10 mM HEPES pH 7.4, 1 mM EDTA, 1 mM DTT, 0.1 % BSA, 1 X protease inhibitor cocktail). Cells were lysed using a motorised handheld tissue homogeniser (Kimble 749540-000) for 20 s in fresh mitochondrial isolation buffer. Larger cell pellets were lysed with 15 strokes of a motorised Kontes Teflon pestle (Kontes 19). Lysed cells were centrifuged 5 min at 600 x g at 4 °C to remove cellular debris and nuclei. Post centrifugation, a sample of supernatant was taken as total cell lysate and lysed in RIPA buffer. The remaining supernatant was further cleared by centrifugation at 600 x g for 5 min at 4 °C. Cleared

supernatant was centrifuged 10 min at 10,000 x g at 4 °C to pellet mitochondria. The supernatant was lysed in RIPA buffer and used as the Cytosol/ER/Microsome fraction. The mitochondrial pellet was washed once in fresh mitochondrial isolation buffer and resuspended in RIPA buffer. Protein concentration was determined by Bradford assay (2.3.2).

2.3.5.2 Purification of mitochondria by sucrose gradient

Mitochondria enriched pellets obtained from the 10,000 x g centrifugation, as described above (2.3.5.1), were purified on a discontinuous sucrose gradient. A sucrose gradient was created by overlaying 1.6 M sucrose (1.6 M sucrose, 10 mM HEPES pH 7.4, 1 mM EDTA, 0.1 % BSA) with 1.2 M sucrose (1.2 M sucrose, 10 mM HEPES pH 7.4, 1 mM EDTA, 0.1 % BSA), adapted from (De Vos et al., 2000). Crude mitochondrial extracts were overlaid onto the sucrose gradient. Gradients were centrifuged 1 h at 4 °C at 28,000 rpm (95,272 x g MAX / 74,329 x g AVG) in a SW 55Ti rotor (Beckman). Post centrifugation, purified mitochondria were collected from the interface between the 1.2 M and 1.6 M sucrose and pelleted by dilution with 3 volumes of mitochondrial isolation buffer at 10,000 x g for 10 min at 4 °C. Mitochondrial pellets were washed once in mitochondrial isolation buffer. Mitochondrial pellets were resuspended in RIPA buffer and protein concentration was determined by Bradford assay (2.3.2). Conversely, for use in downstream assays, recovered mitochondria were resuspended in mitochondrial isolation buffer.

2.3.5.3 Isolation of mitochondria from rat liver

Whole liver was dissected from adult CD IGS rat and washed 2 times in PBS. Liver was diced and washed 2 further times in PBS and once in mitochondrial isolation buffer. Liver was homogenized using a motorised 30 mL Wheaton pestle in mitochondrial isolation buffer. Unlysed cells, nuclei and cell debris were pelleted by centrifugation for 5 min at 600 x g at 4 °C. The supernatant was taken and centrifuged at 600 x g for 5 min at 4 °C to further clear. Mitochondria were pelleted by centrifugation of the cleared supernatant 12 min at 12,000 rpm (14,822 x g MAX / 10,596 x g AVG) in a Type 70Ti rotor (Beckman) at 4 °C. Mitochondria were purified on a 1.2 M/1.6 M discontinuous sucrose gradient by centrifugation at 4 °C for 1 h at 27,000 rpm (131,453 x g MAX / 96,467 x g AVG) in a SW28 rotor (Beckman). Mitochondria were recovered from the interface and pelleted by centrifugation for 12 min at 12,000 rpm (14,822 x g MAX / 10,596 x g AVG) in a Type 70Ti rotor at 4 °C in 3 volumes of mitochondrial isolation buffer. Pellets were washed once in mitochondrial isolation buffer. Mitochondria were resuspended in mitochondrial

isolation buffer and subjected to flash freezing in liquid nitrogen. Frozen mitochondria were stored at -80 °C.

2.3.6 Mitochondrial sub-organelle analysis

2.3.6.1 Membrane integration

Purified mitochondria were treated with sodium carbonate essentially as described previously (De Vos et al., 2012; Ryan et al., 2001) (Figure 2.1A). Briefly, purified mitochondria were resuspended in 300 µL ice cold 100 mM Na₂CO₃ pH 11.5 and incubated 30 min on ice. Following pipetting to promote the release of non-membrane associated proteins, mitochondria were subjected to centrifugation at 50,000 rpm (135,240 x g MAX / 106,120 x g AVG) for 30 min at 4 °C in a TLA100.3 rotor (Beckman). Mitochondrial pellets were resuspended in RIPA buffer and protein concentration determined by Bradford assay (2.3.2).

2.3.6.2 OMM localisation

Purified mitochondria were treated with Proteinase K essentially as described previously to digest cytosol exposed mitochondrial proteins (De Vos et al., 2012; Ryan et al., 2001) (Figure 2.1B). Purified mitochondria were resuspended in 100 µL mitochondrial isolation buffer (without protease inhibitor cocktail) and incubated 10 min with 1 µL 2 mg/mL (equivalent to 80 units) Proteinase K (NEB) on ice. The mitochondria were further incubated with 1 µL 200 mM phenylmethylsulfonyl fluoride (PMSF) (Sigma-Aldrich) for 10 min (final concentration 2 mM) on ice to inhibit Proteinase K activity. Mitochondria were pelleted 10 min at 10,000 x g at 4 °C and washed once in mitochondrial isolation buffer. Mitochondrial pellets were resuspended in RIPA buffer and protein concentration determined by Bradford assay (2.3.2).

2.3.6.3 IMS localisation

Localisation of proteins to the mitochondrial IMS was assayed by permeabilisation the OMM followed by incubation with Proteinase K (Figure 2.1C-D). Permeabilisation of the OMM was achieved by treatment with digitonin, essentially as described by (Badugu et al., 2008). Purified mitochondria were resuspended in mitochondrial isolation buffer (in the absence of protease inhibitor cocktail) and treated with digitonin (Cayman Chemical) (0.5 µg digitonin/ µg mitochondria) 15 min on ice to permeabilise the OMM. Mitochondria were incubated for 10 min with 1 µL 2 mg/mL Proteinase K on ice. The mitochondria were subsequently incubated with 1 µL 200 mM PMSF for 10 min to inhibit Proteinase K activity. Mitochondria were pelleted 10 min at 10,000 x g at 4 °C and washed once in

mitochondrial isolation buffer. Mitochondrial pellets were resuspended in RIPA buffer and protein concentration determined by Bradford assay (2.3.2).

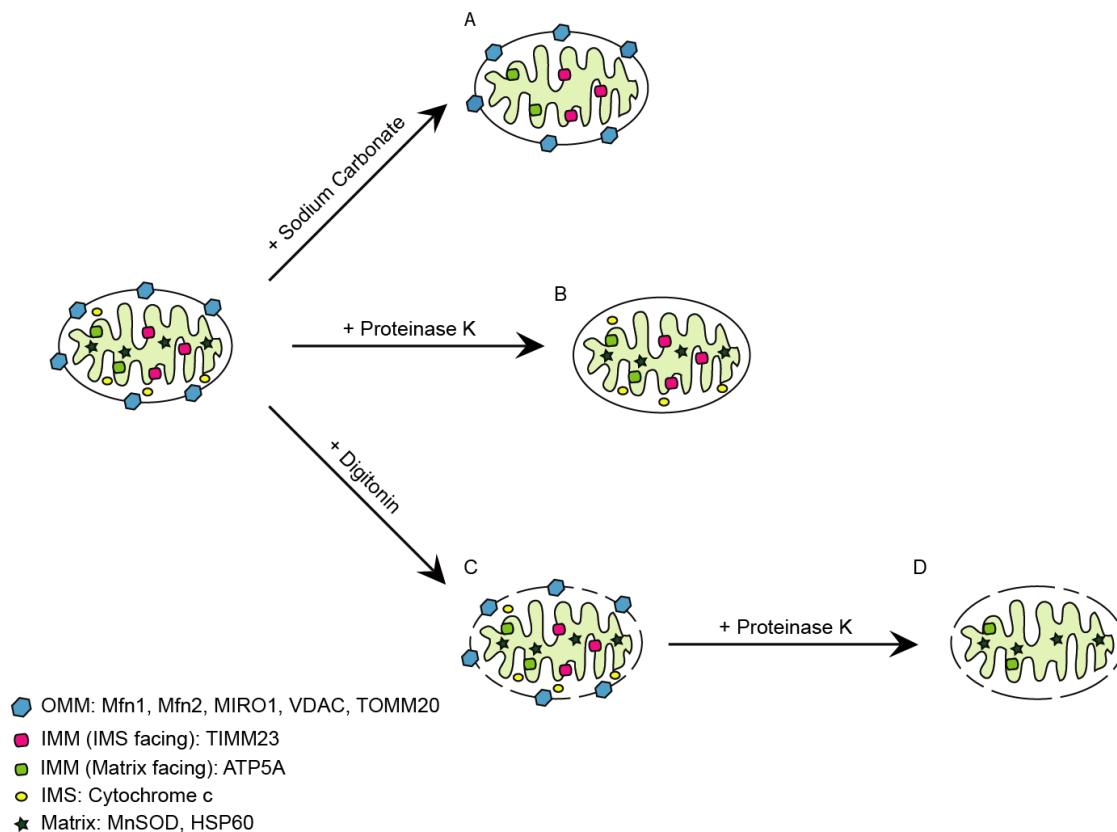


Figure 2.1 Mitochondrial sub-organelle fractionation

A) Investigation of mitochondrial membrane integration using alkaline extraction with sodium carbonate. B) Investigation of OMM localisation by Proteinase K digestion. C – D) Investigation of mitochondrial IMS localisation by permeabilisation of the OMM with digitonin and subsequent digestion of mitochondrial proteins with Proteinase K. The behaviour of known mitochondrial proteins located in each mitochondrial compartment is displayed.

2.4 Immunofluorescence microscopy

2.4.1 Immunostaining

Cells were plated on glass coverslips for use in immunofluorescence experiments. The coverslips were washed once in PBS and fixed for 20 min at room temperature in 3.7 % formaldehyde (Thermo Fisher Scientific) in PBS. Post two PBS washes, coverslips were quenched by washing once with quenching solution (50 mM NH₄Cl in PBS) and incubated a further 10 min at room temperature in quenching solution. When no further staining was required, cells were washed three times in PBS and mounted onto glass

slides using fluorescence mounting medium (Dako). When further staining was required, cells were permeabilised following quenching in 0.2 % Triton X-100 (Thermo Fisher Scientific) in PBS for 3 min at room temperature, washed once in PBS and blocked 20 min at room temperature in PBS containing 0.2 % fish gelatin (PBS-Fish) (Sigma-Aldrich). Coverslips were incubated with primary antibodies in PBS-Fish for 1 h at room temperature in a humidity chamber. The identity and dilution of primary antibodies are outlined in Table 2-13. Coverslips were washed three times in PBS-Fish and incubated for 1 h in secondary antibody in PBS-Fish at room temperature in a humidity chamber. The identity of secondary antibodies used are outlined in Table 2-14. Cells were then washed twice with PBS-Fish and three times with PBS prior to mounting with fluorescence mounting medium. Where nuclear staining was employed, this was achieved by incubation with 1 µg/mL Hoechst 33342 (Thermo Fisher Scientific) for 10 min during the final wash step.

Table 2-13 Primary antibodies used in immunofluorescence

Antibody Target	Supplier	Product code	Host Species	Dilution
anti-Myc	Cell Signaling	2276S	Mouse	1:2,000
anti-Myc	Abcam	ab9106	Rabbit	1:1,000
anti-HA	Sigma-Aldrich	H6908	Rabbit	1:1,000
anti-HA	Sigma-Aldrich	H9658	Mouse	1:5,000
anti-TOMM20	BD Biosciences	612278	Mouse	1:200
anti-MnSOD	Enzo Life Sciences	ADI-SOD-110	Rabbit	1:200
anti-C9orf72	Santa Cruz	sc-138763	Rabbit	1:500

Table 2-14 Secondary antibodies used in immunofluorescence

Antibody	Product Code	Supplier	Dilution
donkey anti-mouse A488	A21202	Invitrogen	1:500
goat anti-rabbit A488	A11008	Invitrogen	1:500
donkey anti-mouse A568	A10037	Invitrogen	1:500
goat anti-rabbit A568	A11011	Invitrogen	1:500

2.4.2 Proximity Ligation Assay

Cells plated on glass coverslips were processed for proximity ligation assay (PLA) according to the manufacturer's protocol (<https://www.sigmaaldrich.com/technical-documents/protocols/biology/duolink-fluorescence-user-manual.html>). Briefly, following fixing, quenching and permeabilisation of cells as described previously for immunofluorescence staining (2.4.1), coverslips were blocked in PBS-Fish for 30 min at room temperature. Coverslips were incubated in primary antibodies for 1 h at room temperature. The primary antibodies were as used previously in immunofluorescence assays and diluted in antibody diluent (Table 2-13). Following 2 washes in wash buffer A (DUO82049-4L, buffer A), samples were incubated with PLA probes (anti-rabbit PLUS (Sigma-Aldrich, DUO92002) and anti-mouse MINUS (Sigma-Aldrich, DUO92004)) for 1 h at 37 °C in a humidity chamber. Following 2 washes in wash buffer A, coverslips were incubated with ligase (Sigma-Aldrich, DUO92007) to anneal the PLA probes for 30 min at 37 °C. Following 2 washes in wash buffer A, PLA signal was amplified by rolling circle PCR via the addition of polymerase for 100 min at 37 °C (Sigma-Aldrich, DUO92007). Following one wash in wash buffer B (Sigma-Aldrich, DUO82049-4L, buffer B), samples were incubated with 1 µg/mL Hoechst 33342 in 0.01 X wash buffer B for 10 min and mounted onto glass slides with fluorescence mounting medium (Dako).

2.4.3 Image acquisition and analysis

2.4.3.1 Image acquisition

Cells were imaged on a Zeiss Axioplan2 microscope fitted with a Hamamatsu multi-format CCD C4880-80 camera, or fitted with a QImaging RetigaR3 camera, using a 63x 1.4 NA Plan Achromat objective (Zeiss). Single cells were selected for analysis based on positive staining in a second channel or from operator-blinded samples.

2.4.3.2 Quantification of mitochondrial morphological parameters

Morphological parameters of the mitochondrial network were analysed in FIJI (Schindelin et al., 2012), according to previously described parameters (De Vos and Sheetz, 2007). Images were imported into FIJI (Figure 2.2A) and split into their separate channels (Figure 2.2B). An ROI was drawn around the cell selected for analysis (Figure 2.2C). Images were filtered using a Hat filter (7x7 kernel) to extract mitochondria (Figure 2.2D) and a default threshold was set to highlight the organelles but not include background (Figure 2.2E). Thresholding was assessed by comparison for correspondence with the original image. Mitochondria were quantified using the 'analyse

particle' function in FIJI, to determine particle area, number, perimeter and aspect ratio (Figure 2.2F).

To analyse the connectivity of the mitochondrial network, the image was converted to a binary image (Figure 2.2G) and skeletonised (Figure 2.2H). The Look Up Table (LUT) was inverted on the image to permit the processing by the binary connectivity analysis plugin (Figure 2.2I - J). The resulting histogram from the binary connectivity analysis was displayed as a table (Figure 2.2K - L). A value of '0' was allocated where there was no positive signal pixel at a given coordinate. A value of '1' was allocated to each coordinate where there was a positive pixel without any neighbouring positive pixels. A value of '2' was allocated to an end-point in the network, where the positive pixel had 1 neighbouring positive pixel. A value of '3' was allocated to positive pixels which had 2 neighbouring positive pixels and was therefore located in the middle of a chain. Positive pixels with either 3 or 4 neighbouring positive pixels were given values of '4' or '5' respectively and represented bifurcations in the network (Figure 2.3). Mitochondrial networking was calculated by dividing the number of endpoints in the network (value '2') by the number of bifurcations (values of '4' and '5').

As a second measure of mitochondrial network branching, mitochondrial form factor was calculated, from the mitochondrial parameters defined by the particle analysis performed in FIJI. Form factor was defined as $\text{Form factor} = (Pm^2)/(4\pi Am)$, where Pm is the perimeter of the mitochondrion and Am is the area of the mitochondrion (Koopman et al., 2005; Mortiboys et al., 2008).

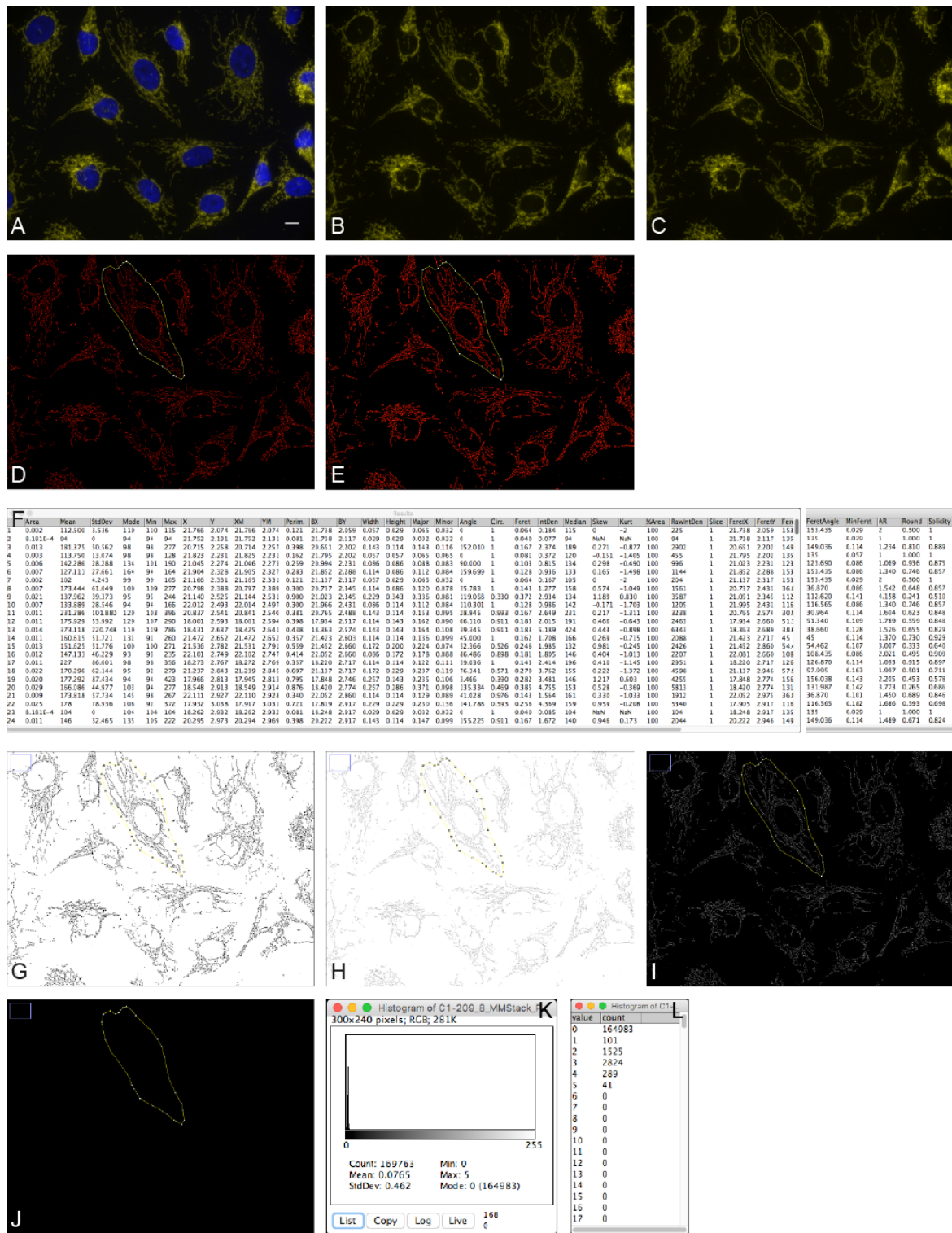


Figure 2.2: Quantification of mitochondrial morphology

A) Composite image (blue: nuclei, yellow: mitochondria) opened in FIJI. Scale bar 10 μm. B) Image split into separate colour channels, yellow (mitochondria) channel shown. C) Region of Interest (ROI) drawn around cell to be analysed. D) Hat 7x7 filter applied to image. E) Default threshold applied to image. F) Excerpt from particle analysis table. G) Image converted to binary. H) Image skeletonized. I) LUT inverted. J) Binary

connectivity add-on ran. K - L) Histogram and table showing the analysis of network connectivity.

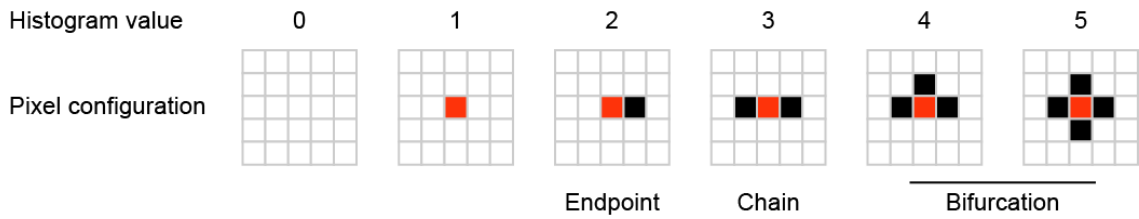


Figure 2.3: Binary connectivity add-on to quantify mitochondrial network connectivity

For any given pixel, the binary connectivity add-on output describes the presence or absence of signal and signal in adjacent pixels. The histogram value of the pixel highlighted in red is indicated.

2.4.3.3 Quantification of PLA

For quantification of PLA puncta, composite images were separated into their individual channels (Figure 2.4A). The ROI for analysis was created on the mitochondrial channel (Figure 2.4B) and applied to the PLA channel (Figure 2.4C). Images of PLA puncta were filtered using a Hat filter (7x7 kernel) to extract single PLA puncta (Figure 2.4D). Thresholding was set to highlight PLA puncta and compared to the original image to ensure correspondence (Figure 2.4E). PLA puncta were quantified using the 'analyse particle' function in FIJI (Figure 2.4F). The number of PLA puncta per cell was quantified.

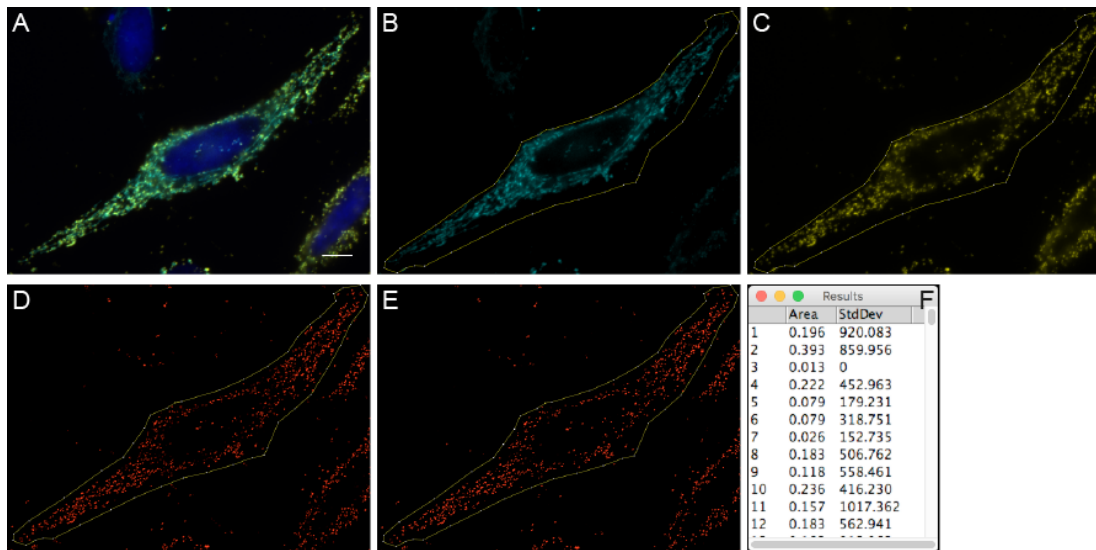


Figure 2.4: Quantification of PLA puncta per cell

A) Image as acquired opened in FIJI. Scale bar 10 μm . B) Image split into separate colour channels. ROI drawn around cell to be analysed on channel showing mitochondria (cyan). C) ROI applied to PLA channel (yellow). D) PLA channel filtered with a Hat 7x7 filter. E) Default threshold applied to image. F) Excerpt from particle analysis table.

2.4.3.4 Quantification of Parkin recruitment

Cells were classified as either having non-recruited cytosolic Parkin or as having recruited Parkin, that which localised to mitochondria in a non-diffuse manner, by a blinded investigator (Figure 2.5). The percentage of cells displaying the recruited EYFP-Parkin phenotype was quantified in each experiment.

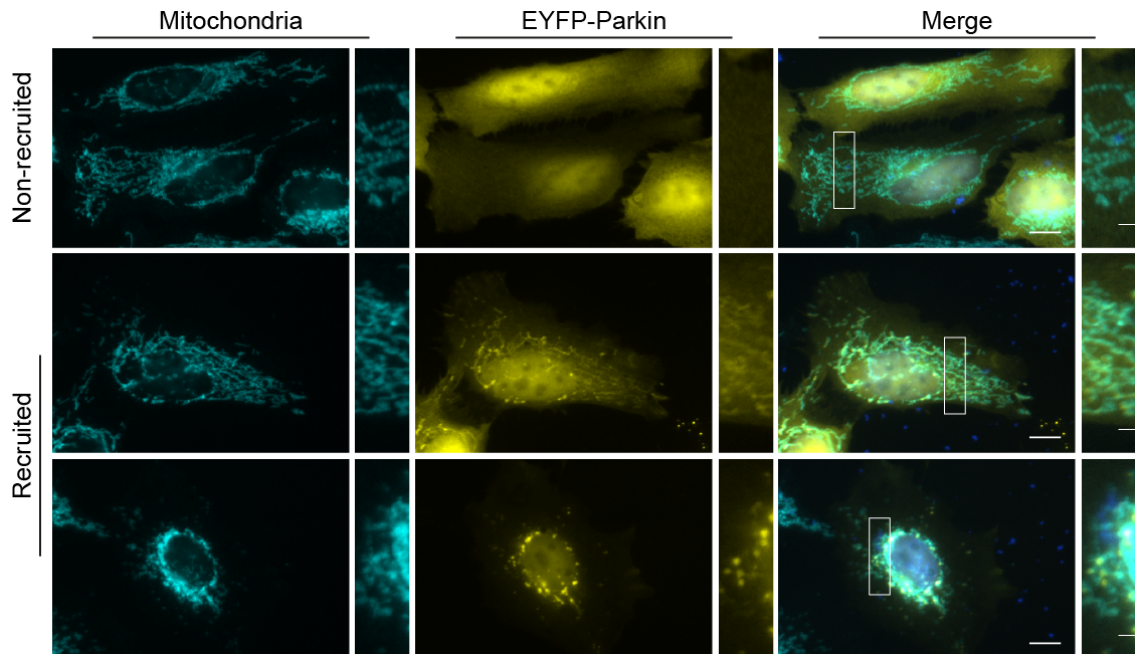


Figure 2.5 Quantification of Parkin recruitment

HeLa cells were transfected with EYFP-Parkin (yellow) and mitochondria were immunostained for TOMM20 (cyan). Recruitment of EYFP-Parkin to damaged mitochondria was elicited by treatment with 10 μ M Oligomycin and 4 μ M Antimycin A. Cytosolic EYFP-Parkin that does not co-localise with TOMM20 classified as 'non-recruited', upper panels. Punctate EYFP-Parkin that co-localised with TOMM20 was classified as 'recruited', lower panels. Scale bar 10 μ m, zoom 2 μ m.

2.4.3.5 Quantification of mitophagy

To analyse the clearance of mitochondria during mitophagy, cells treated with mitophagy inducing treatments were subjected to immunostaining to reveal the remaining mitochondrial content. Cells were classified as having a high, intermediate or low mitochondrial content on a cell by cell basis by a blinded investigator (Figure 2.6). The number of cells for each category were totalled in each condition. The mitophagy index was calculated as the percentage of cells displaying the ‘full’ mitochondrial content in each condition.

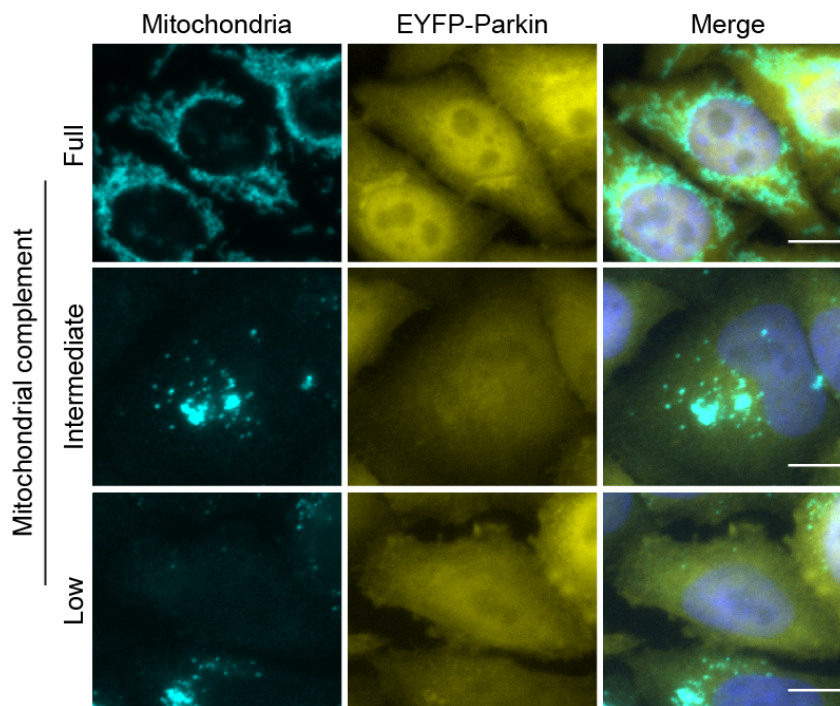


Figure 2.6: Quantification of mitophagy

EYFP-Parkin (yellow) HeLa cells were treated 23 h with 10 μ M Oligomycin and 4 μ M Antimycin A and were subjected to TOMM20 immunostain (cyan), to reveal mitochondrial content. Cells were classified as having a full mitochondrial complement (top panel, ‘full’), reduced mitochondrial complement (middle panel, ‘intermediate’) or low mitochondrial complement (lower panel, ‘low’). Cells with either a partial or full mitochondrial clearance, ‘intermediate’ and ‘low’ mitochondrial complement respectively, were categorised as having undertaken mitophagy. Scale bar 10 μ m.

2.4.4 Analysis of mitochondrial membrane potential

2.4.4.1 Plating

HeLa cells were plated onto 96-well plates (Greiner) at a density of 7,000 cells per well. Cells were transfected the day following plating using Lipofectamine 2000 (as described previously 2.1.3). Triplicate wells were transfected per condition.

2.4.4.2 TMRM dye loading

Three hours prior to analysis, triplicate wells of control cells were treated with 10 μ M CCCP to induce mitochondrial depolarisation. To load Tetramethylrhodamine, methyl ester (TMRM) dye (Thermo Fisher Scientific) and to stain nuclei, cells were incubated for 30 min with 30 nM TMRM and 1 μ g/mL Hoechst 33342. CCCP induced mitochondrial depolarisation was maintained during TMRM loading. Prior to imaging, unloaded TMRM was removed by washing the cells in twice in Phenol-Red free DMEM (Gibco). Cells were placed in Phenol-Red free DMEM for imaging.

2.4.4.3 Automated image acquisition

96 well plates were imaged in an InCell2000 Imager (GE Healthcare) at 5 % CO₂ and 37 °C by automated image acquisition with a 60x 0.95 NA objective. Well acquisition order was determined in a serpentine fashion to distribute the conditions equally along the acquisition timeline. Twenty-five random fields were acquired from each well per experimental run. Cells were imaged using the DAPI filter to acquire images of nuclear staining, FITC to image EGFP transfected constructs and TRITC to image TMRM staining of mitochondria.

2.4.4.4 Automated analysis of TMRM staining

Analysis of MMP was performed automatically using the InCell Developer Software package (GE Healthcare). Images acquired from the InCell2000 Imager were loaded directly into the InCell Developer Software package. Individual cells were identified based on the presence of nuclear staining within a FITC positive area (by intensity of transfected EGFP construct). The limits of the cell were determined by the FITC fluorescence. Mitochondria were identified by intensity in the TRITC channel within the identified cells and an ROI was placed around the individual mitochondria. TRITC intensity and area were then measured to give an integrated intensity value for TMRM staining. Mitochondrial TMRM was calculated by subtracting TMRM signal from CCCP treated cells from that of the untreated cells.

2.5 RT-qPCR

RT-qPCR was used to determine knockdown of targets where antibodies against the endogenous targets were unreliable. The knockdown of C9orf72 following siRNA transfection was verified using RT-qPCR.

2.5.1 RNA extraction

RNA was extracted from HEK293, EYFP-Parkin or HeLa cells with TRIzol reagent (Invitrogen) according to the manufacturer's protocol. Briefly, cells were scraped into TRIzol reagent and incubated for 5 min at room temperature, to allow dissociation of the nucleoprotein complex. A fifth of the volume of TRIzol reagent of chloroform (Thermo Fisher Scientific) was added and mixed by shaking. Samples were incubated 3 min at room temperature and centrifuged 15 min at 12,000 x g at 4 °C, resulting in phase separation between aqueous and phenol-chloroform phases. The RNA containing aqueous layer was removed and the RNA precipitated by incubation with isopropanol (Thermo Fisher Scientific) for 10 min at room temperature and centrifugation at 12,000 x g for 10 min at 4 °C. The supernatant was discarded and the RNA pellet washed once with 75 % ethanol and pelleted by centrifugation at 7,500 x g for 5 min at 4 °C. RNA pellets were air dried for 10 min at room temperature, and resuspended in nuclease free water (Qiagen) for 15 min at 55 °C.

RNA concentration was determined using a Nanodrop ND-1000 spectrophotometer. RNA purity was assessed by looking at the A260/A280 ratio, for protein contamination, and the A260/A230 ratio for solvent (phenol) contamination. A ratio above 2.0 was considered clean.

2.5.2 Reverse transcription of RNA to cDNA

Two µg of RNA was resuspended in 8 µL of nuclease free water. Residual DNA was removed by incubation for 10 min at 37 °C with 1 µL of DNase I enzyme (NEB). DNase I was inactivated by incubation at 75 °C for 10 min in the presence of 1 µL 25 mM EDTA pH 8 (Ameresco). The reverse transcriptase PCR was primed by incubation with 2 µL 25 mM dNTPs (NEB) and 1 µL 0.5 µg/µL Oligo(dT)₁₈ primer (Thermo Fisher Scientific) for 5 min at 65 °C. Oligo(dT)₁₈ primes the poly-A tail of mRNAs resulting in the synthesis of cDNA from mature mRNAs. cDNA was synthesised in a final volume of 20 µL with 2 µL DTT 100 mM and 4 µL 5 X reverse transcriptase buffer (Invitrogen) using 0.5 µL SuperScript III Reverse Transcriptase (Invitrogen). PCR cycle conditions were as follows: 5 min at 25 °C, 60 min at 50 °C and 15 min at 75 °C. Assuming a 100 %

conversion from RNA to cDNA, 20 μL of 100 ng/ μL cDNA was obtained from the reverse transcription PCR. cDNA was stored at 4 $^{\circ}\text{C}$.

2.5.3 RT-qPCR

cDNA was diluted to 10 ng/ μL in nuclease free water. qPCR reactions were performed in triplicate and a master mix produced for each primer set. qPCR primers were designed using Primer3 (<http://primer3.ut.ee/>) and purchased from Sigma-Aldrich. Stock primers were diluted to 100 μM and were further diluted in nuclease free water as required (Table 2-15). Master mixes comprised of 5 X HOT FIREPol EvaGreen qPCR Mix Plus (08-25-00001, Solis Biodyne), desired forward and reverse primers and nuclease free water were produced for each primer set (Table 2-16). RT-qPCR reactions were performed in a Stratagene Mx3000P or a Bio-Rad CFX96 Touch thermocycler and analysed using MxPro v4.10 or Bio-Rad CFX Manger software respectively. Cycling conditions for the RT-qPCR were as follows: 95 $^{\circ}\text{C}$ for 5 min to denature followed by 39 cycles of 95 $^{\circ}\text{C}$ for 30 s and 60 $^{\circ}\text{C}$ for 1 min. RT-qPCR cycles were followed by a melt curve cycle to ensure single products were generated. Conditions for the melt curve were 1 min at 95 $^{\circ}\text{C}$, followed by 60 cycles of 0.5 $^{\circ}\text{C}/\text{cycle}$ from 65 $^{\circ}\text{C}$. mRNA levels were determined comparatively to the GAPDH control via the $\Delta\Delta\text{Ct}$ method (Livak and Schmittgen, 2001).

Table 2-15 Sequences of primers used for RT-qPCR

Primer	Sequence (5' – 3')	Dilution from 100 μM stock	Reference
C9orf72 fwd	GTTGATAGATTAACACATATAATCCGG	1:40	(Webster et al., 2016a)
C9orf72 rev	CAGTAAGCATTGGAATAATACTCTGA	1:40	(Webster et al., 2016a)
GAPDH fwd	GGGTGGGGCTCATTTGCAGGG	1:33	(Webster et al., 2016a)
GAPDH rev	TGGGGGCATCAGCAGAGGGG	1:33	(Webster et al., 2016a)

Table 2-16 Master mix for RT-qPCR

	Mix (per well) (μL)	Master Mix (μL)
5 X HOT FIREPol	4	48
H ₂ O	11	132
Diluted Fwd primer	2	24
Diluted Rev primer	2	24
Final Volume	19	228

2.6 *In vitro* binding assay

2.6.1 Production of GST-tagged proteins

GST, GST-C9orf72L and GST-C9orf72S were expressed from a pGEX6p1 vector in Rosetta PLysS cells. Bacteria were grown overnight from glycerol stocks in 20 mL of Terrific broth (TB) (1.2 % Tryptone, 2.4 % yeast extract, 17 mM KH₂PO₄, 72 mM K₂HPO₄, 0.4 % glycerol) at 37 °C with constant shaking. Rosetta PLysS cells were selected for by inclusion of 34 $\mu\text{g}/\text{mL}$ Chloramphenicol (Sigma-Aldrich) in the broth, whereas selection for the GST containing plasmid transformed cells was achieved with 100 $\mu\text{g}/\text{mL}$ Ampicillin (Melford).

Ten mL of bacterial starter culture was placed in 750 mL of TB containing Ampicillin 100 $\mu\text{g}/\text{mL}$ and an optical density (O.D.) reading obtained at 600 nm. Additional bacterial starter culture was added until an O.D. reading of 0.050 arbitrary units (AU) was achieved. Bacterial cultures were grown at 37 °C with constant shaking for 2 h. After 2 h, O.D. readings were taken at 600 nm to assess growth of the culture. O.D. readings were taken every 30 min until an O.D. of 0.700 AU was reached. Once an O.D. 0.700 AU was attained, production of the GST protein was induced by addition of 0.5 mM Isopropyl- β -D-thiogalactoside (IPTG) for 3 h. Bacterial pellets were obtained by centrifugation at 6,000 rpm (6,371 x g MAX / 3,951 x g AVG) in an Avanti J26 centrifuge using a JA-10 rotor for 10 min. Bacterial pellets were frozen and stored at -20 °C until use.

2.6.2 Polyacrylamide gel and Coomassie stain to check GST expression

To verify the expression of the GST-tagged constructs, uninduced and IPTG induced GST-construct expressing bacteria were lysed in 5 X sample buffer and subjected to SDS-PAGE on a 10 % polyacrylamide gel, as described previously (2.3.4.1).

Polyacrylamide gels were stained for 20 min in Coomassie solution (0.1 % Coomassie Blue R-250, 50 % methanol, 10 % acetic acid). Gels were destained by briefly heating for 15 s and incubating 10 min in destain solution (30 % methanol, 10 % acetic acid) until the gel was clear. The gel was washed 2 times in ddH₂O and imaged on a SynGene G:Box (Figure 2.7).

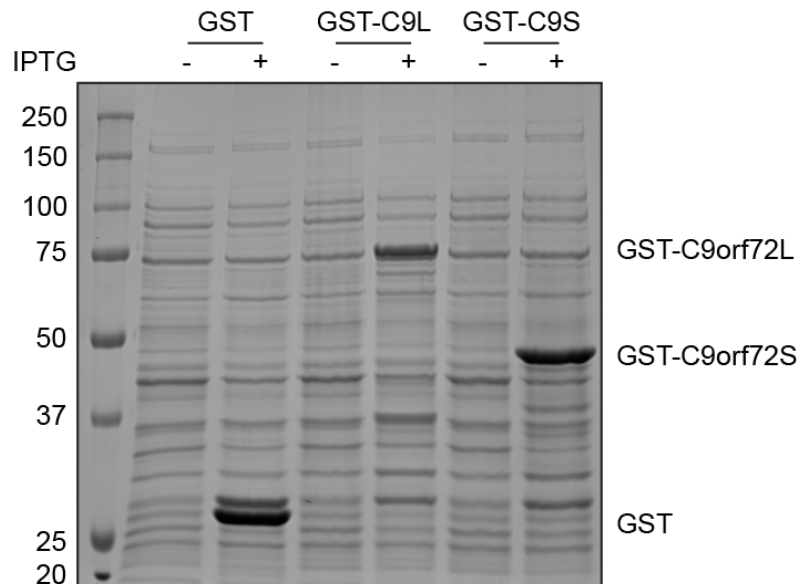


Figure 2.7: Coomassie stained polyacrylamide gel verifying the expression of GST-tagged proteins

Uninduced and IPTG induced samples of bacteria expressing GST, GST-C9orf72L (C9L) and GST-C9orf72S (C9S) were run on a 10 % polyacrylamide gel and were subjected to Coomassie staining.

2.6.3 *In vitro* binding assay

2.6.3.1 *In vitro* translation in reticulocytes

0.5 µg of DNA was incubated at 37 °C for 90 min with 0.5 µL ³⁵S-labelled Methionine and 8 µL of Reticulocyte master mix from the T7 TnT Quick Coupled Transcription/Translation kit (Promega).

2.6.3.2 Bacterial lysis

Per binding reaction, 0.1 g GST, 0.3 g GST-C9orf72L or 0.2 g GST-C9orf72S expressing bacterial pellet was lysed by sonication in 1 mL RB100 buffer (25 mM HEPES pH 7.5, 100 mM KOAc, 10 mM MgCl₂, 1 mM DTT, 0.05 % Triton X-100, 10 % glycerol). To minimise variability in lysis, GST expressing bacteria were lysed as a pool for all reactions. Hence for 3 binding reactions, 0.3 g GST, 0.9 g GST-C9orf72L or 0.6 g GST-

C9orf72S expressing bacterial pellet was lysed in 3 mL RB100, at 100 % sonication for 15 s, repeated 3 times at 30 s intervals. Lysates were clarified by centrifugation for 5 min at 17,000 x g at 4 °C.

2.6.3.3 Binding assay

Lysed bacteria were incubated with 30 µL glutathione-agarose beads (GSH beads) (GE Healthcare) per reaction, to allow binding of the GST-tagged protein to the bead. Beads and bacterial lysate were incubated 30 min at 4 °C with constant rotation. Beads were washed 2 times in ice cold RB100 buffer and pelleted at 2,000 x g for 1 min.

For binding reactions, 8 µL of the *in vitro* translation reaction was incubated with 30 µL of 50 % GSH beads for 1 h at 4 °C with constant rotation in 400 µL RB100 buffer. GSH beads were subsequently washed twice in RB100 and eluted in 40 µL of glutathione elution buffer (50 mM Tris-HCl pH 7.5, 100 mM NaCl, 40 mM reduced glutathione). Samples were prepared for SDS-PAGE by addition of 5 X sample buffer.

Eluted samples were analysed by polyacrylamide SDS-PAGE. 0.5 µL of reticulocyte lysate was used as input. Samples were run on a 10 % polyacrylamide gel as described previously (2.3.4.1). Coomassie staining was used to visualise GST-tagged proteins as described above (2.6.2). Polyacrylamide gels were imaged using a digital camera. Gels were mounted onto filter paper and dried in a vacuum for 15 min. Gels were exposed to a phosphoscreen for 7 days. ³⁵S-labelled proteins were detected on a Phosphoimager.

2.7 Online bioinformatics tools

2.7.1 TMHMM

The TMHMM online platform was used to investigate the presence of transmembrane domains. The protein sequence of the query protein was uploaded in FASTA format to the TMHMM Server v. 2.0., <http://www.cbs.dtu.dk/services/TMHMM/> (Krogh et al., 2001; Sonnhammer et al., 1998). The default settings were used to run the analysis.

2.7.2 MitoMiner

The MitoMiner 4.0 online platform was used to predict the presence of mitochondrial targeting sequences in the protein of interest, <http://mitominer.mrc-mbu.cam.ac.uk/release-4.0/begin.do> (Smith and Robinson, 2016). The gene symbol of the protein of interest was queried on the database. The analysis was ran with the default settings.

2.7.3 Clustal Omega

The Clustal Omega online platform was used to produce multiple sequence alignments. FASTA format protein sequences for the alignment were identified in Ensembl (<https://www.ensembl.org/index.html>), and uploaded onto the Clustal Omega platform, <https://www.ebi.ac.uk/Tools/msa/clustalo/>, (Sievers et al., 2011). The default parameters were used to perform alignments.

2.8 Statistical analysis

Statistical analysis was performed using the Prism 7 (version 7.0c) software package (GraphPad Software, Inc., US). All data presented as mean \pm SEM unless otherwise stated. Statistical analysis performed by one-way ANOVA with Fisher's LSD test unless otherwise stated.

Chapter 3. Investigating the interaction between C9orf72 and mitochondrial proteins

3.1 Introduction

The *C9orf72* gene is predicted to encode 2 protein isoforms: C9orf72L and C9orf72S (reviewed in Haeusler et al., 2016). At the start of this project, there was little evidence supporting the cellular localisation of the C9orf72 protein. Immunostaining for C9orf72 revealed diffuse cytosolic staining, but with refinement of C9orf72 antibodies it was shown that whilst C9orf72L was cytosolic, C9orf72S was localised to the nuclear membrane (Xiao et al., 2015). Early reports revealed that C9orf72 interacts with several Rab GTPases, which suggested that C9orf72 may play a role in endosomal trafficking events and autophagy (Farg et al., 2014). Indeed, the role of C9orf72 in autophagy has now been investigated by multiple groups (Chitiprolu et al., 2018; Sellier et al., 2016; Sullivan et al., 2016; Webster et al., 2016a; Yang et al., 2016). During the course of this project, new data emerged regarding the cellular localisation of C9orf72. C9orf72 was shown to localise to lysosomes upon starvation and regulate lysosomal activity (Amick et al., 2016; Ugolino et al., 2016). More recently, C9orf72 was shown to be enriched in presynapses (Frick et al., 2018), where it may regulate synaptic plasticity (Sivadasan et al., 2016).

The lack of information regarding the localisation of C9orf72 initially rendered the identification of the function of the C9orf72 protein more challenging. In order to aid in the determination of the function of the C9orf72 protein, the identities of C9orf72 interacting proteins were investigated. In the first instance, a yeast two-hybrid (Y2H) screen was carried out by our laboratory (unpublished). A number of these interactors were initially validated by Dr Christopher Webster in our lab (Webster et al., 2016a). In addition to these validated hits, the Y2H screen revealed a number of mitochondrial proteins as potential C9orf72 interacting partners.

The initial aim of this project was to validate and characterise the interactions between C9orf72 and mitochondrial proteins identified in the Y2H screen. We hypothesised that if C9orf72 interacts with mitochondrial proteins, this may indicate that C9orf72 localises to mitochondria. Therefore, we further investigated the subcellular localisation of the C9orf72 protein. Finally, we explored how the C9orf72 protein may achieve its cellular distribution.

3.2 C9orf72 interacts with mitochondrial proteins

Our lab carried out Y2H screens to identify interacting partners of both the C9orf72L and C9orf72S protein isoforms. In the Y2H screens, C9orf72L or C9orf72S was used as bait and screened against a human brain cDNA library. In the C9orf72L Y2H screen, two mitochondrial proteins were identified as potential interacting proteins. In the C9orf72S Y2H screen, eight mitochondrial proteins were identified as potential interacting partners (Table 3-1). In addition, Ubiquitin specific peptidase 8 (USP8), previously implicated in mitochondrial quality control (Durcan et al., 2014), was also identified as a hit in the C9orf72S Y2H screen (Table 3-1). In addition to our Y2H screens, an immunoprecipitation coupled mass spectrometry approach performed in house identified several mitochondrial proteins as interacting partners of C9orf72L (Table 3-2) (Dr Guillaume Hautbergue, unpublished, SITraN, Sheffield). The full details of the interacting partners of C9orf72 identified in these screens can be found in the thesis of Dr Christopher Webster (unpublished, Sheffield).

Whilst we were undertaking this project, the results of a number of additional proteomics screens investigating C9orf72 interacting partners were published. Supporting our previous screening approaches, these screens also identified mitochondrial proteins as interacting partners of C9orf72 (Table 3-3) (Blokhuys et al., 2016; Sellier et al., 2016; Sullivan et al., 2016).

As mitochondrial dysfunction, including mitochondrial quality control, is a prevalent feature of ALS, we hypothesised that the interaction between C9orf72 and mitochondria may be important for cellular function.

Table 3-1 Mitochondria associated hits from C9orf72 yeast two-hybrid screens

Bait	Prey	Prey description	Mitochondrial localisation	Number of times isolated
C9orf72L	COX6C	Cytochrome c oxidase subunit Vlc	IMM	2
	HRK	Activator of apoptosis harakiri	OMM	1
C9orf72S	MRPL48	39S ribosomal protein L48, mitochondrial	IMM	3
	OAT	Ornithine aminotransferase	Matrix	2
	ATP5I	ATP synthase, H ⁺ transporting, mitochondrial F0 complex, subunit E	IMM	1
	PITRM1	Pitriysin metallopeptidase 1	Matrix	1
	PPP2R2 B	Protein phosphatase 2 (formerly 2A), regulatory subunit B, beta isoform	OMM	1
	HSPD1	Heat shock 60kDa protein 1 (chaperonin)	Matrix	1
	NDUFA10	NADH dehydrogenase (ubiquinone) 1 alpha subcomplex, 10, 42kDa	Matrix	1
	SLC25A39	Solute carrier family 25 member 39	IMM	1
	USP8	Ubiquitin specific peptidase 8	Cytosol	2

Mitochondrial localisation was determined from the subcellular localisation listed on UniProt (www.uniprot.org) or reactome (www.reactome.org). Abbreviations: IMM: inner mitochondrial membrane, OMM: outer mitochondrial membrane.

Table 3-2 Mitochondrial interacting partners of C9orf72L identified in mass spectrometry screens (Dr Guillaume Hautbergue, SITraN, Sheffield)

Common name	Protein name	Mitochondrial localisation
ADCY10	Adenylate cyclase type 10	Matrix
ATP5A1	ATP synthase subunit alpha, mitochondrial	IMM
mtHSP70	Stress-70 protein, mitochondrial	Matrix
RPS3	40S ribosomal protein S3	IMM
SLC25A5	ADP/ATP translocase 2	IMM
ATP5B	ATP synthase subunit beta, mitochondrial	IMM
TIMM50	Mitochondrial import inner membrane translocase subunit TIM50	IMM

FLAG pull down was performed in induced Flp-In FLAG-C9orf72L HEK293 cell lysate. Co-immunoprecipitating proteins were identified by MS/MS mass spectrometry. The mitochondrial localisation of co-immunoprecipitating proteins was determined from the subcellular localisation listed on UniProt (www.uniprot.org) or reactome (www.reactome.org). Abbreviation: IMM: inner mitochondrial membrane.

Table 3-3 Mitochondrial interacting partners of C9orf72L from the published proteomics screens

Reference	Common name	Protein name	Mitochondrial localisation
(Blokhuys et al., 2016)	CHCHD3	MICOS complex subunit MIC19	IMM
	IMMT	MICOS complex subunit MIC60	IMM
	ATAD3	ATPase family, domain-containing protein 3A	IMM

Reference	Common name	Protein name	Mitochondrial localisation
	ATP5A1	ATP synthase subunit alpha, mitochondrial	IMM
	ATP5C1	ATP synthase subunit gamma, mitochondrial	IMM
	DNAJA1	DnaJ homolog subfamily A member 1	Unspecified
	PDHA1	Pyruvate dehydrogenase E1 component subunit alpha, somatic form, mitochondrial	Matrix
	PDHB	Pyruvate dehydrogenase E1 component subunit beta, mitochondrial	Matrix
	PDHX	Pyruvate dehydrogenase protein X component, mitochondrial	Matrix
	SDHA	Succinate dehydrogenase [ubiquinone] flavoprotein subunit, mitochondrial	IMM
	SLC25A12	Calcium-binding mitochondrial carrier protein Aralar1	IMM
	SLC25A3	Phosphate carrier protein, mitochondrial	IMM
	SLC25A4	ADP/ATP translocase 1	IMM
	SLC25A5	ADP/ATP translocase 2	IMM
	TIMM50	Mitochondrial import inner membrane translocase subunit TIM50	IMM
	VDAC3	Voltage-dependent anion-selective channel protein 3	OMM

Reference	Common name	Protein name	Mitochondrial localisation
(Sullivan et al., 2016)	CHCHD3	MICOS complex subunit MIC19	IMM
	DNAJA1	DnaJ homolog subfamily A member 1	Unspecified
	IMMT	MICOS complex subunit MIC60	IMM
	KARS	Lysine--tRNA ligase	Matrix
	SLC25A4	ADP/ATP translocase 1	IMM
	SLC25A5	ADP/ATP translocase 2	IMM
	SLC25A11	Mitochondrial oxoglutarate/malate carrier protein	2- IMM
	SLC25A12	Calcium-binding mitochondrial carrier protein Aralar1	IMM
	VDAC3	Voltage-dependent anion-selective channel protein 3	OMM
(Sellier et al., 2016)	SAMM50	Sorting and assembly machinery component 50 homolog	OMM

Blokhuis *et al.* performed a Biotin-Streptavidin pull down from N2A cells expressing bioGFP-C9orf72L, followed by mass spectrometry to identify interacting proteins. Sullivan *et al.* performed a GFP immunoprecipitation from N2A cells transfected with GFP-C9orf72L and analysed co-immunoprecipitating proteins by mass spectrometry. Sellier *et al.* transfected N2A cells with C9orf72L-FLAG-HA and performed HA-FLAG tandem purification. Interacting proteins were identified using NanoESI_Ion Trap mass spectrometry. The mitochondrial localisation of co-precipitating proteins was determined from the subcellular localisation listed on UniProt (www.uniprot.org) or reactome (www.reactome.org). Abbreviations: IMM: inner mitochondrial membrane, OMM: outer mitochondrial membrane.

3.2.1 Transient expression of C9orf72 in cell lines

Two protein isoforms of C9orf72 have been suggested; C9orf72 long isoform 1 – 481 aa (C9orf72L) and C9orf72 short isoform 1 – 222 aa (C9orf72S). As a DENN domain protein, C9orf72L is composed of 3 separate DENN domains; the N-terminal uDENN, central DENN and C-terminal dDENN. C9orf72S is composed of the uDENN domain only (1.3.2). To investigate the localisation of the C9orf72 protein and the role of the DENN domains in its localisation, 3 C9orf72 constructs were generated: C9orf72L, C9orf72S and C9orf72DdD (Figure 3.1A). C9orf72DdD is composed of the central DENN and C-terminal dDENN domains of C9orf72L (205 – 481 aa), and hence corresponds to the domains of C9orf72L that are lacking in C9orf72S.

To verify the expression of the C9orf72 constructs, HEK293 cells were transfected with pCI-neo empty vector, Myc-C9orf72L, Myc-C9orf72S or Myc-C9orf72DdD. The predicted molecular weights of Myc-C9orf72L, Myc-C9orf72S and Myc-C9orf72DdD proteins were 54 kDa, 25 kDa and 32 kDa respectively. Myc immunoblot revealed that Myc-C9orf72L, Myc-C9orf72S and Myc-C9orf72DdD expressed efficiently and had the expected molecular weight on immunoblot (Figure 3.1B).

To observe the cellular localisation of the Myc-tagged C9orf72 constructs, HeLa cells were transfected with pCI-neo empty vector, Myc-C9orf72L, Myc-C9orf72S or Myc-C9orf72DdD and immunostained with anti-Myc antibody (Ab). Immunostaining using Ab to the Myc-tag revealed that both Myc-C9orf72L and Myc-C9orf72S appeared diffuse and cytosolic in cells. In contrast, alongside the cytoplasmic staining, punctate structures were apparent in cells transfected with Myc-C9orf72DdD (Figure 3.1C).

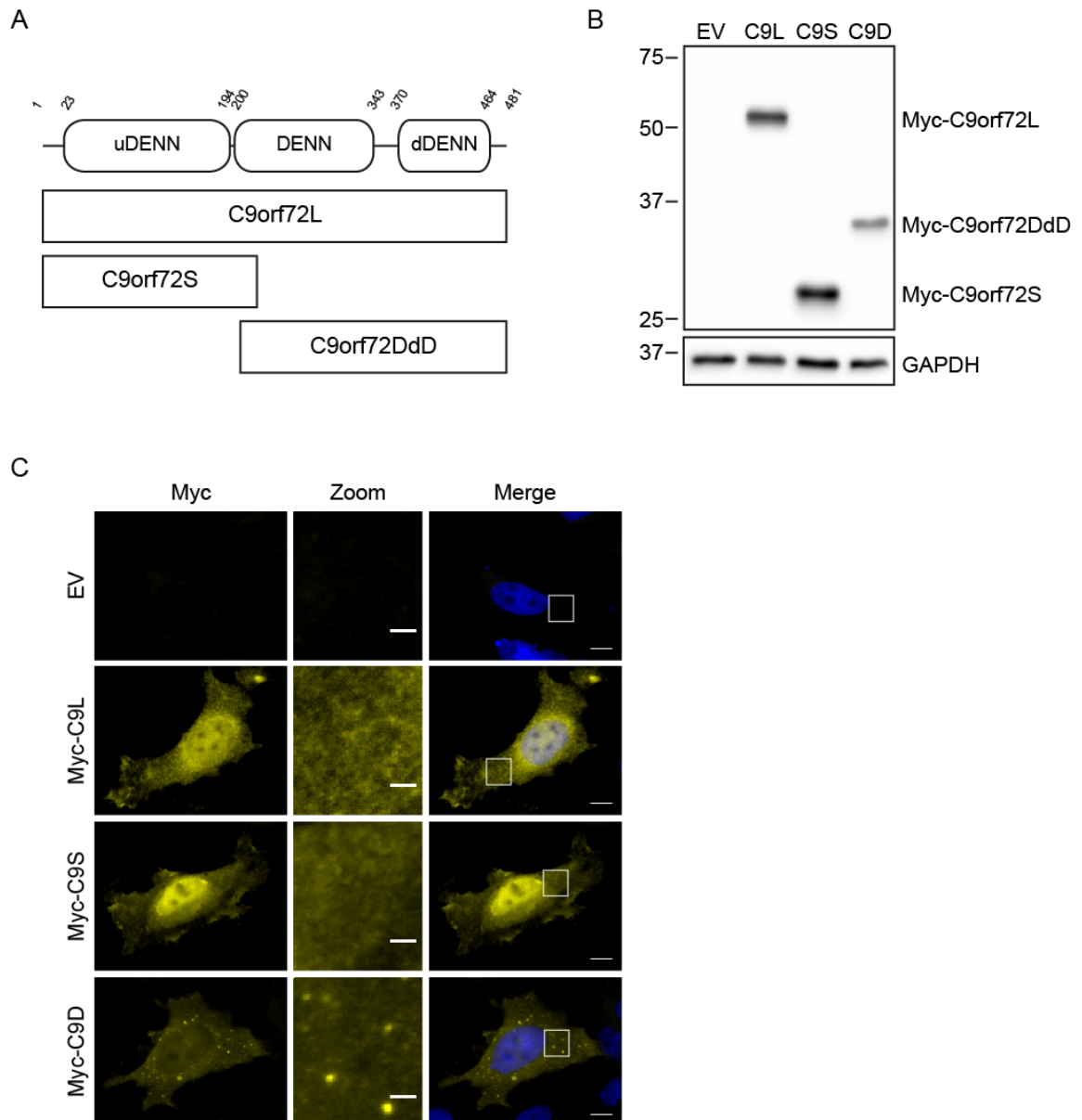


Figure 3.1 Myc-tagged C9orf72 constructs express efficiently in cells

A) Schematic of the C9orf72 protein revealing the position of the uDENN, DENN and dDENN domains. Below is shown the alignment of the C9orf72L, C9orf72S and C9orf72DdD constructs. B) HEK293 cells were transfected with pCI-neo empty vector (EV), Myc-C9orf72L (C9L), Myc-C9orf72S (C9S) or Myc-C9orf72DdD (C9D) and were subjected to Myc immunoblot. C) HeLa cells were transfected with pCI-neo empty vector (EV), Myc-C9orf72L (C9L), Myc-C9orf72S (C9S) or Myc-C9orf72DdD (C9D) and were subjected to immunostaining with anti-Myc Ab (yellow). Scale bar 10 μ m, zoom 2 μ m.

3.2.2 Ornithine Aminotransferase

Ornithine aminotransferase (OAT) was identified as an interacting partner of C9orf72S in the Y2H screen (Table 3-1). OAT is a mitochondrial matrix residing protein responsible for the conversion of ornithine to glutamic acid gamma-semialdehyde and glutamate from alpha-ketoglutarate, for the synthesis of the excitatory and inhibitory neurotransmitters glutamate and GABA. OAT also regulates the conversion of ornithine to proline and may additionally be involved in the synthesis of ornithine from glutamic acid gamma-semialdehyde in an organ specific manner (reviewed in Ginguay et al., 2017). Supporting its role in neurotransmitter synthesis, high levels of OAT have been found at nerve terminals (Wong et al., 1981). Mutations in OAT result in Gyrate Atrophy, an autosomal recessive eye disease (Doimo et al., 2013). Two isoforms of OAT have been identified; hepatic and renal, which were proposed to differ in enzymatic properties. However, the existence of the 2 isoenzymes is controversial and are not consistently reported in all studies (reviewed in Ginguay et al., 2017). Initially the 2 isoforms were also reported to possess 2 different length N-terminal mitochondrial targeting sequences (Figure 3.2A). However, this has been disputed in contrasting reports. It is now thought that multi-step cleavage may play a role in the maturation of OAT, resulting in a single OAT isoform (reviewed in Ginguay et al., 2017).

In the Y2H screen the region of OAT interacting with C9orf72 corresponded to the C-terminus of the protein (Figure 3.2A). To validate the interaction between C9orf72 and OAT, HEK293 cells were co-transfected with pCI-neo empty vector, Myc-C9orf72L or Myc-C9orf72S and with pCI-neo empty vector or OAT-MycDDK. OAT-MycDDK was immunoprecipitated using anti-FLAG Ab, raised against the FLAG peptide sequence DYKDDDDK. Immunoprecipitates were subjected to Myc immunoblot which revealed that neither Myc-C9orf72L nor Myc-C9orf72S co-immunoprecipitated with OAT (Figure 3.2B). Hence the interaction identified in the Y2H screen between C9orf72S and OAT appeared to be a false positive. However, it should be noted that the Y2H screen identified the C-terminal portion of OAT as interacting with C9orf72S and that here we used a C-terminal tagged OAT construct to probe this interaction. It is possible that the C-terminal MycDDK tag on OAT interfered with the interaction with C9orf72. Therefore, to verify whether the interaction was indeed a false hit, the co-immunoprecipitation should be carried out with an endogenous OAT antibody or using an untagged construct.

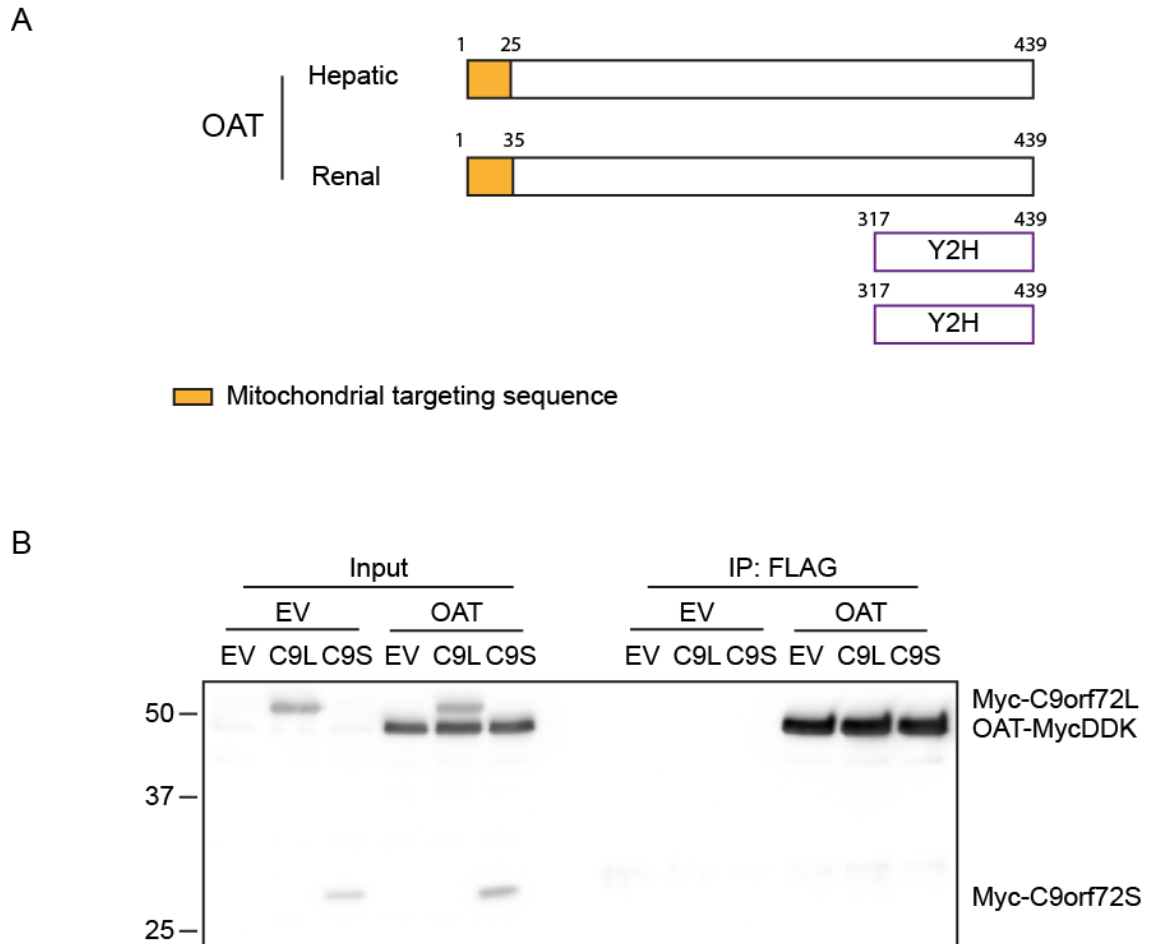


Figure 3.2 C9orf72 does not interact with OAT

A) The two isoforms of OAT, hepatic and renal, are shown with the differing mitochondrial targeting sequences (orange). The two hits from the C9orf72S Y2H screen are shown below, both corresponding to the C-terminal region of OAT. B) HEK293 cells were co-transfected with pCI-neo empty vector (EV), Myc-C9orf72L (C9L) or Myc-C9orf72S (C9S) and EV or OAT-MycDDK and were subjected to immunoprecipitation with anti-FLAG Ab. Immunoprecipitates were probed with anti-Myc Ab. Input represents 10% of lysate subjected to immunoprecipitation.

3.2.3 Cytochrome c oxidase subunit 6c

The Cytochrome c oxidase (COX) IV complex is the terminal complex in the electron transport chain. COX IV is a heteromeric complex formed of 13 subunits. The 3 largest subunits which are involved in catalytic core activity, electron transport and proton pumping are encoded by the mtDNA. The remainder of the subunits are encoded in the nuclear DNA and have regulatory or structural functions (reviewed in Kadenbach and Huttemann, 2015). The Y2H screen identified the COX IV subunit Cytochrome c oxidase 6c (COX6C) as a potential interacting partner of C9orf72L. COX6C is a nuclear encoded subunit of COX IV (Lenka et al., 1998), which is inserted into COX IV after the assembly of the catalytic core (Fornuskova et al., 2010). To date no specific function of the COX6C subunit has been identified, however it has been noted to be tightly bound to the catalytic subunits (Kadenbach and Huttemann, 2015). Within the COX IV complex, COX6C spans the IMM, with the N-terminus located in the mitochondrial matrix and the C-terminus in the IMS (Figure 3.3A). The region of COX6C identified in the Y2H screen as interacting with C9orf72 corresponds to the transmembrane and IMS region of COX6C (highlighted in Figure 3.3A).

To validate the interaction between C9orf72 and COX6C, HEK293 cells were co-transfected with pCI-neo empty vector, Myc-C9orf72L, Myc-C9orf72S or Myc-C9orf72DdD and with either pCI-neo empty vector or COX6C-MycDDK. COX6C-MycDDK was immunoprecipitated using anti-FLAG Ab. Myc immunoblot revealed that Myc-C9orf72L co-immunoprecipitated with COX6C-MycDDK. Interestingly Myc-C9orf72S did not co-immunoprecipitate with COX6C-MycDDK. C9orf72S lacks the central DENN and C-terminal dDENN domains found in C9orf72L. Myc-C9orf72DdD, which corresponds to these domains, co-immunoprecipitated with COX6C-MycDDK, thus the DENN and dDENN domains of C9orf72 may be required to mediate the interaction between C9orf72L and COX6C (Figure 3.3B).

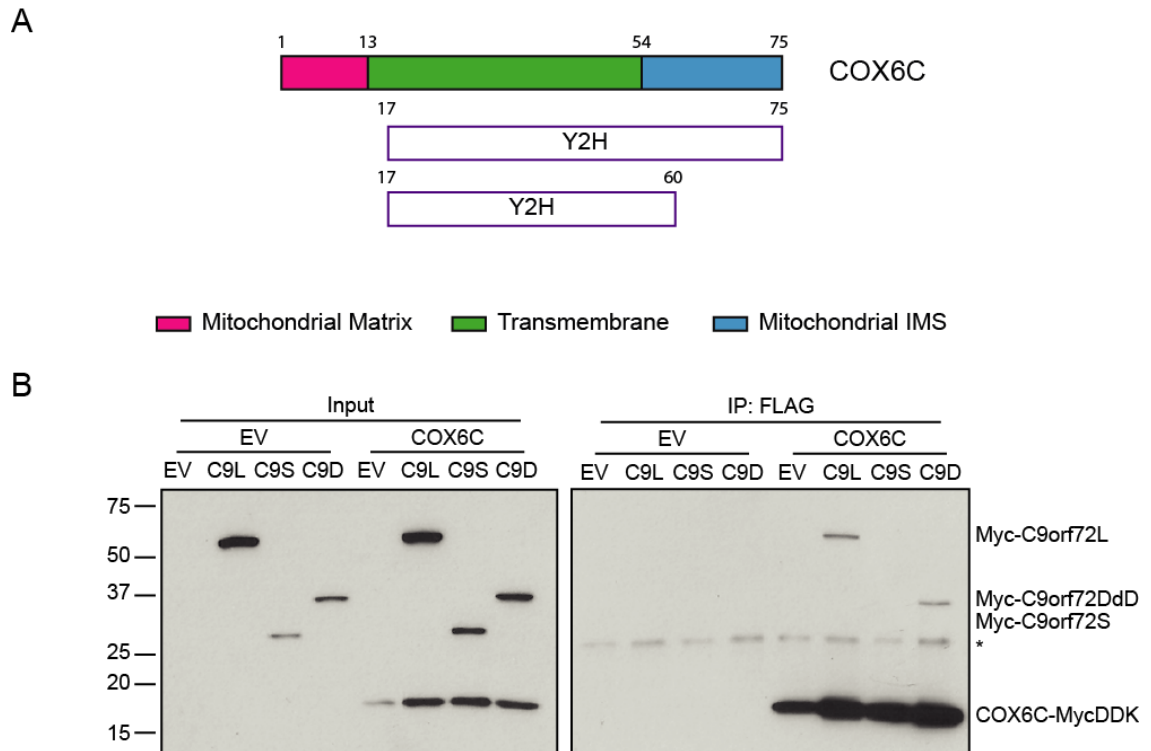


Figure 3.3 C9orf72L and C9orf72DdD but not C9orf72S interact with COX6C

A) The structure of COX6C is shown with the mitochondrial localisation of each domain; the mitochondrial matrix residing N-terminus (pink), transmembrane region (green) and the mitochondrial IMS residing C-terminus (blue). The hits from the C9orf72L Y2H screen are highlighted below. B) HEK293 cells were co-transfected with pCI-neo empty vector (EV), Myc-C9orf72L (C9L), Myc-C9orf72S (C9S) or Myc-C9orf72DdD (C9D) and EV or COX6C-MycDDK and were subjected to immunoprecipitation with anti-FLAG Ab. Immunoprecipitates were subjected to Myc immunoblot. Input represents 5.7 % of lysate subjected to immunoprecipitation. * indicates a band corresponding to Ig light chain.

To further confirm the interaction of C9orf72L with COX6C, proximity ligation assay (PLA) was employed. PLA assesses the proximity of proteins *in situ*, with a signal generated when the two target proteins are 40 nm or less apart (Leuchowius et al., 2011). HeLa cells were co-transfected with pCI-neo empty vector, HA-C9orf72L, HA-C9orf72S or HA-C9orf72DdD and with pCI-neo empty vector or COX6C-MycDDK. To aid in the selection of cells for analysis, transfections were doped with pAcGFP1-Mito. PLA using antibodies against the HA and Myc tags was performed, and the number of PLA puncta in pAcGFP1-Mito positive cells was quantified. There was no significant difference in number of PLA puncta in cells expressing HA-C9orf72L, HA-C9orf72S, HA-C9orf72DdD or COX6C-MycDDK alone compared to empty vector control cells. When compared to cells expressing COX6C-MycDDK alone, cells co-expressing HA-C9orf72L, HA-C9orf72S or HA-C9orf72DdD and COX6C-MycDDK displayed a significant increase in the number of PLA puncta, indicative of proximity of the two proteins *in situ* (Figure 3.4). The increase in PLA puncta in cells co-expressing HA-C9orf72L or HA-C9orf72DdD and COX6C-MycDDK supported the interaction identified in the co-immunoprecipitation assay (Figure 3.3B). Surprisingly, cells expressing HA-C9orf72S and COX6C-MycDDK also showed an increase in PLA puncta number compared to the control cells. Therefore, C9orf72S may also interact with COX6C.

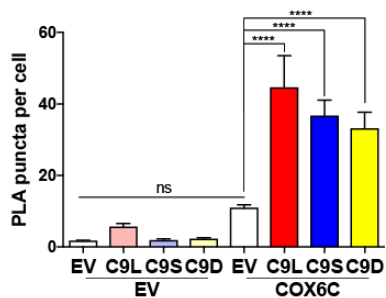
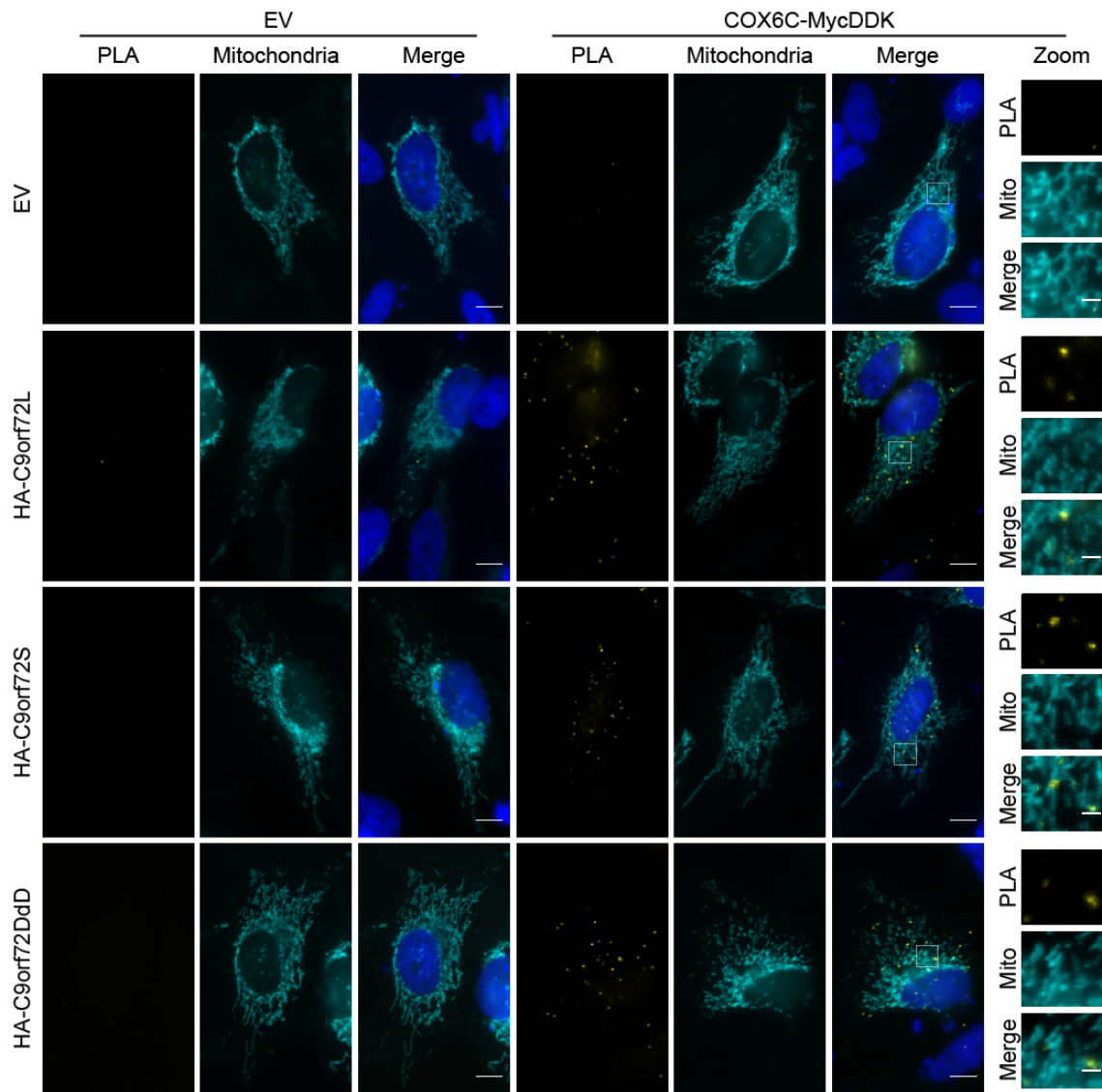


Figure 3.4 C9orf72L, C9orf72S and C9orf72DdD interact with COX6C *in situ*

A) HeLa cells were co-transfected with pCI-neo empty vector (EV), HA-C9orf72L (C9L), HA-C9orf72S (C9S) or HA-C9orf72DdD (C9D) and EV or COX6C-MycDDK. Transfections were doped with pAcGFP1-Mito (cyan) to visualise the mitochondrial network. Cells were subjected to PLA using anti-Myc and anti-HA Ab (yellow). The number of PLA puncta per cell was quantified. Scale bar 10 μ m, zoom 2 μ m. Graph displays mean \pm SEM. Cells were quantified from 3 independent experiments (EV/EV:

116, C9L/EV: 104, C9S/EV: 106, C9D/EV: 106, EV/COX6C: 116, C9L/COX6C: 99, C9S/COX6C: 119, C9D/COX6C: 83 cells). Statistical analysis was performed by one-way ANOVA with Fisher's LSD; **** $P \leq 0.0001$.

3.2.4 ATP Synthase

ATP Synthase (Complex V) is a multi-subunit complex that utilises the proton gradient set up by the electron transport chain complexes I - IV, to generate ATP from ADP and P_i . ATP Synthase is formed of two complexes; the F_1 complex, a catalytic core located in the mitochondrial matrix and the F_0 complex, a proton channel through the IMM (Jonckheere et al., 2012). Several subunits of ATP Synthase were identified as interacting partners of C9orf72. F_0 complex subunit E (ATP5I) was identified as an interactor of C9orf72S in the Y2H screen (Table 3-1). The mass spectrometry screen identified the β subunit of the F_1 complex, ATP5B, as a C9orf72L binding partner (Table 3-2). The mass spectrometry screen also identified ATP5A1 as an interactor of C9orf72L (Table 3-2). ATP5A1 was identified alongside ATP5C1 as an interacting partner of C9orf72 in the subsequently published mass spectrometry screen (Table 3-3) (Blokhuys et al., 2016). ATP5A1 and ATP5C1 encode the F_1 complex subunits α and γ respectively. The subunits of ATP Synthase identified in the Y2H and mass spectrometry screens as potential C9orf72 interacting partners are highlighted in Figure 3.5A.

To confirm the interaction between C9orf72 and ATP Synthase, HEK293 cells were transfected with pCI-neo empty vector, Myc-C9orf72L, Myc-C9orf72S or Myc-C9orf72DdD and subjected to immunoprecipitation with anti-Myc Ab. Immunoprecipitates were probed for endogenous ATP5A, the α subunit of the F_1 complex. Endogenous ATP5A was efficiently co-immunoprecipitated with Myc-C9orf72L, Myc-C9orf72S and Myc-C9orf72DdD (Figure 3.5B).

To further verify the interaction between C9orf72 and ATP Synthase, the reverse co-immunoprecipitation was carried out by immunoprecipitation of endogenous ATP5A. HEK293 cells were transfected with pCI-neo empty vector, Myc-C9orf72L, Myc-C9orf72S or Myc-C9orf72DdD. Endogenous ATP5A was immunoprecipitated with anti-ATP5A Ab. Myc immunoblot revealed that Myc-C9orf72L, but neither Myc-C9orf72S nor Myc-C9orf72DdD co-immunoprecipitated with ATP5A (Figure 3.5C). Together this data showed that C9orf72 interacts with the ATP Synthase complex.

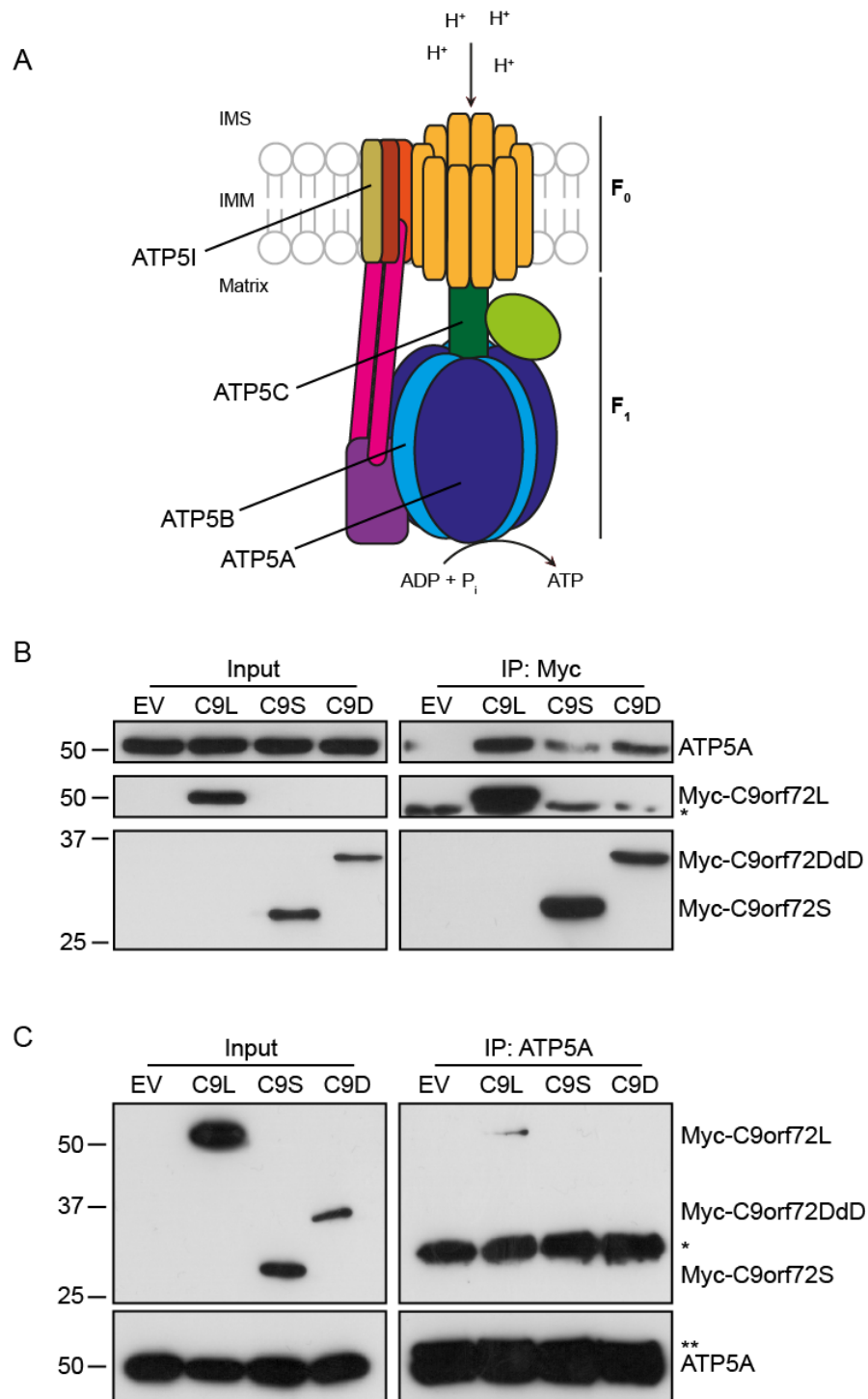


Figure 3.5 C9orf72 interacts with the ATP Synthase complex

A) The structure of the ATP Synthase complex is shown with the potential F_0 and F_1 subunits that may interact with C9orf72 highlighted. B) HEK293 cells were transfected with pCI-neo empty vector (EV), Myc-C9orf72L (C9L), Myc-C9orf72S (C9S) or Myc-C9orf72DdD (C9D) and were subjected to immunoprecipitation with anti-Myc Ab. Immunoprecipitates were probed by ATP5A immunoblot (identical immunoprecipitation sample as probed in Figure 3.6B for TIMM23). Input represents 2 % of lysate subjected

to immunoprecipitation. * indicates a band corresponding to Ig heavy chain. C) HEK293 cells were transfected with pCI-neo empty vector (EV), Myc-C9orf72L (C9L), Myc-C9orf72S (C9S) or Myc-C9orf72DdD (C9D) and were subjected to immunoprecipitation with anti-ATP5A Ab. Immunoprecipitates were probed by Myc immunoblot. Input represents 1 % of lysate subjected to immunoprecipitation. * indicates a band corresponding to Ig light chain. ** indicates a band corresponding to Ig heavy chain.

3.2.5 TIM23 complex

TIMM50 was identified as a potential interacting partner of C9orf72 in both the mass spectrometry screen (Table 3-2) and subsequently in the screen published by the Pasterkamp and Van den Berg (Table 3-3) (Blokhuis et al., 2016). TIMM50 is a subunit of the TIM23 import complex, responsible for the transport of proteins across the IMM into the mitochondrial matrix. The TIMM50 subunit plays a role in recognition of mitochondrial import sequences for proteins destined for the IMM or mitochondrial matrix (Mokranjac and Neupert, 2010) (Figure 3.6A).

The interaction of C9orf72 with the TIM23 complex was investigated by co-immunoprecipitation. HEK293 cells were transfected with pCI-neo empty vector, Myc-C9orf72L, Myc-C9orf72S or Myc-C9orf72DdD and subjected to immunoprecipitation with anti-Myc Ab. TIMM23 immunoblot, a subunit of the TIM23 complex, revealed TIMM23 to co-immunoprecipitate with Myc-C9orf72L, Myc-C9orf72S and Myc-C9orf72DdD (Figure 3.6B).

To further confirm the interaction between C9orf72 and the TIM23 complex, the reverse co-immunoprecipitation was performed. HEK293 cells were transfected with pCI-neo empty vector, Myc-C9orf72L, Myc-C9orf72S or Myc-C9orf72DdD and subjected to immunoprecipitation with anti-TIMM23 Ab. Myc immunoblot revealed that Myc-C9orf72L, but neither Myc-C9orf72S nor Myc-C9orf72DdD co-immunoprecipitated with TIMM23 (Figure 3.6C). Together this showed that C9orf72 interacts with the TIM23 complex.

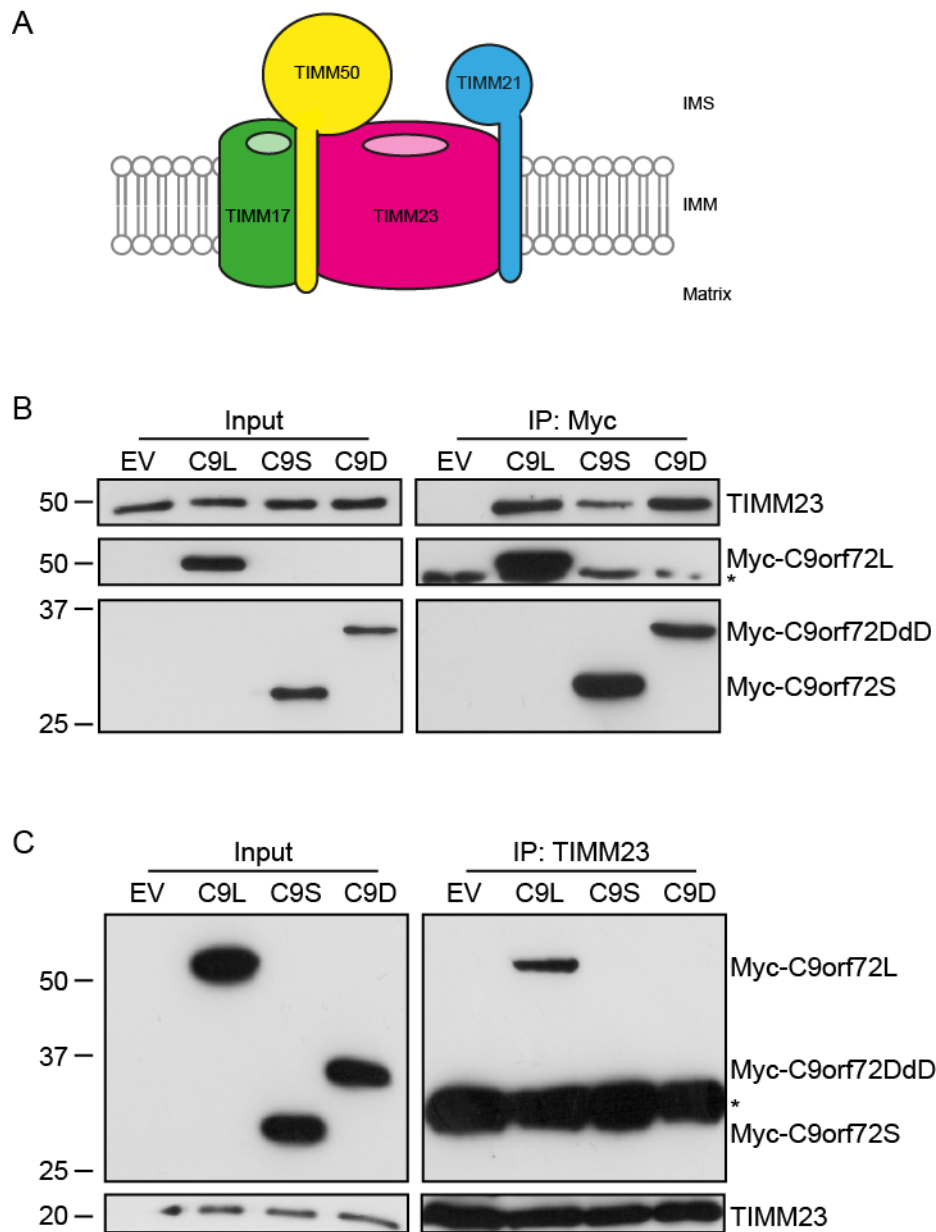


Figure 3.6 C9orf72 interacts with the TIM23 complex

A) Structure of the TIM23 complex is shown with the major subunits indicated. C9orf72 was identified as a potential interactor of the TIMM50 subunit. B) HEK293 cells were transfected with pCI-neo empty vector (EV), Myc-C9orf72L (C9L), Myc-C9orf72S (C9S) or Myc-C9orf72DdD (C9D) and subjected to immunoprecipitation with anti-Myc Ab. Immunoprecipitates were probed by TIMM23 immunoblot (identical immunoprecipitation sample as probed in Figure 3.5B for ATP5A). Input represents 2 % of lysate subjected to immunoprecipitation. * indicates a band corresponding to Ig heavy chain. C) HEK293 cells were transfected with pCI-neo empty vector (EV), Myc-C9orf72L (C9L), Myc-C9orf72S (C9S) or Myc-C9orf72DdD (C9D) and subjected to immunoprecipitation with anti-TIMM23 Ab. Immunoprecipitates were probed by Myc immunoblot. Input represents 1 %

of lysate subjected to immunoprecipitation. * indicates a band corresponding to Ig light chain.

3.3 C9orf72 localises to mitochondria

As C9orf72 interacts with mitochondrial proteins and complexes, we hypothesised that the C9orf72 protein may localise to mitochondria. To begin to investigate if C9orf72 is found on mitochondria, HEK293 cells were transfected with pCI-neo empty vector, Myc-C9orf72L or Myc-C9orf72S and a mitochondrial enriched fraction was produced by centrifugation. The enrichment of mitochondria was verified by immunoblot for the cytosolic protein Tubulin and the mitochondrial protein COX IV. Myc immunoblot revealed that whilst Myc-C9orf72L and Myc-C9orf72S were found in the cytosol/microsome fraction, a proportion of Myc-C9orf72L and Myc-C9orf72S was located in the mitochondrial fraction (Figure 3.7A).

To verify that C9orf72 localised to mitochondria, HEK293 cells were transfected with pCI-neo empty vector, Myc-C9orf72L, Myc-C9orf72S, Myc-C9orf72DdD or Myc-MIRO1, a known OMM protein (Reis et al., 2009), and mitochondria were purified on a discontinuous sucrose gradient, essentially as described in (De Vos et al., 2000). The purity of the mitochondria was tested by Tubulin (cytosol) and MnSOD and COX IV (mitochondria) immunoblot. As expected of an OMM protein, Myc immunoblot showed that Myc-MIRO1 was found in the mitochondrial fraction. Myc immunoblot showed that Myc-C9orf72L, Myc-C9orf72S and Myc-C9orf72DdD were also found in the mitochondrial fraction (Figure 3.7B). Myc-C9orf72L and Myc-C9orf72DdD were more abundant in the mitochondria fraction compared to Myc-C9orf72S. Therefore, the DENN and dDENN domains of C9orf72 may be involved in the localisation of C9orf72 to mitochondria.

As C9orf72DdD was found in the mitochondrial fraction, we hypothesised that the punctate structures seen in Myc-C9orf72DdD expressing cells may be found on mitochondria. To investigate whether the Myc-C9orf72DdD puncta localised to mitochondria, HeLa cells were transfected with pCI-neo empty vector or Myc-C9orf72DdD and immunostained with anti-TOMM20 antibody to visualise the mitochondrial network. Myc-C9orf72DdD puncta appeared to co-localise with the mitochondrial staining (Figure 3.7C). Taken together this data showed that C9orf72 localises to mitochondria.

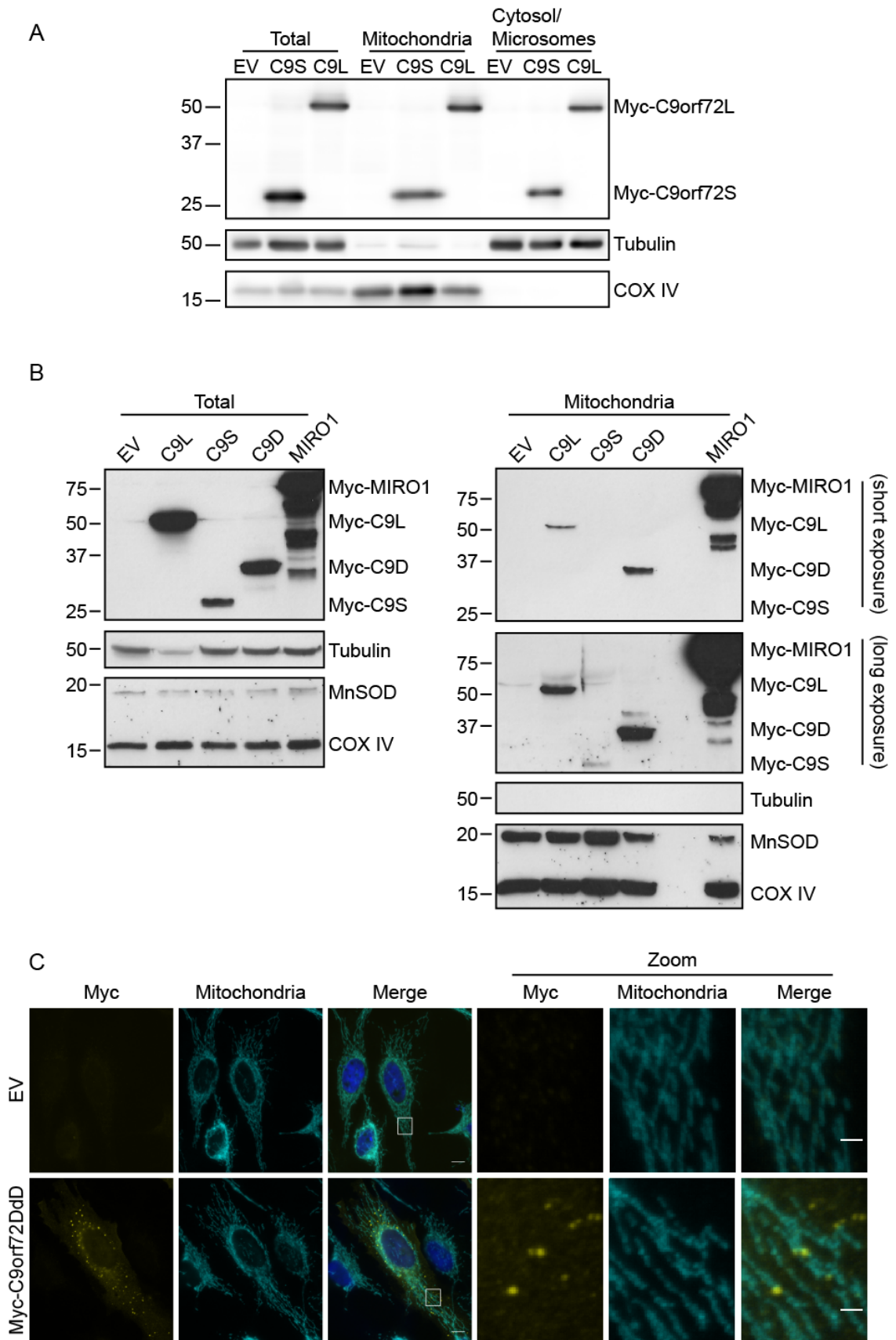


Figure 3.7 Overexpressed C9orf72 localises to mitochondria

A) HEK293 cells were transfected with pCI-neo empty vector (EV), Myc-C9orf72S (C9S) or Myc-C9orf72L (C9L) and mitochondrial enriched fractions were produced. Fractions (15 µg of each fraction) were subjected to Myc, Tubulin (cytosol) and COX IV (mitochondria) immunoblot. B) HEK293 cells were transfected with pCI-neo empty vector (EV), Myc-C9orf72L (C9L), Myc-C9orf72S (C9S), Myc-C9orf72DdD (C9D) or Myc-MIRO1 and mitochondrial enriched fractions were produced and purified by sucrose gradient. Myc-MIRO1 was used as a positive control for the mitochondrial localisation of the Myc-tagged C9orf72 constructs. Mitochondria were subjected to Myc, Tubulin (cytosol), MnSOD and COX IV (mitochondria) immunoblot. Twenty µg of total cell lysate and mitochondrial fractions were subjected to immunoblot. C) HeLa cells were transfected with pCI-neo empty vector (EV) or Myc-C9orf72DdD (yellow) and were subjected to immunostaining with anti-TOMM20 Ab (cyan) to reveal mitochondria. Scale bar 10 µm, zoom 2 µm.

To exclude the possibility that the mitochondrial localisation of Myc-C9orf72 was an artefact of C9orf72 overexpression, the localisation of endogenous C9orf72 protein was investigated. Mitochondria were isolated from HEK293 cells and purified by discontinuous gradient. To verify the identity of the endogenous C9orf72 protein upon C9orf72 immunoblot, mitochondria were also isolated and purified from C9orf72 knockout HEK293 cells (C9orf72^{KO}). Mitochondria were subjected to Tubulin (cytosol), HSP60, TIMM23 and TOMM20 (mitochondria) immunoblot to verify purity. C9orf72 immunoblot revealed C9orf72 to be found in the mitochondrial fraction. The localisation of endogenous C9orf72 in the mitochondrial fraction supported the localisation found with the C9orf72 overexpression constructs and that the latter was not an artefact of overexpression.

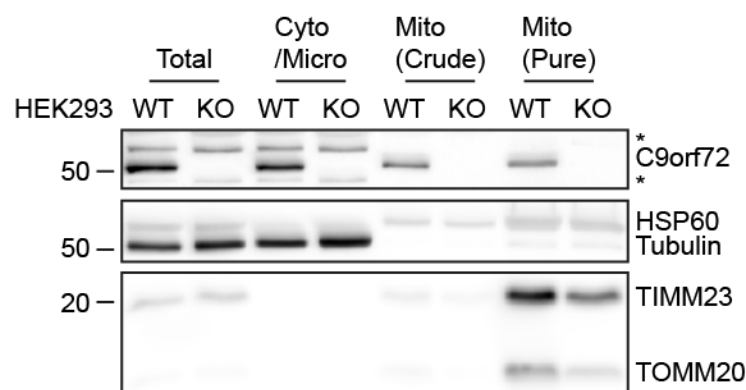


Figure 3.8 Endogenous C9orf72 is located in mitochondria

Mitochondria were isolated and purified from HEK293 (WT) or C9orf72^{KO} (KO) HEK293 cells and were subjected to immunoblotting with endogenous C9orf72 Ab. The

*enrichment of mitochondria was verified by immunoblot for Tubulin (cytosol) and the mitochondrial proteins HSP60 (matrix), TIMM23 (IMM) and TOMM20 (OMM). The cellular fractions subjected to immunoblotting were total cell lysate (total), cytosol and ER/microsomes (Cyto/Micro), crude mitochondria (Mito (Crude)) and purified mitochondria (Mito (Pure)). Fifteen µg of each fraction was subjected to immunoblot. * indicates aspecific bands on C9orf72 immunoblot.*

3.4 Investigating the sub-mitochondrial localisation of C9orf72

Mitochondria are double membraned organelles, comprised of the OMM and IMM. The mitochondrial IMS is located between the OMM and IMM. The mitochondrial matrix is enclosed by the IMM. The mitochondrial compartments each play roles in specific mitochondrial functions and therefore harbour specific mitochondrial proteins (Vogtle et al., 2017). As C9orf72 was found in the mitochondrial fraction (3.3) and interacted with proteins of the IMM (3.2), the mitochondrial sub-compartment to which C9orf72 localises was examined further.

3.4.1 C9orf72 is a peripheral mitochondrial protein

Mitochondrial proteins can be divided into 3 groups: integral, peripheral and soluble proteins. Proteins inserted the IMM or OMM are called integral mitochondrial proteins. Integral proteins include subunits of the TIM/TOM import complexes, COX subunits (Burri et al., 2006; Vogtle et al., 2017) and proteins involved in ER-mitochondrial tethers; such as PTPIP51 (De Vos et al., 2012). Proteins that are not integrated into a mitochondrial membrane but that are also found in or on mitochondria, are either peripheral or soluble mitochondrial proteins. Peripheral mitochondrial proteins are closely associated with the OMM or the IMM and interact with integral mitochondrial proteins, but themselves are not inserted into the mitochondrial membrane. The most characterised peripheral mitochondrial protein is Cytochrome c (Singer, 1974). Finally, the soluble mitochondrial proteins are proteins which do not associate with the mitochondrial membranes. These are found in both the IMS and mitochondrial matrix and include the Tim9-Tim10 chaperone complex of the IMS and the proteins involved in the Krebs cycle in the matrix (Vogtle et al., 2017).

First, we investigated whether C9orf72 is an integral mitochondrial membrane protein. Integral mitochondrial proteins often contain hydrophobic transmembrane domains (Ramasarma, 1996). Online bioinformatics tools can be used to identify potential transmembrane domains in proteins (Moller et al., 2001). Using the TMHMM online bioinformatics tool, the presence of a predicted transmembrane domain in C9orf72 was

investigated. TMHMM analysis of C9orf72 did not predict the presence of a transmembrane domain (Figure 3.9), suggesting that C9orf72 was unlikely to be an integral mitochondrial protein.

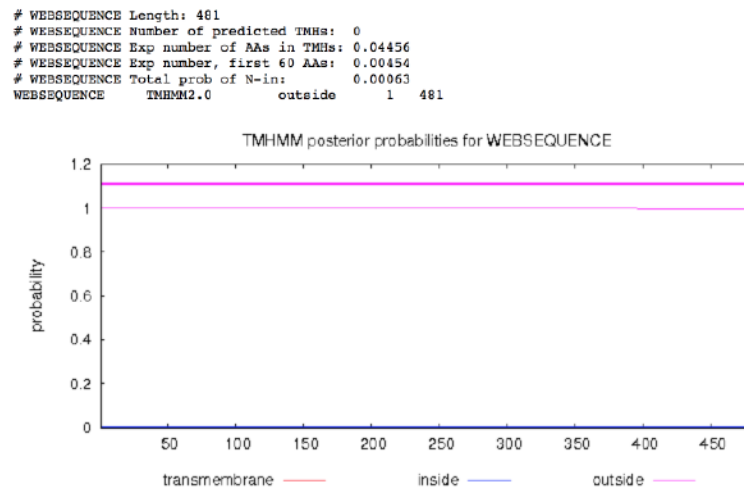


Figure 3.9 C9orf72 is not predicted to contain a transmembrane domain

The C9orf72 protein was analysed for the presence of possible transmembrane domains using the TMHMM platform. C9orf72 was not predicted to contain any transmembrane regions.

To experimentally determine whether C9orf72 is an integral or peripheral/soluble mitochondrial protein, alkaline extraction was performed on mitochondria. Alkaline pH decreases noncovalent interactions between proteins. This results in the release of peripheral and soluble but not integral mitochondrial proteins from mitochondria (Fujiki et al., 1982; Kim et al., 2015b). Mitochondria were purified from Flp-In FLAG-C9orf72L HEK293 cells which were induced to express FLAG-C9orf72L. Purified mitochondria were subjected to alkaline extraction. The purity of the mitochondria was verified by Tubulin immunoblot. Mitochondria were subjected to immunoblot for known integral mitochondrial proteins TOMM20, PTPIP51, TIMM23 and COX IV, the peripheral mitochondrial protein Cytochrome c, and the soluble mitochondrial matrix proteins MnSOD and HSP60 (Figure 3.10). As expected, the integral mitochondrial proteins were not affected by alkaline extraction, whereas the peripheral mitochondrial protein Cytochrome c and the soluble mitochondrial protein MnSOD were extracted from the mitochondria. FLAG immunoblot revealed FLAG-C9orf72L to also be removed from the mitochondria following alkaline extraction. Together this data showed that C9orf72L was either a peripheral or soluble mitochondrial protein. As C9orf72 interacts with mitochondrial proteins and complexes of the IMM (3.2), C9orf72 is a peripheral mitochondrial protein.

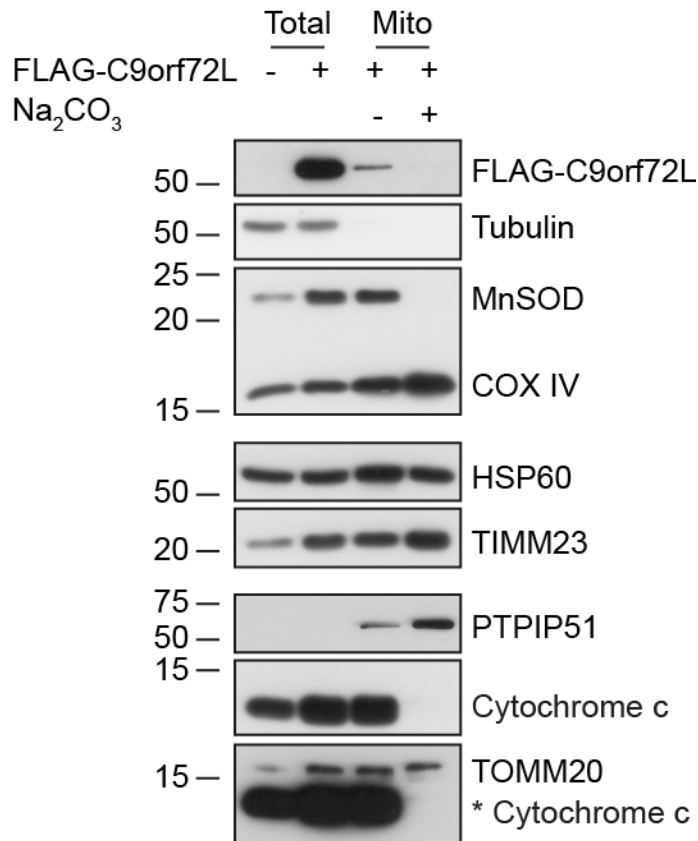


Figure 3.10 C9orf72L is a peripheral mitochondrial protein

Purified mitochondria (mito) from Flp-In FLAG-C9orf72L HEK293 cells were subjected to alkaline extraction (Na₂CO₃). Mitochondria were immunoblotted with Ab against FLAG, Tubulin (cytosol) and the mitochondrial proteins PTPIP51 (OMM), TOMM20 (OMM), Cytochrome c (IMS), TIMM23 (IMM), COX IV (IMM), HSP60 (matrix), MnSOD (matrix). Fifteen µg of total cell lysate and mitochondrial fractions were subjected to immunoblot. * indicates Cytochrome c from previous immunoblot upon TOMM20 immunoblot.

3.4.2 C9orf72 is localised in the mitochondrial intermembrane space

Peripheral mitochondrial proteins may be associated with the OMM and be located in the cytosol or IMS. Peripheral protein may also interact with the IMM, these proteins are located in the IMS or mitochondrial matrix. As C9orf72 interacts with proteins and complexes of the IMM (3.2), we hypothesised that C9orf72 is located either in the IMS or the mitochondrial matrix. To determine whether C9orf72 resides in the IMS, mitochondria were subjected to sequential permeabilisation of the OMM and digestion of cytosol exposed proteins.

The OMM and IMM display differing susceptibility to digitonin permeabilisation owing to their differing cholesterol content (Cheng and Kimura, 1983; Frenkel et al., 2014). This

property can be exploited to assess the localisation of proteins to the IMS (Ryan et al., 2001). Proteinase K is a broad-spectrum proteinase (Ebeling et al., 1974). Treatment of mitochondria with Proteinase K results in the digestion of cytosol exposed proteins. When mitochondria are intact, only OMM proteins are exposed to the cytosol and are hence digested by Proteinase K. However, upon digitonin permeabilisation of the OMM, both IMS and IMM IMS facing proteins are exposed to the cytosol and are therefore also digested by Proteinase K (Ryan et al., 2001). Before investigating the localisation of the C9orf72 protein, the conditions for digitonin permeabilisation of the OMM and the digestion of mitochondrial proteins with Proteinase K were optimised.

The Proteinase K mediated digestion of mitochondrial proteins was optimised by investigating the digestion of the OMM protein Mfn1. Mitochondria were isolated from rat liver and subjected to digestion with Proteinase K. To optimise the conditions for Proteinase K digestion, 2 mg/mL and 0.2 mg/mL Proteinase K were tested. The serine protease inhibitor Phenylmethylsulfonyl fluoride (PMSF) was used to inhibit Proteinase K activity. The conditions for PMSF inhibition of Proteinase K were simultaneously optimised with 2 μ M, 20 μ M and 2 mM PMSF tested. In order to verify that any degradation of Mfn1 protein was due to the activity of Proteinase K, samples were also treated with PMSF prior to Proteinase K addition to inhibit protease activity. Mitochondria were subject to Mfn1 (OMM), MnSOD (matrix) and COX IV (IMM) immunoblot (Figure 3.11). As an OMM protein protruding into the cytosol, Mfn1 should be degraded upon Proteinase K treatment. In contrast, COX IV and MnSOD are located within mitochondria and therefore should not be degraded upon Proteinase K treatment in intact mitochondria. Treatment of mitochondria with 2 mg/mL Proteinase K resulted in the digestion of Mfn1 (Figure 3.11, lanes 3 – 8). Prior treatment of mitochondria with 2 mM (Figure 3.11, lane 7), but neither 2 μ M nor 20 μ M (Figure 3.11, lanes 3 and 5) PMSF was sufficient to inhibit Proteinase K activity. Although, treatment of mitochondria with 0.2 mg/mL Proteinase K resulted in the digestion of Mfn1, for the same incubation period this was reduced markedly from the 2 mg/mL Proteinase K mediated digestion (Figure 3.11, lanes 9 – 12). Therefore, 2 mg/mL Proteinase K and 2 mM PMSF were selected for characterisation of the mitochondrial localisation of C9orf72.

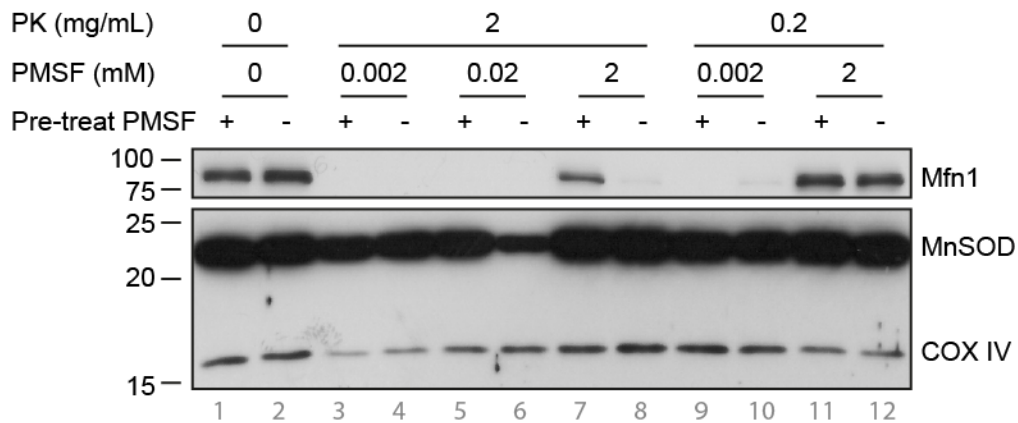


Figure 3.11 Optimisation of Proteinase K and PMSF conditions

Mitochondria were isolated from rat liver and subjected to Proteinase K (PK) digestion. Mitochondria were treated with either 2 mg/mL (lanes 3 – 8) or 0.2 mg/mL (lanes 9 – 12) PK. To inhibit the activity of PK, mitochondria were incubated with 2 μ M (lanes 3, 4, 9, 10), 20 μ M (lanes 5, 6) and 2 mM (lanes 7, 8, 11, 12) PMSF. Mitochondria were also incubated with PMSF prior to the incubation with PK to inhibit PK activity and prevent digestion of OMM proteins (pre-treat, lanes 1, 3, 5, 7, 9 and 11). Mitochondria were subjected to Mfn1 (OMM), MnSOD (matrix) and COX IV (IMM) immunoblot. Fifteen μ g of mitochondria was subjected to immunoblot.

To optimise the permeabilisation of the OMM using digitonin, mitochondria were extracted from rat liver and were permeabilised with increasing amounts of digitonin per μ g of mitochondria. The previously optimised conditions for Proteinase K digestion of mitochondrial proteins was used to digest cytosol exposed proteins. Mitochondria were subjected to immunoblot to reveal Proteinase K mediated digestion of PTPIP51 (OMM) and TIMM23 (IMS facing IMM). IMM integrity was verified by MnSOD and HSP60 (matrix), and COX IV and ATP5A (matrix facing IMM) immunoblot (Figure 3.12). In unpermeabilised mitochondria, Proteinase K digested only the OMM protein PTPIP51 (Figure 3.12, lane 2). Permeabilisation of the OMM with 0.5 μ g digitonin / μ g mitochondria resulted in the Proteinase K digestion of both PTPIP51 and TIMM23 (Figure 3.12, lane 4). The digestion of TIMM23 by Proteinase K indicated that the OMM was successfully permeabilised. Permeabilisation of the OMM with 1 μ g digitonin / μ g mitochondria similarly resulted in the degradation of TIMM23 upon Proteinase K treatment. However, levels of the matrix protein MnSOD were also reduced by Proteinase K treatment suggesting that IMM integrity may have been affected (Figure 3.12, lane 6). Permeabilisation of the OMM with 2 μ g digitonin / μ g mitochondria led to loss of MnSOD, in both Proteinase K untreated and treated mitochondria, again suggesting the loss of IMM integrity (Figure 3.12, lanes 7 and 8). Permeabilisation of the

OMM with 4 μg digitonin / μg mitochondria led to loss of PTPIP51 from the mitochondria in the absence of Proteinase K treatment, indicating that the OMM may have been removed from the mitochondria (Figure 3.12, lane 9). Indeed, digitonin treatment of mitochondria can also be employed to separate mitoplasts (IMM and matrix) from the OMM (Nishimura and Yano, 2014). Furthermore, the loss of MnSOD and the vulnerability of COX IV, ATP5A and HSP60 to Proteinase K digestion showed that IMM integrity was compromised (Figure 3.12, lane 10). Hence a concentration of 0.5 μg digitonin / μg mitochondria was selected for permeabilisation of the OMM, as it was found to result in the permeabilisation of the OMM without affecting the integrity of the IMM.

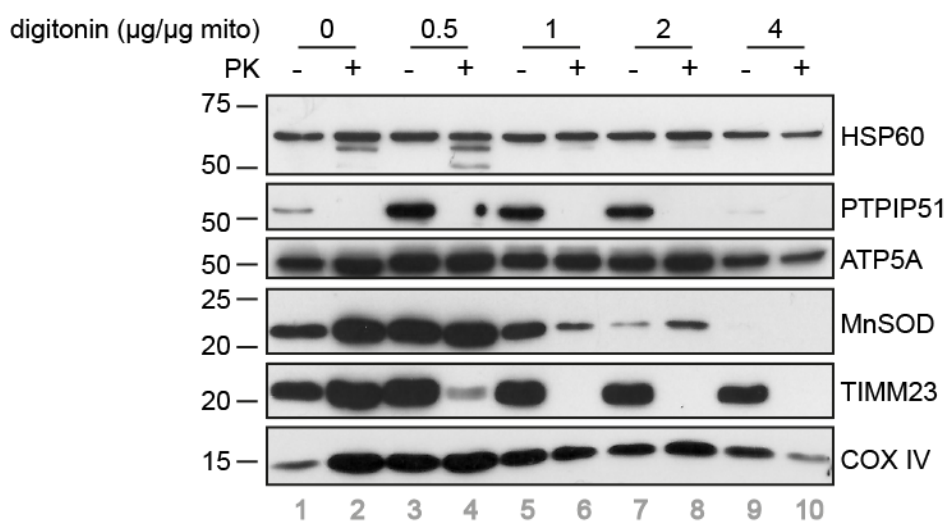


Figure 3.12 Optimisation of digitonin permeabilisation of the OMM

Mitochondria were isolated from rat liver and were subjected to the sequential permeabilisation of the OMM with digitonin and the digestion of cytosol exposed proteins with Proteinase K (PK). To optimise the permeabilisation of the OMM, 4 concentrations of digitonin were tested: 0.5 μg digitonin / μg mitochondria (lanes 3, 4), 1 μg digitonin / μg mitochondria (lanes 5, 6), 2 μg digitonin / μg mitochondria (lanes 7, 8) and 4 μg digitonin / μg mitochondria (lanes 9, 10). Mitochondria were subjected to PTPIP51 (OMM), TIMM23 (IMM, IMS facing), ATP5A (IMM, matrix facing), COX IV (IMM, matrix facing), HSP60 (matrix) and MnSOD (matrix) immunoblot. Twelve μg of mitochondria was subjected to immunoblot.

To investigate whether C9orf72 resided in the mitochondria IMS or matrix, mitochondria were purified from induced Flp-In FLAG-C9orf72L HEK293 cells. The purity of the mitochondria was verified by Tubulin immunoblot. The purified mitochondria were subjected to OMM permeabilisation with digitonin and the subsequent digestion of

cytosol exposed proteins with Proteinase K. Mitochondria were subjected to immunoblot for the mitochondrial proteins PTPIP51 and TOMM20 (OMM), Cytochrome c (IMS), TIMM23 (IMM, IMS facing) and COX IV (IMM, matrix facing), MnSOD and HSP60 (matrix). FLAG-C9orf72L was revealed by FLAG immunoblot. In unpermeabilised mitochondria, Proteinase K digested the OMM proteins PTPIP51 and TOMM20, but did not digest the proteins of the IMS, IMM or matrix. FLAG immunoblot revealed that FLAG-C9orf72L was similarly not digested by Proteinase K. Thus in intact cells, C9orf72L is not found on the OMM and is found in either the IMS or matrix. Permeabilisation of the OMM with digitonin resulted in the digestion of the OMM proteins PTPIP51 and TOMM20 and the IMS facing IMM protein TIMM23 by Proteinase K. In contrast, the matrix facing IMM protein COX IV and the matrix protein HSP60 were not digested by Proteinase K in OMM permeabilised mitochondria. FLAG immunoblot revealed that FLAG-C9orf72L was digested by Proteinase K upon permeabilisation of the OMM (Figure 3.13). Therefore, C9orf72L is found in the mitochondrial IMS.

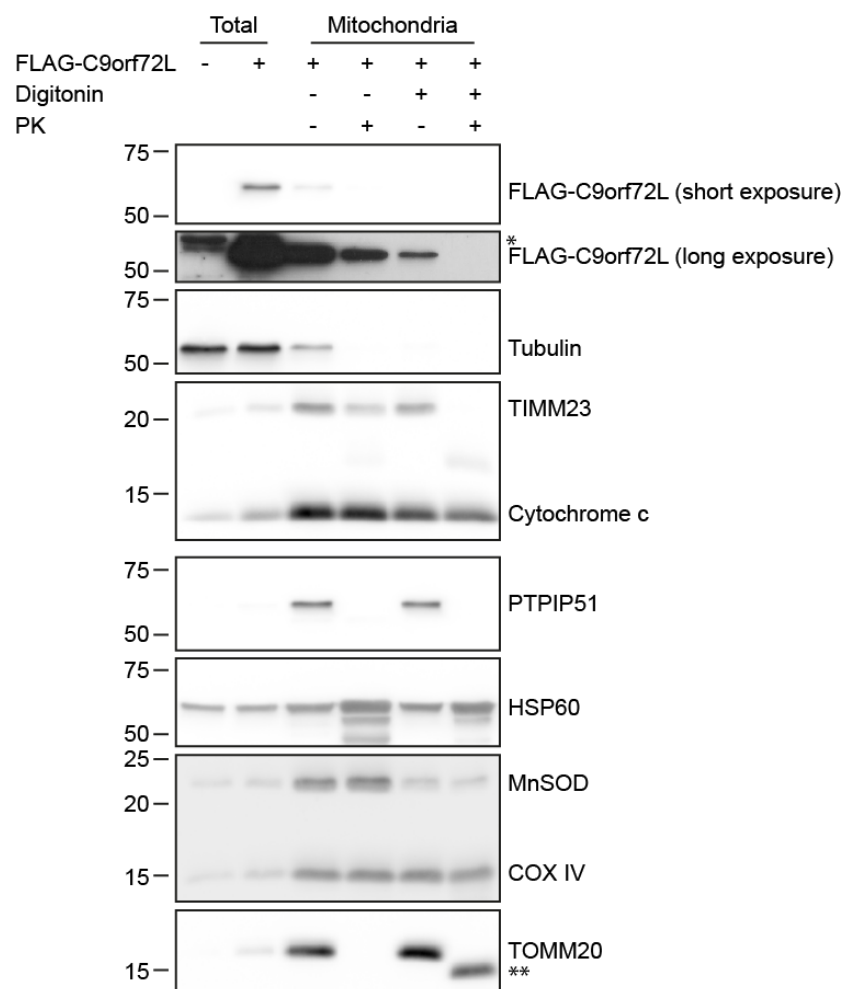


Figure 3.13 C9orf72L resides in the mitochondrial IMS

*Mitochondria were purified from induced Flp-In FLAG-C9orf72L HEK293 cells and were subjected to sequential permeabilisation of the OMM with digitonin and degradation of cytosol exposed proteins with Proteinase K (PK). Mitochondria were subjected to FLAG, Tubulin (cytosol), PTPIP51 (OMM), TOMM20 (OMM), Cytochrome c (IMS), TIMM23 (IMM, IMS facing), COX IV (IMM, matrix facing), HSP60 (matrix) and MnSOD (matrix) immunoblot. * indicates an aspecific band on FLAG immunoblot. Fifteen µg of total cell lysate and mitochondrial fractions were subjected to immunoblot. ** indicates a TOMM20 cleavage product.*

3.5 Targeting C9orf72 to the mitochondrial intermembrane space

The majority of mitochondrial proteins are encoded by the nuclear genome and are synthesised in the cytosol. These proteins are then targeted to mitochondria and transported into their specific mitochondrial sub-compartment (reviewed in Dudek et al., 2013). IMS proteins are classified into three categories according to the mechanism by which they are imported; Class I, II and III (reviewed in Herrmann and Hell, 2005; Herrmann and Riemer, 2012). These mechanisms were initially identified and characterised in yeast but are conserved in mammals. The mechanism by which C9orf72 localises to the IMS was investigated in the final section of this chapter.

3.5.1 Class I IMS protein import

The precursors of Class I IMS proteins harbour an N-terminal targeting sequence and are imported into the mitochondria through the TOM complex into the IMS. Once in the IMS, the N-terminal sequence is recognised by the TIM23 complex and the precursor is directed towards import through the IMM. A second hydrophobic internal sequence results in the arrest of partially imported proteins in TIM23. The arrested proteins are translocated laterally into the IMM. The N-terminal mitochondrial targeting sequence, located in the mitochondrial matrix, is cleaved by mitochondria processing peptidase. The IMP or Pcp1 proteases of the IMS cleave the precursor protein on the IMS side of the IMM, resulting in the release of the C-terminal portion of the protein into the IMS. Class I IMS proteins can be both large and highly folded due to the import being partially driven by TIM23 complex activity (Figure 3.14) (reviewed in Herrmann and Hell, 2005). Proteins that localise to the IMS using this mechanism include the pro-apoptotic proteins Smac/DIABLO and apoptosis-inducing factor, and the mitochondrial fusion protein OPA1 (Burri et al., 2005; Herlan et al., 2003; Sesaki et al., 2003).

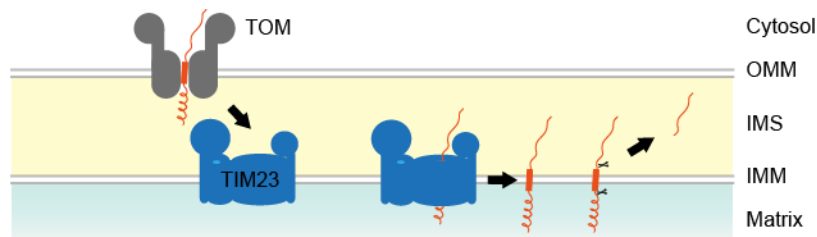


Figure 3.14 Class I IMS protein import

Class I IMS proteins are imported through the TOM complex and undergo partial translocation through the TIM23 complex. Arrested preproteins are transferred laterally into the IMM. Pre-sequences are cleaved in the matrix and proteolytic cleavage on the IMS side of the IMM releases the protein into the IMS.

To investigate whether C9orf72 may be imported by the Class I mechanism, C9orf72 was screened for a predicted N-terminal mitochondrial sequence using the MitoMiner 4.0 platform (Smith and Robinson, 2016). The MitoMiner platform queried 4 separate mitochondrial targeting prediction tools; iPSORT (Bannai et al., 2002), TargetP (Emanuelsson et al., 2000; Petersen et al., 2011), MitoProt (Claros, 1995) and MitoFates (Fukasawa et al., 2015), for a mitochondrial targeting sequence in C9orf72. These prediction tools predict the presence mitochondrial targeting sequences based on the amino acid composition of the N-terminal portion of the input sequence. MitoMiner 4.0 did not identify a mitochondrial targeting sequence in C9orf72 (Table 3-4). Hence, the import of C9orf72 into the IMS is not likely to occur through the Class I mechanism.

Table 3-4 C9orf72 is not predicted to contain a mitochondrial targeting sequence

Protein MTS

2 Proteins											
Primary Accession	Protein Name	Organism	Length	Mito Targeting Seq iPSORT	Mito Targeting Seq TargetP	Mito Targeting Seq TargetP confidence	Mito Targeting Seq MitoProt	MitoProt Cleavage prediction	Mito Targeting Seq MitoFates	MitoFates Cleavage prediction	
Q96LT7	Guanine nucleotide exchange C9orf72	H. sapiens	481 FASTA...	0.0	0.158	_3	0.0373	0.0	0.0	43(MPP)	
Q96LT7-2	Guanine nucleotide exchange C9orf72	H. sapiens	222 FASTA...	0.0	0.158	_3	0.0373	0.0	0.0	43(MPP)	

MitoMiner 4.0 did not predict the presence of a mitochondrial targeting sequence in C9orf72.

3.5.2 Class II IMS protein import

The Class II IMS import mechanism takes advantage of the oxidative environment of the IMS and results in the entrapment of imported proteins through the stabilisation of protein structure via the generation of intramolecular disulphide bonds (reviewed in Backes and Herrmann, 2017; Dudek et al., 2013; Herrmann and Hell, 2005; MacPherson and Tokatlidis, 2017; Schmidt et al., 2010). Class II IMS proteins lack N-terminal cleavable mitochondrial presequences but frequently contain internal cysteine motifs. A twin pair of 2 cysteine residues separated by 3 amino acids (CXXXC) forms the basis of the internal motif and is found in many small TIM and COX proteins (Lutz et al., 2003). Larger Class II IMS proteins with an expanded twin cysteine (CX₉C) motif have been identified (reviewed in Hell and Neupert, 2008; Longen et al., 2009). However, more recently a group of proteins lacking internal cysteine motifs, but which are nevertheless imported into the IMS by the Class II mechanism have been identified. These proteins are rich in cysteine residues and similarly undergo disulphide bond mediated structural changes (Nuebel et al., 2016).

Class II IMS proteins undergo import through the TOM complex whilst the preprotein is in a reduced state (Kurz et al., 1999; Lu et al., 2004; Müller et al., 2008). Once in the IMS, the precursor is folded by the MIA40/ERV1 disulphide relay pathway, that was initially described in yeast (Chacinska et al., 2004; Naoé et al., 2004; Terziyska et al., 2005). Briefly, the imported protein interacts with mitochondrial intermembrane space import and assembly protein 40 (MIA40), with which it forms an intermolecular disulphide bond. The formation of the disulphide bond between precursor and MIA40 results in the reduction of cysteine residues in MIA40. The reduced -SH bonds in cysteines in the imported protein then form intramolecular disulphide bridges, resulting in a structural conformational change in the protein. The structural change results in entrapment of the protein in the IMS. To re-oxidise the cysteine residues in MIA40, MIA40 interacts with Growth factor augments of liver regeneration (ERV1). ERV1 accepts electrons from MIA40 which are then transferred to Cytochrome c and onwards to the electron transport chain. Hence a disulphide relay chain is generated (Figure 3.15) (reviewed in MacPherson and Tokatlidis, 2017). The MIA40/ERV1 pathway is conserved in mammals. The mammalian homologue of MIA40 is coiled-coil-helix-coiled-coil domain 4 (CHCHD4) (Hofmann et al., 2005). The ERV1 mammalian homologue is augments of liver regeneration (ALR), which acts in a similar way to ERV1, and restores the disulphide bond in CHCHD4 (reviewed in Giorda et al., 1996; Hell and Neupert, 2008). Similarly, the binding of imported proteins to co-factors also leads to entrapment of proteins into the IMS (Figure 3.15). The IMS protein SOD1 is imported into the IMS

where it interacts with copper chaperones for SOD (CCS) via an intermolecular disulphide bond. SOD1 subsequently binds copper which results in the formation of an intramolecular disulphide bond in SOD1 and its release from CCS (Kawamata and Manfredi, 2010). The structural change in copper-bound SOD1 results in its entrapment and localisation to the IMS.

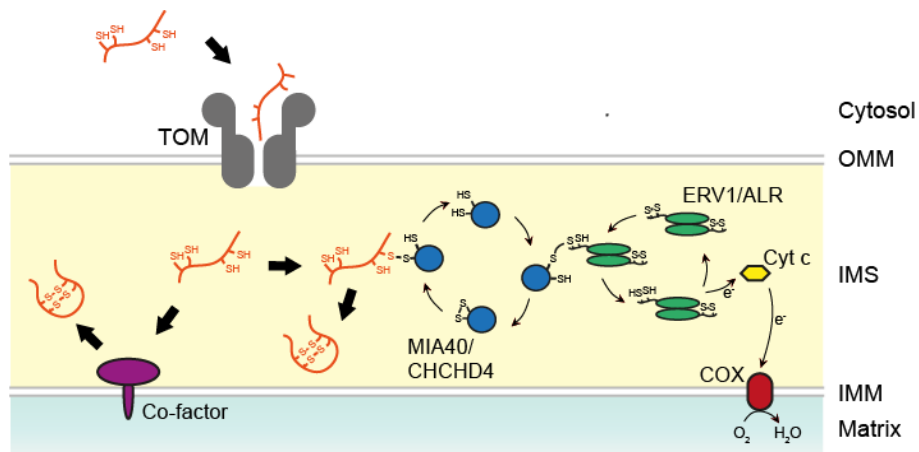
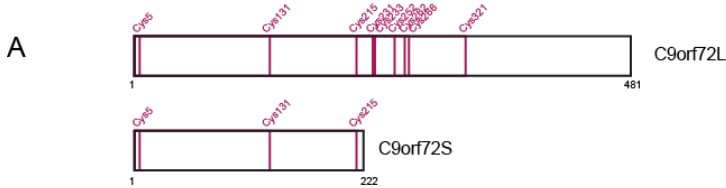


Figure 3.15 Class II IMS protein import

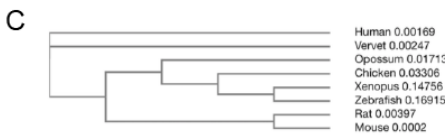
Class II IMS proteins undergo oxidative folding mediated by co-factors or the MIA40/ERV1 (CHCHD4/ALR) disulphide relay. The formation of structural changes in the imported protein through the formation of intramolecular disulphide bonds results in the entrapment of the protein in the IMS.

To begin to investigate if C9orf72 may be imported by the Class II mechanism, first the sequence of C9orf72 was examined for the presence of a cysteine motif or the presence of conserved cysteine residues. C9orf72L and C9orf72S contain 9 and 3 cysteine residues respectively (Figure 3.16A). The amino acid sequence of C9orf72 does not contain a twin cysteine motif, indicating that it may not be a classical Class II IMS protein. However, Clustal O alignment of the C9orf72 protein sequence with the C9orf72 protein of other species, revealed that the cysteine residues of C9orf72 are evolutionally conserved (Figure 3.16B, C). The conservation of the cysteine residues in C9orf72 may hint that disulphide bonds play an important role in the structure or function of the C9orf72 protein.



B

Human	MSTLCPPSPAVAKTEIALSGKSPFLAATPAYWDNILGPRVRHIWAPKTEQV-LLSDGGEI	59
Vervet	MSTLCPPSPAVAKTEIALSGESPLAATPAYWDNILGPRVRHIWAPKTEQV-LLSDGGEI	59
Opossum	MSTLCPPSPAVAKTEIALNGDSPLAATPAYWDNILGPRVRHIWAPKQQL-LLSDGGEI	59
Rat	MSTLCPPSPAVAKTEIALSGESPLAATPAYWDNILGPRVRHIWAPKTDQV-LLSDGGEI	59
Mouse	MSTICPPSPAVAKTEIALSGESPLAATPAYWDNILGPRVRHIWAPKTDQV-LLSDGGEI	59
Chicken	MSALCPPSPAVAKTEISMNGESPLAATPAYWDNILGPRVRHIWAPKTDQV-LLSDGGEI	59
Xenopus	MANLCPPSPAVAKTLISIDGYSPLAATPAYWDNILGPRVRHIWSPKSDHV-LLSDGGEI	59
Zebrafish	MSSACPPQSPAVAKTEVLVDDCCPLAATPAYWDNILGPRVRHIWAPKSGQLLLSDGGEV	60
	*: ***** : ... :*****:*****:*****:*****:*****:*****:	
Human	TFLANHTLNGEILRNAESGAIDVKFFVLSEKGVIIIVSLIPDGNWNGDRSTYGLSIIIPQT	119
Vervet	TFLANHTLNGEILRNAESGAIDVKFFVLSEKGVIIIVSLIPDGNWNGDRSTYGLSIIIPQT	119
Opossum	TFLANHTLNGEILRNAESGAIDVKFFVLSEKGVIIIVSLIPDGNWNGDRSTYGLSIIIPQS	119
Rat	TFLANHTLNGEILRNAESGAIDVKFFVLSEKGVIIIVSLIPDGNWNGDRSTYGLSIIIPQT	119
Mouse	TFLANHTLNGEILRNAESGAIDVKFFVLSEKGVIIIVSLIPDGNWNGDRSTYGLSIIIPQT	119
Chicken	TFLANHTLNGEILRNAESGAIDVKFFVLSEKGVIIIVSLIPDGNWNGDRSTYGLSIIIPQS	119
Xenopus	TFLANHTLNGEILRNAESGAIDVKFFVLSEKGVIIIVSLIPDGNWNGDRSTYGLSIIIPQS	119
Zebrafish	TFLANHTLNGEILRSAESGAVDKFFVLSEKGVIIIVSLIPDGLKGDKNKTCALSIIIPQS	120
	*****:*****:*****:*****:*****:*****:*****:*****:*****:*****:	
Human	ELSFYLP LHRVGVDRDLTHIIRKGRIMHKKERQENVQKIILE--GTERMEDQGSIIIPML	176
Vervet	ELSFYLP LHRVGVDRDLTHIIRKGRIMHKKERQENVQKIILE--GTERMEDQGSIIIPML	176
Opossum	ELSFYLP LHRVGVDRDLTHIIRKGRIMHKKERQENVQKIVLE--GTERMEDQGSIIIPML	176
Rat	ELSFYLP LHRVGVDRDLTHIIRKGRIMHKKERQENVQKIVLE--GTERMEDQGSIIIPML	176
Mouse	ELSFYLP LHRVGVDRDLTHIIRKGRIMHKKERQENVQKIVLE--GTERMEDQGSIIIPML	176
Chicken	ELAFYLP LHRVGVDRDLTHIIRKGRIMHKKERQENVQKIVLE--GTERMEDQGSIIIPML	176
Xenopus	ELAFYLP LHRVGVDRDLTHIIRKGRIMHKKERQENVQKIVLE--GTERMEDQGSIIIPML	179
Zebrafish	ELSFYLP LHRVGVDRDLTHIIRKGRIMHKKERQENVQKIVLE--GTERMEDQGSIIIPML	157
	**:	
Human	TGEVI PVMELLSMKSHSVPEEIDIDTVLNDDDDIGDSCHEGFLLNAISSHLQTCGCSVV	236
Vervet	TGEVI PVMELLSMKSHSVPEEIDIDTVLNDDDDIGDSCHEGFLLNAISSHLQTCGCSVV	236
Opossum	TGEVI PVMELLSMKSHSVPEEINISDTVLNDDDDIGDSCHEGFLLNAISSHLQTCGCSVV	236
Rat	TGEVI PVMELLSMRSHSVPEEDLIDTVLNDDDDIGDSCHEGFLLNAISSHLQTCGCSVV	236
Mouse	TGEVI PVMELLSMKSHSVPEEIDIDTVLNDDDDIGDSCHEGFLLNAISSHLQTCGCSVV	236
Chicken	TGEVI PVMELLSMKSHSVPEEIDISDTVLNDDDDIGDSCHEGFLLNAISSHLQTCGCSVV	236
Xenopus	TGEVI PIMELLSIKSHGVPEEIDITSTVLNDDDDIGDSCHEGFLLINTICNLLKVVCRVM	239
Zebrafish	SSEIVPIMELLSMKSHSVPEEVDLKDITVLNDDDDIGDSCHEDFLHKAISSHLQTCGCSMV	217
	:*:	
Human	VGSS--AEKVNKIVRTLCLFLTPAERKCSRLCAESSFKYESGLFVQGLLKDSTGSPVLP	294
Vervet	VGSS--AEKVNKIVRTLCLFLTPAERKCSRLCAESSFKYESGLFVQGLLKDSTGSPVLP	294
Opossum	VGSS--ADKVNKIVRTLCLFLTPSERKCSRLCRNESSFKYESGLFVQGLLKDSTGSPVLP	294
Rat	VGSS--AEKVNKIVRTLCLFLTPAERKCSRLCAESSFKYESGLFVQGLLKDSTGSPVLP	294
Mouse	VGSS--AEKVNKIVRTLCLFLTPAERKCSRLCAESSFKYESGLFVQGLLKDSTGSPVLP	294
Chicken	VGSS--AEKVNKIVRTLCLFLTPSERKCSRLCRNESSFKYESGLFVQGLLKDSTGSPVLP	294
Xenopus	GWRNIENSLSRMVRTCLFLSPTERKCSRLCRSESSFKYESGLFVQGLLKDSTGSPVLP	299
Zebrafish	VGSN--PEKVNKIVRTLCLFLTPAERKCSRLCHPDGSKFYDGLFVQGLLKDSTGSPVLP	275
	. :*:	
Human	FRQVMYAPYPTTHIDVDVNTVKQMPPCHEHIYNQRRYMRSELTAFWRATSEEDMAQDTII	354
Vervet	FRQVMYAPYPTTHIDVDVNTVKQMPPCHEHIYNQRRYMRSELTAFWRATSEEDMAQDTII	354
Opossum	FRQVMYAPYPTTHIDVDVNTVKQMPPCHEHIYNQRRYMRSELTAFWRATSEEDVAQDTII	354
Rat	FRQVMYAPYPTTHIDVDVNTVKQMPPCHEHIYNQRRYMRSELTAFWRATS-EDMAQDTII	353
Mouse	FRQVMYAPYPTTHIDVDVNTVKQMPPCHEHIYNQRRYMRSELTAFWRATSEEDMAQDTII	354
Chicken	FRQVMYAPYPTTHIDVDVNTVKQMPPCHEHIYNQRRYMRSELTAFWRANSDEEMQDAII	354
Xenopus	FRQVMYAPYPTTHIDVDVNTVKQMPPCHEHIYNQRRYMRSELTAFWRANSDEEIGMDSVI	359
Zebrafish	YRQVLSYPTTHIDVDINTVKQMPPCHEHTYHRRYMRSELSALWKAASEDDFSDNLI	335
	:*:	
Human	YTDSEFTPDLNIFQDVLHR-DTLVKAFLDQVFLKPLGSLRSSTFLAQFLLVLRKALTLI	413
Vervet	YTDSEFTPDLNIFQDVLHR-DTLVKAFLDQVFLKPLGSLRSSTFLAQFLLVLRKALTLI	413
Opossum	YTDSEFTPDLNIFQDVLHR-DTLVKAFLDQVFLKPLGSLRSSTFLAQFLLVLRKALTLI	413
Rat	YTDSEFTPDLNIFQDVLHR-DTLVKAFLDQVFLKPLGSLRSSTFLAQFLLVLRKALTLI	412
Mouse	YTDSEFTPDLNIFQDVLHR-DTLVKAFLDQVFLKPLGSLRSSTFLAQFLLVLRKALTLI	413
Chicken	HTDSEFTPDLNIFQDVLHR-DTLVKAFLDQVFLKPLGSLRSSTFLAQFLLVLRKALTLI	413
Xenopus	HSDEFTPDLNIFQDVLHR-DTLVKAFLDQVFLKPLGSLRSSTFLAQFLLVLRKALTLI	419
Zebrafish	NAQDSYTPDLNIFQDVMHK-DTLVKSFIDEVFLKPLGSLRSSTFLVLSHFLLLVLRKALTLI	394
	:*:	
Human	KYIEDDTQKGGKPFKSLRNLKIDLDLTAEGDLNIMALAEKIKPGLHSFIFGRPFYTSVQ	473
Vervet	KYIEDDTQKGGKPFKSLRNLKIDLDLTAEGDLNIMALAEKIKPGLHSFIFGRPFYTSVQ	473
Opossum	KYIEDDTQKGGKPFKSLRNLKIDLDLTAEGDLNIMALAEKIKPGLHSFIFGRPFYTSVQ	473
Rat	KYIEDDTQKGGKPFKSLRNLKIDLDLTAEGDLNIMALAEKIKPGLHSFIFGRPFYTSVQ	472
Mouse	KYIEDDTQKGGKPFKSLRNLKIDLDLTAEGDLNIMALAEKIKPGLHSFIFGRPFYTSVQ	473
Chicken	KYIEDDTQKGGKPFKSLRNLKIDLDLTAEGDLNIMALAEKIKPGLHSFIFGRPFYTSVQ	473
Xenopus	KYIEDDTQKGGKPFKSLRNLKIDLDLTAEGDLYIMALAEKIKPGLHSFIFGSSPHTSMQ	479
Zebrafish	RYIEDDTQKGGKPFKSLRNLKIDLDLTVGDLNIMAMAEKLRAGLHSFVFGKSPFVTSVQ	454
	:*:	
Human	ERDVLMTF 481	
Vervet	ERDVLMTF 481	
Opossum	ERDVLMTF 481	
Rat	ERDVLMTF 480	
Mouse	ERDVLMTF 481	
Chicken	ERDMLMTF 481	
Xenopus	ERDVLMTF 487	
Zebrafish	ERDLLINF 462	
	**:*:*:*	



C – Conserved cysteine residue
Y – Non-conserved residue, where cysteine is conserved in other species

Figure 3.16 The C9orf72 protein contains conserved cysteine residues

A) The position of cysteine residues in C9orf72L and C9orf72S are shown. B) The amino acid sequence of Human C9orf72 was aligned with that of Vervet, Opossum, Rat, Mouse, Chicken, Xenopus and Zebrafish in CLUSTAL O (v1.2.4.). Cysteine residues that are conserved in all species are highlighted in blue. Alternate amino acid residues that are at the position of cysteine residues conserved in other species are shown in yellow. C) The phylogenetic tree of the species used in the CLUSTAL O alignment is shown.

Next the localisation of C9orf72 to the IMS by the Class II mechanism was investigated experimentally. In yeast knockdown of MIA40 leads to a reduced presence of the Class II imported proteins in mitochondria (Allen et al., 2005; Chacinska et al., 2004; Peleh et al., 2016). In mammalian cells, proteins that are imported into the IMS by the Class II mechanism have been shown to have reduced stability upon CHCHD4 knockdown (Hofmann et al., 2005; Sakowska et al., 2015). As we found C9orf72 to localise to the mitochondrial IMS (3.4.2), we investigated the localisation of C9orf72 in mitochondria in cells with reduced CHCHD4 levels. Mitochondria were isolated from HEK293 cells transfected with non-targeting control or CHCHD4 siRNA. Mitochondria were subjected to immunoblot for Tubulin and the mitochondrial proteins HSP60 and TOMM20 to verify mitochondrial enrichment. The knockdown of CHCHD4 was verified by CHCHD4 immunoblot (Figure 3.17). Loss of CHCHD4 did not alter either the total level of C9orf72 nor the level of mitochondrial C9orf72. Thus, C9orf72 may not be stabilised by the CHCHD4/ALR pathway. However, in contrast to the reports in yeast, the level of known CHCHD4/ALR substrate TIMM9 did not decrease in mitochondria upon the loss of CHCHD4. As we were unable to verify the effect of loss of CHCHD4 on a *bona fide* Class II IMS protein, the localisation of C9orf72 to the IMS via the Class II mechanism cannot be ruled out.

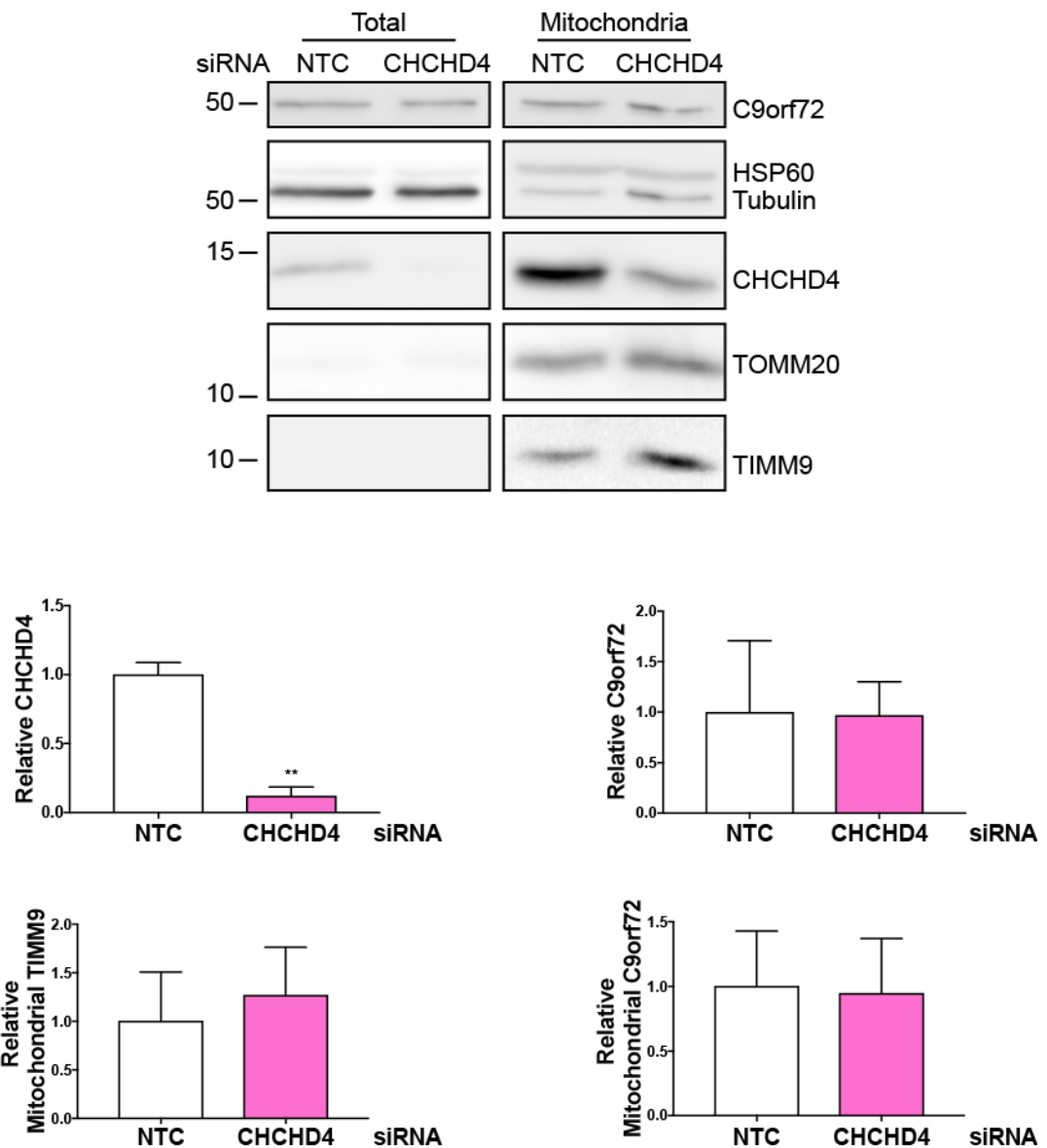


Figure 3.17 Knockdown of CHCHD4 does not affect C9orf72 levels or its localisation in mitochondria

*HEK293 cells were transfected with non-targeting control (NTC) or CHCHD4 siRNA and mitochondria were isolated. Mitochondria were subjected to C9orf72, Tubulin (cytosol), TOMM20 (OMM), HSP60 (matrix) and TIMM9 (IMS) immunoblot. Fifteen μ g of total cell lysate and mitochondrial fractions were subjected to immunoblot. The knockdown of CHCHD4 was verified by CHCHD4 immunoblot. The levels of mitochondrial TIMM9 and total and mitochondrial C9orf72 were quantified from 3 independent experiments. Graphs display mean \pm SEM. Statistical analysis was performed by unpaired t-test; ** $P \leq 0.01$.*

3.5.3 Class III IMS protein import

In contrast to the import of Class I and II IMS proteins, little is known about the mechanism by which Class III proteins localise to the IMS. Class III IMS proteins do not contain N-terminal presequences but may contain internal patterns of hydrophilic residues (Diekert et al., 1999). Class III proteins are associated with proteins of the IMM, which mediates their localisation to the IMS (Figure 3.18). Briefly, Class III IMS proteins are imported through the TOM complex. The import of Class III proteins may be driven by their association with their IMM interacting partners. Mitochondrial function, including OXPHOS activity and cellular ATP levels, are not limiting factors for Class III import. Proteins suggested to be imported into the IMS via the Class III mechanism include COX6B of Complex IV and Qcr8 of Complex III (reviewed in Herrmann and Hell, 2005). The most well characterised Class III IMS proteins are the heme lysases (Steiner et al., 1995), which are targeted to the IMS via an internal hydrophilic amino acid sequence (Diekert et al., 1999). We found C9orf72 interact with several mitochondrial protein complexes (3.2). If C9orf72 is a Class III IMS protein, then these interactions may mediate the localisation of C9orf72 to the IMS.

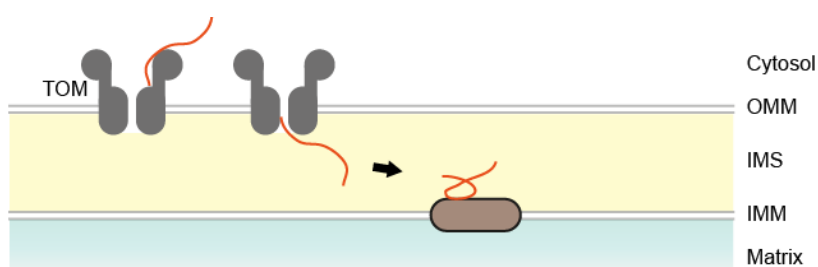


Figure 3.18 Class III IMS protein import

Class III IMS protein are imported through the TOM complex and interact with proteins of the IMM, which drives their IMS localisation.

To begin to investigate whether C9orf72 may be a Class III IMS protein, the requirement of the binding to one of its interacting partners, COX6C, for the mitochondrial localisation of C9orf72 was examined. HEK293 cells were transfected with non-targeting control or COX6C siRNA and were subsequently transfected with pCI-neo empty vector, Myc-C9orf72L, Myc-C9orf72S or Myc-C9orf72DdD. Mitochondrial enriched fractions were produced and subjected to immunoblot for Tubulin and the mitochondrial proteins MnSOD and COX IV to verify the enrichment of mitochondria (Figure 3.19A). Surprisingly, the knockdown of COX6C resulted in a decrease in COX IV levels, which may indicate COX IV instability. The knockdown of COX6C was verified by COX6C immunoblot (Figure 3.19B). Myc immunoblot revealed that the level of Myc-C9orf72L

and Myc-C9orf72DdD in mitochondria was not affected by the knockdown of COX6C. In contrast, the level of Myc-C9orf72S in mitochondria was decreased upon the knockdown of COX6C. Thus, although COX6C is not required for the localisation of C9orf72L and C9orf72DdD to mitochondria, it may be required for the localisation of C9orf72S.

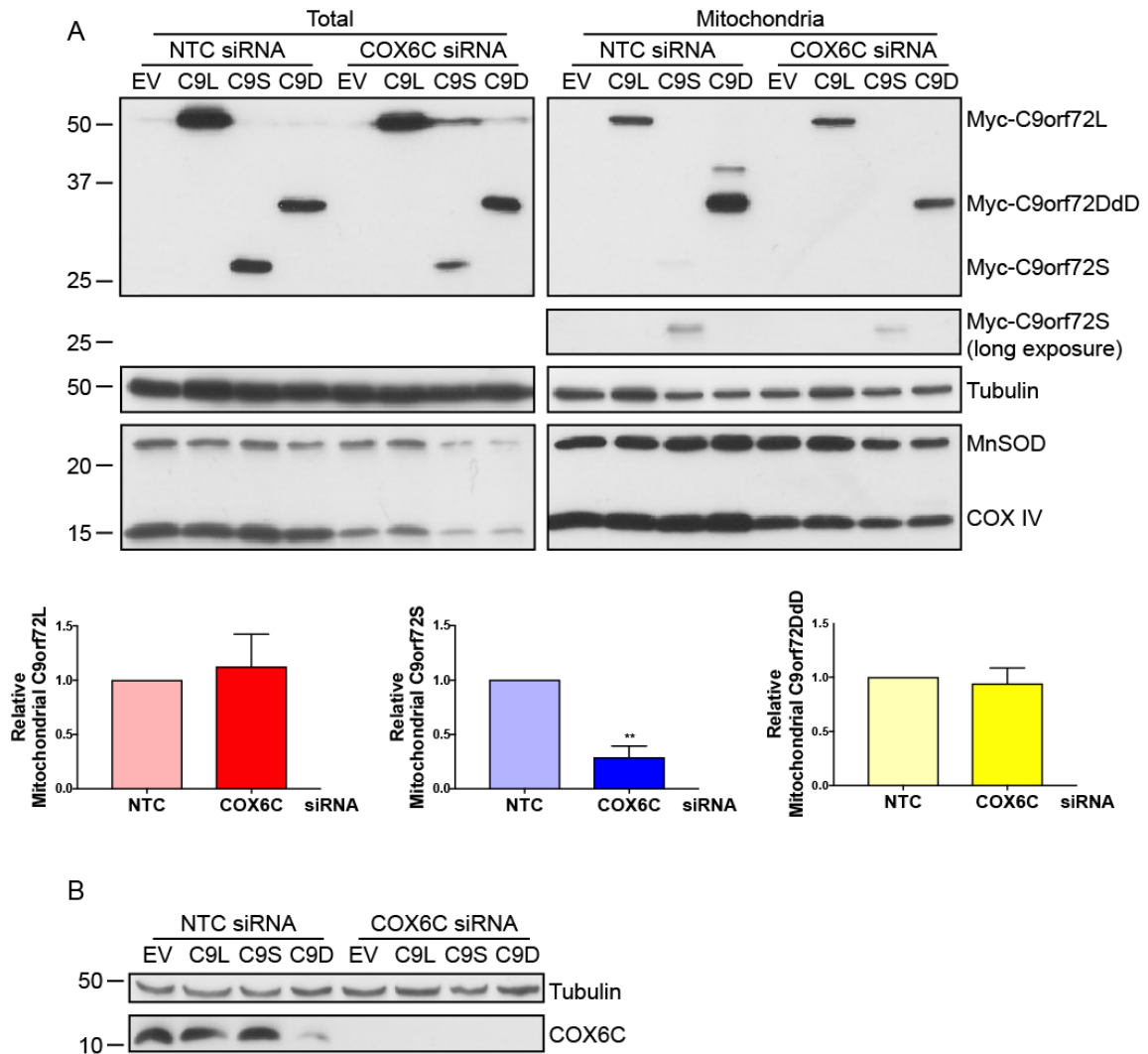


Figure 3.19 COX6C is required for the mitochondrial localisation of C9orf72S

A) HEK293 cells were transfected with non-targeting control (NTC) or COX6C siRNA and were subsequently transfected with pCl-neo empty vector (EV), Myc-C9orf72L (C9L), Myc-C9orf72S (C9S) or Myc-C9orf72DdD (C9D). Mitochondrial enriched fractions were produced and subjected to Myc, Tubulin (cytosol), MnSOD (matrix) and COX IV (IMM) immunoblot. Twenty-five μ g of total cell lysate and mitochondrial fractions were subjected to immunoblot. The level of C9orf72 on the mitochondrial fraction was quantified from 5 (C9L), 3 (C9S) and 3 (C9D) independent experiments. Graphs display mean \pm SEM. Statistical analysis was performed by unpaired *t*-test; ** $P \leq 0.01$. **B)** The knockdown of COX6C was verified by COX6C immunoblot.

To further investigate the role of COX6C in the mitochondrial localisation of C9orf72, HEK293 cells were co-transfected with pCI-neo empty vector, Myc-C9orf72L, Myc-C9orf72S or Myc-C9orf72DdD and with either pCI-neo empty vector or COX6C-MycDDK. Mitochondria enriched fractions were produced and mitochondria were immunoblotted for Tubulin, MnSOD and COX IV to verify the enrichment of mitochondria. Of note, the overexpression of COX6C-MycDDK reduced levels of endogenous COX IV, suggesting that the complex may be destabilised by overexpression of the COX6C subunit. Overexpression of COX6C-MycDDK did not alter the amount of Myc-C9orf72L, Myc-C9orf72S nor Myc-C9orf72DdD on the mitochondrial fraction (Figure 3.20). Taken together, COX6C does not affect the level of C9orf72L or C9orf72DdD in mitochondria but may affect the level of C9orf72S. Therefore, the localisation of C9orf72 to the IMS may in part be governed by the Class III import mechanism, but requires further investigation.

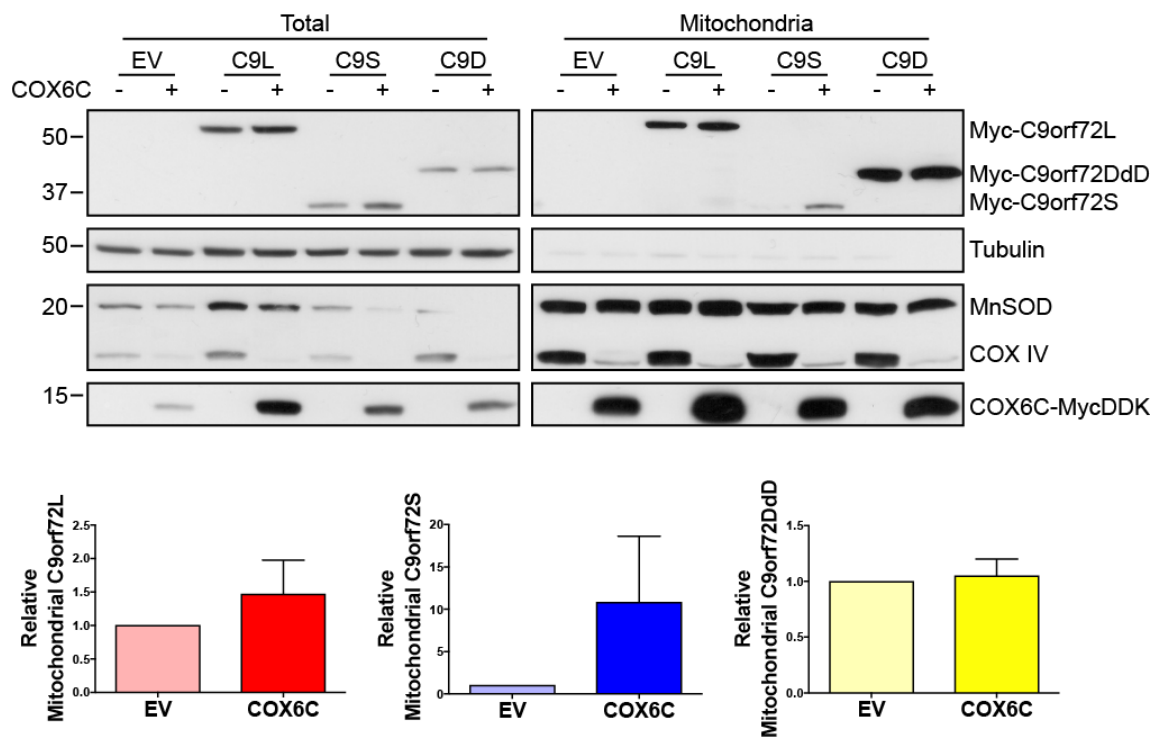


Figure 3.20 Overexpression of COX6C does not affect mitochondrial C9orf72 levels

HEK293 cells were co-transfected with pCI-neo empty vector (EV), Myc-C9orf72L (C9L), Myc-C9orf72S (C9S) or Myc-C9orf72DdD (C9D) and EV (-) or COX6C-MycDDK (+) and mitochondrial enriched fractions were produced. The fractions were subjected to Myc, Tubulin (cytosol), MnSOD (matrix) and COX IV (IMM) immunoblot. Twenty-five μ g of total cell lysate and mitochondrial fractions were subjected to immunoblot. The

level of C9orf72 on the mitochondrial fraction was quantified from 2 independent experiments. Graphs display mean±SEM. Statistical analysis was performed by unpaired t-test.

3.6 Discussion

Mitochondrial dysfunction is a common feature of ALS, including in C9orf72 ALS (Dafinca et al., 2016; Lopez-Gonzalez et al., 2016; Onesto et al., 2016; reviewed in Smith et al., 2017b). We identified and verified an interaction between C9orf72 and mitochondria. In this chapter we show that the C9orf72 protein interacts with the COX IV subunit COX6C, the TIM23 import complex and ATP Synthase. Consistent with an interaction of C9orf72 with IMM complexes, we show additionally that C9orf72 localises to the mitochondrial IMS and attempt to clarify its import mechanism.

The interacting partner of C9orf72 in the TIM23 complex was identified as the TIMM50 subunit (Table 3-2, Table 3-3) (Blokhuis et al., 2016). TIMM50 is involved in the recognition of the preproteins that have been translocated through the TOM20 complex and which are directed towards the TIM23 complex for import across the IMM or into the IMS (Gevorkyan-Airapetov et al., 2009). Therefore, the interaction between C9orf72 and the TIM23 complex may promote the import of C9orf72 into mitochondria and its localisation in the IMS. With the majority mitochondrial proteins synthesised in the cytosol and imported into the mitochondria through the TOM20 complex, C9orf72 associated with TIM23 may interact with proteins that are undergoing import into mitochondria. This includes subunits of COX IV including COX6C (Mehnert et al., 2014; Mick et al., 2012). Therefore, C9orf72 may interact with COX6C during its import and participate in the trafficking of mitochondrial proteins into the organelle. In yeast, the TIM23 complex also interacts with the MIC60 subunit of the mitochondrial contact site and cristae organising system (MICOS), suggesting spatial juxtaposition and interlinked roles in protein import (Mehnert et al., 2014). Indeed, it has been shown that import machineries of the OMM (TOM20 complex) and IMM (TIM23 complex) associate with cristae junctions (Gold et al., 2014) and that MICOS is important for the import of proteins into mitochondria (reviewed in Horvath et al., 2015). Interestingly, the published proteomics screens identified MICOS proteins as interacting partners of C9orf72 (Blokhuis et al., 2016; Sullivan et al., 2016). Thus, C9orf72 may interact with the MICOS and regulate the dynamics of mitochondrial cristae and the complexes found therein.

C9orf72 interacts with the ATP Synthase complex (3.2.4). Proteins that interact with ATP Synthase have been reported to regulate the activity of the complex. Overall these interactions promote the coupling of mitochondrial oxygen consumption and ATP

generation, and regulate the opening of the mitochondrial permeability transition pore (reviewed in Long et al., 2015). Therefore, C9orf72 may play a role in the regulation of ATP Synthase activity. Indeed, C9orf72 ALS patient fibroblasts display increased oxygen consumption and ATP levels (Onesto et al., 2016), but it remains to be seen whether these are due to C9orf72 haploinsufficiency. ATP Synthase also plays a role in the formation of IMM cristae (Paumard et al., 2002). Thus, the interaction between C9orf72 and both the TIM23 and ATP Synthase complexes validated here support a role for C9orf72 in the regulation of mitochondrial IMM structure.

COX6C is thought to be a structural or regulatory subunit of the COX IV complex (Lazarou et al., 2009), which is upregulated in cancer cells and upon ischemia (Llombart et al., 2017; Zhou et al., 2018). Interestingly, reports have implicated COX6C in the mitochondrial apoptotic signalling pathway (Hadife et al., 2013), controlling the levels of Caspase-9, required to activate intrinsic apoptosis after viral infection (Othumpangat et al., 2014). Caspase-9 is also activated as a result of mitochondrial stresses, including the elevation of ROS levels and an inflammatory environment (Guo et al., 2016; Zuo et al., 2009). Furthermore, Caspase-9 has been reported to play a role in promoting autophagy during inflammation (Guo et al., 2016). In ALS, inflammation is reported in the areas of motor neuron loss including the motor cortex and the spinal cord (Kawamata et al., 1992), suggesting that innate immunity pathways are induced. C9orf72 knockout mice display high levels of immunity and a dysregulated immune response (Atanasio et al., 2016; Burberry et al., 2016; O'Rourke et al., 2016; Sudria-Lopez et al., 2016). This implies that C9orf72 haploinsufficiency may lead to the activation of the innate immune system in C9orf72-related ALS (Lall and Baloh, 2017). The interaction between C9orf72 and COX6C may regulate the Caspase-9 autophagy response, which may be altered in C9orf72 ALS/FTD. Whether or not COX6C levels is affected in C9orf72 knockout animal models requires further investigation. Furthermore, the mechanisms underlying the inflammatory phenotype in C9orf72 knockout mice should be investigated to gauge the role of the C9orf72 protein in immune-related autophagy.

C9orf72 was found in mitochondria (Figure 3.8). The mitochondrial localisation of C9orf72 was subsequently reported in the screen by Blokhuis *et al.* (Blokhuis et al., 2016). Investigation of the DENN domains of C9orf72 revealed that the C-terminal fragment of C9orf72L (C9orf72DdD, corresponding to the DENN and dDENN domains) localised more strongly to mitochondria than the uDENN domain (C9orf72S) (Figure 3.7). The DENN and dDENN domains of C9orf72L may also be important for the interaction of C9orf72 with mitochondrial IMM complexes. Indeed in co-immunoprecipitation assays, COX6C only interacted with constructs of C9orf72 which

contained the DENN and dDENN domains (Figure 3.3), whilst ATP5A and TIMM23 interacted more strongly with C9orf72L and C9orf72DdD than with C9orf72S (Figure 3.5, Figure 3.6). Therefore, despite the uDENN, DENN and dDENN domains being frequently reported together and not being described as having separate functions (Levivier et al., 2001); in the context of C9orf72, the DENN and dDENN may mediate the localisation and impart some of the interactions with other proteins. Indeed, it has been reported that the DENN domain of C9orf72 is required to mediate its interaction with both SMCR8 and WDR41 (Yang et al., 2016).

We attempted to identify the mechanism by which C9orf72 localises to the IMS, however this remains unclear. C9orf72 does not have a mitochondrial targeting sequence so the classical mitochondrial targeting pathway (Class I) is unlikely to play a role in the localisation of C9orf72 (Table 3-4). The MIA40/ERV1 pathway (Class II) mechanism has been extensively studied in yeast, however the same level of investigation has not been performed in mammalian cell lines. Knockdown of CHCHD4 in cells did not result in lower levels of C9orf72 in mitochondria, suggesting that the Class II mechanism may not be involved in the IMS localisation of C9orf72. However, it should be noted that unlike in the assays performed in yeast (Allen et al., 2005; Chacinska et al., 2004; Peleh et al., 2016; Sakowska et al., 2015), the knockdown of CHCHD4 did not result in a decrease of a known Class II protein TIMM9 in mitochondria (Figure 3.17). Thus, the Class II IMS import mechanism cannot be excluded for C9orf72. The difference in TIMM9 import could highlight differences in the oxidative folding pathway between yeast and mammalian models that warrants further investigation. Finally, the localisation of C9orf72 to the IMS may be mediated through interactions with the IMM complexes (Class III). The levels of C9orf72L and C9orf72DdD in mitochondria were not altered by changes in the expression of the C9orf72 interacting partner COX6C. In contrast, mitochondrial levels of C9orf72S were affected by the level of COX6C (Figure 3.19). Aside from the interaction with IMM complexes, the mechanism by which Class III proteins are imported into mitochondria remains unclear (Herrmann and Hell, 2005). Thus, it is possible that C9orf72 is imported by the Class III mechanism. We noted the ability of C9orf72DdD to localise readily to mitochondria (Figure 3.7). It may be that the localisation of C9orf72L to mitochondria is regulated by the uDENN domain (essentially C9orf72S). However, it may not be possible to verify the Class III mechanism of C9orf72 import into the IMS without first identifying the full C9orf72 IMM/IMS interactome. This would be required to produce a model in which several interacting partners were knocked-out, to observe any changes in the localisation of C9orf72 in mitochondria. Furthermore, exploration of the localisation of the endogenous C9orf72 protein may aid

in the identification of the import mechanisms, which may be masked by overexpression of C9orf72.

To investigate the sub-mitochondrial localisation of C9orf72, we used Flp-In FLAG-C9orf72L HEK293 cells. This model was used as it provided a reliable level of FLAG-C9orf72L expression, when compared to the transient expression of C9orf72 used in our other assays. However, this model represents nonetheless an overexpression of C9orf72. The overexpression of protein can lead to artefacts and protein mislocalisation, especially in the ER. Therefore to validate our experiments identifying the mitochondrial IMS localisation of C9orf72, our assays need to be reproduced investigating the localisation of the endogenous C9orf72 protein, which is now possible due to the newly available commercial antibodies, including the Proteintech anti-C9orf72 antibody (25757-1-AP) which we used here to identify endogenous C9orf72 on the mitochondrial fraction (Figure 3.8). Another limitation of the methodology is linked to the preparation of the enriched mitochondrial fractions themselves. It is likely that the mitochondrial enriched fractions contain other organelles with similar densities, including lysosomes and peroxisomes. This is especially true for lysosomes which have a similar density to mitochondria on a sucrose gradient (Lodish et al., 2000). Here we identified C9orf72 to be located in the mitochondrial IMS using permeabilisation of the OMM with digitonin and Proteinase K digestion of cytosol exposed proteins (Figure 3.13). However, C9orf72 has previously been shown to be recruited to lysosomes upon starvation (Amick et al., 2016). Lysosomes are single membrane bound organelles and which contain a higher membrane cholesterol content compared to mitochondria and other organelle membranes (Schoer et al., 2000). Therefore, lysosomal membranes would be permeabilised by the treatment with digitonin employed in our assays. Had the C9orf72 we identified on our mitochondrial fraction been of lysosomal origin, then the treatment of the mitochondrial fraction with digitonin alone would have resulted in the loss of FLAG-C9orf72L from the mitochondria pellet, due to the permeabilisation of the lysosomes. As we observed FLAG-C9orf72L to only be removed from the mitochondrial pellet following both digitonin membrane permeabilisation and Proteinase K treatment, this indicated that FLAG-C9orf72L was located in the IMS (Figure 3.13). This was consistent with the interaction of C9orf72 with the IMM proteins.

C9orf72 does not localise exclusively to the mitochondrial fraction, but distributes between mitochondria and the cytosol. This highlights the possibility of a dynamic localisation of the C9orf72 to mitochondria. Indeed, many proteins are recruited to both the OMM and IMM in a temporal and spatial manner. This includes proteins involved in maintaining mitochondrial dynamics (Pagliuso et al., 2018; Yoo and Jung, 2018).

C9orf72 has been previously reported to undergo dynamic cellular redistribution upon amino acid starvation (Amick et al., 2016). Whether the interaction between C9orf72 and mitochondria is a dynamic event with functional consequences will be examined in the following section of this thesis.

Chapter 4. Investigating the role of the C9orf72 protein in mitochondrial function and dynamics

4.1 Introduction

The C9orf72 protein interacts with complexes of the IMM and a proportion of the cellular C9orf72 protein is found in the mitochondrial IMS (3.2, 3.4). We hypothesised that the interaction between C9orf72 and mitochondria may play a role in mitochondrial function.

Interestingly, in our hands C9orf72 does not localise exclusively to the mitochondrial fraction and distributes between mitochondria and the cytosol (Figure 3.7A, Figure 3.8). Therefore, C9orf72 may undergo dynamic changes in localisation depending on the cellular environment. Indeed, the spatiotemporal dynamic recruitment of proteins to mitochondria underlies mitochondrial dynamics, including fission/fusion cycling and mitophagy. Drp1, the GTPase responsible for mitochondrial fission, is recruited to mitochondria upon the triggering of a fission event, including upon mitochondrial damage (reviewed in Hu et al., 2017). Likewise, proteins involved in mitochondrial quality control including Parkin, NDP52, OPTN are recruited to mitochondria upon mitochondrial damage (reviewed in Hamacher-Brady and Brady, 2016). Furthermore, proteins located in the OMM and IMM recruit LC3 positive autophagosomes to mitochondria to promote the clearance of damaged organelles by mitophagy (reviewed in Martinez-Vicente, 2017).

During mitophagy, the autophagy machinery, including the ULK1 initiation complex, is recruited to mitochondria to promote the engulfment of the damaged organelle by an autophagosome (Itakura et al., 2012; Wu et al., 2014). C9orf72 has been shown to interact with the ULK1 initiation complex and regulate its trafficking to phagophores during autophagy via Rab1a (Webster et al., 2016a; Yang et al., 2016). Mitochondrial C9orf72 may similarly recruit the ULK1 initiation complex to mitochondria and promote mitophagy.

In this chapter we aimed to identify the functional relevance of the interaction between C9orf72 and mitochondria.

4.2 C9orf72 protein levels alter mitochondrial network dynamics

Mitochondria are highly dynamic organelles undergoing fission/fusion cycling and transport. Alterations in mitochondrial fission/fusion cycling, transport and mitophagy are features of ALS and are proposed to contribute to the alterations in mitochondrial networks observed in patient derived tissues and cell models (reviewed in Smith et al., 2017b).

To investigate whether C9orf72 may play a role in the maintenance of mitochondrial networks, the effect of altering C9orf72 expression levels on the mitochondrial network was analysed. First, to investigate the effect of an increase in C9orf72 levels on mitochondrial networks, CV1 cells were transfected with pCI-neo empty vector, Myc-C9orf72L or Myc-C9orf72S. To visualise the mitochondrial networks, cells were co-transfected with pAcGFP1-Mito (Figure 4.1A). In control cells, the mitochondrial network appeared branched and tubular. Overexpression of either Myc-C9orf72L or Myc-C9orf72S resulted in more rounded mitochondria, as seen by a decrease in mitochondrial aspect ratio. Myc-C9orf72L and Myc-C9orf72S expression led to a reduction in mitochondrial network connectivity, as seen by a decrease in both form factor and mitochondrial network. A rounding of the mitochondria and reduction in the connectivity of the network was interpreted as a splitting of the mitochondria from the network. Thus, an increase in the level of C9orf72 induced the fragmentation of the mitochondrial network.

To verify that an increase in C9orf72 levels led to a fragmentation of the mitochondrial network in human derived cell lines, HeLa cells were co-transfected with pCI-neo empty vector, Myc-C9orf72L or Myc-C9orf72S and, to visualise the mitochondrial network, pAcGFP1-Mito (Figure 4.1B). As observed in CV1 cells, the overexpression of Myc-C9orf72L and Myc-C9orf72S led to a rounding of the mitochondria, as seen by a decrease in mitochondrial aspect ratio. Overexpression of Myc-C9orf72L and Myc-C9orf72S additionally led to a decrease in mitochondrial network connectivity and form factor. This indicated that overexpression of Myc-C9orf72L and Myc-C9orf72S led to the fragmentation of the mitochondrial network in human derived cell lines.

Next to investigate the effect of loss of C9orf72 on mitochondrial networks, HeLa cells were transfected with non-targeting control or C9orf72 siRNA and immunostained for endogenous TOMM20, an OMM protein, to visualise the mitochondrial network (Figure 4.2A). The efficiency of C9orf72 siRNA knockdown was determined by qPCR (Figure 4.2B). Control cells displayed tubular and branched mitochondrial networks. A reduction in C9orf72 levels resulted in mitochondria appearing more elongated, as seen by an increase in aspect ratio. Mitochondrial network interconnectivity was increased upon the reduction of C9orf72 levels, seen by an increase in both form factor and mitochondrial network. Therefore, reducing the levels of C9orf72 induced mitochondrial networking.

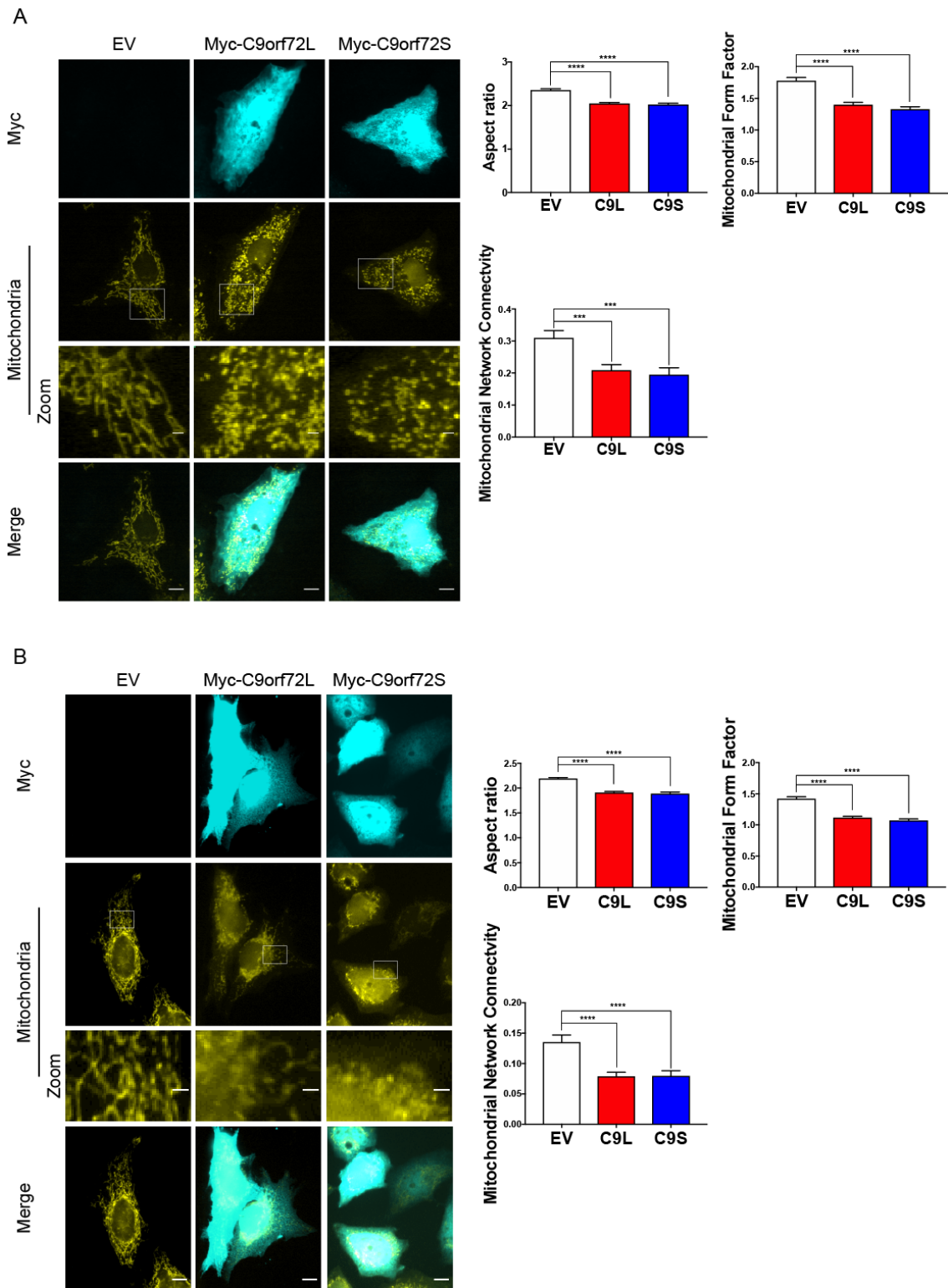


Figure 4.1 Overexpression of C9orf72 leads to the fragmentation of the mitochondrial network

A) CV1 cells were co-transfected with pCI-neo empty vector (EV), Myc-C9orf72L (C9L) or Myc-C9orf72S (C9S) (cyan) and pAcGFP1-Mito (yellow). The shape of the mitochondria (aspect ratio), mitochondrial form factor and mitochondrial network

connectivity were quantified. Cells were quantified from 3 independent experiments (EV: 99, C9L: 92, C9S: 80 cells). Scale bar 10 μm , zoom 2 μm . Graphs display mean \pm SEM. Statistical analysis was performed by one-way ANOVA with Fisher's LSD; *** $P \leq 0.001$, **** $P \leq 0.0001$. B) HeLa cells were co-transfected with pCI-neo empty vector (EV), Myc-C9orf72L (C9L) or Myc-C9orf72S (C9S) (cyan) and pAcGFP1-Mito (yellow). The shape of the mitochondria (aspect ratio), mitochondrial form factor and mitochondrial network connectivity were quantified. Cells were quantified from 3 independent experiments (EV: 65, C9L: 71, C9S: 66 cells). Scale bar 10 μm , zoom 2 μm . Graphs display mean \pm SEM. Statistical analysis was performed by one-way ANOVA with Fisher's LSD; **** $P \leq 0.0001$.

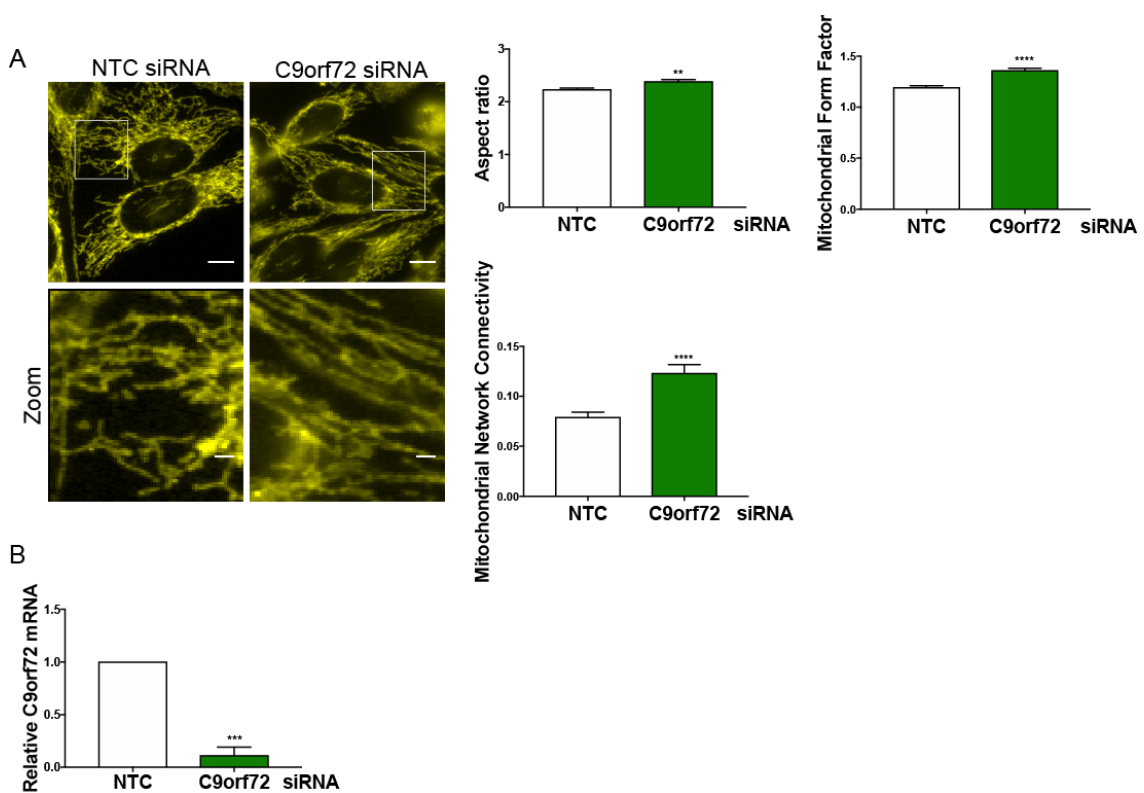


Figure 4.2 Reduced levels of C9orf72 lead to increased mitochondrial networking

A) HeLa cells were transfected with non-targeting control (NTC) or C9orf72 siRNA and were subjected to immunostaining with anti-TOMM20 Ab (yellow) to visualise the mitochondrial network. The mitochondrial shape (aspect ratio), form factor and network connectivity were analysed. Cells were quantified from 3 independent experiments (NTC: 132, C9orf72: 114 cells). Scale bar 10 μm , zoom 2 μm . Graphs display mean \pm SEM. Statistical analysis was performed by unpaired t-test; ** $P \leq 0.01$, **** $P \leq 0.0001$. B) C9orf72 mRNA levels were determined by qPCR. Graph displays mean \pm SEM. Statistical analysis was performed by unpaired t-test; *** $P < 0.001$.

4.2.1 C9orf72 regulates fission/fusion of the mitochondrial network

Changes in the morphology of the mitochondrial networks can be governed by multiple factors, including mitochondrial bioenergetics, the levels of fission/fusion proteins, contacts between mitochondria and ER, and the activity of the mitophagy pathway (reviewed in Elgass et al., 2013; Youle and van der Bliek, 2012). To explore how the change in C9orf72 expression led to changes in the morphology of the mitochondrial network observed, the levels of the proteins involved in the mitochondrial fission/fusion cycling were investigated. It has previously been shown that the fragmentation of the mitochondrial network may be due to a decrease in the levels of the pro-fusions protein Mfn1/2 or an increase in the recruitment of fission mediator Drp1 to mitochondria (Chen et al., 2003; Eura et al., 2003; Labrousse et al., 1999). Conversely, fusion of the mitochondrial network has been reported to be caused by an increase in fusion proteins including Mfn1/2 or a decrease in the level of Drp1 (Mai et al., 2010; Santel and Fuller, 2001).

To investigate the effect an increase in C9orf72 levels on the fission/fusion machinery, initially HeLa cells were co-transfected with pCI-neo empty vector, Myc-C9orf72L or Myc-C9orf72S and Mfn2-MycHis. Mfn2 immunoblot revealed that an increase in C9orf72 levels did not affect the level of the fusion protein Mfn2 (Figure 4.3A). Next to investigate whether an increase in C9orf72 levels induced the fragmentation of the mitochondrial network through the recruitment of Drp1 to mitochondria, HEK293 cells were transfected with pCI-neo empty vector, Myc-C9orf72L or Myc-C9orf72S. To induce the recruitment of Drp1 to mitochondria in control cells, mitochondrial damage was induced by CCCP treatment (Ishihara et al., 2003). Mitochondria were enriched and subjected to Drp1 immunoblot (Figure 4.3B). The treatment of control cells with CCCP resulted in an increase of Drp1 in mitochondria. Increased levels of Myc-C9orf72L or Myc-C9orf72S also resulted in an increase in Drp1 levels in mitochondria indicative of its recruitment. Thus, an increase in C9orf72 levels recruits Drp1 to mitochondria, which may lead to mitochondrial network fragmentation.

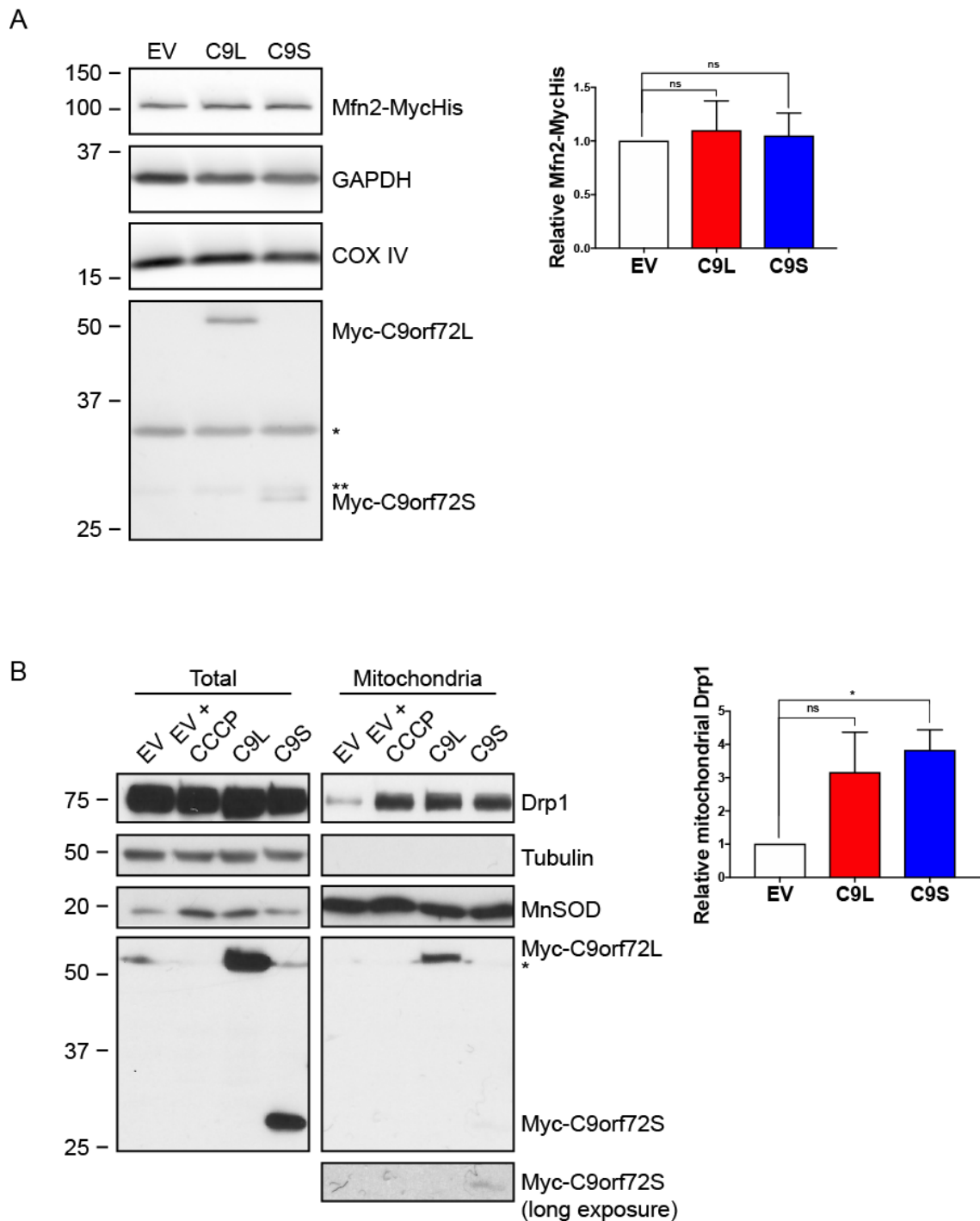


Figure 4.3 Increased C9orf72 levels do not affect the level of fusion protein Mfn2, but induces Drp1 translocation to mitochondria

A) HeLa cells were co-transfected with pCI-neo empty vector (EV), Myc-C9orf72L (C9L) or Myc-C9orf72S (C9S) and Mfn2-MycHis. The level of Mfn2-MycHis was determined by Mfn2 immunoblot and quantified relative to the empty vector control in 3 independent experiments. Twenty μ g of total cell lysate was subjected to immunoblot. Graph displays mean \pm SEM. Statistical analysis was performed by one-way ANOVA with Fisher's LSD.

* indicates the band corresponding to GAPDH upon subsequent Myc immunoblot. ** indicates a non-specific band on Myc immunoblot. B) HEK293 cells were transfected with pCI-neo empty vector (EV), Myc-C9orf72L (C9L) or Myc-C9orf72S (C9S). The recruitment of Drp1 to mitochondria was induced by treatment with 10 μ M CCCP for 4 h in control cells. Mitochondria were subjected to Drp1, Tubulin, MnSOD and Myc immunoblot. Twenty-five μ g of total cell lysate and mitochondrial fractions were subjected to immunoblot. The level of Drp1 recruited to mitochondria was quantified relative to control cells from 3 independent experiments. Graph displays mean \pm SEM. Statistical analysis was performed by one-way ANOVA with Fisher's LSD; * $P \leq 0.05$, (C9L; P Value = 0.0978).

To investigate the fission/fusion machinery upon loss of C9orf72, first HEK293 cells were transfected with non-targeting control or C9orf72 siRNA (Figure 4.4Ai). The efficiency of C9orf72 siRNA knockdown was verified by qPCR (Figure 4.4Aii). The knockdown of C9orf72 did not affect the level of the fission protein Drp1. Thus, loss of C9orf72 did not affect the mitochondrial fission machinery. Secondly to investigate the fusion machinery, HeLa cells were transfected with non-targeting control or C9orf72 siRNA and were subsequently co-transfected with Mfn2-MycHis and EYFP-Parkin (Figure 4.4Bi). The efficiency of C9orf72 siRNA knockdown was verified by qPCR (Figure 4.4Bii). The knockdown of C9orf72 led to an increase in the level of Mfn2-MycHis. Thus, the reduction in C9orf72 levels led to an increase the fusion protein Mfn2, which may underlie the increase in mitochondrial network connectivity observed previously (Figure 4.2).

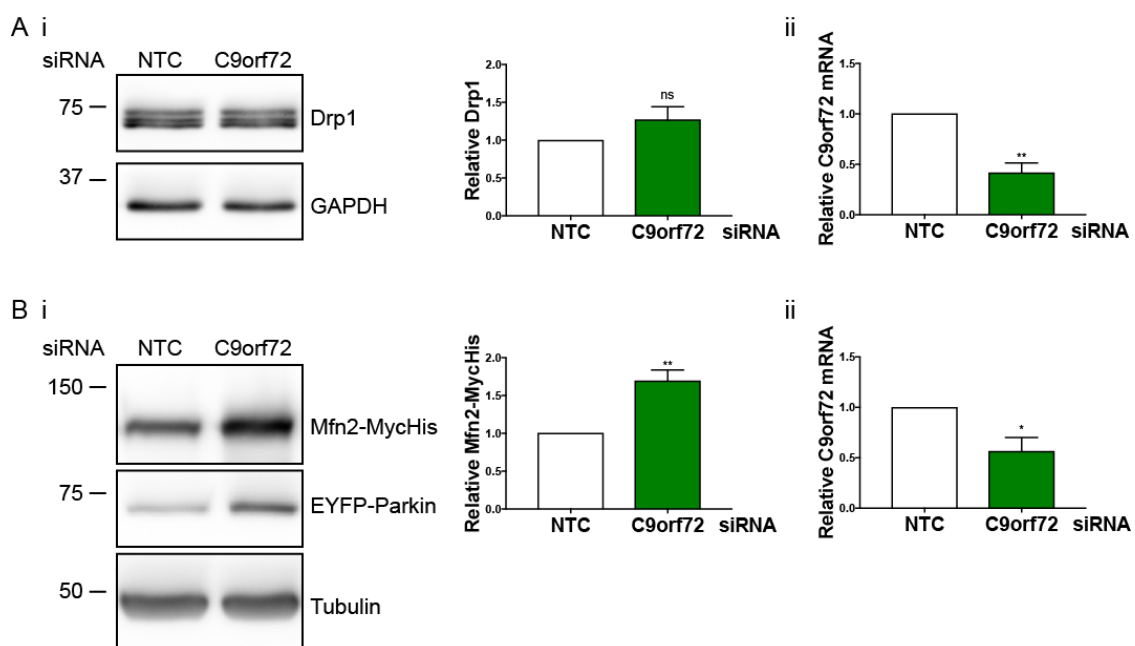


Figure 4.4 The reduction of C9orf72 levels promotes mitochondrial network fusion through increased Mfn2 levels

*A) i) HEK293 cells were transfected with non-targeting control (NTC) or C9orf72 siRNA and were subjected to Drp1 immunoblot. Twenty-five μ g of total cell lysate was subjected to immunoblot. The level of Drp1 in total cell lysate was quantified relative to the control siRNA in 3 independent experiments. Graph displays mean \pm SEM. Statistical analysis was performed by unpaired t-test. ii) C9orf72 mRNA levels were determined by qPCR. Graph displays mean \pm SEM. Statistical analysis was performed by unpaired t-test; ** $P \leq 0.01$. B) i) HeLa cells were transfected with non-targeting control (NTC) or C9orf72 siRNA and were subsequently co-transfected with Mfn2-MycHis and EYFP-Parkin. Mfn2-MycHis levels in total cell lysate were quantified by Mfn2 immunoblot relative to the control siRNA in 3 independent experiments. Twenty μ g of total cell lysate was subjected to immunoblot. Graph displays mean \pm SEM. Statistical analysis was performed by unpaired t-test; ** $P \leq 0.01$. ii) C9orf72 mRNA levels were determined by qPCR. Graph displays mean \pm SEM. Statistical analysis was performed by unpaired t-test; * $P \leq 0.05$.*

4.2.2 Increased C9orf72 expression leads to mitochondrial network fragmentation without altering mitochondrial membrane potential

The MMP is generated by the OXPHOS machinery and drives the production of ATP by mitochondria. Loss of MMP can be induced by mitochondrial damage and triggers dysfunctional organelles to be removed from the cell by mitophagy. To segregate the damaged mitochondrion with a lower MMP from the network, fission of the damaged organelle from the network is promoted by the recruitment of Drp1 (reviewed in Pagliuso et al., 2018). Indeed, damaged mitochondria with a lower MMP display more fragmented mitochondrial networks (reviewed in Youle and van der Bliek, 2012). To investigate whether the fragmentation of the mitochondrial network upon C9orf72 overexpression was as a result of mitochondrial damage, the MMP was measured in cells overexpressing C9orf72. HeLa cells were transfected with EGFP-C2, EGFP-C9orf72L or EGFP-C9orf72S and were subjected to TMRM staining. TMRM is a cell permeable fluorescent dye that accumulates in mitochondria. When used in non-quenching mode, the accumulation of TMRM in mitochondria correlates with MMP (reviewed in Perry et al., 2011). To verify that TMRM fluorescence measured arose from mitochondria, control cells were depolarised with CCCP. CCCP uncouples the proton gradient established by the OXPHOS machinery and thereby inhibits ATP synthesis by ATP Synthase. An increase in the expression level of neither EGFP-C9orf72L nor EGFP-C9orf72S resulted

in a change in TMRM staining intensity compared to the EGFP control (Figure 4.5A). Thus, increased C9orf72 levels did not change MMP. This indicated that overexpression of C9orf72 did not disrupt the proton gradient, suggesting that mitochondrial damage was not induced.

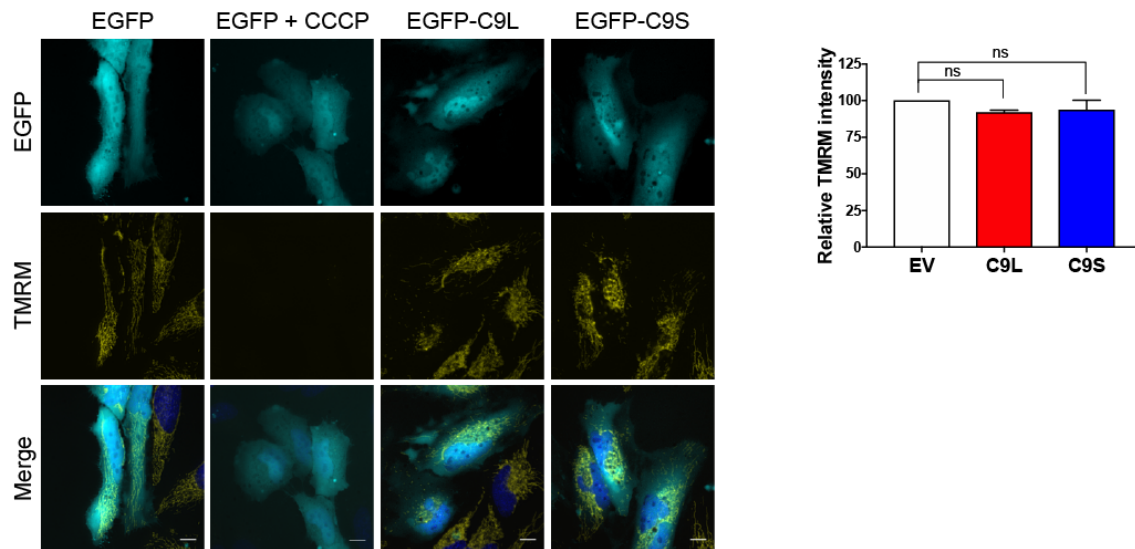


Figure 4.5 Increased C9orf72 levels do not influence mitochondrial membrane potential

HeLa cells were transfected with EGFP-C2 (EGFP), EGFP-C9orf72L (C9L) or EGFP-C9orf72S (C9S) (cyan) and were incubated with 30 nM TMRM (yellow) to determine MMP. MMP was dissipated in control cells by treatment with 10 μ M CCCP for 4 h. Scale bar 10 μ m. The mitochondrial TMRM staining in cells expressing EGFP-C9orf72L or EGFP-C9orf72S was normalised to that of the EGFP control in 3 independent experiments. Statistical analysis was performed by one-way ANOVA with Fisher's LSD.

4.2.3 Mitochondrial fragmentation occurring upon increased C9orf72 levels is a result of the activation of mitophagy

Fission of damaged mitochondria from the mitochondrial network is an important step in mitophagy (reviewed in Hamacher-Brady and Brady, 2016; Ni et al., 2015). We showed that an increase in C9orf72 levels induces the fragmentation of the mitochondrial network (Figure 4.1) and induces the recruitment of Drp1 to mitochondria (Figure 4.3), similar to the effect seen during CCCP induced mitophagy (Ishihara et al., 2003). Therefore, increasing C9orf72 levels in cells may induce mitophagy. During mitophagy, the autophagy machinery is recruited to damaged mitochondria to promote their engulfment by the autophagosome (reviewed in Hamacher-Brady and Brady, 2016). Knockdown of ATG7 or ATG8/LC3 prevents the mitochondrial fragmentation found in

PINK1 knockout cells (Dagda et al., 2009). Knockout of LC3/GABARAP proteins prevents the maturation of mitochondria containing autophagosomes (Nguyen et al., 2016). Furthermore, knockout of the autophagy initiation machinery also affects mitophagy. The initiation complex, comprised of ULK1, FIP200, ATG13 and ATG101 regulates the early stages of autophagy (Figure 1.2). Upon the induction of autophagy, inhibition of mTORC1 results in the dephosphorylation and the activation of ULK1. Activated ULK1 then undergoes autophosphorylation and phosphorylates the other members of the initiation complex and the downstream VPS34 complex to promote the initiation of autophagy (reviewed in Zachari and Ganley, 2017). The interaction of ULK1 with FIP200 or ATG13 is required to improve the stability and kinase activity of ULK1 (Ganley et al., 2009; Hosokawa et al., 2009; Jung et al., 2009). Furthermore, FIP200 is required for the localisation of ULK1 to the isolation membrane (Hara et al., 2008). The knockout of FIP200 in mice leads to the accumulation of misshapen and damaged organelles (Liang et al., 2010), whereas the knockout of ULK1 has been shown to prevent the removal of mitochondria during erythrocyte maturation (Kundu et al., 2008). ULK1 has been shown to be recruited to mitochondria and promote fission via the phosphorylation of Drp1 (Saito and Sadoshima, 2018). C9orf72 has been shown to interact with and mediate the recruitment of the ULK1 initiation complex to the phagophore during autophagy (Sullivan et al., 2016; Webster et al., 2016b; Yang et al., 2016). Thus, the fragmentation of the mitochondrial network upon an increase in C9orf72 levels may be due to activation of mitophagy via ULK1 recruitment to mitochondria.

To begin to investigate, whether the mitochondrial fragmentation induced by an increase in C9orf72 was as a result of the interaction between C9orf72 and the ULK1 initiation complex, HeLa cells were transfected with non-targeting control or ULK1 siRNA. Cells were subsequently co-transfected with pCI-neo empty vector or Myc-C9orf72L and pAcGFP1-Mito, to visualise the mitochondrial network (Figure 4.6Ai). The knockdown of ULK1 was verified by ULK1 immunoblot (Figure 4.6Aii). The loss of ULK1 did not affect the morphology of the mitochondrial network. As observed previously (Figure 4.1), an increase in the level of Myc-C9orf72L led to the rounding of mitochondria and the fragmentation of the mitochondrial network, as seen by a decrease in both mitochondrial aspect ratio and form factor. Loss of ULK1 prevented the rounding of mitochondria and fragmentation upon the expression of Myc-C9orf72L. To verify that the ULK1 initiation complex was required for the mitochondrial fragmentation upon Myc-C9orf72L overexpression, the requirement of the FIP200 protein was investigated. C9orf72 has previously been shown to interact with FIP200 (Sullivan et al., 2016; Webster et al.,

2016a). HeLa cells were transfected with non-targeting control or FIP200 siRNA and were subsequently co-transfected with pCI-neo empty vector or Myc-C9orf72L and pAcGFP1-Mito, to visualise the mitochondrial networks (Figure 4.6Bi). The knockdown of FIP200 was verified by FIP200 immunoblot (Figure 4.6Bii). Loss of FIP200 resulted in a shortening of the mitochondria but did not affect overall branching of the network, which may reflect an accumulation of aggregated mitochondria, as reported previously (Liang et al., 2010). Loss of FIP200 did not affect the mitochondrial shortening and rounding upon expression of Myc-C9orf72L but did prevent the dismantling of the mitochondrial networks. Taken together, the fragmentation of the mitochondrial networks induced by an increase in the level of C9orf72L requires the ULK1 initiation complex.

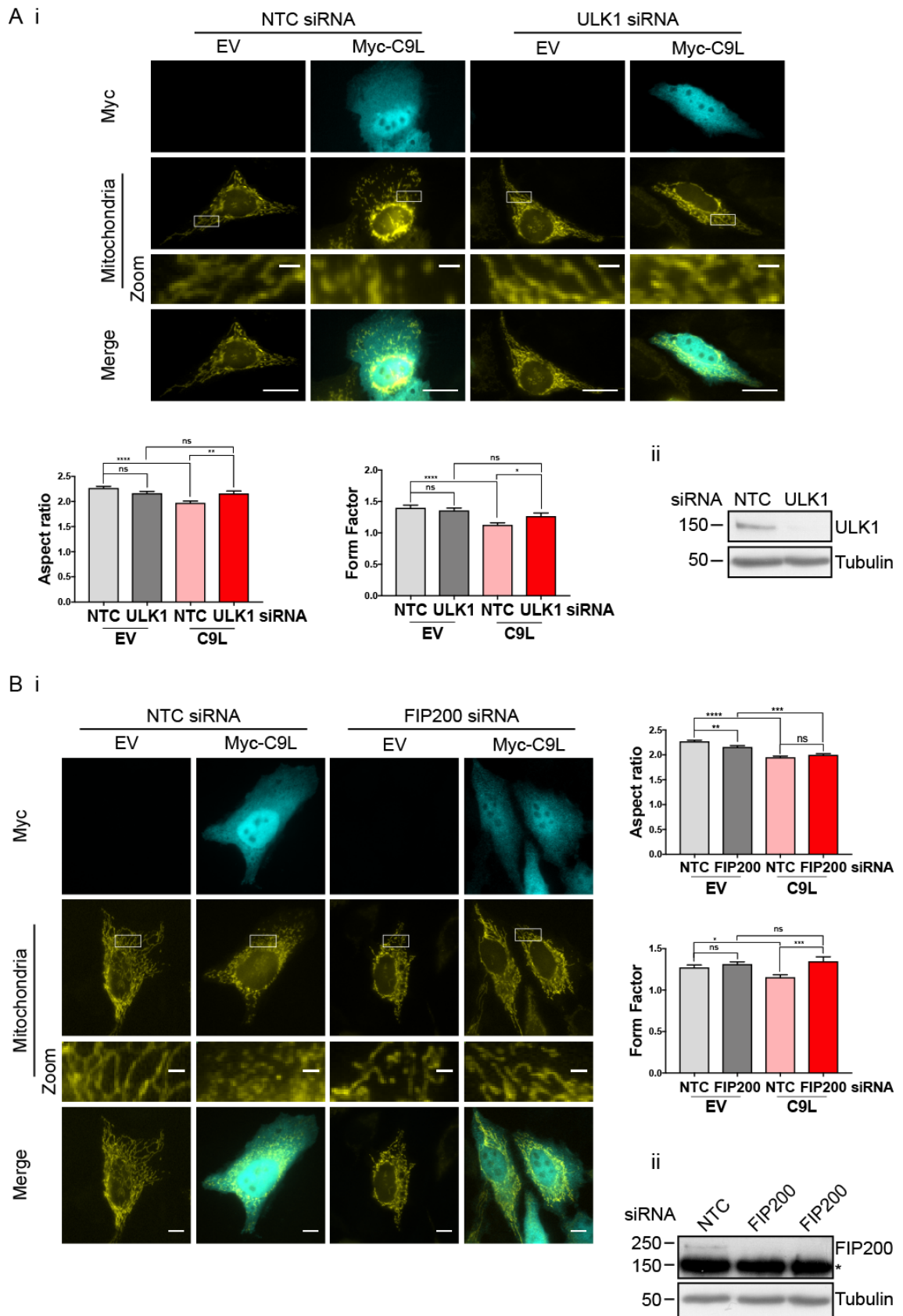


Figure 4.6 The fragmentation of the mitochondrial network upon increased levels of C9orf72L requires the ULK1 initiation complex

A) i) HeLa cells were transfected with non-targeting control (NTC) or ULK1 siRNA and were subsequently co-transfected with pCI-neo empty vector (EV) or Myc-C9orf72L (C9L) (cyan) and pAcGFP1-Mito (yellow). Mitochondrial shape parameters were quantified (aspect ratio and form factor). Cells were analysed from 2 independent experiments (NTC/EV: 30, NTC/C9L: 27, ULK1/EV: 29, ULK1/C9L: 28 cells). Scale bar 10 μ m, zoom 1 μ m. Graphs display mean \pm SEM. Statistical analysis was performed by one-way ANOVA with Fisher's LSD; * $P \leq 0.05$, ** $P \leq 0.01$, **** $P \leq 0.0001$. ii) The knockdown of ULK1 was verified by ULK1 immunoblot. B) i) HeLa cells were transfected with non-targeting control (NTC) or FIP200 siRNA and were subsequently co-transfected with pCI-neo empty vector (EV) or Myc-C9orf72L (C9L) (cyan) and pAcGFP1-Mito (yellow). Mitochondrial shape parameters were quantified (aspect ratio and form factor). Cells were analysed from 3 independent experiments (NTC/EV: 59, NTC/C9L: 53, FIP200/EV: 53, FIP200/C9L: 47 cells). Scale bar 10 μ m, zoom 2 μ m. Graphs display mean \pm SEM. Statistical analysis was performed by one-way ANOVA with Fisher's LSD; * $P \leq 0.05$, ** $P \leq 0.01$, *** $P < 0.001$, **** $P \leq 0.0001$. ii) The knockdown of FIP200 was verified by FIP200 immunoblot. * indicates an aspecific band on FIP200 immunoblot.

The ULK1 initiation complex is recruited to mitochondria upon induction of mitophagy (Itakura et al., 2012; Wu et al., 2014). C9orf72 recruits the ULK1 initiation complex during autophagy (Webster et al., 2016a). To investigate whether C9orf72 may recruit the ULK1 initiation complex to mitochondria and induce mitophagy, HEK293 cells were transfected with pCI-neo empty vector, Myc-C9orf72L or Myc-C9orf72S and mitochondria were isolated. The recruitment of ULK1 to mitochondria was stimulated in control cells by treatment with CCCP to induce mitophagy (Itakura et al., 2012). Mitochondria were subjected to immunoblot for Tubulin and MnSOD to verify the enrichment of mitochondria (Figure 4.7). ULK1 immunoblot revealed that CCCP treated cells displayed increased levels of ULK1 on mitochondria, indicative of induced mitophagy. An increase in the level of Myc-C9orf72L but not of Myc-C9orf72S similarly resulted in an increase in the level of ULK1 found on mitochondria. Thus, the increase in Myc-C9orf72L protein levels led to the recruitment of ULK1 to mitochondria.

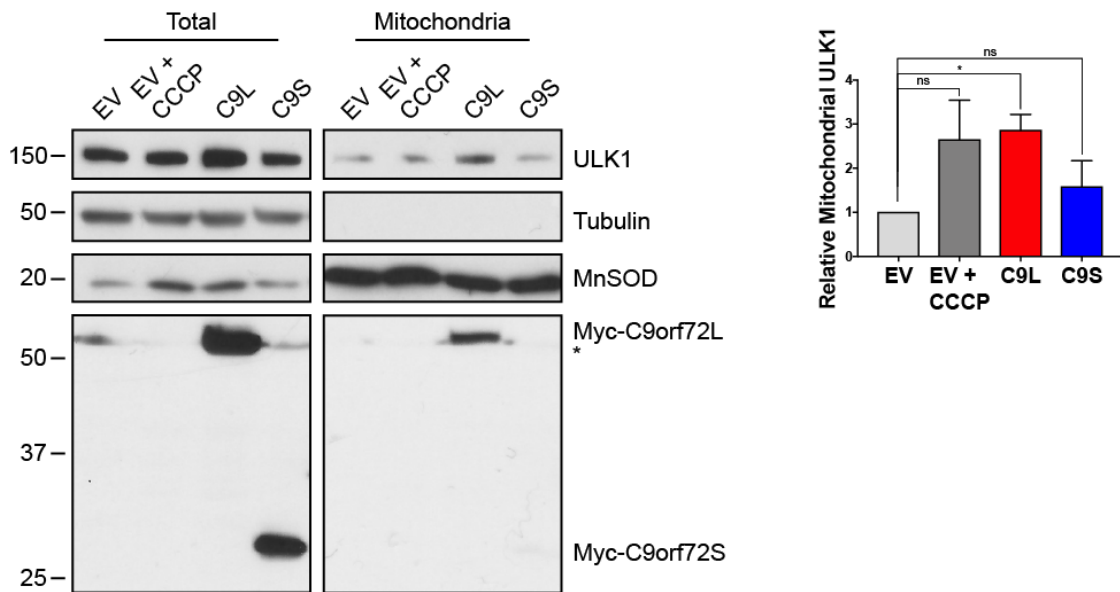


Figure 4.7 ULK1 is recruited to mitochondria by an increase in C9orf72L levels

HEK293 cells were transfected with pCI-neo empty vector (EV), Myc-C9orf72L or Myc-C9orf72S. To induce mitophagy and the translocation of the ULK1 initiation complex to mitochondria, control cells were treated 4 h with 10 μ M CCCP. Mitochondria were isolated and subjected to ULK1, Tubulin, MnSOD and Myc immunoblot. Twenty-five μ g of total cell lysate and mitochondrial fractions were subjected to immunoblot. Mitochondrial ULK1 was quantified relative to the untreated control cells from 3 independent experiments. Graph displays mean \pm SEM. Statistical analysis was performed by one-way ANOVA with Fisher's LSD; * $P \leq 0.05$. * indicates a non-specific band on Myc immunoblot.

4.3 C9orf72 regulates mitochondrial clearance via mitophagy

The recruitment of ULK1 to damaged mitochondria plays an important role in the targeting of damaged organelles for degradation during mitophagy (Itakura et al., 2012; Wu et al., 2014). As increased levels of C9orf72 led to the recruitment of ULK1 to mitochondria, we hypothesised that C9orf72 may regulate mitophagy via the recruitment of ULK1.

First, to investigate whether C9orf72 is involved in the clearance of mitochondria during mitophagy, EYFP-Parkin expressing HeLa cells were transfected with non-targeting control or C9orf72 siRNA and treated 23 h with Oligomycin and Antimycin A (O/A) to induce mitophagy and mitochondrial clearance (Figure 4.8A). Oligomycin is an inhibitor of ATP Synthase (Perlin et al., 1985), whilst Antimycin A is an inhibitor of Complex III of the OXPHOS machinery (Alexandre and Lehninger, 1984). A combination of O/A treatment efficiently induces mitochondrial damage and mitophagy (Lazarou et al., 2015;

Yamano et al., 2016). The remaining mitochondrial content of each cell was scored and the mitophagy index was generated (as described in 2.4.3.5). The knockdown of C9orf72 was verified by C9orf72 immunoblot (Figure 4.8B). In untreated cells, both the control and C9orf72 siRNA transfected cells displayed a mitophagy index value of 100, indicating a full mitochondrial content as expected. In control cells, mitochondrial content was reduced following O/A treatment in 80 % of cells. In contrast, in cells where C9orf72 levels were reduced, only 60 % of cells displayed a reduced mitochondrial content. Thus, loss of C9orf72 impaired mitochondrial clearance. C9orf72 may therefore regulate mitophagy.

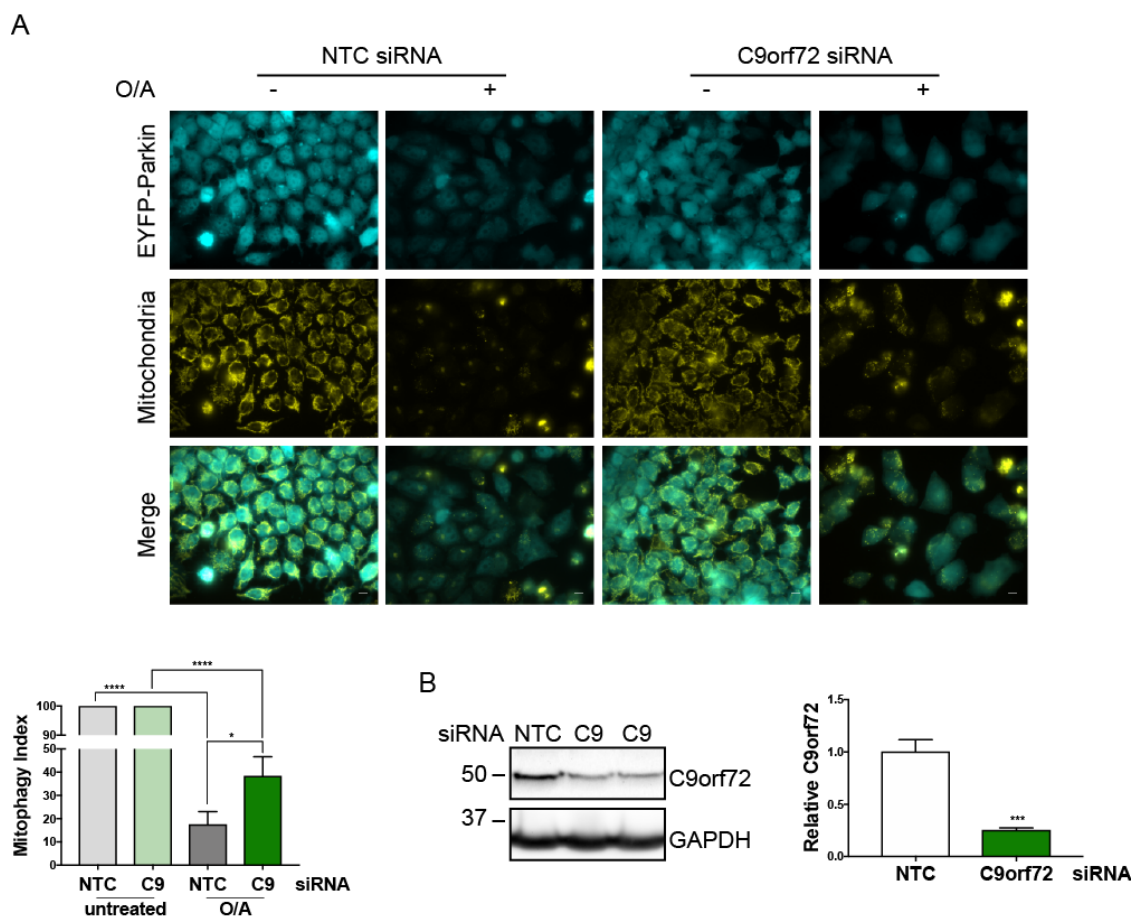


Figure 4.8 Reduced levels of C9orf72 impair mitophagy

A) EYFP-Parkin (cyan) expressing HeLa cells were transfected with non-targeting control (NTC) or C9orf72 siRNA and were treated 23 h with 10 μ M Oligomycin and 4 μ M Antimycin A (O/A) to induce mitophagy. Cells were subjected to immunostain for the OMM protein TOMM20 (yellow) to reveal mitochondrial content. The mitochondrial content of individual cells was quantified at each timepoint and the mitophagy index calculated. Cells were quantified from 15 fields from 4 independent experiments (345 – 864 cells per condition per experiment). Scale bar 10 μ m. Graph displays mean \pm SEM.

*Statistical analysis was performed by one-way ANOVA with Fisher's LSD; * $P \leq 0.05$, **** $P \leq 0.0001$. B) The knockdown of C9orf72 was verified by C9orf72 immunoblot. Relative C9orf72 levels were quantified to the control siRNA. Graph displays mean \pm SEM. Statistical analysis was performed by unpaired t-test; *** $P < 0.001$.*

To investigate how C9orf72 may regulate mitophagy, we investigated the role of C9orf72 in Parkin dependent mitophagy. Briefly, following mitochondrial damage and the depolarisation of the mitochondria, PINK1 is stabilised on the OMM, which leads to the recruitment of the E3 ligase Parkin to mitochondria (Narendra et al., 2008; Narendra et al., 2010a). The ubiquitination of OMM proteins leads to their degradation by the proteasome and to the recruitment of the mitophagy adaptor proteins (Gegg et al., 2010; Lazarou et al., 2015). Finally, the ULK1 initiation complex is recruited to mitochondria and the organelle is engulfed by an autophagosome (Itakura et al., 2012). We next investigated how C9orf72 may regulate mitophagy.

4.3.1 C9orf72 regulates the recruitment of Parkin to mitochondria

The stabilisation of PINK1 on the OMM upon loss of MMP, results in the phosphorylation of mitochondrial ubiquitin residues and the recruitment of the E3 ligase Parkin to damaged mitochondria. Parkin is then phosphorylated resulting in a conformational change and its activation. Parkin ubiquitinates proteins on the OMM surface, resulting in the proteasomal degradation of the proteins involved in mitochondrial fusion and motility (reviewed in Hamacher-Brady and Brady, 2016). The recruitment of Parkin to damaged mitochondria results in an amplification of the mitochondrial damage signal (reviewed in Durcan and Fon, 2015).

To investigate whether C9orf72 is involved in the recruitment of Parkin to mitochondria, first the effect of increasing the level of C9orf72 was explored. In an immunofluorescence approach, HeLa cells were co-transfected with pCI-neo empty vector, Myc-C9orf72L or Myc-C9orf72S and EYFP-Parkin. To induce Parkin recruitment, cells were additionally treated with CCCP to induce mitochondrial damage and Parkin dependent mitophagy. The number of cells displaying EYFP-Parkin recruited to mitochondria was quantified in each condition (Figure 4.9A). Under basal conditions, EYFP-Parkin appeared cytosolic in both control cells and cells expressing either Myc-C9orf72L or Myc-C9orf72S. Upon CCCP treatment, EYFP-Parkin was recruited to mitochondria in control cells. The expression of Myc-C9orf72L or Myc-C9orf72S did not affect the translocation of EYFP-Parkin to mitochondria upon CCCP treatment. One drawback of this immunofluorescence-based approach was the high level of cytosolic EYFP-Parkin under basal conditions. Because it is possible that this may have masked

low levels of Parkin recruitment to mitochondria, the recruitment of Parkin to mitochondria was also investigated by immunoblot. HEK293 cells were co-transfected with pCI-neo empty vector, Myc-C9orf72L or Myc-C9orf72S and EYFP-Parkin. In control cells, EYFP-Parkin translocation to mitochondria was induced by CCCP treatment. Mitochondria were isolated and subjected to immunoblot for Tubulin and COX IV to verify the enrichment of mitochondria (Figure 4.9B). YFP immunoblot revealed a low level of EYFP-Parkin in mitochondria in control cells. The level of EYFP-Parkin in mitochondria increased in control cells upon CCCP treatment, indicative of the translocation of EYFP-Parkin to mitochondria. An increase in the level of C9orf72, upon overexpression of either Myc-C9orf72L or Myc-C9orf72S, led to an increase in the amount of EYFP-Parkin found in the mitochondrial fraction. Thus, increased C9orf72 levels led to the translocation of Parkin to mitochondria.

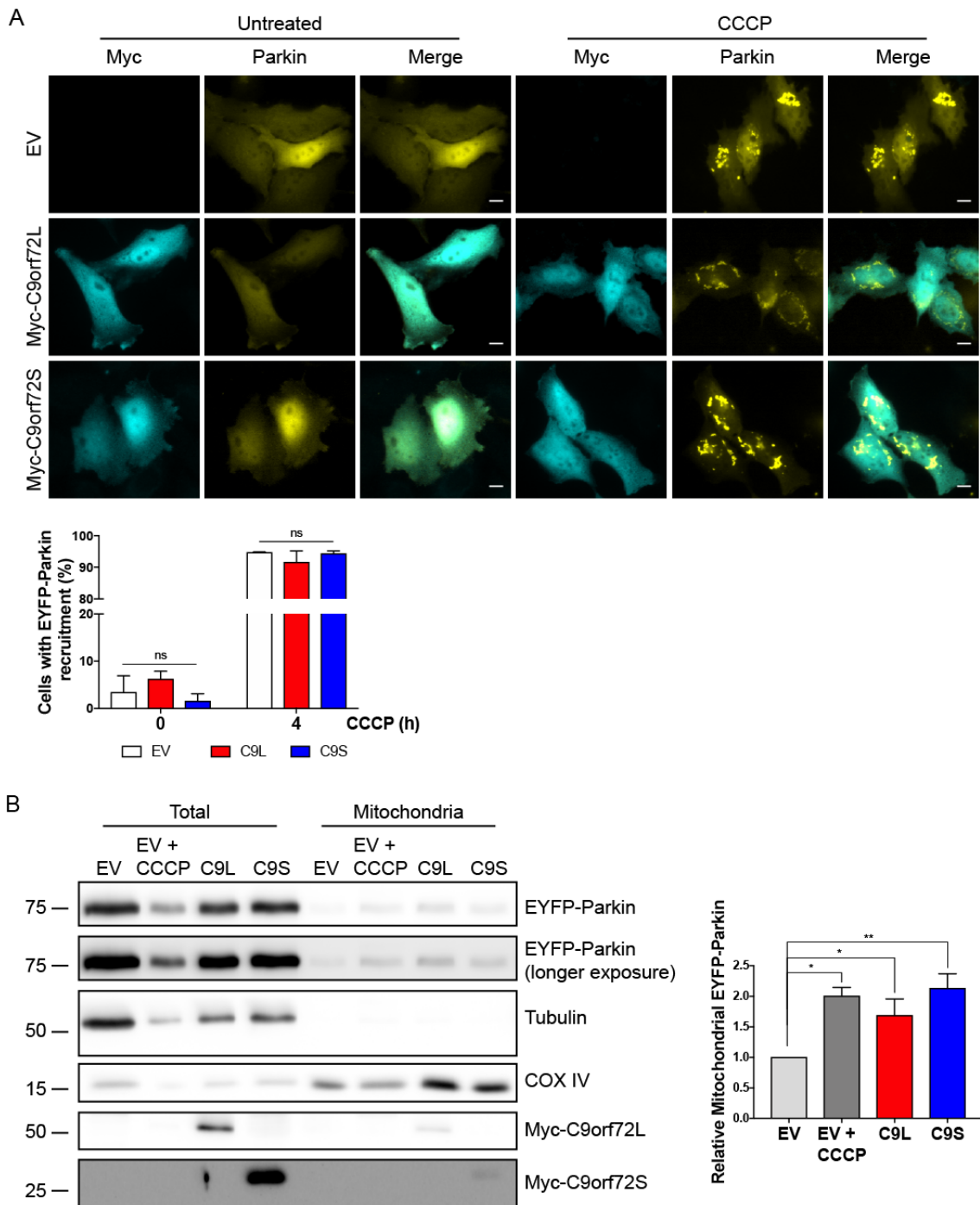


Figure 4.9 An increased C9orf72 level recruits Parkin to mitochondria

A) HeLa cells were co-transfected with pCI-neo empty vector (EV), Myc-C9orf72L (C9L) or Myc-C9orf72S (C9S) (cyan) and EYFP-Parkin (yellow). Subsequently, cells were treated 4 h with 10 μ M CCCP to induce mitochondrial damage and EYFP-Parkin recruitment. The number of cells displaying EYFP-Parkin recruited to mitochondria was quantified at each timepoint. Cells were quantified from 2 independent experiments (29 – 47 cells per experiment). Scale bar 10 μ m. Graph displays mean \pm SEM. Statistical analysis was performed by two-way ANOVA with Fisher's LSD. *B*) Mitochondrial

*enriched fractions were produced from HEK293 cells co-transfected with pCI-neo empty vector (EV), Myc-C9orf72L (C9L) or Myc-C9orf72S (C9S) and EYFP-Parkin. Control cells were treated 4 h with 10 μ M CCCP to induce mitochondrial damage and Parkin translocation to mitochondria. Mitochondria were subject to YFP, Tubulin, COX IV and Myc immunoblot. Twenty μ g of total cell lysate and mitochondrial fractions were subjected to immunoblot. Relative mitochondrial EYFP-Parkin was quantified from the YFP immunoblot relative to the control from 3 independent experiments. Graph displays mean \pm SEM. Statistical analysis was performed by one-way ANOVA with Fisher's LSD; * $P \leq 0.05$, ** $P \leq 0.01$.*

To investigate whether the loss of C9orf72 alters Parkin recruitment and mitophagy initiation, HeLa cells were transfected with non-targeting control or C9orf72 siRNA and were subsequently transfected with EYFP-Parkin. Mitochondrial damage and Parkin translocation were induced by treatment with CCCP treatment and the number of cells displaying recruited EYFP-Parkin was quantified (Figure 4.10Ai). The efficiency of C9orf72 knockdown was verified by qPCR (Figure 4.10Aii). Under basal conditions, control cells and cells lacking C9orf72 displayed cytosolic EYFP-Parkin. At 1 h CCCP treatment, 50 % of control cells displayed EYFP-Parkin recruited to mitochondria. The reduction in C9orf72 levels did not affect the translocation of EYFP-Parkin to mitochondria following 1 h of CCCP treatment. Following 2 h of CCCP treatment, 80 % of control cells displayed EYFP-Parkin recruitment to mitochondria. The loss of C9orf72 did not affect the number of cells displaying the translocation of EYFP-Parkin following 2 h of CCCP treatment. The maintenance of Parkin on mitochondria is required for a robust mitophagy response (reviewed in Durcan and Fon, 2015; Hamacher-Brady and Brady, 2016). To further investigate the role of C9orf72 in Parkin translocation during later stages of mitophagy, HeLa cells were transfected with non-targeting control or C9orf72 siRNA and were subsequently transfected with EYFP-Parkin. Mitochondrial damage and Parkin translocation were induced by treatment with CCCP for 4 h. The number of cells displaying recruited EYFP-Parkin were quantified (Figure 4.10Bi). The efficiency of C9orf72 knockdown was verified by qPCR (Figure 4.10Bii). The loss of C9orf72 led to a decrease in the number of cells displaying EYFP-Parkin translocated to mitochondria compared to control cells following 4 h CCCP treatment. Thus, C9orf72 is not required for the translocation of Parkin during early mitophagy but may be required for maintaining Parkin on mitochondria during late mitophagy.

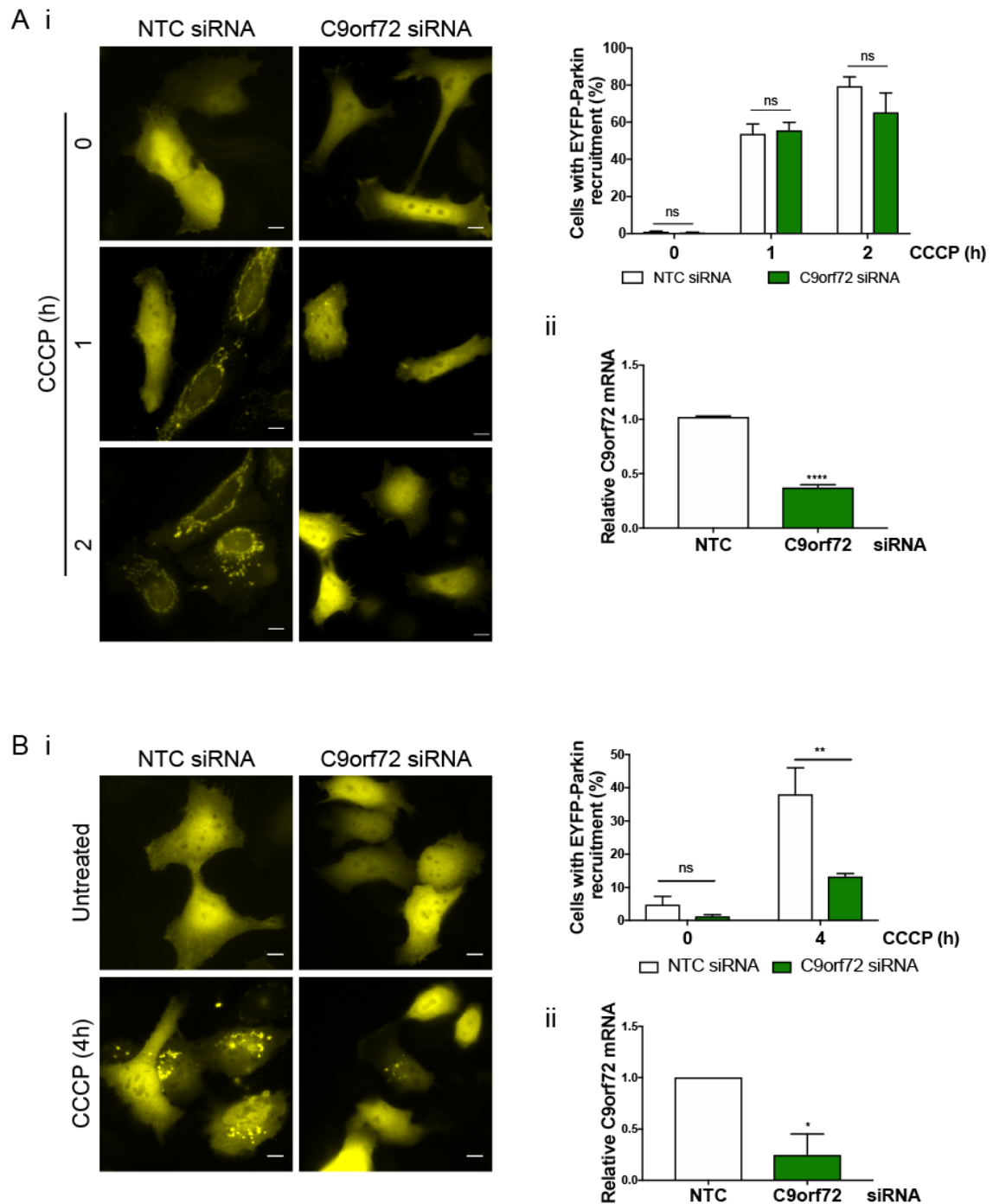


Figure 4.10 The loss of C9orf72 leads to reduced mitochondrially located Parkin at later stages of mitophagy

A) i) HeLa cells were transfected with non-targeting control (NTC) or C9orf72 siRNA and were subsequently transfected with EYFP-Parkin (yellow). Cells were treated 1 or 2 h with 10 μ M CCCP to induce mitochondrial damage and Parkin recruitment. Cells displaying EYFP-Parkin recruited to mitochondria were quantified at each timepoint. Cells were quantified from 5 independent experiments (32 – 79 cells per experiment). Scale bar 10 μ m. Graph displays mean \pm SEM. Statistical analysis was performed by two-

way ANOVA with Fisher's LSD. ii) The level of C9orf72 mRNA was determined by qPCR. Graph displays mean \pm SEM. Statistical analysis was performed by unpaired t-test; **** $P \leq 0.0001$. B) i) HeLa cells were transfected with non-targeting control (NTC) or C9orf72 siRNA and were subsequently transfected with EYFP-Parkin (yellow). Cells were treated 4 h with 10 μ M CCCP to induce mitochondrial damage and Parkin translocation. The number of cells displaying the translocation of EYFP-Parkin to mitochondria was quantified. Cells were quantified from 3 independent experiments. Scale bar 10 μ m. Graph displays mean \pm SEM. Statistical analysis was performed by two-way ANOVA with Fisher's LSD; ** $P \leq 0.01$. ii) The level of C9orf72 mRNA was determined by qPCR. Graph displays mean \pm SEM. Statistical analysis was performed by unpaired t-test; * $P \leq 0.05$.

4.3.2 C9orf72 is not required for the degradation of OMM proteins

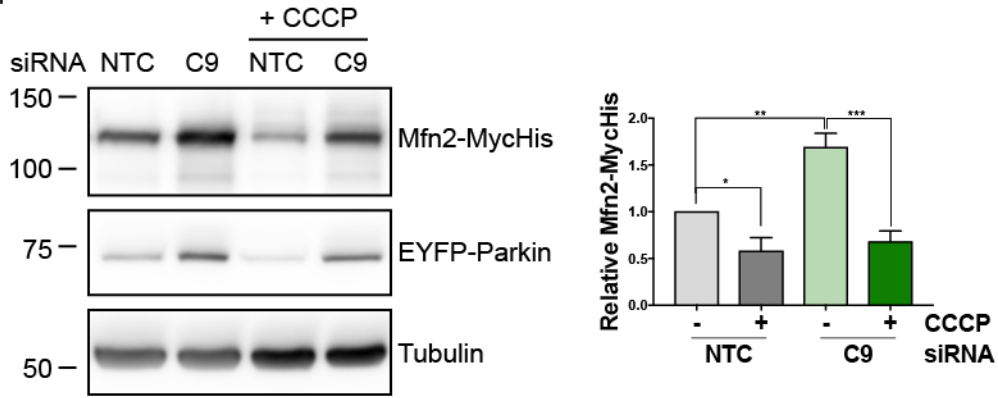
Following the recruitment and activation of Parkin, the OMM proteins involved in mitochondrial fusion and motility are ubiquitinated and degraded by the proteasome. Their degradation leads to the arrest of mitochondrial movement and the isolation of damaged organelles from the network (reviewed in Hamacher-Brady and Brady, 2016). Proteins degraded in this manner include the fusion proteins Mfn1/2 and MIRO1, involved in the anterograde transport of mitochondria (Gegg et al., 2010; Tanaka et al., 2010; Wang et al., 2011). Whether C9orf72 plays a role in this step of mitophagy was next investigated.

Earlier we showed that an increase in C9orf72 expression levels did not alter the levels of OMM protein Mfn2 (Figure 4.3). Thus, despite an increase in the level of Parkin found on mitochondria following the expression of Myc-C9orf72L or Myc-C9orf72S (Figure 4.9), this did not result in the degradation of the OMM protein Mfn2.

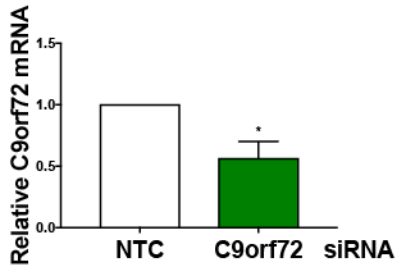
To determine if C9orf72 was required for the Parkin mediated degradation of OMM proteins, HeLa cells were transfected with non-targeting control or C9orf72 siRNA. Cells were subsequently co-transfected Mfn2-MycHis and EYFP-Parkin. To induce mitochondrial damage and the degradation of OMM proteins, cells were treated with CCCP (Figure 4.11Ai). The efficiency of C9orf72 knockdown was verified by qPCR (Figure 4.11Aii). Mfn2 immunoblot revealed that in both control and cells with loss of C9orf72, the treatment with CCCP resulted in a decrease in the level of Mfn2-MycHis. Thus, C9orf72 is not required for the degradation of the OMM protein Mfn2 during mitophagy. To verify that the loss of C9orf72 did not affect the degradation of OMM proteins during mitophagy, a preliminary investigation into the degradation of MIRO1 was performed. HeLa cells were transfected with non-targeting control or C9orf72 siRNA

and were subsequently co-transfected with pCI-neo empty vector or Parkin-MycHis and with Myc-MIRO1. To induce mitophagy cells were treated with CCCP (Figure 4.11Bi). The efficiency of C9orf72 siRNA was verified by qPCR (Figure 4.11Bii). Myc immunoblot revealed that in cells lacking Parkin, the induction of mitophagy with CCCP did not induce a decrease in the level of Myc-MIRO1. Consistent with the role of Parkin in the labelling of OMM proteins for proteasomal degradation, the expression of Parkin-MycHis resulted in a decrease in the level of Myc-MIRO1 upon CCCP treatment in control siRNA transfected cells. Loss of C9orf72 did not affect the reduction in Myc-MIRO1 levels upon mitophagy induction. Hence, C9orf72 is not required for the proteasomal degradation of OMM proteins during mitophagy. We noted that knockdown of C9orf72 resulted in a slight increase in the level of EYFP-Parkin or Parkin-MycHis (Figure 4.11). Parkin has been shown to ubiquitinate itself to regulate its degradation by the autophagy pathway (Durcan et al., 2011; Zhang et al., 2000). Knockdown of C9orf72 has been shown to result in impaired autophagy (Sellier et al., 2016; Webster et al., 2016a; Yang et al., 2016). Hence the elevation in Parkin noted here may correspond to defects in Parkin turnover, which should be explored further. However, Parkin has also been shown to be upregulated upon mitochondrial damage and where mitochondrial fission/fusion cycling is impaired (reviewed in Dorn, 2016). Therefore, this increase may merely reflect a cellular response to defective mitochondrial quality control.

A i



ii



B i

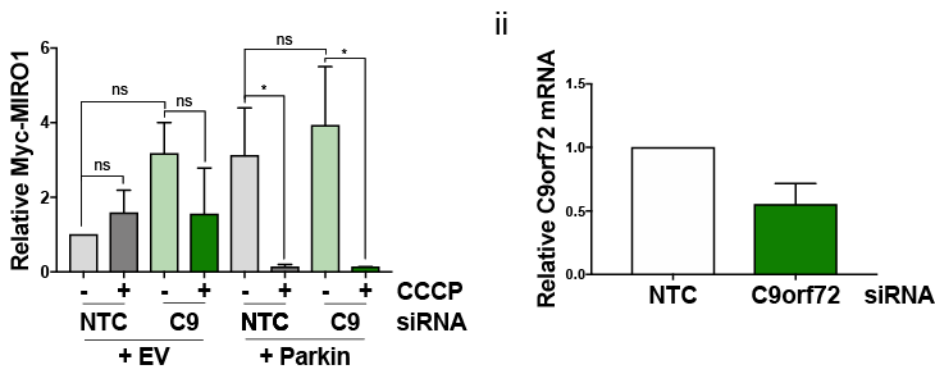
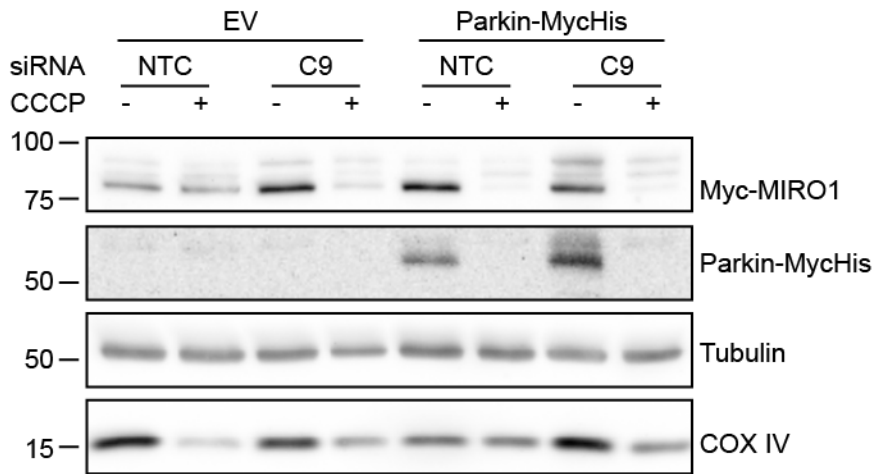


Figure 4.11 Loss of C9orf72 does not impair the degradation of OMM proteins during mitophagy

A) i) HeLa cells were transfected with non-targeting control (NTC) or C9orf72 (C9) siRNA and were subsequently co-transfected with Mfn2-MycHis and EYFP-Parkin. Cells were treated 4 h with 20 μ M CCCP to induce mitochondrial damage and the degradation of OMM proteins. The level of Mfn2-MycHis in total cell lysate was quantified by Mfn2 immunoblot relative to the untreated control in 3 independent experiments. Twenty μ g of total cell lysate was subjected to immunoblot. Graph displays mean \pm SEM. Statistical analysis was performed by one-way ANOVA with Fisher's LSD; * $P \leq 0.05$, ** $P \leq 0.01$, *** $P < 0.001$. ii) The level of C9orf72 mRNA was quantified by qPCR. Graph displays mean \pm SEM. Statistical analysis was performed by unpaired t-test; * $P \leq 0.05$. B) i) HeLa cells were transfected with non-targeting control (NTC) or C9orf72 (C9) siRNA and were subsequently co-transfected with Myc-MIRO1 and pCI-neo empty vector (EV) or Parkin-MycHis. Cells were treated 4 h with 20 μ M CCCP to induce mitochondrial damage and the degradation of OMM proteins. The level of Myc-MIRO1 in total cell lysate was quantified by Myc immunoblot relative to the untreated control in 2 independent experiments. Twenty-five μ g of total cell lysate was subjected to immunoblot. Graph displays mean \pm SEM. Statistical analysis was performed by one-way ANOVA with Fisher's LSD; * $P \leq 0.05$. ii) The level of C9orf72 mRNA was quantified by qPCR. Graph displays mean \pm SEM. Statistical analysis was performed by unpaired t-test; P value = 0.1123.

4.3.3 C9orf72 is recruited to mitochondria upon mitochondrial damage

Mitophagy adaptor proteins and the autophagy machinery are recruited to the damaged organelle upon the induction of mitophagy (reviewed in Hamacher-Brady and Brady, 2016). C9orf72 has previously been shown to relocalise during starvation (Amick et al., 2016). Therefore, the cellular localisation of C9orf72 may be dynamic and respond to the cellular environment. As C9orf72 may be involved in the clearance of mitochondria during mitophagy and may recruit the ULK1 initiation complex to mitochondria, we investigated the possibility that C9orf72 undergoes recruitment to mitochondria upon mitochondrial damage.

To investigate whether C9orf72 may be recruited to mitochondria during mitophagy, HEK293 cells were treated with O/A to induce mitochondrial damage and mitophagy. Mitochondrial enriched fractions were produced and subjected to Tubulin and HSP60 immunoblot to verify the enrichment of mitochondria (Figure 4.12). C9orf72 immunoblot revealed that the induction of mitochondrial damage with O/A resulted in a higher level

of C9orf72 in mitochondria. Thus, C9orf72 is recruited to mitochondria upon mitochondrial damage.



Figure 4.12 C9orf72 is recruited to mitochondrial upon mitochondrial damage

Mitochondria were isolated from HEK293 cells which were treated 3 h with 10 μ M Oligomycin and 4 μ M Antimycin A (O/A) to induce mitochondrial damage. Total cell lysate (Total) and mitochondrial fractions were subjected to C9orf72, Tubulin and HSP60 immunoblot. Twenty-five μ g of total cell lysate and mitochondrial fractions were subjected to immunoblot. The level of mitochondrial C9orf72 was quantified relative to the untreated control in 5 independent experiments. Graph displays mean \pm SEM. Statistical analysis was performed by unpaired t-test; * $P \leq 0.05$. * indicates an aspecific band on C9orf72 immunoblot.

4.4 C9orf72 ALS patient iAstrocytes display altered mitochondrial dynamics

Defects in mitochondrial morphology and mitophagy are common features of ALS patients and cell and animal models (reviewed in Smith et al., 2017b). C9orf72 patient fibroblasts and iPSC motor neurons were reported to have fragmented mitochondrial networks and swollen mitochondria (Dafinca et al., 2016; Onesto et al., 2016). Furthermore, autophagic vacuoles containing mitochondria were reported in C9orf72 fibroblasts, which implied dysregulated mitophagy (Onesto et al., 2016). Non-cell autonomous mechanisms have been shown to contribute to ALS pathogenesis (reviewed in Chen et al., 2018). C9orf72 ALS patient derived astrocytes have been reported to display an impaired ability to support the survival of motor neurons (Meyer et al., 2014). Whether C9orf72 ALS patient astrocytes display mitochondrial quality control defects is currently unknown.

The study of mitochondrial quality control in neuronal cell lines remains controversial (reviewed in Martinez-Vicente, 2017). Therefore, to investigate mitochondrial dysfunction in a disease relevant patient model, mitochondrial network morphology and

mitophagy were investigated in C9orf72 ALS patient derived iAstrocytes. C9orf72 ALS patient skin fibroblasts and age and sex matched controls were reprogrammed into iAstrocytes according to the published protocol (Meyer et al., 2014). C9orf72 ALS patient iAstrocytes display RNA foci, observed in patient tissue and other C9orf72 ALS patient cell models, suggesting that they may recapitulate features of C9orf72 disease (Ferraiuolo lab, University of Sheffield, unpublished data).

4.4.1 C9orf72 patient iAstrocytes have fragmented mitochondrial networks

To investigate whether the C9orf72 patients iAstrocytes display mitochondrial network alterations, C9orf72 ALS patient and control iAstrocytes were immunostained with anti-TOMM20 to visualise mitochondrial networks. The connectivity of the mitochondrial networks was analysed (Figure 4.13). The mitochondrial networks in control cells appeared tubular and branched, whereas the mitochondrial networks in the C9orf72 ALS patient iAstrocytes were more fragmented. Hence C9orf72 patient iAstrocytes recapitulate the fragmented mitochondrial networks reported in other C9orf72 ALS patient models. Therefore, mitochondrial dynamics may be altered in C9orf72 ALS patients.

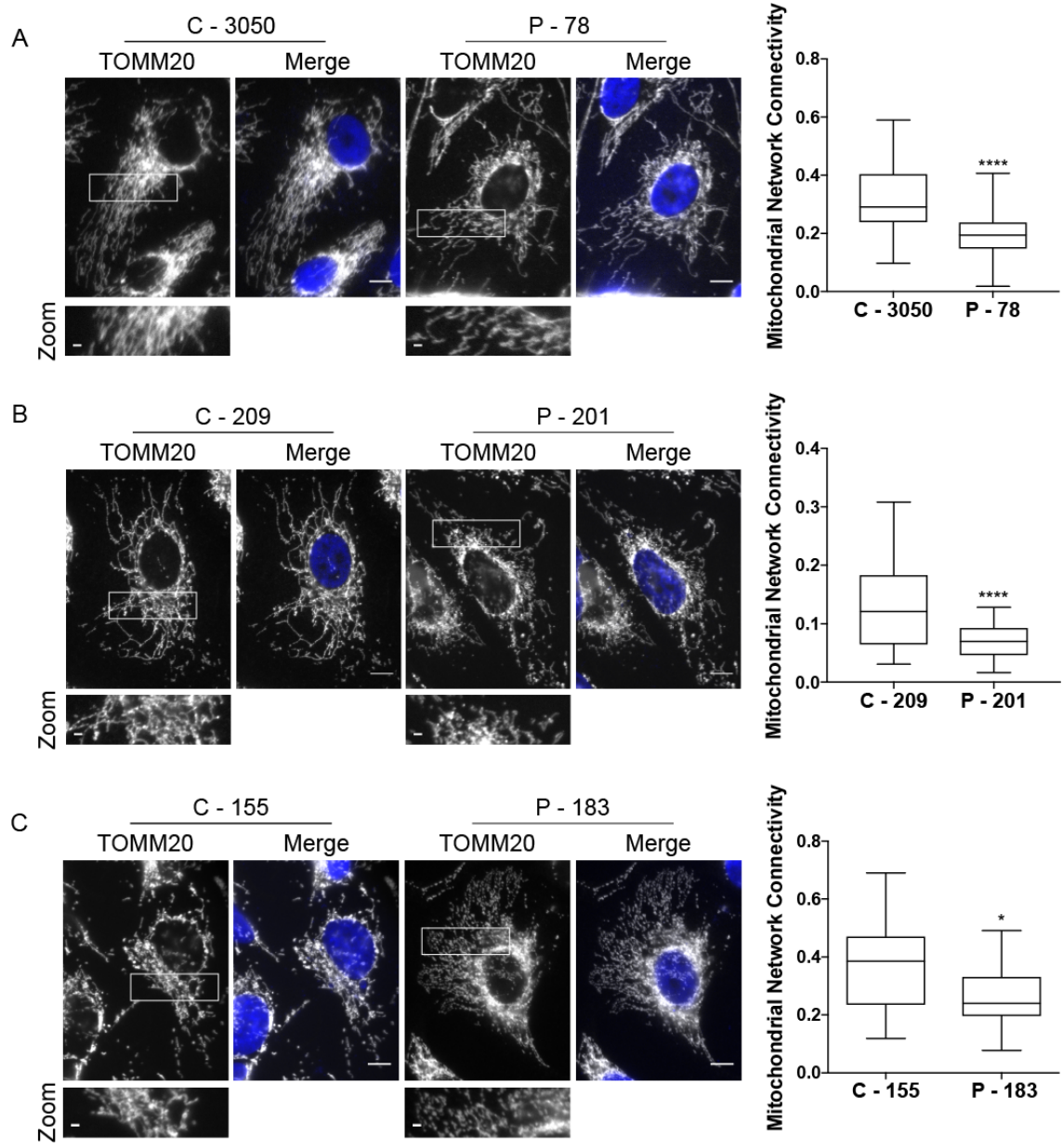


Figure 4.13 C9orf72 patient iAstrocytes display fragmented mitochondrial networks

C9orf72 ALS patient iAstrocytes and matched controls were immunostained with anti-TOMM20 (grey) to reveal mitochondria. Mitochondrial network connectivity was quantified. Scale bar 10 μ m, zoom 2 μ m. Graphs display mean, minimum and maximum values. A) C – 3050/P – 78, cells quantified from 2 independent experiments (C – 3050: 40, P – 78: 40 cells). B) C – 209/P – 201, cells quantified from 2 independent experiments (C – 209: 34, P – 201: 36 cells). C) C – 155/P – 183, cells quantified from 1 experiment (C – 155: 19, P – 183: 19 cells). Statistical analysis was performed by unpaired *t*-test; ** $P \leq 0.01$, **** $P \leq 0.0001$.

4.4.2 Parkin recruitment is delayed in C9orf72 patient iAstrocytes

It was previously reported that iNeurons derived from these same C9orf72 ALS patients (P - 201 and P – 183) exhibit defects in autophagy (Webster et al., 2016a). Defects in autophagy can lead to accumulation of damaged mitochondria through impaired mitophagy (Rambold and Lippincott-Schwartz, 2011). To investigate whether cells from the same C9orf72 ALS patients displayed mitophagy defects, the recruitment of Parkin to damaged mitochondria was analysed. C9orf72 ALS patient and matched control iAstrocytes were transfected with EYFP-Parkin. Mitochondrial damage and the translocation of Parkin was induced by O/A treatment. The number of cells displaying EYFP-Parkin recruited to mitochondria was quantified (Figure 4.14). EYFP-Parkin was translocated to mitochondria in both the control and patient iAstrocytes, indicating that mitophagy had been successfully induced in these cells. Compared to the matched controls, the C9orf72 ALS patient iAstrocytes displayed a reduced number of cells displaying mitochondrially located EYFP-Parkin following both 30 min and 1 h O/A treatment. Following 2 h O/A treatment, C9orf72 ALS patients P – 183 and P – 78 displayed the same level of EYFP-Parkin recruitment as their matched controls. In contrast, patient P – 201 displayed a reduced EYFP-Parkin compared to control C - 209. Hence, C9orf72 ALS patients displayed delayed Parkin recruitment, which may lead to impaired clearance of damaged mitochondria.

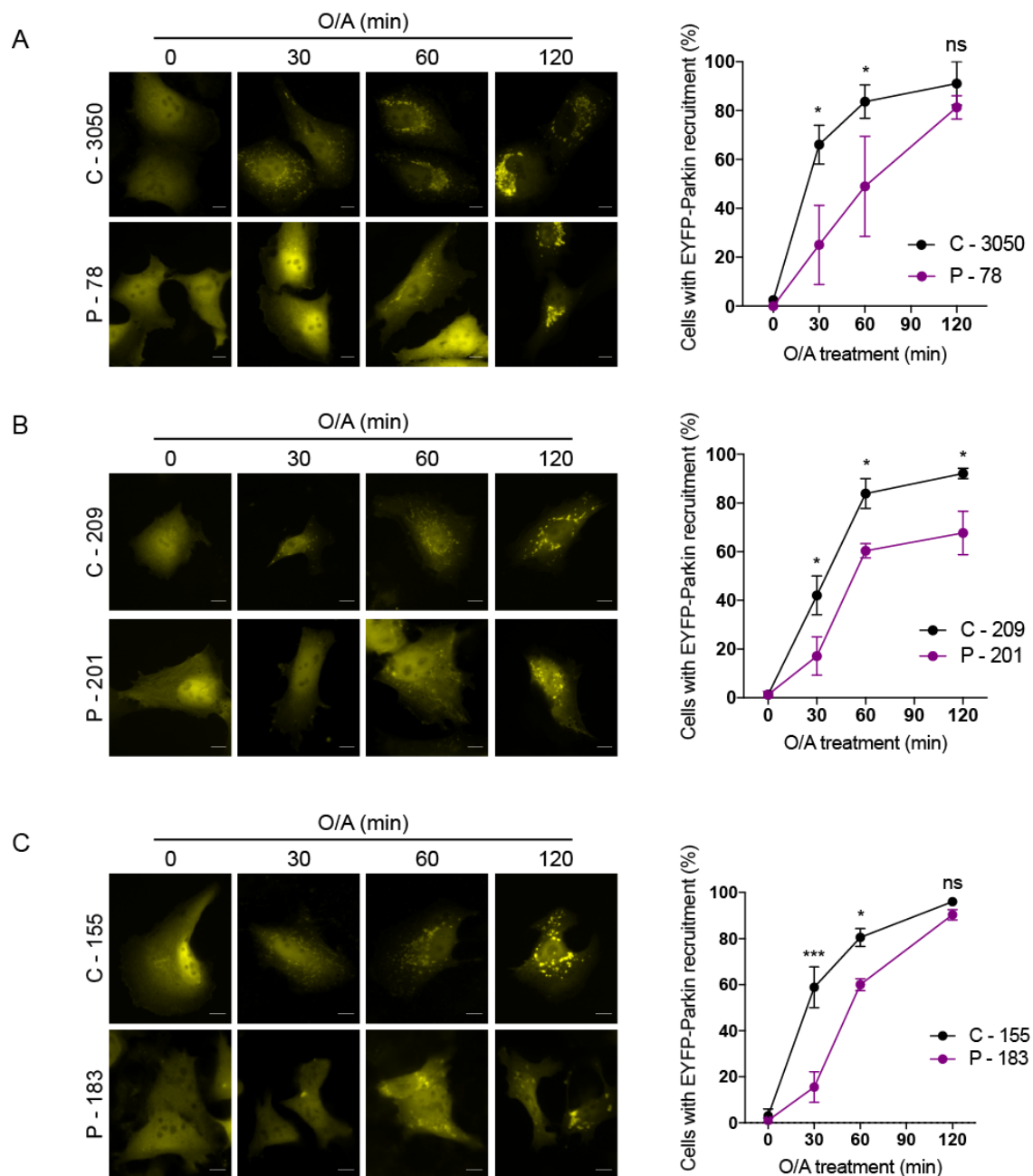


Figure 4.14 C9orf72 patient iAstrocytes have delayed Parkin recruitment

C9orf72 ALS patient (P - 78, P - 201, P - 183) and matched control (C - 3050, C - 209, C - 155) iAstrocytes were transfected with EYFP-Parkin (yellow) and treated with 10 μ M Oligomycin and 4 μ M Antimycin A (O/A) for 30, 60 or 120 min as indicated. The number of cells displaying EYFP-Parkin translocated to mitochondria was quantified at each timepoint. A) C - 3050 / P - 78. B) C - 209 / P - 201. C) C - 155 / P - 183. Scale 10 μ m. Graphs display mean \pm SEM. Cells were quantified from 2 independent experiments (9 - 30 fields per experiment (10 - 114 cells)). Statistical analysis was performed by two-way ANOVA with Fisher's LSD; $P \leq 0.05$, *** $P < 0.001$.

4.5 Discussion

In Chapter 3, we identified an interaction between C9orf72 and mitochondria. In this chapter the relevance of this interaction for mitochondrial health and dynamics was investigated. C9orf72 was found to be recruited to mitochondria following mitochondrial damage (Figure 4.12). An increase in C9orf72 levels induced the fragmentation of the mitochondrial network (Figure 4.1), coupled with Drp1, Parkin and ULK1 recruitment to mitochondria (Figure 4.3B, Figure 4.9, Figure 4.7) but without inducing a decrease in MMP that may indicate damage (Figure 4.5). This indicated that an increase in C9orf72 levels may induce mitophagy. In contrast, loss of C9orf72 led to an increase in mitochondrial fusion (Figure 4.2), associated with increased level of the fusion protein Mfn2 (Figure 4.4A). Loss of C9orf72 impaired the clearance of damaged mitochondria (Figure 4.8), affecting Parkin localisation to mitochondria at later stages of mitophagy (Figure 4.10B).

The localisation of C9orf72 on mitochondria may underlie its role in the regulation of mitochondrial dynamics. C9orf72 has previously been reported to respond to cellular stresses and undergo cellular redistribution during starvation (Amick et al., 2016) and here upon mitochondrial damage (Figure 4.12). An increase in the level of C9orf72 in mitochondria upon induction of mitochondrial damage suggested that C9orf72 may be recruited to damaged mitochondria. Indeed, this is similar to the autophagy and mitophagy adaptor proteins previously implicated in mitophagy (reviewed in Hamacher-Brady and Brady, 2016; Itakura et al., 2012; Lazarou et al., 2015; Wong and Holzbaur, 2014). Damaged mitochondria are targeted for degradation by the recruitment of LC3 positive autophagosomes to mitochondria by the mitophagy adaptor proteins (reviewed in Hamacher-Brady and Brady, 2016). Mitophagy adaptor proteins including OPTN and p62 are recruited to the OMM during mitophagy and in turn recruit LC3 to mitochondria via their LIR (reviewed in Birgisdottir et al., 2013). In addition, mitochondrial proteins which contain an LIR, such as PHB2 of the IMM and FUNDC1 of the OMM have been shown to recruit LC3 to damaged mitochondria (Liu et al., 2012; Wei et al., 2017). PHB2 is located in the IMM and binds LC3 upon rupture of the OMM (Wei et al., 2017). Therefore, despite the interaction of C9orf72 with IMM complexes and a localisation to the IMS, C9orf72 may be involved in recruiting the autophagy machinery to damaged mitochondria. Indeed, rupture of the OMM may promote the mitochondrial localisation of C9orf72 and mitochondrial clearance.

The C9orf72 protein has been previously reported to play a role in the autophagy pathway (Amick et al., 2016; Sellier et al., 2016; Sullivan et al., 2016; Webster et al., 2016a; Yang et al., 2016). As a Rab effector, C9orf72 regulates the trafficking of the

ULK1 initiation complex to the phagophore during autophagy initiation (Sullivan et al., 2016; Webster et al., 2016a; Yang et al., 2016). The recruitment of ULK1 to mitochondria is required for the removal of the damaged organelle (Itakura et al., 2012; Wu et al., 2014) and for the Drp1 mediated fission of mitochondrial networks (Saito and Sadoshima, 2018). The data reported here supports a role for C9orf72 in the clearance of mitochondria via mitophagy. Consistent with a role for the trafficking of the ULK1 initiation complex by C9orf72 in mitophagy, increased levels of C9orf72 led to elevated ULK1 levels on mitochondria (Figure 4.7). Furthermore, ULK1 was required for C9orf72 mediated fission of the mitochondrial network (Figure 4.6). The recruitment of ULK1 to mitochondria has been reported to promote the fission of the network through phosphorylation of Drp1 at Ser616 (Saito and Sadoshima, 2018). Hence trafficking of ULK1 to mitochondria by C9orf72 may result in the fragmentation of the network. Thus, C9orf72 may traffic the ULK1 initiation complex to mitochondria and the activity of the ULK1 complex subsequently results in the fragmentation of the network and promotes mitophagy. Therefore, upon mitochondrial damage, C9orf72 may translocate to mitochondria with the ULK1 initiation complex and promote mitophagy. As an increase in C9orf72 resulted in the fragmentation of the mitochondrial network without inducing mitochondrial damage (Figure 4.1, Figure 4.5), this indicates a role for C9orf72 directly in the targeting of mitochondria for degradation. Indeed, overexpression of PHB2, an IMM protein which also targets mitochondria for degradation (Wei et al., 2017), results in fission of the network without overt mitochondrial damage (Kowno et al., 2014).

We reported an increase in the level of E3 ligase Parkin in mitochondria upon expression of C9orf72 (Figure 4.9). However, this did not correlate with a decrease in the level of known OMM Parkin substrate Mfn2 (Figure 4.3A). To promote the E3 ligase activity, Parkin is phosphorylated by PINK1 and undergoes conformational changes (reviewed in Durcan and Fon, 2015). As MMP was not affected by an increase in C9orf72 expression, it is therefore unlikely that PINK1 is stabilised on the OMM when C9orf72 was expressed. In the absence of PINK1 stabilisation, Parkin activity is repressed, hence the Parkin found on mitochondria upon expression of C9orf72 may not be active and therefore a reduction in the level of Mfn2 may not to be expected. Despite this, this does not preclude the induction of Parkin dependent mitophagy by C9orf72 expression, as low-level Parkin activity has been reported to play a role in the removal of mitochondrial subdomains via MVD formation (1.2.3.2) (McLelland et al., 2014; Sugiura et al., 2014).

Although loss of C9orf72 did not impair the initial recruitment of Parkin to mitochondria (Figure 4.10A), nor the degradation of OMM proteins thereafter (Figure 4.11), at later

stages of mitophagy, loss of C9orf72 led to a decrease in mitochondrially located Parkin (Figure 4.10B). The retention of Parkin on mitochondria is required to produce a whole organelle mitophagy response and the recruitment of the mitophagy adaptor proteins and autophagy machinery (reviewed in Hamacher-Brady and Brady, 2016). Therefore, the impaired mitophagy observed upon loss of C9orf72 may be as a result of two separate events. The loss of Parkin from the mitochondria at an earlier stage during mitophagy, may slow the labelling of OMM proteins with ubiquitin. These may then be targeted by DUBs, including USP30, which remove the ubiquitin residues and prevent the mitochondria from being recognised by the mitophagy adaptor proteins and subsequently promoting the recruitment autophagy machinery (reviewed in Durcan and Fon, 2015) and discussed later in Chapter 5. In a second event, loss of C9orf72 may impair the recruitment of the ULK1 initiation complex to mitochondria, resulting in a further impaired targeting of damaged organelles to autophagosomes. Indeed, depletion of ULK1 impairs mitochondrial clearance (Kundu et al., 2008).

Mitochondrial dysfunction, including mitophagy defects, is a prevalent feature of ALS, including C9orf72 ALS (Dafinca et al., 2016; Lopez-Gonzalez et al., 2016; Onesto et al., 2016; reviewed in Smith et al., 2017b). Here we report mitochondrial defects in C9orf72 ALS patient iAstrocytes. C9orf72 ALS models display fragmented and swollen mitochondria (Figure 4.13) (Dafinca et al., 2016; Onesto et al., 2016). However, it is unclear whether the mitochondrial dysfunction found in these patient cells is as a direct result of C9orf72 haploinsufficiency. Indeed, the poly-GR DPRs were reported to induce mitochondrial damage (Lopez-Gonzalez et al., 2016). In addition, TDP-43 pathology results in ROS induced mitochondrial damage (Hong et al., 2012). ROS can trigger the fragmentation of mitochondrial networks (reviewed in Ježek et al., 2018), which may result directly in the fragmented mitochondria observed in C9orf72 ALS models. Furthermore, TDP-43 pathology may impair Parkin mediated mitophagy through transcriptional alterations and therefore prevent mitochondrial clearance (Lagier-Tourenne et al., 2012; Polymenidou et al., 2011). Therefore, in order to determine the contribution of C9orf72 haploinsufficiency in our C9orf72 ALS/FTD iAstrocytes patient model, it will be necessary to rescue the levels of C9orf72 through expression. Indeed, if the C9orf72 ALS/FTD patient iAstrocytes display fragmented mitochondrial networks and impaired Parkin translocation during mitophagy upon expression of C9orf72L, then it may be that the gain of function mechanisms or TDP-43 pathology play important roles in the impairment of mitochondrial dynamics.

Emerging evidence supports defects in mitophagy to contribute to the mitochondrial dysfunction seen in the C9orf72 ALS patient cells. Indeed, the early stages of mitophagy

were impaired in the C9orf72 ALS iAstrocytes, with a defect in the translocation of Parkin observed (Figure 4.14). In patient fibroblasts, in contrast, mitochondria were found within autophagic vacuoles, suggesting a downstream impairment of mitophagy progression (Onesto et al., 2016). Although also potentially linked to the other C9orf72 disease mechanisms, both the swollen mitochondria and the mitochondria located in autophagic vacuoles may be linked directly to C9orf72 haploinsufficiency. The accumulation of aggregated and swollen mitochondria is a feature of cells in which the initiation of autophagy is impaired. For instance, both FIP200 and ULK1 knockout cells have aggregated and swollen mitochondria (Kundu et al., 2008; Liang et al., 2010). Loss of C9orf72 has been shown to impair autophagy initiation (Webster et al., 2016a), and may therefore also contribute to the mitochondrial morphology changes reported in C9orf72 ALS patient cells. C9orf72 has also been linked to lysosomal function (Amick et al., 2016; Ugolino et al., 2016). Defects in lysosomal function lead to the accumulation of autophagic vacuoles containing mitochondria, a feature prevalent in familial PD (reviewed in Plotegher and Duchen, 2017). Therefore, a double hit effect on mitochondrial clearance may arise from C9orf72 haploinsufficiency in C9orf72 ALS patient cells.

There are several drawbacks arising from our study design that may need to be addressed further. In the first instance we used overexpressed C9orf72 to investigate mitochondrial dynamics. Overexpression of proteins can lead to altered function and cell stress, leading to cellular artefacts being observed. Induction of cell stress pathways may induce the fragmentation of the mitochondrial network, as we observed upon expression of Myc-C9orf72L and Myc-C9orf72S (Figure 4.1). In order to establish whether the mitochondrial network fragmentation was as a result of protein overexpression, attempts to correlate the level of expression with the fragmentation phenotype should be made. In addition, if C9orf72 were to be tagged with an EGFP tag, then expression of EGFP-C9orf72L and EGFP-C9orf72S compared to EGFP empty vector and non-transfected cells could be performed. Second, in our C9orf72 knockdown experiments, we used a pool of 2 siRNAs C9orf72 (C9orf72 #2 and C9orf72 #D). In order to verify that the impaired mitochondrial network connectivity and mitophagy defect were not off-target effects, rescues of the C9orf72 knockdown should be performed through the expression of an siRNA-resistant C9orf72 construct. In addition, the pool of siRNA ought to be split into its component parts to verify that each siRNA gives rise to a similar phenotype. Finally, in Chapter 3 we identified C9orf72 to be distributed between the mitochondria and cytosol (Figure 3.8). Here we did not attempt to distinguish whether the C9orf72 found in the mitochondria plays a separate

role in mitochondrial quality control, compared to C9orf72 found in the cytosol. Therefore, it may be informative to design assays to determine the contribution of each C9orf72 population, either through exclusion of C9orf72 import into mitochondria or via the targeting of C9orf72 exclusively to the mitochondrial IMS.

Chapter 5. Investigating the role of the interaction between C9orf72 and USP8 in mitophagy

5.1 Introduction

Cellular processes including mitophagy are regulated by the post-translational modification of proteins, including by ubiquitination. Ubiquitin is a highly conserved 76 amino acid protein, which is conjugated to Lys residues on the target protein by the action of the E1, E2 and E3 ligase cascade (reviewed in Berndsen and Wolberger, 2014). Although ubiquitin is typically conjugated to Lys residues, ubiquitination of other amino acid residues including Cys has been reported (reviewed in McDowell and Philpott, 2013). The specific ligation of ubiquitin to proteins is regulated by the E3 ligase, of which over 600 have been identified in humans (Li et al., 2008). The addition of ubiquitin to proteins occurs in both mono- and poly-ubiquitination chains. Poly-ubiquitin chains arise from the addition of ubiquitin moieties to one of the 7 Lys residues on a previously conjugated ubiquitin moiety. Eight different ubiquitin linkages have been identified and convey different cellular functions (reviewed in Akutsu et al., 2016). K48- and K63- linked ubiquitin chains are the best characterised and are linked to the degradation of proteins by the proteasome and by autophagy respectively (reviewed in Komander and Rape, 2012).

The progression of mitophagy is controlled in part by the ubiquitination of OMM proteins and their degradation by the proteasome. The labelling of OMM proteins with ubiquitin is performed by the E3 ligase Parkin (Sarraf et al., 2013). K6-, K11-, K48- and K63-linked chains are thought to have particular relevance for mitophagy (reviewed in Durcan and Fon, 2015). K48- linked chains are associated with the degradation of the OMM proteins by the proteasome (Chan et al., 2011), whereas K63- linked ubiquitination has been shown to be involved in mitochondrial clustering and the recruitment p62 to damaged mitochondria (Okatsu et al., 2010). K6- and K11- linked ubiquitin chains have been shown to be required for the normal progression of mitophagy (Cunningham et al., 2015).

The action of E3 ligases and the ubiquitination of proteins is regulated by the opposing action of DUBs. DUBs hydrolyse ubiquitin chains, thus altering the fate and function of ubiquitinated proteins (reviewed in Komander et al., 2009; Mevissen and Komander, 2017). Several DUBs have been implicated in mitophagy. DUB activity of Ubiquitin specific peptidases 15, 30 and 35 (USP15, USP30 and USP35) have been shown to oppose mitophagy (Bingol et al., 2014; Cornelissen et al., 2014; Cunningham et al., 2015; Wang et al., 2015). In contrast, USP8 DUB activity was reported to promote the

recruitment of Parkin to mitochondria following mitochondrial damage (Durcan et al., 2014). The mechanism by which USP8 regulates mitophagy is unclear. On the one hand, USP8 DUB activity may improve the stability of endogenous Parkin in cells and thereby promote mitophagy (reviewed in Bingol and Sheng, 2016). Alternatively, USP8 has been proposed to remove K6- linked ubiquitin chains from Parkin to promote its translocation and thereafter mitochondrial clearance (Durcan et al., 2014). Furthermore, USP8 may be involved in the removal of K6- linked ubiquitin chains that would otherwise prevent the interactions between Parkin, the target mitochondria and the inbound autophagy machinery (Durcan and Fon, 2015).

In addition to its role in mitophagy, USP8 has been shown to play a role in cellular trafficking events including the control of endosome morphology, and early endosome cargo sorting and trafficking (Berlin et al., 2010a; Row et al., 2007; Row et al., 2006). Gain of function mutations in USP8 lead to Cushing's disease, reported to be due to increased epidermal growth factor receptor (EGFR) signalling (Berlin et al., 2010b; Reincke et al., 2015). Furthermore, USP8 has been shown to remove K63- linked ubiquitin chains from α -synuclein, a protein found in Lewy bodies in PD. Persistence of the K63- linked ubiquitin chains prevented the degradation of α -synuclein by the lysosome leading to cellular aggregation and toxicity. Consistent with this, knockdown of USP8 rescued the locomotor defects and cell loss in α -synuclein WT and A53T *Drosophila* models (Alexopoulou et al., 2016).

The USP8 protein is composed of 3 separate domains: the microtubule interacting and trafficking (MIT), the Rhodanese and the USP domains (Figure 5.1A). The MIT domain is involved in many of the functions of USP8 including endosomal localisation, Charged multivesicular body protein 1b (CHMP1B) binding, maintenance of endosomal sorting required for transport complex 0 (ESCRT-0) stability and EGFR degradation (Row et al., 2007). The Rhodanese domain is required to bind the E3 ligase NRDP1 (Wu et al., 2004). Finally, the USP domain conveys the ubiquitin hydrolase activity (Komander et al., 2009).

USP8 was identified as a potential interacting partner of C9orf72S in the Y2H screen (Table 3-1). The interacting region mapped to the C-terminal region of USP8, which corresponds to the USP domain (Figure 5.1A). As both USP8 (Durcan et al., 2014) and C9orf72 (4.3) have been implicated in membrane trafficking events and mitophagy, the interaction between C9orf72 and USP8 in the context of mitochondrial quality control was explored in the final chapter of this thesis.

5.2 C9orf72 interacts with USP8

The interaction between C9orf72 and USP8, as identified in the Y2H screen (Table 3-1), was initially verified by co-immunoprecipitation. HEK293 cells were co-transfected with pCI-neo empty vector, Myc-C9orf72L, Myc-C9orf72S or Myc-C9orf72Dd and either EGFP-C2 or EGFP-USP8. Myc-C9orf72 isoforms were immunoprecipitated using anti-Myc Ab. Immunoprecipitates were probed for co-immunoprecipitation of EGFP-USP8 by GFP immunoblot. EGFP-USP8 co-immunoprecipitated with Myc-C9orf72L, Myc-C9orf72S and Myc-C9orf72Dd. A greater amount of EGFP-USP8 appeared to co-immunoprecipitate with Myc-C9orf72S than with Myc-C9orf72L or Myc-C9orf72Dd. The interaction was not due to the EGFP-tag, as EGFP-USP8 did not co-immunoprecipitate with the empty vector control. Furthermore, the EGFP empty vector control did not co-immunoprecipitate with the empty vector control nor with any of the Myc-C9orf72 constructs (Figure 5.1B).

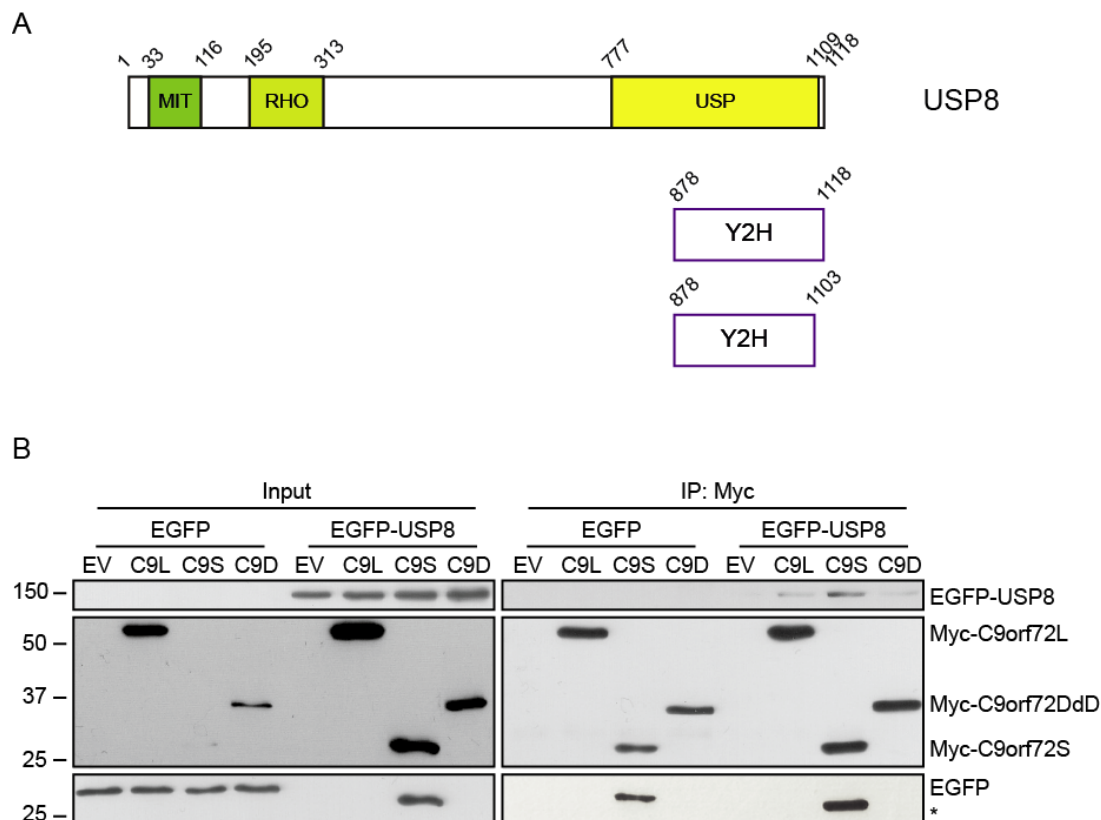


Figure 5.1 C9orf72 interacts with USP8

A) The location of the MIT (green), Rhodanese (RHO) (light green) and USP (yellow) domains of USP8 are depicted on USP8. Below are shown the regions of USP8 that were identified as interacting with C9orf72S in the Y2H screen. B) HEK293 cells were co-transfected with pCI-neo empty vector (EV), Myc-C9orf72L (C9L), Myc-C9orf72S

(C9S) or Myc-C9orf72DdD (C9D) and with EGFP-C2 or EGFP-USP8 and subjected to immunoprecipitation with anti-Myc Ab. Co-immunoprecipitation of EGFP-C2 or EGFP-USP8 was determined by GFP immunoblot. Input represents 5.7 % of lysate subjected to immunoprecipitation. * indicates a band corresponding to Myc-C9orf72S from the Myc immunoblot upon the subsequent GFP immunoblot.

The Y2H screen indicated an interaction between C9orf72S and the USP domain of USP8 (Figure 5.1A). To establish the domain of USP8 which interacts with C9orf72, several fragments of USP8 (USP8^{FL} full length) were generated. To investigate interactions with the N-terminus of USP8, constructs harbouring the MIT domain only (USP8^{MIT}, aa 1-116) and the MIT-RHO domains (USP8^{MIT-RHO}, aa 1-313) were generated. To investigate the interaction with the C-terminus, a USP domain only (USP8^{USP}, aa 776-1118) and a RHO-USP construct (USP8^{RHO-USP}, aa 195-1118) were generated. Finally a RHO domain only (USP8^{RHO}, aa 195-313) fragment was generated (Figure 5.2A).

To establish whether the generation of USP8 fragments had been successful and that these produced the expected products, the USP8 fragments were expressed in cells. HEK293 cells were transfected with either pCI-neo empty vector, Myc-USP8^{MIT}, Myc-USP8^{MIT-RHO} or Myc-USP8^{FL}. The predicted molecular weights of the USP8 fragments were 14 kDa, 37 kDa and 127 kDa for Myc-USP8^{MIT}, Myc-USP8^{MIT-RHO} and Myc-USP8^{FL} respectively. Myc immunoblot revealed that Myc-USP8^{MIT}, Myc-USP8^{MIT-RHO} and Myc-USP8^{FL} expressed efficiently in cells and corresponded to the expected molecular weight (Figure 5.2B). Next, HEK293 cells were transfected with either pCI-neo empty vector, Myc-USP8^{RHO-USP} or Myc-USP8^{FL}. The predicted molecular weights of these fragments were 105 kDa and 127 kDa for Myc-USP8^{RHO-USP} and Myc-USP8^{FL} respectively. Myc immunoblot revealed Myc-USP8^{FL} and Myc-USP8^{RHO-USP} to be expressed efficiently in cells and to correspond to the expected molecular weight (Figure 5.2C). Finally, HEK293 cells were transfected with pCI-neo empty vector, Myc-USP8^{RHO} or Myc-USP8^{USP}. The predicted molecular weights of Myc-USP8^{RHO} and Myc-USP8^{USP} were 14 kDa and 40 kDa respectively. Myc immunoblot revealed that whilst Myc-USP8^{USP} was expressed in cells and corresponded to the expected molecular weight, Myc-USP8^{RHO} was not detected, suggesting that it may not express efficiently in cells (Figure 5.2D).

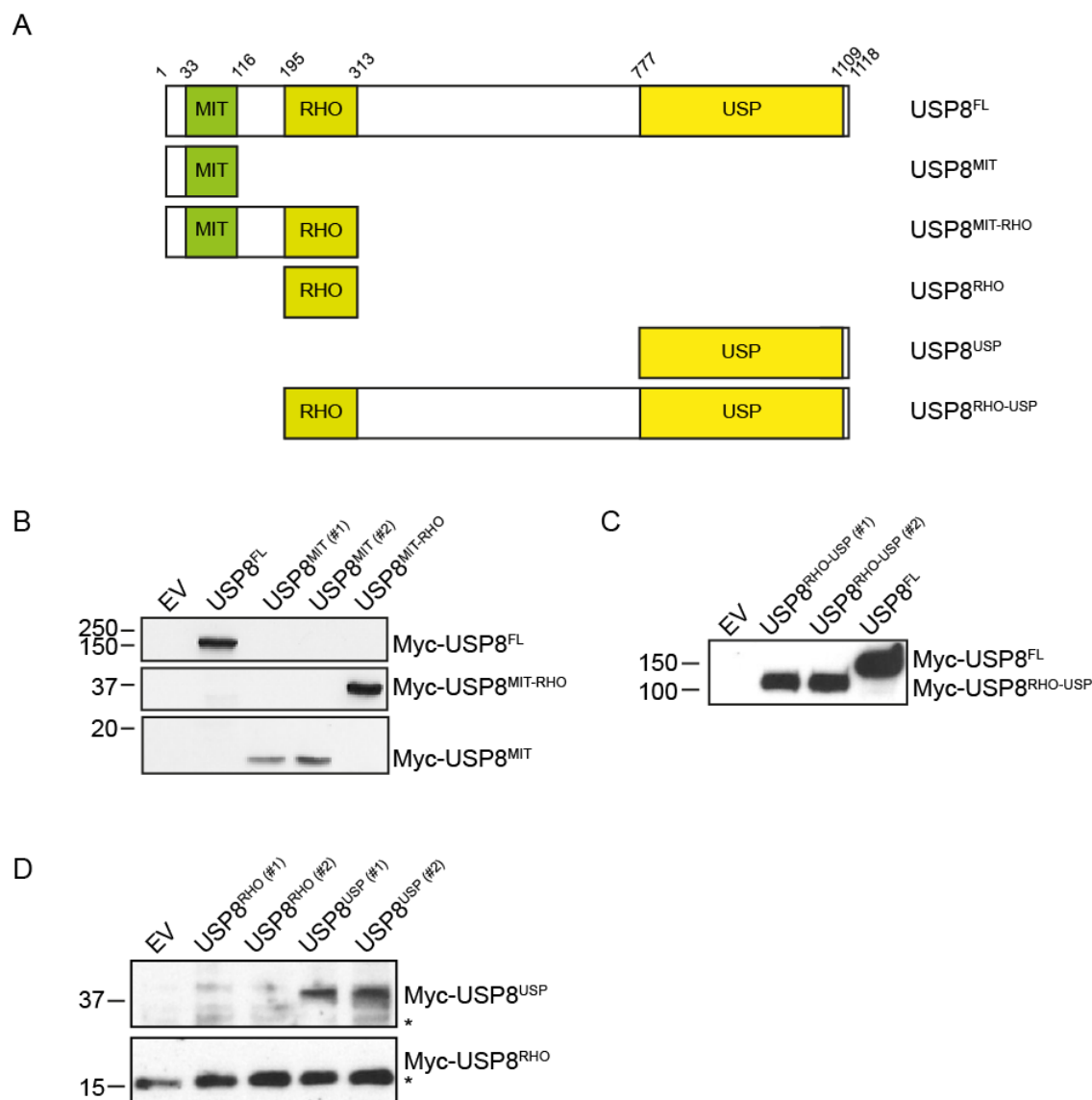


Figure 5.2 The generation and expression of USP8 fragments

A) The domain structure of USP8 full length ($USP8^{FL}$) depicting the MIT domain (green), Rhodanese (RHO) domain (light green) and the USP domain (yellow) is shown. Below are shown the domain fragments of USP8 that were generated. B) HEK293 cells were transfected with pCI-neo empty vector (EV), Myc- $USP8^{FL}$, Myc- $USP8^{MIT}$ or Myc- $USP8^{MIT-RHO}$. The expression of the Myc-tagged USP8 constructs was verified by Myc immunoblot. C) HEK293 cells were transfected with pCI-neo empty vector (EV), Myc- $USP8^{RHO-USP}$ or Myc- $USP8^{FL}$. The expression of the Myc-tagged USP8 constructs was verified by Myc immunoblot. D) HEK293 cells were transfected with pCI-neo empty vector (EV), Myc- $USP8^{RHO}$ or Myc- $USP8^{USP}$. The expression of the Myc-tagged USP8 constructs was verified by Myc immunoblot. * indicates a non-specific band on Myc immunoblot. #1 and #2 correspond to cells transfected with DNA extracted from individual bacterial clones (either clone 1 or 2) expressing the USP8 construct.

To investigate the domain of USP8 which confers its interaction with C9orf72, *in vitro* binding assays were performed. The N-terminal fragments of USP8 (USP8^{MIT} or USP8^{MIT-RHO}), the C-terminal fragments of USP8 (USP8^{RHO-USP} or USP8^{USP}) and USP8 (full length, USP8^{FL}) were translated in a TnT coupled reticulocyte reaction to produce ³⁵S-labelled USP8 fragments. The ³⁵S-labelled USP8 fragments were incubated with GST empty vector, GST-C9orf72S or GST-C9orf72L. GST-tagged constructs were isolated using GSH-beads (Coomassie stain, lower panels). The co-isolation of the ³⁵S-labelled USP8 fragments was detected by phosphoscreen (upper panels). ³⁵S-labelled USP8^{FL} was co-isolated with both GST-C9orf72L and GST-C9orf72S. The co-isolation was due to the interaction with C9orf72 as ³⁵S-labelled USP8^{FL} did not co-isolate with the GST empty vector control (Figure 5.3A, B). The ³⁵S-labelled N-terminal USP8 fragments USP8^{MIT} and USP8^{MIT-RHO} were not co-isolated with the GST empty vector control nor with the GST-tagged C9orf72S or C9orf72L (Figure 5.3A). The ³⁵S-labelled C-terminal USP8 fragments USP8^{RHO-USP} and USP8^{USP} were co-isolated with both GST-C9orf72L and GST-C9orf72S. Neither USP8^{RHO-USP} nor USP8^{USP} were co-isolated with the GST empty vector control (Figure 5.3B). As USP8^{USP} was co-isolated with both GST-C9orf72L and GST-C9orf72S, it appeared that the USP domain of USP8 was sufficient to convey the interaction between C9orf72 and USP8.

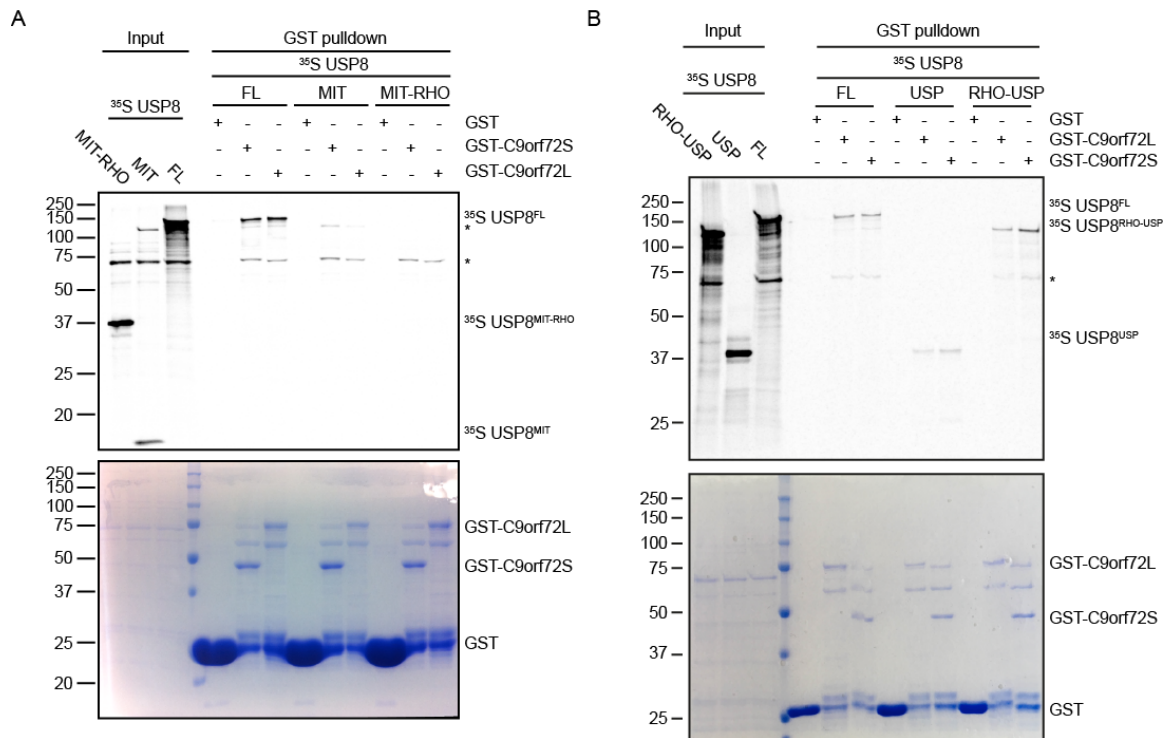


Figure 5.3 C9orf72 interacts with the USP domain of USP8

A) ³⁵S radiolabelled full length USP8 (USP8^{FL} – FL) or the N-terminal MIT fragment of USP8 (USP8^{MIT} – MIT) or MIT-Rhodanese fragment of USP8 (USP8^{MIT-RHO} – MIT-RHO) were incubated with GST empty vector (GST), GST-C9orf72L or GST-C9orf72S. GST pull down was performed with GSH beads and revealed by Coomassie stain (lower panel). The co-isolation of ³⁵S radiolabelled USP8 or USP8 N-terminal fragments was detected on a phosphoscreen (upper panel). Input represents 6.25 % of ³⁵S radiolabelled USP8 fragments incubated in GST pulldown. B) ³⁵S radiolabelled full length USP8 (USP8^{FL} – FL), the C-terminal Rhodanese-USP fragment of USP8 (USP8^{RHO-USP} – RHO-USP) or USP fragment of USP8 (USP8^{USP} – USP) were incubated with GST empty vector (GST), GST-C9orf72L or GST-C9orf72S. GST pull down was performed with GSH beads and revealed by Coomassie stain (lower panel). The co-isolation of ³⁵S radiolabelled USP8 or USP8 C-terminal fragments was detected on a phosphoscreen (upper panel). Input represents 6.25 % of ³⁵S radiolabelled USP8 fragments incubated in GST pulldown. * ³⁵S radiolabelled USP8 products arising from potential alternative start codons. N-terminal USP8 fragments were generated by the introduction of a STOP codon in USP8 following the MIT or Rhodanese domains. These alternative USP8 products are comprised of the C-terminal region of USP8 and likely interact with C9orf72 in a similar manner to the C-terminal USP8 fragments via the USP domain.

To verify if the USP domain confers the interaction between USP8 and C9orf72 in cells, co-immunoprecipitation assays using the N-terminal and C-terminal fragments of USP8 were performed. To investigate the interaction with the N-terminal USP8 fragments, HEK293 cells were co-transfected with pCI-neo empty vector or HA-C9orf72L and with pCI-neo empty vector, Myc-USP8^{MIT}, Myc-USP8^{MIT-RHO} or Myc-USP8^{FL}. To investigate the interaction with the C-terminal USP8 fragments HEK293 cells were co-transfected with pCI-neo empty vector or HA-C9orf72L and with pCI-neo empty vector, Myc-USP8^{RHO}, Myc-USP8^{USP}, Myc-USP8^{RHO-USP} or Myc-USP8^{FL}. Cell lysates were subjected to immunoprecipitation with anti-Myc Ab to immunoprecipitate the Myc-USP8 fragments. Immunoprecipitates were probed with anti-HA Ab to reveal co-immunoprecipitation of HA-C9orf72L. HA-C9orf72L co-immunoprecipitated with Myc-USP8^{FL} (Figure 5.4A, B). HA-C9orf72L was also co-immunoprecipitated with the N-terminal USP8 fragment Myc-USP8^{MIT-RHO} (Figure 5.4A) and the C-terminal USP8 fragment Myc-USP8^{RHO-USP} (Figure 5.4B). HA-C9orf72L was co-immunoprecipitated with the Rhodanese domain fragment (Myc-USP8^{RHO}) (Figure 5.4B). HA-C9orf72L did not co-immunoprecipitate with the fragment corresponding to the MIT domain (Myc-USP8^{MIT}) (Figure 5.4A). Hence the interaction between Myc-USP8^{MIT-RHO} and HA-C9orf72L was likely due to the interaction between C9orf72L and the Rhodanese domain of USP8. HA-C9orf72L also interacted to a lesser extent with the USP domain (Myc-USP8^{USP}) (Figure 5.4B), which recapitulated the finding of the *in vitro* binding assay (Figure 5.3). The interaction between HA-C9orf72L and the Myc-USP8 fragments was specific as HA-C9orf72L was not co-immunoprecipitated in the empty vector control.

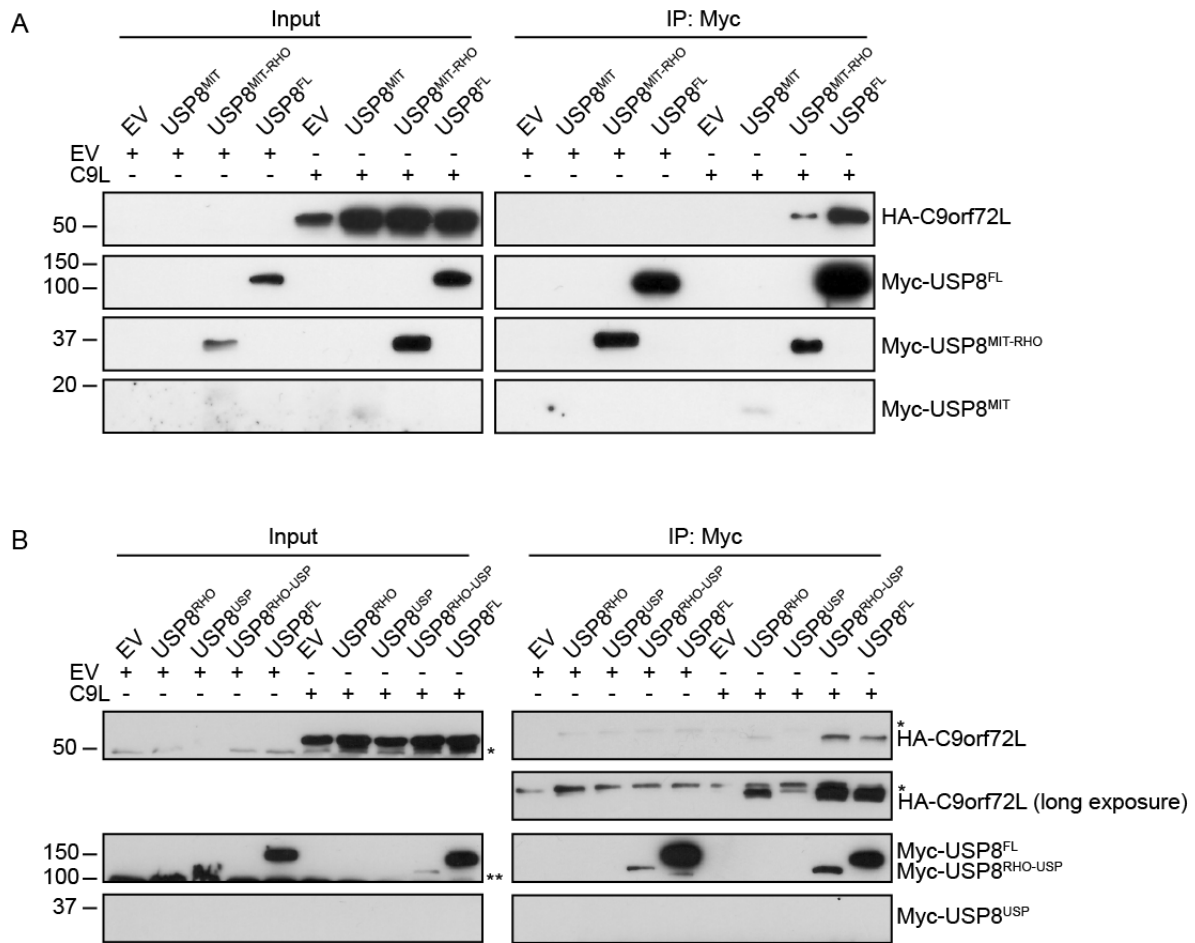


Figure 5.4 C9orf72L interacts with the Rhodanese and USP domains of USP8

A) HEK293 cells were co-transfected with pCI-neo empty vector (EV) or HA-C9orf72L (C9L) and with EV, Myc-USP8^{MIT}, Myc-USP8^{MIT-RHO} or Myc-USP8^{FL} and were subjected to immunoprecipitation with anti-Myc Ab. Immunoprecipitates were subjected to HA immunoblot. Input represents 4 % of lysate subjected to immunoprecipitation. B) HEK293 cells were transfected with pCI-neo empty vector (EV) or HA-C9orf72L (C9L) and with EV, Myc-USP8^{RHO}, Myc-USP8^{USP}, Myc-USP8^{RHO-USP} or Myc-USP8^{FL} and subjected to immunoprecipitation with anti-Myc Ab. Immunoprecipitates were subjected to HA immunoblot. Input represents 4 % of lysate subjected to immunoprecipitation. * indicates a non-specific band on HA immunoblot. ** indicates a non-specific band on Myc immunoblot.

5.3 C9orf72 and USP8 do not have connected roles in maintaining mitochondrial dynamics

DUBs, including USP8, have been shown to play a role in mitochondrial quality control (reviewed in Bingol and Sheng, 2016; Durcan and Fon, 2015). USP8 has been shown to be required for the efficient recruitment of Parkin to damaged mitochondria, with knockdown impairing mitophagy progression (Durcan et al., 2014). We identified a role for C9orf72 in the regulation of mitochondrial dynamics and the removal of damaged mitochondria through the mitophagy pathway (4.3). As C9orf72 interacts with USP8 (Figure 5.1B), and both appear to be involved in the regulation of mitophagy, the role of the interaction between C9orf72 and USP8 in relation to mitochondrial dynamics was investigated.

5.3.1 Knockdown of USP8 does not affect C9orf72 induced fragmentation of the mitochondrial network

Overexpression of C9orf72 resulted in mitochondrial rounding and the fragmentation of the mitochondrial network (Figure 4.1). To investigate whether USP8 is necessary for the fragmentation of the mitochondrial network induced by C9orf72 overexpression, HeLa cells were transfected with non-targeting control or USP8 siRNA and subsequently co-transfected with pCI-neo empty vector or Myc-C9orf72L and pAcGFP1-Mito, to visualise the mitochondrial networks (Figure 5.5A). The reduction of USP8 protein following siRNA knockdown was confirmed by USP8 immunoblot (Figure 5.5B). As observed previously (Figure 4.1), overexpression of Myc-C9orf72L led to the fragmentation of the mitochondrial network in the control siRNA transfected cells. Knockdown of USP8 led an elongation of the mitochondria but did not affect mitochondrial network connectivity. The knockdown of USP8 did not affect the rounding of mitochondria nor the fragmentation of the mitochondrial network upon overexpression of Myc-C9orf72L (Figure 5.5A). Thus, USP8 is not required for C9orf72 mediated changes in mitochondrial network morphology.

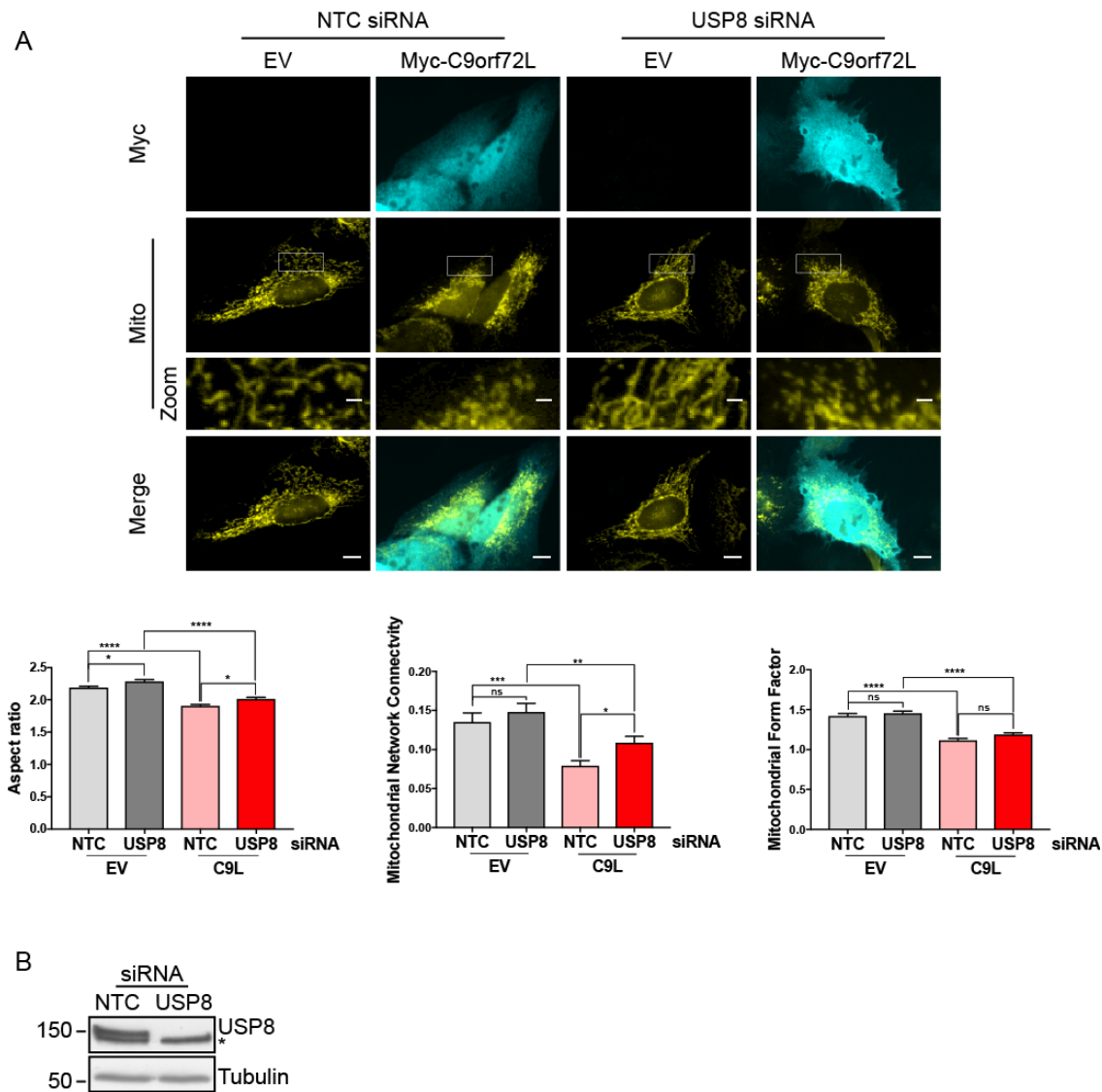


Figure 5.5 Knockdown of USP8 does not prevent C9orf72L overexpression induced fragmentation of the mitochondrial network

A) HeLa cells were transfected with non-targeting control (NTC) or USP8 siRNA and were subsequently co-transfected with pCI-neo empty vector (EV) or Myc-C9orf72L (cyan) and pAcGFP1-Mito (yellow). Scale bar 10 μ m, zoom 2 μ m. Mitochondrial shape (aspect ratio), network connectivity and form factor were quantified from 3 independent experiments (NTC/EV: 62, NTC/C9L: 58, USP8/EV: 60, USP8/C9L: 60 cells). Graphs display mean \pm SEM. Statistical analysis was performed by one-way ANOVA with Fisher's LSD; * $P \leq 0.05$, **** $P \leq 0.0001$. B) The knockdown of USP8 was verified by USP8 immunoblot. * indicates an aspecific band on USP8 immunoblot.

5.3.2 The recruitment of Parkin is differentially regulated by C9orf72 and USP8

Knockdown of USP8 has previously been shown to result in a delay in the recruitment of Parkin to mitochondria following the induction of mitochondrial damage (Durcan et al., 2014). To verify that USP8 knockdown impairs Parkin recruitment, HeLa cells were transfected with non-targeting control or USP8 siRNA and were subsequently transfected with EYFP-Parkin. Mitochondrial damage and the recruitment of EYFP-Parkin to mitochondria was induced by treatment with CCCP (Figure 5.6A). The knockdown of USP8 was confirmed by USP8 immunoblot (Figure 5.6B). At 1 h CCCP treatment, USP8 siRNA transfected cells displayed a reduction in EYFP-Parkin translocation to mitochondria compared to the control siRNA transfected cells. At 2 h CCCP treatment there was no difference in EYFP-Parkin translocation to mitochondria between control and USP8 siRNA transfected cells. This corroborated the previous report that knockdown of USP8 delayed the recruitment of Parkin to mitochondria following mitochondrial damage (Durcan et al., 2014).

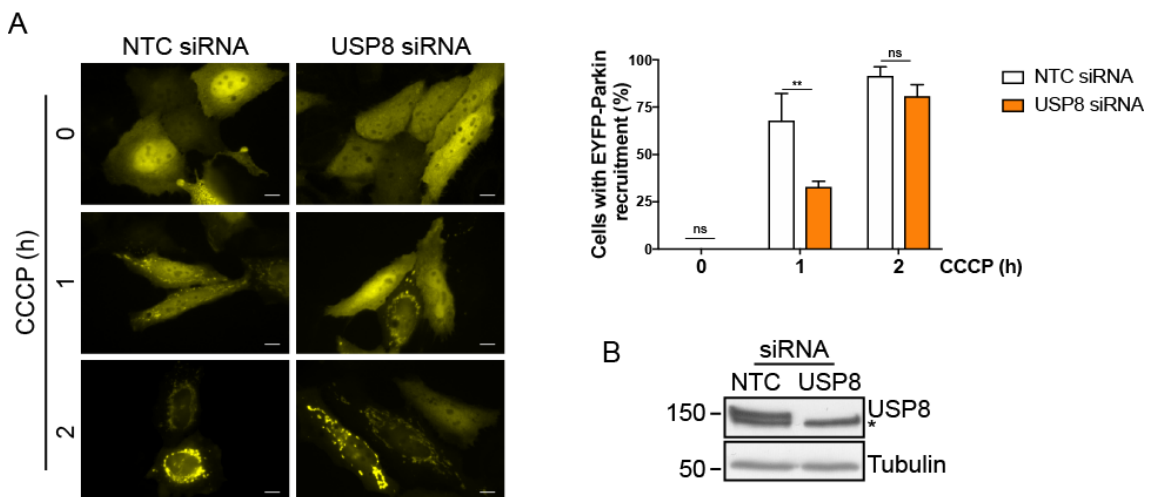


Figure 5.6 Knockdown of USP8 impairs Parkin recruitment

*A) HeLa cells were transfected with non-targeting control (NTC) or USP8 siRNA and subsequently were transfected with EYFP-Parkin (yellow). Cells were treated for 1 or 2 h with 10 μ M CCCP to induce mitochondrial damage and EYFP-Parkin recruitment. The number of cells displaying EYFP-Parkin recruited to mitochondria was quantified at each timepoint. Scale bar 10 μ m. Graph displays mean \pm SEM. Cells were quantified from 3 independent experiments (cells were quantified from 15 – 30 fields per experiment (25 – 92 cells)). Statistical analysis was performed by two-way ANOVA with Fisher's LSD; ** $P \leq 0.01$. B) The knockdown of USP8 was verified by USP8 immunoblot. * indicates an aspecific band on USP8 immunoblot.*

The activation and recruitment of Parkin to damaged mitochondria depends on its phosphorylation and upon cycles of ubiquitination and de-ubiquitination (reviewed in Bingol and Sheng, 2016). Upon mitochondrial damage, Parkin has been proposed to be ubiquitinated at 3 Lys residues: K27-, K48- and K76-, with K6- linked ubiquitin chains. USP8 was reported to remove the K6- linked ubiquitin chains from Parkin to permit it to translocate efficiently to mitochondria (Figure 5.7A, B) (Durcan et al., 2014). To investigate the importance of the ubiquitination of these Lys residues for the translocation of Parkin to mitochondria upon mitochondrial damage, a novel Parkin construct was generated by the mutagenesis of the Lys residues at positions 27, 48 and 76 to Arg. Changes in R group composition between Lys and Arg prevents the ubiquitination of Parkin at these residues. Hence, ubiquitination of Parkin^{K27R/K48R/K76R} (Parkin^{3xKR}) at residues R27, R48 and R76 upon mitochondrial damage would not occur and Parkin^{3xKR} was predicted to be recruited to mitochondria (Figure 5.7C). As the removal of ubiquitin chains on Parkin^{3xKR} was not required for its predicted translocation to mitochondria, we hypothesised that knockdown of USP8 would not affect the recruitment of Parkin^{3xKR} (Figure 5.7D).

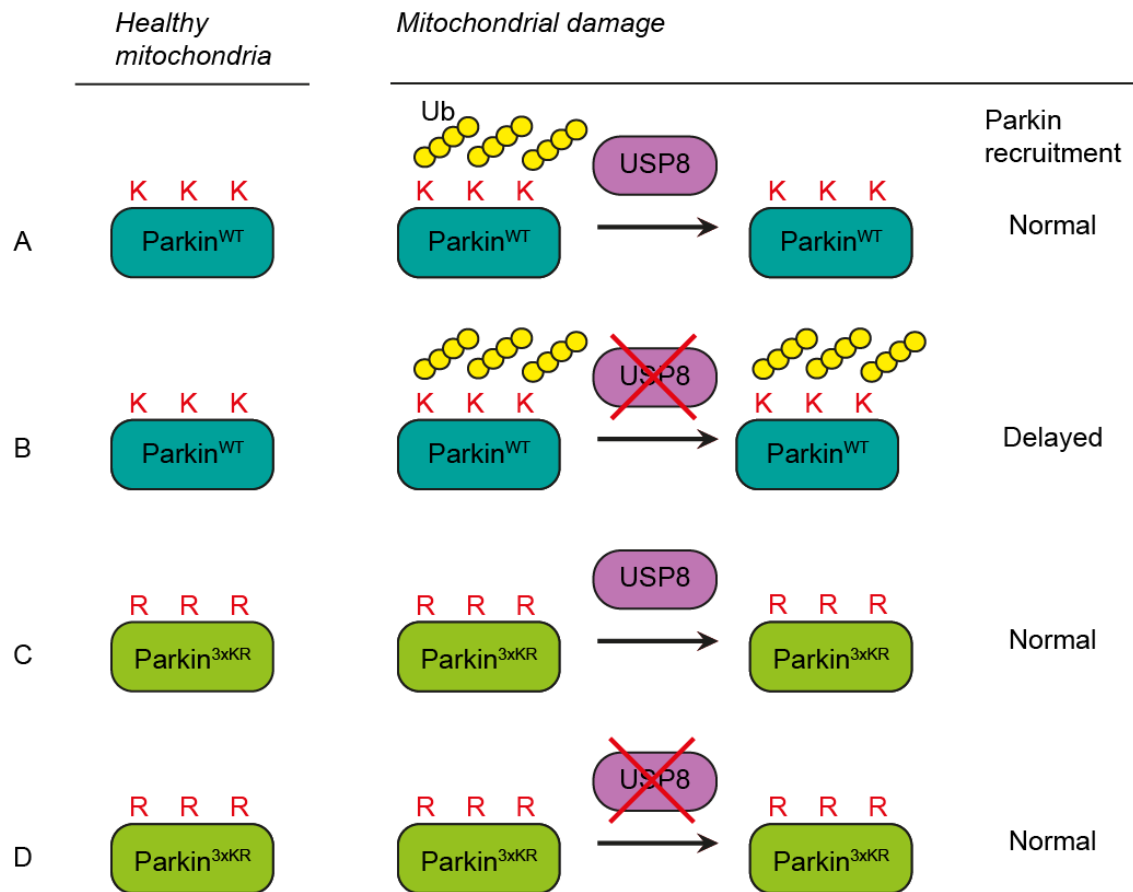


Figure 5.7: The predicted translocation of Parkin^{WT} and Parkin^{3xKR} in mitophagy

A) Wild type Parkin (Parkin^{WT}) is ubiquitinated (Ub) at K27, K48 and K76 upon the induction of mitophagy. The ubiquitin chains are removed by USP8 to permit the translocation of Parkin to damaged mitochondria. B) The knockdown of USP8 prevents the removal of ubiquitin chains from K27, K48 and K76 and delays the recruitment of Parkin during mitophagy. C) Parkin^{K27R/K48R/K76R} (Parkin^{3xKR}) harbours Arg substitutions at the Lys residues that are ubiquitinated upon mitophagy induction. Parkin^{3xKR} is not ubiquitinated upon mitophagy induction and translocates to mitochondria. D) Parkin^{3xKR} does not undergo ubiquitination of the R27, R48 and R76 residues upon mitophagy induction, therefore USP8 is not required to deubiquitinate Parkin^{3xKR} to permit its translocation. Hence knockdown of USP8 does not impair the translocation of Parkin^{3xKR} to mitochondria during mitophagy.

To verify whether the recruitment of Parkin^{3xKR} to mitochondria was affected by the knockdown of USP8, HeLa cells were transfected with non-targeting control or USP8 siRNA and subsequently transfected with EYFP-Parkin^{WT} (wild type) or EYFP-Parkin^{3xKR}. Cells were treated with CCCP to induce mitochondrial damage and Parkin recruitment (Figure 5.8A). The knockdown of USP8 was confirmed by USP8 immunoblot

(Figure 5.8B). CCCP treatment resulted in the translocation of EYFP-Parkin^{WT} to mitochondria at 1 h. The knockdown of USP8 resulted in a decrease in cells displaying recruited EYFP-Parkin^{WT} compared to the control siRNA transfected cells following 1 h CCCP treatment, as reported previously by (Durcan et al., 2014). Surprisingly, compared to the control siRNA cells expressing EYFP-Parkin^{WT}, EYFP-Parkin^{3xKR} recruitment was delayed in both the control and USP8 siRNA transfected cells following 1 h CCCP treatment. Thus, the K27, K48 and K76 residues of Parkin may be important for the translocation of Parkin. There was no difference in the recruitment of EYFP-Parkin^{WT} and EYFP-Parkin^{3xKR} to mitochondria at 1 h CCCP treatment in USP8 siRNA transfected cells. Thus, it is unlikely that the delay in Parkin recruitment upon USP8 knockdown is due to the removal of K6- linked ubiquitin chains from K27, K48 and K76. At 2 h CCCP treatment, the recruitment of EYFP-Parkin^{WT} and EYFP-Parkin^{3xKR} in USP8 knockdown cells was decreased compared to the NTC EYFP-Parkin^{WT} control, in contrast to previous reports (Durcan et al., 2014) and our previous finding (Figure 5.6A). No difference in EYFP-Parkin^{WT} or EYFP-Parkin^{3xKR} translocation was observed between the control and USP8 siRNA transfected cells at 4 h CCCP treatment.

To explore further the role of USP8 and K6- linked ubiquitination in Parkin recruitment during mitophagy, the recruitment of Parkin in cells unable to form K6- linked ubiquitin chains was explored. An HA-Ub construct was mutated at position 6 from Lys to Arg (HA-Ub^{K6R}), rendering it unable to form K6- linked ubiquitin chains. In the study by Durcan *et al.*, expression of HA-Ub^{K6R} rescued the defect in Parkin recruitment reported with USP8 knockdown (Durcan et al., 2014). HeLa cells were transfected with non-targeting control or USP8 siRNA and were subsequently co-transfected with pCI-neo empty vector, HA-Ub^{WT} (wild type) or HA-Ub^{K6R} and with EYFP-Parkin. Cells were treated CCCP to induce mitochondrial damage and EYFP-Parkin translocation (Figure 5.9A). The knockdown of USP8 was confirmed by USP8 immunoblot (Figure 5.9B). Knockdown of USP8 resulted in a decrease in EYFP-Parkin translocation at 1 h CCCP treatment. No difference in the recruitment of EYFP-Parkin to mitochondria was observed with co-expression of either HA-Ub^{WT} or HA-Ub^{K6R} in USP8 siRNA transfected cells. Thus, USP8 may not be involved in the removal of K6- linked ubiquitin chains in mitophagy. Surprisingly, overexpression of HA-Ub^{WT} led to a decrease in EYFP-Parkin translocation to mitochondria in control siRNA transfected cells. Thus, an increase in total cellular ubiquitin levels may impair Parkin recruitment. Whether or not this is due to increased ubiquitination of Parkin remains to be explored. At 2 h CCCP treatment, a decrease in the mitochondrially located EYFP-Parkin persisted in the USP8 knockdown cells transfected with both empty vector and HA-Ub^{K6R}.

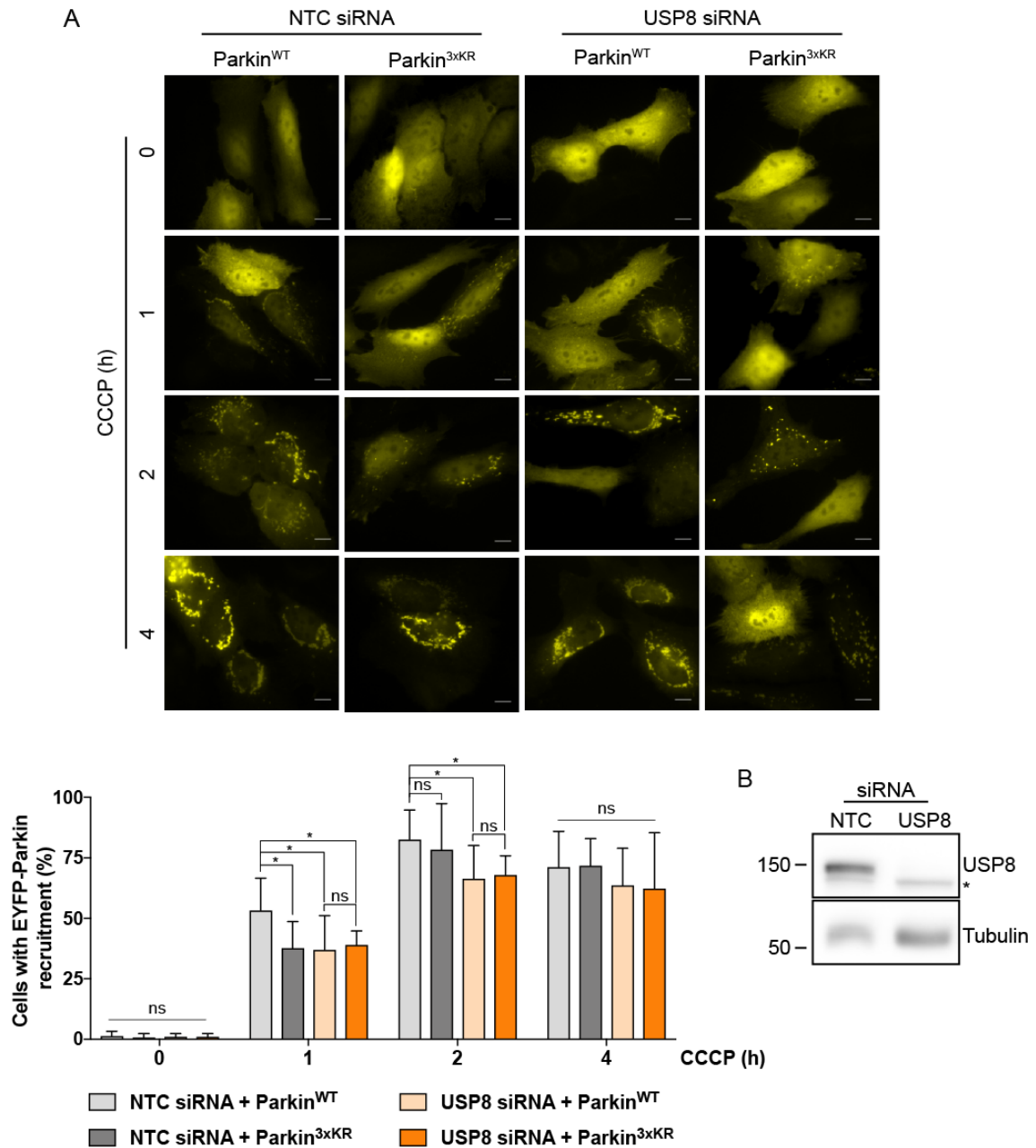


Figure 5.8: Parkin translocation to mitochondria requires K27, K48 and K76 independently of USP8 activity

A) HeLa cells were transfected with non-targeting control (NTC) or USP8 siRNA and were subsequently transfected with EYFP-Parkin^{WT} or EYFP-Parkin^{3xKR} (yellow). Cells were treated 1, 2 or 4 h with 10 μ M CCCP to induce mitochondrial damage and EYFP-Parkin recruitment. Cells displaying EYFP-Parkin recruited to mitochondria at each timepoint was quantified. Scale bar 10 μ m. Graph displays mean \pm SEM. Cells were quantified from 6 coverslips from 3 independent experiments (10 fields quantified per coverslip (18 – 52 cells per coverslip)). Statistical analysis was performed by two-way

*ANOVA with Fisher's LSD; * $P \leq 0.05$. B) Knockdown of USP8 was verified by USP8 immunoblot. * indicates an aspecific band on USP8 immunoblot.*

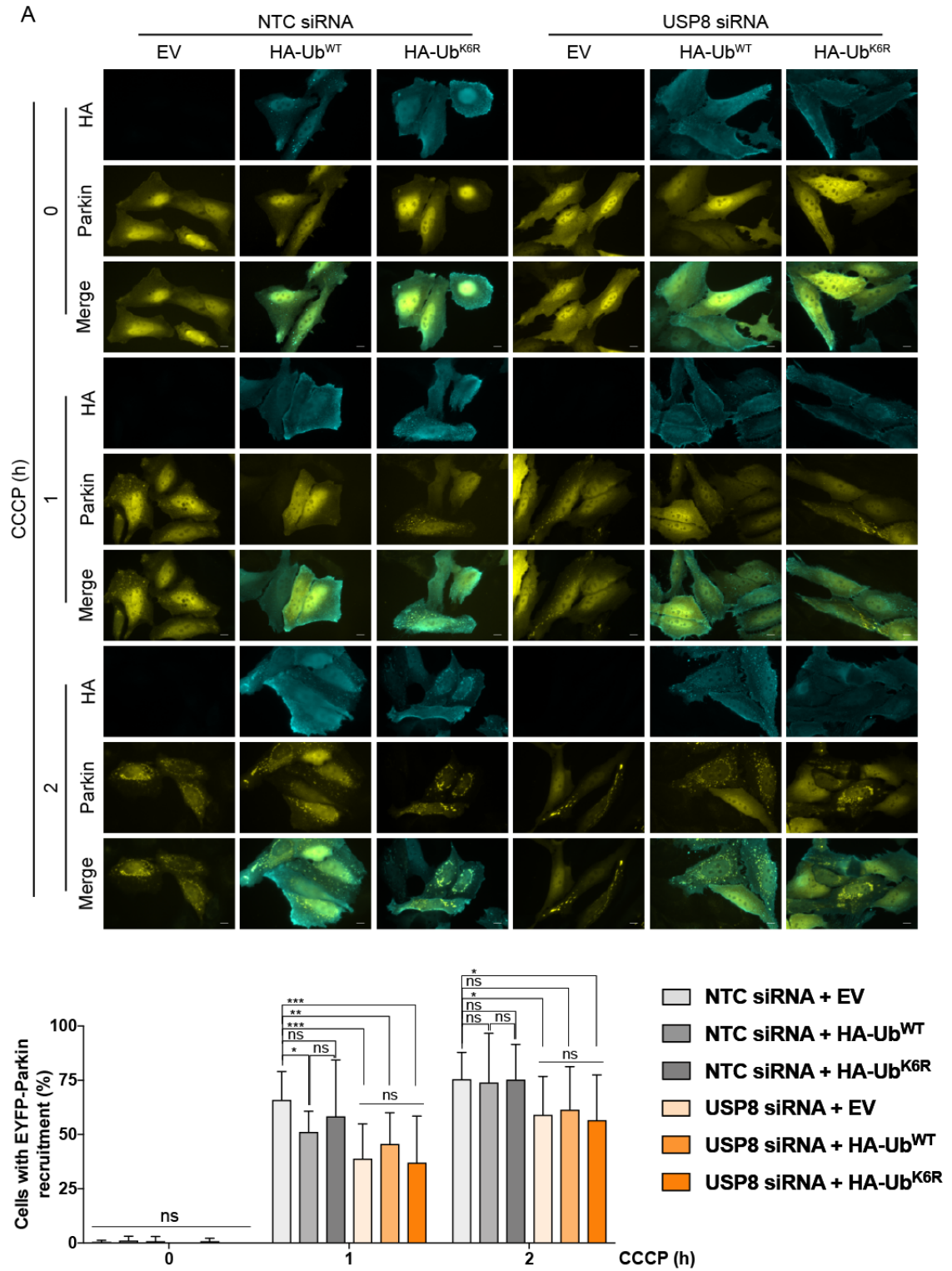


Figure 5.9 Cells unable to form K6- linked ubiquitin chains are equally affected by USP8 knockdown in their ability to recruit Parkin

A) HeLa cells were transfected with non-targeting control (NTC) or USP8 siRNA and were subsequently co-transfected with pCI-neo empty vector (EV), HA-Ub^{WT} or HA-Ub^{K6R} (cyan) and EYFP-Parkin (yellow). Cells were treated for 1 or 2 h with 10 μ M CCCP to induce mitochondrial damage and EYFP-Parkin recruitment. Cells displaying EYFP-Parkin recruitment at each timepoint were quantified. Scale bar 10 μ m. Graph displays mean \pm SEM. Cells were quantified from 8 coverslips from 4 independent experiments (12 – 15 fields quantified per coverslip (27 – 101 cells per coverslip)). Statistical analysis was performed by two-way ANOVA with Fisher's LSD; * $P \leq 0.05$, ** $P \leq 0.01$, *** $P < 0.001$. B) Knockdown of USP8 was verified by USP8 immunoblot. * indicates an aspecific band on USP8 immunoblot.

We previously identified that C9orf72 was involved in the recruitment of Parkin to mitochondria (4.3.1). To investigate whether C9orf72 and USP8 played roles in Parkin recruitment that placed them in the same pathway, the functional relationship between C9orf72 and USP8 was analysed.

First, whether C9orf72 acts downstream of USP8 in the translocation of Parkin during mitophagy was examined. HeLa cells were transfected with non-targeting control or USP8 siRNA and subsequently co-transfected with pCI-neo empty vector, Myc-C9orf72L or Myc-C9orf72S and EYFP-Parkin. Cells were treated with CCCP to induce mitochondrial damage and EYFP-Parkin translocation (Figure 5.10A). The knockdown of USP8 was verified by USP8 immunoblot (Figure 5.10B). The knockdown of USP8 resulted in a decrease in EYFP-Parkin that was translocated to mitochondria following 1 h CCCP treatment. The overexpression of Myc-C9orf72L or Myc-C9orf72S did not affect the translocation of EYFP-Parkin to mitochondria in the control siRNA transfected cells. Furthermore, overexpression of neither Myc-C9orf72L nor Myc-C9orf72S altered the defect in EYFP-Parkin translocation in USP8 siRNA transfected cells.

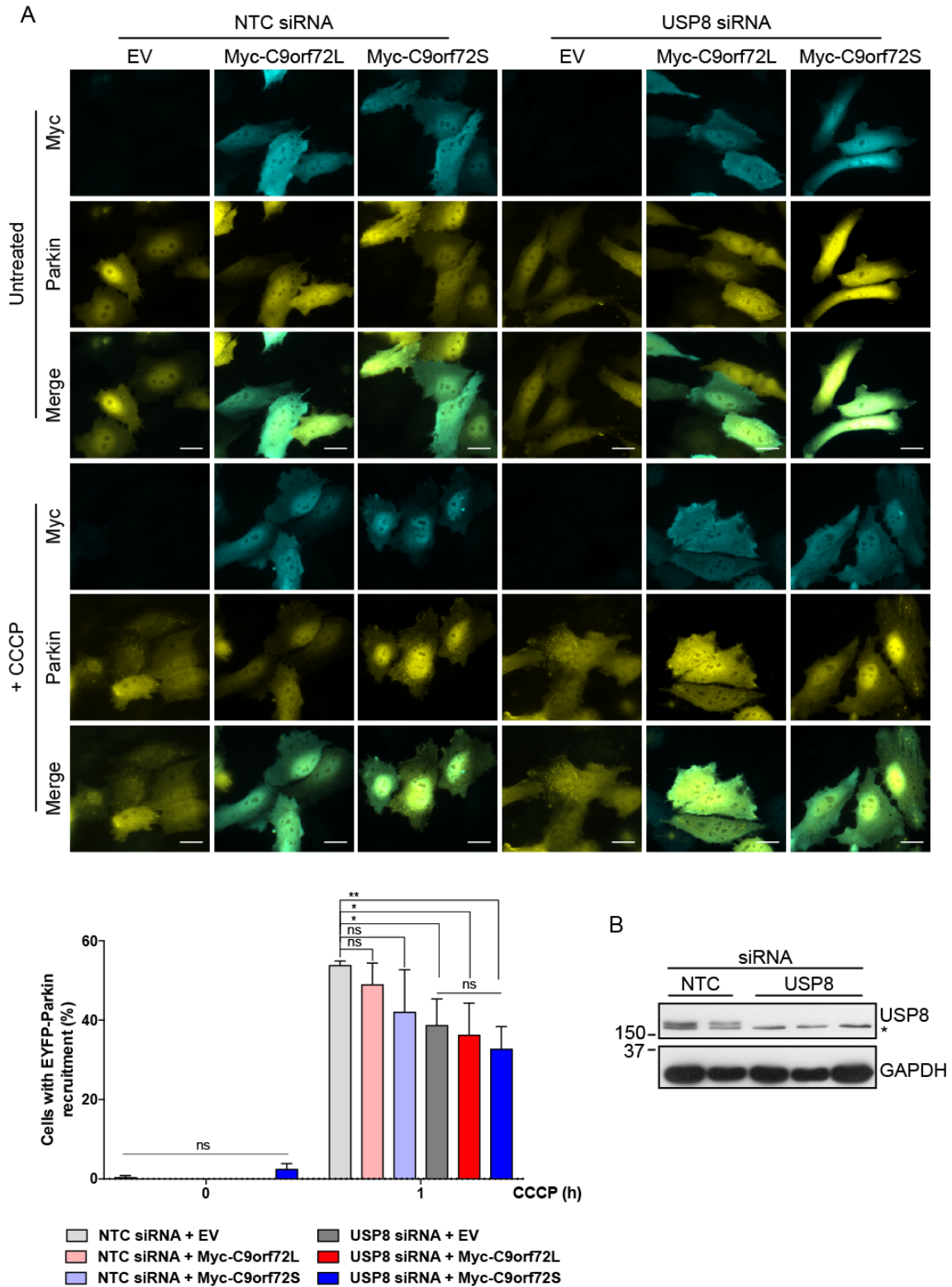


Figure 5.10 Overexpression of C9orf72 does not rescue the USP8 knockdown delay in Parkin translocation

A) HeLa cells were transfected with non-targeting control (NTC) or USP8 siRNA and subsequently co-transfected with pCI-neo empty vector (EV), Myc-C9orf72L (C9L) or Myc-C9orf72S (C9S) (cyan) and EYFP-Parkin (yellow). Cells were treated 1 h with 10

*μM CCCP to induce mitochondrial damage and Parkin recruitment. Cells displaying recruited EYFP-Parkin were quantified at each timepoint. Scale bar 10 μm. Graph displays mean±SEM. Cells were quantified from 3 independent experiments (cells quantified from 15 – 30 fields per experiment (37 – 101 cells)). Statistical analysis was performed by two-way ANOVA with Fisher's LSD; * P ≤ 0.05, ** P ≤ 0.01. B) Knockdown of USP8 was verified by USP8 immunoblot. * indicates an aspecific band on USP8 immunoblot.*

If the C9orf72 and USP8 proteins play sequential roles in Parkin translocation during mitophagy, then knockdown of both USP8 or C9orf72 would result in a delay in Parkin recruitment that was equal to the effect of the knockdown of the downstream protein alone. Conversely, if C9orf72 and USP8 affect different parts of the Parkin translocation pathway, the double knockdown would result in a change in the delay in Parkin translocation from the single knockdown phenotype. To investigate whether knockdown of C9orf72 alters the USP8 knockdown induced delay in Parkin recruitment, HeLa cells were transfected with either non-targeting control, USP8 or a combination of both C9orf72 and USP8 siRNA and were subsequently transfected with EYFP-Parkin. Cells were treated with CCCP to induce mitochondrial damage and EYFP-Parkin translocation (Figure 5.11A). The efficiency of C9orf72 knockdown was confirmed by qPCR (Figure 5.11B), the knockdown of USP8 was verified by USP8 immunoblot (Figure 5.11C). One hour CCCP treatment in USP8 knockdown cells resulted in a decrease in cells displaying EYFP-Parkin recruitment to mitochondria compared to the control siRNA transfected control cells. Double knockdown of C9orf72 and USP8 did not alter the USP8 knockdown induced delay in EYFP-Parkin recruitment. At 2 h CCCP there was no difference between the control cells and the USP8 or C9orf72 and USP8 siRNA transfected cells. Thus, C9orf72 and USP8 may act as parts of the same Parkin translocation pathway.

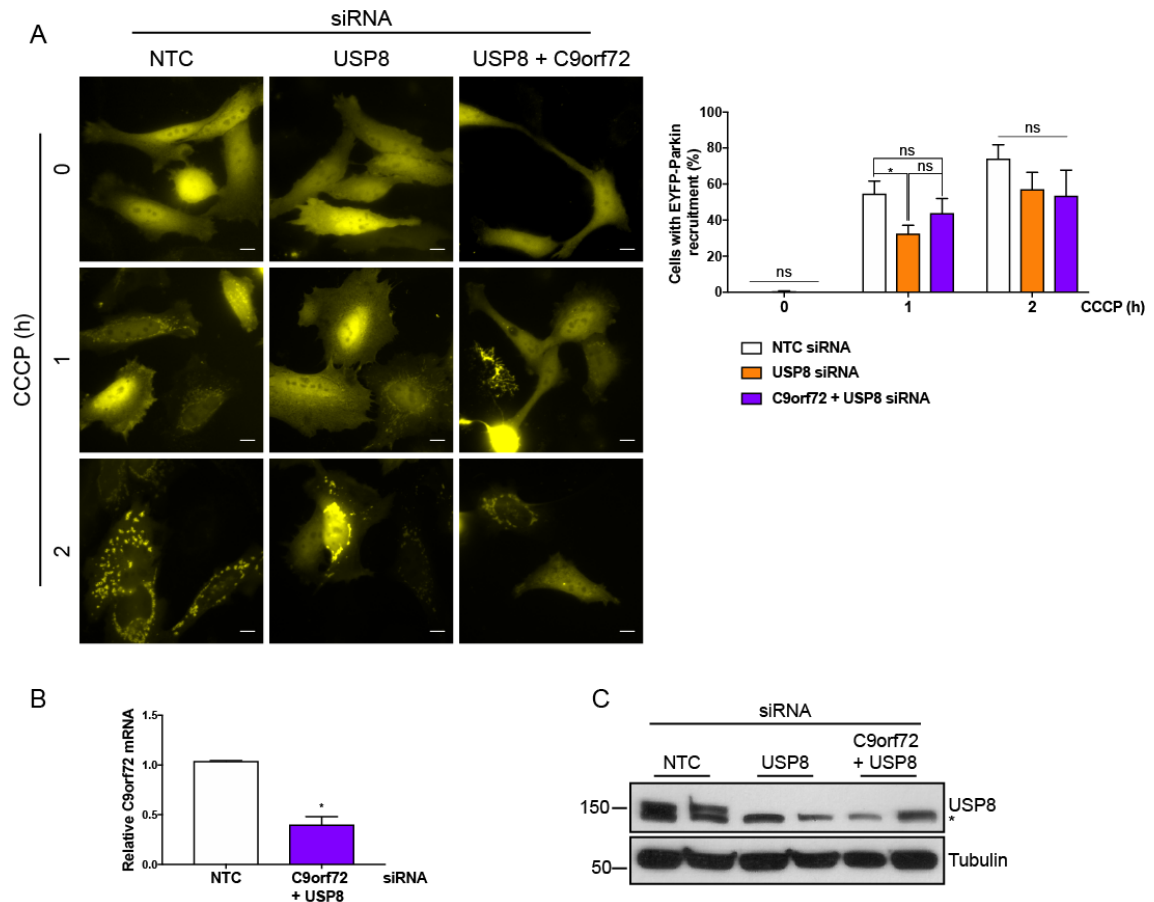


Figure 5.11 Knockdown of C9orf72 does not affect the USP8 knockdown delay in Parkin translocation

*A) HeLa cells were transfected with non-targeting control (NTC), USP8 or a combination of C9orf72 and USP8 siRNA and were subsequently transfected with EYFP-Parkin (yellow). Cells were treated 1 or 2 h with 10 μ M CCCP to induce mitochondrial damage and EYFP-Parkin recruitment. Cells displaying EYFP-Parkin recruited to mitochondria were quantified at each timepoint. Scale bar 10 μ m. Graph displays mean \pm SEM. Cells were quantified from 4 coverslips from 2 independent experiments (10 fields quantified per coverslip (17 – 63 cells per coverslip)). Statistical analysis was performed by two-way ANOVA with Fisher's LSD; * $P \leq 0.05$. B) C9orf72 mRNA levels were determined by qPCR. Graph displays mean \pm SEM. Statistical analysis was performed by unpaired t-test; * $P \leq 0.05$. C) The knockdown of USP8 was verified by USP8 immunoblot. * indicates an aspecific band on USP8 immunoblot.*

5.4 Discussion

In this chapter the interaction between C9orf72 and USP8 was investigated. DUB enzymes, including USP8, feature 3 domains which mediate cellular localisation, interactions and DUB activity (Komander et al., 2009). In USP8, the C-terminal USP

domain interacts with ubiquitin to mediate the cleavage of ubiquitin from the substrate, hence mediating DUB activity. Interactions between substrate and DUB promote substrate specificity (reviewed in Mevissen and Komander, 2017). The Rhodanese domain has been identified to interact with the E3 ligase NRDP1, possibly to regulate the of ubiquitination of substrates or NDPR1 stability (Wu et al., 2004). *In vitro* assays differentially identified the USP and Rhodanese domains of USP8 as potential interacting regions that were required for the interaction with C9orf72 (Figure 5.3, Figure 5.4). The interaction between the Rhodanese domain of USP8 and C9orf72 may promote specific targeting of USP8 DUB activity towards C9orf72. Indeed, C9orf72 is predicted to undergo ubiquitination at Lys14 (prediction from <http://ubpred.org>), which may target it for degradation by the proteasome. As the USP domain interacts with ubiquitin moieties, the USP domain of USP8 may interact preferentially with the ubiquitinated form of C9orf72. Indeed, preliminary data from our lab suggests that USP8 is involved in regulating the turnover of C9orf72 (Dr Christopher Webster, unpublished data), which will be investigated further in our lab by Miss Lily Koryang.

A greater amount of USP8 appeared to co-immunoprecipitate with C9orf72S than with C9orf72L or C9orf72DdD, suggesting that the N-terminal fragment of C9orf72 may interact preferentially with USP8 (Figure 5.1B). As EGFP-USP8 interacted with both C9orf72S and C9orf72DdD, which are composed of either the uDENN or DENN-dDENN domains of C9orf72 respectively, USP8 may interact with multiple sites on C9orf72. Previous data collected in our lab showed that C9orf72L and C9orf72S can interact (Dr Christopher Webster, unpublished data). The formation of C9orf72 dimers may underlie the interaction between USP8 and both the C- and N-terminal C9orf72 proteins. The formation of C9orf72 dimers should be further investigated to determine interacting regions and relevance for the cellular functions of C9orf72.

Next, we investigated the importance of the C9orf72 and USP8 interaction in the regulation of mitochondrial dynamics. The mitochondrial network morphology is in part controlled by the ubiquitination of proteins involved in fission and fusion events. Indeed, ubiquitination of Drp1 regulates the fission of mitochondria, whereas the ubiquitination and proteasomal degradation of OMM targets regulates fusion events. DUBs have been previously found to play a role in regulating the mitochondrial network. Mitochondrially located USP30 regulates mitochondrial morphology, with knockdown of USP30 resulting in elongation of the mitochondria (Nakamura and Hirose, 2008). USP30 has been shown to deubiquitinate OMM proteins including MIRO1, TOMM20 and VDAC and prevent their degradation by the proteasome (Bingol et al., 2014; Cunningham et al., 2015; Liang et al., 2015). It remains unclear how the knockdown of USP30 may lead to elongation of

mitochondria, but may involve dysregulated mitochondrial fusion by Mfn1/2 turnover (Nakamura and Hirose, 2008). In our hands, knockdown of USP8 resulted in a similar elongation of mitochondria and an increase in mitochondrial connectivity (Figure 5.5). Therefore, USP8 may also target OMM proteins and regulate mitochondrial fission/fusion events by a similar undiscovered mechanism. We observed a fragmentation of the mitochondrial network upon C9orf72 overexpression (4.2), which was not influenced by the absence of USP8 (Figure 5.5). Therefore, the regulation of mitochondrial network morphology in C9orf72 expressing cells may not be due to dysregulated ubiquitination of the mitochondrial fission/fusion machinery.

Finally, we investigated the role of the C9orf72 and USP8 interaction in mitophagy. USP8 has been suggested to be involved in the recruitment of the E3 ligase Parkin to mitochondria. USP8 was proposed to remove K6- linked ubiquitin from Parkin to promote its translocation (Durcan et al., 2014). We previously found that C9orf72 may be involved in mitophagy and the translocation of Parkin (4.3). We found no evidence that C9orf72 and USP8 play interlinked roles in Parkin translocation (Figure 5.10, Figure 5.11). Indeed, this would support the finding that C9orf72 may be involved in the recruitment of the ULK1 initiation complex in mitophagy, a downstream event of Parkin translocation. Furthermore, we did not find any direct evidence to support the previously described function of USP8 in mitophagy. Expression of a Parkin unable to undergo ubiquitination at the 3 Lys residues was detrimentally recruited upon stimulation of mitophagy (Figure 5.8). In addition, in our hands the defect in Parkin translocation upon USP8 knockdown was not rescued by expression of ubiquitin unable to form K6- linked chains (Figure 5.9). Thus, USP8 may not regulate the translocation of Parkin to mitochondria though the removal of K6- linked ubiquitin chains.

Although K6- linked ubiquitin linkages were the most abundant poly-ubiquitin chain assembled on Parkin in mitophagy, K11-, K48- and K63- linkages were also identified, which also assembled on K27, K48 and K76 of Parkin (Durcan et al., 2014). Due to the mutation of Lys to Arg, the Parkin^{3xKR} would be also unable to assemble these ubiquitin chains. As the ubiquitination status of Parkin may underlie its activation and translocation, Parkin^{3xKR} cannot undergo the initial translocation events, resulting in the delay reported here (Figure 5.8). Indeed ubiquitination of Parkin was shown to promote the role of Parkin in the clearance of α -synuclein via autophagy (Lonskaya et al., 2013). Hence it may be information to investigate further the ubiquitin linkage sites found on Parkin as well as the nature of the ubiquitin linkage itself, to fully understand the role of ubiquitin in the activation of Parkin during mitophagy.

It is clear that K6- linked ubiquitin chains are important for the regulation of mitophagy. In the context of USP8 regulated mitophagy Durcan *et al.*, speculated K6- linked ubiquitin may impair the interaction between Parkin and PINK1 or phosphorylated ubiquitin chains on mitochondria impairing the translocation of Parkin to mitochondria (Durcan and Fon, 2015). Durcan *et al.*, also proposed that K6- linked ubiquitin chains may impair the interactions between damaged mitochondria and the autophagy machinery and hence prevent autophagic clearance (Durcan and Fon, 2015). However, several other DUB enzymes have been implicated in mitophagy. USP15, USP30 and USP35 have been identified to act in opposition to the progression of mitophagy, with knockdown of these DUBs resulting in increased mitochondrial turnover (Bingol *et al.*, 2014; Cornelissen *et al.*, 2014; Cunningham *et al.*, 2015; Wang *et al.*, 2015). USP30 is located on the OMM, with the catalytic portion of the protein facing the cytosol (Nakamura and Hirose, 2008). Knockdown of USP30 led to an increase levels of ubiquitinated TOMM20 and MIRO1, suggesting that it may act to remove these ubiquitin linkages on OMM targets to prevent mitophagic clearance (Bingol *et al.*, 2014). In addition, knockdown of USP30 was able to rescue the mitophagy defects associated with Parkin mutants, suggesting that its role is downstream of Parkin in mitophagy (Bingol *et al.*, 2014). USP30 has been shown to display a preference for K6- linked ubiquitin chains on mitochondrial proteins (Cunningham *et al.*, 2015). The accumulation of K6- linked ubiquitin chains as a result of USP30 knockdown appeared to accelerate mitophagy (Cunningham *et al.*, 2015). Moreover, expression of a Ub^{K6R} was reported in these studies to result in a delay of mitophagy (Cunningham *et al.*, 2015), which was recapitulated in our results (Figure 5.9). The difference in reported effects of Ub^{K6R} on accelerating or impeding mitophagy was postulated to be due to the substrate on which the K6- linked chain was formed. Thus K6- linked ubiquitin chains on mitochondrial proteins promote mitochondrial clearance, whereas K6- linked chains on Parkin impair its translocation and mitophagy (reviewed in Durcan and Fon, 2015). Clarification as to how ubiquitin regulates mitochondrial turnover via mitophagy requires further investigation.

DUB enzymes do not display selective linkage hydrolysis. Indeed, unlike USP30 that has been shown to show a degree of specificity towards K6- linked ubiquitin chains (Gersch *et al.*, 2017), USP8 does not display linkage specificity (Ritorto *et al.*, 2014). USP8 has been shown to hydrolyse both K48- and K63- ubiquitin chains (Alexopoulou *et al.*, 2016). As multiple types of ubiquitin linkage are involved in mitophagy progression (notably K6-, K11-, K48-, and K63-), the dysregulation of mitophagy induced by knockdown of DUB enzymes may be due to changes in ubiquitination of many cellular

targets, including those involve in trafficking events. The lysosomal targeting of mitochondria during mitophagy was promoted upon knockdown of both USP30 and USP35 (Wang et al., 2015). A process also potentially linked to USP8 mitophagy via its interaction with the E3 ligase NRDP1 which plays a role in the fusion of lysosome during late Parkin mediated mitophagy (Soleimanpour et al., 2014). As C9orf72 was shown to be recruited to lysosomes, the C9orf72 and USP8 interaction may be involved in the regulation lysosomal function and mitophagy at later stages which warrant further investigation. Furthermore, both USP8 and C9orf72 have been shown to be involved in endosomal trafficking events, suggesting additional interconnected roles which will be discussed further (6.2.3).

Although here we identified an interaction between C9orf72 and USP8 in both co-immunoprecipitation and *in vitro* GST binding assays, it would be informative to verify that this interaction is of physiological relevance by performing the co-immunoprecipitation between the endogenous proteins. Similar to our assays in Chapter 4, we investigated the role of USP8 in mitophagy using a pool of siRNA consisting of 2 individual siRNAs targeting USP8. To verify that these did not lead to off target effects, which may also impair mitophagy progression, the rescue of USP8 using siRNA resistant constructs should be performed. Despite this, our assays correspond to the second cell type that USP8 siRNA knockdown has been shown to impair Parkin translocation during mitophagy, indicating that USP8 may indeed play a role in mitophagy, albeit one not yet fully characterised. Furthermore, we were unable to identify a role for the C9orf72 and USP8 interaction in the maintenance of mitochondrial dynamics (5.3). A PLA investigation may clarify the cellular compartment in which the interaction between C9orf72 and USP8 occurs, which may inform on which cellular processes, including mitophagy, lysosomal function and endosomal trafficking, may be regulated by the two proteins.

Chapter 6. Discussion

6.1 Introduction

A repeat expansion in *C9orf72* is the most common genetic defect associated with ALS and FTD (reviewed in Corcia et al., 2017; DeJesus-Hernandez et al., 2011; Renton et al., 2011). The repeat expansion is proposed to contribute to disease via 3 separate mechanisms; an RNA toxicity, a DPR protein toxicity and *C9orf72* haploinsufficiency (reviewed in Gendron and Petrucelli, 2018; Todd and Petrucelli, 2016). *C9orf72* haploinsufficiency has been reported to impact on the survival of motor neurons, indicating that it may play a role in ALS pathogenesis (Shi et al., 2018b). The *C9orf72* protein has been shown to be in a complex with SMCR8 and WDR41 and to play a role in both autophagy and lysosomal function (reviewed in Amick and Ferguson, 2017; Amick et al., 2016; reviewed in Nassif et al., 2017; Sellier et al., 2016; Sullivan et al., 2016; Ugolino et al., 2016; Webster et al., 2016a; Yang et al., 2016). The purpose of this thesis was to investigate the function of the *C9orf72* protein further, by characterising the interaction between *C9orf72* and mitochondrial proteins.

Screens designed to identify interacting partners of the *C9orf72* protein reported several mitochondrial proteins and complexes as hits (Y2H unpublished screen, Dr Guillaume Hautbergue (SITraN) unpublished mass spectrometry screen and in published screens (Blokhuys et al., 2016; Sellier et al., 2016; Sullivan et al., 2016)). In Chapter 3, we verified the interaction between *C9orf72* and mitochondrial proteins and complexes of the IMM, namely COX6C of COX IV and the ATP Synthase and TIM23 complexes (Figure 3.3, Figure 3.5, Figure 3.6). Consistent with these interactions, *C9orf72* was found to localise to the IMS (Figure 3.13). However, the mechanism by which *C9orf72* is imported into the IMS remains unclear (3.5).

We next investigated the function of the interaction between *C9orf72* and mitochondria (Chapter 4). *C9orf72* was found to influence the dynamics of the mitochondrial network (Figure 4.1, Figure 4.2); which can occur as a result of changes in mitochondrial quality control (reviewed in Hamacher-Brady and Brady, 2016). Consistent with a role in mitophagy, loss of *C9orf72* led to impaired clearance of mitochondria (Figure 4.8). *C9orf72* was found to be recruited to mitochondria upon mitochondrial damage (Figure 4.12) and to recruit the mitochondrial fission and the autophagy machinery to mitochondria (Figure 4.3, Figure 4.7). Therefore, *C9orf72* may assist in the segregation of the damaged organelles from the network and in the initiation of phagophore biogenesis, targeting the damaged organelle for degradation (reviewed in Hu et al., 2017; Ishihara et al., 2003; Itakura et al., 2012; reviewed in Yamano et al., 2016).

As C9orf72 haploinsufficiency may contribute to C9orf72 ALS/FTD (Shi et al., 2018b), and the poly(GR) DPR has been shown to induce mitochondrial dysfunction (Lopez-Gonzalez et al., 2016), we investigated the mitochondrial dynamics of a C9orf72 ALS patient iAstrocyte model. C9orf72 ALS patient iAstrocytes were found to have fragmented mitochondrial networks (Figure 4.13) and an impairment in an early stage of mitophagy (Figure 4.14). Therefore, C9orf72 ALS/FTD patients display signs of impaired mitochondrial dynamics, reminiscent of some of the changes observed in the C9orf72 loss and gain of function cell models.

Finally, we characterised the interaction between C9orf72 and a DUB, USP8 (5.2). Both C9orf72 and USP8 were previously implicated in endosomal trafficking events (Berlin et al., 2010a; Farg et al., 2014; Row et al., 2007) and autophagy (Sellier et al., 2016; Sun et al., 2018; Webster et al., 2016a; Yang et al., 2016). We identified a mitochondrial function for C9orf72 (Chapter 4), whilst USP8 had previously been implicated in Parkin dependent mitophagy (Durcan et al., 2014). We found no evidence of interplay between C9orf72 and USP8 in the regulation of mitochondrial dynamics or mitophagy (5.3). Furthermore and in contrast to the previous report, we did not observe the K6- linked specificity of DUB activity of USP8 towards Parkin (Figure 5.8, Figure 5.9) (Durcan et al., 2014). Whilst this does not exclude a role for USP8 and other DUBs in mitophagy, as discussed previously in (5.4), it does highlight the need for further investigation into the role of USP8 in mitochondrial quality control. Further investigations into the functional relevance of the interaction between C9orf72 and USP8 are also required.

6.2 The role of the C9orf72 protein in maintaining mitochondrial function

6.2.1 C9orf72 in mitochondrial function and mitophagy

We found C9orf72 to be recruited to mitochondria following mitochondrial damage (Figure 4.12). We propose that as C9orf72 interacts with and regulates the translocation of the autophagy machinery, C9orf72 may direct the autophagy machinery specifically to damaged organelles during mitophagy. Indeed, an increased expression of C9orf72 led to an increase in the level of ULK1 found on mitochondria (Figure 4.7, Figure 6.1). This is similar to the mitophagy adaptor proteins that are recruited to ubiquitin chains on the OMM of damaged mitochondria (Lazarou et al., 2015). The majority of proteins that direct the autophagy machinery to mitochondria are located on or recruited to the OMM (reviewed in Yamano et al., 2016). However, PHB2 found on the IMM, also interacts with LC3 to promote mitophagy upon the rupture of the OMM (Wei et al., 2017). We identified IMM complexes as interacting partners of C9orf72 (3.2, Figure 3.3, Figure 3.5, Figure 3.6), with C9orf72 residing in the IMS (3.4, Figure 3.13). Following rupture of the

OMM, the IMM is exposed to the cytosol, cytosolic C9orf72 may then interact with COX IV via COX6C and the TIM23 and ATP Synthase complexes, leading to the recruitment of C9orf72 to mitochondria and with it the trafficking of the ULK1 initiation complex. The binding to multiple IMM complexes may indicate that C9orf72 recognises damaged organelles in a redundant manner.

We observed C9orf72 to be found in mitochondria even in the absence of mitochondrial damage (Figure 3.8, Figure 6.1). Whilst, this does not exclude the above statement about the recruitment of C9orf72 to mitochondria upon damage, it rather suggests an additional role for C9orf72 in the regulation of IMM complexes or in the recognition of damaged organelles. Interestingly, C9orf72 has been proposed to interact with VDAC3 (Blokhuis et al., 2016; Sullivan et al., 2016). The oxidation of Cys residues in VDAC3 has been proposed to stimulate mitochondrial quality control pathways including MDV formation and Parkin dependent mitophagy (reviewed in Reina et al., 2016; Soubannier et al., 2012b; Sun et al., 2012). C9orf72 itself contains a number of conserved Cys residues (Figure 3.16), which may become oxidised upon mitochondrial damage and form part of the signalling pathway to detect the accumulation of damaged organelles and promote their subsequent clearance (Figure 6.1). Furthermore, ubiquitinated VDAC3 acts as a Parkin docking site during mitophagy (Sun et al., 2012). Therefore, the proposed interaction between C9orf72 and VDAC3 may be involved in the recognition of damaged organelles and in the recruitment of mitophagy machinery to mitochondria.

C9orf72 has been shown to be in a stable complex with SMCR8 and WDR41 (Amick et al., 2016; Sellier et al., 2016; Sullivan et al., 2016; Ugolino et al., 2016; Yang et al., 2016). In this study we did not investigate the contribution to mitophagy made by either SMCR8 or WDR41. WDR41 has been shown to regulate the trafficking of C9orf72 to lysosome upon amino acid starvation (Amick et al., 2018), but its role in mitophagy is unexplored. The interactions between SMCR8, OPTN and p62; SMCR8, Rab8a and Rab39b; and the phosphorylation of SMCR8 by TBK1 strongly support a role for SMCR8 in mitophagy, driving site specific formation of autophagosomes (Figure 6.1) (Sellier et al., 2016). Indeed, SMCR8 may be recruited to mitochondria by the mitophagy adaptor proteins, OPTN and p62 (Sellier et al., 2016). The amino acid sequence of SMCR8, harbours a potential GABARAP interaction motif; [F]-[V]-[X]-[V]. Therefore, SMCR8 may also interact with GABARAP proteins (Rogov et al., 2017). Like the LC3s, GABARAPs are lipidated during autophagosome maturation and are required for mitophagy progression (Kabeya et al., 2004; Nguyen et al., 2016; Weidberg et al., 2010). Therefore, following mitochondrial damage, SMCR8 may be recruited to mitochondria as part of

the C9orf72 complex or by OPTN/p62. SMCR8 may aid in the recruitment of GABARAP proteins and participate in the elongation and maturation of the phagophore (Figure 6.1).

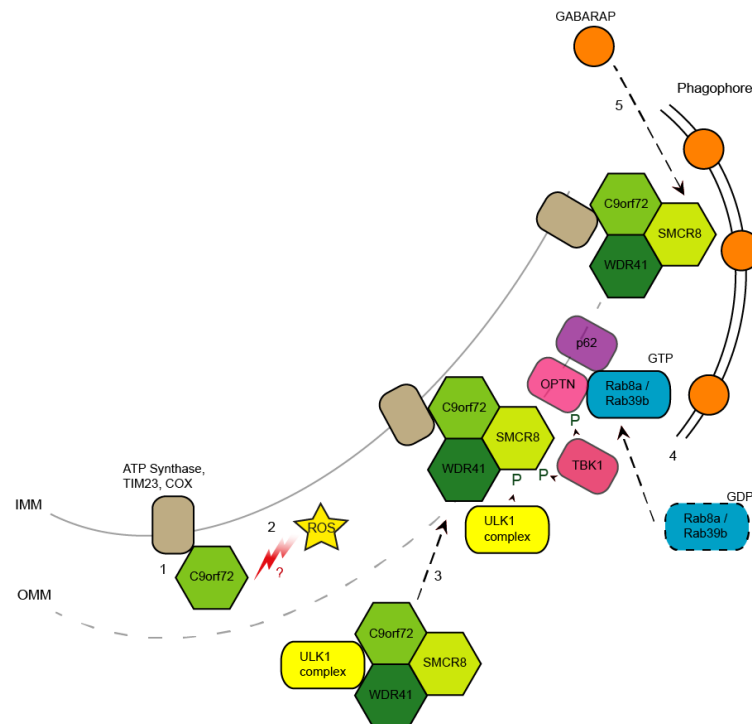


Figure 6.1 A model suggesting how the C9orf72 complex regulates the engulfment of damaged mitochondria by the autophagosome

1) The C9orf72 protein interacts with protein complexes of the IMM. 2) Mitochondrial damage may be sensed by IMS residing C9orf72 and modify IMM complex function. 3) The C9orf72 complex is recruited to mitochondria upon damage and mediates the recruitment of the ULK1 initiation complex. 4) SMCR8 may be recruited to mitochondria by C9orf72, p62 and OPTN. SMCR8 is phosphorylated by TBK1 and ULK1, modifying its GEF activity. SMCR8 acts as GEF for Rab8a and Rab39b and promotes autophagosome elongation. 5) SMCR8 interacts with GABARAP proteins to promote the elongation and maturation of the phagophore.

We identified C9orf72 to play a role in the removal of damaged mitochondria through the mitophagy pathway (Figure 4.8). C9orf72 recruits the autophagy machinery, namely the ULK1 initiation complex, to damaged mitochondria to promote their removal (Figure 6.1). The recruitment of the ULK1 initiation complex to mitochondria is a feature of both Parkin dependent and Parkin independent mitophagy pathways (Itakura et al., 2012; Wu et al., 2014). Therefore, despite the investigation into the role of C9orf72 in Parkin dependent mitophagy here, C9orf72 may also play a role in Parkin independent mitophagy.

Recently attention has turned away from investigating Parkin dependent mitophagy utilising chemical induction, as this relies on an induction of mitophagy which may not employ mechanisms that function *in vivo* to maintain mitochondria. Indeed, animal models have shown that both PINK1 and Parkin are dispensable for the maintenance of mitochondria and basal mitophagy (Lee et al., 2018b; Lin et al., 2017; McWilliams et al., 2018). Therefore, separate mechanisms as yet unexplored, may be of greater relevance *in vivo*, which may also be regulated by the C9orf72 protein.

C9orf72 is expressed in neurons and has been shown to regulate neuronal autophagy, via the translocation of the ULK1 initiation complex (Webster et al., 2016a). Whether or not C9orf72 regulates mitophagy in neurons requires further investigation. Fully understanding the role that the C9orf72 protein may play in the maintenance of neuronal mitochondria presents further challenges, as little evidence supports the function of endogenous Parkin in the maintenance of mitochondria in neurons (reviewed in Cummins and Gotz, 2017). Furthermore, mitophagy is not reliably induced in neurons under cell culture conditions (reviewed in Martinez-Vicente, 2017). Therefore, exploring the role of C9orf72 in neuronal mitochondrial maintenance may therefore require investigations into both Parkin dependent and independent mitophagy mechanisms.

C9orf72 has been shown to regulate lysosomal function (reviewed in Amick and Ferguson, 2017; Amick et al., 2016; Ugolino et al., 2016). Lysosomal function is required for the clearance of autophagy substrates including damaged mitochondria (reviewed in Menzies et al., 2017). Loss of C9orf72 led to the perinuclear clustering of swollen lysosomes suggestive of impaired clearance or lysosomal transport (Amick et al., 2016). Although we did not investigate the role of the downstream effects of lysosomal function on mitophagy in our C9orf72 loss of function model, this does not exclude that disrupted lysosome function may lead to the delayed mitochondrial clearance observed.

The phenotype associated with C9orf72 knockout mice is consistent with a defect in immune system function, rather than neurodegeneration (Atanasio et al., 2016; Burberry et al., 2016; O'Rourke et al., 2016; Sullivan et al., 2016; Ugolino et al., 2016). The changes in lysosomal function associated with loss of C9orf72 in cells may lead directly to the phenotype of the C9orf72 knockout mice (reviewed in Amick and Ferguson, 2017). Furthermore, alterations in immune function are reported in C9orf72 ALS/FTD patients, which may indicate a contribution of C9orf72 haploinsufficiency towards the progression of C9orf72 ALS/FTD (reviewed in Lall and Baloh, 2017). The function of the immune system is intrinsically linked to that of mitochondria (reviewed in Weinberg et al., 2015). Mitochondrial function has not yet been explored and reported in the C9orf72 knockout mice. However, the accumulation of damaged mitochondria through reduced mitophagy,

as reported here in our C9orf72 loss of function cell model (Figure 4.8), may lead to an increase in mitochondrial damage-associated molecular patterns (DAMPs) which activate the inflammasome and promote a pro-inflammatory state (reviewed in Broz and Dixit, 2016), similar to that observed in the C9orf72 knockout mice (Atanasio et al., 2016; O'Rourke et al., 2016). Consistent with defects in mitophagy stimulating the inflammatory system, the loss of Parkin and/or the downstream mitophagy effector p62 in macrophages led to an increase in pro-inflammatory IL-1 β following stimulation of the inflammasome (Zhong et al., 2016). Furthermore, PINK1 and Parkin knockout mouse models display elevated levels of pro-inflammatory cytokines following mitochondrial stress (Sliter et al., 2018). Therefore, reduced mitophagy through C9orf72 haploinsufficiency, may in concert with the increased cellular stresses associated with C9orf72 ALS/FTD, including DPRs, TDP-43 aggregates and p62 pathology, promote mitochondrial induced activation of the inflammatory response and result in the inflammation observed in C9orf72 ALS/FTD patients.

6.2.2 Rab GTPases in mitochondrial dynamics and mitophagy

C9orf72 and SMCR8 are DENN domain containing proteins (Levine et al., 2013; Zhang et al., 2012). As such C9orf72 and SMCR8 have been shown to act in Rab GTPase cascades (reviewed in Webster et al., 2016b). Consistent with this role, C9orf72 has been shown to interact with multiple Rab GTPases (Table 1-3). Rab cascades have been implicated in the maintenance of mitochondrial health, through the regulation of both mitochondrial network dynamics and the removal of damaged organelles (Alto et al., 2002; Bui et al., 2010; Caza et al., 2014; Lai et al., 2015; Landry et al., 2014; Ortiz-Sandoval et al., 2014; Yamano et al., 2018). As a Rab effector or GEF, C9orf72 may be responsible for the targeting of Rabs to specific cellular membranes or their activity (Grosshans et al., 2006). As C9orf72 is found on mitochondria, it may direct Rabs to damaged mitochondria and regulate mitochondrial dynamics.

The Rab cascade involving C9orf72 and SMCR8 has so far been studied in the context of autophagy. C9orf72 has been shown to act as an effector for Rab1a (Webster et al., 2016a). Consistent with a Rab cascade, C9orf72 may then recruit the downstream GEF (SMCR8) and Rabs (Rab8a and Rab39b) which promotes the elongation of the phagophore (reviewed in Nassif et al., 2017; Sellier et al., 2016; Yang et al., 2016). This Rab cascade may also be of relevance in the clearance of mitochondria. Indeed, the interaction of Rab8a and Rab39b with OPTN and p62 suggest a role in the selective degradation of autophagic cargos and damaged mitochondria (Pilli et al., 2012; Sellier et al., 2016; Vaibhava et al., 2012). Rab8a is phosphorylated upon the induction of

mitochondrial damage, downstream of PINK1 and Parkin activation, by an unknown kinase (Lai et al., 2015). Although the role of this phosphorylation event in mitophagy is unclear, it has been shown to impair the activation of Rab8a by its GEF Rabin (Lai et al., 2015). Furthermore, SMCR8 has been shown to be phosphorylated by TBK1, mTOR, AMPK and ULK1 (Figure 6.1) (Hoffman et al., 2015; Hsu et al., 2011; Sellier et al., 2016). The phosphorylation of SMCR8 may alter its GEF activity and regulate site directed autophagosome synthesis (Jung and Behrends, 2017; Sellier et al., 2016).

Mitochondrial network morphology has been shown to be regulated by the Rab32 family and Rab11, through the modulation of Drp1 (Alto et al., 2002; Bui et al., 2010; Landry et al., 2014; Ortiz-Sandoval et al., 2014). We found that overexpression of C9orf72 led to the recruitment of Drp1 to mitochondria (Figure 4.3) and to the fragmentation of the mitochondrial network (Figure 4.1). The Rab32 family, which includes Rab38 and Rab29, are localised to the mitochondria and MAM (Bui et al., 2010; Ortiz-Sandoval et al., 2014), where they regulate the recruitment of calnexin to maintain Ca^{2+} homeostasis (Bui et al., 2010). MAM is also important for the regulation of mitochondrial dynamics and fission (reviewed in Paillusson et al., 2016). Rab32, and to a lesser extent Rab38 and Rab29, were found to interact with Drp1, with dominant active Rab32 promoting the interaction indicating that Drp1 may be an effector for this family of Rabs. Furthermore, the expression of the dominant negative Rab32 family led to the collapse of mitochondria around the nucleus (Ortiz-Sandoval et al., 2014), similar to that found in Drp1 knockout cells (Ishihara et al., 2009). Ortiz-Sandoval *et al.* proposed that the Rab32 family mediated the redistribution of Drp1 on ER membranes to mediate mitochondrial fission. Although the C9orf72 complex was not found to interact with Rab32, it was found to interact with family members Rab29 and Rab38, which play a similar role in Drp1 recruitment. Therefore, C9orf72 may also play a role in the trafficking of these Rabs during mitochondrial network fission events (Figure 6.2) (Aoki et al., 2017; Ortiz-Sandoval et al., 2014; Sellier et al., 2016). In addition, Rab32 has been shown to play a role in autophagosome membrane elongation (Hirota and Tanaka, 2009), which may indicate further involvement of C9orf72 in autophagy Rab cascades. C9orf72 was also shown to co-localise and interact with Rab11 (Farg et al., 2014), which has also linked to Drp1 mediated mitochondrial fission following viral insult. Rab11 was shown to regulate the remodelling of the cytoskeleton and mitochondria in an SFK dependent manner. In this model the trafficking of Drp1 to mitochondria dependent on Rab11 and its effector FIP1/RCP (Landry et al., 2014). Rabs have been shown to be regulated by multiple effectors. Furthermore, the interaction of a single effector with multiple Rabs permits the coupling of the Rab activity and allows crosstalk between membrane

compartments (reviewed in Grosshans et al., 2006; Pylypenko et al., 2018). Therefore, although currently C9orf72 has not been linked to these Rabs in the context of mitochondrial dynamics, this does not exclude a role for the C9orf72/SMCR8/WRD41 complex in the localisation and mitochondrial function of Rab11, Rab29 and Rab38 (Figure 6.2).

Following PINK1 activation and the labelling of OMM proteins with ubiquitin chains, RABGEF1 is recruited to mitochondria and directs downstream Rab5 to mitochondria. Rab5 and its effectors then mediate the recruitment of the downstream Rab, Rab7. Rab7 mediates the recruitment of ATG9A membranes to the mitochondrion and promotes the formation and elongation of the phagophore in a mechanism that is specific to PINK1/Parkin mitophagy. Rab7 is inactivated by TBC1D15 and TBC1D17 (GAPs) which are recruited to mitochondria by Fis1 (Yamano et al., 2018). Rab7 has been shown to interact with Mfn2, which is increased during starvation, to promote the use of mitochondrial membranes as sources of autophagosome membrane (Zhao et al., 2012). C9orf72 has been shown to interact with both Rab5 and Rab7 (Aoki et al., 2017; Farg et al., 2014; Frick et al., 2018). The effector for Rab7 mediating the recruitment of ATG9A during mitophagy has not been identified, therefore it is possible that C9orf72 could fulfil such a role. This could lead to a two-step recruitment of autophagy machinery by C9orf72 to damaged mitochondria, recruiting both ULK1 during initiation and ATG9A for phagophore elongation, inducing phagophore biogenesis specifically at the damaged mitochondrion (Figure 6.2). In addition to this role in the initiation of mitophagy, Rab7 has also been implicated in autophagosome maturation regulating the fusion with the lysosome (Gutierrez et al., 2004), the transport of lysosomes (Pu et al., 2016) and SNPH MDV transport (Lin et al., 2017). These also impact on mitochondrial dynamics and mitophagy (1.2.3.2). Investigations into the nature of the interaction between C9orf72 and Rab7 will explore whether C9orf72 is involved in these processes and will clarify the extent to which C9orf72 is involved in mitochondrial quality control.

Rab4 has been reported to influence mitochondrial clearance; regulating Drp1 levels and the formation of autophagosomes on the mitochondria (Caza et al., 2014; Talaber et al., 2014). Rab4, LC3 and mitochondria were found to co-localise upon starvation and the inhibition of mTOR (Talaber et al., 2014). To date no interaction has been found between C9orf72 and Rab4. However, loss of C9orf72 perturbs signalling of mTOR during starvation and amino acid re-feeding, resulting in altered lysosomal function (Amick et al., 2016; Ugolino et al., 2016). Therefore, C9orf72 may have an indirect effect on Rab4 mediated autophagosome biogenesis during starvation and impair autophagy and mitophagy.

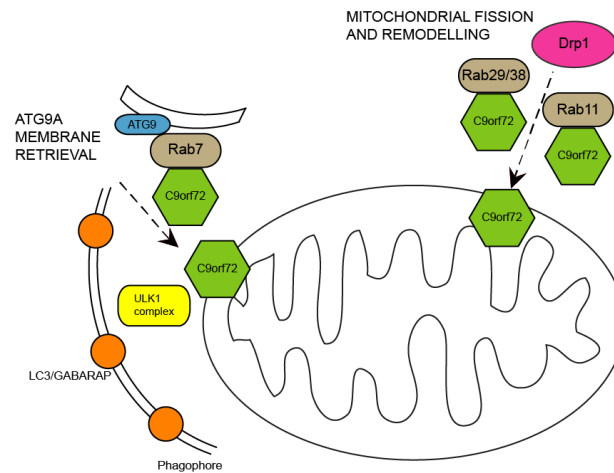


Figure 6.2 C9orf72 may regulate Rab GTPases governing mitochondrial dynamics
C9orf72 may act as a GEF or effector for Rab11, Rab29 and Rab38 and promote the recruitment of the pro-fission protein Drp1 to mitochondria. The recruitment of Drp1 results in mitochondrial network fragmentation and remodelling. In mitophagy, C9orf72 regulates the recruitment of the ULK1 initiation complex to mitochondria. In addition, C9orf72 may also act as a GEF or effector for Rab7, which retrieves ATG9A membranes during mitophagy, to promote the elongation of the phagophore.

6.2.3 The role of the C9orf72 and USP8 interaction

We identified an interaction between C9orf72 and the DUB USP8 (5.2), however we did not identify a common function in mitochondrial quality control (Figure 5.10, Figure 5.11, 5.3). Interestingly both USP8 and C9orf72 have been reported to co-localise with Rab5 (Alexopoulou et al., 2016; Farg et al., 2014; Frick et al., 2018; Xia et al., 2012), which is involved in the trafficking of early endosomes (Jovic et al., 2010). Consistent with an interaction with Rab5, both C9orf72 and USP8 have been implicated in endosomal trafficking (Farg et al., 2014; Row et al., 2007; Row et al., 2006; Yeates and Tesco, 2016). Constitutively active Rab5 was able to improve the survival of C9orf72 ALS patient iMN, indicative that defective endosomal trafficking may contribute to C9orf72 ALS/FTD (Shi et al., 2018b). The activity of Rab cycles is regulated by PTMs, including ubiquitination, which can alter cellular localisation and activity (reviewed in de la Vega et al., 2011). Rab5 has been shown to undergo ubiquitination which can impair the interaction between Rab5 and its effector, as well as GDP/GTP exchange activity (Shin et al., 2017). Hence USP8 may be involved in the regulation of the ubiquitination state of endosomal Rabs, including those trafficked by the C9orf72 complex.

In contrast, ubiquitination can also regulate protein turnover (reviewed in Komander and Rape, 2012). The interaction between USP8 and C9orf72 may therefore regulate the

turnover of C9orf72. It is unclear whether this is the case, but this is currently under investigation by Miss Lily Koryang in our lab. If C9orf72 turnover is regulated by USP8, then USP8 may be an attractive therapeutic target for C9orf72 ALS/FTD, to increase C9orf72 levels. Targeting the activity of USP8 has previously been identified as a therapeutic target for neurodegenerative diseases, including PD and ALS. USP8 has been shown to regulate the clearance of α -synuclein aggregates, with knockdown of USP8 resulting in a decrease in α -synuclein aggregates and eye toxicity in a *Drosophila* model of PD (Alexopoulou et al., 2016). USP8 has also been shown to interact with TDP-43, with USP8 regulating the turnover of TDP-43 by the proteasome. Consistent with this, knockdown of USP8 was reported to increase the severity of the fly eye phenotype in TDP-43 expressing *Drosophila* (Hans et al., 2014). This would indicate that silencing USP8 may not be a catch-all therapy and although beneficial for some conditions, may increase the pathology associated with other neurodegenerative diseases, especially TDP-43 pathologies including ALS/FTD.

6.3 Defective mitochondrial dynamics in ALS

6.3.1 ALS proteins interact with mitochondria and mediate mitochondrial dysfunction

A number of ALS-linked genes products have been shown to interact with mitochondria and regulate mitochondrial function, including, SOD1, TDP-43, FUS and the C9orf72 repeat expansion-associated DPR poly-GR (Blokhuys et al., 2016; Deng et al., 2015; Higgins et al., 2002; Lopez-Gonzalez et al., 2016; Mattiazzi et al., 2002; Wang et al., 2016). The interaction between these proteins, especially the ALS mutant forms, have been implicated directly in the dysregulation of mitochondria (reviewed in Smith et al., 2017b).

Here we found C9orf72 to be located to the IMS and to interact with OXPHOS and the TIM23 complexes (Figure 3.5, Figure 3.6). At present it is unknown whether C9orf72 regulates the function of the mitochondrial import or OXPHOS complexes. Mitochondria in C9orf72 ALS patient fibroblasts and iPSC motor neurons have been reported to be hyperpolarised (Lopez-Gonzalez et al., 2016; Onesto et al., 2016), although this is contested by others (Dafinca et al., 2016). Hyperpolarised mitochondria can be indicative of OXPHOS dysfunction (Forkink et al., 2014; Perl et al., 2004). The hyperpolarisation of mitochondria in C9orf72 ALS patients is in stark contrast to the majority of ALS cases, including SOD1, TDP-43, FUS, VCP and SQSTM1 ALS, where mitochondria have been reported to be depolarised (reviewed in Smith et al., 2017b). Therefore, a specific C9orf72-linked mechanism may result in the changes in MMP

observed. If the interaction between C9orf72 and ATP Synthase plays a regulatory role in the latter's function, then C9orf72 haploinsufficiency may lead to dysregulation of the OXPHOS machinery. However, the C9orf72 repeat expansion associated poly-GR DPRs have been shown to interact with mitochondrial ribosomal proteins and induce mitochondrial stress (Lopez-Gonzalez et al., 2016). Therefore, a combination of C9orf72 repeat expansion-associated disease mechanisms may lead ultimately to the mitochondrial dysfunction found in C9orf72 ALS/FTD patients. As cellular ROS are generated through the activity of the OXPHOS machinery (reviewed in Murphy, 2009; Turrens, 2003), a higher MMP may drive elevated ROS levels through increased OXPHOS activity, establishing a pathological cycle. The poly-GR DPRs may also interact with mitochondria and induce further ROS generation (Figure 6.3).

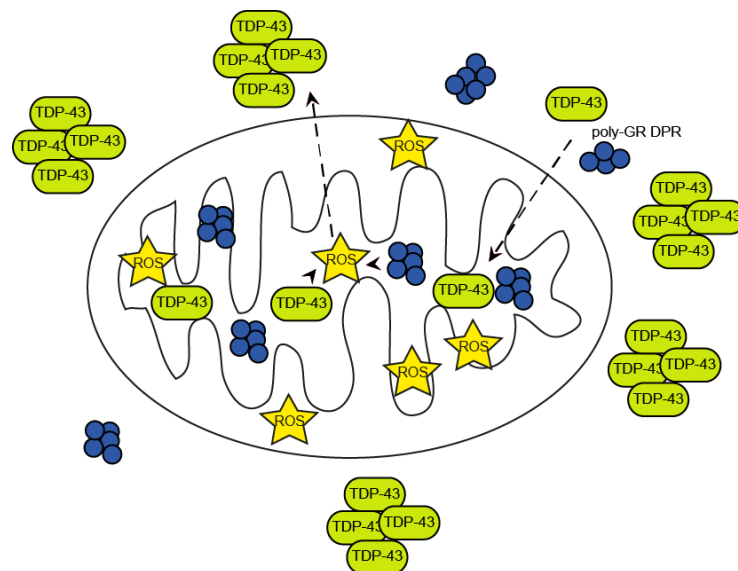


Figure 6.3 Mitochondrial damage establishes a pathological cycle

C9orf72 repeat associated poly-GR DPRs and cytosolic TDP-43 are imported into mitochondria and associate with mitochondrial ribosomal proteins and mRNA respectively. These aberrant associations induce mitochondrial damage and drive the generation of ROS. Excessive ROS generation induces mitochondrial dysfunction but also perpetuates the mislocalisation and aggregation of TDP-43 establishing a pathological cycle.

The production of ROS has been shown to lead to the mislocalisation and aggregation of TDP-43 (Colombrita et al., 2009; McDonald et al., 2011; Meyerowitz et al., 2011), which may then exacerbate cellular and mitochondrial dysfunction and ROS generation (Figure 6.3). Indeed, TDP-43 and to a greater extent ALS mutant TDP-43 accumulates in mitochondria where it preferentially binds the mRNAs of the mtDNA-encoded complex

I subunits, resulting in complex I disassembly (Wang et al., 2016). Since cytoplasmic TDP-43 accumulation is a hallmark pathology in most ALS cases, including C9orf72 ALS, this may also explain the mitochondrial defects observed in sporadic ALS and other familial ALS cases. Therefore it may be key to determine the contribution to mitochondrial dysfunction that can be attributed to the mutated ALS protein itself, in contrast to the TDP-43 pathology associated changes.

6.3.2 Import of mitochondrial proteins in ALS

We identified C9orf72 to be located in the IMS, however we did not identify the mechanism by which its import was achieved (3.5). As C9orf72 haploinsufficiency is implicated in C9orf72 ALS/FTD it is possible that levels of IMS C9orf72 are reduced in disease. This may then result in a 2-fold effect on mitochondrial function. First, as described here (Chapter 4), the clearance of damaged mitochondria may be impaired. Second, if the C9orf72 protein is found to play a role in the function of mitochondria, then these may also be impaired in disease.

The mislocalisation of IMS proteins SOD1 and CHCHD10 has been implicated in SOD1 and CHCHD10 ALS (reviewed in Muyderman and Chen, 2014; Ramesh and Pandey, 2017). Loss of CHCHD10 import was proposed to underlie the changes in cristae morphology found in CHCHD10 ALS patient fibroblasts (Bannwarth et al., 2014). However, the exact role of CHCHD10 in the IMS is unclear, as CHCHD10 knockout mice displayed no mitochondrial substructure alterations (Burstein et al., 2018). Secondly, the accumulation of ALS mutant SOD1 in the IMS is thought to primarily be driven by the formation of aggregates (Kawamata and Manfredi, 2008). However, it has been shown that increased levels of CCS worsened the ALS phenotype and mitochondrial swelling of SOD1 G93A mice, highlighting a role for Class II IMS import in SOD1 ALS pathogenesis (Son et al., 2007). Hence the potential loss of C9orf72 from the IMS either directly as a result of haploinsufficiency or as a result of impaired import, may affect mitochondrial function and mitochondrial architecture.

6.3.3 Structural alterations of mitochondrial networks in ALS

We found C9orf72 patient iAstrocytes to have fragmented mitochondrial networks (Figure 4.13). This is consistent with previous reports of fragmented mitochondria being observed in C9orf72 ALS patient fibroblasts mitochondria contained within autophagic vesicles (Onesto et al., 2016) and swollen mitochondria found in C9orf72 ALS patient iPSC motor neurons (Dafinca et al., 2016). As most ALS models, including C9orf72 ALS, display mitochondrial fragmentation this suggests that mitochondrial dysfunction is a

prevalent and core feature of disease (Table 1-2) (reviewed in Smith et al., 2017b). Fragmented mitochondria are indicative of defects in mitochondrial function (reviewed in Youle and van der Bliek, 2012).

In SOD1 and TDP-43 ALS, imbalances in mitochondrial fission and fusion machinery were reported to induce the mitochondrial fragmentation, with the balance shifted towards an increase in fission proteins, although this remains controversial (Ferri et al., 2010; Liu et al., 2013; Luo et al., 2013; Xu et al., 2010; Xu et al., 2011). Interestingly, in C9orf72 ALS patient fibroblasts, elevated levels of Mfn1 were reported (Onesto et al., 2016). This is counterintuitive as this would suggest a shift towards mitochondrial fusion, as opposed to the fragmented mitochondrial networks observed (Onesto et al., 2016). In our C9orf72 loss of function cell model, we observed an increase in Mfn2 levels which correlated with mitochondrial network fusion (Figure 4.4). Therefore, C9orf72 haploinsufficiency may induce the increase in pro-fusion proteins, as seen in the C9orf72 ALS patient fibroblasts and our C9orf72 loss of function model (Onesto et al., 2016). However, it is likely that the other repeat expansion mechanisms influence mitochondria function in C9orf72 ALS/FTD, resulting in an overall decrease in mitochondrial network connectivity. For instance, the interaction between the poly-GR DRP and mitochondria proteins is likely to induce mitochondrial dysfunction, as seen by the increase in mitochondrial ROS, leading to mitochondrial fragmentation (Lopez-Gonzalez et al., 2016). In addition, C9orf72 ALS/FTD patients present with TDP-43 pathology, which itself may contribute to mitochondrial dysfunction and mitochondrial fragmentation (Wang et al., 2016).

IMM cristae play important roles in mitochondrial function, supporting import of proteins through the TOM20/TIM23 complexes and the activity of the OXPHOS machinery (reviewed in Cogliati et al., 2016). We identified the C9orf72 protein to interact with IMM complexes that are located within mitochondrial cristae (Figure 3.5, Figure 3.6). Furthermore, a BioIP screen identified MICOS subunits, CHCHD3 and IMMT, as potential interacting partners of C9orf72 (Blokhuys et al., 2016). CHCHD3, also known as MIC19, regulates the assembly of the MICOS complex (Sakowska et al., 2015). IMMT, also referred to as MIC60, regulates the remodelling of membranes for cristae formation and is regulated by MIC19 (Hessenberger et al., 2017). Therefore, C9orf72 may be involved in the regulation of cristae structure. Therefore, C9orf72 haploinsufficiency may disrupt cristae formation, resulting the deformed cristae observed in C9orf72 patient cell models (Dafinca et al., 2016; Onesto et al., 2016). This may impair mitochondrial function, which may then lead to the fragmentation of the mitochondrial network. The deformation of mitochondrial cristae has been reported in

SOD1, TDP-43, FUS, Alsin and CHCHD10 ALS cell and animal models (Bannwarth et al., 2014; Deng et al., 2015; Gautam et al., 2016; Genin et al., 2016; Kirkinos et al., 2005; Stribl et al., 2014). In SOD1 and FUS ALS models, these defects are associated with early disease stages indicating that early changes in mitochondrial function may underlie disease pathogenesis (Kong and Xu, 1998; Sharma et al., 2016).

Interestingly, the fragmentation of the mitochondrial network is also a feature of ageing. Mitochondrial function declines with age (reviewed in Seo et al., 2010), which could contribute to the progression of neurodegenerative diseases. Importantly fragmentation of mitochondria is also associated with PD, AD and HD (Cai and Tammineni, 2016; Martin et al., 2015; Ryan et al., 2015). The similarity in mitochondrial dysfunction between neurodegenerative diseases, highlights potential crossover between disease pathways despite the varying clinical phenotypes and endpoints, that may inform on therapeutic avenues.

6.3.4 Defective mitochondrial quality control in ALS

Mitochondrial quality control is impaired in neurodegenerative diseases including ALS (reviewed in Rodolfo et al., 2018). Indeed, the accumulations of mitochondria seen in ALS patient tissue, and ALS cell and animal models point towards defective clearance of mitochondria (reviewed in Smith et al., 2017b).

In C9orf72 ALS patient iAstrocytes expressing Parkin, we observed a delay in the recruitment of Parkin to mitochondria upon mitochondrial damage (Figure 4.14). This may lead to a decrease in the recognition of damaged organelles for clearance by mitophagy. A decrease in the recruitment of Parkin to mitochondria could also lead to an increase in the level of OMM proteins that are normally regulated by Parkin mediated degradation by the proteasome as part of basal mitochondrial maintenance (reviewed in Martinez-Vicente, 2017). This may account for the increase in the level of Mfn1 observed in C9orf72 ALS patient fibroblasts (Onesto et al., 2016) and the increase in Mfn2 levels we observed upon C9orf72 knockdown (Figure 4.4). Parkin dependent mitophagy may be impaired in TDP-43 and FUS ALS, as both have been shown to regulate the expression of Parkin (Lagier-Tourenne et al., 2012; Polymenidou et al., 2011). As TDP-43 mislocalisation to the cytosol is a feature of most ALS cases, defects in Parkin expression may be a common feature of ALS. Consequently, the induction of mitophagy may be affected in most ALS cases. In contrast, a recent study in SOD1 G93A mice revealed a chronic induction of Parkin dependent mitophagy, which resulted in a lower mitochondrial mass. The knockout of Parkin in SOD1 G93A mice improved the survival and delayed onset of pathology (Palomo et al., 2018). Palomo *et al.*

suggested that the knockout of Parkin delayed the chronic accelerated turnover of mitochondria in SOD1 G93A mice, thereby improving mitochondrial dynamics. In agreement with this, the knockout of PINK1 or Parkin in a FUS P525L Drosophila model led to an improvement in motor phenotype and survival (Chen et al., 2016b). As neither SOD1 nor FUS ALS are associated with the mislocalisation of TDP-43, it is likely that this may explain the increase in Parkin activity and differentiate these forms of ALS from those associated with TDP-43 pathology. Nevertheless, improving mitochondrial dynamics may present an attractive therapeutic strategy for ALS.

We established C9orf72 as an IMS protein that may recruit directly the ULK1 autophagy machinery to mitochondria upon mitochondrial damage (Figure 4.7). C9orf72 haploinsufficiency may therefore impair the recruitment of the ULK1 initiation complex to mitochondria. Indeed, C9orf72 haploinsufficiency has been shown to impair autophagy in C9orf72 patient iNeurons through a similar mechanism (Webster et al., 2016a). The disrupted targeting of mitochondria for degradation appears to be a common feature in ALS. The expression of the autophagy adaptors p62 and BNIP3, were found to be reduced in SOD1 G93A mice (Rogers et al., 2017). Furthermore, the recognition of mitochondria with ruptured OMM is mediated by the IMM protein PBH2 (Wei et al., 2017). TDP-43 has been shown to interact with PHB2 and regulate its expression during mitophagy (Davis et al., 2018). It is unknown how this interaction may be affected by ALS mutations in TDP-43. However, due to the widespread prevalence of TDP-43 mislocalisation in ALS, this pathway for the recognition of damaged mitochondria may be affected in ALS as a whole. Finally, the autophagy machinery is recruited to mitochondria indirectly by the mitophagy adaptor proteins including, p62 and OPTN (reviewed in Yamano et al., 2016). Both ALS mutant forms of p62 and OPTN lead to decreased recognition of the organelle by LC3 (Fecto et al., 2011; Maruyama et al., 2010). OPTN and p62 are phosphorylated by TBK1 to increase the affinity of the interaction with LC3 (reviewed in Majcher et al., 2015; Richter et al., 2016) (Wild et al., 2011a). ALS-linked loss of function mutations in TBK1 impair the interaction between TBK1 and OPTN impair the clearance of damaged mitochondria (Li et al., 2016; Moore and Holzbaur, 2016; Richter et al., 2016).

Not all mitochondrial turnover occurs via the removal of whole organelles (reviewed in Martinez-Vicente, 2017). The budding of MDV from neuronal mitochondria has been reported to deliver damaged mitochondria directly to lysosomes (McLelland et al., 2014; Soubannier et al., 2012a; Sugiura et al., 2014). SOD1 G93A mice were shown to have increased formation of SNPH mitochondrial vesicles (Lin et al., 2017). It is unknown if this is also the case in C9orf72 ALS/FTD. However, the transport of MDV to lysosomes

is regulated by Rab7 (Lin et al., 2017). If C9orf72 is found to regulate Rab7 mediated trafficking events through its interaction (Farg et al., 2014; Frick et al., 2018), then this mechanism of mitochondrial quality control may also be affected in disease.

Defects in autophagy lead to the accumulation of damaged mitochondria. Autophagy defects linked to ALS are present in multiple steps of the pathway and C9orf72 has been implicated several of these including phagophore initiation and downstream in lysosomal function (reviewed in Amick and Ferguson, 2017; Nassif et al., 2017; Webster et al., 2017). C9orf72 ALS patients have been shown to have altered autophagic flux and an accumulation of autophagic vacuoles, including some containing mitochondria (O'Rourke et al., 2016; Onesto et al., 2016; Sellier et al., 2016; Sullivan et al., 2016; Ugolino et al., 2016; Webster et al., 2016b). These findings suggest that the lysosomal function of C9orf72 ALS patients is impaired, which could be as a direct result of C9orf72 haploinsufficiency. The clearance of mitochondria is dependent on the lysosomal degradation of both autophagosomes containing mitochondria and MDV (reviewed in Martinez-Vicente, 2017). Thus, C9orf72 haploinsufficiency may lead to a two-step impairment of mitochondrial clearance; occurring at both initiation and degradation stages. Changes in lysosome function have repeatedly been implicated in neurodegenerative diseases, including ALS (reviewed in Wang et al., 2018). Compounding the potential effect of C9orf72 haploinsufficiency, is the altered lysosomal function associated with C9orf72 ALS/FTD risk factor TMEM106B (Amick and Ferguson, 2017). However although loss of TMEM106B has been reported to affect lysosomal trafficking, it did not affect mitochondrial trafficking or mass (Schwenk et al., 2014), suggesting that it does not itself play a role in the regulation of mitochondrial dynamics.

As C9orf72 haploinsufficiency impairs mitochondrial clearance (Figure 4.8) and the DPR proteins induce mitochondrial damage (Lopez-Gonzalez et al., 2016) a 2-hit mechanism impairing mitochondrial dynamics may arise in C9orf72 ALS/FTD. Indeed, the DPRs may lead to an accumulation of mitochondria that are targeted for mitophagy, but that fail to be removed as a result of C9orf72 haploinsufficiency. The accumulation of damaged mitochondria, which generate ROS, may then act feed-forward and induce further cellular dysfunction.

C9orf72 patient fibroblasts have been shown to have increased mitochondrial mass and upregulated PGC-1 α (Onesto et al., 2016). PGC-1 α is the master regulator of mitochondrial biogenesis (reviewed in Jornayvaz and Shulman, 2010). Therefore, whilst an increased mitochondrial mass could be explained by an impairment of the removal of damaged organelles by mitophagy, it may also be due to increased generation of new organelles. In C9orf72 ALS patient cells, mitochondrial biogenesis may be promoted to

produce new organelles due to poor mitochondrial health. However, coincidentally, cells are unable to remove the damaged organelles, leading to the accumulation of damaged fragmented mitochondria as seen in our iAstrocyte model (Figure 4.13) and reported in the C9orf72 ALS patient fibroblasts and iPSC motor neurons (Dafinca et al., 2016; Lopez-Gonzalez et al., 2016; Onesto et al., 2016). The mechanism underlying the increase in PGC-1 α in C9orf72 ALS patient fibroblast is unknown. However, disrupted mitochondrial biogenesis has been implicated in other ALS models. TDP-43 located in mitochondria regulates the transcription of mtDNA encoded proteins (Izumikawa et al., 2017). Mutant TDP-43 and TDP-43 ALS pathology have been shown to impair mitochondrial function and biogenesis (Wang et al., 2016). As TDP-43 pathology is a feature of all ALS cases, with the exception of SOD1 and FUS ALS, it is likely that dysregulated mitochondrial biogenesis plays a role in ALS pathogenesis. In contrast to the report in C9orf72 ALS fibroblasts, SOD1 G93A mice and sporadic ALS patients were reported to have lower levels of PGC-1 α expression (Thau et al., 2012). In PD, activation of PGC-1 α has been proposed as a therapeutic target as it has been shown to prevent the death of dopaminergic neurons in cell models of disease (reviewed in Corona and Duchon, 2015). However, SOD1 G37R mice with elevated PGC-1 α levels, generated through a cross with an MCK-PGC1 α mouse, displayed improved motor function without any extension of lifespan (Da Cruz et al., 2012). Therefore, early indications suggest that increasing mitochondrial biogenesis may not be beneficial for SOD1-linked ALS, potentially due to the numerous other cellular pathologies.

The high level of redundancy in the mitophagy pathway supports a multi-hit hypothesis for mitochondrial dysfunction in C9orf72 ALS. ALS is a progressive disease affecting individuals over the age of 55 – 65 (Orsini et al., 2015). Mitochondrial function declines naturally with age (reviewed in Bratic and Larsson, 2013; Payne and Chinnery, 2015), in addition declines in autophagy and lysosomal function also occur (reviewed in Carmona-Gutierrez et al., 2016; Martinez-Lopez et al., 2015). C9orf72 haploinsufficiency may impair mitochondrial quality control in C9orf72 ALS patients. Therefore, in early life, C9orf72 ALS patients may be able to remove damaged mitochondria through non-C9orf72 related mitophagy pathways. However as cellular dysfunction increases over age, perpetuated by the RNA and protein toxicities associated with the C9orf72 repeat expansion and the aggregation of autophagic cargos, mitochondrial clearance further declines, and damaged mitochondria accumulate.

C9orf72 ALS/FTD is likely caused by a contribution of all 3 repeat expansion disease mechanisms. Indeed, no model investigating a single disease mechanism recapitulates

the features of C9orf72 ALS/FTD fully (reviewed in Batra and Lee, 2017; Gitler and Tsuiji, 2016; Moens et al., 2017). The poly-GR DPRs have been shown to interact with mitochondrial ribosomes and induce mitochondrial derived ROS (Lopez-Gonzalez et al., 2016). Apart from these direct effects, the gain of function of mechanisms may have indirect effects on mitochondrial function. The sequestration of RNA binding proteins by the repeat expansion leads to the dysregulation of nuclear encoded genes (Cooper-Knock et al., 2015a; reviewed in Kumar et al., 2017; Prudencio et al., 2015; Sareen et al., 2013). As the majority of mitochondrial proteins are encoded by the nuclear genome, it is possible that the RNA toxicity leads to expression changes of mitochondrial proteins. The DPR proteins induce cell stress responses (reviewed in Freibaum and Taylor, 2017). For instance, the poly-GA DPR has been shown to induce ER stress (Zhang et al., 2014). ER stress is modulated by the contacts between mitochondria and ER at MAM, which then affect mitochondrial function (van Vliet and Agostinis, 2018). In ALS, ER – mitochondria contacts have been found to be reduced (Bernard-Marissal et al., 2015; reviewed in Smith et al., 2017b; Stoica et al., 2014; Stoica et al., 2016). It is currently unknown how ER - mitochondria contacts are affected in C9orf72 ALS/FTD. But dysregulation of ER-mitochondrial contacts and induction of ER stress could likely lead to further mitochondrial stress and ROS generation.

Cortical hyperexcitability has been reported in C9orf72 ALS patients and synaptic dysfunction reported in several of the DPR and repeat expansion models (Starr and Sattler, 2018). Synaptic dysfunction can be linked to mitochondrial dysfunction and has been proposed to contribute to AD and ALS/FTD (reviewed in Guo et al., 2017; Ling, 2018). Indeed, mitochondria are responsible for local ATP synthesis and Ca^{2+} buffering at the synapse (reviewed in Lee et al., 2018a). ALS-linked mutations in the mitochondrial IMS protein CHCHD10 lead to ALS and FTD, potentially as due to a loss of function (Bannwarth et al., 2014; Woo et al., 2017), however this remains contested (Burstein et al., 2018). Loss of CHCHD10 and the expression of ALS mutant CHCHD10 led to changes in expression of synaptic markers (Woo et al., 2017). This may indicate a direct link between mitochondrial and synaptic dysfunction. However, this may merely reflect the dysfunction in TDP-43 that was reported upon loss of CHCHD10 and the ALS mutant proteins (Woo et al., 2017). Indeed, TDP-43 at the synapse is involved in the transport of mRNAs to the synapse and their localised translation at the synapse, both of which may be impaired by the aggregation of TDP-43 in ALS and FTD (reviewed in Ling, 2018). C9orf72 has been shown to be found in synaptosomes and interact with the Rab3 family, which suggests that C9orf72 may play a role in the regulating the trafficking of

synaptic vesicles (Atkinson et al., 2015; Frick et al., 2018). The function of C9orf72 at the synapse is currently being investigated by Miss Rebecca Cohen in our laboratory.

6.4 Future Directions

Here we investigated the role of C9orf72 in Parkin dependent mitophagy upon the induction of mitochondrial damage using chemical inhibitors in cell lines. The recruitment of ULK1 has been reported in Parkin independent mitophagy mechanisms and upon the stimulation of mitophagy by other types of mitochondrial damage (Laker et al., 2017; Wu et al., 2014). As the recruitment of ULK1 appears to be a feature of multiple mitophagy pathways, C9orf72 may also be involved in these. Establishing whether C9orf72 is involved in Parkin independent mitophagy pathways may be important due to the high levels of redundancy in the mitophagy quality control pathways and the paucity of data supporting a single mitochondrial quality control mechanism to be active in neurons (reviewed in Cummins and Gotz, 2017; Martinez-Vicente, 2017).

Basal mitophagy may be regulated by alternate mechanisms to that induced by mitochondrial stress (Lee et al., 2018b; McWilliams et al., 2018). The monitoring of basal mitophagy can be assayed using constructs measuring the delivery of mitochondria to lysosomes, including mt-Keima and mito-QC (McWilliams et al., 2016; Sun et al., 2017; Sun et al., 2015). As C9orf72 has been implicated in the regulation of lysosomal function (Amick et al., 2016), it will be informative to explore the role of C9orf72 in the delivery of mitochondria to lysosomes in basal mitophagy, as this may help decipher between upstream and downstream roles for C9orf72 in mitophagy. The investigations into basal mitophagy should also be extended to C9orf72 ALS/FTD patient models.

To fully investigate the role of the C9orf72 protein in mitophagy, experiments should be carried out to identify Rab GTPases for which C9orf72 and the C9orf72/SMCR8/WDR41 complex may be a GEF or effector. These Rabs may include those already identified to interact with the C9orf72 complex in autophagy, namely Rab1a, Rab8a and Rab39b (reviewed in Nassif et al., 2017; Sellier et al., 2016; Webster et al., 2016a). Other Rabs that should be investigated include those that have been shown to co-localise or interact with C9orf72 including Rab5, Rab7, Rab11, Rab29 and Rab38 (Aoki et al., 2017; Farg et al., 2014; Sellier et al., 2016), which have also been shown to regulate mitochondrial dynamics (Alto et al., 2002; Bui et al., 2010; Landry et al., 2014; Ortiz-Sandoval et al., 2014; Yamano et al., 2014; Yamano et al., 2018). Although targeted investigations into these Rabs may yield informative results, it may additionally be useful to perform a Rab siRNA screen to fully identify Rabs that are involved in C9orf72 activity in mitophagy. Furthermore, whilst we concentrated of the role of C9orf72 in mitophagy, it will be

interesting to dissect the roles of SMCR8 and WDR41 in mitophagy and mitochondrial function.

Whilst here we used cell lines to investigate the function of C9orf72, this may be of limited relevance for the study of neurodegenerative disease (Schlachetzki et al., 2013). C9orf72 is ubiquitously expressed and regulates autophagy in neurons (Sellier et al., 2016; Webster et al., 2016a). The study of mitophagy in neurons has proven more controversial than in cell lines (reviewed in Cummins and Gotz, 2017; Martinez-Vicente, 2017). Establishing the role of C9orf72 in the maintenance of mitochondria in neurons should be carried out in both the context of Parkin dependent and independent mechanisms, in order to determine its potential as a target for therapeutic strategy in ALS/FTD. Furthermore, as ALS has been linked to non-cell autonomous mechanisms (reviewed in Lee et al., 2016a), exploring the role of C9orf72 in the maintenance of mitochondria in astrocytes and microglia may also lead to targets for therapeutic strategy.

C9orf72 was found to interact with several IMM complexes (3.2). However, many other potential interacting partners have been identified which still require validation (Blokhuys et al., 2016; Sellier et al., 2016; Sullivan et al., 2016). Establishing the full C9orf72 interactome could clarify the role of C9orf72 in mitochondria. The effect of the C9orf72 interaction with the complexes on mitochondrial function should also be investigated. For instance, import through the TIM23 complex in the presence and absence of C9orf72 could be explored to investigate the role of C9orf72 in protein import.

Whilst we concentrated on the role of C9orf72 in mitochondrial quality control, C9orf72 has been identified to play roles in autophagy, lysosome function, endosome trafficking, synaptic function and the regulation of the immune response (reviewed in Amick and Ferguson, 2017; Nassif et al., 2017). In addition, considerable overlap exists between autophagy, mitophagy and xenophagy (reviewed in Randow and Youle, 2014). To fully understand the function of C9orf72, these additional avenues of research should be pursued. Indeed, these may inform on both C9orf72 ALS/FTD pathology and therapeutic strategy.

Mitochondrial defects are a prevalent feature of ALS, including C9orf72 ALS (reviewed in Smith et al., 2017b). So far investigations into mitochondrial network connectivity, ROS production and MMP have been performed in C9orf72 ALS/FTD patient models (Figure 4.13) (Dafinca et al., 2016; Lopez-Gonzalez et al., 2016; Onesto et al., 2016). Further studies into extent mitochondrial dysfunction found in C9orf72 ALS should be carried out to determine the degree of similarity with other ALS cases. This may then

help in the development of therapeutics either for ALS as a whole or towards gene specific therapy for ALS.

Finally, if C9orf72 haploinsufficiency plays a role in C9orf72 ALS/FTD, it will be important to quantify the contribution of this towards the mitochondrial dysfunction observed in C9orf72 ALS/FTD patient cells. Indeed, the contribution of each C9orf72 repeat expansion mechanisms towards mitochondrial dysfunction should be explored using cell models and patient derived cells. These models may then be used in drug screening assays to identify compounds that improve mitochondrial function and cell survival.

References

- Abel, O., Powell, J.F., Andersen, P.M., and Al-Chalabi, A. (2012). ALSod: A user-friendly online bioinformatics tool for amyotrophic lateral sclerosis genetics. *Human Mutation* 33, 1345-1351.
- Abramoff, M.D., Magalhaes, P.J., and Ram, S.J. (2004). Image processing with imageJ. *Biophotonics International Volume 11*, 36-41.
- Akutsu, M., Dikic, I., and Bremm, A. (2016). Ubiquitin chain diversity at a glance. *Journal of Cell Science* 129, 875.
- Al-Saif, A., Al-Mohanna, F., and Bohlega, S. (2011). A mutation in sigma-1 receptor causes juvenile amyotrophic lateral sclerosis. *Ann Neurol* 70, 913-919.
- Alami, N.H., Smith, R.B., Carrasco, M.A., Williams, L.A., Winborn, C.S., Han, S.S., Kiskinis, E., Winborn, B., Freibaum, B.D., Kanagaraj, A., *et al.* (2014). Axonal transport of TDP-43 mRNA granules is impaired by ALS-causing mutations. *Neuron* 81, 536-543.
- Alexandre, A., and Lehninger, A.L. (1984). Bypasses of the antimycin a block of mitochondrial electron transport in relation to ubisemiquinone function. *Biochim Biophys Acta* 767, 120-129.
- Alexianu, M.E., Ho, B.K., Mohamed, A.H., La Bella, V., Smith, R.G., and Appel, S.H. (1994). The role of calcium-binding proteins in selective motoneuron vulnerability in amyotrophic lateral sclerosis. *Annals of Neurology* 36, 846-858.
- Alexopoulou, Z., Lang, J., Perrett, R.M., Elschami, M., Hurry, M.E.D., Kim, H.T., Mazaraki, D., Szabo, A., Kessler, B.M., Goldberg, A.L., *et al.* (2016). Deubiquitinase Usp8 regulates α -synuclein clearance and modifies its toxicity in Lewy body disease. *Proceedings of the National Academy of Sciences* 113, E4688.
- Allen, S., Balabanidou, V., Sideris, D.P., Lisowsky, T., and Tokatlidis, K. (2005). Erv1 mediates the Mia40-dependent protein import pathway and provides a functional link to the respiratory chain by shuttling electrons to cytochrome c. *J Mol Biol* 353, 937-944.
- Allen, S.P., Hall, B., Castelli, L.M., Francis, L., Woof, R., Siskos, A.P., Kouloura, E., Gray, E., Thompson, A.G., Talbot, K., *et al.* (2019). Astrocyte adenosine deaminase loss increases motor neuron toxicity in amyotrophic lateral sclerosis. *Brain* 142, 586-605.
- Allen, S.P., Rajan, S., Duffy, L., Mortiboys, H., Higginbottom, A., Grierson, A.J., and Shaw, P.J. (2014). Superoxide dismutase 1 mutation in a cellular model of amyotrophic lateral sclerosis shifts energy generation from oxidative phosphorylation to glycolysis. *Neurobiology of Aging* 35, 1499-1509.
- Alto, N.M., Soderling, J., and Scott, J.D. (2002). Rab32 is an A-kinase anchoring protein and participates in mitochondrial dynamics. *J Cell Biol* 158, 659-668.
- Amick, J., and Ferguson, S.M. (2017). C9orf72: At the intersection of lysosome cell biology and neurodegenerative disease. *Traffic (Copenhagen, Denmark)* 18, 267-276.
- Amick, J., Roczniak-Ferguson, A., and Ferguson, S.M. (2016). C9orf72 binds SMCR8, localizes to lysosomes, and regulates mTORC1 signaling. *Molecular Biology of the Cell* 27, 3040-3051.
- Amick, J., Tharkeshwar, A.K., Amaya, C., and Ferguson, S.M. (2018). WDR41 Supports Lysosomal Response to Changes in Amino Acid Availability. *Mol Biol Cell*, mbcE17120703.
- Anagnostou, G., Akbar, M.T., Paul, P., Angelinetta, C., Steiner, T.J., and de Bellerche, J. (2010). Vesicle associated membrane protein B (VAPB) is decreased in ALS spinal cord. *Neurobiology of Aging* 31, 969-985.

- Andersen, J.K. (2004). Oxidative stress in neurodegeneration: cause or consequence? *Nature Medicine* 10 Suppl, S18-25.
- Andrus, P.K., Fleck, T.J., Gurney, M.E., and Hall, E.D. (1998). Protein oxidative damage in a transgenic mouse model of familial amyotrophic lateral sclerosis. *Journal of Neurochemistry* 71, 2041-2048.
- Aoki, Y., Manzano, R., Lee, Y., Dafinca, R., Aoki, M., Douglas, A.G.L., Varela, M.A., Sathyaprakash, C., Scaber, J., Barbagallo, P., *et al.* (2017). C9orf72 and RAB7L1 regulate vesicle trafficking in amyotrophic lateral sclerosis and frontotemporal dementia. *Brain* 140, 887-897.
- Arai, T., Hasegawa, M., Akiyama, H., Ikeda, K., Nonaka, T., Mori, H., Mann, D., Tsuchiya, K., Yoshida, M., Hashizume, Y., *et al.* (2006). TDP-43 is a component of ubiquitin-positive tau-negative inclusions in frontotemporal lobar degeneration and amyotrophic lateral sclerosis. *Biochemical and Biophysical Research Communications* 351, 602-611.
- Ash, P., Bieniek, K., Gendron, T., Caulfield, T., Lin, W.L., DeJesus-Hernandez, M., Van Blitterswijk, M., Jansen-West, K., Paul, J., Rademakers, R., *et al.* (2013). Unconventional Translation of C9ORF72 GGGGCC Expansion Generates Insoluble Polypeptides Specific to c9FTD/ALS. *Neuron* 77, 639-646.
- Ashkenazi, A., and Salvesen, G. (2014). Regulated cell death: signaling and mechanisms. *Annual Review of Cell and Developmental Biology* 30, 337-356.
- Atanasio, A., Decman, V., White, D., Ramos, M., Ikiz, B., Lee, H.C., Siao, C.J., Brydges, S., LaRosa, E., Bai, Y., *et al.* (2016). C9orf72 ablation causes immune dysregulation characterized by leukocyte expansion, autoantibody production, and glomerulonephropathy in mice. *Sci Rep* 6, 23204.
- Atkinson, R.A.K., Fernandez-Martos, C.M., Atkin, J.D., Vickers, J.C., and King, A.E. (2015). C9ORF72 expression and cellular localization over mouse development. *Acta Neuropathologica Communications* 3, 59.
- Atsumi, T. (1981). The ultrastructure of intramuscular nerves in amyotrophic lateral sclerosis. *Acta Neuropathologica* 55, 193-198.
- Aulas, A., and Vande Velde, C. (2015). Alterations in stress granule dynamics driven by TDP-43 and FUS: a link to pathological inclusions in ALS? *Front Cell Neurosci* 9, 423.
- Avci, D., and Lemberg, M.K. (2015). Clipping or Extracting: Two Ways to Membrane Protein Degradation. *Trends in Cell Biology* 25, 611-622.
- Axe, E.L., Walker, S.A., Manifava, M., Chandra, P., Roderick, H.L., Habermann, A., Griffiths, G., and Ktistakis, N.T. (2008). Autophagosome formation from membrane compartments enriched in phosphatidylinositol 3-phosphate and dynamically connected to the endoplasmic reticulum. *J Cell Biol* 182, 685-701.
- Ayers, J.I., Xu, G., Pletnikova, O., Troncoso, J.C., Hart, P.J., and Borchelt, D.R. (2014). Conformational specificity of the C4F6 SOD1 antibody; low frequency of reactivity in sporadic ALS cases. *Acta Neuropathologica Communications* 2, 55.
- Backes, S., and Herrmann, J.M. (2017). Protein Translocation into the Intermembrane Space and Matrix of Mitochondria: Mechanisms and Driving Forces. *Front Mol Biosci* 4, 83.
- Badugu, R., Garcia, M., Bondada, V., Joshi, A., and Geddes, J.W. (2008). N terminus of calpain 1 is a mitochondrial targeting sequence. *J Biol Chem* 283, 3409-3417.
- Ban, T., Ishihara, T., Kohno, H., Saita, S., Ichimura, A., Maenaka, K., Oka, T., Mihara, K., and Ishihara, N. (2017). Molecular basis of selective mitochondrial fusion by heterotypic action between OPA1 and cardiolipin. *Nature Cell Biology* 19, 856.

- Bang, J., Spina, S., and Miller, B.L. (2015). Non-Alzheimer's dementia 1: Frontotemporal dementia. *Lancet* (London, England) 386, 1672-1682.
- Bannai, H., Tamada, Y., Maruyama, O., Nakai, K., and Miyano, S. (2002). Extensive feature detection of N-terminal protein sorting signals. *Bioinformatics* 18, 298-305.
- Bannwarth, S., Ait-El-Mkadem, S., Chausseot, A., Genin, E.C., Lacas-Gervais, S., Fragaki, K., Berg-Alonso, L., Kageyama, Y., Serre, V., Moore, D.G., *et al.* (2014). A mitochondrial origin for frontotemporal dementia and amyotrophic lateral sclerosis through CHCHD10 involvement. *Brain* 137, 2329-2345.
- Barber, S.C., and Shaw, P.J. (2010). Oxidative stress in ALS: Key role in motor neuron injury and therapeutic target. *Free Radical Biology and Medicine* 48, 629-641.
- Barker, H.V., Niblock, M., Lee, Y.-B., Shaw, C.E., and Gallo, J.-M. (2017). RNA Misprocessing in C9orf72-Linked Neurodegeneration. *Frontiers in Cellular Neuroscience* 11, 195.
- Barmada, S.J. (2015). Linking RNA Dysfunction and Neurodegeneration in Amyotrophic Lateral Sclerosis. *Neurotherapeutics* 12, 340-351.
- Bartolome, F., Wu, H.C., Burchell, V.S., Preza, E., Wray, S., Mahoney, C.J., Fox, N.C., Calvo, A., Canosa, A., Moglia, C., *et al.* (2013). Pathogenic VCP Mutations Induce Mitochondrial Uncoupling and Reduced ATP Levels. *Neuron* 78, 57-64.
- Batra, R., and Lee, C.W. (2017). Mouse Models of C9orf72 Hexanucleotide Repeat Expansion in Amyotrophic Lateral Sclerosis/ Frontotemporal Dementia. *Frontiers in Cellular Neuroscience* 11, 196.
- Beck, J., Poulter, M., Hensman, D., Rohrer, J.D., Mahoney, C.J., Adamson, G., Campbell, T., Uphill, J., Borg, A., Fratta, P., *et al.* (2013). Large C9orf72 hexanucleotide repeat expansions are seen in multiple neurodegenerative syndromes and are more frequent than expected in the UK population. *American Journal of Human Genetics* 92, 345-353.
- Beers, D.R., Henkel, J.S., Zhao, W., Wang, J., Huang, A., Wen, S., Liao, B., and Appel, S.H. (2011). Endogenous regulatory T lymphocytes ameliorate amyotrophic lateral sclerosis in mice and correlate with disease progression in patients with amyotrophic lateral sclerosis. *Brain* 134, 1293-1314.
- Belzil, V.V., Bauer, P.O., Prudencio, M., Gendron, T.F., Stetler, C.T., Yan, I.K., Pregent, L., Daugherty, L., Baker, M.C., Rademakers, R., *et al.* (2013). Reduced C9orf72 gene expression in c9FTD/ALS is caused by histone trimethylation, an epigenetic event detectable in blood. *Acta Neuropathologica* 126, 895-905.
- Benard, G., and Karbowski, M. (2009). Mitochondrial fusion and division: regulation and role in cell viability. *Seminars in cell & developmental biology* 20, 365-374.
- Bendotti, C., Marino, M., Cheroni, C., Fontana, E., Crippa, V., Poletti, A., and De Biasi, S. (2012). Dysfunction of constitutive and inducible ubiquitin-proteasome system in amyotrophic lateral sclerosis: implication for protein aggregation and immune response. *Prog Neurobiol* 97, 101-126.
- Berlin, I., Higginbotham, K.M., Dise, R.S., Sierra, M.I., and Nash, P.D. (2010a). The deubiquitinating enzyme USP8 promotes trafficking and degradation of the chemokine receptor 4 at the sorting endosome. *J Biol Chem* 285, 37895-37908.
- Berlin, I., Schwartz, H., and Nash, P.D. (2010b). Regulation of Epidermal Growth Factor Receptor Ubiquitination and Trafficking by the USP8-STAM Complex. *The Journal of Biological Chemistry* 285, 34909-34921.

- Bernard-Marissal, N., Medard, J.J., Azzedine, H., and Chrast, R. (2015). Dysfunction in endoplasmic reticulum-mitochondria crosstalk underlies SIGMAR1 loss of function mediated motor neuron degeneration. *Brain* 138, 875-890.
- Berndsen, C.E., and Wolberger, C. (2014). New insights into ubiquitin E3 ligase mechanism. *Nature Structural & Molecular Biology* 21, 301.
- Bilsland, L.G., Sahai, E., Kelly, G., Golding, M., Greensmith, L., and Schiavo, G. (2010). Deficits in axonal transport precede ALS symptoms in vivo. *Proceedings of the National Academy of Sciences of the United States of America* 107, 20523-20528.
- Bingol, B., and Sheng, M. (2016). Mechanisms of mitophagy: PINK1, Parkin, USP30 and beyond. *Free Radical Biology and Medicine* 100, 210-222.
- Bingol, B., Tea, J.S., Phu, L., Reichelt, M., Bakalarski, C.E., Song, Q., Foreman, O., Kirkpatrick, D.S., and Sheng, M. (2014). The mitochondrial deubiquitinase USP30 opposes parkin-mediated mitophagy. *Nature* 510, 370-375.
- Binotti, B., Jahn, R., and Chua, J.J. (2016). Functions of Rab Proteins at Presynaptic Sites. *Cells* 5.
- Birgisdottir, A.B., Lamark, T., and Johansen, T. (2013). The LIR motif - crucial for selective autophagy. *J Cell Sci* 126, 3237-3247.
- Blokhuis, A.M., Groen, E.J.N., Koppers, M., van den Berg, L.H., and Pasterkamp, R.J. (2012). Protein aggregation in amyotrophic lateral sclerosis. *Acta Neuropathol* 125, 777-794.
- Blokhuis, A.M., Groen, E.J.N., Koppers, M., van den Berg, L.H., and Pasterkamp, R.J. (2013). Protein aggregation in amyotrophic lateral sclerosis. *Acta Neuropathol* 125, 777-794.
- Blokhuis, A.M., Koppers, M., Groen, E.J., van den Heuvel, D.M., Dini Modigliani, S., Anink, J.J., Fumoto, K., van Diggelen, F., Snelting, A., Sooda, P., *et al.* (2016). Comparative interactomics analysis of different ALS-associated proteins identifies converging molecular pathways. *Acta Neuropathologica* 132, 175-196.
- Boeynaems, S., Bogaert, E., Michiels, E., Gijssels, I., Sieben, A., Jovicic, A., De Baets, G., Scheveneels, W., Steyaert, J., Cuijt, I., *et al.* (2016). *Drosophila* screen connects nuclear transport genes to DPR pathology in c9ALS/FTD. *Sci Rep* 6, 20877.
- Bogdanov, M., Brown Jr, R.H., Matson, W., Smart, R., Hayden, D., O'Donnell, H., Flint Beal, M., and Cudkowicz, M. (2000). Increased oxidative damage to DNA in ALS patients. *Free Radical Biology and Medicine* 29, 652-658.
- Borthwick, G.M., Johnson, M.A., Ince, P.G., Shaw, P.J., and Turnbull, D.M. (1999). Mitochondrial enzyme activity in amyotrophic lateral sclerosis: Implications for the role of mitochondria in neuronal cell death. *Annals of Neurology* 46, 787-790.
- Bosco, D.A., Morfini, G., Karabacak, N.M., Song, Y., Gros-Louis, F., Pasinelli, P., Goolsby, H., Fontaine, B.A., Lemay, N., McKenna-Yasek, D., *et al.* (2010). Wild-type and mutant SOD1 share an aberrant conformation and a common pathogenic pathway in ALS. *Nature Neuroscience* 13, 1396-1403.
- Bowling, A.C., Schulz, J.B., Brown Jr, R.H., and Beal, M.F. (1993). Superoxide dismutase activity, oxidative damage, and mitochondrial energy metabolism in familial and sporadic amyotrophic lateral sclerosis. *Journal of Neurochemistry* 61, 2322-2325.
- Boya, P., Reggiori, F., and Codogno, P. (2013). Emerging regulation and functions of autophagy. *Nature Cell Biology* 15, 713.

- Bradford, M.M. (1976). A rapid and sensitive method for the quantitation of microgram quantities of protein utilizing the principle of protein-dye binding. *Analytical biochemistry* 72, 248-254.
- Bratic, A., and Larsson, N.-G. (2013). The role of mitochondria in aging. *The Journal of Clinical Investigation* 123, 951-957.
- Brickley, K., Smith, M.J., Beck, M., and Stephenson, F.A. (2005). GRIF-1 and OIP106, members of a novel gene family of coiled-coil domain proteins: association in vivo and in vitro with kinesin. *Journal of Biological Chemistry* 280, 14723-14732.
- Brickley, K., and Stephenson, F.A. (2011). Trafficking kinesin protein (TRAK)-mediated transport of mitochondria in axons of hippocampal neurons. *Journal of Biological Chemistry* 286, 18079-18092.
- Brighouse, A., Dacks, J.B., and Field, M.C. (2010). Rab protein evolution and the history of the eukaryotic endomembrane system. *Cell Mol Life Sci* 67, 3449-3465.
- Brooks, C., Wei, Q., Feng, L., Dong, G., Tao, Y., Mei, L., Xie, Z.J., and Dong, Z. (2007). Bak regulates mitochondrial morphology and pathology during apoptosis by interacting with mitofusins. *Proc Natl Acad Sci U S A* 104, 11649-11654.
- Brotherton, T.E., Li, Y., Cooper, D., Gearing, M., Julien, J.P., Rothstein, J.D., Boylan, K., and Glass, J.D. (2012). Localization of a toxic form of superoxide dismutase 1 protein to pathologically affected tissues in familial ALS. *Proceedings of the National Academy of Sciences of the United States of America* 109, 5505-5510.
- Browne, S.E., Bowling, A.C., Baik, M.J., Gurney, M., Brown Jr, R.H., and Beal, M.F. (1998). Metabolic dysfunction in familial, but not sporadic, amyotrophic lateral sclerosis. *Journal of Neurochemistry* 71, 281-287.
- Broz, P., and Dixit, V.M. (2016). Inflammasomes: mechanism of assembly, regulation and signalling. *Nature reviews Immunology* 16, 407-420.
- Bui, M., Gilady, S.Y., Fitzsimmons, R.E., Benson, M.D., Lynes, E.M., Gesson, K., Alto, N.M., Strack, S., Scott, J.D., and Simmen, T. (2010). Rab32 modulates apoptosis onset and mitochondria-associated membrane (MAM) properties. *J Biol Chem* 285, 31590-31602.
- Burberry, A., Suzuki, N., Wang, J.Y., Moccia, R., Mordes, D.A., Stewart, M.H., Suzuki-Uematsu, S., Ghosh, S., Singh, A., Merkle, F.T., *et al.* (2016). Loss-of-function mutations in the C9ORF72 mouse ortholog cause fatal autoimmune disease. *Sci Transl Med* 8, 347ra393.
- Burguete, A.S., Almeida, S., Gao, F.-B., Kalb, R., Akins, M.R., and Bonini, N.M. (2015). GGGGCC microsatellite RNA is neuritically localized, induces branching defects, and perturbs transport granule function. *eLife* 4, e08881.
- Burri, L., Strahm, Y., Hawkins, C.J., Gentle, I.E., Puryer, M.A., Verhagen, A., Callus, B., Vaux, D., and Lithgow, T. (2005). Mature DIABLO/Smac is produced by the IMP protease complex on the mitochondrial inner membrane. *Mol Biol Cell* 16, 2926-2933.
- Burri, L., Vascotto, K., Gentle, I.E., Chan, N.C., Beilharz, T., Stapleton, D.I., Ramage, L., and Lithgow, T. (2006). Integral membrane proteins in the mitochondrial outer membrane of *Saccharomyces cerevisiae*. *The FEBS Journal* 273, 1507-1515.
- Burstein, S.R., Valsecchi, F., Kawamata, H., Bourens, M., Zeng, R., Zuberi, A., Milner, T.A., Cloonan, S.M., Lutz, C., Barrientos, A., *et al.* (2018). In vitro and in vivo studies of the ALS-FTLD protein CHCHD10 reveal novel mitochondrial topology and protein interactions. *Hum Mol Genet* 27, 160-177.

- Busch, J.I., Unger, T.L., Jain, N., Tyler Skrinak, R., Charan, R.A., and Chen-Plotkin, A.S. (2016). Increased expression of the frontotemporal dementia risk factor TMEM106B causes C9orf72-dependent alterations in lysosomes. *Hum Mol Genet* 25, 2681-2697.
- Bylund, L., Kytola, S., Lui, W.O., Larsson, C., and Weber, G. (2004). Analysis of the cytogenetic stability of the human embryonal kidney cell line 293 by cytogenetic and STR profiling approaches. *Cytogenet Genome Res* 106, 28-32.
- Cai, Q., and Tammineni, P. (2016). Alterations in mitochondrial quality control in Alzheimer's disease. *Frontiers in Cellular Neuroscience* 10.
- Carmona-Gutierrez, D., Hughes, A.L., Madeo, F., and Ruckenstein, C. (2016). The crucial impact of lysosomes in aging and longevity. *Ageing Research Reviews* 32, 2-12.
- Carri, M.T., Ferri, A., Battistoni, A., Famhy, L., Gabbianelli, R., Poccia, F., and Rotilio, G. (1997). Expression of a Cu,Zn superoxide dismutase typical of familial amyotrophic lateral sclerosis induces mitochondrial alteration and increase of cytosolic Ca²⁺ concentration in transfected neuroblastoma SH-SY5Y cells. *FEBS Letters* 414, 365-368.
- Caza, T.N., Fernandez, D.R., Talaber, G., Oaks, Z., Haas, M., Madaio, M.P., Lai, Z.W., Miklossy, G., Singh, R.R., Chudakov, D.M., *et al.* (2014). HRES-1/Rab4-mediated depletion of Drp1 impairs mitochondrial homeostasis and represents a target for treatment in SLE. *Annals of the rheumatic diseases* 73, 1888-1897.
- Chacinska, A., Pfannschmidt, S., Wiedemann, N., Kozjak, V., Sanjuan Szklarz, L.K., Schulze-Specking, A., Truscott, K.N., Guiard, B., Meisinger, C., and Pfanner, N. (2004). Essential role of Mia40 in import and assembly of mitochondrial intermembrane space proteins. *Embo j* 23, 3735-3746.
- Chan, N.C., Salazar, A.M., Pham, A.H., Sweredoski, M.J., Kolawa, N.J., Graham, R.L.J., Hess, S., and Chan, D.C. (2011). Broad activation of the ubiquitin-proteasome system by Parkin is critical for mitophagy. *Human Molecular Genetics* 20, 1726-1737.
- Chang, Y., Kong, Q., Shan, X., Tian, G., Ilieva, H., Cleveland, D.W., Rothstein, J.D., Borchelt, D.R., Wong, P.C., and Lin, C.L.G. (2008). Messenger RNA oxidation occurs early in disease pathogenesis and promotes motor neuron degeneration in ALS. *PLoS ONE* 3.
- Chen, H., Detmer, S.A., Ewald, A.J., Griffin, E.E., Fraser, S.E., and Chan, D.C. (2003). Mitofusins Mfn1 and Mfn2 coordinately regulate mitochondrial fusion and are essential for embryonic development. *J Cell Biol* 160, 189-200.
- Chen, H., Kankel, M.W., Su, S.C., Han, S.W.S., and Ofengeim, D. (2018). Exploring the genetics and non-cell autonomous mechanisms underlying ALS/FTLD. *Cell Death & Differentiation* 25, 646-660.
- Chen, W.-W., Zhang, X.I.A., and Huang, W.-J. (2016a). Role of neuroinflammation in neurodegenerative diseases (Review). *Molecular Medicine Reports* 13, 3391-3396.
- Chen, Y., Deng, J., Wang, P., Yang, M., Chen, X., Zhu, L., Liu, J., Lu, B., Shen, Y., Fushimi, K., *et al.* (2016b). PINK1 and Parkin are genetic modifiers for FUS-induced neurodegeneration. *Human Molecular Genetics* 25, 5059-5068.
- Cheng, B., and Kimura, T. (1983). The distribution of cholesterol and phospholipid composition in submitochondrial membranes from bovine adrenal cortex: fundamental studies of steroidogenic mitochondria. *Lipids* 18, 577-584.
- Chio, A., Logroscino, G., Hardiman, O., Swingler, R., Mitchell, D., Beghi, E., Traynor, B.G., and Eurals, C. (2009). Prognostic factors in ALS: A critical review. *Amyotrophic lateral sclerosis : official publication of the World Federation of Neurology Research Group on Motor Neuron Diseases* 10, 310-323.

- Chiò, A., Logroscino, G., Traynor, B.J., Collins, J., Simeone, J.C., Goldstein, L.A., and White, L.A. (2013). Global Epidemiology of Amyotrophic Lateral Sclerosis: a Systematic Review of the Published Literature. *Neuroepidemiology* 41, 118-130.
- Chitiprolu, M., Jagow, C., Tremblay, V., Bondy-Chorney, E., Paris, G., Savard, A., Palidwor, G., Barry, F.A., Zinman, L., Keith, J., *et al.* (2018). A complex of C9ORF72 and p62 uses arginine methylation to eliminate stress granules by autophagy. *Nature Communications* 9, 2794.
- Choi, S.Y., Huang, P., Jenkins, G.M., Chan, D.C., Schiller, J., and Frohman, M.A. (2006). A common lipid links Mfn-mediated mitochondrial fusion and SNARE-regulated exocytosis. *Nat Cell Biol* 8, 1255-1262.
- Chow, C.Y., Landers, J.E., Bergren, S.K., Sapp, P.C., Grant, A.E., Jones, J.M., Everett, L., Lenk, G.M., McKenna-Yasek, D.M., Weisman, L.S., *et al.* (2009). Deleterious Variants of FIG4, a Phosphoinositide Phosphatase, in Patients with ALS. *American Journal of Human Genetics* 84, 85-88.
- Ciura, S., Lattante, S., Le Ber, I., Latouche, M., Tostivint, H., Brice, A., and Kabashi, E. (2013). Loss of function of C9orf72 causes motor deficits in a zebrafish model of amyotrophic lateral sclerosis. *Annals of Neurology* 74, 180-187.
- Claros, M.G. (1995). MitoProt, a Macintosh application for studying mitochondrial proteins. *Computer applications in the biosciences : CABIOS* 11, 441-447.
- Cogliati, S., Enriquez, J.A., and Scorrano, L. (2016). Mitochondrial Cristae: Where Beauty Meets Functionality. *Trends in Biochemical Sciences* 41, 261-273.
- Cohen, T.J., Hwang, A.W., Restrepo, C.R., Yuan, C.X., Trojanowski, J.Q., and Lee, V.M. (2015). An acetylation switch controls TDP-43 function and aggregation propensity. *Nature Communications* 6, 5845.
- Cohen, T.J., Hwang, A.W., Unger, T., Trojanowski, J.Q., and Lee, V.M. (2012). Redox signalling directly regulates TDP-43 via cysteine oxidation and disulphide cross-linking. *EMBO Journal* 31, 1241-1252.
- Colombo, E., and Farina, C. (2016). Astrocytes: Key Regulators of Neuroinflammation. *Trends in Immunology* 37, 608-620.
- Colombrita, C., Onesto, E., Megiorni, F., Pizzuti, A., Baralle, F.E., Buratti, E., Silani, V., and Ratti, A. (2012). TDP-43 and FUS RNA-binding proteins bind distinct sets of cytoplasmic messenger RNAs and differently regulate their post-transcriptional fate in motoneuron-like cells. *Journal of Biological Chemistry* 287, 15635-15647.
- Colombrita, C., Zennaro, E., Fallini, C., Weber, M., Sommacal, A., Buratti, E., Silani, V., and Ratti, A. (2009). TDP-43 is recruited to stress granules in conditions of oxidative insult. *Journal of Neurochemistry* 111, 1051-1061.
- Conlon, E.G., Lu, L., Sharma, A., Yamazaki, T., Tang, T., Shneider, N.A., and Manley, J.L. (2016). The C9ORF72 GGGGCC expansion forms RNA G-quadruplex inclusions and sequesters hnRNP H to disrupt splicing in ALS brains. *eLife* 5.
- Cooper, T.A., Wan, L., and Dreyfuss, G. (2009). RNA and Disease. *Cell* 136, 777-793.
- Cooper-Knock, J., Bury, J.J., Heath, P.R., Wyles, M., Higginbottom, A., Gelsthorpe, C., Highley, J.R., Hautbergue, G., Rattray, M., Kirby, J., *et al.* (2015a). C9ORF72 GGGGCC Expanded Repeats Produce Splicing Dysregulation which Correlates with Disease Severity in Amyotrophic Lateral Sclerosis. *PLoS One* 10, e0127376.
- Cooper-Knock, J., Hewitt, C., Highley, J.R., Brockington, A., Milano, A., Man, S., Martindale, J., Hartley, J., Walsh, T., Gelsthorpe, C., *et al.* (2012). Clinico-pathological features in amyotrophic lateral sclerosis with expansions in C9ORF72. *Brain* 135, 751-764.

- Cooper-Knock, J., Higginbottom, A., Stopford, M.J., Highley, J.R., Ince, P.G., Wharton, S.B., Pickering-Brown, S., Kirby, J., Hautbergue, G.M., and Shaw, P.J. (2015b). Antisense RNA foci in the motor neurons of C9ORF72-ALS patients are associated with TDP-43 proteinopathy. *Acta Neuropathol* 130, 63-75.
- Cooper-Knock, J., Walsh, M.J., Higginbottom, A., Highley, J.R., Dickman, M.J., Edbauer, D., Ince, P.G., Wharton, S.B., Wilson, S.A., Kirby, J., *et al.* (2014). Sequestration of multiple RNA recognition motif-containing proteins by C9orf72 repeat expansions. *Brain* 137, 2040-2051.
- Corbo, M., and Hays, A.P. (1992). Peripherin and neurofilament protein coexist in spinal spheroids of motor neuron disease. *J Neuropathol Exp Neurol* 51, 531-537.
- Corcia, P., Couratier, P., Blasco, H., Andres, C.R., Beltran, S., Meininger, V., and Vourc'h, P. (2017). Genetics of amyotrophic lateral sclerosis. *Revue neurologique* 173, 254-262.
- Corcia, P., Tauber, C., Vercoullie, J., Arlicot, N., Prunier, C., Praline, J., Nicolas, G., Venel, Y., Hommet, C., Baulieu, J.L., *et al.* (2012). Molecular imaging of microglial activation in amyotrophic lateral sclerosis. *PLoS One* 7, e52941.
- Cornelissen, T., Haddad, D., Wauters, F., Van Humbeeck, C., Mandemakers, W., Koentjoro, B., Sue, C., Gevaert, K., De Strooper, B., Verstreken, P., *et al.* (2014). The deubiquitinase USP15 antagonizes Parkin-mediated mitochondrial ubiquitination and mitophagy. *Human molecular genetics* 23, 5227-5242.
- Corona, J.C., and Duchen, M.R. (2015). PPAR γ and PGC-1 α as Therapeutic Targets in Parkinson's. *Neurochemical Research* 40, 308-316.
- Coussee, E., De Smet, P., Bogaert, E., Elens, I., Van Damme, P., Willems, P., Koopman, W., Van Den Bosch, L., and Callewaert, G. (2011). G37R SOD1 mutant alters mitochondrial complex I activity, Ca $^{2+}$ uptake and ATP production. *Cell Calcium* 49, 217-225.
- Crugnola, V., Lamperti, C., Lucchini, V., Ronchi, D., Peverelli, L., Prella, A., Sciacco, M., Bordoni, A., Fassone, E., Fortunato, F., *et al.* (2010). Mitochondrial respiratory chain dysfunction in muscle from patients with amyotrophic lateral sclerosis. *Archives of Neurology* 67, 849-854.
- Cui, H., Kong, Y., and Zhang, H. (2012). Oxidative stress, mitochondrial dysfunction, and aging. *Journal of Signal Transduction* 2012, 646354.
- Cummins, N., and Gotz, J. (2017). Shedding light on mitophagy in neurons: what is the evidence for PINK1/Parkin mitophagy in vivo? *Cell Mol Life Sci*.
- Cunningham, C.N., Baughman, J.M., Phu, L., Tea, J.S., Yu, C., Coons, M., Kirkpatrick, D.S., Bingol, B., and Corn, J.E. (2015). USP30 and parkin homeostatically regulate atypical ubiquitin chains on mitochondria. *Nature Cell Biology* 17, 160-169.
- Custer, S.K., Neumann, M., Lu, H., Wright, A.C., and Taylor, J.P. (2010). Transgenic mice expressing mutant forms VCP/p97 recapitulate the full spectrum of IBMPFD including degeneration in muscle, brain and bone. *Hum Mol Genet* 19, 1741-1755.
- Da Cruz, S., Parone, P.A., Lopes, V.S., Lillo, C., McAlonis-Downes, M., Lee, S.K., Vetto, A.P., Petrosyan, S., Marsala, M., Murphy, A.N., *et al.* (2012). Elevated PGC-1 α activity sustains mitochondrial biogenesis and muscle function without extending survival in a mouse model of inherited ALS. *Cell Metab* 15, 778-786.
- Dafinca, R., Scaber, J., Ababneh, N.a., Lalic, T., Weir, G., Christian, H., Vowles, J., Douglas, A.G.L., Fletcher-Jones, A., Browne, C., *et al.* (2016). C9orf72 Hexanucleotide Expansions Are Associated with Altered Endoplasmic Reticulum Calcium Homeostasis and Stress Granule Formation in Induced Pluripotent Stem Cell-Derived Neurons from

Patients with Amyotrophic Lateral Sclerosis and Frontotemporal Dementia. *Stem Cells* 34, 2063–2078.

Dagda, R.K., Cherra, S.J., 3rd, Kulich, S.M., Tandon, A., Park, D., and Chu, C.T. (2009). Loss of PINK1 function promotes mitophagy through effects on oxidative stress and mitochondrial fission. *J Biol Chem* 284, 13843-13855.

Dal Canto, M.C., and Gurney, M.E. (1994). Development of central nervous system pathology in a murine transgenic model of human amyotrophic lateral sclerosis. *American Journal of Pathology* 145, 1271-1279.

Damiano, M., Starkov, A.A., Petri, S., Kipiani, K., Kiaei, M., Mattiazzi, M., Flint Beal, M., and Manfredi, G. (2006). Neural mitochondrial Ca²⁺ capacity impairment precedes the onset of motor symptoms in G93A Cu/Zn-superoxide dismutase mutant mice. *Journal of Neurochemistry* 96, 1349-1361.

Davidson, Y.S., Barker, H., Robinson, A.C., Thompson, J.C., Harris, J., Troakes, C., Smith, B., Al-Saraj, S., Shaw, C., Rollinson, S., *et al.* (2014). Brain distribution of dipeptide repeat proteins in frontotemporal lobar degeneration and motor neurone disease associated with expansions in C9ORF72. *Acta Neuropathol Commun* 2, 70.

Davidson, Y.S., Robinson, A.C., Rollinson, S., Pickering-Brown, S., Xiao, S., Robertson, J., and Mann, D.M.A. (2017). Immunohistochemical detection of C9orf72 protein in frontotemporal lobar degeneration and motor neurone disease: patterns of immunostaining and an evaluation of commercial antibodies. *Amyotrophic lateral sclerosis & frontotemporal degeneration*, 1-10.

Davis, S.A., Itaman, S., Khalid-Janney, C.M., Sherard, J.A., Dowell, J.A., Cairns, N.J., and Gitcho, M.A. (2018). TDP-43 interacts with mitochondrial proteins critical for mitophagy and mitochondrial dynamics. *Neuroscience Letters* 678, 8-15.

de la Vega, M., Burrows, J.F., and Johnston, J.A. (2011). Ubiquitination. *Small GTPases* 2, 192-201.

De Vos, K., Severin, F., Van Herreweghe, F., Vancompernelle, K., Goossens, V., Hyman, A., and Grooten, J. (2000). Tumor necrosis factor induces hyperphosphorylation of kinesin light chain and inhibits kinesin-mediated transport of mitochondria. *Journal of Cell Biology* 149, 1207-1214.

De Vos, K.J., Chapman, A.L., Tennant, M.E., Manser, C., Tudor, E.L., Lau, K.F., Brownlees, J., Ackerley, S., Shaw, P.J., McLoughlin, D.M., *et al.* (2007). Familial amyotrophic lateral sclerosis-linked SOD1 mutants perturb fast axonal transport to reduce axonal mitochondria content. *Human Molecular Genetics* 16, 2720-2728.

De Vos, K.J., Grierson, A.J., Ackerley, S., and Miller, C.C.J. (2008). Role of axonal transport in neurodegenerative diseases. In *Annual Review of Neuroscience*, pp. 151-173.

De Vos, K.J., and Hafezparast, M. (2017). Neurobiology of axonal transport defects in motor neuron diseases: opportunities for translational research? . *Neurobiology of Disease*.

De Vos, K.J., Mórotz, G.M., Stoica, R., Tudor, E.L., Lau, K., Ackerley, S., Warley, A., Shaw, C.E., and Miller, C.C. (2012). VAPB interacts with the mitochondrial protein PTPIP51 to regulate calcium homeostasis. *Human Molecular Genetics* 21, 1299-1311.

De Vos, K.J., and Sheetz, M.P. (2007). Visualization and quantification of mitochondrial dynamics in living animal cells. *Methods Cell Biol* 80, 627-682.

DeJesus-Hernandez, M., Mackenzie, I., Boeve, B., Boxer, A., Baker, M., Rutherford, N., Nicholson, A., Finch, N., Flynn, H., Adamson, J., *et al.* (2011). Expanded GGGGCC

Hexanucleotide Repeat in Noncoding Region of C9ORF72 Causes Chromosome 9p-Linked FTD and ALS. *Neuron* 72, 245-256.

Del Dotto, V., Mishra, P., Vidoni, S., Fogazza, M., Maresca, A., Caporali, L., McCaffery, J.M., Cappelletti, M., Baruffini, E., Lenaers, G., *et al.* (2017). OPA1 Isoforms in the Hierarchical Organization of Mitochondrial Functions. *Cell Rep* 19, 2557-2571.

Deng, H.X., Chen, W., Hong, S.T., Boycott, K.M., Gorrie, G.H., Siddique, N., Yang, Y., Fecto, F., Shi, Y., Zhai, H., *et al.* (2011). Mutations in UBQLN2 cause dominant X-linked juvenile and adult-onset ALS and ALS/dementia. *Nature* 477, 211-215.

Deng, J., Yang, M., Chen, Y., Chen, X., Liu, J., Sun, S., Cheng, H., Li, Y., Bigio, E.H., Mesulam, M., *et al.* (2015). FUS Interacts with HSP60 to Promote Mitochondrial Damage. *PLoS Genetics* 11, e1005357.

Devine, M.J., Birsa, N., and Kittler, J.T. (2016). Miro sculpts mitochondrial dynamics in neuronal health and disease. *Neurobiology of Disease* 90, 27-34.

Diekert, K., Kispal, G., Guiard, B., and Lill, R. (1999). An internal targeting signal directing proteins into the mitochondrial intermembrane space. *Proceedings of the National Academy of Sciences of the United States of America* 96, 11752-11757.

Dini Modigliani, S., Morlando, M., Errichelli, L., Sabatelli, M., and Bozzoni, I. (2014). An ALS-associated mutation in the FUS 3'-UTR disrupts a microRNA-FUS regulatory circuitry. *Nature Communications* 5, 4335.

Dissmeyer, N., Rivas, S., and Graciet, E. (2018). Life and death of proteins after protease cleavage: protein degradation by the N-end rule pathway. *The New phytologist* 218, 929-935.

Doimo, M., Desbats, M.A., Baldoin, M.C., Lenzini, E., Basso, G., Murphy, E., Graziano, C., Seri, M., Burlina, A., Sartori, G., *et al.* (2013). Functional analysis of missense mutations of OAT, causing gyrate atrophy of choroid and retina. *Hum Mutat* 34, 229-236.

Dong, X.-x., Wang, Y., and Qin, Z.-h. (2009). Molecular mechanisms of excitotoxicity and their relevance to pathogenesis of neurodegenerative diseases. *Acta Pharmacologica Sinica* 30, 379-387.

Donnelly, C.J., Zhang, P.W., Pham, J.T., Heusler, A.R., Mistry, N.A., Vidensky, S., Daley, E.L., Poth, E.M., Hoover, B., Fines, D.M., *et al.* (2013). RNA Toxicity from the ALS/FTD C9ORF72 Expansion Is Mitigated by Antisense Intervention. *Neuron* 80, 415-428.

Dorn, G.W., 2nd (2016). Parkin-dependent mitophagy in the heart. *Journal of molecular and cellular cardiology* 95, 42-49.

Duan, W., Li, X., Shi, J., Guo, Y., Li, Z., and Li, C. (2010). Mutant TAR DNA-binding protein-43 induces oxidative injury in motor neuron-like cell. *Neuroscience* 169, 1621-1629.

Dudek, J., Rehling, P., and van der Laan, M. (2013). Mitochondrial protein import: common principles and physiological networks. *Biochim Biophys Acta* 1833, 274-285.

Durcan, T.M., and Fon, E.A. (2015). The three 'P's of mitophagy: PARKIN, PINK1, and post-translational modifications. *Genes & Development* 29, 989-999.

Durcan, T.M., Kontogiannea, M., Thorarinsdottir, T., Fallon, L., Williams, A.J., Djarmati, A., Fantaneanu, T., Paulson, H.L., and Fon, E.A. (2011). The machado-joseph disease-associated mutant form of ataxin-3 regulates parkin ubiquitination and stability. *Human Molecular Genetics* 20, 141-154.

- Durcan, T.M., Tang, M.Y., Pérusse, J.R., Dashti, E.A., Aguilera, M.A., McLelland, G.L., Gros, P., Shaler, T.A., Faubert, D., Coulombe, B., *et al.* (2014). USP8 regulates mitophagy by removing K6-linked ubiquitin conjugates from parkin. *EMBO Journal* 33, 2473-2491.
- Ebeling, W., Hennrich, N., Klockow, M., Metz, H., Orth, H.D., and Lang, H. (1974). Proteinase K from *Tritirachium album* Limber. *European Journal of Biochemistry* 47, 91-97.
- Elden, A.C., Kim, H.J., Hart, M.P., Chen-Plotkin, A.S., Johnson, B.S., Fang, X., Armakola, M., Geser, F., Greene, R., Lu, M.M., *et al.* (2010). Ataxin-2 intermediate-length polyglutamine expansions are associated with increased risk for ALS. *Nature* 466, 1069-1075.
- Elgass, K., Pakay, J., Ryan, M.T., and Palmer, C.S. (2013). Recent advances into the understanding of mitochondrial fission. *Biochimica et Biophysica Acta (BBA) - Molecular Cell Research* 1833, 150-161.
- Emanuelsson, O., Nielsen, H., Brunak, S., and von Heijne, G. (2000). Predicting subcellular localization of proteins based on their N-terminal amino acid sequence. *J Mol Biol* 300, 1005-1016.
- Eura, Y., Ishihara, N., Oka, T., and Mihara, K. (2006). Identification of a novel protein that regulates mitochondrial fusion by modulating mitofusin (Mfn) protein function. *J Cell Sci* 119, 4913-4925.
- Eura, Y., Ishihara, N., Yokota, S., and Mihara, K. (2003). Two mitofusin proteins, mammalian homologues of FZO, with distinct functions are both required for mitochondrial fusion. *J Biochem* 134, 333-344.
- Evans, C.S., and Holzbaur, E.L.F. (2018). Autophagy and mitophagy in ALS. *Neurobiology of Disease*.
- Farg, M.A., Sundaramoorthy, V., Sultana, J.M., Yang, S., Atkinson, R.A., Levina, V., Halloran, M.A., Gleeson, P.A., Blair, I.P., Soo, K.Y., *et al.* (2014). C9ORF72, implicated in amyotrophic lateral sclerosis and frontotemporal dementia, regulates endosomal trafficking. *Hum Mol Genet* 23, 3579-3595.
- Featherstone, D.E. (2010). Intercellular Glutamate Signaling in the Nervous System and Beyond. *ACS Chemical Neuroscience* 1, 4-12.
- Fecto, F., Yan, J., Vemula, S.P., Liu, E., Yang, Y., Chen, W., Zheng, J.G., Shi, Y., Siddique, N., Arrat, H., *et al.* (2011). SQSTM1 mutations in familial and sporadic amyotrophic lateral sclerosis. *Archives of Neurology* 68, 1440-1446.
- Feldmann, A., Bekbulat, F., Huesmann, H., Ulbrich, S., Tatzelt, J., Behl, C., and Kern, A. (2017). The RAB GTPase RAB18 modulates macroautophagy and proteostasis. *Biochemical and Biophysical Research Communications* 486, 738-743.
- Ferraiuolo, L., Kirby, J., Grierson, A.J., Sendtner, M., and Shaw, P.J. (2011). Molecular pathways of motor neuron injury in amyotrophic lateral sclerosis. *Nature Reviews Neurology* 7, 616-630.
- Ferri, A., Cozzolino, M., Crosio, C., Nencini, M., Casciati, A., Gralla, E.B., Rotilio, G., Valentine, J.S., and Carri, M.T. (2006). Familial ALS-superoxide dismutases associate with mitochondria and shift their redox potentials. *Proceedings of the National Academy of Sciences of the United States of America* 103, 13860-13865.
- Ferri, A., Fiorenzo, P., Nencini, M., Cozzolino, M., Pesaresi, M.G., Valle, C., Sepe, S., Moreno, S., and Carri, M.T. (2010). Glutaredoxin 2 prevents aggregation of mutant SOD1 in mitochondria and abolishes its toxicity. *Human Molecular Genetics* 19, 4529-4542.

- Figlewicz, D.A., Krizus, A., Martinoli, M.G., Meininger, V., Dib, M., Rouleau, G.A., and Julien, J.P. (1994). Variants of the heavy neurofilament subunit are associated with the development of amyotrophic lateral sclerosis. *Human Molecular Genetics* 3, 1757-1761.
- Finelli, M.J., Liu, K.X., Wu, Y., Oliver, P.L., and Davies, K.E. (2015). Oxr1 improves pathogenic cellular features of ALS-associated FUS and TDP-43 mutations. *Human Molecular Genetics* 24, 3529-3544.
- Fitzmaurice, P.S., Shaw, I.C., Kleiner, H.E., Miller, R.T., Monks, T.J., Lau, S.S., Mitchell, J.D., and Lynch, P.G. (1996). Evidence for DNA damage in amyotrophic lateral sclerosis. *Muscle & nerve* 19, 797-798.
- Fomin, V., Richard, P., Hoque, M., Li, C., Gu, Z., Fissore, O., Leary, M., Tian, B., Prives, C., and Manley, J.L. (2018). The C9orf72 Gene, Implicated in Amyotrophic Lateral Sclerosis and Frontotemporal Dementia, Encodes a Protein That Functions in Control of Endothelin and Glutamate Signaling. *Molecular and Cellular Biology* 38, e00155-00118.
- Foran, E., and Trotti, D. (2009). Glutamate transporters and the excitotoxic path to motor neuron degeneration in amyotrophic lateral sclerosis. *Antioxidants and Redox Signaling* 11, 1587-1602.
- Forkink, M., Manjeri, G.R., Liemburg-Apers, D.C., Nibbeling, E., Blanchard, M., Wojtala, A., Smeitink, J.A.M., Wieckowski, M.R., Willems, P.H.G.M., and Koopman, W.J.H. (2014). Mitochondrial hyperpolarization during chronic complex I inhibition is sustained by low activity of complex II, III, IV and V. *Biochimica et Biophysica Acta (BBA) - Bioenergetics* 1837, 1247-1256.
- Fornuskova, D., Stiburek, L., Wenchich, L., Vinsova, K., Hansikova, H., and Zeman, J. (2010). Novel insights into the assembly and function of human nuclear-encoded cytochrome c oxidase subunits 4, 5a, 6a, 7a and 7b. *The Biochemical journal* 428, 363-374.
- Francy, C.A., Clinton, R.W., Fröhlich, C., Murphy, C., and Mears, J.A. (2017). Cryo-EM Studies of Drp1 Reveal Cardiolipin Interactions that Activate the Helical Oligomer. *Scientific Reports* 7, 10744.
- Fransson, S., Ruusala, A., and Aspenstrom, P. (2006). The atypical Rho GTPases Miro-1 and Miro-2 have essential roles in mitochondrial trafficking. *Biochemical and Biophysical Research Communications* 344, 500-510.
- Fratta, P., Poulter, M., Lashley, T., Rohrer, J.D., Polke, J.M., Beck, J., Ryan, N., Hensman, D., Mizielinska, S., Waite, A.J., *et al.* (2013). Homozygosity for the C9orf72 GGGGCC repeat expansion in frontotemporal dementia. *Acta Neuropathologica* 126, 401-409.
- Freibaum, B.D., Lu, Y., Lopez-Gonzalez, R., Kim, N.C., Almeida, S., Lee, K.H., Badders, N., Valentine, M., Miller, B.L., Wong, P.C., *et al.* (2015). GGGGCC repeat expansion in C9orf72 compromises nucleocytoplasmic transport. *Nature* 525, 129-133.
- Freibaum, B.D., and Taylor, J.P. (2017). The Role of Dipeptide Repeats in C9ORF72-Related ALS-FTD. *Frontiers in Molecular Neuroscience* 10, 35.
- Freischmidt, A., Müller, K., Ludolph, A.C., and Weishaupt, J.H. (2013). Systemic dysregulation of TDP-43 binding microRNAs in amyotrophic lateral sclerosis. *Acta Neuropathologica Communications* 1, 42-42.
- Freischmidt, A., Wieland, T., Richter, B., Ruf, W., Schaeffer, V., Muller, K., Marroquin, N., Nordin, F., Hubers, A., Weydt, P., *et al.* (2015). Haploinsufficiency of TBK1 causes familial ALS and fronto-temporal dementia. *Nature Neuroscience* 18, 631-636.

- Frenkel, N., Makky, A., Sudji, I.R., Wink, M., and Tanaka, M. (2014). Mechanistic investigation of interactions between steroidal saponin digitonin and cell membrane models. *The journal of physical chemistry B* 118, 14632-14639.
- Frick, P., Sellier, C., Mackenzie, I.R.A., Cheng, C.-Y., Tahraoui-Bories, J., Martinat, C., Pasterkamp, R.J., Prudlo, J., Edbauer, D., Oulad-Abdelghani, M., *et al.* (2018). Novel antibodies reveal presynaptic localization of C9orf72 protein and reduced protein levels in C9orf72 mutation carriers. *Acta Neuropathologica Communications* 6, 72.
- Friedman, J.R., Lackner, L.L., West, M., DiBenedetto, J.R., Nunnari, J., and Voeltz, G.K. (2011). ER tubules mark sites of mitochondrial division. *Science* 334, 358-362.
- Fujiki, Y., Hubbard, A.L., Fowler, S., and Lazarow, P.B. (1982). Isolation of intracellular membranes by means of sodium carbonate treatment: application to endoplasmic reticulum. *J Cell Biol* 93, 97-102.
- Fukasawa, Y., Tsuji, J., Fu, S.C., Tomii, K., Horton, P., and Imai, K. (2015). MitoFates: improved prediction of mitochondrial targeting sequences and their cleavage sites. *Molecular & cellular proteomics : MCP* 14, 1113-1126.
- Fukunaga, K., Shinoda, Y., and Tagashira, H. (2015). The role of SIGMAR1 gene mutation and mitochondrial dysfunction in amyotrophic lateral sclerosis. *Journal of Pharmaceutical Sciences* 127, 36-41.
- Gallagher, M.D., Suh, E., Grossman, M., Elman, L., McCluskey, L., Van Swieten, J.C., Al-Sarraj, S., Neumann, M., Gelpi, E., Ghetti, B., *et al.* (2014). TMEM106B is a genetic modifier of frontotemporal lobar degeneration with C9orf72 hexanucleotide repeat expansions. *Acta Neuropathologica* 127, 407-418.
- Gandhi, S., and Abramov, A.Y. (2012). Mechanism of oxidative stress in neurodegeneration. *Oxidative Medicine and Cellular Longevity* 2012, 428010.
- Ganley, I.G., Lam du, H., Wang, J., Ding, X., Chen, S., and Jiang, X. (2009). ULK1.ATG13.FIP200 complex mediates mTOR signaling and is essential for autophagy. *J Biol Chem* 284, 12297-12305.
- Gargiulo, S., Anzilotti, S., Coda, A.R., Gramanzini, M., Greco, A., Panico, M., Vinciguerra, A., Zannetti, A., Vicidomini, C., Dolle, F., *et al.* (2016). Imaging of brain TSPO expression in a mouse model of amyotrophic lateral sclerosis with (18)F-DPA-714 and micro-PET/CT. *European journal of nuclear medicine and molecular imaging* 43, 1348-1359.
- Gautam, M., Jara, J.H., Sekerkova, G., Yasvoina, M.V., Martina, M., and Ozdinler, P.H. (2016). Absence of alsin function leads to corticospinal motor neuron vulnerability via novel disease mechanisms. *Human Molecular Genetics* 25, 1074-1087.
- Gegg, M.E., Cooper, J.M., Chau, K.Y., Rojo, M., Schapira, A.H.V., and Taanman, J.W. (2010). Mitofusin 1 and mitofusin 2 are ubiquitinated in a PINK1/parkin-dependent manner upon induction of mitophagy. *Human Molecular Genetics* 19, 4861-4870.
- Gendron, T.F., Bieniek, K.F., Zhang, Y.J., Jansen-West, K., Ash, P.E.A., Caulfield, T., Daugherty, L., Dunmore, J.H., Castanedes-Casey, M., Chew, J., *et al.* (2013). Antisense transcripts of the expanded C9ORF72 hexanucleotide repeat form nuclear RNA foci and undergo repeat-associated non-ATG translation in c9FTD/ALS. *Acta Neuropathologica* 126, 829-844.
- Gendron, T.F., and Petrucelli, L. (2018). Disease Mechanisms of C9ORF72 Repeat Expansions. *Cold Spring Harbor perspectives in medicine* 8.
- Gendron, T.F., van Blitterswijk, M., Bieniek, K.F., Daugherty, L.M., Jiang, J., Rush, B.K., Pedraza, O., Lucas, J.A., Murray, M.E., Desaro, P., *et al.* (2015). Cerebellar c9RAN

proteins associate with clinical and neuropathological characteristics of C9ORF72 repeat expansion carriers. *Acta Neuropathologica* 130, 559-573.

Genin, E.C., Plutino, M., Bannwarth, S., Villa, E., Cisneros-Barroso, E., Roy, M., Ortega-Vila, B., Fragaki, K., Lespinasse, F., Pinero-Martos, E., *et al.* (2016). *CHCHD10* mutations promote loss of mitochondrial cristae junctions with impaired mitochondrial genome maintenance and inhibition of apoptosis. *EMBO Molecular Medicine* 8, 58–72.

Gersch, M., Gladkova, C., Schubert, A.F., Michel, M.A., Maslen, S., and Komander, D. (2017). Mechanism and regulation of the Lys6-selective deubiquitinase USP30. *Nat Struct Mol Biol* 24, 920-930.

Gevorgyan-Airapetov, L., Zohary, K., Popov-Celeketic, D., Mapa, K., Hell, K., Neupert, W., Azem, A., and Mokranjac, D. (2009). Interaction of Tim23 with Tim50 is essential for protein translocation by the mitochondrial TIM23 complex. *J Biol Chem* 284, 4865-4872.

Ghiasi, P., Hosseinkhani, S., Noori, A., Nafissi, S., and Khajeh, K. (2012). Mitochondrial complex I deficiency and ATP/ADP ratio in lymphocytes of amyotrophic lateral sclerosis patients. *Neurological Research* 34, 297-303.

Gijssels, I., Van Mossevelde, S., van der Zee, J., Sieben, A., Engelborghs, S., De Bleecker, J., Ivanoiu, A., Deryck, O., Edbauer, D., Zhang, M., *et al.* (2015). The C9orf72 repeat size correlates with onset age of disease, DNA methylation and transcriptional downregulation of the promoter. *In Mol Psychiatry*.

Ginguay, A., Cynober, L., Curis, E., and Nicolis, I. (2017). Ornithine Aminotransferase, an Important Glutamate-Metabolizing Enzyme at the Crossroads of Multiple Metabolic Pathways. *Biology* 6, 18.

Giorda, R., Hagiya, M., Seki, T., Shimonishi, M., Sakai, H., Michaelson, J., Francavilla, A., Starzl, T.E., and Trucco, M. (1996). Analysis of the structure and expression of the augments of liver regeneration (ALR) gene. *Molecular medicine (Cambridge, Mass)* 2, 97-108.

Gitcho, M.A., Strider, J., Carter, D., Taylor-Reinwald, L., Forman, M.S., Goate, A.M., and Cairns, N.J. (2009). VCP mutations causing frontotemporal lobar degeneration disrupt localization of TDP-43 and induce cell death. *Journal of Biological Chemistry* 284, 12384-12398.

Gitler, A.D., and Tsuiji, H. (2016). There has been an awakening: Emerging mechanisms of C9orf72 mutations in FTD/ALS. *Brain Research* 1647, 19-29.

Gladkova, C., Maslen, S.L., Skehel, J.M., and Komander, D. (2018). Mechanism of parkin activation by PINK1. *Nature* 559, 410-414.

Glater, E.E., Megeath, L.J., Stowers, R.S., and Schwarz, T.L. (2006). Axonal transport of mitochondria requires mltin to recruit kinesin heavy chain and is light chain independent. *Journal of Cell Biology* 173, 545-557.

Gold, V.A.M., Ieva, R., Walter, A., Pfanner, N., van der Laan, M., and Kühlbrandt, W. (2014). Visualizing active membrane protein complexes by electron cryotomography. *Nature Communications* 5, 4129.

Goode, A., Butler, K., Long, J., Cavey, J., Scott, D., Shaw, B., Sollenberger, J., Gell, C., Johansen, T., Oldham, N.J., *et al.* (2016). Defective recognition of LC3B by mutant SQSTM1/p62 implicates impairment of autophagy as a pathogenic mechanism in ALS-FTLD. *Autophagy* 12, 1094-1104.

Gosselin, R.D., Meylan, P., and Decosterd, I. (2013). Extracellular microvesicles from astrocytes contain functional glutamate transporters: regulation by protein kinase C and cell activation. *Front Cell Neurosci* 7, 251.

- Green, K.M., Linsalata, A.E., and Todd, P.K. (2016). RAN translation—What makes it run? *Brain Research* 1647, 30-42.
- Greenway, M.J., Alexander, M.D., Ennis, S., Traynor, B.J., Corr, B., Frost, E., Green, A., and Hardiman, O. (2004). A novel candidate region for ALS on chromosome 14q11.2. *Neurology* 63, 1936-1938.
- Groh, M., Silva, L.M., and Gromak, N. (2014). Mechanisms of transcriptional dysregulation in repeat expansion disorders. *Biochemical Society transactions* 42, 1123-1128.
- Gros-Louis, F., Larivière, R., Gowing, G., Laurent, S., Camu, W., Bouchard, J.P., Meininger, V., Rouleau, G.A., and Julien, J.P. (2004). A frameshift deletion in peripherin gene associated with amyotrophic lateral sclerosis. *Journal of Biological Chemistry* 279, 45951-45956.
- Grosshans, B.L., Ortiz, D., and Novick, P. (2006). Rabs and their effectors: Achieving specificity in membrane traffic. *Proceedings of the National Academy of Sciences of the United States of America* 103, 11821-11827.
- Grosskreutz, J., Van Den Bosch, L., and Keller, B.U. (2010). Calcium dysregulation in amyotrophic lateral sclerosis. *Cell Calcium* 47, 165-174.
- Guedes-Dias, P., Pinho, B.R., Soares, T.R., de Proenca, J., Duchen, M.R., and Oliveira, J.M. (2016). Mitochondrial dynamics and quality control in Huntington's disease. *Neurobiol Dis* 90, 51-57.
- Guo, H., Chitiprolu, M., Gagnon, D., Meng, L., Perez-Iratxeta, C., Lagace, D., and Gibbings, D. (2014). Autophagy supports genomic stability by degrading retrotransposon RNA. *Nat Commun* 5, 5276.
- Guo, L., Tian, J., and Du, H. (2017). Mitochondrial Dysfunction and Synaptic Transmission Failure in Alzheimer's Disease. *Journal of Alzheimer's disease : JAD* 57, 1071-1086.
- Guo, R., Lin, B., Pan, J.F., Liang, E.C., Xu, A.M., Youdim, M., Fung, M.L., So, K.F., and Tipoe, G.L. (2016). Inhibition of caspase-9 aggravates acute liver injury through suppression of cytoprotective autophagy. *Scientific Reports* 6, 32447.
- Gutierrez, M.G., Munafó, D.B., Berón, W., and Colombo, M.I. (2004). Rab7 is required for the normal progression of the autophagic pathway in mammalian cells. *Journal of Cell Science* 117, 2687.
- Hadano, S., Benn, S.C., Kakuta, S., Otomo, A., Sudo, K., Kunita, R., Suzuki-Utsunomiya, K., Mizumura, H., Shefner, J.M., Cox, G.A., *et al.* (2006). Mice deficient in the Rab5 guanine nucleotide exchange factor ALS2/alsin exhibit age-dependent neurological deficits and altered endosome trafficking. *Human Molecular Genetics* 15, 233-250.
- Hadano, S., Hand, C.K., Osuga, H., Yanagisawa, Y., Otomo, A., Devon, R.S., Miyamoto, N., Showguchi-Miyata, J., Okada, Y., Singaraja, R., *et al.* (2001). A gene encoding a putative GTPase regulator is mutated in familial amyotrophic lateral sclerosis 2. *Nature Genetics* 29, 166-173.
- Hadano, S., Otomo, A., Kunita, R., Suzuki-Utsunomiya, K., Akatsuka, A., Koike, M., Aoki, M., Uchiyama, Y., Itoyama, Y., and Ikeda, J.E. (2010). Loss of ALS2/Alsin exacerbates motor dysfunction in a SOD1H46R-expressing mouse ALS model by disturbing endolysosomal trafficking. *PLoS ONE* 5.
- Hadife, N., Nemos, C., Fripiat, J.P., Hamade, T., Perrot, A., and Dalloul, A. (2013). Interleukin-24 mediates apoptosis in human B-cells through early activation of cell cycle

arrest followed by late induction of the mitochondrial apoptosis pathway. *Leuk Lymphoma* 54, 587-597.

Haeusler, A.R., Donnelly, C.J., Periz, G., Simko, E.A.J., Shaw, P.G., Kim, M.S., Maragakis, N.J., Troncoso, J.C., Pandey, A., Sattler, R., *et al.* (2014). C9orf72 nucleotide repeat structures initiate molecular cascades of disease. *Nature* 507, 195-200.

Haeusler, A.R., Donnelly, C.J., and Rothstein, J.D. (2016). The expanding biology of the C9orf72 nucleotide repeat expansion in neurodegenerative disease. *Nature Reviews Neuroscience* 17, 383.

Hajek, P., Chomyn, A., and Attardi, G. (2007). Identification of a novel mitochondrial complex containing mitofusin 2 and stomatin-like protein 2. *J Biol Chem* 282, 5670-5681.

Hamacher-Brady, A., and Brady, N.R. (2016). Mitophagy programs: mechanisms and physiological implications of mitochondrial targeting by autophagy. *Cellular and Molecular Life Sciences* 73, 775-795.

Hand, C.K., Khoris, J., Salachas, F., Gros-Louis, F., Simões Lopes, A.A., Mayeux-Portas, V., Brown R.H, Jr., Meininger, V., Camu, W., and Rouleau, G.A. (2002). A novel locus for familial amyotrophic lateral sclerosis, on chromosome 18q. *American Journal of Human Genetics* 70, 251-256.

Hans, F., Fiesel, F.C., Strong, J.C., Jackel, S., Rasse, T.M., Geisler, S., Springer, W., Schulz, J.B., Voigt, A., and Kahle, P.J. (2014). UBE2E ubiquitin-conjugating enzymes and ubiquitin isopeptidase Y regulate TDP-43 protein ubiquitination. *J Biol Chem* 289, 19164-19179.

Hara, T., Takamura, A., Kishi, C., Iemura, S., Natsume, T., Guan, J.L., and Mizushima, N. (2008). FIP200, a ULK-interacting protein, is required for autophagosome formation in mammalian cells. *J Cell Biol* 181, 497-510.

Harper, P.S., Harley, H.G., Reardon, W., and Shaw, D.J. (1992). Anticipation in myotonic dystrophy: New light on an old problem. *American Journal of Human Genetics* 51, 10-16.

Hart, M.N., Cancilla, P.A., Frommes, S., and Hirano, A. (1977). Anterior horn cell degeneration and Bunina-type inclusions associated with dementia. *Acta Neuropathologica* 38, 225-228.

Hatch, A.L., Gurel, P.S., and Higgs, H.N. (2014). Novel roles for actin in mitochondrial fission. *Journal of Cell Science* 127, 4549.

Hautbergue, G.M., Castelli, L.M., Ferraiuolo, L., Sanchez-Martinez, A., Cooper-Knock, J., Higginbottom, A., Lin, Y.-H., Bauer, C.S., Dodd, J.E., Myszczyńska, M.A., *et al.* (2017). SRSF1-dependent nuclear export inhibition of C9ORF72 repeat transcripts prevents neurodegeneration and associated motor deficits. *Nature Communications* 8, 16063.

Hebron, M.L., Lonskaya, I., Sharpe, K., Weerasinghe, P.P., Algarzae, N.K., Shekoyan, A.R., and Moussa, C.E. (2013). Parkin ubiquitinates Tar-DNA binding protein-43 (TDP-43) and promotes its cytosolic accumulation via interaction with histone deacetylase 6 (HDAC6). *Journal of Biological Chemistry* 288, 4103-4115.

Hell, K., and Neupert, W. (2008). Oxidative protein folding in mitochondria. *Oxidative Folding of Peptides and Proteins*.

Henkel, J.S., Beers, D.R., Wen, S., Rivera, A.L., Toennis, K.M., Appel, J.E., Zhao, W., Moore, D.H., Powell, S.Z., and Appel, S.H. (2013). Regulatory T-lymphocytes mediate amyotrophic lateral sclerosis progression and survival. *EMBO Mol Med* 5, 64-79.

- Hentati, A., Bejaoui, K., Pericak-Vance, M.A., Hentati, F., Speer, M.C., Hung, W.Y., Figlewicz, D.A., Haines, J., Rimmler, J., Ben Hamida, C., *et al.* (1994). Linkage of recessive familial amyotrophic lateral sclerosis to chromosome 2q33-q35. *Nat Genet* 7, 425-428.
- Heo, J.M., Ordureau, A., Paulo, J.A., Rinehart, J., and Harper, J.W. (2015). The PINK1-PARKIN Mitochondrial Ubiquitylation Pathway Drives a Program of OPTN/NDP52 Recruitment and TBK1 Activation to Promote Mitophagy. *Molecular Cell* 60, 7-20.
- Herlan, M., Vogel, F., Bornhövd, C., Neupert, W., and Reichert, A.S. (2003). Processing of Mgm1 by the rhomboid-type protease Pcp1 is required for maintenance of mitochondrial morphology and of mitochondrial DNA. *Journal of Biological Chemistry* 278, 27781-27788.
- Herrmann, J.M., and Hell, K. (2005). Chopped, trapped or tacked--protein translocation into the IMS of mitochondria. *Trends Biochem Sci* 30, 205-211.
- Herrmann, J.M., and Riemer, J. (2012). Mitochondrial Disulfide Relay: Redox-regulated Protein Import into the Intermembrane Space. *The Journal of Biological Chemistry* 287, 4426-4433.
- Hessenberger, M., Zerbes, R.M., Rampelt, H., Kunz, S., Xavier, A.H., Purfürst, B., Lilie, H., Pfanner, N., van der Laan, M., and Daumke, O. (2017). Regulated membrane remodeling by Mic60 controls formation of mitochondrial crista junctions. *Nature Communications* 8, 15258.
- Higgins, C.M., Jung, C., Ding, H., and Xu, Z. (2002). Mutant Cu, Zn superoxide dismutase that causes motoneuron degeneration is present in mitochondria in the CNS. *Journal of Neuroscience* 22.
- Higgins, C.M.J., Jung, C., and Xu, Z. (2003). ALS-associated mutant SOD1G93A causes mitochondrial vacuolation by expansion of the intermembrane space by involvement of SOD1 aggregation and peroxisomes. *BMC Neuroscience* 4.
- Hirota, Y., and Tanaka, Y. (2009). A small GTPase, human Rab32, is required for the formation of autophagic vacuoles under basal conditions. *Cell Mol Life Sci* 66, 2913-2932.
- Hoffman, N.J., Parker, B.L., Chaudhuri, R., Fisher-Wellman, K.H., Kleinert, M., Humphrey, S.J., Yang, P., Holliday, M., Trefely, S., Fazakerley, D.J., *et al.* (2015). Global Phosphoproteomic Analysis of Human Skeletal Muscle Reveals a Network of Exercise-Regulated Kinases and AMPK Substrates. *Cell Metab* 22, 922-935.
- Hofmann, S., Rothbauer, U., Muhlenbein, N., Baiker, K., Hell, K., and Bauer, M.F. (2005). Functional and mutational characterization of human MIA40 acting during import into the mitochondrial intermembrane space. *J Mol Biol* 353, 517-528.
- Hoitzing, H., Johnston, I.G., and Jones, N.S. (2015). What is the function of mitochondrial networks? A theoretical assessment of hypotheses and proposal for future research. *Bioessays* 37, 687-700.
- Honda, S., Arakawa, S., Nishida, Y., Yamaguchi, H., Ishii, E., and Shimizu, S. (2014). Ulk1-mediated Atg5-independent macroautophagy mediates elimination of mitochondria from embryonic reticulocytes. *Nature Communications* 5.
- Hong, K., Li, Y., Duan, W., Guo, Y., Jiang, H., Li, W., and Li, C. (2012). Full-length TDP-43 and its C-terminal fragments activate mitophagy in NSC34 cell line. *Neuroscience Letters* 530, 144-149.
- Hornberger, M., and Piguet, O. (2012). Episodic memory in frontotemporal dementia: a critical review. *Brain* 135, 678-692.

- Horvath, S.E., Rampelt, H., Oeljeklaus, S., Warscheid, B., van der Laan, M., and Pfanner, N. (2015). Role of membrane contact sites in protein import into mitochondria. *Protein Sci* 24, 277-297.
- Hosokawa, N., Sasaki, T., Iemura, S., Natsume, T., Hara, T., and Mizushima, N. (2009). Atg101, a novel mammalian autophagy protein interacting with Atg13. *Autophagy* 5, 973-979.
- Hsu, P.P., Kang, S.A., Rameseder, J., Zhang, Y., Ottina, K.A., Lim, D., Peterson, T.R., Choi, Y., Gray, N.S., Yaffe, M.B., *et al.* (2011). The mTOR-regulated phosphoproteome reveals a mechanism of mTORC1-mediated inhibition of growth factor signaling. *Science* 332, 1317-1322.
- Hu, C., Huang, Y., and Li, L. (2017). Drp1-Dependent Mitochondrial Fission Plays Critical Roles in Physiological and Pathological Progresses in Mammals. *International Journal of Molecular Sciences* 18, 144.
- Hutagalung, A.H., and Novick, P.J. (2011). Role of Rab GTPases in Membrane Traffic and Cell Physiology. *Physiological reviews* 91, 119-149.
- Ince, P., Stout, N., Shaw, P., Slade, J., Hunziker, W., Heizmann, C.W., and Baimbridge, K.G. (1993). Parvalbumin and calbindin D-28k in the human motor system and in motor neuron disease. *Neuropathology and Applied Neurobiology* 19, 291-299.
- Ishihara, N., Eura, Y., and Mihara, K. (2004). Mitofusin 1 and 2 play distinct roles in mitochondrial fusion reactions via GTPase activity. *J Cell Sci* 117, 6535-6546.
- Ishihara, N., Jofuku, A., Eura, Y., and Mihara, K. (2003). Regulation of mitochondrial morphology by membrane potential, and DRP1-dependent division and FZO1-dependent fusion reaction in mammalian cells. *Biochem Biophys Res Commun* 301, 891-898.
- Ishihara, N., Nomura, M., Jofuku, A., Kato, H., Suzuki, S.O., Masuda, K., Otera, H., Nakanishi, Y., Nonaka, I., Goto, Y.-i., *et al.* (2009). Mitochondrial fission factor Drp1 is essential for embryonic development and synapse formation in mice. *Nature Cell Biology* 11, 958.
- Israelson, A., Arbel, N., Da Cruz, S., Ilieva, H., Yamanaka, K., Shoshan-Barmatz, V., and Cleveland, D.W. (2010). Misfolded mutant SOD1 directly inhibits VDAC1 conductance in a mouse model of inherited ALS. *Neuron* 67, 575-587.
- Itakura, E., Kishi-Itakura, C., Koyama-Honda, I., and Mizushima, N. (2012). Structures containing Atg9A and the ULK1 complex independently target depolarized mitochondria at initial stages of Parkin-mediated mitophagy. *J Cell Sci* Jan 24.
- Itoh, T., Fujita, N., Kanno, E., Yamamoto, A., Yoshimori, T., and Fukuda, M. (2008). Golgi-resident small GTPase Rab33B interacts with Atg16L and modulates autophagosome formation. *Mol Biol Cell* 19, 2916-2925.
- Izumikawa, K., Nobe, Y., Yoshikawa, H., Ishikawa, H., Miura, Y., Nakayama, H., Nonaka, T., Hasegawa, M., Egawa, N., Inoue, H., *et al.* (2017). TDP-43 stabilises the processing intermediates of mitochondrial transcripts. *Scientific Reports* 7, 7709.
- Jaiswal, M.K. (2013). Calcium, mitochondria, and the pathogenesis of ALS: the good, the bad, and the ugly. *Frontiers in Cellular Neuroscience* 7, 199.
- Ježek, J., Cooper, K.F., and Strich, R. (2018). Reactive Oxygen Species and Mitochondrial Dynamics: The Yin and Yang of Mitochondrial Dysfunction and Cancer Progression. *Antioxidants* 7, 13.
- Jiang, J., Zhu, Q., Gendron, T.F., Saberi, S., McAlonis-Downes, M., Seelman, A., Stauffer, J.E., Jafar-Nejad, P., Drenner, K., Schulte, D., *et al.* (2016). Gain of Toxicity

from ALS/FTD-Linked Repeat Expansions in C9ORF72 Is Alleviated by Antisense Oligonucleotides Targeting GGGGCC-Containing RNAs. *Neuron* 90, 535-550.

Jin, S.M., Lazarou, M., Wang, C., Kane, L.A., Narendra, D.P., and Youle, R.J. (2010). Mitochondrial membrane potential regulates PINK1 import and proteolytic destabilization by PARL. *Journal of Cell Biology* 191, 933-942.

Johnson, J.O., Glynn, S.M., Gibbs, J.R., Nalls, M.A., Sabatelli, M., Restagno, G., Drory, V.E., Chio, A., Rogaeva, E., and Traynor, B.J. (2014a). Mutations in the CHCHD10 gene are a common cause of familial amyotrophic lateral sclerosis. *Brain* 137, e311.

Johnson, J.O., Mandrioli, J., Benatar, M., Abramzon, Y., Van Deerlin, V.M., Trojanowski, J.Q., Gibbs, J.R., Brunetti, M., Gronka, S., Wu, J., *et al.* (2010). Exome Sequencing Reveals VCP Mutations as a Cause of Familial ALS. *Neuron* 68, 857-864.

Johnson, J.O., Piro, E.P., Boehringer, A., Chia, R., Feit, H., Renton, A.E., Pliner, H.A., Abramzon, Y., Marangi, G., Winborn, B.J., *et al.* (2014b). Mutations in the Matrin 3 gene cause familial amyotrophic lateral sclerosis. *Nat Neurosci* 17, 664-666.

Jonckheere, A.I., Smeitink, J.A.M., and Rodenburg, R.J.T. (2012). Mitochondrial ATP synthase: architecture, function and pathology. *Journal of Inherited Metabolic Disease* 35, 211-225.

Jornayvaz, F.R., and Shulman, G.I. (2010). Regulation of mitochondrial biogenesis. *Essays in biochemistry* 47, 10.1042/bse0470069.

Joshi, A.U., Saw, N.L., Vogel, H., Cunnigham, A.D., Shamloo, M., and Mochly-Rosen, D. (2018). Inhibition of Drp1/Fis1 interaction slows progression of amyotrophic lateral sclerosis. *EMBO Molecular Medicine* 10, e8166.

Jovic, M., Sharma, M., Rahajeng, J., and Caplan, S. (2010). The early endosome: a busy sorting station for proteins at the crossroads. *Histology and histopathology* 25, 99-112.

Jovicic, A., Mertens, J., Boeynaems, S., Bogaert, E., Chai, N., Yamada, S.B., Paul, J.W., 3rd, Sun, S., Herdy, J.R., Bieri, G., *et al.* (2015). Modifiers of C9orf72 dipeptide repeat toxicity connect nucleocytoplasmic transport defects to FTD/ALS. *Nat Neurosci* 18, 1226-1229.

Ju, J.S., Fuentealba, R.A., Miller, S.E., Jackson, E., Piwnica-Worms, D., Baloh, R.H., and Weihl, C.C. (2009). Valosin-containing protein (VCP) is required for autophagy and is disrupted in VCP disease. *J Cell Biol* 187, 875-888.

Jung, C.H., Jun, C.B., Ro, S.H., Kim, Y.M., Otto, N.M., Cao, J., Kundu, M., and Kim, D.H. (2009). ULK-Atg13-FIP200 complexes mediate mTOR signaling to the autophagy machinery. *Mol Biol Cell* 20, 1992-2003.

Jung, J., and Behrends, C. (2017). Multifaceted role of SMCR8 as autophagy regulator. *Small GTPases*, 1-9.

Jung, J., Nayak, A., Schaeffer, V., Starzetz, T., Kirsch, A.K., Muller, S., Dikic, I., Mittelbronn, M., and Behrends, C. (2017). Multiplex image-based autophagy RNAi screening identifies SMCR8 as ULK1 kinase activity and gene expression regulator. *eLife* 6.

Kabeya, Y., Mizushima, N., Yamamoto, A., Oshitani-Okamoto, S., Ohsumi, Y., and Yoshimori, T. (2004). LC3, GABARAP and GATE16 localize to autophagosomal membrane depending on form-II formation. *J Cell Sci* 117, 2805-2812.

Kabuta, C., Kono, K., Wada, K., and Kabuta, T. (2015). 4-Hydroxynonenal induces persistent insolubilization of TDP-43 and alters its intracellular localization. *Biochemical and Biophysical Research Communications* 463, 82-87.

- Kadenbach, B., and Huttemann, M. (2015). The subunit composition and function of mammalian cytochrome c oxidase. *Mitochondrion* 24, 64-76.
- Kanekura, K., Yagi, T., Cammack, A.J., Mahadevan, J., Kuroda, M., Harms, M.B., Miller, T.M., and Urano, F. (2016). Poly-dipeptides encoded by the C9ORF72 repeats block global protein translation. *Hum Mol Genet* 25, 1803-1813.
- Kang, J.S., Tian, J.H., Pan, P.Y., Zald, P., Li, C., Deng, C., and Sheng, Z.H. (2008). Docking of axonal mitochondria by syntaphilin controls their mobility and affects short-term facilitation. *Cell* 132, 137-148.
- Kapeli, K., Martinez, F.J., and Yeo, G.W. (2017). Genetic mutations in RNA-binding proteins and their roles in ALS. *Human Genetics* 136, 1193-1214.
- Karanasios, E., Stapleton, E., Manifava, M., Kaizuka, T., Mizushima, N., Walker, S.A., and Ktistakis, N.T. (2013). Dynamic association of the ULK1 complex with omegasomes during autophagy induction. *J Cell Sci* 126, 5224-5238.
- Karbowski, M., Norris, K.L., Cleland, M.M., Jeong, S.Y., and Youle, R.J. (2006). Role of Bax and Bak in mitochondrial morphogenesis. *Nature* 443, 658-662.
- Kawamata, H., and Manfredi, G. (2008). Different regulation of wild-type and mutant Cu,Zn superoxide dismutase localization in mammalian mitochondria. *Human Molecular Genetics* 17, 3303-3317.
- Kawamata, H., and Manfredi, G. (2010). Import, Maturation, and Function of SOD1 and Its Copper Chaperone CCS in the Mitochondrial Intermembrane Space. *Antioxidants & Redox Signaling* 13, 1375-1384.
- Kawamata, T., Akiyama, H., Yamada, T., and McGeer, P.L. (1992). Immunologic reactions in amyotrophic lateral sclerosis brain and spinal cord tissue. *American Journal of Pathology* 140, 691-707.
- Kazlauskaite, A., Kondapalli, C., Gourlay, R., Campbell, D.G., Ritorto, M.S., Hofmann, K., Alessi, D.R., Knebel, A., Trost, M., and Muqit, M.M. (2014). Parkin is activated by PINK1-dependent phosphorylation of ubiquitin at Ser65. *The Biochemical journal* 460, 127-139.
- Kenna, K.P., van Doormaal, P.T., Dekker, A.M., Ticozzi, N., Kenna, B.J., Diekstra, F.P., van Rheenen, W., van Eijk, K.R., Jones, A.R., Keagle, P., *et al.* (2016). NEK1 variants confer susceptibility to amyotrophic lateral sclerosis. *Nat Genet* 48, 1037-1042.
- Kerr, J.S., Adriaanse, B.A., Greig, N.H., Mattson, M.P., Cader, M.Z., Bohr, V.A., and Fang, E.F. (2017). Mitophagy and Alzheimer's disease: cellular and molecular mechanisms. *Trends in neurosciences* 40, 151-166.
- Khalil, B., Cabirol-Pol, M.J., Miguel, L., Whitworth, A.J., Lecourtois, M., and Lievens, J.C. (2017). Enhancing Mitofusin/Marf ameliorates neuromuscular dysfunction in *Drosophila* models of TDP-43 proteinopathies. *Neurobiol Aging* 54, 71-83.
- Khalil, B., and Liévens, J.-C. (2017). Mitochondrial quality control in amyotrophic lateral sclerosis: towards a common pathway? *Neural Regeneration Research* 12, 1052-1061.
- Kiernan, M.C., Vucic, S., Cheah, B.C., Turner, M.R., Eisen, A., Hardiman, O., Burrell, J.R., and Zoing, M.C. (2011). Amyotrophic lateral sclerosis. *The Lancet* 377, 942-955.
- Kim, G.H., Kim, J.E., Rhie, S.J., and Yoon, S. (2015a). The Role of Oxidative Stress in Neurodegenerative Diseases. *Experimental Neurobiology* 24, 325-340.
- Kim, H., Botelho, S.C., Park, K., and Kim, H. (2015b). Use of carbonate extraction in analyzing moderately hydrophobic transmembrane proteins in the mitochondrial inner membrane. *Protein Science : A Publication of the Protein Society* 24, 2063-2069.

- Kim, H.J., Kim, N.C., Wang, Y.D., Scarborough, E.A., Moore, J., Diaz, Z., MacLea, K.S., Freibaum, B., Li, S., Molliex, A., *et al.* (2013a). Mutations in prion-like domains in hnRNPA2B1 and hnRNPA1 cause multisystem proteinopathy and ALS. *Nature* 495, 467-473.
- Kim, J., Kundu, M., Viollet, B., and Guan, K.L. (2011). AMPK and mTOR regulate autophagy through direct phosphorylation of Ulk1. *Nat Cell Biol* 13, 132-141.
- Kim, N.C., Tresse, E., Kolaitis, R.M., Molliex, A., Thomas, R.E., Alami, N.H., Wang, B., Joshi, A., Smith, R.B., Ritson, G.P., *et al.* (2013b). VCP Is Essential for Mitochondrial Quality Control by PINK1/Parkin and this Function Is Impaired by VCP Mutations. *Neuron* 78, 65-80.
- Kirkinezos, I.G., Bacman, S.R., Hernandez, D., Oca-Cossio, J., Arias, L.J., Perez-Pinzon, M.A., Bradley, W.G., and Moraes, C.T. (2005). Cytochrome c association with the inner mitochondrial membrane is impaired in the CNS of G93A-SOD1 mice. *Journal of Neuroscience* 25, 164-172.
- Klein, C., and Westenberger, A. (2012). Genetics of Parkinson's Disease. *Cold Spring Harbor perspectives in medicine* 2, a008888.
- Komander, D., Clague, M.J., and Urbe, S. (2009). Breaking the chains: structure and function of the deubiquitinases. *Nat Rev Mol Cell Biol* 10, 550-563.
- Komander, D., and Rape, M. (2012). The ubiquitin code. *Annual review of biochemistry* 81, 203-229.
- Kong, J., and Xu, Z. (1998). Massive mitochondrial degeneration in motor neurons triggers the onset of amyotrophic lateral sclerosis in mice expressing a mutant SOD1. *Journal of Neuroscience* 18, 3241-3250.
- Koopman, W.J., Visch, H.J., Verkaart, S., van den Heuvel, L.W., Smeitink, J.A., and Willems, P.H. (2005). Mitochondrial network complexity and pathological decrease in complex I activity are tightly correlated in isolated human complex I deficiency. *Am J Physiol Cell Physiol* 289, C881-890.
- Koppers, M., van Blitterswijk, M.M., Vlam, L., Rowicka, P.A., van Vught, P.W.J., Groen, E.J.N., Spliet, W.G.M., Engelen-Lee, J., Schelhaas, H.J., de Visser, M., *et al.* (2012). VCP mutations in familial and sporadic amyotrophic lateral sclerosis. *Neurobiology of Aging* 33, 837.e837-837.e813.
- Koshiba, T., Detmer, S.A., Kaiser, J.T., Chen, H., McCaffery, J.M., and Chan, D.C. (2004). Structural basis of mitochondrial tethering by mitofusin complexes. *Science* 305, 858-862.
- Kowno, M., Watanabe-Susaki, K., Ishimine, H., Komazaki, S., Enomoto, K., Seki, Y., Wang, Y.Y., Ishigaki, Y., Ninomiya, N., Noguchi, T.-a.K., *et al.* (2014). Prohibitin 2 Regulates the Proliferation and Lineage-Specific Differentiation of Mouse Embryonic Stem Cells in Mitochondria. *PLoS ONE* 9, e81552.
- Kraus, F., and Ryan, M.T. (2017). The constriction and scission machineries involved in mitochondrial fission. *Journal of Cell Science*.
- Krogh, A., Larsson, B., von Heijne, G., and Sonnhammer, E.L. (2001). Predicting transmembrane protein topology with a hidden Markov model: application to complete genomes. *J Mol Biol* 305, 567-580.
- Kumar, V., Hasan, G.M., and Hassan, M.I. (2017). Unraveling the Role of RNA Mediated Toxicity of C9orf72 Repeats in C9-FTD/ALS. *Frontiers in Neuroscience* 11, 711.
- Kundu, M., Lindsten, T., Yang, C.Y., Wu, J., Zhao, F., Zhang, J., Selak, M.A., Ney, P.A., and Thompson, C.B. (2008). Ulk1 plays a critical role in the autophagic clearance of mitochondria and ribosomes during reticulocyte maturation. *Blood* 112, 1493-1502.

- Kuroda, S., Ishizu, H., Kawai, K., and Otsuki, S. (1990). Bunina bodies in dendrites of patients with amyotrophic lateral sclerosis. *Acta medica Okayama* 44, 41-45.
- Kurz, M., Martin, H., Rassow, J., Pfanner, N., and Ryan, M.T. (1999). Biogenesis of Tim proteins of the mitochondrial carrier import pathway: Differential targeting mechanisms and crossing over with the main import pathway. *Molecular Biology of the Cell* 10, 2461-2474.
- Kwiatkowski Jr, T.J., Bosco, D.A., LeClerc, A.L., Tamrazian, E., Vanderburg, C.R., Russ, C., Davis, A., Gilchrist, J., Kasarskis, E.J., Munsat, T., *et al.* (2009). Mutations in the FUS/TLS gene on chromosome 16 cause familial amyotrophic lateral sclerosis. *Science* 323, 1205-1208.
- Kwon, I., Xiang, S., Kato, M., Wu, L., Theodoropoulos, P., Wang, T., Kim, J., Yun, J., Xie, Y., and McKnight, S.L. (2014). Poly-dipeptides encoded by the C9orf72 repeats bind nucleoli, impede RNA biogenesis, and kill cells. *Science* 345, 1139-1145.
- La Spada, A.R., and Taylor, J.P. (2010). Repeat expansion disease: Progress and puzzles in disease pathogenesis. *Nature Reviews Genetics* 11, 247-258.
- Labbadia, J., and Morimoto, R.I. (2015). The Biology of Proteostasis in Aging and Disease. *Annual review of biochemistry* 84, 435-464.
- Labrousse, A.M., Zappaterra, M.D., Rube, D.A., and van der Blik, A.M. (1999). C. elegans Dynamin-Related Protein DRP-1 Controls Severing of the Mitochondrial Outer Membrane. *Molecular Cell* 4, 815-826.
- Labzin, L.I., Heneka, M.T., and Latz, E. (2018). Innate Immunity and Neurodegeneration. *Annual review of medicine* 69, 437-449.
- Laemmli, U.K. (1970). Cleavage of structural proteins during the assembly of the head of bacteriophage T4. *Nature* 227, 680-685.
- Lagier-Tourenne, C., Baughn, M., Rigo, F., Sun, S., Liu, P., Li, H.R., Jiang, J., Watt, A.T., Chun, S., Katz, M., *et al.* (2013). Targeted degradation of sense and antisense C9orf72 RNA foci as therapy for ALS and frontotemporal degeneration. *Proceedings of the National Academy of Sciences of the United States of America* 110, E4530-E4539.
- Lagier-Tourenne, C., Polymenidou, M., Hutt, K.R., Vu, A.Q., Baughn, M., Huelga, S.C., Clutario, K.M., Ling, S.C., Liang, T.Y., Mazur, C., *et al.* (2012). Divergent roles of ALS-linked proteins FUS/TLS and TDP-43 intersect in processing long pre-mRNAs. *Nature Neuroscience* 15, 1488-1497.
- Lai, Y.C., Kondapalli, C., Lehneck, R., Procter, J.B., Dill, B.D., Woodroof, H.I., Gourlay, R., Peggie, M., Macartney, T.J., Corti, O., *et al.* (2015). Phosphoproteomic screening identifies Rab GTPases as novel downstream targets of PINK1. *Embo j* 34, 2840-2861.
- Laker, R.C., Drake, J.C., Wilson, R.J., Lira, V.A., Lewellen, B.M., Ryall, K.A., Fisher, C.C., Zhang, M., Saucerman, J.J., Goodyear, L.J., *et al.* (2017). Ampk phosphorylation of Ulk1 is required for targeting of mitochondria to lysosomes in exercise-induced mitophagy. *Nature Communications* 8, 548.
- Lall, D., and Baloh, R.H. (2017). Microglia and C9orf72 in neuroinflammation and ALS and frontotemporal dementia. *J Clin Invest* 127, 3250-3258.
- Landry, M.C., Champagne, C., Boulanger, M.C., Jette, A., Fuchs, M., Dziengelewski, C., and Lavoie, J.N. (2014). A functional interplay between the small GTPase Rab11a and mitochondria-shaping proteins regulates mitochondrial positioning and polarization of the actin cytoskeleton downstream of Src family kinases. *J Biol Chem* 289, 2230-2249.

- Lazarou, M., Sliter, D.A., Kane, L.A., Sarraf, S.A., Wang, C., Burman, J.L., Sideris, D.P., Fogel, A.I., and Youle, R.J. (2015). The ubiquitin kinase PINK1 recruits autophagy receptors to induce mitophagy. *Nature* 524, 309-314.
- Lazarou, M., Smith, S.M., Thorburn, D.R., Ryan, M.T., and McKenzie, M. (2009). Assembly of nuclear DNA-encoded subunits into mitochondrial complex IV, and their preferential integration into supercomplex forms in patient mitochondria. In *FEBS J* (England), pp. 6701-6713.
- Le Ber, I. (2013). Genetics of frontotemporal lobar degeneration: an up-date and diagnosis algorithm. *Revue neurologique* 169, 811-819.
- Lee, A., Hirabayashi, Y., Kwon, S.-K., Lewis, T.L., and Polleux, F. (2018a). Emerging roles of mitochondria in synaptic transmission and neurodegeneration. *Current Opinion in Physiology* 3, 82-93.
- Lee, J., Hyeon, S.J., Im, H., Ryu, H., Kim, Y., and Ryu, H. (2016a). Astrocytes and Microglia as Non-cell Autonomous Players in the Pathogenesis of ALS. *Experimental neurobiology* 25, 233-240.
- Lee, J.E., Westrate, L.M., Wu, H., Page, C., and Voeltz, G.K. (2016b). Multiple dynamin family members collaborate to drive mitochondrial division. *Nature* 540, 139-143.
- Lee, J.J., Sanchez-Martinez, A., Zarate, A.M., Beninca, C., Mayor, U., Clague, M.J., and Whitworth, A.J. (2018b). Basal mitophagy is widespread in *Drosophila* but minimally affected by loss of Pink1 or parkin. *J Cell Biol* 217, 1613-1622.
- Lee, K.H., Zhang, P., Kim, H.J., Mitrea, D.M., Sarkar, M., Freibaum, B.D., Cika, J., Coughlin, M., Messing, J., Molliex, A., *et al.* (2016c). C9orf72 Dipeptide Repeats Impair the Assembly, Dynamics, and Function of Membrane-Less Organelles. *Cell* 167, 774-788.e717.
- Lee, V.M.Y., Goedert, M., and Trojanowski, J.Q. (2001). Neurodegenerative Tauopathies. *Annual Review of Neuroscience* 24, 1121-1159.
- Lenka, N., Vijayasarathy, C., Mullick, J., and Avadhani, N.G. (1998). Structural organization and transcription regulation of nuclear genes encoding the mammalian cytochrome c oxidase complex. *Progress in nucleic acid research and molecular biology* 61, 309-344.
- Leuchowius, K.J., Weibrecht, I., and Soderberg, O. (2011). In situ proximity ligation assay for microscopy and flow cytometry. *Current protocols in cytometry Chapter 9*, Unit 9.36.
- Leung, C.L., He, C.Z., Kaufmann, P., Chin, S.S., Naini, A., Liem, R.K., Mitsumoto, H., and Hays, A.P. (2004). A pathogenic peripherin gene mutation in a patient with amyotrophic lateral sclerosis. *Brain Pathol* 14, 290-296.
- Levine, B., Mizushima, N., and Virgin, H.W. (2011). Autophagy in immunity and inflammation. *Nature* 469, 323-335.
- Levine, T.P., Daniels, R.D., Gatta, A.T., Wong, L.H., and Hayes, M.J. (2013). The product of C9orf72, a gene strongly implicated in neurodegeneration, is structurally related to DENN Rab-GEFs. *Bioinformatics* 29, 499-503.
- Levivier, E., Goud, B., Souchet, M., Calmels, T.P.G., Mornon, J.-P., and Callebaut, I. (2001). uDENN, DENN, and dDENN: Indissociable Domains in Rab and MAP Kinases Signaling Pathways. *Biochemical and Biophysical Research Communications* 287, 688-695.
- Li, F., Xie, X., Wang, Y., Liu, J., Cheng, X., Guo, Y., Gong, Y., Hu, S., and Pan, L. (2016). Structural insights into the interaction and disease mechanism of neurodegenerative disease-associated optineurin and TBK1 proteins. *Nat Commun* 7, 12708.

- Li, W., Bengtson, M.H., Ulbrich, A., Matsuda, A., Reddy, V.A., Orth, A., Chanda, S.K., Batalov, S., and Joazeiro, C.A.P. (2008). Genome-Wide and Functional Annotation of Human E3 Ubiquitin Ligases Identifies MULAN, a Mitochondrial E3 that Regulates the Organelle's Dynamics and Signaling. *PLOS ONE* 3, e1487.
- Liang, C.-C., Wang, C., Peng, X., Gan, B., and Guan, J.-L. (2010). Neural-specific Deletion of FIP200 Leads to Cerebellar Degeneration Caused by Increased Neuronal Death and Axon Degeneration. *The Journal of Biological Chemistry* 285, 3499-3509.
- Liang, J.-R., Martinez, A., Lane, J.D., Mayor, U., Clague, M.J., and Urbé, S. (2015). USP30 deubiquitylates mitochondrial Parkin substrates and restricts apoptotic cell death. *EMBO Reports* 16, 618-627.
- Lin, M.-Y., Cheng, X.-T., Tammineni, P., Xie, Y., Zhou, B., Cai, Q., and Sheng, Z.-H. (2017). Releasing Syntaphilin Removes Stressed Mitochondria from Axons Independent of Mitophagy under Pathophysiological Conditions. *Neuron* 94, 595-610.e596.
- Lin, Y., Mori, E., Kato, M., Xiang, S., Wu, L., Kwon, I., and McKnight, S.L. (2016). Toxic PR Poly-Dipeptides Encoded by the C9orf72 Repeat Expansion Target LC Domain Polymers. *Cell* 167, 789-802.e712.
- Ling, S.C. (2018). Synaptic Paths to Neurodegeneration: The Emerging Role of TDP-43 and FUS in Synaptic Functions. *Neural plasticity* 2018, 8413496.
- Liu, E.Y., Russ, J., Wu, K., Neal, D., Suh, E., McNally, A.G., Irwin, D.J., Van Deerlin, V.M., and Lee, E.B. (2014). C9orf72 hypermethylation protects against repeat expansion-associated pathology in ALS/FTD. *Acta Neuropathologica* 128, 525-541.
- Liu, J., and Wang, F. (2017). Role of Neuroinflammation in Amyotrophic Lateral Sclerosis: Cellular Mechanisms and Therapeutic Implications. *Frontiers in Immunology* 8, 1005.
- Liu, L., Feng, D., Chen, G., Chen, M., Zheng, Q., Song, P., Ma, Q., Zhu, C., Wang, R., Qi, W., *et al.* (2012). Mitochondrial outer-membrane protein FUNDC1 mediates hypoxia-induced mitophagy in mammalian cells. *Nature Cell Biology* 14, 177-185.
- Liu, W., Tian, F., Morimoto, N., Yamashita, T., Ikeda, Y., Deguchi, K., and Abe, K. (2013). Dynamic changes of mitochondrial fusion and fission proteins in a murine model of amyotrophic lateral sclerosis. *Current Neurovascular Research* 10, 222-230.
- Liu, Y.-J., Tsai, P.-Y., and Chern, Y. (2017). Energy Homeostasis and Abnormal RNA Metabolism in Amyotrophic Lateral Sclerosis. *Frontiers in Cellular Neuroscience* 11, 126.
- Livak, K.J., and Schmittgen, T.D. (2001). Analysis of relative gene expression data using real-time quantitative PCR and the 2(-Delta Delta C(T)) Method. In *Methods* (United States: 2001 Elsevier Science (USA).), pp. 402-408.
- Llombart, V., Trejo, S.A., Bronsoms, S., Morancho, A., Feifei, M., Faura, J., Garcia-Berrocso, T., Simats, A., Rosell, A., Canals, F., *et al.* (2017). Profiling and identification of new proteins involved in brain ischemia using MALDI-imaging-mass-spectrometry. *Journal of proteomics* 152, 243-253.
- Lodish, H., Berk, A., Zipursky, S.L., Matsudaira, P., Baltimore, D., and Darnell, J. (2000). Section 5.2 Purification of Cells and Their Parts. In *Molecular Cell Biology* 4th edition, F. W.H., ed. (New York).
- Long, Q., Yang, K., and Yang, Q. (2015). Regulation of mitochondrial ATP synthase in cardiac pathophysiology. *American Journal of Cardiovascular Disease* 5, 19-32.
- Longen, S., Bien, M., Bihlmaier, K., Kloeppe, C., Kauff, F., Hammermeister, M., Westermann, B., Herrmann, J.M., and Riemer, J. (2009). Systematic Analysis of the Twin Cx9C Protein Family. *Journal of Molecular Biology* 393, 356-368.

- Lonskaya, I., Desforges, N.M., Hebron, M.L., and Moussa, C.E.H. (2013). Ubiquitination Increases Parkin Activity to Promote Autophagic α -Synuclein Clearance. *PLOS ONE* 8, e83914.
- Lopez-Gonzalez, R., Lu, Y., Gendron, T.F., Karydas, A., Tran, H., Yang, D., Petrucelli, L., Miller, B.L., Almeida, S., and Gao, F.B. (2016). Poly(GR) in C9ORF72-Related ALS/FTD Compromises Mitochondrial Function and Increases Oxidative Stress and DNA Damage in iPSC-Derived Motor Neurons. *Neuron* 92, 383-391.
- Loson, O.C., Song, Z., Chen, H., and Chan, D.C. (2013). Fis1, Mff, MiD49, and MiD51 mediate Drp1 recruitment in mitochondrial fission. *Mol Biol Cell* 24, 659-667.
- Lowe, J., Lennox, G., Jefferson, D., Morrell, K., McQuire, D., Gray, T., Landon, M., Doherty, F.J., and Mayer, R.J. (1988). A filamentous inclusion body within anterior horn neurones in motor neurone disease defined by immunocytochemical localisation of ubiquitin. *Neuroscience Letters* 94, 203-210.
- Lu, H., Allen, S., Wardleworth, L., Savory, P., and Tokatlidis, K. (2004). Functional TIM10 Chaperone Assembly Is Redox-regulated in Vivo. *Journal of Biological Chemistry* 279, 18952-18958.
- Lu, J., Duan, W., Guo, Y., Jiang, H., Li, Z., Huang, J., Hong, K., and Li, C. (2012). Mitochondrial dysfunction in human TDP-43 transfected NSC34 cell lines and the protective effect of dimethoxy curcumin. *Brain Research Bulletin* 89, 185-190.
- Luo, G., Yi, J., Ma, C., Xiao, Y., Yi, F., Yu, T., and Zhou, J. (2013). Defective mitochondrial dynamics is an early event in skeletal muscle of an amyotrophic lateral sclerosis mouse model. *PLoS One* 8, e82112.
- Lutz, T., Neupert, W., and Herrmann, J.M. (2003). Import of small Tim proteins into the mitochondrial intermembrane space. *EMBO Journal* 22, 4400-4408.
- MacAskill, A.F., Brickley, K., Stephenson, F.A., and Kittler, J.T. (2009a). GTPase dependent recruitment of Grif-1 by Miro1 regulates mitochondrial trafficking in hippocampal neurons. *Molecular and Cellular Neuroscience* 40, 301-312.
- Macaskill, A.F., Rinholm, J.E., Twelvetrees, A.E., Arancibia-Carcamo, I.L., Muir, J., Fransson, A., Aspenstrom, P., Attwell, D., and Kittler, J.T. (2009b). Miro1 is a calcium sensor for glutamate receptor-dependent localization of mitochondria at synapses. *Neuron* 61, 541-555.
- MacKenzie, I.R., Arzberger, T., Kremmer, E., Troost, D., Lorenzl, S., Mori, K., Weng, S.M., Haass, C., Kretzschmar, H.A., Edbauer, D., *et al.* (2013). Dipeptide repeat protein pathology in C9ORF72 mutation cases: Clinico-pathological correlations. *Acta Neuropathologica* 126, 859-879.
- Mackenzie, I.R., Frick, P., Grasser, F.A., Gendron, T.F., Petrucelli, L., Cashman, N.R., Edbauer, D., Kremmer, E., Prudlo, J., Troost, D., *et al.* (2015). Quantitative analysis and clinico-pathological correlations of different dipeptide repeat protein pathologies in C9ORF72 mutation carriers. *Acta Neuropathol* 130, 845-861.
- Mackenzie, I.R., and Neumann, M. (2016). Molecular neuropathology of frontotemporal dementia: insights into disease mechanisms from postmortem studies. *J Neurochem* 138 Suppl 1, 54-70.
- Mackenzie, I.R., Nicholson, A.M., Sarkar, M., Messing, J., Purice, M.D., Pottier, C., Annu, K., Baker, M., Perkerson, R.B., Kurti, A., *et al.* (2017). TIA1 Mutations in Amyotrophic Lateral Sclerosis and Frontotemporal Dementia Promote Phase Separation and Alter Stress Granule Dynamics. *Neuron* 95, 808-816.e809.
- Mackenzie, I.R.A., Bigio, E.H., Ince, P.G., Geser, F., Neumann, M., Cairns, N.J., Kwong, L.K., Forman, M.S., Ravits, J., Stewart, H., *et al.* (2007). Pathological TDP-43

distinguishes sporadic amyotrophic lateral sclerosis from amyotrophic lateral sclerosis with SOD1 mutations. *Annals of Neurology* 61, 427-434.

MacPherson, L., and Tokatlidis, K. (2017). Protein trafficking in the mitochondrial intermembrane space: mechanisms and links to human disease. *The Biochemical journal* 474, 2533-2545.

Magnuson, B., Ekim, B., and Fingar, D.C. (2012). Regulation and function of ribosomal protein S6 kinase (S6K) within mTOR signalling networks. *The Biochemical journal* 441, 1-21.

Magrané, J., Cortez, C., Gan, W., and Manfredi, G. (2014). Abnormal mitochondrial transport and morphology are common pathological denominators in SOD1 and TDP43 ALS mouse models. *Human Molecular Genetics* 23, 1413-1424.

Magrané, J., Hervias, I., Henning, M.S., Damiano, M., Kawamata, H., and Manfredi, G. (2009). Mutant SOD1 in neuronal mitochondria causes toxicity and mitochondrial dynamics abnormalities. *Human Molecular Genetics* 18, 4552-4564.

Magrané, J., Sahawneh, M.A., Przedborski, S., Estévez, A.G., and Manfredi, G. (2012). Mitochondrial dynamics and bioenergetic dysfunction is associated with synaptic alterations in mutant sod1 motor neurons. *Journal of Neuroscience* 32, 229-242.

Mai, S., Klinkenberg, M., Auburger, G., Bereiter-Hahn, J., and Jendrach, M. (2010). Decreased expression of Drp1 and Fis1 mediates mitochondrial elongation in senescent cells and enhances resistance to oxidative stress through PINK1. *J Cell Sci* 123, 917-926.

Majcher, V., Goode, A., James, V., and Layfield, R. (2015). Autophagy receptor defects and ALS-FTLD. *Molecular and Cellular Neuroscience* 66, 43-52.

Manfredi, G., and Kawamata, H. (2016). Mitochondria and endoplasmic reticulum crosstalk in amyotrophic lateral sclerosis. *Neurobiology of Disease* 90, 35-42.

Mankodi, A., Takahashi, M.P., Jiang, H., Beck, C.L., Bowers, W.J., Moxley, R.T., Cannon, S.C., and Thornton, C.A. (2002). Expanded CUG repeats trigger aberrant splicing of CIC-1 chloride channel pre-mRNA and hyperexcitability of skeletal muscle in myotonic dystrophy. *Molecular Cell* 10, 35-44.

Marat, A.L., Dokainish, H., and McPherson, P.S. (2011). DENN domain proteins: regulators of Rab GTPases. *J Biol Chem* 286, 13791-13800.

Marin, B., Boumédiene, F., Logroscino, G., Couratier, P., Babron, M.-C., Leutenegger, A.L., Copetti, M., Preux, P.-M., and Beghi, E. (2017). Variation in worldwide incidence of amyotrophic lateral sclerosis: a meta-analysis. *International Journal of Epidemiology* 46, 57-74.

Marinković, P., Reuter, M.S., Brill, M.S., Godinho, L., Kerschensteiner, M., and Miggelid, T. (2012). Axonal transport deficits and degeneration can evolve independently in mouse models of amyotrophic lateral sclerosis. *Proceedings of the National Academy of Sciences of the United States of America* 109, 4296-4301.

Martin, D.D., Ladha, S., Ehrnhoefer, D.E., and Hayden, M.R. (2015). Autophagy in Huntington disease and huntingtin in autophagy. *Trends in Neurosciences* 38, 26-35.

Martinez-Lopez, N., Athonvarangkul, D., and Singh, R. (2015). Autophagy and Aging. *Advances in experimental medicine and biology* 847, 73-87.

Martinez-Vicente, M. (2017). Neuronal Mitophagy in Neurodegenerative Diseases. *Frontiers in Molecular Neuroscience* 10, 64.

- Maruyama, H., Morino, H., Ito, H., Izumi, Y., Kato, H., Watanabe, Y., Kinoshita, Y., Kamada, M., Nodera, H., Suzuki, H., *et al.* (2010). Mutations of optineurin in amyotrophic lateral sclerosis. *Nature* 465, 223-226.
- Matheoud, D., Sugiura, A., Bellemare-Pelletier, A., Laplante, A., Rondeau, C., Chemali, M., Fazel, A., Bergeron, J.J., Trudeau, L.E., Burelle, Y., *et al.* (2016). Parkinson's Disease-Related Proteins PINK1 and Parkin Repress Mitochondrial Antigen Presentation. *Cell* 166, 314-327.
- Matsunaga, K., Saitoh, T., Tabata, K., Omori, H., Satoh, T., Kurotori, N., Maejima, I., Shirahama-Noda, K., Ichimura, T., Isobe, T., *et al.* (2009). Two Beclin 1-binding proteins, Atg14L and Rubicon, reciprocally regulate autophagy at different stages. *Nat Cell Biol* 11, 385-396.
- Mattiazzi, M., D'Aurelio, M., Gajewski, C.D., Martushova, K., Kiaei, M., Flint Beal, M., and Manfredi, G. (2002). Mutated human SOD1 causes dysfunction of oxidative phosphorylation in mitochondria of transgenic mice. *Journal of Biological Chemistry* 277, 29626-29633.
- May, S., Hornburg, D., Schludi, M.H., Arzberger, T., Rentzsch, K., Schwenk, B.M., Grasser, F.A., Mori, K., Kremmer, E., Banzhaf-Strathmann, J., *et al.* (2014). C9orf72 FTL/ALS-associated Gly-Ala dipeptide repeat proteins cause neuronal toxicity and Unc119 sequestration. *Acta Neuropathol* 128, 485-503.
- McDonald, K.K., Aulas, A., Destroismaisons, L., Pickles, S., Beleac, E., Camu, W., Rouleau, G.A., and Vande Velde, C. (2011). TAR DNA-binding protein 43 (TDP-43) regulates stress granule dynamics via differential regulation of G3BP and TIA-1. *Human Molecular Genetics* 20, 1400-1410.
- McDowell, G.S., and Philpott, A. (2013). Non-canonical ubiquitylation: Mechanisms and consequences. *The International Journal of Biochemistry & Cell Biology* 45, 1833-1842.
- McLelland, G.L., Soubannier, V., Chen, C.X., McBride, H.M., and Fon, E.A. (2014). Parkin and PINK1 function in a vesicular trafficking pathway regulating mitochondrial quality control. *EMBO Journal* 33, 282-295.
- McWilliams, T.G., Prescott, A.R., Allen, G.F., Tamjar, J., Munson, M.J., Thomson, C., Muqit, M.M., and Ganley, I.G. (2016). mito-QC illuminates mitophagy and mitochondrial architecture in vivo. *J Cell Biol* 214, 333-345.
- McWilliams, T.G., Prescott, A.R., Montava-Garriga, L., Ball, G., Singh, F., Barini, E., Muqit, M.M.K., Brooks, S.P., and Ganley, I.G. (2018). Basal Mitophagy Occurs Independently of PINK1 in Mouse Tissues of High Metabolic Demand. *Cell Metab* 27, 439-449.e435.
- Medinas, D.B., Valenzuela, V., and Hetz, C. (2017). Proteostasis disturbance in amyotrophic lateral sclerosis. *Hum Mol Genet* 26, R91-r104.
- Mehnert, C.S., Rampelt, H., Gebert, M., Oeljeklaus, S., Schrempp, S.G., Kochbeck, L., Guiard, B., Warscheid, B., and van der Laan, M. (2014). The Mitochondrial ADP/ATP Carrier Associates with the Inner Membrane Presequence Translocase in a Stoichiometric Manner. *The Journal of Biological Chemistry* 289, 27352-27362.
- Mehta, P., Kaye, W., Bryan, L., Larson, T., Copeland, T., Wu, J., Muravov, O., and Horton, K. (2016). Prevalence of Amyotrophic Lateral Sclerosis - United States, 2012-2013. *MMWR Surveillance Summaries* 65, 1-12.
- Menzies, F.M., Cookson, M.R., Taylor, R.W., Turnbull, D.M., Chrzanowska-Lightowlers, Z.M., Dong, L., Figlewicz, D.A., and Shaw, P.J. (2002). Mitochondrial dysfunction in a cell culture model of familial amyotrophic lateral sclerosis. *Brain* 125, 1522-1533.

Menzies, F.M., Fleming, A., Caricasole, A., Bento, C.F., Andrews, S.P., Ashkenazi, A., Fullgrave, J., Jackson, A., Jimenez Sanchez, M., Karabiyik, C., *et al.* (2017). Autophagy and Neurodegeneration: Pathogenic Mechanisms and Therapeutic Opportunities. *Neuron* 93, 1015-1034.

Mercer, C.A., Kaliappan, A., and Dennis, P.B. (2009). A novel, human Atg13 binding protein, Atg101, interacts with ULK1 and is essential for macroautophagy. *Autophagy* 5, 649-662.

Merkwirth, C., Dargazanli, S., Tatsuta, T., Geimer, S., Lower, B., Wunderlich, F.T., von Kleist-Retzow, J.C., Waisman, A., Westermann, B., and Langer, T. (2008). Prohibitins control cell proliferation and apoptosis by regulating OPA1-dependent cristae morphogenesis in mitochondria. *Genes Dev* 22, 476-488.

Mevissen, T.E.T., and Komander, D. (2017). Mechanisms of Deubiquitinase Specificity and Regulation. *Annual review of biochemistry* 86, 159-192.

Meyer, H., and Weihl, C.C. (2014). The VCP/p97 system at a glance: connecting cellular function to disease pathogenesis. *Journal of Cell Science* 127, 3877-3883.

Meyer, K., Ferraiuolo, L., Miranda, C.J., Likhite, S., McElroy, S., Rensch, S., Ditsworth, D., Lagier-Tourenne, C., Smith, R.A., Ravits, J., *et al.* (2014). Direct conversion of patient fibroblasts demonstrates non-cell autonomous toxicity of astrocytes to motor neurons in familial and sporadic ALS. *Proceedings of the National Academy of Sciences of the United States of America* 111, 829-832.

Meyer, T., Schwan, A., Dullinger, J.S., Brocke, J., Hoffmann, K.T., Nolte, C.H., Hopt, A., Kopp, U., Andersen, P., Epplen, J.T., *et al.* (2005). Early-onset ALS with long-term survival associated with spastin gene mutation. *Neurology* 65, 141-143.

Meyerowitz, J., Parker, S.J., Vella, L.J., Ng, D.C., Price, K.A., Liddell, J.R., Caragounis, A., Li, Q.X., Masters, C.L., Nonaka, T., *et al.* (2011). C-Jun N-terminal kinase controls TDP-43 accumulation in stress granules induced by oxidative stress. *Molecular Neurodegeneration* 6.

Mick, David U., Dennerlein, S., Wiese, H., Reinhold, R., Pacheu-Grau, D., Lorenzi, I., Sasarman, F., Weraarpachai, W., Shoubridge, Eric A., Warscheid, B., *et al.* (2012). MITRAC Links Mitochondrial Protein Translocation to Respiratory-Chain Assembly and Translational Regulation. *Cell* 151, 1528-1541.

Migheli, A., Attanasio, A., and Schiffer, D. (1994). Ubiquitin and neurofilament expression in anterior horn cells in amyotrophic lateral sclerosis: possible clues to the pathogenesis. *Neuropathol Appl Neurobiol* 20, 282-289.

Migheli, A., Pezzulo, T., Attanasio, A., and Schiffer, D. (1993). Peripherin immunoreactive structures in amyotrophic lateral sclerosis. Laboratory investigation; a journal of technical methods and pathology 68, 185-191.

Millecamps, S., Barroca, S.D., Cazeneuve, C., Salachas, F., Pradat, P.F., Danel-Brunaud, V., Vandenberghe, N., Lacomblez, L., Le Forestier, N., Bruneteau, G., *et al.* (2010). Questioning on the role of D amino acid oxidase in familial amyotrophic lateral sclerosis. *Proceedings of the National Academy of Sciences of the United States of America* 107.

Mitchell, J., Paul, P., Chen, H.J., Morris, A., Payling, M., Falchi, M., Habgood, J., Panoutsou, S., Winkler, S., Tisato, V., *et al.* (2010). Familial amyotrophic lateral sclerosis is associated with a mutation in D-amino acid oxidase. *Proceedings of the National Academy of Sciences of the United States of America* 107, 7556-7561.

Mitne-Neto, M., Machado-Costa, M., Marchetto, M.C., Bengtson, M.H., Joazeiro, C.A., Tsuda, H., Bellen, H.J., Silva, H.C., Oliveira, A.S., Lazar, M., *et al.* (2011).

Downregulation of VAPB expression in motor neurons derived from induced pluripotent stem cells of ALS8 patients. *Human Molecular Genetics* 20, 3642-3652.

Mitsumoto, H., Santella, R., Liu, X., Bogdanov, M., Zipprich, J., Wu, H.C., Mahata, J., Kilty, M., Bednarz, K., Bell, D., *et al.* (2008). Oxidative stress biomarkers in sporadic ALS. *Amyotrophic Lateral Sclerosis* 9, 177-183.

Mizielinska, S., Gronke, S., Niccoli, T., Ridler, C.E., Clayton, E.L., Devoy, A., Moens, T., Norona, F.E., Woollacott, I.O., Pietrzyk, J., *et al.* (2014). C9orf72 repeat expansions cause neurodegeneration in *Drosophila* through arginine-rich proteins. *Science* 345, 1192-1194.

Mizielinska, S., Lashley, T., Norona, F.E., Clayton, E.L., Ridler, C.E., Fratta, P., and Isaacs, A.M. (2013). C9orf72 frontotemporal lobar degeneration is characterised by frequent neuronal sense and antisense RNA foci. *Acta Neuropathologica* 126, 845-857.

Mizusawa, H. (1993). Hyaline and Skein-like Inclusions in Amyotrophic Lateral Sclerosis. *Neuropathology* 13, 201-208.

Mizushima, N., Noda, T., Yoshimori, T., Tanaka, Y., Ishii, T., George, M.D., Klionsky, D.J., Ohsumi, M., and Ohsumi, Y. (1998). A protein conjugation system essential for autophagy. *Nature* 395, 395.

Moens, T.G., Partridge, L., and Isaacs, A.M. (2017). Genetic models of C9orf72: what is toxic? *Current Opinion in Genetics & Development* 44, 92-101.

Mohandas, E., and Rajmohan, V. (2009). Frontotemporal dementia: An updated overview. *Indian Journal of Psychiatry* 51, S65-S69.

Mokranjac, D., and Neupert, W. (2010). The many faces of the mitochondrial TIM23 complex. *Biochim Biophys Acta* 1797, 1045-1054.

Moller, S., Croning, M.D., and Apweiler, R. (2001). Evaluation of methods for the prediction of membrane spanning regions. *Bioinformatics* 17, 646-653.

Moloney, E.B., de Winter, F., and Verhaagen, J. (2014). ALS as a distal axonopathy: molecular mechanisms affecting neuromuscular junction stability in the presymptomatic stages of the disease. *Frontiers in Neuroscience* 8.

Moore, A.S., and Holzbaur, E.L.F. (2016). Dynamic recruitment and activation of ALS-associated TBK1 with its target optineurin are required for efficient mitophagy. *Proceedings of the National Academy of Sciences of the United States of America* 113, E3349-E3358.

Mori, K., Arzberger, T., Grasser, F.A., Gijssels, I., May, S., Rentzsch, K., Weng, S.M., Schludi, M.H., van der Zee, J., Cruts, M., *et al.* (2013a). Bidirectional transcripts of the expanded C9orf72 hexanucleotide repeat are translated into aggregating dipeptide repeat proteins. *Acta Neuropathol* 126, 881-893.

Mori, K., Lammich, S., Mackenzie, I.R.A., Forné, I., Zilow, S., Kretschmar, H., Edbauer, D., Janssens, J., Kleinberger, G., Cruts, M., *et al.* (2013b). HnRNP A3 binds to GGGGCC repeats and is a constituent of p62-positive/TDP43-negative inclusions in the hippocampus of patients with C9orf72 mutations. *Acta Neuropathologica* 125, 413-423.

Mori, K., Weng, S.M., Arzberger, T., May, S., Rentzsch, K., Kremmer, E., Schmid, B., Kretschmar, H.A., Cruts, M., Van Broeckhoven, C., *et al.* (2013c). The C9orf72 GGGGCC repeat is translated into aggregating dipeptide-repeat proteins in FTL/ALS. *Science* 339, 1335-1338.

Morlino, G., Barreiro, O., Baixauli, F., Robles-Valero, J., Gonzalez-Granado, J.M., Villa-Bellosta, R., Cuenca, J., Sanchez-Sorzano, C.O., Veiga, E., Martin-Cofreces, N.B., *et al.* (2014). Miro-1 links mitochondria and microtubule Dynein motors to control lymphocyte migration and polarity. *Molecular and Cellular Biology* 34, 1412-1426.

- Mórotz, G.M., De Vos, K.J., Vagnoni, A., Ackerley, S., Shaw, C.E., and Miller, C.C.J. (2012). Amyotrophic lateral sclerosis-associated mutant VAPBP56s perturbs calcium homeostasis to disrupt axonal transport of mitochondria. *Human Molecular Genetics* 21, 1979-1988.
- Mortiboys, H., Thomas, K.J., Koopman, W.J., Klaffke, S., Abou-Sleiman, P., Olpin, S., Wood, N.W., Willems, P.H., Smeitink, J.A., Cookson, M.R., *et al.* (2008). Mitochondrial function and morphology are impaired in parkin-mutant fibroblasts. *Ann Neurol* 64, 555-565.
- Müller, J.M., Milenkovic, D., Guiard, B., Pfanner, N., and Chacinska, A. (2008). Precursor oxidation by Mia40 and Erv1 promotes vectorial transport of proteins into the mitochondrial intermembrane space. *Molecular Biology of the Cell* 19, 226-236.
- Münch, C. (2018). The different axes of the mammalian mitochondrial unfolded protein response. *BMC Biology* 16, 81.
- Murphy, M.P. (2009). How mitochondria produce reactive oxygen species. *Biochemical Journal* 417, 1-13.
- Muyderman, H., and Chen, T. (2014). Mitochondrial dysfunction in amyotrophic lateral sclerosis - a valid pharmacological target? *Br J Pharmacol* 171, 2191-2205.
- Nakamura, N., and Hirose, S. (2008). Regulation of mitochondrial morphology by USP30, a deubiquitinating enzyme present in the mitochondrial outer membrane. *Mol Biol Cell* 19, 1903-1911.
- Nakamura, S., and Yoshimori, T. (2017). New insights into autophagosome-lysosome fusion. *J Cell Sci* 130, 1209-1216.
- Naoé, M., Ohwa, Y., Ishikawa, D., Ohshima, C., Nishikawa, S.I., Yamamoto, H., and Endo, T. (2004). Identification of Tim40 that mediates protein sorting to the mitochondrial intermembrane space. *Journal of Biological Chemistry* 279, 47815-47821.
- Napolitano, G., and Ballabio, A. (2016). TFEB at a glance. *Journal of Cell Science* 129, 2475-2481.
- Narendra, D., Tanaka, A., Suen, D.F., and Youle, R.J. (2008). Parkin is recruited selectively to impaired mitochondria and promotes their autophagy. *J Cell Biol* 183, 795-803.
- Narendra, D.P., Jin, S.M., Tanaka, A., Suen, D.F., Gautier, C.A., Shen, J., Cookson, M.R., and Youle, R.J. (2010a). PINK1 is selectively stabilized on impaired mitochondria to activate Parkin. *Plos Biol*, 8.
- Narendra, D.P., Kane, L.A., Hauser, D.N., Fearnley, I.M., and Youle, R.J. (2010b). p62/SQSTM1 is required for Parkin-induced mitochondrial clustering but not mitophagy; VDAC1 is dispensable for both. *Autophagy* 6, 1090-1106.
- Nassif, M., Woehlbier, U., and Manque, P.A. (2017). The Enigmatic Role of C9ORF72 in Autophagy. *Frontiers in Neuroscience* 11, 442.
- Netea-Maier, R.T., Plantinga, T.S., van de Veerdonk, F.L., Smit, J.W., and Netea, M.G. (2016). Modulation of inflammation by autophagy: Consequences for human disease. *Autophagy* 12, 245-260.
- Neumann, M., Sampathu, D.M., Kwong, L.K., Truax, A.C., Micsenyi, M.C., Chou, T.T., Bruce, J., Schuck, T., Grossman, M., Clark, C.M., *et al.* (2006). Ubiquitinated TDP-43 in frontotemporal lobar degeneration and amyotrophic lateral sclerosis. *Science* 314, 130-133.
- Nguyen, T.N., Padman, B.S., Usher, J., Oorschot, V., Ramm, G., and Lazarou, M. (2016). Atg8 family LC3/GAB ARAP proteins are crucial for autophagosome-lysosome

fusion but not autophagosome formation during PINK1/Parkin mitophagy and starvation. *Journal of Cell Biology* 215, 857-874.

Ni, H.-M., Williams, J.A., and Ding, W.-X. (2015). Mitochondrial dynamics and mitochondrial quality control. *Redox Biology* 4, 6-13.

Nishimura, A.L., Mitne-Neto, M., Silva, H.C.A., Richieri-Costa, A., Middleton, S., Cascio, D., Kok, F., Oliveira, J.R.M., Gillingwater, T., Webb, J., *et al.* (2004). A mutation in the vesicle-trafficking protein VAPB causes late-onset spinal muscular atrophy and amyotrophic lateral sclerosis. *American Journal of Human Genetics* 75, 822-831.

Nishimura, N., and Yano, M. (2014). Separation of the Inner and Outer Mitochondrial Membrane in HeLa Cells. *Bio-protocol* 4, e1299.

Nuebel, E., Manganas, P., and Tokatlidis, K. (2016). Orphan proteins of unknown function in the mitochondrial intermembrane space proteome: New pathways and metabolic cross-talk. *Biochim Biophys Acta* 1863, 2613-2623.

O'Rourke, J.G., Bogdanik, L., Yanez, A., Lall, D., Wolf, A.J., Muhammad, A.K., Ho, R., Carmona, S., Vit, J.P., Zarrow, J., *et al.* (2016). C9orf72 is required for proper macrophage and microglial function in mice. *Science* 351, 1324-1329.

Okamoto, K., Hirai, S., Amari, M., Watanabe, M., and Sakurai, A. (1993). Bunina bodies in amyotrophic lateral sclerosis immunostained with rabbit anti-cystatin C serum. *Neuroscience Letters* 162, 125-128.

Okamoto, K., Hirai, S., Shoji, M., Senoh, Y., and Yamazaki, T. (1990). Axonal swellings in the corticospinal tracts in amyotrophic lateral sclerosis. *Acta Neuropathologica* 80, 222-226.

Okamoto, K., Mizuno, Y., and Fujita, Y. (2008). Bunina bodies in amyotrophic lateral sclerosis. *Neuropathology* 28, 109-115.

Okatsu, K., Oka, T., Iguchi, M., Imamura, K., Kosako, H., Tani, N., Kimura, M., Go, E., Koyano, F., Funayama, M., *et al.* (2012). PINK1 autophosphorylation upon membrane potential dissipation is essential for Parkin recruitment to damaged mitochondria. *Nature Communications* 3.

Okatsu, K., Saisho, K., Shimanuki, M., Nakada, K., Shitara, H., Sou, Y., Kimura, M., Sato, S., Hattori, N., Komatsu, M., *et al.* (2010). P62/SQSTM1 cooperates with Parkin for perinuclear clustering of depolarized mitochondria. *Genes to Cells* 15, 887-900.

Onesto, E., Colombrita, C., Gumina, V., Borghi, M.O., Dusi, S., Doretto, A., Fagiolari, G., Invernizzi, F., Moggio, M., Tiranti, V., *et al.* (2016). Gene-specific mitochondria dysfunctions in human TARDBP and C9ORF72 fibroblasts. *Acta Neuropathologica Communications* 4, 47.

Orlacchio, A., Babalini, C., Borreca, A., Patrono, C., Massa, R., Basaran, S., Munhoz, R.P., Rogaeva, E.A., St George-Hyslop, P.H., Bernardi, G., *et al.* (2010). SPATACSN mutations cause autosomal recessive juvenile amyotrophic lateral sclerosis. *Brain* 133, 591-598.

Orr, M.E., Sullivan, A.C., and Frost, B. (2017). A Brief Overview of Tauopathy: Causes, Consequences, and Therapeutic Strategies. *Trends in Pharmacological Sciences* 38, 637-648.

Orsini, M., Oliveira, A.B., Nascimento, O.J., Reis, C.H., Leite, M.A., de Souza, J.A., Pupe, C., de Souza, O.G., Bastos, V.H., de Freitas, M.R., *et al.* (2015). Amyotrophic Lateral Sclerosis: New Perspectives and Update. *Neurology International* 7, 5885.

Ortiz-Sandoval, C.G., Hughes, S.C., Dacks, J.B., and Simmen, T. (2014). Interaction with the effector dynamin-related protein 1 (Drp1) is an ancient function of Rab32 subfamily proteins. *Cellular Logistics* 4, e986399.

- Otera, H., Ishihara, N., and Mihara, K. (2013). New insights into the function and regulation of mitochondrial fission. *Biochimica et Biophysica Acta (BBA) - Molecular Cell Research* 1833, 1256-1268.
- Othumpangat, S., Noti, J.D., and Beezhold, D.H. (2014). Lung epithelial cells resist influenza A infection by inducing the expression of cytochrome c oxidase VIc which is modulated by miRNA 4276. In *Virology (United States: Published by Elsevier Inc.)*, pp. 256-264.
- Otomo, A., Kunita, R., Suzuki-Utsunomiya, K., Ikeda, J.E., and Hadano, S. (2011). Defective relocalization of ALS2/alsin missense mutants to Rac1-induced macropinosomes accounts for loss of their cellular function and leads to disturbed amphisome formation. *FEBS Lett* 585, 730-736.
- Pagliuso, A., Cossart, P., and Stavru, F. (2018). The ever-growing complexity of the mitochondrial fission machinery. *Cellular and Molecular Life Sciences* 75, 355-374.
- Paillusson, S., Stoica, R., Gomez-Suaga, P., Lau, D.H., Mueller, S., Miller, T., and Miller, C.C. (2016). There's Something Wrong with my MAM; the ER-Mitochondria Axis and Neurodegenerative Diseases. *Trends in Neurosciences* 39, 146-157.
- Palecek, J., Lips, M.B., and Keller, B.U. (1999). Calcium dynamics and lowering in motoneurons of the mouse spinal cord. *Journal of Physiology* 520, 485-502.
- Palomo, G.M., Granatiero, V., Kawamata, H., Konrad, C., Kim, M., Arreguin, A.J., Zhao, D., Milner, T.A., and Manfredi, G. (2018). Parkin is a disease modifier in the mutant SOD1 mouse model of ALS. *EMBO Molecular Medicine*.
- Park, J.-S., Davis, R.L., and Sue, C.M. (2018). Mitochondrial Dysfunction in Parkinson's Disease: New Mechanistic Insights and Therapeutic Perspectives. *Current Neurology and Neuroscience Reports* 18, 21.
- Park, S., Choi, S.G., Yoo, S.M., Son, J.H., and Jung, Y.K. (2014). Choline dehydrogenase interacts with SQSTM1/p62 to recruit LC3 and stimulate mitophagy. *Autophagy* 10, 1906-1920.
- Parkinson, N., Ince, P.G., Smith, M.O., Highley, R., Skibinski, G., Andersen, P.M., Morrison, K.E., Pall, H.S., Hardiman, O., Collinge, J., *et al.* (2006). ALS phenotypes with mutations in CHMP2B (charged multivesicular body protein 2B). In *Neurology (United States)*, pp. 1074-1077.
- Pasinelli, P., Belford, M.E., Lennon, N., Bacskai, B.J., Hyman, B.T., Trotti, D., and Brown Jr, R.H. (2004). Amyotrophic lateral sclerosis-associated SOD1 mutant proteins bind and aggregate with Bcl-2 in spinal cord mitochondria. *Neuron* 43, 19-30.
- Paumard, P., Vaillier, J., Coulary, B., Schaeffer, J., Soubannier, V., Mueller, D.M., Brèthes, D., di Rago, J.-P., and Velours, J. (2002). The ATP synthase is involved in generating mitochondrial cristae morphology. *The EMBO Journal* 21, 221-230.
- Payne, B.A., and Chinnery, P.F. (2015). Mitochondrial dysfunction in aging: Much progress but many unresolved questions. *Biochimica et Biophysica Acta* 1847, 1347-1353.
- Pedrini, S., Sau, D., Guareschi, S., Bogush, M., Brown Jr, R.H., Naniche, N., Kia, A., Trotti, D., and Pasinelli, P. (2010). ALS-linked mutant SOD1 damages mitochondria by promoting conformational changes in Bcl-2. *Human Molecular Genetics* 19, 2974-2986.
- Peleh, V., Cordat, E., and Herrmann, J.M. (2016). Mia40 is a trans-site receptor that drives protein import into the mitochondrial intermembrane space by hydrophobic substrate binding. *eLife* 5.

- Perl, A., Gergely, P., Nagy, G., Koncz, A., and Banki, K. (2004). Mitochondrial hyperpolarization: a checkpoint of T-cell life, death and autoimmunity. *Trends in immunology* 25, 360-367.
- Perlin, D.S., Latchney, L.R., and Senior, A.E. (1985). Inhibition of *Escherichia coli* H⁺-ATPase by venturicidin, oligomycin and ossamycin. *Biochim Biophys Acta* 807, 238-244.
- Perry, S.W., Norman, J.P., Barbieri, J., Brown, E.B., and Gelbard, H.A. (2011). Mitochondrial membrane potential probes and the proton gradient: a practical usage guide. *BioTechniques* 50, 98-115.
- Pesiridis, G.S., Lee, V.M., and Trojanowski, J.Q. (2009). Mutations in TDP-43 link glycine-rich domain functions to amyotrophic lateral sclerosis. *Hum Mol Genet* 18, R156-162.
- Petersen, T.N., Brunak, S., von Heijne, G., and Nielsen, H. (2011). SignalP 4.0: discriminating signal peptides from transmembrane regions. *Nat Meth* 8, 785-786.
- Pfeffer, S.R., and Kellogg, D. (2017). Rab GTPases: master regulators that establish the secretory and endocytic pathways. *Molecular Biology of the Cell* 28, 712-715.
- Pickles, S., Destroismaisons, L., Peyrard, S.L., Cadot, S., Rouleau, G.A., Brown, R.H., Julien, J.P., Arbour, N., and Velde, C.V. (2013). Mitochondrial damage revealed by immunoselection for ALS-linked misfolded SOD1. *Human Molecular Genetics* 22, 3947-3959.
- Pickles, S., Semmler, S., Broom, H.R., Destroismaisons, L., Legroux, L., Arbour, N., Meiering, E., Cashman, N.R., and Vande Velde, C. (2016). ALS-linked misfolded SOD1 species have divergent impacts on mitochondria. *Acta Neuropathologica Communications* 4, 43.
- Pickles, S., Vigié, P., and Youle, R.J. (2018). Mitophagy and Quality Control Mechanisms in Mitochondrial Maintenance. *Current Biology* 28, R170-R185.
- Pilli, M., Arko-Mensah, J., Ponpuak, M., Roberts, E., Master, S., Mandell, M.A., Dupont, N., Ornatowski, W., Jiang, S., Bradfute, S.B., *et al.* (2012). TBK-1 promotes autophagy-mediated antimicrobial defense by controlling autophagosome maturation. *Immunity* 37, 223-234.
- Plotegher, N., and Duchen, M.R. (2017). Crosstalk between Lysosomes and Mitochondria in Parkinson's Disease. *Frontiers in Cell and Developmental Biology* 5, 110.
- Polymenidou, M., Lagier-Tourenne, C., Hutt, K.R., Huelga, S.C., Moran, J., Liang, T.Y., Ling, S.C., Sun, E., Wancewicz, E., Mazur, C., *et al.* (2011). Long pre-mRNA depletion and RNA missplicing contribute to neuronal vulnerability from loss of TDP-43. *Nature Neuroscience* 14, 459-468.
- Protter, D.S.W., and Parker, R. (2016). Principles and Properties of Stress Granules. *Trends in Cell Biology* 26, 668-679.
- Prudencio, M., Belzil, V.V., Batra, R., Ross, C.A., Gendron, T.F., Pregent, L.J., Murray, M.E., Overstreet, K.K., Piazza-Johnston, A.E., Desaro, P., *et al.* (2015). Distinct brain transcriptome profiles in C9orf72-associated and sporadic ALS. *Nature neuroscience* 18, 1175-1182.
- Pu, J., Guardia, C.M., Keren-Kaplan, T., and Bonifacino, J.S. (2016). Mechanisms and functions of lysosome positioning. *Journal of Cell Science* 129, 4329-4339.
- Puls, I., Jonnakuty, C., LaMonte, B.H., Holzbaur, E.L.F., Tokito, M., Mann, E., Floeter, M.K., Bidus, K., Drayna, D., Oh, S.J., *et al.* (2003). Mutant dynactin in motor neuron disease. *Nature Genetics* 33, 455-456.

Pylypenko, O., Hammich, H., Yu, I.M., and Houdusse, A. (2018). Rab GTPases and their interacting protein partners: Structural insights into Rab functional diversity. *Small GTPases* 9, 22-48.

Rakhit, R., Cunningham, P., Furtos-Matei, A., Dahan, S., Qi, X.F., Crow, J.P., Cashman, N.R., Kondejewski, L.H., and Chakrabarty, A. (2002). Oxidation-induced misfolding and aggregation of superoxide dismutase and its implications for amyotrophic lateral sclerosis. *Journal of Biological Chemistry* 277, 47551-47556.

Ramasarma, T. (1996). Transmembrane domains participate in functions of integral membrane proteins. *Indian journal of biochemistry & biophysics* 33, 20-29.

Rambold, A.S., and Lippincott-Schwartz, J. (2011). Mechanisms of mitochondria and autophagy crosstalk. *Cell Cycle* 10, 4032-4038.

Ramesh, N., and Pandey, U.B. (2017). Autophagy Dysregulation in ALS: When Protein Aggregates Get Out of Hand. *Frontiers in Molecular Neuroscience* 10, 263.

Randow, F., and Youle, R.J. (2014). Self and non-self: How autophagy targets mitochondria and bacteria. *Cell host & microbe* 15, 403-411.

Ravikumar, B., Imarisio, S., Sarkar, S., O'Kane, C.J., and Rubinsztein, D.C. (2008). Rab5 modulates aggregation and toxicity of mutant huntingtin through macroautophagy in cell and fly models of Huntington disease. *J Cell Sci* 121, 1649-1660.

Reddy, K., Zamiri, B., Stanley, S.Y.R., Macgregor Jr, R.B., and Pearson, C.E. (2013). The disease-associated r(GGGGCC)_n repeat from the C9orf72 gene forms tract length-dependent uni- and multimolecular RNA G-quadruplex structures. *Journal of Biological Chemistry* 288, 9860-9866.

Reina, S., Guarino, F., Magrì, A., and De Pinto, V. (2016). VDAC3 As a Potential Marker of Mitochondrial Status Is Involved in Cancer and Pathology. *Frontiers in Oncology* 6, 264.

Reincke, M., Sbiera, S., Hayakawa, A., Theodoropoulou, M., Osswald, A., Beuschlein, F., Meitinger, T., Mizuno-Yamasaki, E., Kawaguchi, K., Saeki, Y., *et al.* (2015). Mutations in the deubiquitinase gene USP8 cause Cushing's disease. *Nat Genet* 47, 31-38.

Reis, K., Fransson, Å., and Aspenström, P. (2009). The Miro GTPases: At the heart of the mitochondrial transport machinery. *FEBS Letters* 583, 1391-1398.

Renton, A., Majounie, E., Waite, A., Simón-Sánchez, J., Rollinson, S., Gibbs, J., Schymick, J., Laaksovirta, H., van Swieten, J., Myllykangas, L., *et al.* (2011). A hexanucleotide repeat expansion in C9ORF72 is the cause of chromosome 9p21-linked ALS-FTD. *Neuron* 72, 257-268.

Renton, A.E., Chiò, A., and Traynor, B.J. (2014). State of play in amyotrophic lateral sclerosis genetics. *Nature Neuroscience* 17, 17-23.

Riar, A.K., Burstein, S.R., Palomo, G.M., Arreguin, A., Manfredi, G., and Germain, D. (2017). Sex specific activation of the ER α axis of the mitochondrial UPR (UPR(mt)) in the G93A-SOD1 mouse model of familial ALS. *Human Molecular Genetics* 26, 1318-1327.

Richardson, K., Allen, S.P., Mortiboys, H., Grierson, A.J., Wharton, S.B., Ince, P.G., Shaw, P.J., and Heath, P.R. (2013). The effect of SOD1 mutation on cellular bioenergetic profile and viability in response to oxidative stress and influence of mutation-type. *PLoS One* 8, e68256.

Richter, B., Sliter, D.A., Herhaus, L., Stolz, A., Wang, C., Beli, P., Zaffagnini, G., Wild, P., Martens, S., Wagner, S.A., *et al.* (2016). Phosphorylation of OPTN by TBK1 enhances its binding to Ub chains and promotes selective autophagy of damaged

mitochondria. *Proceedings of the National Academy of Sciences of the United States of America* 113, 4039-4044.

Ridley, R.M., Frith, C.D., Crow, T.J., and Conneally, P.M. (1988). Anticipation in Huntington's disease is inherited through the male line but may originate in the female. *Journal of Medical Genetics* 25, 589.

Ritorto, M.S., Ewan, R., Perez-Oliva, A.B., Knebel, A., Buhrlage, S.J., Wightman, M., Kelly, S.M., Wood, N.T., Virdee, S., Gray, N.S., *et al.* (2014). Screening of DUB activity and specificity by MALDI-TOF mass spectrometry. *Nature Communications* 5, 4763.

Rodolfo, C., Campello, S., and Cecconi, F. (2018). Mitophagy in neurodegenerative diseases. *Neurochemistry International* 117, 156-166.

Rogers, R.S., Tungtur, S., Tanaka, T., Nadeau, L.L., Badawi, Y., Wang, H., Ni, H.M., Ding, W.X., and Nishimune, H. (2017). Impaired Mitophagy Plays a Role in Denervation of Neuromuscular Junctions in ALS Mice. *Front Neurosci* 11, 473.

Rogov, V., Dotsch, V., Johansen, T., and Kirkin, V. (2014). Interactions between autophagy receptors and ubiquitin-like proteins form the molecular basis for selective autophagy. *Mol Cell* 53, 167-178.

Rogov, V.V., Stolz, A., Ravichandran, A.C., Rios-Szwed, D.O., Suzuki, H., Kniss, A., Lohr, F., Wakatsuki, S., Dotsch, V., Dikic, I., *et al.* (2017). Structural and functional analysis of the GABARAP interaction motif (GIM). *EMBO Rep* 18, 1382-1396.

Rohrer, J.D., Guerreiro, R., Vandrovicova, J., Uphill, J., Reiman, D., Beck, J., Isaacs, A.M., Authier, A., Ferrari, R., Fox, N.C., *et al.* (2009). The heritability and genetics of frontotemporal lobar degeneration. *Neurology* 73, 1451-1456.

Rosen, D.R., Siddique, T., Patterson, D., Figlewicz, D.A., Sapp, P., Hentati, A., Donaldson, D., Goto, J., O'Regan, J.P., Deng, H.X., *et al.* (1993). Mutations in Cu/Zn superoxide dismutase gene are associated with familial amyotrophic lateral sclerosis. *Nature* 362, 59-62.

Rossi, S., Serrano, A., Gerbino, V., Giorgi, A., Di Francesco, L., Nencini, M., Bozzo, F., Schinina, M.E., Bagni, C., Cestra, G., *et al.* (2015). Nuclear accumulation of mRNAs underlies G4C2-repeat-induced translational repression in a cellular model of C9orf72 ALS. *J Cell Sci* 128, 1787-1799.

Rothstein, J.D., Martin, L.J., and Kuncl, R.W. (1992). Decreased glutamate transport by the brain and spinal cord in amyotrophic lateral sclerosis. *New England Journal of Medicine* 326, 1464-1468.

Row, P.E., Liu, H., Hayes, S., Welchman, R., Charalabous, P., Hofmann, K., Clague, M.J., Sanderson, C.M., and Urbe, S. (2007). The MIT domain of UBPY constitutes a CHMP binding and endosomal localization signal required for efficient epidermal growth factor receptor degradation. *J Biol Chem* 282, 30929-30937.

Row, P.E., Prior, I.A., McCullough, J., Clague, M.J., and Urbé, S. (2006). The ubiquitin isopeptidase UBPY regulates endosomal ubiquitin dynamics and is essential for receptor down-regulation. *Journal of Biological Chemistry* 281, 12618-12624.

Ryan, B.J., Hoek, S., Fon, E.A., and Wade-Martins, R. (2015). Mitochondrial dysfunction and mitophagy in Parkinson's: from familial to sporadic disease. *Trends in Biochemical Sciences* 40, 200-210.

Ryan, M.T., Voos, W., and Pfanner, N. (2001). Assaying protein import into mitochondria. *Methods Cell Biol* 65, 189-215.

Saberi, S., Stauffer, J.E., Schulte, D.J., and Ravits, J. (2015). "Neuropathology of amyotrophic lateral sclerosis and its variants". *Neurologic clinics* 33, 855-876.

Saito, T., and Sadoshima, J. (2018). Abstract 19501: Ulk1 Induces Mitochondrial Autophagy by Regulating Mitochondrial Fission and Alternative Autophagy in the Heart. *Circulation Research* 134, A19501.

Saitoh, T., Fujita, N., Jang, M.H., Uematsu, S., Yang, B.G., Satoh, T., Omori, H., Noda, T., Yamamoto, N., Komatsu, M., *et al.* (2008). Loss of the autophagy protein Atg16L1 enhances endotoxin-induced IL-1 β production. *Nature* 456, 264-268.

Sakowska, P., Jans, D.C., Mohanraj, K., Riedel, D., Jakobs, S., and Chacinska, A. (2015). The Oxidation Status of Mic19 Regulates MICOS Assembly. *Mol Cell Biol* 35, 4222-4237.

Santel, A., and Fuller, M.T. (2001). Control of mitochondrial morphology by a human mitofusin. *Journal of Cell Science* 114, 867.

Sapp, P.C., Hosler, B.A., McKenna-Yasek, D., Chin, W., Gann, A., Genise, H., Gorenstein, J., Huang, M., Sailer, W., Scheffler, M., *et al.* (2003). Identification of two novel loci for dominantly inherited familial amyotrophic lateral sclerosis. *American Journal of Human Genetics* 73, 397-403.

Sareen, D., O'Rourke, J.G., Meera, P., Muhammad, A.K.M.G., Grant, S., Simpkinson, M., Bell, S., Carmona, S., Ornelas, L., Sahabian, A., *et al.* (2013). Targeting RNA foci in iPSC-derived motor neurons from ALS patients with a C9ORF72 repeat expansion. *Science Translational Medicine* 5.

Sarraf, S.A., Raman, M., Guarani-Pereira, V., Sowa, M.E., Huttlin, E.L., Gygi, S.P., and Harper, J.W. (2013). Landscape of the PARKIN-dependent ubiquitylome in response to mitochondrial depolarization. *Nature* 496, 372-376.

Sasaki, S., and Iwata, M. (1996). Ultrastructural study of synapses in the anterior horn neurons of patients with amyotrophic lateral sclerosis. *Neuroscience Letters* 204, 53-56.

Sasaki, S., and Iwata, M. (2007). Mitochondrial alterations in the spinal cord of patients with sporadic amyotrophic lateral sclerosis. *Journal of Neuropathology and Experimental Neurology* 66, 10-16.

Sasaki, S., Maruyama, S., Yamane, K., Sakuma, H., and Takeishi, M. (1989). Swellings of proximal axons in a case of motor neuron disease. *Ann Neurol* 25, 520-522.

Sato, T., Iwano, T., Kunii, M., Matsuda, S., Mizuguchi, R., Jung, Y., Hagiwara, H., Yoshihara, Y., Yuzaki, M., Harada, R., *et al.* (2014). Rab8a and Rab8b are essential for several apical transport pathways but insufficient for ciliogenesis. *J Cell Sci* 127, 422-431.

Schaaf, M.B., Keulers, T.G., Vooijs, M.A., and Rouschop, K.M. (2016). LC3/GABARAP family proteins: autophagy-(un)related functions. *FASEB journal : official publication of the Federation of American Societies for Experimental Biology* 30, 3961-3978.

Schagger, H. (2006). Tricine-SDS-PAGE. *Nature protocols* 1, 16-22.

Schindelin, J., Arganda-Carreras, I., Frise, E., Kaynig, V., Longair, M., Pietzsch, T., Preibisch, S., Rueden, C., Saalfeld, S., Schmid, B., *et al.* (2012). Fiji: an open-source platform for biological-image analysis. *Nature methods* 9, 676-682.

Schlachetzki, J.C., Saliba, S.W., and Oliveira, A.C. (2013). Studying neurodegenerative diseases in culture models. *Revista brasileira de psiquiatria (Sao Paulo, Brazil : 1999)* 35 Suppl 2, S92-100.

Schluter, O.M., Basu, J., Sudhof, T.C., and Rosenmund, C. (2006). Rab3 superprimes synaptic vesicles for release: implications for short-term synaptic plasticity. *J Neurosci* 26, 1239-1246.

- Schmidt, O., Pfanner, N., and Meisinger, C. (2010). Mitochondrial protein import: From proteomics to functional mechanisms. *Nature Reviews Molecular Cell Biology* 11, 655-667.
- Schoer, J.K., Gallegos, A.M., McIntosh, A.L., Starodub, O., Kier, A.B., Billheimer, J.T., and Schroeder, F. (2000). Lysosomal Membrane Cholesterol Dynamics. *Biochemistry* 39, 7662-7677.
- Schratt, G. (2009). microRNAs at the synapse. *Nature Reviews Neuroscience* 10, 842.
- Schrepfer, E., and Scorrano, L. (2016). Mitofusins, from Mitochondria to Metabolism. *Mol Cell* 61, 683-694.
- Schroder, B., Wrocklage, C., Pan, C., Jager, R., Kusters, B., Schafer, H., Elsasser, H.P., Mann, M., and Hasilik, A. (2007). Integral and associated lysosomal membrane proteins. *Traffic (Copenhagen, Denmark)* 8, 1676-1686.
- Schweers, R.L., Zhang, J., Randall, M.S., Loyd, M.R., Li, W., Dorsey, F.C., Kundu, M., Opferman, J.T., Cleveland, J.L., Miller, J.L., *et al.* (2007). NIX is required for programmed mitochondrial clearance during reticulocyte maturation. *Proc Natl Acad Sci U S A* 104, 19500-19505.
- Schwenk, B.M., Lang, C.M., Hognl, S., Tahirovic, S., Orozco, D., Rentzsch, K., Lichtenthaler, S.F., Hoogenraad, C.C., Capell, A., Haass, C., *et al.* (2014). The FTL risk factor TMEM106B and MAP6 control dendritic trafficking of lysosomes. *The EMBO Journal* 33, 450-467.
- Scotter, E.L., Chen, H.J., and Shaw, C.E. (2015). TDP-43 Proteinopathy and ALS: Insights into Disease Mechanisms and Therapeutic Targets. *Neurotherapeutics* 12, 352-363.
- Seibenhener, M.L., Du, Y., Diaz-Meco, M.T., Moscat, J., Wooten, M.C., and Wooten, M.W. (2013). A role for sequestosome 1/p62 in mitochondrial dynamics, Import and genome integrity. *Biochimica et Biophysica Acta - Molecular Cell Research* 1833, 452-459.
- Sellier, C., Campanari, M.L., Julie Corbier, C., Gaucherot, A., Kolb-Cheynel, I., Oulad-Abdelghani, M., Ruffenach, F., Page, A., Ciura, S., Kabashi, E., *et al.* (2016). Loss of C9ORF72 impairs autophagy and synergizes with polyQ Ataxin-2 to induce motor neuron dysfunction and cell death. *EMBO J* 35, 1276-1297.
- Selvaraj, B.T., Livesey, M.R., and Chandran, S. (2017). Modeling the C9ORF72 repeat expansion mutation using human induced pluripotent stem cells. *Brain Pathol* 27, 518-524.
- Seo, A.Y., Joseph, A.M., Dutta, D., Hwang, J.C., Aris, J.P., and Leeuwenburgh, C. (2010). New insights into the role of mitochondria in aging: mitochondrial dynamics and more. *J Cell Sci* 123, 2533-2542.
- Sesaki, H., Southard, S.M., Aiken Hobbs, A.E., and Jensen, R.E. (2003). Cells lacking Pcp1p/Ugo2p, a rhomboid-like protease required for Mgm1p processing, lose mtDNA and mitochondrial structure in a Dnm1p-dependent manner, but remain competent for mitochondrial fusion. *Biochemical and Biophysical Research Communications* 308, 276-283.
- Seto, S., Sugaya, K., Tsujimura, K., Nagata, T., Horii, T., and Koide, Y. (2013). Rab39a interacts with phosphatidylinositol 3-kinase and negatively regulates autophagy induced by lipopolysaccharide stimulation in macrophages. *PLoS One* 8, e83324.
- Settembre, C., Zoncu, R., Medina, D.L., Vetrini, F., Erdin, S., Erdin, S., Huynh, T., Ferron, M., Karsenty, G., Vellard, M.C., *et al.* (2012). A lysosome-to-nucleus signalling

mechanism senses and regulates the lysosome via mTOR and TFEB. *Embo j* 31, 1095-1108.

Shahheydari, H., Ragagnin, A., Walker, A.K., Toth, R.P., Vidal, M., Jagaraj, C.J., Perri, E.R., Konopka, A., Sultana, J.M., and Atkin, J.D. (2017). Protein Quality Control and the Amyotrophic Lateral Sclerosis/Frontotemporal Dementia Continuum. *Frontiers in Molecular Neuroscience* 10, 119.

Shaid, S., Brandts, C.H., Serve, H., and Dikic, I. (2013). Ubiquitination and selective autophagy. *Cell death and differentiation* 20, 21-30.

Shan, X., Chiang, P.M., Price, D.L., and Wong, P.C. (2010). Altered distributions of Gemini of coiled bodies and mitochondria in motor neurons of TDP-43 transgenic mice. *Proceedings of the National Academy of Sciences of the United States of America* 107, 16325-16330.

Shanbhag, R., Shi, G., Rujiviphat, J., and McQuibban, G.A. (2012). The Emerging Role of Proteolysis in Mitochondrial Quality Control and the Etiology of Parkinson's Disease. *Parkinson's Disease* 2012, 382175.

Shang, Y., and Huang, E.J. (2016). Mechanisms of FUS Mutations in Familial Amyotrophic Lateral Sclerosis. *Brain research* 1647, 65-78.

Sharma, A., Lyashchenko, A.K., Lu, L., Nasrabad, S.E., Elmaleh, M., Mendelsohn, M., Nemes, A., Tapia, J.C., Mentis, G.Z., and Shneider, N.A. (2016). ALS-associated mutant FUS induces selective motor neuron degeneration through toxic gain of function. *Nature Communications* 7, 10465.

Shaw, P.J., and Eggett, C.J. (2000). Molecular factors underlying selective vulnerability of motor neurons to neurodegeneration in amyotrophic lateral sclerosis. *Journal of Neurology, Supplement* 247, 17-27.

Shaw, P.J., Ince, P.G., Falkous, G., and Mantle, D. (1995). Oxidative damage to protein in sporadic motor neuron disease spinal cord. *Annals of Neurology* 38, 691-695.

Shen, W.C., Li, H.Y., Chen, G.C., Chern, Y., and Tu, P.H. (2015). Mutations in the ubiquitin-binding domain of OPTN/optineurin interfere with autophagy-mediated degradation of misfolded proteins by a dominant-negative mechanism. *Autophagy* 11, 685-700.

Shi, P., Ström, A.-L., Gal, J., and Zhu, H. (2010). Effects of ALS-related SOD1 mutants on dynein- and KIF5-mediated retrograde and anterograde axonal transport. *Biochimica et Biophysica Acta (BBA) - Molecular Basis of Disease* 1802, 707-716.

Shi, R., Guberman, M., and Kirshenbaum, L.A. (2018a). Mitochondrial quality control: The role of mitophagy in aging. *Trends in Cardiovascular Medicine* 28, 246-260.

Shi, R.Y., Zhu, S.H., Li, V., Gibson, S.B., Xu, X.S., and Kong, J.M. (2014). BNIP3 interacting with LC3 triggers excessive mitophagy in delayed neuronal death in stroke. *CNS neuroscience & therapeutics* 20, 1045-1055.

Shi, Y., Lin, S., Staats, K.A., Li, Y., Chang, W.H., Hung, S.T., Hendricks, E., Linares, G.R., Wang, Y., Son, E.Y., *et al.* (2018b). Haploinsufficiency leads to neurodegeneration in C9ORF72 ALS/FTD human induced motor neurons. *Nat Med*.

Shiba-Fukushima, K., Imai, Y., Yoshida, S., Ishihama, Y., Kanao, T., Sato, S., and Hattori, N. (2012). PINK1-mediated phosphorylation of the Parkin ubiquitin-like domain primes mitochondrial translocation of Parkin and regulates mitophagy. *Scientific Reports* 2.

Shibata, N., Nagai, R., Uchida, K., Horiuchi, S., Yamada, S., Hirano, A., Kawaguchi, M., Yamamoto, T., Sasaki, S., and Kobayashi, M. (2001). Morphological evidence for lipid

peroxidation and protein glycooxidation in spinal cords from sporadic amyotrophic lateral sclerosis patients. *Brain Research* 917, 97-104.

Shin, D., Na, W., Lee, J.-H., Kim, G., Baek, J., Park, S.H., Choi, C.Y., and Lee, S. (2017). Site-specific monoubiquitination downregulates Rab5 by disrupting effector binding and guanine nucleotide conversion. *eLife* 6, e29154.

Shlevkov, E., Kramer, T., Schapansky, J., LaVoie, M.J., and Schwarz, T.L. (2016). Miro phosphorylation sites regulate Parkin recruitment and mitochondrial motility. *Proceedings of the National Academy of Sciences of the United States of America* 113, E6097-E6106.

Shpilka, T., and Haynes, C.M. (2017). The mitochondrial UPR: mechanisms, physiological functions and implications in ageing. *Nature Reviews Molecular Cell Biology* 19, 109.

Sicot, G., and Gomes-Pereira, M. (2013). RNA toxicity in human disease and animal models: From the uncovering of a new mechanism to the development of promising therapies. *Biochimica et Biophysica Acta (BBA) - Molecular Basis of Disease* 1832, 1390-1409.

Sievers, F., Wilm, A., Dineen, D., Gibson, T.J., Karplus, K., Li, W., Lopez, R., McWilliam, H., Remmert, M., Soding, J., *et al.* (2011). Fast, scalable generation of high-quality protein multiple sequence alignments using Clustal Omega. *Molecular systems biology* 7, 539.

Siklós, L., Engelhardt, J., Harati, Y., Smith, R.G., Joó, F., and Appel, S.H. (1996). Ultrastructural evidence for altered calcium in motor nerve terminals in amyotrophic lateral sclerosis. *Annals of Neurology* 39, 203-216.

Siklos, L., Engelhardt, J.I., Alexianu, M.E., Gurney, M.E., Siddique, T., and Appel, S.H. (1998). Intracellular calcium parallels motoneuron degeneration in SOD-1 mutant mice. *Journal of Neuropathology & Experimental Neurology* 57, 571-587.

Simone, R., Balendra, R., Moens, T.G., Preza, E., Wilson, K.M., Heslegrave, A., Woodling, N.S., Niccoli, T., Gilbert-Jaramillo, J., Abdelkarim, S., *et al.* (2018). G-quadruplex-binding small molecules ameliorate C9orf72 FTD/ALS pathology in vitro and in vivo. *EMBO Mol Med* 10, 22-31.

Simpson, C.L., Lemmens, R., Miskiewicz, K., Broom, W.J., Hansen, V.K., van Vught, P.W., Landers, J.E., Sapp, P., Van Den Bosch, L., Knight, J., *et al.* (2009). Variants of the elongator protein 3 (ELP3) gene are associated with motor neuron degeneration. *Hum Mol Genet* 18, 472-481.

Simpson, E.P., Henry, Y.K., Henkel, J.S., Smith, R.G., and Appel, S.H. (2004). Increased lipid peroxidation in sera of ALS patients: A potential biomarker of disease burden. *Neurology* 62, 1758-1765.

Singer, S.J. (1974). The Molecular Organization of Membranes. *Annual review of biochemistry* 43, 805-833.

Sivadasan, R., Hornburg, D., Drepper, C., Frank, N., Jablonka, S., Hansel, A., Lojewski, X., Sternecker, J., Hermann, A., Shaw, P.J., *et al.* (2016). C9ORF72 interaction with cofilin modulates actin dynamics in motor neurons. *Nat Neurosci* 19, 1610-1618.

Skourti-Stathaki, K., and Proudfoot, N.J. (2014). A double-edged sword: R loops as threats to genome integrity and powerful regulators of gene expression. *Genes Dev* 28, 1384-1396.

Sliter, D.A., Martinez, J., Hao, L., Chen, X., Sun, N., Fischer, T.D., Burman, J.L., Li, Y., Zhang, Z., Narendra, D.P., *et al.* (2018). Parkin and PINK1 mitigate STING-induced inflammation. *Nature*.

- Smith, A.C., and Robinson, A.J. (2016). MitoMiner v3.1, an update on the mitochondrial proteomics database. *Nucleic Acids Res* *44*, D1258-1261.
- Smith, B.N., Ticozzi, N., Fallini, C., Gkazi, A.S., Topp, S., Kenna, K.P., Scotter, E.L., Kost, J., Keagle, P., Miller, J.W., *et al.* (2014). Exome-wide rare variant analysis identifies TUBA4A mutations associated with familial ALS. *Neuron* *84*, 324-331.
- Smith, B.N., Topp, S.D., Fallini, C., Shibata, H., Chen, H.J., Troakes, C., King, A., Ticozzi, N., Kenna, K.P., Soragia-Gkazi, A., *et al.* (2017a). Mutations in the vesicular trafficking protein annexin A11 are associated with amyotrophic lateral sclerosis. *Sci Transl Med* *9*.
- Smith, E.F., Shaw, P.J., and De Vos, K.J. (2017b). The role of mitochondria in amyotrophic lateral sclerosis. *Neurosci Lett*.
- Smith, R.G., Henry, Y.K., Mattson, M.P., and Appel, S.H. (1998). Presence of 4-hydroxynonenal in cerebrospinal fluid of patients with sporadic amyotrophic lateral sclerosis. *Annals of Neurology* *44*, 696-699.
- Soleimanpour, S.A., Gupta, A., Bakay, M., Ferrari, A.M., Groff, D.N., Fadista, J., Spruce, L.A., Kushner, J.A., Groop, L., Seeholzer, S.H., *et al.* (2014). The diabetes susceptibility gene Clec16a regulates mitophagy. *Cell* *157*, 1577-1590.
- Son, J.H., Shim, J.H., Kim, K.H., Ha, J.Y., and Han, J.Y. (2012). Neuronal autophagy and neurodegenerative diseases. *Experimental & molecular medicine* *44*, 89-98.
- Son, M., Puttappathi, K., Kawamata, H., Rajendran, B., Boyer, P.J., Manfredi, G., and Elliott, J.L. (2007). Overexpression of CCS in G93A-SOD1 mice leads to accelerated neurological deficits with severe mitochondrial pathology. *Proceedings of the National Academy of Sciences of the United States of America* *104*, 6072-6077.
- Song, W., Song, Y., Kincaid, B., Bossy, B., and Bossy-Wetzler, E. (2013). Mutant SOD1G93A triggers mitochondrial fragmentation in spinal cord motor neurons: Neuroprotection by SIRT3 and PGC-1 α . *Neurobiology of Disease* *51*, 72-81.
- Sonnhammer, E.L., von Heijne, G., and Krogh, A. (1998). A hidden Markov model for predicting transmembrane helices in protein sequences. *Proceedings International Conference on Intelligent Systems for Molecular Biology* *6*, 175-182.
- Sotelo-Silveira, J.R., Lepanto, P., Elizondo, V., Horjales, S., Palacios, F., Martinez-Palma, L., Marin, M., Beckman, J.S., and Barbeito, L. (2009). Axonal mitochondrial clusters containing mutant SOD1 in transgenic models of ALS. *Antioxidants and Redox Signaling* *11*, 1535-1545.
- Soubannier, V., McLelland, G.L., Zunino, R., Braschi, E., Rippstein, P., Fon, E.A., and McBride, H.M. (2012a). A vesicular transport pathway shuttles cargo from mitochondria to lysosomes. *Current Biology* *22*, 135-141.
- Soubannier, V., Rippstein, P., Kaufman, B.A., Shoubridge, E.A., and McBride, H.M. (2012b). Reconstitution of mitochondria derived vesicle formation demonstrates selective enrichment of oxidized cargo. *Plos One*, *7*.
- Sowter, H.M., Ratcliffe, P.J., Watson, P., Greenberg, A.H., and Harris, A.L. (2001). HIF-1-dependent regulation of hypoxic induction of the cell death factors BNIP3 and NIX in human tumors. *Cancer Research* *61*, 6669-6673.
- Spence, E.F., and Soderling, S.H. (2015). Actin Out: Regulation of the Synaptic Cytoskeleton. *J Biol Chem* *290*, 28613-28622.
- Sproul, D., and Meehan, R.R. (2013). Genomic insights into cancer-associated aberrant CpG island hypermethylation. *Briefings in Functional Genomics* *12*, 174-190.

- Sreedharan, J., Blair, I.P., Tripathi, V.B., Hu, X., Vance, C., Rogelj, B., Ackerley, S., Durnall, J.C., Williams, K.L., Buratti, E., *et al.* (2008). TDP-43 mutations in familial and sporadic amyotrophic lateral sclerosis. *Science* 319, 1668-1672.
- Stagi, M., Klein, Z.A., Gould, T.J., Bewersdorf, J., and Strittmatter, S.M. (2014). Lysosome size, motility and stress response regulated by fronto-temporal dementia modifier TMEM106B. *Mol Cell Neurosci* 61, 226-240.
- Starr, A., and Sattler, R. (2018). Synaptic dysfunction and altered excitability in C9ORF72 ALS/FTD. *Brain Research* 1693, 98-108.
- Steiner, H., Zollner, A., Haid, A., Neupert, W., and Lill, R. (1995). Biogenesis of mitochondrial heme lyases in yeast. Import and folding in the intermembrane space. *Journal of Biological Chemistry* 270, 22842-22849.
- Stewart, H., Rutherford, N.J., Briemberg, H., Krieger, C., Cashman, N., Fabros, M., Baker, M., Fok, A., DeJesus-Hernandez, M., Eisen, A., *et al.* (2012). Clinical and pathological features of amyotrophic lateral sclerosis caused by mutation in the C9ORF72 gene on chromosome 9p. *Acta Neuropathologica* 123, 409-417.
- Stoica, R., De Vos, K.J., Paillusson, S., Mueller, S., Sancho, R.M., Lau, K.F., Vizcay-Barrena, G., Lin, W.L., Xu, Y.F., Lewis, J., *et al.* (2014). ER-mitochondria associations are regulated by the VAPB-PTPIP51 interaction and are disrupted by ALS/FTD-associated TDP-43. *Nature Communications* 5, 3996.
- Stoica, R., Paillusson, S., Gomez-Suaga, P., Mitchell, J.C., Lau, D.H., Gray, E.H., Sancho, R.M., Vizcay-Barrena, G., De Vos, K.J., Shaw, C.E., *et al.* (2016). ALS/FTD-associated FUS activates GSK-3beta to disrupt the VAPB-PTPIP51 interaction and ER-mitochondria associations. *EMBO Reports* 17, 1326-1342.
- Strappazzon, F., Nazio, F., Corrado, M., Cianfanelli, V., Romagnoli, A., Fimia, G.M., Campello, S., Nardacci, R., Piacentini, M., Campanella, M., *et al.* (2015). AMBRA1 is able to induce mitophagy via LC3 binding, regardless of PARKIN and p62/SQSTM1. *Cell Death and Differentiation* 22, 419-432.
- Stribl, C., Samara, A., Trümbach, D., Peis, R., Neumann, M., Fuchs, H., Gailus-Durner, V., Hrabě de Angelis, M., Rathkolb, B., Wolf, E., *et al.* (2014). Mitochondrial Dysfunction and Decrease in Body Weight of a Transgenic Knock-in Mouse Model for TDP-43. *Journal of Biological Chemistry* 289, 10769–10784.
- Sudria-Lopez, E., Koppers, M., de Wit, M., van der Meer, C., Westeneng, H.J., Zundel, C.A., Youssef, S.A., Harkema, L., de Bruin, A., Veldink, J.H., *et al.* (2016). Full ablation of C9orf72 in mice causes immune system-related pathology and neoplastic events but no motor neuron defects. *Acta Neuropathol* 132, 145-147.
- Sugiura, A., McLelland, G.L., Fon, E.A., and McBride, H.M. (2014). A new pathway for mitochondrial quality control: mitochondrial-derived vesicles. *Embo j* 33, 2142-2156.
- Suh, E., Lee, E.B., Neal, D., Wood, E.M., Toledo, J.B., Rennert, L., Irwin, D.J., McMillan, C.T., Krock, B., Elman, L.B., *et al.* (2015). Semi-automated quantification of C9orf72 expansion size reveals inverse correlation between hexanucleotide repeat number and disease duration in frontotemporal degeneration. *Acta Neuropathol* 130, 363-372.
- Sullivan, P.M., Zhou, X., Robins, A.M., Paushter, D.H., Kim, D., Smolka, M.B., and Hu, F. (2016). The ALS/FTLD associated protein C9orf72 associates with SMCR8 and WDR41 to regulate the autophagy-lysosome pathway. *Acta Neuropathologica Communications* 4, 51.
- Sun, J., Hu, Q., Peng, H., Peng, C., Zhou, L., Lu, J., and Huang, C. (2018). The ubiquitin-specific protease USP8 deubiquitinates and stabilizes Cx43. *J Biol Chem* 293, 8275-8284.

- Sun, N., Malide, D., Liu, J., Rovira, I., Combs, C.A., and Finkel, T. (2017). A fluorescence-based imaging method to measure in vitro and in vivo mitophagy using mt-Keima. *Nature protocols* 12, 1576-1587.
- Sun, N., Youle, R.J., and Finkel, T. (2016). The Mitochondrial Basis of Aging. *Molecular cell* 61, 654-666.
- Sun, N., Yun, J., Liu, J., Malide, D., Liu, C., Rovira, I., Holmstrom, K.M., Fergusson, M.M., Yoo, Y.H., Combs, C.A., *et al.* (2015). Measuring In Vivo Mitophagy. *Mol Cell* 60, 685-696.
- Sun, Y., Vashisht, A.A., Tchieu, J., Wohlschlegel, J.A., and Dreier, L. (2012). Voltage-dependent Anion Channels (VDACs) Recruit Parkin to Defective Mitochondria to Promote Mitochondrial Autophagy. *The Journal of Biological Chemistry* 287, 40652-40660.
- Sung, H., Tandarich, L.C., Nguyen, K., and Hollenbeck, P.J. (2016). Compartmentalized Regulation of Parkin-Mediated Mitochondrial Quality Control in the Drosophila Nervous System In Vivo. *J Neurosci* 36, 7375-7391.
- Swinnen, B., and Robberecht, W. (2014). The phenotypic variability of amyotrophic lateral sclerosis. *Nature Reviews Neurology* 10, 661-670.
- Szatmari, Z., Kis, V., Lippai, M., Hegedus, K., Farago, T., Lorincz, P., Tanaka, T., Juhasz, G., and Sass, M. (2014). Rab11 facilitates cross-talk between autophagy and endosomal pathway through regulation of Hook localization. *Mol Biol Cell* 25, 522-531.
- Tadic, V., Prell, T., Lautenschlaeger, J., and Grosskreutz, J. (2014). The ER mitochondria calcium cycle and ER stress response as therapeutic targets in amyotrophic lateral sclerosis. *Frontiers in Cellular Neuroscience* 8, 147.
- Tagashira, H., Shinoda, Y., Shioda, N., and Fukunaga, K. (2014). Methyl pyruvate rescues mitochondrial damage caused by SIGMAR1 mutation related to amyotrophic lateral sclerosis. *Biochimica et Biophysica Acta* 1840, 3320-3334.
- Takahashi, Y., Fukuda, Y., Yoshimura, J., Toyoda, A., Kurppa, K., Moritoyo, H., Belzil, V.V., Dion, P.A., Higasa, K., Doi, K., *et al.* (2013). ERBB4 mutations that disrupt the neuregulin-ErbB4 pathway cause amyotrophic lateral sclerosis type 19. *Am J Hum Genet* 93, 900-905.
- Talaber, G., Miklossy, G., Oaks, Z., Liu, Y., Tooze, S.A., Chudakov, D.M., Banki, K., and Perl, A. (2014). HRES-1/Rab4 Promotes the Formation of LC3+ Autophagosomes and the Accumulation of Mitochondria during Autophagy. *PLOS ONE* 9, e84392.
- Tan, W., Nanche, N., Bogush, A., Pedrini, S., Trotti, D., and Pasinelli, P. (2013). Small peptides against the mutant SOD1/Bcl-2 toxic mitochondrial complex restore mitochondrial function and cell viability in mutant SOD1-mediated ALS. *Journal of Neuroscience* 33, 11588-11598.
- Tanaka, A., Cleland, M.M., Xu, S., Narendra, D.P., Suen, D.F., Karbowski, M., and Youle, R.J. (2010). Proteasome and p97 mediate mitophagy and degradation of mitofusins induced by Parkin. *Journal of Cell Biology* 191, 1367-1380.
- Tanaka, K. (2009). The proteasome: Overview of structure and functions. *Proceedings of the Japan Academy Series B, Physical and Biological Sciences* 85, 12-36.
- Tang, W.K., and Xia, D. (2016). Mutations in the Human AAA+ Chaperone p97 and Related Diseases. *Frontiers in Molecular Biosciences* 3, 79.
- Tao, Z., Wang, H., Xia, Q., Li, K., Li, K., Jiang, X., Xu, G., Wang, G., and Ying, Z. (2015). Nucleolar stress and impaired stress granule formation contribute to C9orf72 RAN translation-induced cytotoxicity. *Hum Mol Genet* 24, 2426-2441.

- Tateno, M., Kato, S., Sakurai, T., Nukina, N., Takahashi, R., and Araki, T. (2009). Mutant SOD1 impairs axonal transport of choline acetyltransferase and acetylcholine release by sequestering KAP3. *Human Molecular Genetics* 18, 942-955.
- Taylor, J.P., Brown Jr, R.H., and Cleveland, D.W. (2016). Decoding ALS: from genes to mechanism. *Nature* 539, 197.
- Terziyska, N., Lutz, T., Kozany, C., Mokranjac, D., Mesecke, N., Neupert, W., Herrmann, J.M., and Hell, K. (2005). Mia40, a novel factor for protein import into the intermembrane space of mitochondria is able to bind metal ions. *FEBS Letters* 579, 179-184.
- Thau, N., Knippenberg, S., Körner, S., Rath, K.J., Dengler, R., and Petri, S. (2012). Decreased mRNA expression of PGC-1 α and PGC-1 α regulated factors in the SOD1G93A ALS mouse model and in human sporadic ALS. *Journal of Neuropathology and Experimental Neurology* 71, 1064-1074.
- Therrien, M., Rouleau, G.A., Dion, P.A., and Parker, J.A. (2013). Deletion of C9ORF72 results in motor neuron degeneration and stress sensitivity in *C. elegans*. *PLoS ONE* 8.
- Thys, R.G., and Wang, Y.H. (2015). DNA Replication Dynamics of the GGGGCC Repeat of the C9orf72 Gene. *J Biol Chem* 290, 28953-28962.
- Tian, W., Li, W., Chen, Y., Yan, Z., Huang, X., Zhuang, H., Zhong, W., Chen, Y., Wu, W., Lin, C., *et al.* (2015). Phosphorylation of ULK1 by AMPK regulates translocation of ULK1 to mitochondria and mitophagy. *FEBS Lett* 589, 1847-1854.
- Ticozzi, N., Vance, C., Leclerc, A.L., Keagle, P., Glass, J.D., McKenna-Yasek, D., Sapp, P.C., Silani, V., Bosco, D.A., Shaw, C.E., *et al.* (2011). Mutational analysis reveals the FUS homolog TAF15 as a candidate gene for familial amyotrophic lateral sclerosis. *American journal of medical genetics Part B, Neuropsychiatric genetics : the official publication of the International Society of Psychiatric Genetics* 156b, 285-290.
- Tilokani, L., Nagashima, S., Paupe, V., and Prudent, J. (2018). Mitochondrial dynamics: overview of molecular mechanisms. *Essays Biochem* 62, 341-360.
- Todd, T.W., and Petrucelli, L. (2016). Insights into the pathogenic mechanisms of Chromosome 9 open reading frame 72 (C9orf72) repeat expansions. *Journal of Neurochemistry* 138, 145-162.
- Topp, J.D., Gray, N.W., Gerard, R.D., and Horazdovsky, B.F. (2004). Alsin is a Rab5 and Rac1 guanine nucleotide exchange factor. *J Biol Chem* 279, 24612-24623.
- Torralba, D., Baixauli, F., and Sánchez-Madrid, F. (2016). Mitochondria Know No Boundaries: Mechanisms and Functions of Intercellular Mitochondrial Transfer. *Frontiers in Cell and Developmental Biology* 4, 107.
- Tran, H., Almeida, S., Moore, J., Gendron, T.F., Chalasani, U., Lu, Y., Du, X., Nickerson, J.A., Petrucelli, L., Weng, Z., *et al.* (2015). Differential Toxicity of Nuclear RNA Foci versus Dipeptide Repeat Proteins in a *Drosophila* Model of C9ORF72 FTD/ALS. *Neuron* 87, 1207-1214.
- Tresse, E., Salomons, F.A., Vesa, J., Bott, L.C., Kimonis, V., Yao, T.P., Dantuma, N.P., and Taylor, J.P. (2010). VCP/p97 is essential for maturation of ubiquitin-containing autophagosomes and this function is impaired by mutations that cause IBMPFD. *Autophagy* 6, 217-227.
- Turner, M.R., Cagnin, A., Turkheimer, F.E., Miller, C.C., Shaw, C.E., Brooks, D.J., Leigh, P.N., and Banati, R.B. (2004). Evidence of widespread cerebral microglial activation in amyotrophic lateral sclerosis: an [11C](R)-PK11195 positron emission tomography study. *Neurobiol Dis* 15, 601-609.
- Turrens, J.F. (2003). Mitochondrial formation of reactive oxygen species. *Journal of Physiology* 552, 335-344.

- Ugolino, J., Ji, Y.J., Conchina, K., Chu, J., Nirujogi, R.S., Pandey, A., Brady, N.R., Hamacher-Brady, A., and Wang, J. (2016). Loss of C9orf72 Enhances Autophagic Activity via Deregulated mTOR and TFEB Signaling. *PLoS Genet* 12, e1006443.
- Uhlen, M., Fagerberg, L., Hallstrom, B.M., Lindskog, C., Oksvold, P., Mardinoglu, A., Sivertsson, A., Kampf, C., Sjostedt, E., Asplund, A., *et al.* (2015). Proteomics. Tissue-based map of the human proteome. *Science* 347, 1260419.
- Vaibhava, V., Nagabhushana, A., Chalasani, M.L., Sudhakar, C., Kumari, A., and Swarup, G. (2012). Optineurin mediates a negative regulation of Rab8 by the GTPase-activating protein TBC1D17. *J Cell Sci* 125, 5026-5039.
- Van Blitterswijk, M., DeJesus-Hernandez, M., Niemantsverdriet, E., Murray, M.E., Heckman, M.G., Diehl, N.N., Brown, P.H., Baker, M.C., Finch, N.A., Bauer, P.O., *et al.* (2013). Association between repeat sizes and clinical and pathological characteristics in carriers of C9ORF72 repeat expansions (Xpansize-72): A cross-sectional cohort study. *The Lancet Neurology* 12, 978-988.
- Van Blitterswijk, M., DeJesus-Hernandez, M., and Rademakers, R. (2012). How do C9ORF72 repeat expansions cause ALS and FTD: can we learn from other non-coding repeat expansion disorders? *Current Opinion in Neurology* 25, 689-700.
- Van Blitterswijk, M., Gendron, T.F., Baker, M.C., DeJesus-Hernandez, M., Finch, N.A., Brown, P.H., Daugherty, L.M., Murray, M.E., Heckman, M.G., Jiang, J., *et al.* (2015). Novel clinical associations with specific C9ORF72 transcripts in patients with repeat expansions in C9ORF72. *Acta neuropathologica* 130, 863-876.
- Van Blitterswijk, M., Mullen, B., Nicholson, A.M., Bieniek, K.F., Heckman, M.G., Baker, M.C., DeJesus-Hernandez, M., Finch, N.A., Brown, P.H., Murray, M.E., *et al.* (2014a). TMEM106B protects C9ORF72 expansion carriers against frontotemporal dementia. *Acta Neuropathol* 127, 397-406.
- Van Blitterswijk, M., Mullen, B., Wojtas, A., Heckman, M.G., Diehl, N.N., Baker, M.C., DeJesus-Hernandez, M., Brown, P.H., Murray, M.E., Hsiung, G.-Y.R., *et al.* (2014b). Genetic modifiers in carriers of repeat expansions in the C9ORF72 gene. *Molecular neurodegeneration* 9, 38-38.
- Van Den Bosch, L., Van Damme, P., Bogaert, E., and Robberecht, W. (2006). The role of excitotoxicity in the pathogenesis of amyotrophic lateral sclerosis. *Biochim Biophys Acta* 1762, 1068-1082.
- Van Den Bosch, L., Vandenberghe, W., Klaassen, H., Van Houtte, E., and Robberecht, W. (2000). Ca²⁺-permeable AMPA receptors and selective vulnerability of motor neurons. *Journal of the Neurological Sciences* 180, 29-34.
- van Es, M.A., Veldink, J.H., Saris, C.G.J., Blauw, H.M., Van Vught, P.W.J., Birve, A., Lemmens, R., Schelhaas, H.J., Groen, E.J.N., Huisman, M.H.B., *et al.* (2009). Genome-wide association study identifies 19p13.3 (UNC13A) and 9p21.2 as susceptibility loci for sporadic amyotrophic lateral sclerosis. *Nature Genetics* 41, 1083-1087.
- Van Humbeeck, C., Cornelissen, T., Hofkens, H., Mandemakers, W., Gevaert, K., De Strooper, B., and Vandenberghe, W. (2011). Parkin interacts with Ambra1 to induce mitophagy. *J Neurosci* 31, 10249-10261.
- Van Mossevelde, S., van der Zee, J., Gijssels, I., and *et al.* (2017). Clinical evidence of disease anticipation in families segregating a c9orf72 repeat expansion. *JAMA Neurology* 74, 445-452.
- van Rheenen, W., Shatunov, A., Dekker, A.M., McLaughlin, R.L., Diekstra, F.P., Pulit, S.L., van der Spek, R.A., Vosa, U., de Jong, S., Robinson, M.R., *et al.* (2016). Genome-wide association analyses identify new risk variants and the genetic architecture of amyotrophic lateral sclerosis. *Nat Genet* 48, 1043-1048.

- van Spronsen, M., Mikhaylova, M., Lipka, J., Schlager, M.A., van den Heuvel, D.J., Kuijpers, M., Wulf, P.S., Keijzer, N., Demmers, J., Kapitein, L.C., *et al.* (2013). TRAK/Milton motor-adaptor proteins steer mitochondrial trafficking to axons and dendrites. *Neuron* 77, 485-502.
- van Vliet, A.R., and Agostinis, P. (2018). Mitochondria-Associated Membranes and ER Stress. *Current topics in microbiology and immunology* 414, 73-102.
- Vance, C., Rogelj, B., Hortobágyi, T., De Vos, K.J., Nishimura, A.L., Sreedharan, J., Hu, X., Smith, B., Ruddy, D., Wright, P., *et al.* (2009). Mutations in FUS, an RNA processing protein, cause familial amyotrophic lateral sclerosis type 6. *Science* 323, 1208-1211.
- Vance, J.E. (1990). Phospholipid synthesis in a membrane fraction associated with mitochondria. *J Biol Chem* 265, 7248-7256.
- Vande Velde, C., McDonald, K.K., Boukhedimi, Y., McAlonis-Downes, M., Lobsiger, C.S., Bel Hadj, S., Zandona, A., Julien, J.-P., Shah, S.B., and Cleveland, D.W. (2011). Misfolded SOD1 Associated with Motor Neuron Mitochondria Alters Mitochondrial Shape and Distribution Prior to Clinical Onset. *PLoS One* 6, e22031.
- Varcianna, A., Myszczyńska, M.A., Castelli, L.M., O'Neill, B., Kim, Y., Talbot, J., Nyberg, S., Nyamali, I., Heath, P.R., Stopford, M.J., *et al.* (2019). Micro-RNAs secreted through astrocyte-derived extracellular vesicles cause neuronal network degeneration in C9orf72 ALS. *EBioMedicine*.
- Vielhaber, S., Kunz, D., Winkler, K., Wiedemann, F.R., Kirches, E., Feistner, H., Heinze, H.J., Elger, C.E., Schubert, W., and Kunz, W.S. (2000). Mitochondrial DNA abnormalities in skeletal muscle of patients with sporadic amyotrophic lateral sclerosis. *Brain* 123, 1339-1348.
- Vogtle, F.N., Burkhart, J.M., Gonczarowska-Jorge, H., Kucukkose, C., Taskin, A.A., Kopczynski, D., Ahrends, R., Mossmann, D., Sickmann, A., Zahedi, R.P., *et al.* (2017). Landscape of submitochondrial protein distribution. *Nat Commun* 8, 290.
- Waite, A.J., Bäumer, D., East, S., Neal, J., Morris, H.R., Ansorge, O., and Blake, D.J. (2014). Reduced C9orf72 protein levels in frontal cortex of amyotrophic lateral sclerosis and frontotemporal degeneration brain with the C9ORF72 hexanucleotide repeat expansion. *Neurobiology of Aging* 35, 1779e1775-1779e1713.
- Walensky, L.D. (2006). BCL-2 in the crosshairs: tipping the balance of life and death. *Cell Death & Differentiation* 13, 1339-1350.
- Wang, C., Telpoukhovskaia, M.A., Bahr, B.A., Chen, X., and Gan, L. (2018). Endolysosomal dysfunction: a converging mechanism in neurodegenerative diseases. *Current Opinion in Neurobiology* 48, 52-58.
- Wang, W., Li, L., Lin, W.L., Dickson, D.W., Petrucelli, L., Zhang, T., and Wang, X. (2013). The ALS disease-associated mutant TDP-43 impairs mitochondrial dynamics and function in motor neurons. *Human Molecular Genetics* 22, 4706-4719.
- Wang, W., Wang, L., Lu, J., Siedlak, S.L., Fujioka, H., Liang, J., Jiang, S., Ma, X., Jiang, Z., da Rocha, E.L., *et al.* (2016). The inhibition of TDP-43 mitochondrial localization blocks its neuronal toxicity. *Nature Medicine* 22, 869-878.
- Wang, X., and Schwarz, T.L. (2009). The mechanism of Ca²⁺-dependent regulation of kinesin-mediated mitochondrial motility. *Cell* 136, 163-174.
- Wang, X., Winter, D., Ashrafi, G., Schlehe, J., Wong, Y.L., Selkoe, D., Rice, S., Steen, J., LaVoie, M.J., and Schwarz, T.L. (2011). PINK1 and Parkin target Miro for phosphorylation and degradation to arrest mitochondrial motility. *Cell* 147, 893-906.

- Wang, Y., Serricchio, M., Jauregui, M., Shanbhag, R., Stoltz, T., Di Paolo, C.T., Kim, P.K., and McQuibban, G.A. (2015). Deubiquitinating enzymes regulate PARK2-mediated mitophagy. *Autophagy* 11, 595-606.
- Watanabe, S., Ilieva, H., Tamada, H., Nomura, H., Komine, O., Endo, F., Jin, S., Mancias, P., Kiyama, H., and Yamanaka, K. (2016). Mitochondria-associated membrane collapse is a common pathomechanism in SIGMAR1- and SOD1-linked ALS. *EMBO Molecular Medicine* 8, 1421-1437.
- Webster, C.P., Smith, E.F., Bauer, C.S., Moller, A., Hautbergue, G.M., Ferraiuolo, L., Myszczyńska, M.A., Higginbottom, A., Walsh, M.J., Whitworth, A.J., *et al.* (2016a). The C9orf72 protein interacts with Rab1a and the ULK1 complex to regulate initiation of autophagy. *EMBO Journal* 35, 1656-1676.
- Webster, C.P., Smith, E.F., Grierson, A.J., and De Vos, K.J. (2016b). C9orf72 plays a central role in Rab GTPase-dependent regulation of autophagy. *Small GTPases*, 1-10.
- Webster, C.P., Smith, E.F., Shaw, P.J., and De Vos, K.J. (2017). Protein homeostasis in amyotrophic lateral sclerosis: therapeutic opportunities? *Frontiers in Neuroscience*.
- Wei, Y., Chiang, W.C., Sumpter, R., Jr., Mishra, P., and Levine, B. (2017). Prohibitin 2 Is an Inner Mitochondrial Membrane Mitophagy Receptor. *Cell* 168, 224-238.e210.
- Weidberg, H., Shvets, E., Shpilka, T., Shimron, F., Shinder, V., and Elazar, Z. (2010). LC3 and GATE-16/GABARAP subfamilies are both essential yet act differently in autophagosome biogenesis. *The EMBO Journal* 29, 1792-1802.
- Weihofen, A., Thomas, K.J., Ostaszewski, B.L., Cookson, M.R., and Selkoe, D.J. (2009). Pink1 forms a multiprotein complex with Miro and Milton, linking Pink1 function to mitochondrial trafficking. *Biochemistry* 48, 2045-2052.
- Weinberg, S.E., Sena, L.A., and Chandel, N.S. (2015). Mitochondria in the regulation of innate and adaptive immunity. *Immunity* 42, 406-417.
- Wen, X., Tan, W., Westergard, T., Krishnamurthy, K., Markandaiah, S.S., Shi, Y., Lin, S., Shneider, Neil A., Monaghan, J., Pandey, Udai B., *et al.* (2014). Antisense Proline-Arginine RAN Dipeptides Linked to C9ORF72-ALS/FTD Form Toxic Nuclear Aggregates that Initiate In Vitro and In Vivo Neuronal Death. *Neuron* 84, 1213-1225.
- Wiedemann, F.R., Manfredi, G., Mawrin, C., Flint Beal, M., and Schon, E.A. (2002). Mitochondrial DNA and respiratory chain function in spinal cords of ALS patients. *Journal of Neurochemistry* 80, 616-625.
- Wiedemann, F.R., Winkler, K., Kuznetsov, A.V., Bartels, C., Vielhaber, S., Feistner, H., and Kunz, W.S. (1998). Impairment of mitochondrial function in skeletal muscle of patients with amyotrophic lateral sclerosis. *Journal of the Neurological Sciences* 156, 65-72.
- Wild, P., Farhan, H., McEwan, D.G., Wagner, S., Rogov, V.V., Brady, N.R., Richter, B., Korac, J., Waidmann, O., Choudhary, C., *et al.* (2011a). Phosphorylation of the autophagy receptor optineurin restricts Salmonella growth. *Science* 333, 228-233.
- Wild, P., Farhan, H., McEwan, D.G., Wagner, S., Rogov, V.V., Brady, N.R., Richter, B., Korac, J., Waidmann, O., Choudhary, C., *et al.* (2011b). Phosphorylation of the autophagy receptor optineurin restricts Salmonella growth. *Science* 333, 228-233.
- Williams, K.L., Topp, S., Yang, S., Smith, B., Fifita, J.A., Warraich, S.T., Zhang, K.Y., Farrarwell, N., Vance, C., Hu, X., *et al.* (2016). CCNF mutations in amyotrophic lateral sclerosis and frontotemporal dementia. *Nat Commun* 7, 11253.
- Williams, T.L., Day, N.C., Ince, P.G., Kamboj, R.K., and Shaw, P.J. (1997). Calcium-permeable α -amino-3-hydroxy-5-methyl-4-isoxazole propionic acid receptors: A

molecular determinant of selective vulnerability in amyotrophic lateral sclerosis. *Annals of Neurology* 42, 200-207.

Wong, P.T., McGeer, E.G., and McGeer, P.L. (1981). A sensitive radiometric assay for ornithine aminotransferase: regional and subcellular distributions in rat brain. *J Neurochem* 36, 501-505.

Wong, Y.C., and Holzbaur, E.L.F. (2014). Optineurin is an autophagy receptor for damaged mitochondria in parkin-mediated mitophagy that is disrupted by an ALS-linked mutation. *Proceedings of the National Academy of Sciences of the United States of America* 111, E4439-E4448.

Woo, J.-A.A., Liu, T., Trotter, C., Fang, C.C., De Narvaez, E., LePochat, P., Maslar, D., Bukhari, A., Zhao, X., Deonarine, A., *et al.* (2017). Loss of function CHCHD10 mutations in cytoplasmic TDP-43 accumulation and synaptic integrity. *Nature Communications* 8, 15558.

Wu, C.H., Fallini, C., Ticozzi, N., Keagle, P.J., Sapp, P.C., Piotrowska, K., Lowe, P., Koppers, M., McKenna-Yasek, D., Baron, D.M., *et al.* (2012). Mutations in the profilin 1 gene cause familial amyotrophic lateral sclerosis. *Nature* 488, 499-503.

Wu, W., Tian, W., Hu, Z., Chen, G., Huang, L., Li, W., Zhang, X., Xue, P., Zhou, C., Liu, L., *et al.* (2014). ULK1 translocates to mitochondria and phosphorylates FUNDC1 to regulate mitophagy. *EMBO Rep* 15, 566-575.

Wu, X., Yen, L., Irwin, L., Sweeney, C., and Carraway, K.L., 3rd (2004). Stabilization of the E3 ubiquitin ligase Nrdp1 by the deubiquitinating enzyme USP8. *Mol Cell Biol* 24, 7748-7757.

Xi, Z., van Blitterswijk, M., Zhang, M., McGoldrick, P., McLean, J.R., Yunusova, Y., Knock, E., Moreno, D., Sato, C., McKeever, P.M., *et al.* (2015). Jump from pre-mutation to pathologic expansion in C9orf72. *Am J Hum Genet* 96, 962-970.

Xi, Z., Zinman, L., Moreno, D., Schymick, J., Liang, Y., Sato, C., Zheng, Y., Ghani, M., Dib, S., Keith, J., *et al.* (2013). Hypermethylation of the CpG island near the G4C2 repeat in ALS with a C9orf72 expansion. *American Journal of Human Genetics* 92, 981-989.

Xia, R., Jia, H., Fan, J., Liu, Y., and Jia, J. (2012). USP8 Promotes Smoothed Signaling by Preventing Its Ubiquitination and Changing Its Subcellular Localization. *PLoS Biology* 10, e1001238.

Xiao, S., MacNair, L., McGoldrick, P., McKeever, P.M., McLean, J.R., Zhang, M., Keith, J., Zinman, L., Rogaeva, E., and Robertson, J. (2015). Isoform-specific antibodies reveal distinct subcellular localizations of C9orf72 in amyotrophic lateral sclerosis. *Ann Neurol* 78, 568-583.

Xiao, S., McLean, J., and Robertson, J. (2006). Neuronal intermediate filaments and ALS: A new look at an old question. *Biochimica et Biophysica Acta (BBA) - Molecular Basis of Disease* 1762, 1001-1012.

Xiao, S., Sanelli, T., Dib, S., Sheps, D., Findlater, J., Bilbao, J., Keith, J., Zinman, L., Rogaeva, E., and Robertson, J. (2011). RNA targets of TDP-43 identified by UV-CLIP are deregulated in ALS. *Molecular and Cellular Neuroscience* 47, 167-180.

Xu, J., Fotouhi, M., and McPherson, P.S. (2015). Phosphorylation of the exchange factor DENND3 by ULK in response to starvation activates Rab12 and induces autophagy. *EMBO Rep* 16, 709-718.

Xu, Y.F., Gendron, T.F., Zhang, Y.J., Lin, W.L., D'Alton, S., Sheng, H., Casey, M.C., Tong, J., Knight, J., Yu, X., *et al.* (2010). Wild-type human TDP-43 expression causes TDP-43 phosphorylation, mitochondrial aggregation, motor deficits, and early mortality in transgenic mice. *Journal of Neuroscience* 30, 10851-10859.

- Xu, Y.F., Zhang, Y.J., Lin, W.L., Cao, X., Stetler, C., Dickson, D.W., Lewis, J., and Petrucelli, L. (2011). Expression of mutant TDP-43 induces neuronal dysfunction in transgenic mice. *Molecular Neurodegeneration* 6.
- Yamano, K., Fogel, A.I., Wang, C., van der Bliek, A.M., and Youle, R.J. (2014). Mitochondrial Rab GAPs govern autophagosome biogenesis during mitophagy. *eLife* 3, e01612.
- Yamano, K., Matsuda, N., and Tanaka, K. (2016). The ubiquitin signal and autophagy: an orchestrated dance leading to mitochondrial degradation. *EMBO Reports* 17, 300-316.
- Yamano, K., Wang, C., Sarraf, S.A., Munch, C., Kikuchi, R., Noda, N.N., Hizukuri, Y., Kanemaki, M.T., Harper, W., Tanaka, K., *et al.* (2018). Endosomal Rab cycles regulate Parkin-mediated mitophagy. *eLife* 7.
- Yamano, K., and Youle, R.J. (2013). PINK1 is degraded through the N-end rule pathway. *Autophagy* 9, 1758-1769.
- Yang, M., Liang, C., Swaminathan, K., Herrlinger, S., Lai, F., Shiekhhattar, R., and Chen, J.F. (2016). A C9ORF72/SMCR8-containing complex regulates ULK1 and plays a dual role in autophagy. *Science Advances* 2, e1601167.
- Yeates, E.F.A., and Tesco, G. (2016). The Endosome-associated Deubiquitinating Enzyme USP8 Regulates BACE1 Enzyme Ubiquitination and Degradation. *Journal of Biological Chemistry* 291, 15753-15766.
- Yoo, S.-M., and Jung, Y.-K. (2018). A Molecular Approach to Mitophagy and Mitochondrial Dynamics. *Molecules and Cells* 41, 18-26.
- Yoshii, S.R., Kishi, C., Ishihara, N., and Mizushima, N. (2011). Parkin Mediates Proteasome-dependent Protein Degradation and Rupture of the Outer Mitochondrial Membrane. *The Journal of Biological Chemistry* 286, 19630-19640.
- Yoshii, S.R., and Mizushima, N. (2015). Autophagy machinery in the context of mammalian mitophagy. *Biochimica et Biophysica Acta (BBA) - Molecular Cell Research* 1853, 2797-2801.
- Youle, R.J., and van der Bliek, A.M. (2012). Mitochondrial fission, fusion, and stress. *Science* 337, 1062-1065.
- Zachari, M., and Ganley, I.G. (2017). The mammalian ULK1 complex and autophagy initiation. *Essays in biochemistry* 61, 585-596.
- Zarei, S., Carr, K., Reiley, L., Diaz, K., Guerra, O., Altamirano, P.F., Pagani, W., Lodin, D., Orozco, G., and Chinaea, A. (2015). A comprehensive review of amyotrophic lateral sclerosis. *Surgical Neurology International* 6, 171.
- Zhang, D., Iyer, L.M., He, F., and Aravind, L. (2012). Discovery of Novel DENN Proteins: Implications for the Evolution of Eukaryotic Intracellular Membrane Structures and Human Disease. *Front Genet* 3, 283.
- Zhang, F., Strom, A.L., Fukada, K., Lee, S., Hayward, L.J., and Zhu, H. (2007). Interaction between familial amyotrophic lateral sclerosis (ALS)-linked SOD1 mutants and the dynein complex. *Journal of Biological Chemistry* 282, 16691-16699.
- Zhang, F., Wang, W., Siedlak, S.L., Liu, Y., Liu, J., Jiang, K., Perry, G., Zhu, X., and Wang, X. (2015a). Miro1 deficiency in amyotrophic lateral sclerosis. *Frontiers in Aging Neuroscience* 7, 100.
- Zhang, K., Donnelly, C.J., Haeusler, A.R., Grima, J.C., Machamer, J.B., Steinwald, P., Daley, E.L., Miller, S.J., Cunningham, K.M., Vidensky, S., *et al.* (2015b). The C9orf72 repeat expansion disrupts nucleocytoplasmic transport. *Nature* 525, 56-61.

- Zhang, Y., Burberry, A., Wang, J.Y., Sandoe, J., Ghosh, S., Udeshi, N.D., Svinkina, T., Mordes, D.A., Mok, J., Charlton, M., *et al.* (2018). The C9orf72-interacting protein Smcr8 is a negative regulator of autoimmunity and lysosomal exocytosis. *Genes Dev* 32, 929-943.
- Zhang, Y., Gao, J., Chung, K.K.K., Huang, H., Dawson, V.L., and Dawson, T.M. (2000). Parkin functions as an E2-dependent ubiquitin– protein ligase and promotes the degradation of the synaptic vesicle-associated protein, CDCrel-1. *Proceedings of the National Academy of Sciences* 97, 13354.
- Zhang, Y.J., Jansen-West, K., Xu, Y.F., Gendron, T.F., Bieniek, K.F., Lin, W.L., Sasaguri, H., Caulfield, T., Hubbard, J., Daughrity, L., *et al.* (2014). Aggregation-prone c9FTD/ALS poly(GA) RAN-translated proteins cause neurotoxicity by inducing ER stress. *Acta Neuropathol* 128, 505-524.
- Zhao, T., Huang, X., Han, L., Wang, X., Cheng, H., Zhao, Y., Chen, Q., Chen, J., Cheng, H., Xiao, R., *et al.* (2012). Central role of mitofusin 2 in autophagosome-lysosome fusion in cardiomyocytes. *J Biol Chem* 287, 23615-23625.
- Zhao, Z.H., Chen, W.Z., Wu, Z.Y., Wang, N., Zhao, G.X., Chen, W.J., and Murong, S.X. (2009). A novel mutation in the senataxin gene identified in a Chinese patient with sporadic amyotrophic lateral sclerosis. *Amyotrophic Lateral Sclerosis* 10, 118-122.
- Zhen, Y., and Stenmark, H. (2015). Cellular functions of Rab GTPases at a glance. *Journal of Cell Science* 128, 3171.
- Zhong, Y., Wang, Q.J., Li, X., Yan, Y., Backer, J.M., Chait, B.T., Heintz, N., and Yue, Z. (2009). Distinct regulation of autophagic activity by Atg14L and Rubicon associated with Beclin 1-phosphatidylinositol-3-kinase complex. *Nat Cell Biol* 11, 468-476.
- Zhong, Z., Umemura, A., Sanchez-Lopez, E., Liang, S., Shalpour, S., Wong, J., He, F., Boassa, D., Perkins, G., Ali, S.R., *et al.* (2016). NF-kappaB Restricts Inflammasome Activation via Elimination of Damaged Mitochondria. *Cell* 164, 896-910.
- Zhou, B., Liu, C., Geng, Y., and Zhu, G. (2015). Topology of a G-quadruplex DNA formed by C9orf72 hexanucleotide repeats associated with ALS and FTD. *Scientific Reports* 5, 16673.
- Zhou, C., Ma, K., Gao, R., Mu, C., Chen, L., Liu, Q., Luo, Q., Feng, D., Zhu, Y., and Chen, Q. (2016). Regulation of mATG9 trafficking by Src- and ULK1-mediated phosphorylation in basal and starvation-induced autophagy. *Cell Research* 27, 184.
- Zhou, Q., Lehmer, C., Michaelsen, M., Mori, K., Alterauge, D., Baumjohann, D., Schludi, M.H., Greiling, J., Farny, D., Flatley, A., *et al.* (2017). Antibodies inhibit transmission and aggregation of C9orf72 poly-GA dipeptide repeat proteins. *EMBO Mol Med* 9, 687-702.
- Zhou, Q.H., Deng, C.Z., Li, Z.S., Chen, J.P., Yao, K., Huang, K.B., Liu, T.Y., Liu, Z.W., Qin, Z.K., Zhou, F.J., *et al.* (2018). Molecular characterization and integrative genomic analysis of a panel of newly established penile cancer cell lines. *Cell death & disease* 9, 684.
- Zhu, H., Foretz, M., Xie, Z., Zhang, M., Zhu, Z., Xing, J., Leclerc, J., Gaudry, M., Viollet, B., and Zou, M.H. (2014). PRKAA1/AMPKalpha1 is required for autophagy-dependent mitochondrial clearance during erythrocyte maturation. *Autophagy* 10, 1522-1534.
- Zu, T., Liu, Y., Bañez-Coronel, M., Reid, T., Pletnikova, O., Lewis, J., Miller, T.M., Harms, M.B., Falchook, A.E., Subramony, S.H., *et al.* (2013). RAN proteins and RNA foci from antisense transcripts in C9ORF72 ALS and frontotemporal dementia. *Proceedings of the National Academy of Sciences of the United States of America* 110, E4968-E4977.

Zuo, Y., Xiang, B., Yang, J., Sun, X., Wang, Y., Cang, H., and Yi, J. (2009). Oxidative modification of caspase-9 facilitates its activation via disulfide-mediated interaction with Apaf-1. *Cell Res* 19, 449-457.